

General Disclaimer

One or more of the Following Statements may affect this Document

- This document has been reproduced from the best copy furnished by the organizational source. It is being released in the interest of making available as much information as possible.
- This document may contain data, which exceeds the sheet parameters. It was furnished in this condition by the organizational source and is the best copy available.
- This document may contain tone-on-tone or color graphs, charts and/or pictures, which have been reproduced in black and white.
- This document is paginated as submitted by the original source.
- Portions of this document are not fully legible due to the historical nature of some of the material. However, it is the best reproduction available from the original submission.

954668

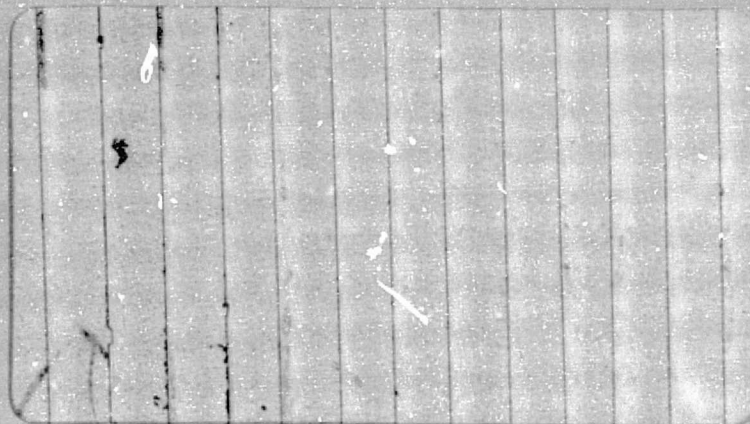
OCEAN DATA SYSTEMS, INC.

(NASA-CR-157327) ATMOSPHERIC MODEL
DEVELOPMENT IN SUPPORT OF SEASAT. VOLUME 1:
SUMMARY OF FINDINGS Final Technical Report
(Ocean Data Systems, Inc.) 303 p HC A14/MF
A01

N78-28579

Unclas
25955

CSCL 22A G3/43





OCEAN DATA SYSTEMS, INC.

2400 GARDEN ROAD, MONTEREY, CALIFORNIA 93940 • 408/649-1133

Submitted to
JET PROPULSION LABORATORY
Pasadena, California

ATMOSPHERIC MODEL DEVELOPMENT
IN SUPPORT OF SEASAT

VOLUME I - SUMMARY OF FINDINGS

Final Technical Report

Prepared under
JPL Contract Number 954668
(Subcontract of NASA Contract Number NAS7-100)

September 30, 1977

Prepared by
Philip G. Kesel
OCEAN DATA SYSTEMS, INC.
Monterey, California

EXECUTIVE SUMMARY

This Final Report (in five volumes) was prepared by Ocean Data Systems, Inc. for the Jet Propulsion Laboratory under Contract No. 954668 (as amended) in support of the SEASAT Program.

The objective was to develop atmospheric analysis and prediction models of varying (grid) resolution, and to test the models using real observational data for the purpose of assessing the impact of grid resolution on short-range numerical weather prediction. Secondly, the discretionary model procedures had to be examined so that the computational viability of SEASAT data might be enhanced during the conduct of (future) sensitivity tests.

ODSI has: (1) completed and tested an entire sequence of objective analysis models; (2) developed and tested four versions of an atmospheric prediction model on grids of differing horizontal and/or vertical resolution; (3) prepared a real data base consisting of two four-day meteorological scenarios (using the analysis models); (4) exercised all analysis and prediction models (on the CYBER 175 at FNWC and the CDC 7600 at NASA Ames); and (5) conducted sensitivity studies with the forecast model to order the impacts of individual procedures and effects.

A. General Description

These hemispheric models were designed for use on either of two horizontal grids: (1) a 63 x 63 coarse-mesh grid (CMG); and (2) a 187 x 187 fine-mesh grid (FMG). On the CMG, the true-earth mesh distance varies from 204 kilometers at the equator to 408 kilometers at the pole. On the FMG, it varies from 68 to 136 kilometers. The scales of meteorological interest can be handled very well on the FMG.

The objective analysis models are based on a Pattern Conserving Technique (PCT) which accommodates observations while preserving differential properties of the first-guess field (under a system of weights). In the multi-level upper-air analysis, the 1000- to 100-MB region was resolved with ten layers for better representation of stable layers in the lower troposphere. Stratospheric extensions (from 100 to 10 MBS) to the mass structure were obtained using regression equations. Although analyses were performed on the FMG, the forecast models were initialized using interpolated CMG values. In the analysis effort, ODSI: (1) examined procedures for allowing data to influence the analysis; (2) examined the effects of varying the weights in the analysis procedure; (3) tested and implemented procedures for solving the minimization equation in an optimal way; (4) described the impact of grid resolution on analysis; and (5) devised and implemented numerous practical solutions to analysis problems, generally.

The hemispheric prediction models contain suitable numerics and physics for generating operationally-competitive forecasts. Each model was exercised in either a 5-layer or 10-layer mode on either the CMG or FMG. The contribution of each process, procedure and parameter to a forecast was ordered and examined. Clearly, the primary consideration in prediction is to pose the initial conditions properly (through adequate data, resolution and initialization methods). Complex forecast models, however, employ "computational devices" (such as smoothers, tendency truncators, mountain shaping, diffusion operators, temporal filters) for both stability and cosmetic purposes. The use/misuse of such devices can mask the effects of modeled processes and effects.

The effects of resolution on prediction modeling are presented in terms of: (1) forecast charts; (2) forecast change/error charts; (3) forecast difference charts (10-layer minus 5-layer or 187 x 187 forecast minus 63 x 63 forecast); and (4) statistical/graphical information describing model performance and model behavior (energetics).

B. Summary of Findings

Increases in horizontal resolution are computationally expensive, but they lead to significant improvements in model performance and behavior. For a given number of vertical

layers, the three-fold increase in horizontal resolution represents a 27X problem. Numerically, the benefits are: (1) more realistic phase speeds of fronts/troughs; (2) better representation of gradients; (3) the possibility of treating additional smaller scales; and (4) the reduction of harmful effects of computational devices. In terms of the physics, the benefits are: (1) the scale of dissipation becomes further removed from those scales producing eddy kinetic energy; (2) the effects of parameterized physical processes are better retained in small scales, instead of being smeared upscale; (3) a 100% increase in modeled precipitation; and (4) better treatment of energy conversions in baroclinic scales (cyclogenesis).

Increases in vertical resolution tend to produce smaller effects. The ten-layer models predicted 10-20% less precipitation than the five-layer models (on both the FMG and CMG). There was no significant improvement indicated with respect to prediction of pressure system intensity. Increased vertical resolution permits improved specification of high-altitude conditions, but the impact on sea-level pressure forecasts is minimal.

Analysis models must be capable of distributing observed information into scales which are computationally viable in the prediction models. More study of data influence functions and dynamic coupling of atmospheric variables is needed.

In the prediction models, the need for dynamic initialization is readily apparent. Such procedures may be computationally expensive, but they are needed to: (1) minimize the harmful effects of initialization shock; (2) improve model energetics; and (3) stabilize the model context to prevent "wash out" of information in the smaller scales (such as SEASAT data).

Finally, the effects of discretionary procedures in prediction models must be understood, ordered and exploited. Physical effects are often small compared to the effects of "cosmetic operators".

TABLE OF CONTENTS

<u>Section</u>	<u>Page</u>
EXECUTIVE SUMMARY.....	ii
LIST OF FIGURES.....	x
LIST OF TABLES.....	xv
LIST OF CHARTS.....	xviii
I. INTRODUCTION.....	I-1
II. SCOPE OF WORK.....	II-1
A. General Certification.....	II-2
B. Definitions and Cross-References.....	II-3
1. Analyses.....	II-4
2. Forecasts.....	II-5
III. ANALYSIS MODEL DEVELOPMENT.....	III-1
1. Vertical Resolution.....	III-2
2. Horizontal Resolution.....	III-2
A. Objective Analysis: Discussion.....	III-3
B. A Scheme for Objective Analysis: Pattern Conservation Technique (PCT)....	III-5
1. Solution Method for PCT Equations.....	III-7
2. Analysis Code Sequence and Computer Requirements.....	III-11
C. Data Influence Region.....	III-13
D. The Effects of Varying the Weights.....	III-15
E. Some Practical Solutions to Analysis Problems.....	III-17
1. Problems in Low Latitudes.....	III-18
2. Analyzed vs. Retrieved Temperatures.....	III-20
F. Data Base Preparation.....	III-22
G. Charts and Tables.....	III-24
1. Scenario A Discussion.....	III-24
2. Scenario B Discussion.....	III-27
H. Effects of Grid Resolution.....	III-29
1. Scenario A.....	III-29
2. Scenario B.....	III-30
3. Sea-Surface Temperature (SST).....	III-31

TABLE OF CONTENTS (Continued)

<u>Section</u>	<u>Page</u>
IV. PREDICTION MODEL DEVELOPMENT.....	IV-1
A. Model Description.....	IV-2
B. Special Characteristics.....	IV-6
1. Geostrophic 50-MB Winds.....	IV-6
2. Moisture Initialization Algorithm...	IV-6
3. Special Processing of Outputs.....	IV-7
4. Special Processing of Inputs to Fine-Mesh (187 x 187) Models.....	IV-7
5. Lateral Boundary Conditions and Tendency Truncation.....	IV-8
6. Pressure-Gradient Force (PGF) Time-Averaging in Momentum Equations.....	IV-8
7. Temporal Filtering of Thermo- dynamic and Moisture Equations.....	IV-9
8. Non-Linear Pressure (Tendency Equation) Smoothing.....	IV-9
9. Horizontal Diffusion.....	IV-10
10. Temporal Differencing.....	IV-10
11. Diabatic Heating in Low Latitudes...	IV-11
12. Tapered Terrain.....	IV-11
C. Computer Utilization.....	IV-11
V. PREDICTION MODEL TEST RESULTS.....	V-1
A. Scenario A: Forecasts, Forecast Changes, Forecast Errors.....	V-2
1. Run F22 (PEFHCV).....	V-3
2. Run F18 (PECHCV).....	V-4
3. Run T4 (PECHFV).....	V-5
4. Run F20 (PECHCV).....	V-6
5. Run T6 (PECHFV).....	V-7
B. Scenario B: Forecasts, Forecast Changes, Forecast Errors.....	V-8
1. Run F24 (PEFHCV).....	V-8
2. Run F19 (PECHCV).....	V-9
3. Run T5 (PECHFV).....	V-10
C. Scenario A: Comparative Performance Data.....	V-11
1. Intensity of Pressure Systems at Sea Level.....	V-11
2. Performance Statistics.....	V-12

TABLE OF CONTENTS (Continued)

<u>Section</u>	<u>Page</u>
3. Kinetic Energy (KE).....	V-12
4. Square Vorticity.....	V-14
5. Square Divergence.....	V-14
6. Temperature.....	V-15
7. Precipitation.....	V-15
D. Scenario B: Comparative Performance	
Data.....	V-15
1. Intensity of Pressure Systems at Sea Level.....	V-15
2. Performance Statistics.....	V-16
3. Kinetic Energy (KE).....	V-16
4. Square Vorticity.....	V-18
5. Square Divergence.....	V-18
6. Temperature.....	V-18
7. Precipitation.....	V-19
E. Effects of Changes in Model Vertical Resolution on Sea-Level Pressure and 500-MB Height Forecasts.....	V-19
1. Scenario A Comparisons.....	V-19
2. Scenario B Comparisons.....	V-21
F. Effects of Changes in Model Horizontal Resolution on Sea-Level Pressure and 500-MB Height Forecasts.....	V-22
1. Scenario A Comparison.....	V-22
2. Scenario B Comparison.....	V-22
VI. FIGURES.....	VI-1
VII. TABLES.....	VII-1
VIII. CHARTS.....	VIII-1

LIST OF FIGURES

Figure

- VI-1 KINETIC ENERGY 24-HOUR FORECAST CHANGE (%), BY MODEL VERSION AND LEVEL. SCENARIO A.
- VI-2 KINETIC ENERGY ($\times 10$) 24-HOUR FORECAST CROSS-SECTION. RUN T4. MODEL PECHFV. SCENARIO A.
- VI-3 KINETIC ENERGY ($\times 10$) 24-HOUR FORECAST CROSS-SECTION. RUN F18. MODEL PECHCV. SCENARIO A.
- VI-4 KINETIC ENERGY ($\times 10$) 24-HOUR FORECAST CROSS-SECTION. RUN F22. MODEL PEFHCV. SCENARIO A.
- VI-5 TIME VARIATION OF KINETIC ENERGY FOR THREE MODEL VERSIONS AT SIGMA=0.9 LEVEL. SCENARIO A.
- VI-6 TIME VARIATION OF KINETIC ENERGY FOR THREE MODEL VERSIONS AT SIGMA=0.7 LEVEL. SCENARIO A.
- VI-7 TIME VARIATION OF KINETIC ENERGY FOR THREE MODEL VERSIONS AT SIGMA=0.5 LEVEL. SCENARIO A.
- VI-8 TIME VARIATION OF KINETIC ENERGY FOR THREE MODEL VERSIONS AT SIGMA=0.3 LEVEL. SCENARIO A.
- VI-9 TIME VARIATION OF KINETIC ENERGY FOR THREE MODEL VERSIONS AT SIGMA=0.1 LEVEL. SCENARIO A.
- VI-10 SQUARE VORTICITY 24-HOUR FORECAST CHANGE (%), BY MODEL VERSION AND LEVEL. SCENARIO A.
- VI-11 TIME VARIATION OF SQUARE VORTICITY FOR THREE MODEL VERSIONS AT SIGMA=0.9 LEVEL. SCENARIO A.

LIST OF FIGURES (Continued)

Figure

- VI-12 TIME VARIATION OF SQUARE VORTICITY FOR THREE
MODEL VERSIONS AT SIGMA=0.7 LEVEL. SCENARIO A.
- VI-13 TIME VARIATION OF SQUARE VORTICITY FOR THREE
MODEL VERSIONS AT SIGMA=0.5 LEVEL. SCENARIO A.
- VI-14 TIME VARIATION OF SQUARE VORTICITY FOR THREE
MODEL VERSIONS AT SIGMA=0.3 LEVEL. SCENARIO A.
- VI-15 TIME VARIATION OF SQUARE VORTICITY FOR THREE
MODEL VERSIONS AT SIGMA=0.1 LEVEL. SCENARIO A.
- VI-16 TIME VARIATION OF SQUARE DIVERGENCE FOR THREE
MODEL VERSIONS AT SIGMA=0.9 LEVEL. SCENARIO A.
- VI-17 TIME VARIATION OF SQUARE DIVERGENCE FOR THREE
MODEL VERSIONS AT SIGMA=0.7 LEVEL. SCENARIO A.
- VI-18 TIME VARIATION OF SQUARE DIVERGENCE FOR THREE
MODEL VERSIONS AT SIGMA=0.5 LEVEL. SCENARIO A.
- VI-19 TIME VARIATION OF SQUARE DIVERGENCE FOR THREE
MODEL VERSIONS AT SIGMA=0.3 LEVEL. SCENARIO A.
- VI-20 TIME VARIATION OF SQUARE DIVERGENCE FOR THREE
MODEL VERSIONS AT SIGMA=0.1 LEVEL. SCENARIO A.
- VI-21 KINETIC ENERGY 24-HOUR FORECAST CHANGE (%), BY
MODEL VERSION AND LEVEL. SCENARIO B.
- VI-22 KINETIC ENERGY (x10) 24-HOUR FORECAST CROSS-
SECTION. RUN T5. MODEL PECHFV. SCENARIO B.

LIST OF FIGURES (Continued)

Figure

- VI-23 KINETIC ENERGY ($\times 10$) 24-HOUR FORECAST CROSS-SECTION. RUN F19. MODEL PECHCV. SCENARIO B.
- VI-24 KINETIC ENERGY ($\times 10$) 24-HOUR FORECAST CROSS-SECTION. RUN F24. MODEL PEFHCV. SCENARIO B.
- VI-25 TIME VARIATION OF KINETIC ENERGY FOR THREE MODEL VERSIONS AT SIGMA=0.9 LEVEL. SCENARIO B.
- VI-26 TIME VARIATION OF KINETIC ENERGY FOR THREE MODEL VERSIONS AT SIGMA=0.7 LEVEL. SCENARIO B.
- VI-27 TIME VARIATION OF KINETIC ENERGY FOR THREE MODEL VERSIONS AT SIGMA=0.5 LEVEL. SCENARIO B.
- VI-28 TIME VARIATION OF KINETIC ENERGY FOR THREE MODEL VERSIONS AT SIGMA=0.3 LEVEL. SCENARIO B.
- VI-29 TIME VARIATION OF KINETIC ENERGY FOR THREE MODEL VERSIONS AT SIGMA=0.1 LEVEL. SCENARIO B.
- VI-30 SQUARE VORTICITY 24-HOUR FORECAST CHANGE (%), BY MODEL VERSION AND LEVEL. SCENARIO B.
- VI-31 TIME VARIATION OF SQUARE VORTICITY FOR THREE MODEL VERSIONS AT SIGMA=0.9 LEVEL. SCENARIO B.
- VI-32 TIME VARIATION OF SQUARE VORTICITY FOR THREE MODEL VERSIONS AT SIGMA=0.7 LEVEL. SCENARIO B.
- VI-33 TIME VARIATION OF SQUARE VORTICITY FOR THREE MODEL VERSIONS AT SIGMA=0.5 LEVEL. SCENARIO B.

LIST OF FIGURES (Continued)

Figure

- VI-34 TIME VARIATION OF SQUARE VORTICITY FOR THREE MODEL
VERSIONS AT SIGMA=0.3 LEVEL. SCENARIO B.
- VI-35 TIME VARIATION OF SQUARE VORTICITY FOR THREE MODEL
VERSIONS AT SIGMA=0.1 LEVEL. SCENARIO B.
- VI-36 TIME VARIATION OF SQUARE DIVERGENCE FOR THREE MODEL
VERSIONS AT SIGMA=0.9 LEVEL. SCENARIO B.
- VI-37 TIME VARIATION OF SQUARE DIVERGENCE FOR THREE MODEL
VERSIONS AT SIGMA=0.7 LEVEL. SCENARIO B.
- VI-38 TIME VARIATION OF SQUARE DIVERGENCE FOR THREE MODEL
VERSIONS AT SIGMA=0.5 LEVEL. SCENARIO B.
- VI-39 TIME VARIATION OF SQUARE DIVERGENCE FOR THREE MODEL
VERSIONS AT SIGMA=0.3 LEVEL. SCENARIO B.
- VI-40 TIME VARIATION OF SQUARE DIVERGENCE FOR THREE MODEL
VERSIONS AT SIGMA=0.1 LEVEL. SCENARIO B.
- VI-41 TEMPERATURE 24-HOUR FORECAST CHANGE ($^{\circ}\text{C}$), BY
LATITUDE AND LEVEL. RUN T4. MODEL PECHFV.
SCENARIO A.
- VI-42 TEMPERATURE 24-HOUR FORECAST CHANGE ($^{\circ}\text{C}$), BY
LATITUDE AND LEVEL. RUN F18. MODEL PECHCV.
SCENARIO A.
- VI-43 TEMPERATURE 24-HOUR FORECAST CHANGE ($^{\circ}\text{C}$), BY
LATITUDE AND LEVEL. RUN F22. MODEL PEPHCV.
SCENARIO A.

LIST OF FIGURES (Continued)

Figure

- VI-44 TEMPERATURE 24-HOUR FORECAST CHANGE ($^{\circ}\text{C}$), BY
LATITUDE AND LEVEL. RUN T5. MODEL PECHV.
SCENARIO B.
- VI-45 TEMPERATURE 24-HOUR FORECAST CHANGE ($^{\circ}\text{C}$), BY
LATITUDE AND LEVEL. RUN F19. MODEL PEPHEV.
SCENARIO B.
- VI-46 TEMPERATURE 24-HOUR FORECAST CHANGE ($^{\circ}\text{C}$), BY
LATITUDE AND LEVEL. RUN F24. MODEL PEPHEV.
SCENARIO B.
- VI-47 PRECIPITATION (PER GRID POINT) FOR THREE MODEL
VERSIONS. SCENARIO A.
- VI-48 PRECIPITATION (PER GRID POINT) FOR THREE MODEL
VERSIONS. SCENARIO B.

LIST OF TABLES

Table

- VII-1 24-HOUR FORECAST CENTRAL PRESSURES (MBS) USING THREE MODELS OF DIFFERING RESOLUTION. SCENARIO A.
- VII-2 24-HOUR FORECAST CENTRAL PRESSURES (MBS) USING THREE MODELS OF DIFFERING RESOLUTION. SCENARIO B.
- VII-3 PERFORMANCE STATISTICS FOR FORECAST MODELS OF DIFFERING RESOLUTION: 500 MB HEIGHTS (METERS).
- VII-4 PERFORMANCE STATISTICS FOR FORECAST MODELS OF DIFFERING RESOLUTION: SEA-LEVEL PRESSURE (MBS).
- VII-5 KINETIC ENERGY 24-HOUR FORECAST CHANGES, FOR MODELS OF VARYING RESOLUTION AND TWO SCENARIOS (GIVEN IN PERCENT).
- VII-6 SQUARE VORTICITY 24-HOUR FORECAST CHANGES, FOR MODELS OF VARYING RESOLUTION AND TWO SCENARIOS (GIVEN IN PERCENT).
- VII-7 THE EFFECT OF (FORECAST) MODEL RESOLUTION ON PRECIPITATION.
- VII-8 STATISTICAL DIFFERENCES BETWEEN 187 x 187 AND 63 x 63 ANALYSES.
- VII-9 STATISTICAL DIFFERENCES BETWEEN 187 x 187 FORECAST AND 63 x 63 FORECAST. SCENARIO A.
- VII-10 STATISTICAL DIFFERENCES BETWEEN 187 x 187 FORECAST AND 63 x 63 FORECAST. SCENARIO B.

LIST OF TABLES (Continued)

Table

VII-11	ACTUAL CHANGES (FINAL MINUS INITIAL ANALYSIS). SCENARIO <u>A</u> .
VII-12	MODEL STATISTICS. RUN <u>F22</u> . MODEL <u>PEFHCV</u> . SCENARIO <u>A</u> . TEST SERIES B ANALYSES.
VII-13	MODEL STATISTICS. RUN <u>F18</u> . MODEL <u>PECHCV</u> . SCENARIO <u>A</u> . TEST SERIES B ANALYSES.
VII-14	MODEL STATISTICS. RUN <u>T4</u> . MODEL <u>PECHFV</u> . SCENARIO <u>A</u> . TEST SERIES B ANALYSES.
VII-15	MODEL STATISTICS. RUN <u>F20</u> . MODEL <u>PECHCV</u> . SCENARIO <u>A</u> . PRODUCTION SERIES C ANALYSES.
VII-16	MODEL STATISTICS. RUN <u>T6</u> . MODEL <u>PECHFV</u> . SCENARIO <u>A</u> . PRODUCTION SERIES C ANALYSES.
VII-17	ACTUAL CHANGES (FINAL MINUS INITIAL ANALYSIS). SCENARIO <u>B</u> .
VII-18	MODEL STATISTICS. RUN <u>F24</u> . MODEL <u>PEFHCV</u> . SCENARIO <u>B</u> . PRODUCTION SERIES C ANALYSES.
VII-19	MODEL STATISTICS. RUN <u>F19</u> . MODEL <u>PECHCV</u> . SCENARIO <u>B</u> . PRODUCTION SERIES C ANALYSES.
VII-20	MODEL STATISTICS. RUN <u>T5</u> . MODEL <u>PECHFV</u> . SCENARIO <u>B</u> . PRODUCTION SERIES C ANALYSES.
VII-21	PECHFV FORECAST MINUS PECHCV FORECAST. SCENARIO <u>A</u> . PRODUCTION SERIES C ANALYSES.

LIST OF TABLES (Continued)

Table

VII-22	PECHFV FORECAST MINUS PECHCV FORECAST. <u>A.</u> TEST SERIES B ANALYSES.	SCENARIO
VII-23	PECHFV FORECAST MINUS PECHCV FORECAST. <u>B.</u> PRODUCTION SERIES C ANALYSES.	SCENARIO

LIST OF CHARTS

CHART VIII-1	SEA-LEVEL PRESSURE ANALYSIS, 63 x 63 GRID, 1200Z, 22 APRIL 1976.
CHART VIII-2	SEA-LEVEL PRESSURE ANALYSIS, 63 x 63 GRID, 1200Z, 23 APRIL 1976.
CHART VIII-3	SEA-LEVEL PRESSURE ANALYSIS, 63 x 63 GRID, 1200Z, 24 APRIL 1976.
CHART VIII-4	SEA-LEVEL PRESSURE ANALYSIS, 187 x 187 GRID, 1200Z, 22 APRIL 1976.
CHART VIII-5	500 MB HEIGHT ANALYSIS, 63 x 63 GRID, 1200Z, 22 APRIL 1976.
CHART VIII-6	500 MB HEIGHT ANALYSIS, 63 x 63 GRID, 1200Z, 23 APRIL 1976.
CHART VIII-7	500 MB HEIGHT ANALYSIS, 63 x 63 GRID, 1200Z, 24 APRIL 1976.
CHART VIII-8	500 MB HEIGHT ANALYSIS, 187 x 187 GRID, 1200Z, 22 APRIL 1976.
CHART VIII-9	500 MB TEMPERATURE ANALYSIS, 63 x 63 GRID, 1200Z, 22 APRIL 1976.
CHART VIII-10	500 MB WIND VECTOR ANALYSIS, 63 x 63 GRID, 1200Z, 22 APRIL 1976.
CHART VIII-11	500 MB TEMPERATURE ANALYSIS, 187 x 187 GRID, 1200Z, 22 APRIL 1976.
CHART VIII-12	900 MB WIND VECTOR ANALYSIS, 63 x 63 GRID, 1200Z, 22 APRIL 1976. WITH REPORTS.

LIST OF CHARTS (Continued)

CHART VIII-13 SEA-LEVEL PRESSURE ANALYSIS, 63 x 63 GRID,
1200Z, 20 MAY 1976.

CHART VIII-14 SEA-LEVEL PRESSURE ANALYSIS, 63 x 63 GRID,
1200Z, 21 MAY 1976.

CHART VIII-15 SEA-LEVEL PRESSURE ANALYSIS, 63 x 63 GRID,
1200Z, 22 MAY 1976.

CHART VIII-16 SEA-LEVEL PRESSURE ANALYSIS, 187 x 187 GRID,
1200Z, 20 MAY 1976.

CHART VIII-17 500 MB HEIGHT ANALYSIS, 63 x 63 GRID, 1200Z,
20 MAY 1976.

CHART VIII-18 500 MB HEIGHT ANALYSIS, 63 x 63 GRID, 1200Z,
21 MAY 1976.

CHART VIII-19 500 MB HEIGHT ANALYSIS, 63 x 63 GRID, 1200Z,
22 MAY 1976.

CHART VIII-20 500 MB HEIGHT ANALYSIS, 187 x 187 GRID, 1200Z,
20 MAY 1976.

CHART VIII-21 500 MB TEMPERATURE ANALYSIS, 63 x 63 GRID,
1200Z, 20 MAY 1976.

CHART VIII-22 500 MB WIND VECTOR ANALYSIS. 63 x 63 GRID,
1200Z, 20 MAY 1976.

CHART VIII-23 500 MB TEMPERATURE ANALYSIS, 187 x 187 GRID,
1200Z, 20 MAY 1976.

CHART VIII-24 500 MB WIND VECTOR ANALYSIS, 187 x 187 GRID,
1200Z, 20 MAY 1976.

LIST OF CHARTS (Continued)

CHART VIII-25	FNWC SEA-LEVEL PRESSURE ANALYSIS, 1200Z, 22 APRIL 1976.
CHART VIII-26	FNWC SEA-LEVEL PRESSURE ANALYSIS, 1200Z, 23 APRIL 1976.
CHART VIII-27	FNWC 500 MB HEIGHT ANALYSIS, 1200Z, 22 APRIL 1976.
CHART VIII-28	FNWC 500 MB HEIGHT ANALYSIS, 1200Z, 23 APRIL 1976.
CHART VIII-29	FNWC 24-HOUR SEA-LEVEL PRESSURE FORECAST FROM 1200Z, 22 APRIL 1976.
CHART VIII-30	FNWC 24-HOUR 500 MB HEIGHT FORECAST FROM 1200Z, 22 APRIL 1976.
CHART VIII-31	FNWC SEA-LEVEL PRESSURE ANALYSIS, 1200Z, 20 MAY 1976.
CHART VIII-32	FNWC SEA-LEVEL PRESSURE ANALYSIS, 1200Z, 21 MAY 1976.
CHART VIII-33	FNWC 500 MB HEIGHT ANALYSIS, 1200Z, 20 MAY 1976.
CHART VIII-34	FNWC 500 MB HEIGHT ANALYSIS, 1200Z, 21 MAY 1976.
CHART VIII-35	FNWC 24-HOUR SEA-LEVEL PRESSURE FORECAST FROM 1200Z, 20 MAY 1976.
CHART VIII-36	FNWC 24-HOUR 500 MB HEIGHT FORECAST FROM 1200Z, 20 MAY 1976.

LIST OF CHARTS (Continued)

- CHART VIII-37 DIFFERENCE BETWEEN TEN-LEVEL AND FIVE-LEVEL
24-HOUR SEA-LEVEL PRESSURE FORECASTS.
PRODUCTION SERIES C ANALYSES. SCENARIO A.
- CHART VIII-38 DIFFERENCE BETWEEN TEN-LEVEL AND FIVE-LEVEL
24-HOUR 500 MB HEIGHT FORECASTS. PRODUCTION
SERIES C ANALYSES. SCENARIO A.
- CHART VIII-39 DIFFERENCE BETWEEN TEN-LEVEL AND FIVE-LEVEL
24-HOUR SEA-LEVEL PRESSURE FORECASTS. TEST
SERIES B ANALYSES. SCENARIO A.
- CHART VIII-40 DIFFERENCE BETWEEN TEN-LEVEL AND FIVE-LEVEL
24-HOUR 500 MB HEIGHT FORECASTS. TEST
SERIES B ANALYSES. SCENARIO A.
- CHART VIII-41 DIFFERENCE BETWEEN TEN-LEVEL AND FIVE-LEVEL
24-HOUR SEA-LEVEL PRESSURE FORECASTS. FNWC
GUESS-FIELD ANALYSES. SCENARIO A.
- CHART VIII-42 DIFFERENCE BETWEEN TEN-LEVEL AND FIVE-LEVEL
24-HOUR 500 MB HEIGHT FORECASTS. FNWC
GUESS-FIELD ANALYSES. SCENARIO A.
- CHART VIII-43 DIFFERENCE BETWEEN TEN-LEVEL AND FIVE-LEVEL
24-HOUR SEA-LEVEL PRESSURE FORECASTS.
PRODUCTION SERIES C ANALYSES. SCENARIO B.
- CHART VIII-44 DIFFERENCE BETWEEN TEN-LEVEL AND FIVE-LEVEL
24-HOUR 500 MB HEIGHT FORECASTS. PRODUCTION
SERIES C ANALYSES. SCENARIO B.
- CHART VIII-45 DIFFERENCE BETWEEN 187 x 187 and 63 x 63
FIVE-LAYER 24-HOUR FORECASTS. SEA-LEVEL
PRESSURE. SCENARIO A.

LIST OF CHARTS (Continued)

- CHART VIII-46 DIFFERENCE BETWEEN 187 x 187 AND 63 x 63
FIVE-LAYER 24-HOUR FORECASTS. 500 MB HEIGHT.
SCENARIO A.
- CHART VIII-47 DIFFERENCE BETWEEN 187 x 187 AND 63 x 63
FIVE-LAYER 24-HOUR FORECASTS. SEA-LEVEL
PRESSURE. SCENARIO B.
- CHART VIII-48 DIFFERENCE BETWEEN 187 x 187 AND 63 x 63
FIVE-LAYER 24-HOUR FORECASTS. 500 MB HEIGHT.
SCENARIO B.
- CHART VIII-49 700 MB TEMPERATURE ANALYSIS FOR 1200Z,
15 APRIL 1976 (EARLY VERSION).
- CHART VIII-50 700 MB HEIGHT ANALYSIS FOR 1200Z, 15 APRIL
1976 (EARLY VERSION).
- CHART VIII-51 SEA-LEVEL PRESSURE ANALYSIS FOR 1200Z,
22 APRIL 1976 (EARLY VERSION).
- CHART VIII-52 SEA-LEVEL PRESSURE ANALYSIS FOR 1200Z,
23 APRIL 1976 (EARLY VERSION).
- CHART VIII-53 RETRIEVED TEMPERATURES FOR 950 MBS AT 1200Z,
22 APRIL 1976 (EARLY VERSION).
- CHART VIII-54 ANALYZED TEMPERATURES FOR 950 MBS AT 1200Z,
22 APRIL 1976 (EARLY VERSION).
- CHART VIII-55 SEA-LEVEL PRESSURE ANALYSIS DIFFERENCE CHART:
187 x 187 GRID MINUS 63 x 63 GRID.
SCENARIO A.

LIST OF CHARTS (Continued)

- CHART VIII-56 500 MB HEIGHT ANALYSIS DIFFERENCE CHART:
187 x 187 GRID MINUS 63 x 63 GRID.
SCENARIO A.
- CHART VIII-57 SEA-LEVEL PRESSURE ANALYSIS DIFFERENCE CHART:
187 x 187 GRID MINUS 63 x 63 GRID.
SCENARIO B.
- CHART VIII-58 500 MB HEIGHT ANALYSIS DIFFERENCE CHART:
187 x 187 GRID MINUS 63 x 63 GRID.
SCENARIO B.
- CHART VIII-59 SEA-LEVEL PRESSURE ACTUAL CHANGES OVER 24
HOURS. SCENARIO A.
- CHART VIII-60 500 MB HEIGHT ACTUAL CHANGES OVER 24 HOURS.
SCENARIO A.
- CHART VIII-61 SEA-LEVEL PRESSURE ACTUAL CHANGES OVER 48
HOURS. SCENARIO A.
- CHART VIII-62 500 MB HEIGHT ACTUAL CHANGES OVER 48 HOURS.
SCENARIO A.
- CHART VIII-63 RUN F22. SCENARIO A. MODEL PEFHCV. 24-HOUR
FORECAST CHANGE IN SEA-LEVEL PRESSURE.
- CHART VIII-64 RUN F22. SCENARIO A. MODEL PEFHCV. 24-HOUR
FORECAST ERROR IN SEA-LEVEL PRESSURE.
- CHART VIII-65 RUN F22. SCENARIO A. MODEL PEFHCV. 24-HOUR
FORECAST CHANGE IN 500 MB HEIGHT.

LIST OF CHARTS (Continued)

CHART VIII-66	RUN F22. SCENARIO A. MODEL <u>PEFHCV</u> . 24-HOUR FORECAST ERROR IN 500 MB HEIGHT.
CHART VIII-67	RUN F18. SCENARIO A. MODEL <u>PECHCV</u> . 24-HOUR FORECAST CHANGE IN SEA-LEVEL PRESSURE.
CHART VIII-68	RUN F18. SCENARIO A. MODEL <u>PECHCV</u> . 24-HOUR FORECAST ERROR IN SEA-LEVEL PRESSURE.
CHART VIII-69	RUN F18. SCENARIO A. MODEL <u>PECHCV</u> . 24-HOUR FORECAST CHANGE IN 500 MB HEIGHT.
CHART VIII-70	RUN F18. SCENARIO A. MODEL <u>PECHCV</u> . 24-HOUR FORECAST ERROR IN 500 MB HEIGHT.
CHART VIII-71	RUN F18. SCENARIO A. MODEL <u>PECHCV</u> . 48-HOUR FORECAST CHANGE IN SEA-LEVEL PRESSURE.
CHART VIII-72	RUN F18. SCENARIO A. MODEL <u>PECHCV</u> . 48-HOUR FORECAST ERROR IN SEA-LEVEL PRESSURE.
CHART VIII-73	RUN F18. SCENARIO A. MODEL <u>PECHCV</u> . 48-HOUR FORECAST CHANGE IN 500 MB HEIGHT.
CHART VIII-74	RUN F18. SCENARIO A. MODEL <u>PECHCV</u> . 48-HOUR FORECAST ERROR IN 500 MB HEIGHT.
CHART VIII-75	RUN T4. SCENARIO A. MODEL <u>PECHFV</u> . 24-HOUR FORECAST CHANGE IN SEA-LEVEL PRESSURE.
CHART VIII-76	RUN T4. SCENARIO A. MODEL <u>PECHFV</u> . 24-HOUR FORECAST ERROR IN SEA-LEVEL PRESSURE.

LIST OF CHARTS (Continued)

CHART VIII-77	RUN <u>T4</u> . SCENARIO A. MODEL <u>PECHFV</u> . 24-HOUR FORECAST CHANGE IN 500 MB HEIGHT.
CHART VIII-78	RUN <u>T4</u> . SCENARIO A. MODEL <u>PECHFV</u> . 24-HOUR FORECAST ERROR IN 500 MB HEIGHT.
CHART VIII-79	RUN <u>T4</u> . SCENARIO A. MODEL <u>PECHFV</u> . 48-HOUR FORECAST CHANGE IN SEA-LEVEL PRESSURE.
CHART VIII-80	RUN <u>T4</u> . SCENARIO A. MODEL <u>PECHFV</u> . 48-HOUR FORECAST ERROR IN SEA-LEVEL PRESSURE.
CHART VIII-81	RUN <u>T4</u> . SCENARIO A. MODEL <u>PECHFV</u> . 48-HOUR FORECAST CHANGE IN 500 MB HEIGHT.
CHART VIII-82	RUN <u>T4</u> . SCENARIO A. MODEL <u>PECHFV</u> . 48-HOUR FORECAST ERROR IN 500 MB HEIGHT.
CHART VIII-83	RUN <u>F20</u> . SCENARIO A. MODEL <u>PECHCV</u> . 24-HOUR FORECAST CHANGE IN SEA-LEVEL PRESSURE.
CHART VIII-84	RUN <u>F20</u> . SCENARIO A. MODEL <u>PECHCV</u> . 24-HOUR FORECAST ERROR IN SEA-LEVEL PRESSURE.
CHART VIII-85	RUN <u>F20</u> . SCENARIO A. MODEL <u>PECHCV</u> . 24-HOUR FORECAST CHANGE IN 500 MB HEIGHT.
CHART VIII-86	RUN <u>F20</u> . SCENARIO A. MODEL <u>PECHCV</u> . 24-HOUR FORECAST ERROR IN 500 MB HEIGHT.
CHART VIII-87	RUN <u>F20</u> . SCENARIO A. MODEL <u>PECHCV</u> . 48-HOUR FORECAST CHANGE IN SEA-LEVEL PRESSURE.

LIST OF CHARTS (Continued)

CHART VIII-88	RUN <u>F20</u> . SCENARIO A. MODEL <u>PECHCV</u> . 48-HOUR FORECAST ERROR IN SEA-LEVEL PRESSURE.
CHART VIII-89	RUN <u>F20</u> . SCENARIO A. MODEL <u>PECHCV</u> . 48-HOUR FORECAST CHANGE IN 500 MB HEIGHT.
CHART VIII-90	RUN <u>F20</u> . SCENARIO A. MODEL <u>PECHCV</u> . 48-HOUR FORECAST ERROR IN 500 MB HEIGHT.
CHART VIII-91	RUN <u>T6</u> . SCENARIO A. MODEL <u>PECHFV</u> . 24-HOUR FORECAST CHANGE IN SEA-LEVEL PRESSURE.
CHART VIII-92	RUN <u>T6</u> . SCENARIO A. MODEL <u>PECHFV</u> . 24-HOUR FORECAST ERROR IN SEA-LEVEL PRESSURE.
CHART VIII-93	RUN <u>T6</u> . SCENARIO A. MODEL <u>PECHFV</u> . 24-HOUR FORECAST CHANGE IN 500 MB HEIGHT.
CHART VIII-94	RUN <u>T6</u> . SCENARIO A. MODEL <u>PECHFV</u> . 24-HOUR FORECAST ERROR IN 500 MB HEIGHT.
CHART VIII-95	RUN <u>T6</u> . SCENARIO A. MODEL <u>PECHFV</u> . 48-HOUR FORECAST CHANGE IN SEA-LEVEL PRESSURE.
CHART VIII-96	RUN <u>T6</u> . SCENARIO A. MODEL <u>PECHFV</u> . 48-HOUR FORECAST ERROR IN SEA-LEVEL PRESSURE.
CHART VIII-97	RUN <u>T6</u> . SCENARIO A. MODEL <u>PECHFV</u> . 48-HOUR FORECAST CHANGE IN 500 MB HEIGHT.
CHART VIII-98	RUN <u>T6</u> . SCENARIO A. MODEL <u>PECHFV</u> . 48-HOUR FORECAST ERROR IN 500 MB HEIGHT.

LIST OF CHARTS (Continued)

CHART VIII-99	SEA-LEVEL PRESSURE ACTUAL CHANGES OVER 24 HOURS. SCENARIO B.
CHART VIII-100	500 MB HEIGHT ACTUAL CHANGES OVER 24 HOURS. SCENARIO B.
CHART VIII-101	SEA-LEVEL PRESSURE ACTUAL CHANGES OVER 48 HOURS. SCENARIO B.
CHART VIII-102	500 MB HEIGHT ACTUAL CHANGES OVER 48 HOURS. SCENARIO B.
CHART VIII-103	RUN <u>F24</u> . SCENARIO B. MODEL <u>PEFHCV</u> . 24-HOUR FORECAST CHANGE IN SEA-LEVEL PRESSURE.
CHART VIII-104	RUN <u>F24</u> . SCENARIO B. MODEL <u>PEFHCV</u> . 24-HOUR FORECAST ERROR IN SEA-LEVEL PRESSURE.
CHART VIII-105	RUN <u>F24</u> . SCENARIO B. MODEL <u>PEFHCV</u> . 24-HOUR FORECAST CHANGE IN 500 MB HEIGHT.
CHART VIII-106	RUN <u>F24</u> . SCENARIO B. MODEL <u>PEFHCV</u> . 24-HOUR FORECAST ERROR IN 500 MB HEIGHT.
CHART VIII-107	RUN <u>F19</u> . SCENARIO B. MODEL <u>PECHCV</u> . 24-HOUR FORECAST CHANGE IN SEA-LEVEL PRESSURE.
CHART VIII-108	RUN <u>F19</u> . SCENARIO B. MODEL <u>PECHCV</u> . 24-HOUR FORECAST ERROR IN SEA-LEVEL PRESSURE.
CHART VIII-109	RUN <u>F19</u> . SCENARIO B. MODEL <u>PECHCV</u> . 24-HOUR FORECAST CHANGE IN 500 MB HEIGHT.

LIST OF CHARTS (Continued)

CHART VIII-110	RUN F19. SCENARIO B. MODEL PECHCV. 24-HOUR FORECAST ERROR IN 500 MB HEIGHT.
CHART VIII-111	RUN F19. SCENARIO B. MODEL PECHCV. 48-HOUR FORECAST CHANGE IN SEA-LEVEL PRESSURE.
CHART VIII-112	RUN F19. SCENARIO B. MODEL PECHCV. 48-HOUR FORECAST ERROR IN SEA-LEVEL PRESSURE.
CHART VIII-113	RUN F19. SCENARIO B. MODEL PECHCV. 48-HOUR FORECAST CHANGE IN 500 MB HEIGHT.
CHART VIII-114	RUN F19. SCENARIO B. MODEL PECHCV. 48-HOUR FORECAST ERROR IN 500 MB HEIGHT.
CHART VIII-115	RUN T5. SCENARIO B. MODEL PECHFV. 24-HOUR FORECAST CHANGE IN SEA-LEVEL PRESSURE.
CHART VIII-116	RUN T5. SCENARIO B. MODEL PECHFV. 24-HOUR FORECAST ERROR IN SEA-LEVEL PRESSURE.
CHART VIII-117	RUN T5. SCENARIO B. MODEL PECHFV. 24-HOUR FORECAST CHANGE IN 500 MB HEIGHT.
CHART VIII-118	RUN T5. SCENARIO B. MODEL PECHFV. 24-HOUR FORECAST ERROR IN 500 MB HEIGHT.
CHART VIII-119	RUN T5. SCENARIO B. MODEL PECHFV. 48-HOUR FORECAST CHANGE IN SEA-LEVEL PRESSURE.

LIST OF CHARTS (Continued)

CHART VIII-120	RUN T5. SCENARIO B. MODEL PECHFV. 48-HOUR FORECAST ERROR IN SEA-LEVEL PRESSURE.
CHART VIII-121	RUN T5. SCENARIO B. MODEL PECHFV. 48-HOUR FORECAST CHANGE IN 500 MB HEIGHT.
CHART VIII-122	RUN T5. SCENARIO B. MODEL PECHFV. 48-HOUR FORECAST ERROR IN 500 MB HEIGHT.
CHART VIII-123	SST ANALYSIS, 1200Z, 22 APRIL 1976, 187 x 187 GRID.
CHART VIII-124	SST ANALYSIS, 1200Z, 22 APRIL 1976, 63 x 63 GRID.
CHART VIII-125	SST ANALYSIS, 1200Z, 23 APRIL 1976, 63 x 63 GRID.
CHART VIII-126	SST ANALYSIS, 1200Z, 24 APRIL 1976, 63 x 63 GRID.
CHART VIII-127	SST ANALYSIS, 1200Z, 20 MAY 1976, 187 x 187 GRID.
CHART VIII-128	SST ANALYSIS, 1200Z, 20 MAY 1976, 63 x 63 GRID.
CHART VIII-129	SST ANALYSIS, 1200Z, 21 MAY 1976, 63 x 63 GRID.
CHART VIII-130	SST ANALYSIS, 1200Z, 22 MAY 1976, 63 x 63 GRID.

LIST OF CHARTS (Continued)

CHART VIII-131 SEA-LEVEL PRESSURE 24-HOUR FORECAST.
RUN F22. MODEL PEFHCV. SCENARIO A.

CHART VIII-132 500 MB HEIGHT 24-HOUR FORECAST. RUN F22.
MODEL PEFHCV. SCENARIO A.

CHART VIII-133 500 MB TEMPERATURE 24-HOUR FORECAST.
RUN F22. MODEL PEFHCV. SCENARIO A.

CHART VIII-134 SEA-LEVEL PRESSURE 24-HOUR FORECAST.
RUN F18. MODEL PECHCV. SCENARIO A.

CHART VIII-135 500 MB HEIGHT 24-HOUR FORECAST. RUN F18.
MODEL PECHCV. SCENARIO A.

CHART VIII-136 500 MB TEMPERATURE 24-HOUR FORECAST.
RUN F18. MODEL PECHCV. SCENARIO A.

CHART VIII-137 SEA-LEVEL PRESSURE 48-HOUR FORECAST.
RUN F18. MODEL PECHCV. SCENARIO A.

CHART VIII-138 500 MB HEIGHT 48-HOUR FORECAST. RUN F18.
MODEL PECHCV. SCENARIO A.

CHART VIII-139 500 MB TEMPERATURE 48-HOUR FORECAST.
RUN F18. MODEL PECHCV. SCENARIO A.

CHART VIII-140 SEA-LEVEL PRESSURE 24-HOUR FORECAST.
RUN T4. MODEL PECHFV. SCENARIO A.

CHART VIII-141 500 MB HEIGHT 24-HOUR FORECAST. RUN T4.
MODEL PECHFV. SCENARIO A.

LIST OF CHARTS (Continued)

CHART VIII-142 500 MB TEMPERATURE 24-HOUR FORECAST.
RUN T4. MODEL PECHFV. SCENARIO A.

CHART VIII-143 SEA-LEVEL PRESSURE 48-HOUR FORECAST.
RUN T4. MODEL PECHFV. SCENARIO A.

CHART VIII-144 500 MB HEIGHT 48-HOUR FORECAST. RUN T4.
MODEL PECHFV. SCENARIO A.

CHART VIII-145 500 MB TEMPERATURE 48-HOUR FORECAST.
RUN T4. MODEL PECHFV. SCENARIO A.

CHART VIII-146 SEA-LEVEL PRESSURE 24-HOUR FORECAST.
RUN F20. MODEL PECHCV. SCENARIO A.

CHART VIII-147 500 MB HEIGHT 24-HOUR FORECAST. RUN F20.
MODEL PECHCV. SCENARIO A.

CHART VIII-148 500 MB TEMPERATURE 24-HOUR FORECAST.
RUN F20. MODEL PECHCV. SCENARIO A.

CHART VIII-149 SEA-LEVEL PRESSURE 48-HOUR FORECAST.
RUN F20. MODEL PECHCV. SCENARIO A.

CHART VIII-150 500 MB HEIGHT 48-HOUR FORECAST. RUN F20.
MODEL PECHCV. SCENARIO A.

CHART VIII-151 500 MB TEMPERATURE 48-HOUR FORECAST.
RUN F20. MODEL PECHCV. SCENARIO A.

CHART VIII-152 SEA-LEVEL PRESSURE 24-HOUR FORECAST.
RUN T6. MODEL PECHFV. SCENARIO A.

LIST OF CHARTS (Continued)

CHART VIII-153	500 MB HEIGHT 24-HOUR FORECAST. RUN <u>T6</u> . MODEL <u>PECHFV</u> . SCENARIO A.
CHART VIII-154	500 MB TEMPERATURE 24-HOUR FORECAST. RUN <u>T6</u> . MODEL <u>PECHFV</u> . SCENARIO A.
CHART VIII-155	SEA-LEVEL PRESSURE 48-HOUR FORECAST. RUN <u>T6</u> . MODEL <u>PECHFV</u> . SCENARIO A.
CHART VIII-156	500 MB HEIGHT 48-HOUR FORECAST. RUN <u>T6</u> . MODEL <u>PECHFV</u> . SCENARIO A.
CHART VIII-157	500 MB TEMPERATURE 48-HOUR FORECAST. RUN <u>T6</u> . MODEL <u>PECHFV</u> . SCENARIO A.
CHART VIII-158	SEA-LEVEL PRESSURE 24-HOUR FORECAST. RUN <u>F24</u> . MODEL <u>PEFHCV</u> . SCENARIO B.
CHART VIII-159	500 MB HEIGHT 24-HOUR FORECAST. RUN <u>F24</u> . MODEL <u>PEFHCV</u> . SCENARIO B.
CHART VIII-160	500 MB TEMPERATURE 24-HOUR FORECAST. RUN <u>F24</u> . MODEL <u>PEFHCV</u> . SCENARIO B.
CHART VIII-161	SEA-LEVEL PRESSURE 24-HOUR FORECAST. RUN <u>F19</u> . MODEL <u>PECHCV</u> . SCENARIO B.
CHART VIII-162	500 MB HEIGHT 24-HOUR FORECAST. RUN <u>F19</u> . MODEL <u>PECHCV</u> . SCENARIO B.
CHART VIII-163	500 MB TEMPERATURE 24-HOUR FORECAST. RUN <u>F19</u> . MODEL <u>PECHCV</u> . SCENARIO B.

LIST OF CHARTS (Continued)

CHART VIII-164 SEA-LEVEL PRESSURE 48-HOUR FORECAST.
RUN F19. MODEL PECHCV. SCENARIO B.

CHART VIII-165 500 MB HEIGHT 48-HOUR FORECAST. RUN F19.
MODEL PECHCV. SCENARIO B.

CHART VIII-166 500 MB TEMPERATURE 48-HOUR FORECAST.
RUN F19. MODEL PECHCV. SCENARIO B.

CHART VIII-167 SEA-LEVEL PRESSURE 24-HOUR FORECAST.
RUN T5. MODEL PECHFV. SCENARIO B.

CHART VIII-168 500 MB HEIGHT 24-HOUR FORECAST. RUN T5.
MODEL PECHFV. SCENARIO B.

CHART VIII-169 500 MB TEMPERATURE 24-HOUR FORECAST.
RUN T5. MODEL PECHFV. SCENARIO B.

CHART VIII-170 SEA-LEVEL PRESSURE 48-HOUR FORECAST.
RUN T5. MODEL PECHFV. SCENARIO B.

CHART VIII-171 500 MB HEIGHT 48-HOUR FORECAST. RUN T5.
MODEL PECHFV. SCENARIO B.

CHART VIII-172 500 MB TEMPERATURE 48-HOUR FORECAST.
RUN T5. MODEL PECHFV. SCENARIO B.

I. INTRODUCTION

This is the Final Report of Ocean Data Systems, Inc. (ODSI) for the Jet Propulsion Laboratory (JPL) under Contract No. 954668 in support of the SEASAT Program of the National Aeronautics and Space Administration (NASA). The Final Report is in five volumes, and describes: (1) atmospheric analysis and prediction models for grids of varying resolution; (2) model test results when executed using real data scenarios; and (3), sensitivity studies with a coarse-mesh prediction model.

Volume I is the Summary of Findings for all aspects of the work defined in the original Statement of Work; i.e., the development and testing of analysis models and the first three (of four) versions of a prediction model. Volumes II and III contain rather detailed descriptions of the analysis and prediction models, respectively. Volume IV summarizes the results of sensitivity studies conducted with a coarse-mesh prediction model. Volume V contains an update of portions of Volume I to reflect the tests conducted with a fourth version of the prediction model (the 187 x 187 x 10 layer model).

The NASA-JPL-ODSI atmospheric modeling effort derives from the need to develop and test an operationally-oriented model capability for assessing the impact of SEASAT data on objective analysis and short-range (a few days) numerical weather prediction. As a practical matter, it means that a proper model context has to be assembled which facilitates the necessary sensitivity studies. Problem areas (numerics, physics, data) have to be identified, sized and solved (in turn) according to their (separate) contributions to a forecast. The goal, of course, is to prevent such problems from masking the effects of SEASAT data. Although the primary objective of this contract effort was to examine the effects of grid resolution on analysis and prediction using real data, its nature and scope became much broader as the work progressed. In addition to being able to document such grid effects, ODSI can also make a statement about the effects of: (1) variations in analysis procedures; and (2), variations in many discretionary procedures and parameters in prediction. Finally, this modeling experience has significantly increased the probability that valuable SEASAT data will not get "washed out" of modeled atmospheric structures; i.e., the computational viability of such data will be greatly improved as a consequence of the insight gained in this contract effort.

II. SCOPE OF WORK

The original Statement of Work, as contained in Article 1 of JPL Contract No. 954668, provided that:

- ODSI shall complete and test an analysis "scheme" (i.e., a set of computer programs to perform objective analyses of certain atmospheric parameters) needed to initialize four versions of an atmospheric prediction model. The design should permit the handling of both real and simulated observations.
- ODSI shall develop and test three (out of four) versions of a primitive-equation prediction model. The grids to be used are: 63 x 63 x 5 layers; 63 x 63 x 10 layers; 187 x 187 x 5 layers. The model should contain appropriate attributes (numerics and physics) for generating "operationally-competitive" forecasts of periods of one or two days.
- ODSI shall exercise the analysis and prediction models with real data for two meteorological scenarios, the observations for which shall be provided by Fleet Numerical Weather Central.
- ODSI shall verify, describe and document forecast model performance in both an objective (statistics, charts) and subjective (narrative) manner, emphasizing those differences caused by variation in resolution.
- ODSI shall perform such model development and testing on either the CYBER 175 (at FNWC) or the CDC 7600 (at NASA Ames) to the extent that computer resources permit.

This Statement of Work was subsequently modified to include:

- The development and testing of a fourth version (187 x 187 x 10 layers) of a prediction model.
- A task to conduct sensitivity tests with the coarse-mesh (63 x 63 x 5 layers) prediction model in order to determine and order the factors which might mask or impair the utility of SEASAT data.

A. General Certification

The terms and conditions of the Statement of Work (as amended) have been fulfilled completely. In fact, the scope of work actually performed goes well beyond the provisions of the statement, especially in those activities undertaken to develop/refine the outputs of the analysis and prediction models. The Scenario A data set was used several times, for example, to determine the cumulative/interactive impact of model changes on a sequence of twelve-hourly analyses and forecasts. Another example would be the extra efforts to introduce and to examine the effects of procedural changes in the models in order to improve the quality of model outputs. Many of these improvements were incorporated in the final analysis production series.

With respect to the forecast model runs, only eight production forecasts were needed to satisfy the augmented work statement, since there are four model versions and two data sets. In practice, about 30-40 production forecasts were made. Most of these were coarse-mesh model forecasts, because not enough CDC 7600 time was available to perform extra runs with the $187 \times 187 \times 5$ or $187 \times 187 \times 10$ model versions.

During the contract period, it became necessary to shift the programming/production efforts from one type of computer to another (in order to accommodate GFE availability). Thus, some of the total effort was related to such system changes.

B. Definitions and Cross-References

Table II-1 is the "road map" for reviewing Volume I. It contains descriptors, identifiers, and cross-reference information needed to facilitate the examination of study results. With respect to the figures, tables and charts which are referenced, Table II-1 is not intended to be exhaustive.

1. Analyses

The analysis descriptors and selected chart references are located at the top of Table II-1. There are two meteorological scenarios for which time: objective analyses were produced. For each scenario, twelve-hourly analyses were produced for each of two grids (63 x 63 and 187 x 187). Production series analyses are interactive sequences of analyses (those which are coupled with first-guess fields produced by a 12-hour forecast from the previous analysis). Others are "test series" analyses for a single date-time which are non-interactive analyses (the cumulative effects of the analysis-prediction sequence were not determined).

As indicated earlier, analyses were made using the 187 x 187 grid, but these were not actually employed to initialize the fine-mesh forecasts for two important reasons: (1) the comparison of fine-mesh and coarse-mesh forecasts would be affected (in ways not easily assessed) by the presence of additional (small) scales in the fine-mesh analyses; and (2) there was not enough CDC 7600 computer time to run both types of fine-mesh forecasts (those using interpolated coarse-mesh initial values and those using fine-mesh initial values). The fine-mesh forecast models were initialized, therefore, with interpolated coarse-mesh values to facilitate comparisons.

During the analysis development effort, several test and production series analyses were improved upon and discarded. This included Production Series A and B, and Test Series A. One of the difficulties with early analysis versions was related to the procedure used to "assemble" each datum to the nearest grid point. Later versions allow each datum to influence more than one grid point according to an area influence function.

Selected ODSI analyses are shown in Section VIII. Charts VIII-1 through VIII-12 are key analyses in Scenario A. Charts VIII-13 through VIII-24 are key analyses in Scenario B. These may be compared to FNWC analyses provided as Charts VIII-25 to VIII-29, and VIII-31 to VIII-34, respectively.

2. Forecasts

Table II-1 also provides model descriptors and run numbers for both the five-layer and ten-layer forecasts treated in this report. These are distributed by scenario. In addition, the table indicates the type of analysis model outputs used for forecast model initialization, as well as the key references (tables, figures, and charts).

The major runs for Scenario A are F18 (63 x 63 x 5), F22 (187 x 187 x 5) and T4 (63 x 63 x 10). Test Series B analysis outputs were used to initialize all three forecasts.

(The 187 x 187 x 10 forecasts will be treated in Volume V of this Final Report.) Other runs in Scenario A are provided for assessing the impact of (varying) analysis procedures on short-range forecasts. Thus, F18 can be compared to F20 to assess the impact of analysis-forecast interaction.

For Scenario B, Production Series C analyses were used throughout. The key runs are F19 (63 x 63 x 5), F24 (187 x 187 x 5), and T5 (63 x 63 x 10).

TABLE II-1: DEFINITIONS AND CROSS-REFERENCES

TYPE	ITEM	SCENARIO A			SCENARIO B	
		63 x 63		187 x 187	63 x 63	187 x 187
ANALYSES	• DESCRIPTORS	TEST SERIES B	PRODUCTION SERIES C	TEST SERIES B	PRODUCTION SERIES C	PRODUCTION SERIES C
	• CHARTS (SECTION VIII) -- SEA LEVEL PRESSURE -- 500 MB HEIGHT -- 24-HR, 48-HR CHANGES	1-3 5-7 59-62	- - -	4 8 -	13-15 17-19 99-102	16 20 -
PREDICTION MODELS	• FIVE-LAYER MODEL DESCRIPTORS	PECHCV	PECHCV	PEFHCV	PECHCV	PEFHCV
	• RUN NUMBERS	F18	F20	F22	F19	F24
	• FIGURES (SECTION VI)	3,42		4,43	23,45	24,46
	• TABLES (SECTION VII)	13	15	12	19	18
	• CHARTS (SECTION VIII) -- FORECASTS -- FORECAST CHANGES/ERRORS	134-139 67-74	146-151 83-90	131-133 63-66	161-166 107-114	158-160 103-106
	• TEN-LAYER MODEL DESCRIPTORS	PECHFV	PECHFV	N/A	PECHFV	N/A
	• RUN NUMBERS	T4	T6		T5	
	• FIGURES (SECTION VI)	2,41			22,44	
	• TABLES (SECTION VII)	14	16		20	
	• CHARTS (SECTION VIII) -- FORECASTS -- FORECAST CHANGES/ERRORS	140-145 75-82	152-157 91-98		167-172 115-122	

III. ANALYSIS MODEL DEVELOPMENT

Objective analysis models were designed, developed and tested (on the FNWC CYBER 175) using real observational data. Each of the analysis programs may be executed on either the 63 x 63 coarse-mesh grid (CMG) or the 187 x 187 fine-mesh grid (FMG). These CMG and FMG polar-stereographic mappings of the Northern Hemisphere are true at 60N where the mesh distances are 381 and 127 kilometers, respectively. Elsewhere, the map factor

$$m(\phi) = \frac{1 + \sin 60}{1 + \sin \phi}$$

is required to obtain true-earth distances.

The parameters for analysis include: sea-surface temperature; twelve levels of wind, temperature and geopotential height (from 1000 to 100 millibars); and sea-level pressure. Stratospheric (50 to 10 millibars) temperatures and heights were generated using regression equations. Before objective analyses could be performed at the 950 MB and 900 MB levels, it was necessary to merge/check significant-level and mandatory-level radiosonde information for each analysis time.

The primary objective of this modeling effort is to examine the effects of grid resolution on analysis and short-range weather prediction. A short discussion of and rationale for the model resolutions chosen will be presented in the following paragraphs.

The writers assume that the reader will become familiar with the technical aspects of the analysis models as presented in Volume II of this Final Report.

1. Vertical Resolution

With respect to the 1000-100 MB mass structure analysis, FNWC partitions each vertical column into eight layers -- each of which is assigned a value of static stability. In that model, the lowest layer (from 1000 - 775 MBS) is quite gross. The shallow stable layers (inversions) in the lower troposphere cannot be depicted. ODSI retained the upper seven layers but divided the 1000 - 775 MB layer into three sub-layers, each of which is assigned a value of static stability. The new layer interfaces occur at 925 MBS and 875 MBS. Thus, ODSI designed a ten-layer, twelve-level mass structure model. This led to the aforementioned requirement for inputs at 950 MBS and 900 MBS.

2. Horizontal Resolution

In the horizontal, ODSI selected the one-third mesh (187 x 187) grid for both analysis and prediction. On this grid, the true-earth mesh distance varies from 68 kilometers at the equator to 90 kilometers at 45N to 136 kilometers at the pole. It permits significantly better depiction of smaller scales in analysis. It dramatically reduces spatial truncation error in prediction. Indeed, for the shorter baroclinic waves the undermovement should be no greater than one or two percent.

A. Objective Analysis: Discussion

The procedure (or scheme) used in objective analysis of atmospheric-state parameters is to invoke a set of rules to obtain a value at each discrete grid point by blending several types of information: (1) new observations (which are irregularly-spaced, non-representative of the scales being modeled, and contain an assortment of errors); (2) guess-field functional values and differential properties; and (3), control-field information (climatology). [If variational techniques are employed, it is possible to impose dynamical constraints on the relationship between two or more parameters for analysis.] The relative impact of each type of information may be specified according to a set of weights. The objective of an atmospheric analysis is to describe/depict the "relevant" scales of motion, processes and effects consistent with problem characteristics, available resources (computer power, time, data), and the needs of the users. In numerical weather prediction, one performs an analysis in order to pose the initial state.

An objective analysis scheme tends to follow the same rules that a trained meteorologist follows as he produces a subjective (manual) analysis. An objective analysis, however, should be devoid of day-to-day, person-to-person variations in quality. Since the first-guess field embodies all of the

retained information of the parameter to be analyzed prior to receipt of current observations, both methods should and do exploit that resource. Since an analysis is primarily concerned with the locations and shapes of features (as refined through use of gradient and curvature information), both methods may downgrade the importance of any single reported value. In some ways, the task is easier for a meteorologist. He can arbitrarily modify the procedure, smooth a given contour, or assign a measure of confidence to a report. These things can be done in objective analyses, but not as easily.

The grid resolution is extremely important in the objective analysis because it tends to define the range of spatial scales for treatment. Fine-resolution grids permit the depiction of more of the total atmospheric variation, but they also increase the accommodation of non-representative and/or erroneous reports. Few, if any, surface observations are truly representative of the spatial scales of interest in NWP. The "local" content of observations tends to be aliased into the larger, permissible scales of motion. As the model resolution is changed, so must the grid-dependent procedures and coefficients. The impact of each report on the analysis, for example, should depend more on the scales of features being represented than on the grid size. Thus, it

becomes important to determine the influence functions for various observational classes and analysis types. Finally, an objective analysis should be able to introduce and distribute information into spatial scales which are computationally viable (in the prediction model), and to enhance that viability through dynamic coupling and/or numerical consistency. Failing this, small-scale information may get "washed out" in the adjustment period of a primitive-equation forecast model.

B. A Scheme for Objective Analysis: Pattern Conservation Technique (PCT)

ODSI has completed an objective analysis scheme, and has tested the scheme using a real data base assembled in conjunction with the Fleet Numerical Weather Central (FNWC). All of the analysis programs use this Pattern-Conservation Technique (PCT), which preserves specified differential properties of the first-guess field while fitting the observations under a system of weights. ODSI selected this scheme because it exhibits many of the desirable characteristics of a good manual analysis procedure.

The goal of a PCT scalar analysis is to blend the following information: the new data; the most recent past analysis or forecast value (the first guess); the gradients

of the first guess field in eight directions from each grid point; and the Laplacian of the first guess field. The contribution of each such piece of information or term is specified by a set of weights.

The desired fit of all analysis elements is realized by minimizing the sum of the squared deviations of the various characteristics of the analysis from their counterparts in the first guess. The minimization is accomplished with an elementary application of the calculus of variations.

Information is spread through space by the gradient and Laplacian terms. In a sea-level pressure analysis, for example, there are sometimes natural obstacles (mountain ridges, coastlines) beyond which a meteorologist would not allow a new observation to influence the analysis. This kind of constraint can be simulated in the objective analysis by reducing the influence of the gradients and Laplacian along the demarcation zone.

Each PCT analysis "cycle" consists of three steps: (1) assemble the data at grid points using some specified influence function; (2) solve an appropriate minimization equation; and (3), re-evaluate the weight of each report. At least two cycles are needed to re-evaluate the weights. Indeed, an additional cycle (for a total of three) will often cause a rejected/downgraded report to re-enter the analysis.

Vector applications of PCT may be regarded as extensions to the scalar procedures. In the objective wind analysis, for example, the vector application requires solution of two minimization equations (u-component and v-component equations) simultaneously. Also, the method preserves the vorticity and divergence of the first-guess wind field while fitting reported winds (under a system of weights).

The reader should review the contents of Sections I and II of Volume II which describe the scalar and vector applications of PCT in analysis.

1. Solution Method for PCT Equations

In the previous section, it was pointed out that the PCT scheme required solution of a "minimization equation" peculiar to the analysis type. Originally, the method of successive over-relaxation (SOR) was used. When tests were made to determine the impact of a single observation on the analysis, it was obvious that the SOR method was not distributing the information as would be expected from numerical and meteorological considerations.

Several approaches were made to the solution of the minimization equation. The criteria by which the success of an approach was measured were of two kinds. One was the speed of convergence of iterative methods together with the

length of time until convergence. The second was the degree to which the solution obtained agreed with meteorological expectations in the three cases: using only one data report for a constant guess field; using only four data reports for a constant guess field (one report in each quadrant; and using a complete (typical) set of reports.

The methods of solution which were explored were: Poisson fast solve method; successive over-relaxation by points; successive over-relaxation by lines; Jacobi iterations; Gauss iterations; block iterations; successive over-relaxation in 5-block scanning order; and successive over-relaxation scanning by spiral (the relaxation methods for the vector minimization equations required under-relaxation). Further description of each method follows.

The Poisson fast solve method uses the routine POIS 2 developed at NCAR. Although the minimization equation is not a Poisson equation -- or even elliptic -- it is possible to extract a Poisson part of the equation and to attempt to solve it by iteration. More precisely, and in general, given the linear matrix equation $Ax = B$, one may write $A = P - Q$ and the equation may be written $Px = Qx + B$. If the matrix P is amenable to some quick solution method, then one may attempt to find a solution via iteration:

$$Px^{(v)} = Qx^{(v-1)} + B.$$

In the Poisson method, we choose P to be the Poisson matrix part of the equation. As is well known, a solution by iteration is possible for all initial guesses of x if and only if the eigenvalues of $P^{-1}Q$ are all of modulus less than unity. This was not the case for the minimization equation, and iterative attempts at solutions diverged.

The method of Jacobi iteration is a simultaneous relaxation method. In terms of the general method above, we write our equation as $Ax = 0$ and $A = (a_{i,j})$ as $(a_{i,i}\delta_{i,j} - a_{i,j})$, where $\delta_{i,j} = \begin{bmatrix} 0 & i \neq j \\ 1 & i = j \end{bmatrix}$. This method failed to converge.

Gauss iteration is Jacobi iteration but using the updated values of the unknown as soon as they are available. This corresponds to splitting A as $A = (L + I) + u$ where L is the lower triangular part of A , u is the upper triangular part, and I the main diagonal. Gauss iteration converged, but quite slowly. This had the undesirable effect of spreading data too far from the location of the report.

The method of successive over-relaxation by points is an accelerated Gauss iteration method. In general, an iterative method may possibly be accelerated by taking the splitting $A = P - Q$ and rewriting it as $A = (P + \alpha Q) - (Q + \alpha Q)$ for some choice of real number $\alpha \neq -1$. For a

suitable choice of α , this method converges quite rapidly, but nevertheless, allows data to spread in anomalous ways.

Successive over-relaxation by lines is as above for points, but instead of updating the unknown as soon as each new x_i is computed, update only after a line of x_i 's corresponding to a line of grid points is computed. This method failed to converge.

The method of block iteration involves a splitting $A = P - Q$ where P is block pentadiagonal. Since a block pentadiagonal matrix equation can be solved directly and rapidly, this method is suitable. It yielded the fastest convergence of all in the number of iterations, but took a longer execution time than the fastest method. In addition, there was a somewhat anomalous pattern in the spread of the data.

The last two methods are both successive-over-relaxation but differ from the above in the order of the unknowns in the equation. This involves permuting rows of the matrix of the equation -- but because of the splitting -- this yields different effects.

The 5-block scan involves grouping the unknowns into 5 groups and scanning them in order in each group, from group 1 to group 5. This method converged fairly rapidly -- but not most rapidly -- and yielded some anomalous data spread.

The method of spiral scan was designed and tested. It requires scanning the grid from the center (pole) point in a counter-clockwise spiral outward to the edges. It converged fastest (of all) and yielded the least anomalous pattern of data spreading.

Thus, the best result was obtained by SOR using a spiral scan with variable over-relaxation factor. Indeed, under-relaxation was found to converge more quickly in the simultaneous solution of the u- and v-component minimization equations in the objective wind analysis. This method has been implemented in all PCT codes in current use.

2. Analysis Code Sequence and Computer Requirements

The entire set of analysis codes outputs about fifty fields per horizontal grid per analysis time. The sequence of analysis codes commences with the 12-hour forecast outputs of the coarse-mesh PE Model (PECHCV) as initialized with analysis outputs for the time twelve hours previous to the current (analysis) time. Each program in the sequence is necessary either for a subsequent analysis code or for the forecast model, as listed below:

- a. Program to merge/check radiosonde observations, and to interpolate the given profile to those pressure levels not already included in the observation;

- b. Program to analyze the sea-surface temperature (SST);
- c. Program to generate the first-guess sea-level pressure and upper-level temperature fields;
- d. Program to analyze the sea-level pressure;
- e. Program to analyze temperatures at twelve pressure levels from 1000 to 100 MBS;
- f. Program to generate the first-guess upper-level geopotential-height fields (using outputs from d and e, above);
- g. Program to analyze the geopotential-heights at twelve pressure levels from 1000 to 100 MBS, to "retrieve" hydrostatically-consistent virtual temperature profiles (if desired), and to generate 50-, 30- and 10-MB temperatures and heights using regression equations;
- h. Program to analyze the reported winds (satellite cloud vectors, rawinsondes, aircraft reports, pilot balloons) at twelve pressure levels from 1000 to 100 MBS;
- i. Program which assembles the forecast model input fields.

A substantial amount of CYBER 175 computer time was needed to develop these analysis codes. For the contract year, analysis model development and production runs consumed about 150 CP-hours (about 400 wall-clock hours).

The program sequence shown above (exclusive of the 12-hour forecast) uses about six CP-minutes (twenty-three wall-clock minutes) on the coarse-mesh grid, and thirty-three CP-minutes (100 wall-clock minutes) on the fine-mesh grid per analysis time. There are nine analysis periods per scenario, and two scenarios. Each analysis requires a coarse-mesh, twelve-hour forecast -- which takes seven CP-minutes and seventeen wall-clock minutes. This forecast is used for analyses on both grids. Thus, each analysis scenario takes about 400 CP-minutes or about 1,400 wall-clock minutes to complete. There are two scenarios. For the first scenario (April 1976), the entire scenario was run three times altogether, in order to implement and test the cumulative effects of certain procedures.

C. Data Influence Region

The analysis procedure in use at the outset of this study permitted a report to be assembled in the analysis at the nearest grid point. On the coarse-mesh (63 x 63) grid, the procedure appears to be satisfactory in that it tended to accommodate the observations while preserving the smoothly-varying differential properties of the first-guess field.

Once the fine-mesh (187 x 187) analysis codes were exercised, however, it became obvious that the procedure had to be altered in such a way as to cause an observation to impact on the analysis in the same geographical/meteorological scales -- regardless of the grid size. As a report was introduced in the 187 x 187 analysis, the information was being distributed to the same number of gridpoints as in the 63 x 63 analysis, but the geographical distance/area was much less than in the 63 x 63 analysis.

Procedures were implemented and tested in both the 63 x 63 and 187 x 187 analysis codes which distributed observational information within a circular neighborhood in a manner which may be specified. (This action then pointed out the need to re-evaluate the weights of observations in a similar manner.) For the 63 x 63 code, the implementation of this change was rather straightforward. The radius of the influence circle was chosen to be three, two, and one (coarse) grid lengths for the first, second and third analysis cycles, respectively. For the 187 x 187 code, the same geographical areas were influenced, but the number of grid points affected could be as large as 296, 112, or 32, depending on the cycle number.

D. The Effects of Varying the Weights

The constants which determine the relative importance of observations and the guess-field (and its differential properties) were examined. Tests showed the weights to be grid dependent. They also showed that the amount of computer time needed to arrive at a solution can vary markedly with changes in the weights. This is especially so in the case of the weight assigned to the Laplacian terms (in the pressure analysis). Trial and error constitutes the only way to determine the optimum weights. There are no guarantees, however, that the minimization equation will even converge for some choices of weights.

Tests were made to see if one can determine the combination of weights which produces a valid, visually-pleasing analysis in a computationally-efficient way. The results of these tests were not particularly encouraging. Indeed, it appears to be the case that a substantial quality-control effort is required to prevent deterioration of the analyzed structures in data-poor areas. Two special cases can be discussed. First, it should be stated and understood that the primitive-equation forecast models do not predict the observed changes in the equatorial/subtropical latitudes with any degree of skill. Systematic, if only slight, errors are common in low latitudes where the initialization

problem is acute. Over an analysis-prediction-analysis scenario of several days in length, the gradual departures from reality can become rather large in data-poor regions. If, after several days, an observation is received, it may be sufficiently different from the value(s) in the first-guess field as to be downgraded or discarded. The opposite situation is also troublesome. That is to say, an analysis scheme may accept a report which, because of its difference from the first-guess values, may lead to a perturbation in the analysis (it could be real, but it is probably spurious). The primitive-equation forecast model will, more than likely, amplify such a perturbation into quite an intense, unreal circulation. The problem, of course, is to develop techniques for distributing observed information into appropriate ranges of scale (wholesale updating of guess-field values) rather than to allow a report to create a spurious circulation/system. If such techniques cannot be developed, it would be better not to introduce isolated data at all in sparse-data regions which are characterized by weak horizontal gradients (generally) and large horizontal scales.

E. Some Practical Solutions to Analysis Problems

As in any undertaking of this scope and complexity, many problems were encountered, and either solved or circumvented. At first, the problems tended to be related to the implementation of model procedures in terms of correct/efficient code. But, once these difficulties were overcome, the problems centered on the effects of sparse and/or bad data (especially in the tropics) and on the procedures for distributing information in isolated reports (spatially) into larger meteorological scales. On the other hand, no amount of effort can solve the fundamental problem in objective analysis: how do you handle an unsupported observation of an unexpected change/event? Another important problem arises from any procedure which relies too heavily upon either the reports or upon the guess field. Even though it can be argued that the guess field represents the cumulative knowledge of the atmosphere prior to receipt of the latest observations, the guess field often departs from reality in data-poor regions so much so that perfectly good observations will be downgraded or rejected altogether. The use of (satellite) cloud photographs, therefore, is vital to the required quality control effort in operational analysis. Even so, the design (and redesign) of data toss-out criteria (with provision for manual override) represents an important and open-ended aspect of analysis modeling.

1. Problems in Low Latitudes

During the early stages of the analysis development effort, analysis outputs contained unrealistic, small-scale features in low latitudes, generally, and in the lateral boundary areas, specifically. SIRS soundings caused the general problem, because the actual horizontal gradients in the tropical regions tend to be small compared to fictitious gradients caused by errors in the SIRS measurements. Once the small-scale features get into the analyzed structure, the primitive-equation model has a tendency to produce (forecast) structures which are even less realistic. Since the analysis sequence (over several days) is maintained with 12-hour forecasts, each analysis can become increasingly unrealistic.

Charts VIII-49 and VIII-50 illustrate the low-latitude analysis problem. Chart VIII-49 is a 700 MB temperature analysis for 1200Z, 15 April 1976. It contains numerous satellite temperature soundings. Chart VIII-50 is the corresponding 700 MB height analysis containing SIRS height observations. An early version of the analysis procedure was used for these outputs. The non-meteorological character of these outputs is clearly indicated in the ocean regions south of (about) 30° North.

Charts VIII-51 and VIII-52 were also generated using the same (early) versions of the analysis models. Chart VIII-51 contains the sea-level pressure analysis for 1200Z, 22 April 1976. It is quite noisy in appearance, especially in low latitudes. Chart VIII-52 contains the sea-level pressure analysis twenty-four hours later (1200Z, 23 April). Because of the interaction with the forecast model (described above), this pressure pattern has become quite unrealistic generally, but totally unacceptable on the lower/upper boundaries. This illustrates how seemingly innocuous errors (shown in Chart VIII-51) can amplify after only two (subsequent) 12-hour forecasts and analyses (each).

Several remedial procedures were implemented and tested in the analyses. These included: (1) Fourier filtering; (2) Shapiro filtering; (3) Laplacian-type smoothing with latitudinal variation; and (4), removal of SIRS reports south of a prescribed latitude (about 20N). The first two measures were discarded. Some remedial steps were also taken in the forecast model. These included: (1) use of a tendency truncator which does not permit forecast changes south of 5N, but which leaves the tendencies unaltered north of 15N (with linear variation between these limits); (2) application of a low-pass filter to model outputs (with no feedback to the integrations); (3) use of thermal/momentum

diffusion in the integrations; and (4), use of latitudinally-dependent Laplacian-type smoothing (between 5N and 30N) of model outputs.

Chart VIII-2 illustrates the cumulative benefits of these remedial actions. This 1200Z, 23 April PS analysis should be compared to Chart VIII-52. On the basis of many model tests, it was concluded that the entire 63 x 63 analysis-prediction scenario could be carried out without further modifications to the analysis procedure.

2. Analyzed vs. Retrieved Temperatures

The original analysis technique called for modeling the 1000-100 MB mass structure in terms of eight (or ten) static-stability layers. Once the heights, $Z(p)$, were determined for the column, the solution of a matrix transformation equation yielded a corresponding set of virtual temperatures, $T^*(p)$, which could be integrated hydrostatically to produce the heights, $Z(p)$. These so-called "retrieved" temperatures tend to differ, however, from analyzed temperatures at any given pressure level.

Chart VIII-53 shows the retrieved temperatures at 950 MBS for 1200Z, 22 April 1976. In Chart VIII-54, we show the 950 MB analyzed temperatures. These show that the retrieved temperatures are not only noisy in appearance, but

they also lose much of the structure normally found in carefully-drawn subjective analyses. Analyzed temperatures were used thereafter to initialize the prediction model with no apparent negative effects.

F. Data Base Preparation

The analysis program sequence described in Section III.B.2 was executed using real observations in order to prepare the data base needed to initialize the several versions of the prediction model. The CYBER 175 at FNWC was utilized for all aspects of observation processing and objective analysis.

There are two meteorological scenarios of four days duration each. Scenario A covers the period from 1200Z, 21 April 1976 through 1200Z, 25 April 1976. Scenario B covers the period from 1200Z, 19 May 1976 through 1200Z, 23 May 1976. The analyses are performed at twelve-hourly intervals. Thus, there are nine analyses in each four-day scenario. As noted earlier, Scenario A was the subject of special investigations leading to improved procedures in analysis. The analyses were performed on both the 63 x 63 coarse-mesh and the 187 x 187 fine-mesh grids.

Table II-1 indicated that the Test Series B analyses were used to initialize the forecasts in Scenario A. These are non-interactive analyses. Specifically, analyses were made for individual date-times using an area-influence procedure without allowing the forecast model to propagate such

effects to a subsequent analysis. In contrast, the Production Series C analyses were fully interactive. (By examining the F20 and F18 forecasts, one can assess the impact of such interactive procedures on a short-range forecast.)

The scenarios were selected for periods during which interesting (and large) changes were taking place. All available conventional and satellite data at FNWC, together with corresponding FNWC analyses and forecasts, were collected with the help of FNWC personnel. The data counts for 1200Z, 22 April 1976 are representative. Included are: (1) 4,706 sea-level pressure reports; (2) 442 sea-surface temperatures; and (3), upper-air temperature, height and wind reports in numbers shown in the table below:

<u>Number of Reports</u>			
<u>Pressure</u>	<u>Temperature</u>	<u>Height</u>	<u>Wind</u>
1000	402	476	266
950	530	496	326
900	562	504	691
850	637	647	MSG
700	651	654	551
500	644	649	550
400	637	640	557
300	631	632	604
250	MSG	MSG	899
200	593	595	976
150	566	567	476
100	489	491	470

At this date-time, there were about 500 radiosonde/rawinsonde soundings, but values at specific levels were sometimes missing or garbled. Counts in excess of 500 generally indicate the presence of SIRS soundings/winds. Satellite wind vectors are available at 900 MBS, and in large numbers at/near the 200-MB level.

G. Charts and Tables

Recall that the analysis models output approximately fifty distributions/fields at each analysis time on each horizontal grid. Thus, the charts provided in this Final Report represent only a small fraction of the total. In addition to presenting selected analyses, analysis actual change charts (the difference between analyses at two times) and analysis difference charts (the difference between analyses on two grids) will be presented, as appropriate. Statistical measures of such changes/differences will also be provided.

1. Scenario A Discussion

Although this scenario commences at 1200Z, 21 April 1976, the forecasts were initialized with analysis model outputs for 1200Z, 22 April 1976.

Charts VIII-1 through VIII-3 contain the sea-level pressure (PS) analyses for 22 April through 24 April, respectively. These were produced on the 63 x 63 grid. During this

period, the atmosphere underwent some rather large changes. Chart VIII-59, for example, shows the PS actual changes (using a 4-MB contour interval) during the first day. There are several change centers with magnitudes greater than twenty millibars (about 1 MB per hour). Charts VIII-5 through VIII-7 contain the 500 MB height analyses for the 22-24 April period. The main feature is the blocking high southeast of Iceland, which leads to height falls over southern Europe (downstream of the block). In contrast, the Pacific region undergoes some rather large adjustments in the open-wave pattern. The Pacific Ocean atmospheric changes are clearly more interesting than those in the Atlantic. For the most part, they reflect system intensity changes. In contrast, the intense low pressure system in the Atlantic (near 45N/40W) changes intensity and location only slightly. In fact, the Atlantic and European sectors are comparatively inactive during this period. Chart VIII-60 contains the corresponding changes in the 500 MB heights. This shows a maximum change of -360 meters over China, with several change centers in excess of ± 180 meters. The 48-hour changes are shown in Charts VIII-61 and VIII-62.

Table VII-11 contains some statistical measures of the atmospheric changes taking place in this 48-hour period. The RMS pressure difference increases from 4.81 MBS to

6.01 MBS after one and two days, respectively. The RMS 500 MB height difference increases from 54.7 meters to 67.7 meters after one and two days, respectively.

In the evaluation of prediction model outputs, emphasis will be given to the system over China and to the system in the Gulf of Alaska. The former deepened 19 MBS in the first day, and the latter deepened 23 MBS in the first day. The Atlantic low may be used as a standard -- since it did not change in intensity during the period.

Chart VIII-9 contains the 500 MB temperature analysis for 1200Z, 22 April 1976. Note the SIRS reports over the oceans north of 20N.

Chart VIII-10 contains the 500 MB wind analysis for 1200Z, 22 April 1976. Reports are shown as heavy barbs. Chart VIII-12 contains the 900 MB wind analysis for the same time. This contains many satellite wind vectors.

The reader may compare the aforementioned PS and Z500 analysis outputs to FNWC analyses. See Charts VIII-25 and VIII-26 for the PS charts for 22 and 23 April, respectively. See Charts VIII-27 and VIII-28 for the corresponding 500 MB height analyses.

2. Scenario B Discussion

Although this scenario commences at 1200Z, 19 May 1976, the forecasts were initialized with analysis model outputs for 1200Z, 20 May 1976.

Charts VIII-13 through VIII-15 contain the sea-level pressure (PS) analyses for 20 May through 22 May 1976, respectively. These were produced on the 63 x 63 grid. Charts VIII-99 and VIII-101 contain the PS actual changes for the first day and total period, respectively. The reader will note that a typhoon (present near 12N/146E) accounts for the rise-fall pair of centers on Chart VIII-99.

Charts VIII-17 through VIII-19 contain the 500 MB height analyses for 20-22 May. Charts VIII-100 and VIII-102 contain the Z500 actual changes (60-meter contours) for the first day and total period, respectively. For the most part, the actual changes for Scenario B are smaller than those indicated in Scenario A, but they are still large enough to be of use in this study. In Chart VIII-102, for example, two Z500 change centers exceed 300 meters in magnitude.

As Charts VIII-13 and VIII-14 are examined, one finds that the intensity of centers did not change dramatically. One secondary center between Iceland and England deepened from 1004 to 996 MBS. The deep low over China

remained constant at 988 MBS. The low center east of Kamchatka and the low center in the Gulf of Alaska each filled about four millibars. In the central Atlantic (near 40N/40W), the low deepened a little from 1009 to 1006 MBS. Thus, the displacement of systems was a significant consideration in this scenario.

Selected additional parameters are also provided at the (base) time of 1200, 20 May 1976. Chart VIII-21 contains a 500 MB temperature analysis. Chart VIII-22 contains the corresponding wind analysis. Both were performed on the 63 x 63 grid.

The charts for Scenario B may be compared to FNWC analyses. Charts VIII-31 and VIII-32 contain the PS analyses for 20 and 21 May, respectively. Charts VIII-33 and VIII-34 contain the Z500 analyses for these same dates. As would be expected, the correspondence between ODSI and FNWC analyses is quite good, especially in regions with adequate observational counts.

Table VII-17 contains some statistical measures of the actual changes at sea level and 500 MBS in Scenario B. The RMS pressure change amounts to 3.34 MBS in the first day (20-21 May), and increases slightly to 4.35 MBS for the two-day period (20-22 May). These are somewhat smaller than the RMS changes (of 4.81 and 6.01 MBS) in Scenario A.

H. Effects of Grid Resolution

Selected analysis model outputs using the 187 x 187 grid are provided in order to facilitate comparison with the 63 x 63 outputs.

1. Scenario A

Chart VIII-4 contains the 187 x 187 sea-level pressure analysis for 1200Z, 22 April 1976. It may be compared to Chart VIII-1. In fact, the (small) differences between these two analyses are contained in Chart VIII-55. (The contour interval is 1 MB.)

Chart VIII-8 contains the 187 x 187 500 MB height analysis for 1200Z, 22 April 1976. Compare this with the 63 x 63 version shown in Chart VIII-5. The differences between these analyses are shown on Chart VIII-56. (The contour interval is 10 meters.) Here, one starts to see differences of 10-30 meters in places. Note that in dense-data areas, the differences between the 187 x 187 and 63 x 63 outputs occur in small scales (as expected, because of the ability of the FMG to accommodate those reports better). In sparse-data regions, the differences appear to be in larger (meteorological) scales. This is due to the fact that: (1) filtering action on the 63 x 63 affects a broader geographical

region than on a 187 x 187 grid; and (2), the percent of the difference (between the reported value and the first-guess value) which gets applied to a grid point will tend to be larger for the 187 x 187 grid because of proximity (alone).

Chart VIII-11 contains the 500 MB temperature analysis for 1200Z, 22 April 1976 for the 187 x 187 grid. Compare this to Chart VIII-9.

2. Scenario B

Chart VIII-16 contains the 187 x 187 sea-level pressure analysis for 1200Z, 20 May 1976. Compare this output to Chart VIII-13 containing the 63 x 63 output. The differences between these two analyses are shown on Chart VIII-57. There are two small regions of 2 MB differences (central Pacific and Ethiopia). Otherwise, the differences are minimal.

Chart VIII-20 contains the 187 x 187 500 MB height analysis for 1200Z, 20 May. Compare this to Chart VIII-17. The differences between these outputs are shown in Chart VIII-58. Once again, the differences are in very small scales in dense-data regions. In sparse-data areas (such as the central Pacific), the differences lie in larger spatial scales. The 90-meter difference near 45N/170W is the result of a single report (which produced a minor trough) in the 187 x 187 analysis.

Chart VIII-23 contains the 187 x 187 500 MB temperature analysis for 20 May. Compare this to Chart VIII-21.

Chart VIII-24 contains the 187 x 187 500 MB wind vector analysis for 20 May. Compare this to Chart VIII-22.

3. Sea-Surface Temperature (SST)

Eight sea-surface temperature analyses are provided. Charts VIII-123 through VIII-126 pertain to Scenario A. Charts VIII-123 is the 187 x 187 SST analysis, which should be compared to Chart VIII-124 containing the 63 x 63 SST analysis for the same date-time. The ability of the FMG to resolve strong gradients is extremely good.

Charts VIII-127 through VIII-130 pertain to Scenario B. In this sequence, compare the 187 x 187 analysis in Chart VIII-127 with the 63 x 63 analysis in Chart VIII-128.

IV. PREDICTION MODEL DEVELOPMENT

The primary objective of this modeling effort was to examine the impact of grid resolution on short-range weather prediction (with real data). In so doing, ODSI has prepared a more effective/efficient model context for assessing the impact of SEASAT data on weather prediction. The models possess many of the characteristics of existing operational models at Fleet Numerical Weather Central, Monterey. This will facilitate the applicability and transferability of study results to that computational environment. This is particularly true with respect to the procedures in analysis codes and to the physics in prediction codes. With respect to data management and computational procedures in the prediction models, ODSI has implemented alternative approaches in order to be able to execute high-resolution versions on available computer systems.

These tests have pointed out the importance of "engineering" in prediction model development. Computational devices (smoothers and filters, tendency truncators, mountain shaping, diffusion operators) are needed to control noise in the solutions. But, the repetitive use of such devices can/does produce effects which mask (or overwhelm) the effects of physical processes being modeled. Thus, the impact of each discretionary procedure needs to be ordered, understood and exploited.

Observations are deficient in both number and distribution. Ocean-area data coverage is a critical issue in objective analysis. Satellite measurements are intended to satisfy ocean-area data requirements eventually, but model development can/must proceed in the interim. When the full potential of this data resource is realized, there should be significant improvement both in the specification of the initial state for prediction and in our understanding of the underlying physics. The point, of course, is that special care must be taken to ensure the computational viability of observed information.

A. Model Description

A complete description of the various forecast model versions (and programs) is provided in Volume III of this Final Report. For reader convenience, however, some important attributes and procedures will be described briefly in the following paragraphs.

The model requires a computer solution, using numerical methods, to a set of non-linear, partial difference equations at each grid point in the three-dimensional domain each integration time step. The time step is 4 minutes (12 minutes) in the 187 x 187 (63 x 63) model versions. The horizontal domain is a polar-stereographic mapping of the Northern

Hemisphere. Terrain-following "sigma" surfaces are used to map variables vertically. PECHFV has ten sigma surfaces ($\sigma = 0.95, 0.85, \dots, 0.05$). PEFHCV and PECHCV have five sigma surfaces ($\sigma = 0.9, 0.7, \dots, 0.1$).

The set of equations contains mathematical terms which represent relevant physical/dynamical processes and effects. The equations are written in flux form to facilitate the use of a second-order differencing scheme with special conservation properties. For temporal differencing, each twelve hours of integrations is initiated with an Euler-backward step and carried forward with centered steps (leapfrog). Consecutive solutions are time-filtered using a procedure devised by Robert in order to minimize solution separation while selectively dissipating high-frequency computational modes. The pressure-gradient force terms in the momentum equations are time-averaged to permit a slightly larger integration time step than would be acceptable ordinarily.

Some of the more important physical/dynamical processes represented in the model are: evaporation and condensation (cyclone-scale and cumulus-scale); sensible heat exchanges (air-ocean; air-ground); and solar and terrestrial radiation. The cumulus parameterization is based on a 1968 Arakawa algorithm, and redistributes heat and moisture in each column if certain (conditional-instability) criteria are met. Dry-

convective adjustments are invoked as necessary to preclude hydrostatic instability. Both mountain and frictional effects lend realism to flows. The quadratic friction term vanishes at $\sigma = 0.8$ (0.9) level in the 5-layer (10-layer) model. Mountain gradients cannot exceed 2,000 meters per meshlength. A land-sea-ice discriminator is employed, as appropriate. Terms representing the three-dimensional transport and vergence of heat, moisture and momentum are present, of course. Adiabatic temperature changes are modeled.

The diabatic heating rates are calculated (each hour) in a manner similar to that used at UCLA, as outlined by Langlois and Kwok (1969). Moisture is carried out at the lowest three (six) levels in the 5-level (10-level) models. Initial moistures are parameterized in terms of the patterns of geostrophic relative vorticity (the flow patterns). Heating rates are calculated for two gross layers (between $\sigma = 1.0$ and 0.6 , and between 0.6 and 0.2). A gross cloud is modeled after Smagorinsky (1960), and used to apportion the clear-sky and cloudy-sky rates. The solar calculations follow Joseph (1966). Infra-red fluxes are based on Mintz and Arakawa, after approximate fluxes are calculated using the approach of Danard (1969).

The model is initialized using the objective analysis model outputs described earlier. Recall that vertical

interpolation is needed to initialize sigma-surface points using pressure-surface information. Winds come from an objective analysis in which the first-guess values are non-divergent geostrophic winds.

Both explicit and implicit smoothing/filtering are present in this model. Without thermal and momentum diffusion terms, it would be difficult to control noise (hence, stability). A non-linear pressure smoother is also employed. In addition, a tendency truncator is used to eliminate forecast changes south of 5° latitude, and to gradually increase (with latitude) the permissible amount of forecast change up to 20° latitude (above which all forecast changes are allowed). [Such limiters are motivated and justified by problems with the data, (artificial) boundary conditions, and initialization procedures in tropical latitudes.]

This class of model has been in operational use by FNWC since 1970. It produces forecasts with skill (compared to a persistence forecast) for periods up to several days. Short baroclinic waves tend to be undermoved by 10-20 percent on the 63 x 63 grid, but only 1-4 percent on the 187 x 187 grid. Precipitation tends to be modeled well, especially in maritime cyclones. Indeed, the model handles cyclogenesis quite well, especially in the western Pacific Ocean.

B. Special Characteristics

Although a complete model description is provided in Volume III of the Final Report, brief explanations of special model characteristics will be provided in this section.

1. Geostrophic 50-MB Winds

In both PECHCV and PEFHCV, the sigma = 0.1 surface is often above 100 MBS, especially over high terrain where it can reach to 50 MBS. With PECHFV, the uppermost computational surface lies in the 50- to 25-MB stratum. Since the wind analysis model provides winds up to 100 MBS only, one can either extrapolate from available levels or use a non-divergent geostrophic wind above 100 MBS. Tests showed the latter procedure to be quite satisfactory (and an improvement over extrapolation).

2. Moisture Initialization Algorithm

As pointed out earlier, the initial relative humidity (RH) values are parameterized using geostrophic relative vorticity values from the flow patterns. This has proved to be superior to any so-called moisture analysis (which has few if any reports over the oceans), or to climatology values.

3. Special Processing of Outputs

Early tests showed that noise and/or unrealistic structures tended to build up in tropical regions during the course of the analysis-prediction cycle.

The remedial procedures included restoring the initial boundary conditions for output distributions, with Laplacian smoothing (latitudinally dependent) south of 30° latitude. (In an operational context, this procedure would have to be replaced with one involving a return to climatology in analysis in data-sparse regions.)

4. Special Processing of Inputs to Fine-Mesh (187 x 187) Models

Because of the large data base with the 187 x 187 grid (about one million words), it is more efficient to sort the input (analysis) data into vertical sections (I,K) for which pressure is the vertical coordinate (same as in the analysis codes) prior to performing the vertical interpolation to sigma surfaces. A separate program named PEPREP performs this task and generates an appropriate file for use in the initialization overlay of the PE model. PEPREP uses both rotating mass storage and either ECS or LCM (about 250,000 words) for temporary storage.

The 187 x 187 model may be initialized with 187 x 187 analysis outputs, or with 63 x 63 analysis outputs which have been interpolated to the 187 x 187 grid.

5. Lateral Boundary Conditions and Tendency Truncation

Forecast tendencies for each integration time step are reduced/eliminated south of 20N according to an array of coefficients. South of 5N the tendencies are set to zero (producing a persistence forecast). Between 5N and 20N, the coefficients vary according to the latitude θ as follows:

$$\left[\frac{(\sin \theta - \sin 5^\circ)}{(\sin 20^\circ - \sin 5^\circ)} \right]^2$$

Within each integration step, however, the boundary walls are assumed to be rigid, insulated and slippery. No boundary fluxes are allowed. Tangential flow is permitted.

6. Pressure-Gradient Force (PGF) Time-Averaging in Momentum Equations

To allow for a slightly lengthened integration time step, the pressure-gradient force (PGF) terms in the momentum equations are time-averaged. The procedure requires that the integrations be re-ordered as follows: (1) integrate all of the equations except the momentum equations [in order to

produce new (T+1) geopotentials]; (2) time-average the PGF terms, using

$$\overline{\text{PGF}}^T = (1-\alpha) \text{PGF}^T + \frac{\alpha}{2} (\text{PGF}^{T-1} + \text{PGF}^{T+1});$$

and (3), integrate the momentum equations containing the time-averaged PGF terms.

7. Temporal Filtering of Thermodynamic and Moisture Equations

In the temperature and moisture equations, consecutive solutions are time-filtered using a method devised by Robert (1966). The method is used to minimize solution separation, as well as to damp undesirable short-wave components. It is not applied to the momentum equations.

8. Non-Linear Pressure (Tendency Equation) Smoothing

Oliger and Welck (1970) describe a non-linear pressure-smoother which we apply in the pressure-tendency equation each time step. Since the operator is actually applied to stencils of sea-level pressure values about each point, the terrain pressure must first be reduced to sea level, then recovered from sea-level values, using a specified algorithm.

9. Horizontal Diffusion

Temperature diffusion, D_T , and momentum diffusion, D_M , were added to the model equations to redistribute/attenuate high-frequency components. The former (D_T) varies in magnitude according to the diffusion coefficient, K , given by

$$K = \begin{cases} 10^6 & \text{on the CMG} \\ 4 \times 10^5 & \text{on the FMG} \end{cases}$$

The latter (D_M) varies with both latitude and model level, in addition to the aforementioned grid-dependent coefficient.

10. Temporal Differencing

Centered (leapfrog) differencing is used, except for the step which initiates a new integration period (normally every twelve forecast hours). For this step, we use an Euler-backward step (which is selectively dissipative). In the 187 x 187 model versions, a provision has been made to employ an Euler-backward step at other specified times, as well.

Due to the interaction of the various computational devices being used, the integration is fifteen minutes in the 63 x 63 models, and four minutes in the 187 x 187 models. We refer to: (1) PGF time-averaging; (2) Robert time-filtering; (3) non-linear pressure smoothing; and (4) lateral diffusion.

11. Diabatic Heating in Low Latitudes

The diabatic heating/cooling is turned off south of 25° North. This is primarily an economy measure which is consistent with other aspects of these forecasts (forecast length; initialization in low latitudes; use of tendency truncation). We refer to: (1) radiation; (2) latent and sensible heating; and (3) the cumulus parameterization.

12. Tapered Terrain

As a general rule, one should not introduce trauma into models in scales that the model cannot resolve handle well. Terrain gradients are a source of trauma. In order to minimize this difficulty, two actions were taken: (1) the terrain gradients were not permitted to exceed 2,000 meters per coarse meshlength; and (2) the terrain was tapered from 5° to 20° North and allowed to vanish below 5° North. See Chart IV-1 for the terrain specification so modified. The contour interval is 250 meters.

C. Computer Utilization

To be able to accomplish all of the analysis and prediction model development and production testing in this contractual effort required a substantial amount of computer support.

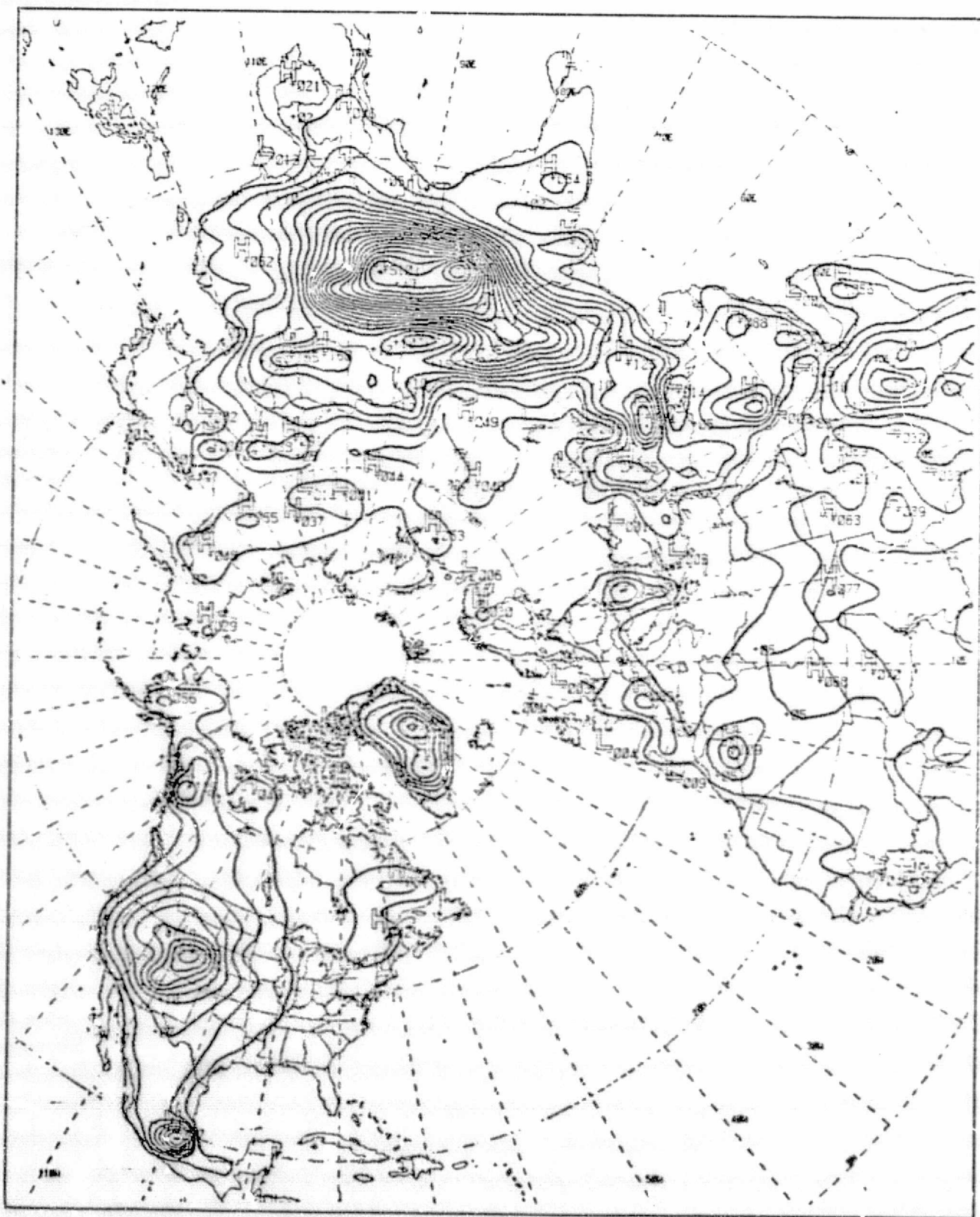


CHART IV-1: TERRAIN HEIGHT. MAXIMUM GRADIENT
EQUALS 2,000 METERS PER MESH LENGTH.

ORIGINAL PAGE
IS OF POOR QUALITY

IV-12

ORIGINAL PAGE IS
OF POOR QUALITY

All of the analysis and coarse-mesh (63 x 63) prediction modeling was performed on the CYBER 175 at Fleet Numerical Weather Central, Monterey. In this contract period, this amounted to about 200 CP-hours and about 600 wall-clock hours. Table IV-1 shows the CYBER 175 utilization for typical 24-hour forecasts using either the 63 x 63 x 5-level or 63 x 63 x 10-level prediction models.

The fine-mesh (187 x 187) prediction modeling was performed on the CDC 7600 at NASA Ames. Table IV-2 shows the time it takes to execute these high-resolution model versions. These tables indicate that it takes about 12-13 times longer to execute the one-third mesh version on the 7600 than it does to execute a standard-mesh model on the 175. Since the 7600 is about twice as fast as the 175 for such codes, this suggests that the fine-mesh problem is a 25X problem. Theoretically, it is a 27X problem. Thus, some economies of scale were realized.

The lack of 7600 time prevented ODSI from executing the fine-mesh models on more data sets or for longer forecast periods.

During the contract period, it became necessary to shift the programming/production efforts from one type of computer to another (in order to accommodate GFE availability). Thus, some of the total effort was related to such system changes.

TABLE IV-1: CYBER 175 UTILIZATION FOR
COARSE-MESH PREDICTION.

MODEL/ITEM	CYBER 175 EXECUTION TIMES	
	WALL	CP
63 x 63 x 10 PEM (PECHFV)		
-- Initialization	--	5 Sec.
-- Each 12-hour Integration	--	11.5 Min.
-- Each 12-hour Output	--	17 Sec.
-- Total 24-hour Forecast	50 Min.	23.5 Min.
63 x 63 x 5 PEM (PECHCV)		
-- Initialization	--	3 Sec.
-- Each 12-hour Integration	--	5.9 Min.
-- Each 12-hour Output	--	15 Sec.
-- Total 24-hour Forecast	33 Min.	12.5 Min.

NOTES:

1. Used 12-minute timesteps.
2. FNWC provided 200 CP-hours (about 600 wall-clock hours) in this contract year.

TABLE IV-2: CDC 7600 UTILIZATION FOR
FINE-MESH PREDICTION.

MODEL/ITEM	CDC 7600 EXECUTION TIMES	
	WALL	CP
187 x 187 x 10 PEM (PEHFV)		
-- Initialization	44 Sec.	13 Sec.
-- Each 6-hour Integration	3.5 Hr.	1.2 Hr.
-- Each 6-hour Output	14 Min.	1.5 Min.
-- Total 24-hour Forecast	15 Hr.	4.8 Hr.
187 x 187 x 5 PEM (PEFHCV)		
-- Initialization	23 Sec.	8 Sec.
-- Each 6-hour Integration	67 Min.	39 Min.
-- Each 6-hour Output	9 Min.	1.3 Min.
-- Total 24-hour Forecast	5.2 Hr.	2.7 Hr.

NOTES:

1. Used 4-minute timesteps.
2. Runs were made at NASA Ames.

V. PREDICTION MODEL TEST RESULTS

Table II-1 provides the model descriptors, run numbers and selected chart, table and figure references for those prediction model results to be presented in this Final Report. The coarse-mesh (63 x 63 x 5 or 63 x 63 x 10) forecasts are all two-day forecasts. The fine-mesh (187 x 187 x 5) forecasts are one-day forecasts. There are three major runs in each of two scenarios. In Scenario A, all forecasts were initialized with Test Series B analyses. The major runs for Scenario A are: F18 (63 x 63 x 5), F22 (187 x 187 x 5) and T4 (63 x 63 x 10). Runs F20 (63 x 63 x 5) and T6 (63 x 63 x 10) were initialized with Production Series C analyses, and may be compared to the major runs, as appropriate, to determine the effects of interactive analyses. In Scenario B, all forecasts were initialized with Production Series C analyses. The major runs for Scenario B are: F19 (63 x 63 x 5), F24 (187 x 187 x 5) and T5 (63 x 63 x 10).

Several classes of exhibits will be provided to aid in the examination and evaluation of these results: (1) forecast charts; (2) forecast change charts (forecast minus starting analysis); (3) forecast error charts (forecast minus verification analysis); (4) forecast difference charts (ten-layer forecast minus five-layer forecast and fine-mesh forecast minus

coarse-mesh forecast); (5) starting/verification analysis charts; (6) actual change charts (to be compared to either forecast error charts or forecast change charts); (7) statistical information describing model performance and model behavior (energetics); and (8) graphical information describing model behavior.

A. Scenario A: Forecasts, Forecast Changes, Forecast Errors

Several types of comparisons may be made in this scenario. The forecast charts may be verified against the appropriate verification analyses. Forecasts from a five-layer model (for a given initial analysis type) may be compared to forecasts from a ten-layer model. Forecasts (from a given model version) using one type of initial analysis may be compared to forecasts using a different type of initial analysis. Ideally, the forecast changes and actual changes should correspond quite well. Also, the pattern of forecast errors should be less dense/smaller in size than the pattern of actual changes. Such qualitative assessments may be augmented by detailed comparisons of statistical measures presented herein.

1. Run F22 (PEFHCV)

Charts VIII-131 through VIII-133 contain the 24-hour sea-level pressure (PS), 500-MB height (Z500) and 500-MB temperature (T500) forecasts, respectively, using the 187 x 187 x 5 model version and Test Series B analyses. Charts VIII-2 and VIII-6 may be used to verify the PS and Z500 forecasts, respectively. The forecasts may be compared also to Charts VIII-134 through VIII-136 to ascertain the impact of horizontal resolution.

Charts VIII-63 through VIII-66 contain the forecast error/change patterns at both sea level and 500 MBS. In addition, the actual change patterns are shown in Charts VIII-59 and VIII-60. Table VII-11 contains the actual change statistics.

Table VII-12 contains model statistics for Run F22. At sea level, the 4.78-MB RMS forecast change compares well to the 4.81-MB RMS actual change, and the 3.61-MB RMS forecast error is much less than the actual change. At 500 MBS, the 53.7-meter RMS forecast change compares well to the 54.7-meter actual change, while the 36.3-meter RMS error is much smaller than the actual change.

2. Run F18 (PECHCV)

Charts VIII-13^A through VIII-136 contain the 24-hour sea-level pressure, 500-MB height and 500-MB temperature forecasts, respectively, using the 63 x 63 x 5 model version. Charts VIII-2 and VIII-6 may be used to verify the PS and Z500 forecasts, respectively. Charts VIII-137 through VIII-139 contain the 48-hour PS, Z500 and T500 forecasts, respectively. Verify the PS and Z500 forecasts using Charts VIII-3 and VIII-7, respectively.

Charts VIII-67 through VIII-74 contain the forecast change/error patterns. Twenty-four hour changes/errors at both sea level and 500 MBS are shown in Charts VIII-67 through VIII-70. Forty-eight hour changes/errors are shown in Charts VIII-71 through VIII-74. These patterns may be compared to the actual changes shown in Charts VIII-59 through VIII-62.

Table VII-13 contains model statistics for Run F18. At sea level, the 5.74-MB RMS forecast change is slightly less than the 6.01-MB actual change after 48 hours. Also, the 4.16-MB RMS error shows good skill compared to the actual change. At 500 MBS, the statistics are consistent. The 64.1-meter RMS forecast change is slightly less than the 67.7-meter RMS actual change. And, the 51.2-meter RMS error shows skill compared to the actual change.

3. Run T4 (PECHFV)

Charts VIII-140 through VIII-142 contain the 24-hour PS, Z500 and T500 forecasts, respectively, using the 63 x 63 x 10 model version. Charts VIII-2 and VIII-6 may be used to verify the PS and Z500 forecasts, respectively. Charts VIII-143 through VIII-145 contain the corresponding 48-hour forecasts. Verify the PS and Z500 forecasts using Charts VIII-3 and VIII-7, respectively.

Charts VIII-75 through VIII-82 contain the forecast change/error patterns. Twenty-four hour changes/errors at both sea level and 500 MBS are shown in Charts VIII-75 through VIII-78. Forty-eight hour changes/errors are shown in Charts VIII-79 through VIII-82. These patterns may be compared to the actual changes shown in Charts VIII-59 through VIII-62.

Table VIII-14 contains model statistics for Run T4. At sea level, the 5.81-MB RMS forecast change compares well to the 6.01-MB RMS actual change, while the 4.15-MB RMS error is much smaller than the actual change. At 500 MBS, the 64.9-meter RMS forecast change compares well to the 67.7-meter RMS actual change, while the 50.9-meter RMS forecast error shows good skill after 48 hours.

4. Run F20 (PECHCV)

Charts VIII-146 through VIII-148 contain the 24-hour PS, Z500 and T500 forecasts, respectively, using the 63 x 63 x 5 model version and Production Series C analyses. Charts VIII-2 and VIII-6 may be used to verify the PS and Z500 forecasts, respectively. The forecasts may be compared also to Charts VIII-134 through VIII-136 to ascertain the differences due to variations in the initial analyses.

Charts VIII-149 through VIII-151 contain the 48-hour PS, Z500 and T500 forecasts, respectively, for Run F20. Verify these forecasts against Charts VIII-3 and VIII-7, respectively. Compare these forecasts against VIII-137 through VIII-139 to ascertain the impact of initial analyses on 48-hour forecasts.

Charts VIII-83 through VIII-90 contain the F20 forecast change/error patterns. Compare these charts to the actual change patterns shown in Charts VIII-59 through VIII-62.

Table VIII-15 contains model statistics for Run F20. At sea level, the 4.26-MB RMS error shows skill compared to the 6.01-MB RMS actual change. At 500 MBS, the 56.9-meter RMS error shows skill compared to the 67.7-meter RMS actual change.

5. Run T6 (PECHFV)

Charts VIII-152 through VIII-154 contain the 24-hour PS, Z500 and T500 forecasts, respectively, using the 63 x 63 x 10 model version and Production Series C analyses. Charts VIII-2 and VIII-6 may be used to verify the PS and Z500 forecasts, respectively. The T6 forecasts may be compared also to Run F20 forecasts to ascertain vertical resolution effects, or to Run T4 forecasts to ascertain initial analysis effects.

Charts VIII-155 through VIII-157 contain the 48-hour PS, Z500 and T500 forecasts, respectively, for Run T6. Verify these against Charts VIII-3 and VIII-7. Comparisons to appropriate charts for Runs F20 and T4 may be made also.

Charts VIII-91 through VIII-98 contain the T6 forecast change/error patterns. Compare these patterns to the actual change patterns shown in Charts VIII-59 through VIII-62.

Table VII-16 contains model statistics for Run T6. At sea level, the 4.13-MB RMS forecast error shows skill compared to the 6.01-MB RMS actual change. At 500 MBS, the 56.6-meter RMS forecast error shows skill compared to the 67.7-meter RMS actual change. In both cases, the forecast change was only slightly less than the actual change.

B. Scenario B: Forecasts, Forecast Changes, Forecast Errors

All of the Scenario B forecasts were made from the same starting analyses. The 187 x 187 x 5 model version was initialized with values that were obtained by interpolation of 63 x 63 analysis model outputs.

1. Run F24 (PEFHCV)

Charts VIII-158 through VIII-160 contain the 24-hour PS, Z500 and T500 forecasts, respectively, using the 187 x 187 x 5 model version and interpolated Production Series C 63 x 63 analyses. Charts VIII-14 and VIII-18 may be used to verify the PS and Z500 forecasts, respectively. These forecasts may be compared also to Run F19 forecasts, shown as Charts VIII-161 through VIII-163, to assess the effects of horizontal resolution.

Charts VIII-103 through VIII-106 contain the forecast change/error patterns at both sea level and 500 MBS. In addition, the actual change patterns are shown as Charts VIII-99 through VIII-102. Table VII-17 contains the actual change statistics.

Table VII-18 contains the model statistics for Run F24. At sea level, both the forecast change and the forecast error exceed the actual change. The RMS forecast

error was 3.89 MBS while the RMS actual change was 3.34 MBS. At 500 MBS, the 38.2-meter RMS error is only slightly smaller than the 38.6-meter RMS actual change.

2. Run F19 (PECHCV)

Charts VIII-161 through VIII-163 contain the 24-hour PS, Z500 and T500 forecasts, respectively, using the 63 x 63 x 5 model version. Verify the PS and Z500 forecasts against Charts VIII-14 and VIII-18, respectively. Compare the F19 forecasts to the T5 forecasts to assess the effect of vertical resolution. Charts VIII-164 through VIII-166 contain the corresponding 48-hour forecasts for Run F19. Verify these against Charts VIII-15 and VIII-19, as appropriate.

Charts VIII-107 through VIII-114 contain the 24-hour and 48-hour forecast change/error patterns. These patterns may be compared to the actual changes shown in Charts VIII-99 through VIII-102. Table VII-17 contains the actual change statistics.

Table VII-19 contains the model statistics for Run F19. At both sea level and 500 MBS, F19 shows slight skill after 48 hours. At sea level, the 3.83-MB RMS forecast error is slightly smaller than the 4.35-MB RMS actual change.

At 500 MBS, the 50.8-meter RMS forecast error is slightly smaller than the 52.3-meter RMS actual change. This is true in spite of the fact that the forecast error exceeded the actual change during the first 24 hours of the forecast.

3. Run T5 (PECHFV)

Charts VIII-167 through VIII-169 contain the 24-hour PS, Z500 and T500 forecasts, respectively, using the 63 x 63 x 10 model version. Verify the PS and Z500 forecasts against Charts VIII-14 and VIII-18, respectively. Charts VIII-170 through VIII-172 contain the corresponding 48-hour PS, Z500 and T500 forecasts. Verify these against Charts VIII-15 and VIII-19, as appropriate.

Charts VIII-115 through VIII-122 contain the 24-hour and 48-hour forecast change/error patterns. These may be compared to the actual changes shown in Charts VIII-99 through VIII-102. Table VII-17 contains the actual change statistics.

Table VII-20 contains the model statistics for Run T5. At sea level, the 3.34-MB RMS forecast error after 24 hours exactly equals the actual change, but the 3.70-MB RMS error after 48 hours is smaller than the 4.35-MB RMS actual change. At 500 MBS, the forecast error is slightly smaller than the actual change. After 24 hours, the 38.0-meter

RMS error may be compared to the 38.6-meter RMS change. After 48 hours, the 50.4-meter RMS error may be compared to the 52.3-meter RMS change.

In general, the models did not exhibit as much skill in Scenario B (the May case) as they did in Scenario A (the April case).

C. Scenario A: Comparative Performance Data

1. Intensity of Pressure Systems at Sea Level

Table VII-1 contains the 24-hour forecast central pressures (in millibars) using three models of differing resolution. Eight significant low-pressure systems are considered. The starting and verification pressures for each system are provided. The average algebraic error is also shown for each model version.

Run F22, the 187 x 187 x 5 model, exhibits the best overall performance in terms of algebraic error (-0.8 MBS per system), due in part to large compensating errors (+11 MBS in the Alaskan Gulf low and -10 MBS in the China low). Both F18 and T4 exhibited the same +6 MB average error, more or less. Indeed, the effects of doubling the vertical resolution appear to be minimal. Both coarse-mesh models did not deepen several of the lows enough.

2. Performance Statistics

Tables VII-3 and VII-4 contain comparative performance statistics at 500 MBS and sea level, respectively.

In Table VII-3, Scenario A, Run F22 has the best 24-hour performance, with an RMS height error of only 36.3 meters. F22 also has an RMS forecast change of 53.7 meters, which compares very favorably to an actual RMS change of 54.7 meters. At 48 hours, the 63 x 63 models (F18 and T4) exhibit RMS errors which are quite comparable to one another.

In Table VII-4, Scenario A, Run F22 has a slightly larger RMS error (3.61 MBS) than the 63 x 63 models. It did, however, produce an RMS forecast change which compares very well to the RMS actual change. Both 63 x 63 models tended to produce small error as a consequence of a less-courageous (smoother) forecast.

3. Kinetic Energy (KE)

Table VII-5 contains the layer-mean kinetic energy 24-hour forecast changes (expressed in percent) for models of varying resolution. Consider the Scenario A part. Run F22 produced large increases in KE in the lower (moisture bearing) levels, as compared to the 63 x 63 models which both predicted KE losses at all levels. Figure VI-1 shows the percent forecast change in KE by model level.

Figures VI-2 through VI-4 contain KE 24-hour forecast cross-sections (latitude vs. model level), in energy units. Figure VI-2 pertains to Run T4, which exhibits a maximum of 18 units near 300 MBS at 40°N. Figure VI-3 pertains to Run F18, and exhibits a 16+ unit maximum near 400 MBS at 40°N. Altitude differences are due to vertical resolution. Figure VI-4 exhibits a stronger maximum (22+ units) near 300 MBS and 40°N. Thus, the 187 x 187 x 5 model and 63 x 63 x 5 model exhibit comparable KE core locations, but the 187 x 187 model produces a much greater core magnitude.

Figures VI-5 through VI-9 show the time variations of KE by model/model level for Scenario A. In Figure VI-5, Run F22 exhibits a continuing growth with time at sigma=0.9 level, as compared to Runs F18 and T4 which decrease after reaching a 6-hour maximum. In Figure VI-6, one sees the same type of behavior at sigma=0.7 level. In Figure VI-7, Run F22 exhibits some oscillatory behavior without the large net increase observed at lower levels. Runs F18 and T4 show net decreases. In Figure VI-8, one can see that all three models behave in like manner -- with a large initial decrease followed by oscillatory behavior. (This appears to be typical at the sigma=0.3 level.) Finally, the somewhat less-remarkable behavior at the sigma=0.1 level is shown in Figure VI-9.

4. Square Vorticity

Figure VI-10 shows the square vorticity 24-hour forecast changes (in percent) by model version and level. PEFHCV (Run F22) produced large increases in the lower levels compared to PECHCV (F18) and PECHFV (T4). (Table VII-6 contains the source percentages.)

Figures VI-11 through VI-15 contain the time variations of square vorticity at each level for Scenario A. Run F22 (187 x 187 model) generates much more vorticity than the two 63 x 63 models in the lowest three levels. In Figure VI-14, one can observe a decrease in square vorticity in the first six hours (in all models) at the $\sigma=0.3$ level. Compare this to the KE behavior at this level shown previously in Figure VI-8.

5. Square Divergence

Figures VI-16 through VI-20 contain the time variations of square divergence in Scenario A at the five model levels, respectively. Run F22 (the 187 x 187 model) behaves quite differently from 63 x 63 models, especially at low levels. The effects of vertical resolution and horizontal resolution appear to be (more) alike at higher levels.

6. Temperature

Figures VI-41 through VI-43 contain 24-hour forecast temperature-change ($^{\circ}\text{C}$) cross-sections (latitude versus model level) for Scenario A forecasts. Figure VI-41, which pertains to Run T4, and Figure VI-42, which pertains to Run F18, are in qualitative agreement. Figure VI-43, which pertains to Run F22, shows a greater (positive) forecast change (near 500 MBS at 40°N) than the 63 x 63 model versions.

7. Precipitation

Figure VI-47 shows the average precipitation (centimeters) per grid point for three model versions in Scenario A. The source numbers are contained in Table VII-7. The effects of vertical resolution changes are small compared to the effects of horizontal resolution changes.

D. Scenario B: Comparative Performance Data

1. Intensity of Pressure Systems at Sea Level

Table VII-2 contains the twenty-four hour forecast central pressures (in millibars) using three models of differing resolution. Six significant low-pressure centers are considered in this scenario. The starting and verification pressures for each system are provided. The average algebraic error for each model version is also tabulated.

Runs T5 and F19, the 63 x 63 models, exhibit the best overall performance. As in Table VII-1, the effects of vertical resolution appear to be minimal. In contrast, Run F24 (the 187 x 187 x 5 model) produced lows which were slightly too deep (~3 MBS on the average).

2. Performance Statistics

Table VII-3 and VII-4 contain comparative performance statistics at 500 MBS and sea level, respectively.

In Table VII-3, Scenario B, all three model versions perform in the same manner. The RMS error at 500 MBS is equal to the RMS change (no skill compared to persistence) at 24 hours, but slightly less at 48 hours.

In Table VII-4, Scenario B, T5 exhibits the smallest RMS error, but mainly as a consequence of a less-courageous (smoother) forecast. Run F24 does not exhibit skill compared to persistence at 24 hours. It predicted too much change. The 63 x 63 models show slight skill at 48 hours, however.

3. Kinetic Energy (KE)

Table VII-5 contains the layer-mean kinetic energy 24-hour forecast changes (expressed in percent). Consider the part for Scenario B. F24 produced a large increase in KE (27.8%) at sigma=0.9 level, compared to KE decreases in

the 63 x 63 models. At other levels, F24 produced smaller decreases in KE than the 63 x 63 models. Figure VI-21 shows the percent forecast change in KE by model level.

Figures VI-22 through VI-24 contain KE 24-hour forecast cross-sections (latitude versus model level) in energy units. Figure VI-22 shows the Run T5 cross-section with a core magnitude of 12+ units near 300 MBS at 40°N. Figure VI-23 shows the Run F19 cross-section with a core magnitude of 12+ units near 350 MBS and 45°N. Figure VI-24 shows the Run F24 section with a core magnitude of 12+ units near 350 MBS at 45°N. In this May case, the core magnitudes are quite comparable. The ten-level model places the core slightly higher in altitude than the five-level models.

Figures VI-25 through VI-29 contain the time variations of kinetic energy by model/model level for Scenario B. In many ways, the KE behavior is comparable to the behavior described for Scenario A earlier. In Figure VI-25, one observes that the sigma=0.9 level net increase by Run F24 (187 x 187 model) is much less than that shown in Figure VI-5 (by Run F22). The modal value at forecast hour six remains for the 63 x 63 models. In Figure VI-26, however, the F24 behavior at sigma=0.7 level is much better than F22 behavior shown previously in Figure VI-6. In Figure VI-28, one sees the (same) large decreases in the first six hours at the sigma=0.3 level.

4. Square Vorticity

Figure VI-30 shows the square vorticity 24-hour forecast changes (in percent), by model version and level. PEFHCV (Run F24) produced a large increase at the $\sigma=0.9$ level. Compare this to the behavior of the 63 x 63 models shown. (Table VII-6 contains the source percentages.)

Figures VI-31 through VI-35 contain the time variations of square vorticity at each level for Scenario B. Run F24 (the 187 x 187 model) behavior is quite different from the 63 x 63 models.

5. Square Divergence

Figures VI-36 through VI-40 contain the time variations of square divergence in Scenario B at the five model levels, respectively. Run F24 behaves quite differently from 63 x 63 models, especially at low levels. The effects of vertical resolution and horizontal resolution appear to be comparable at higher levels.

6. Temperature

Figures VI-44 through VI-46 contain 24-hour forecast temperature-change ($^{\circ}\text{C}$) cross-sections (latitude versus model level) for Scenario B forecasts. Run T5 in Figure VI-44

shows qualitative agreement with Run F19 in Figure VI-45, but it is not as smooth. Run F24 in Figure VI-46 corresponds very well with F18 but tends to show larger amplitudes near 35°N.

7. Precipitation

Figure VI-48 shows the average precipitation (centimeters) per grid point for three model versions in Scenario B. The source numbers are shown in Table VII-7. As in Scenario A, the effects of vertical resolution changes are demonstrated to be small compared to horizontal resolution changes.

E. Effects of Changes in Model Vertical Resolution on Sea-Level Pressure and 500-MB Height Forecasts

1. Scenario A Comparisons

Three comparisons can be made (in Scenario A) between five-layer and ten-layer models: (1) Runs F19 and T4 which were both initialized with Test Series B analyses; (2) Runs F20 and T6 which were both initialized with Production Series C analyses; and (3), an additional set of forecasts which were initialized with analyses using FNWC first-guess fields. (The comparison between Run F22 and its ten-layer counterpart will be covered in a separate volume.)

Charts VIII-37 and VIII-38 show the differences between Runs F20 (63 x 63 x 5) and T6 (63 x 63 x 10) at sea level and 500 MBS, respectively. (Chart VIII-37 has a 2-MB contour interval; and Chart VIII-38 has a 30-meter contour interval.) Table VII-21 contains statistical measures of the differences between F20 and T6 at the 24-hour and 48-hour forecast times at both sea level and 500 MBS. The RMS pressure difference is 0.96 MBS at hours 24 and 48 (no additional differences after the first 24 hours). At 500 MBS, the RMS height difference increases from 8.34 meters at hour 24 to 9.32 meters at hour 48. From Chart VIII-37, note that a maximum 24-hour difference of 5.15 MBS is located 35N/160E.

Charts VIII-38 and VIII-39 show the differences between Runs F18 and T4. Table VII-22 contains statistical measures of the differences. In this case, the RMS pressure difference is 0.92 MBS at hour 24 and 1.02 MBS at hour 48. The maximum difference, however, is 7.29 MBS near 35N/160E. At 500 MBS, the RMS height difference increases from 8.19 meters at hour 24 to 9.79 meters at hour 48.

Charts VIII-41 and VIII-42 show the differences between a five-layer and ten-layer forecast, both of which were initialized with analyses that started with FNWC first-guess fields. From visual appearances, the differences appear to be slightly smaller than those observed in the previous cases.

These differences appear to be small in both magnitude and areal extent. They can be compared to differences between a 187 x 187 forecast and a 63 x 63 forecast which were approximately twice as large in magnitude. Finally, one can also assess the forecast differences brought about by differences in the initialization. In an RMS sense, such differences appear to be small compared to the differences brought about by changing the vertical resolution.

2. Scenario B Comparison

Charts VIII-43 and VIII-44 show the differences between Runs F19 and T5. Table VII-23 contains statistical measures of the differences at sea level and 500 MBS. The RMS pressure difference of 0.76 MBS at hour 24 increases to 0.82 MBS at hour 48. The maximum 24-hour difference is +4.88 MBS south of Japan. At 500 MBS, the RMS height difference of 7.27 meters at hour 24 increases to 8.66 meters at hour 48. NOTE: The effects of differing vertical resolution on model energetics, precipitation and forecast accuracy were discussed earlier. Suffice to say that the differences due to vertical resolution were consistently small (or even negligible) compared to the differences due to horizontal resolution. Refer to Table VII-7, for example, which shows the precipitation amounts from each model.

F. Effects of Changes in Model Horizontal Resolution
on Sea-Level Pressure and 500-MB Height Forecasts

1. Scenario A Comparison

Charts VIII-45 and VIII-46 show the differences between Runs F22 (187 x 187 x 5) and F18 (63 x 63 x 5) at sea level and 500 MBS, respectively. (The sea-level pressure contour interval is 2 MBS. The 500-MB contour interval is 30 meters.) Table VII-9 contains statistical measures of the differences. The RMS pressure difference is 2.01 MBS, with a maximum difference of -16.5 MBS near Japan. At 500 MBS, the RMS height difference is 14.1 meters, with a maximum difference of -148.0 meters near Japan. These differences are "of meteorological scale". They tend to contour nicely. The differences in the subtropics are small.

2. Scenario B Comparison

Charts VIII-47 and VIII-48 show the differences between Runs F24 (187 x 187 x 5) and F19 (63 x 63 x 5) at sea level and 500 MBS, respectively. Table VII-10 contains statistical measures of the differences. The RMS pressure difference is 1.58 MBS, with a maximum difference of -9.6 MBS. At 500 MBS, the RMS height difference is 9.8 meters, with a maximum difference of -69.6 meters.

NOTE: Differences in model energetics, precipitation, and forecast accuracy as a consequence of changes in horizontal resolution were discussed earlier. Such differences are large compared to other causes of differences, generally.

VI. FIGURES

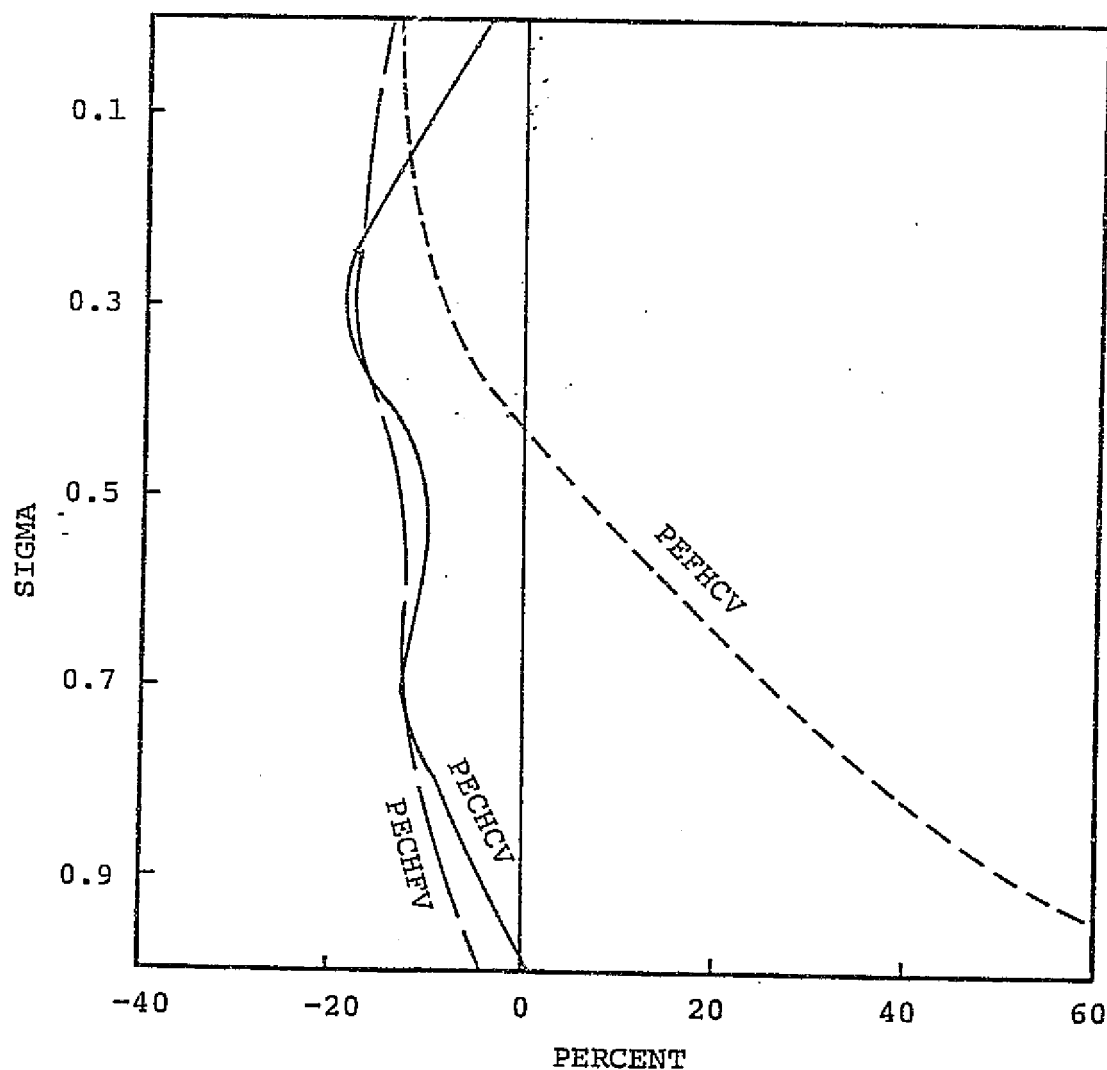


FIGURE VI-1: KINETIC ENERGY 24-HOUR FORECAST
CHANGE (%), BY MODEL VERSION
AND LEVEL. SCENARIO A.

ORIGINAL PAGE IS
OF POOR QUALITY

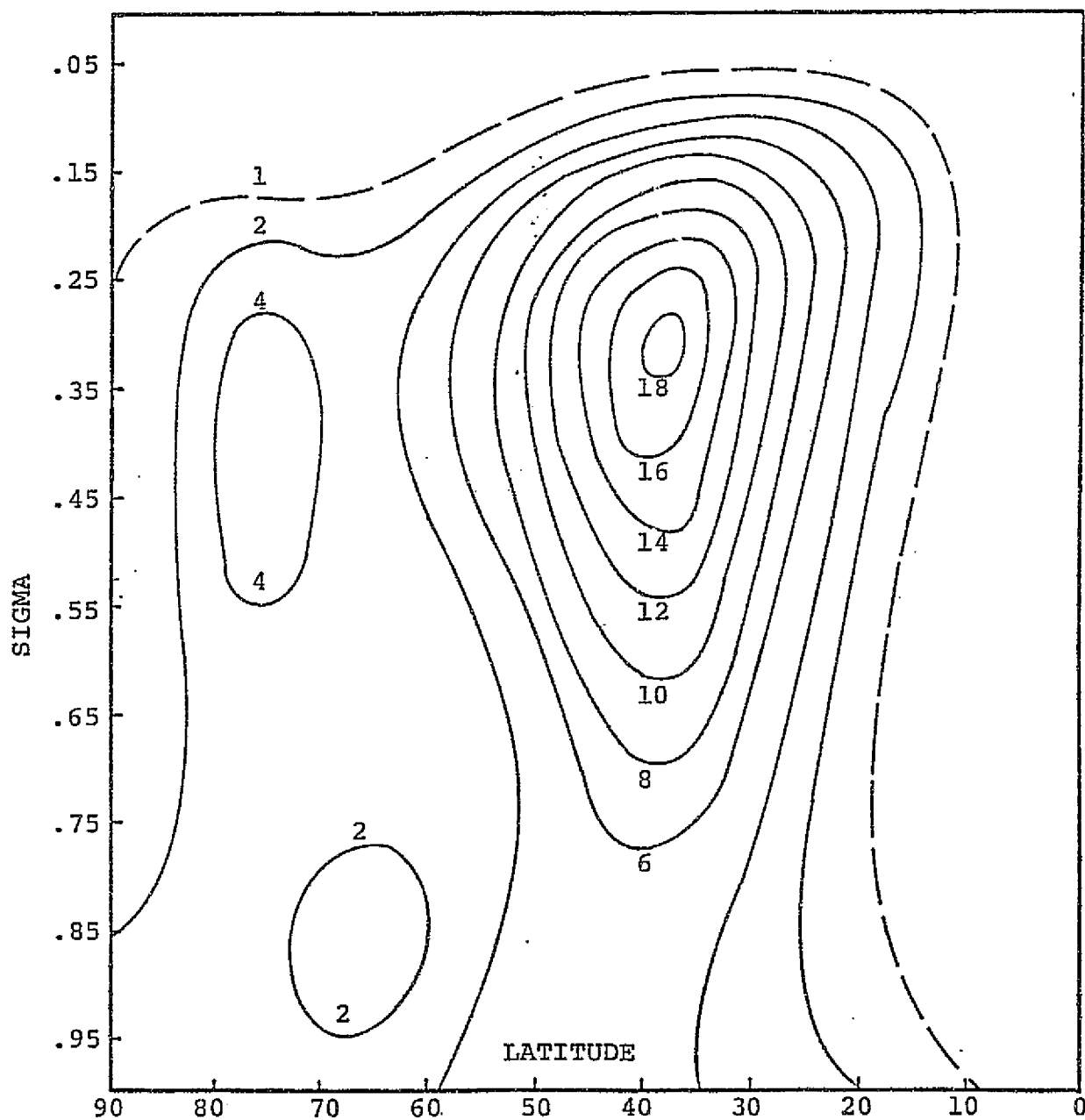


FIGURE VI-2: KINETIC ENERGY ($\times 10$) 24-HOUR FORECAST CROSS-SECTION. RUN T4.
MODEL PECHFV. SCENARIO A.

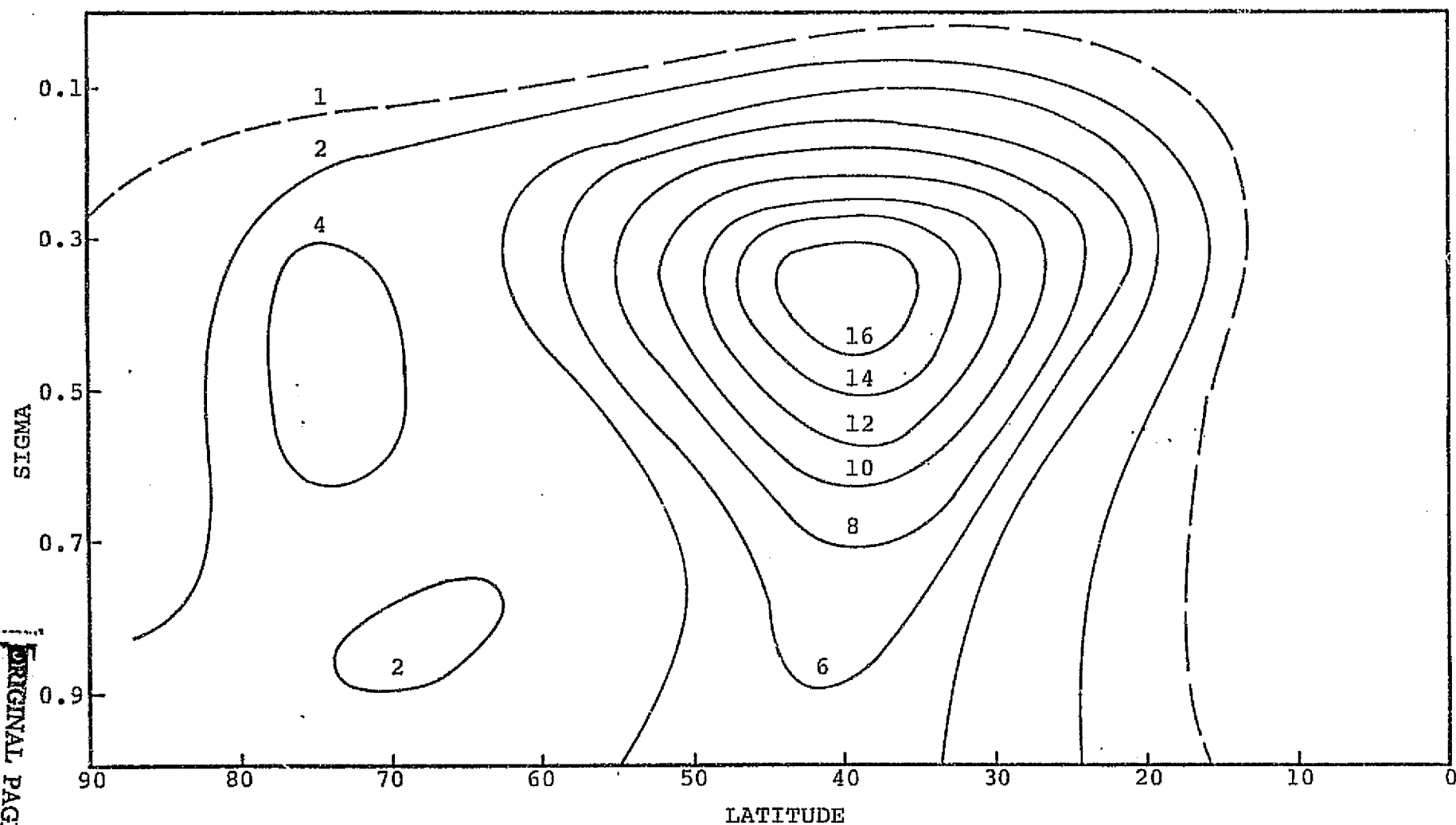


FIGURE VI-3: KINETIC ENERGY ($\times 10$) 24-HOUR FORECAST CROSS-SECTION.
 RUN F18. MODEL PECHCV. SCENARIO A.

ORIGINAL PAGE IS
 OF POOR QUALITY

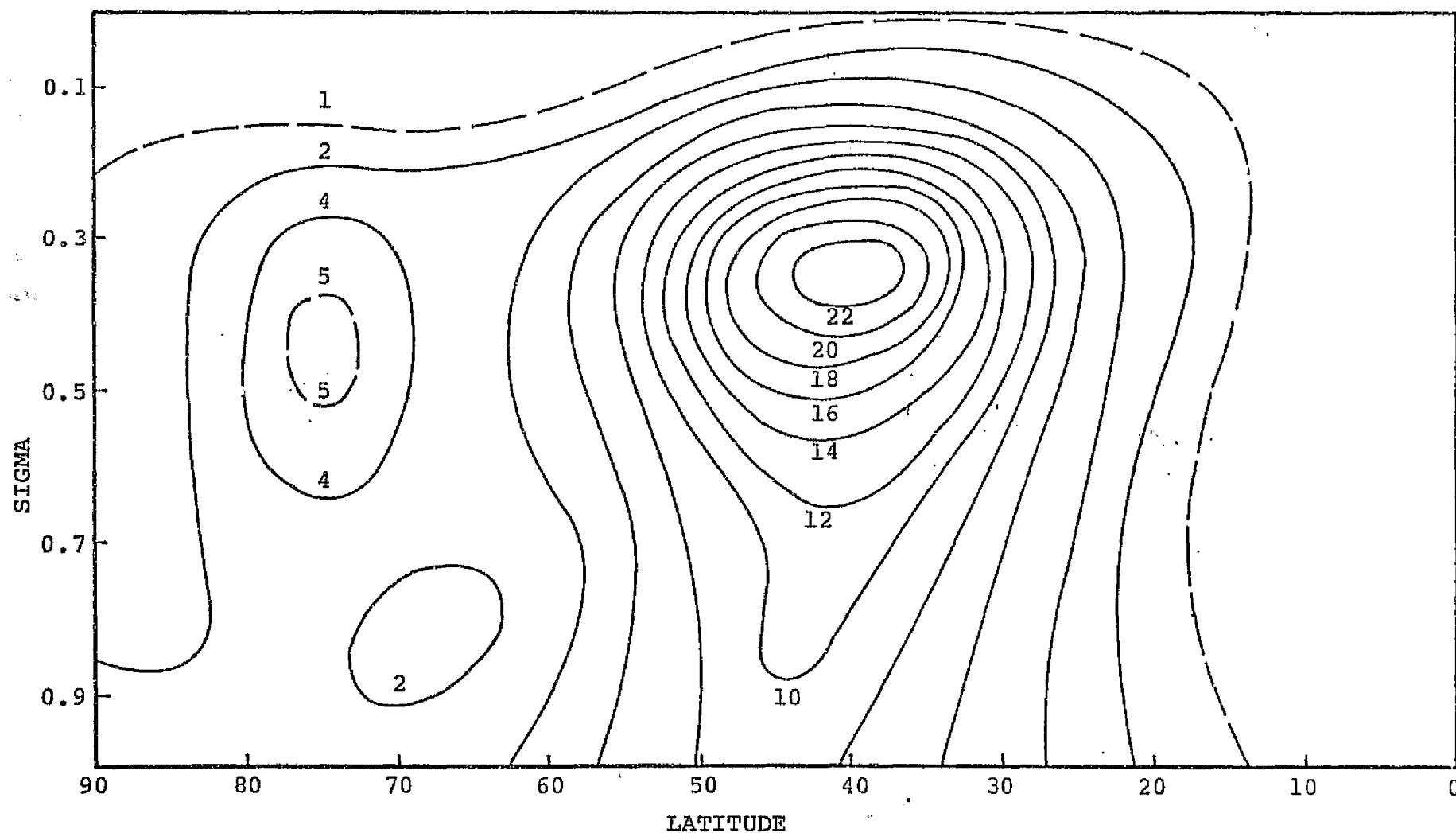


FIGURE VI-4: KINETIC ENERGY ($\times 10$) 24-HOUR FORECAST CROSS-SECTION.
 RUN F22. MODEL PEFHCV. SCENARIO A.

SIGMA=0.9

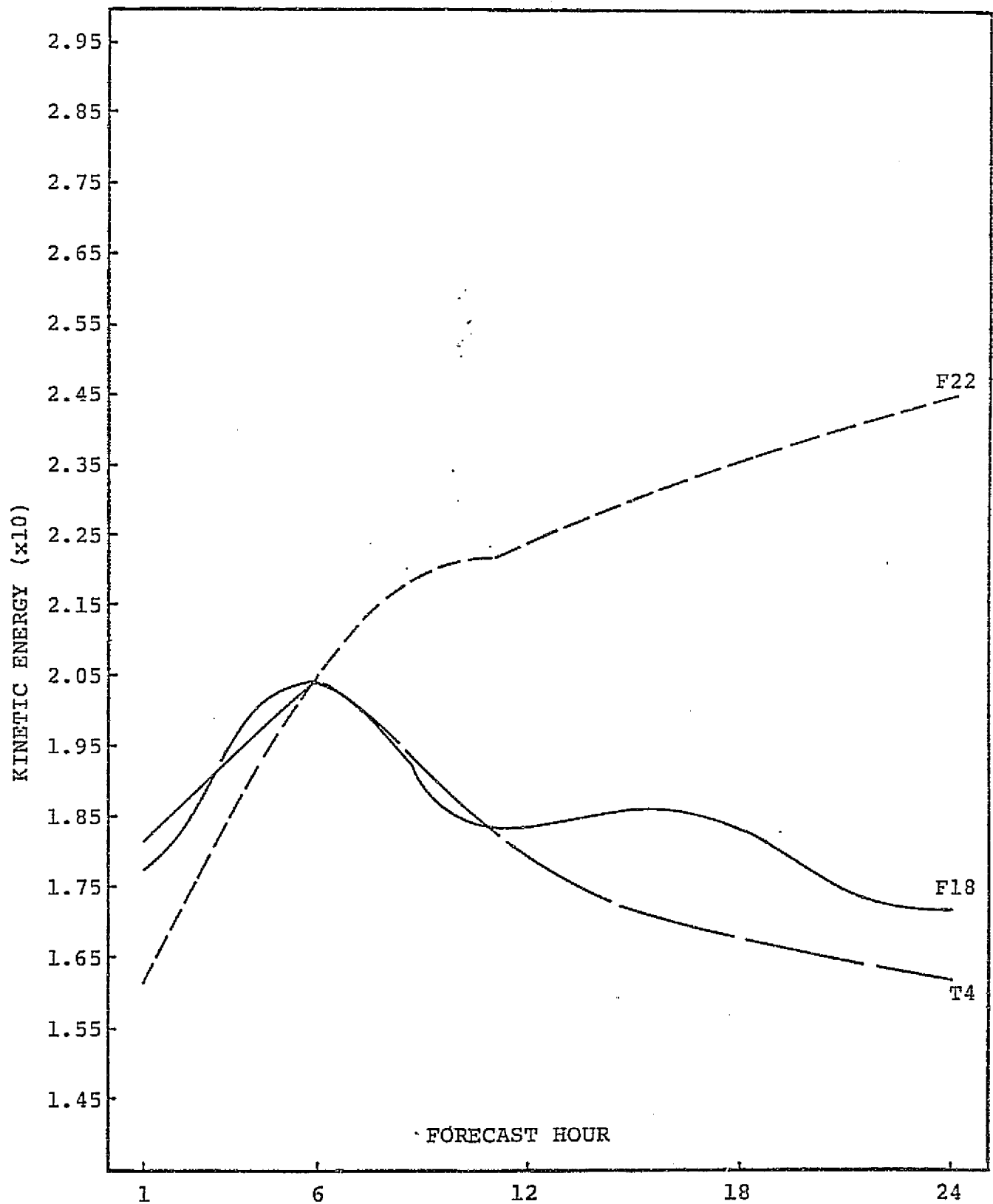


FIGURE VI-5: TIME VARIATION OF KINETIC ENERGY FOR THREE MODEL VERSIONS AT SIGMA=0.9 LEVEL. SCENARIO A.

SIGMA=0.7

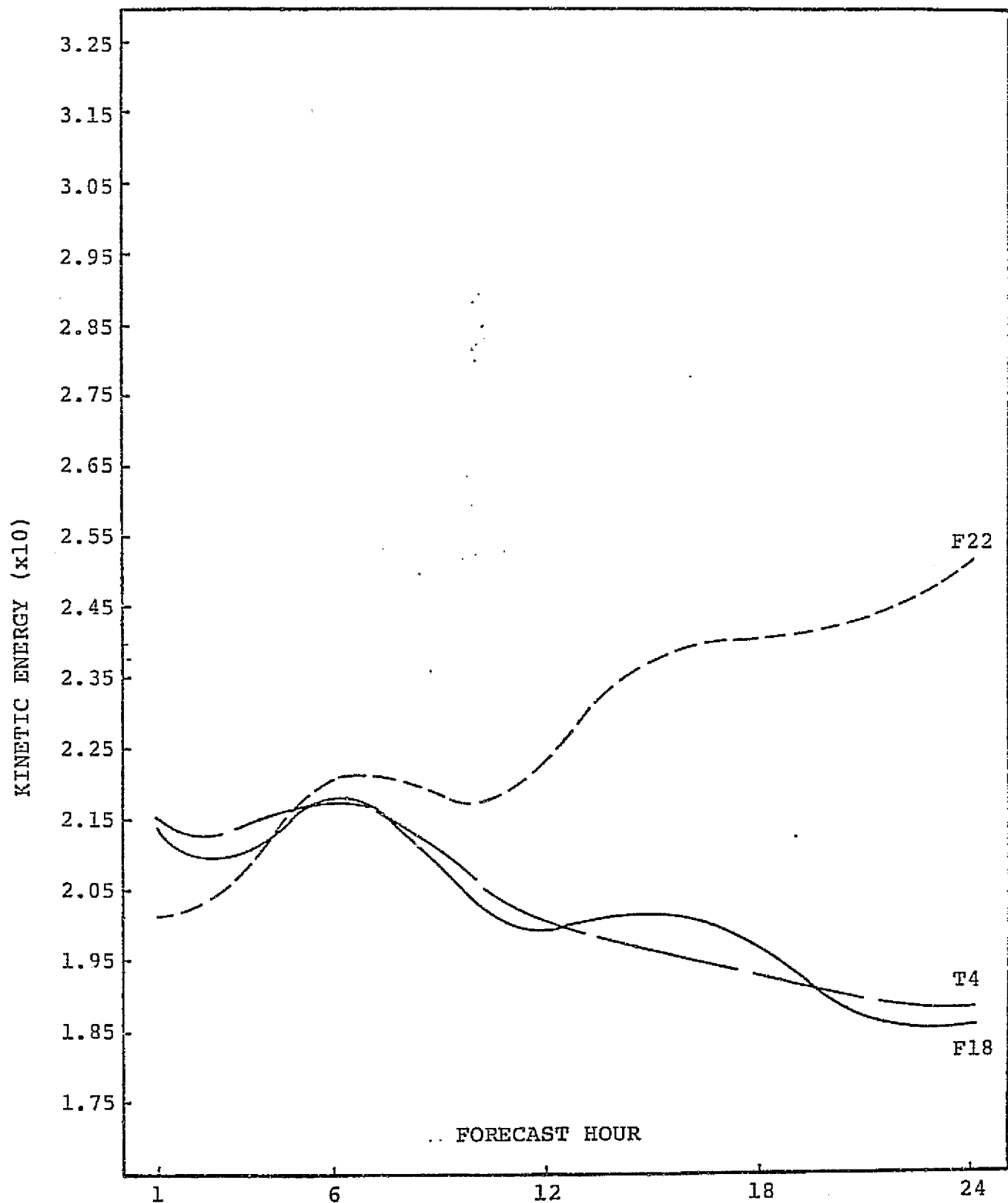


FIGURE VI-6: TIME VARIATION OF KINETIC ENERGY FOR THREE MODEL VERSIONS AT SIGMA=0.7 LEVEL. SCENARIO A.

SIGMA=0.5

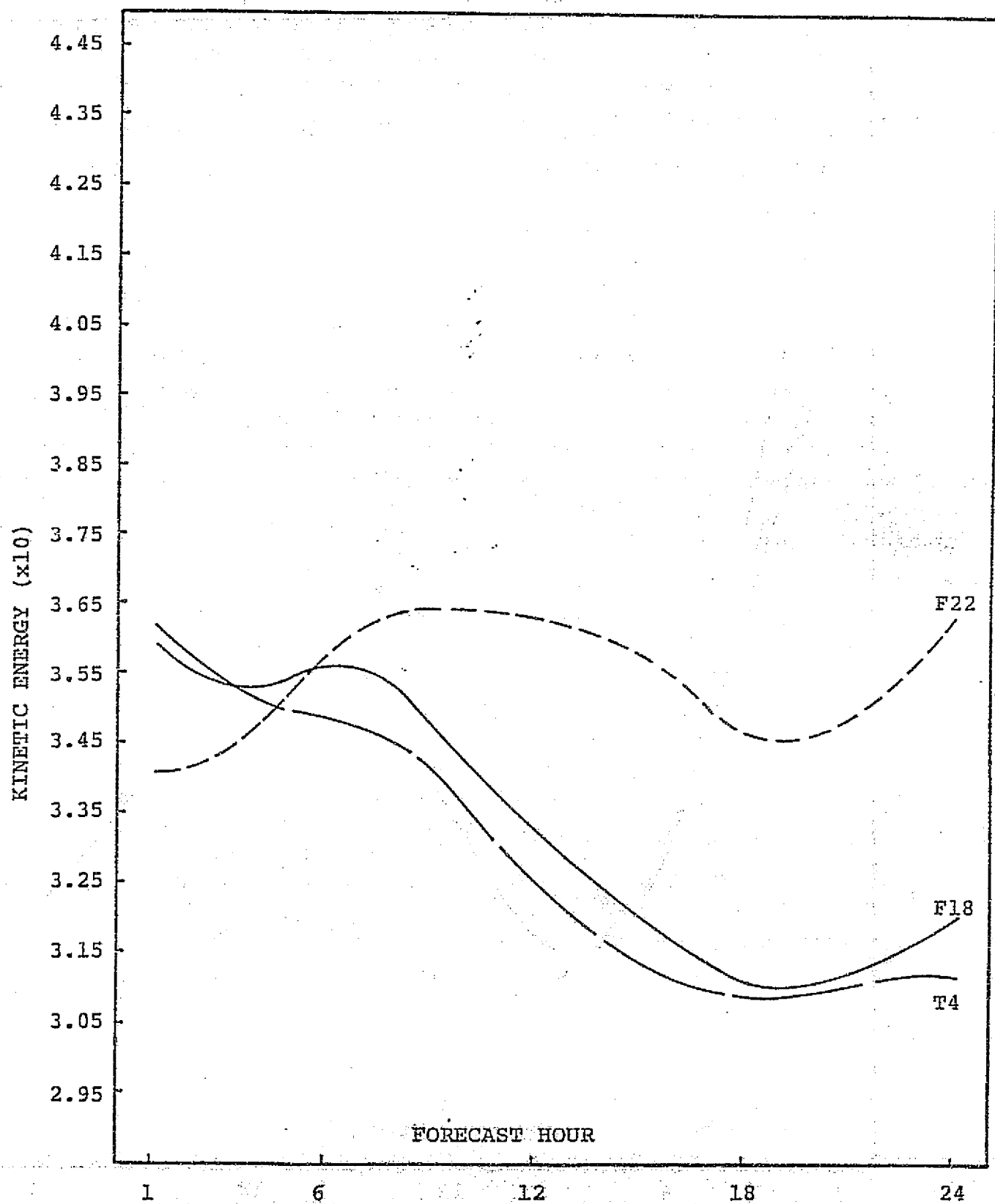


FIGURE VI-7: TIME VARIATION OF KINETIC ENERGY FOR THREE MODEL VERSIONS AT SIGMA=0.5 LEVEL. SCENARIO A.

SIGMA=0.3

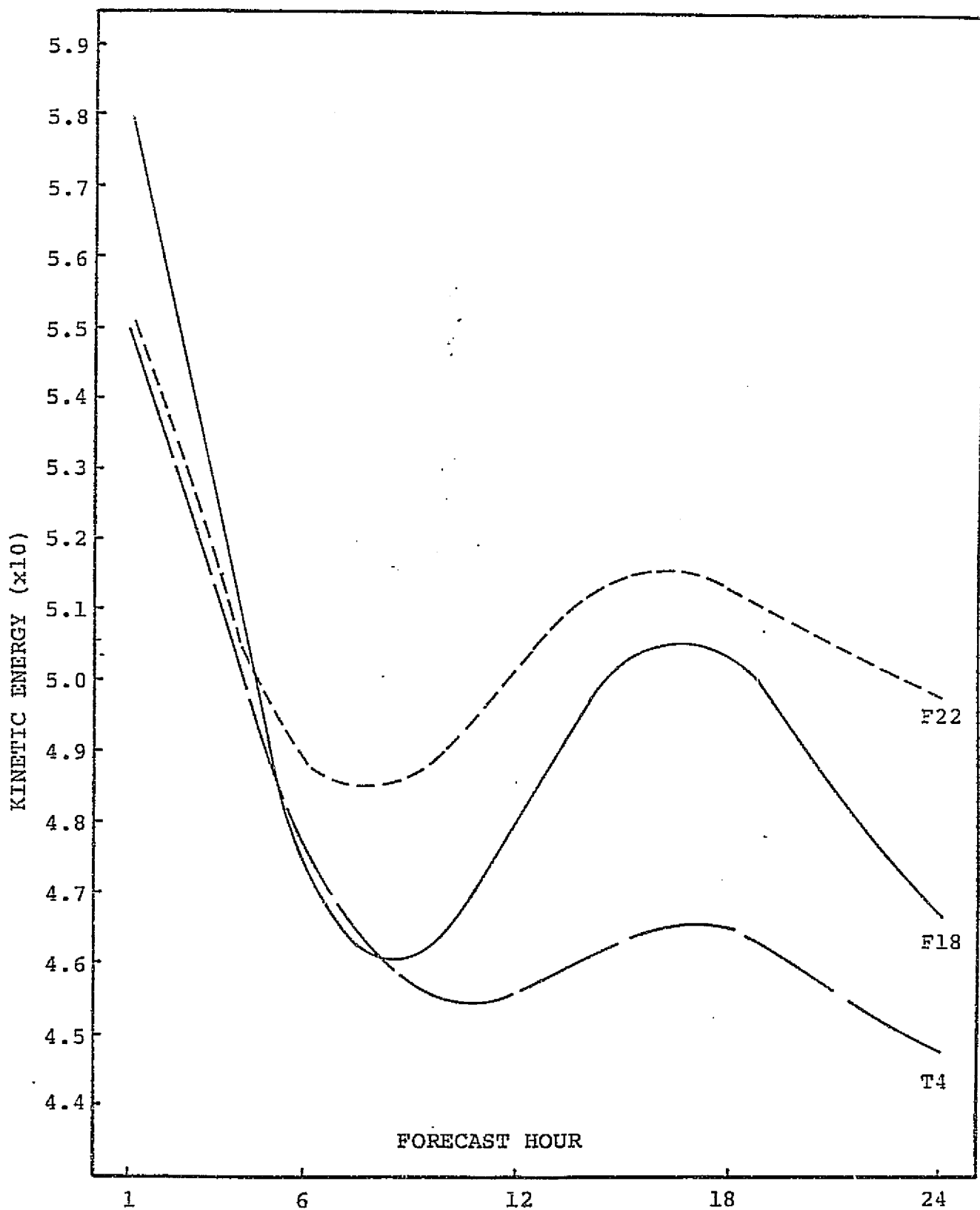


FIGURE VI-8: TIME VARIATION OF KINETIC ENERGY FOR THREE MODEL VERSIONS AT SIGMA=0.3 LEVEL. SCENARIO A.

SIGMA=0.1

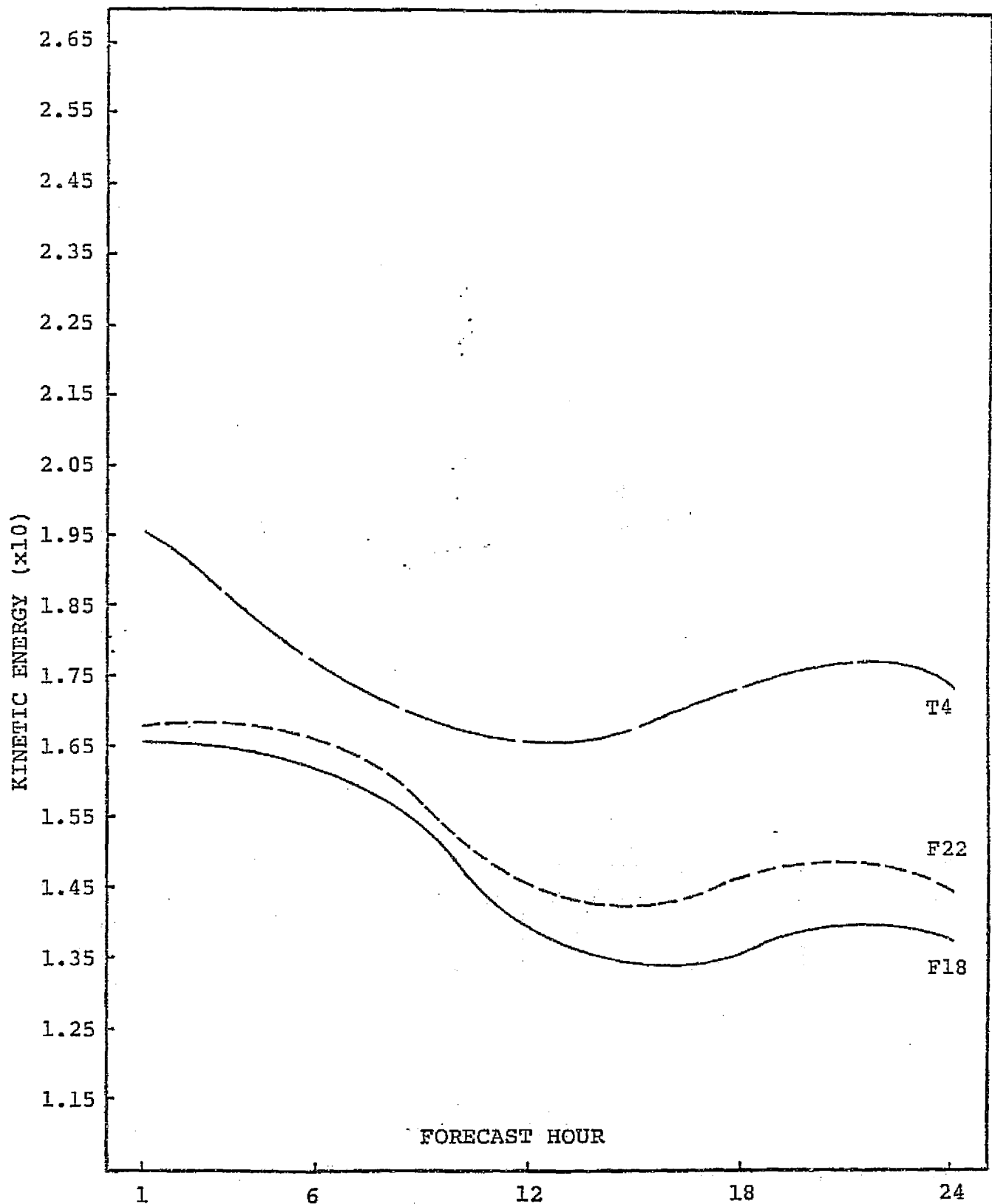


FIGURE VI-9: TIME VARIATION OF KINETIC ENERGY FOR THREE MODEL VERSIONS AT SIGMA=0.1 LEVEL. SCENARIO A.

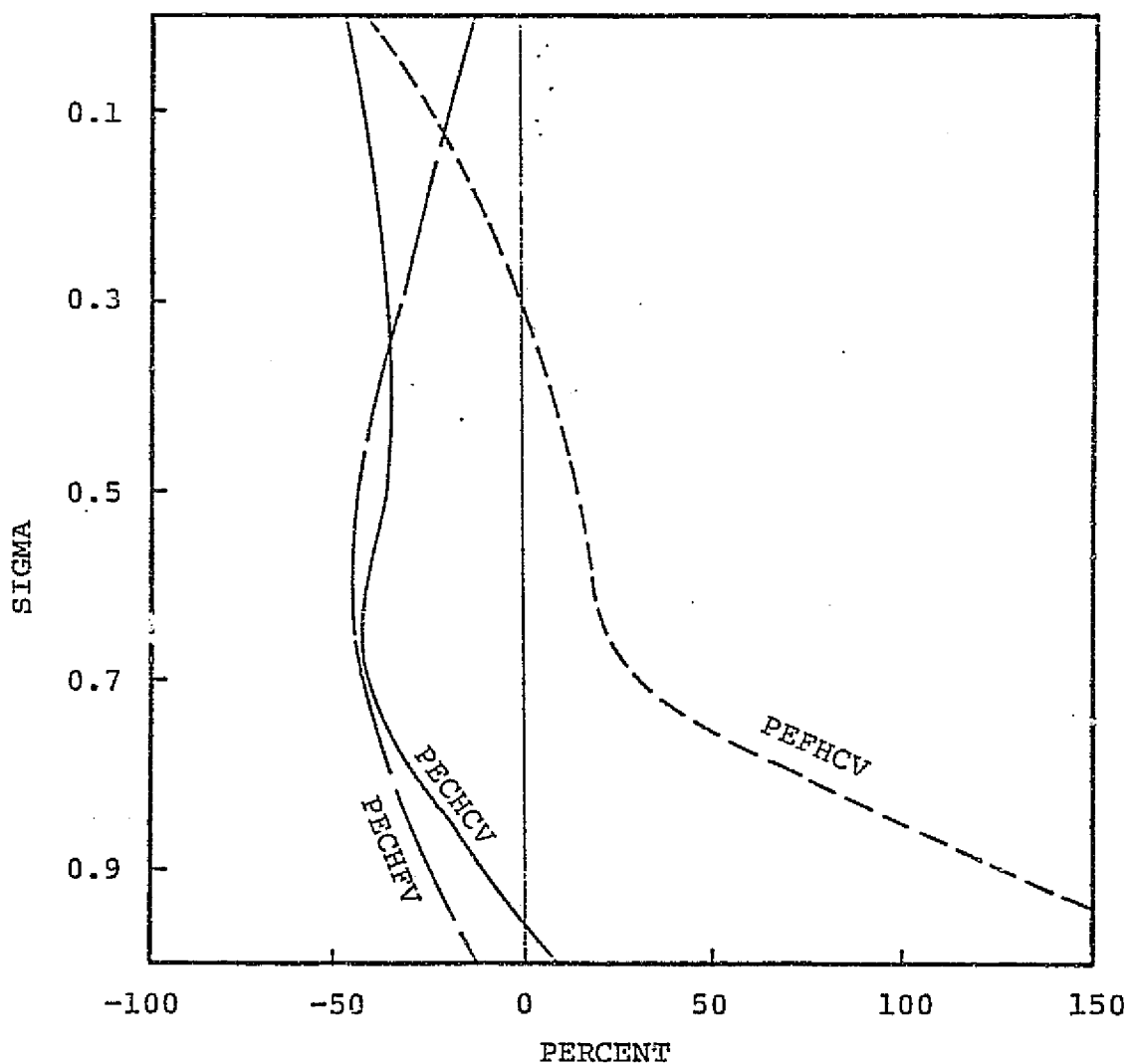


FIGURE VI-10: SQUARE VORTICITY 24-HOUR FORECAST CHANGE (%), BY MODEL VERSION AND LEVEL. SCENARIO A.

SIGMA=0.9

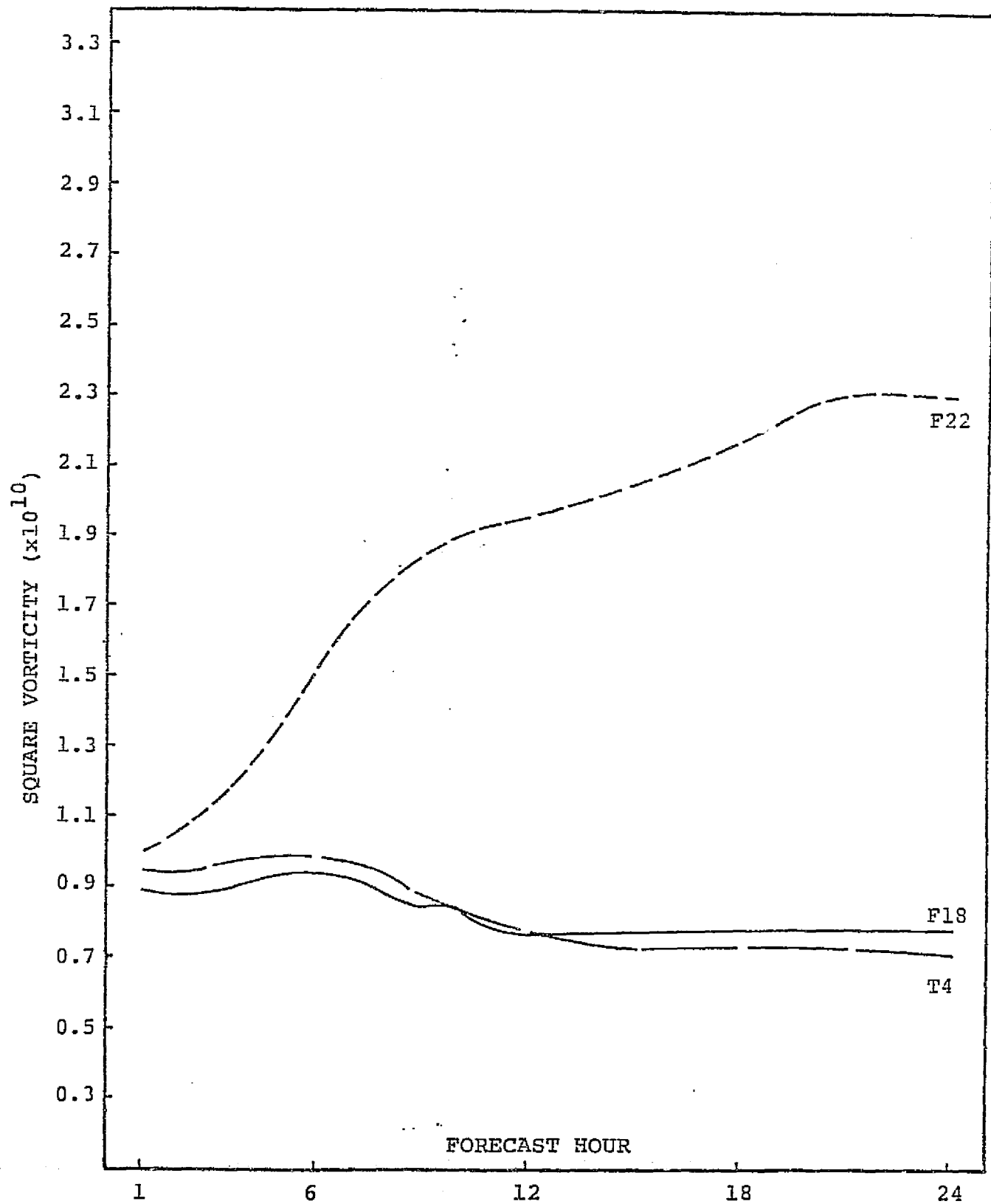


FIGURE VI-11: TIME VARIATION OF SQUARE VORTICITY FOR THREE MODEL VERSIONS AT SIGMA=0.9 LEVEL. SCENARIO A.

SIGMA=0.7

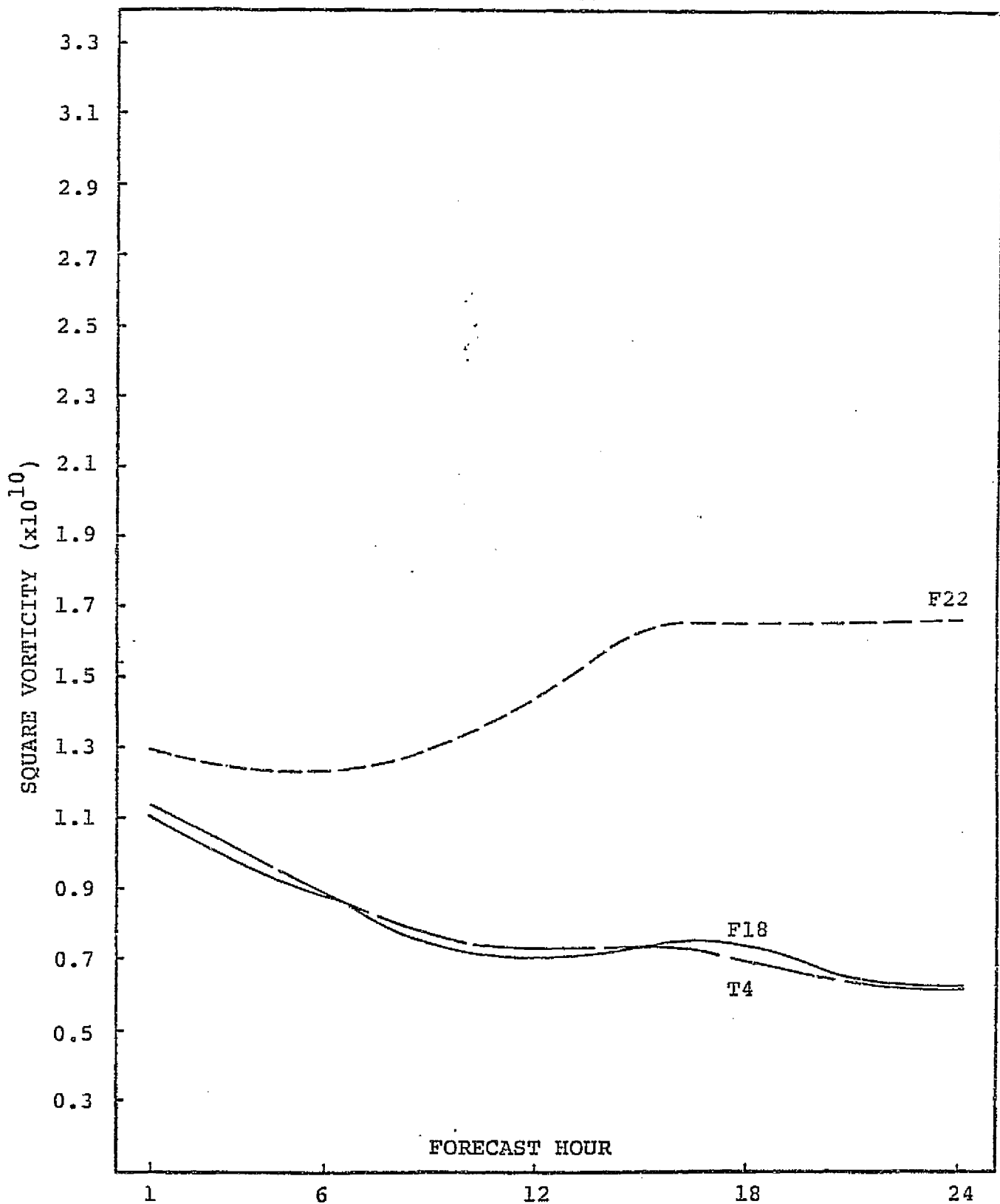


FIGURE VI-12: TIME VARIATION OF SQUARE VORTICITY FOR THREE MODEL VERSIONS AT SIGMA=0.7 LEVEL. SCENARIO A.

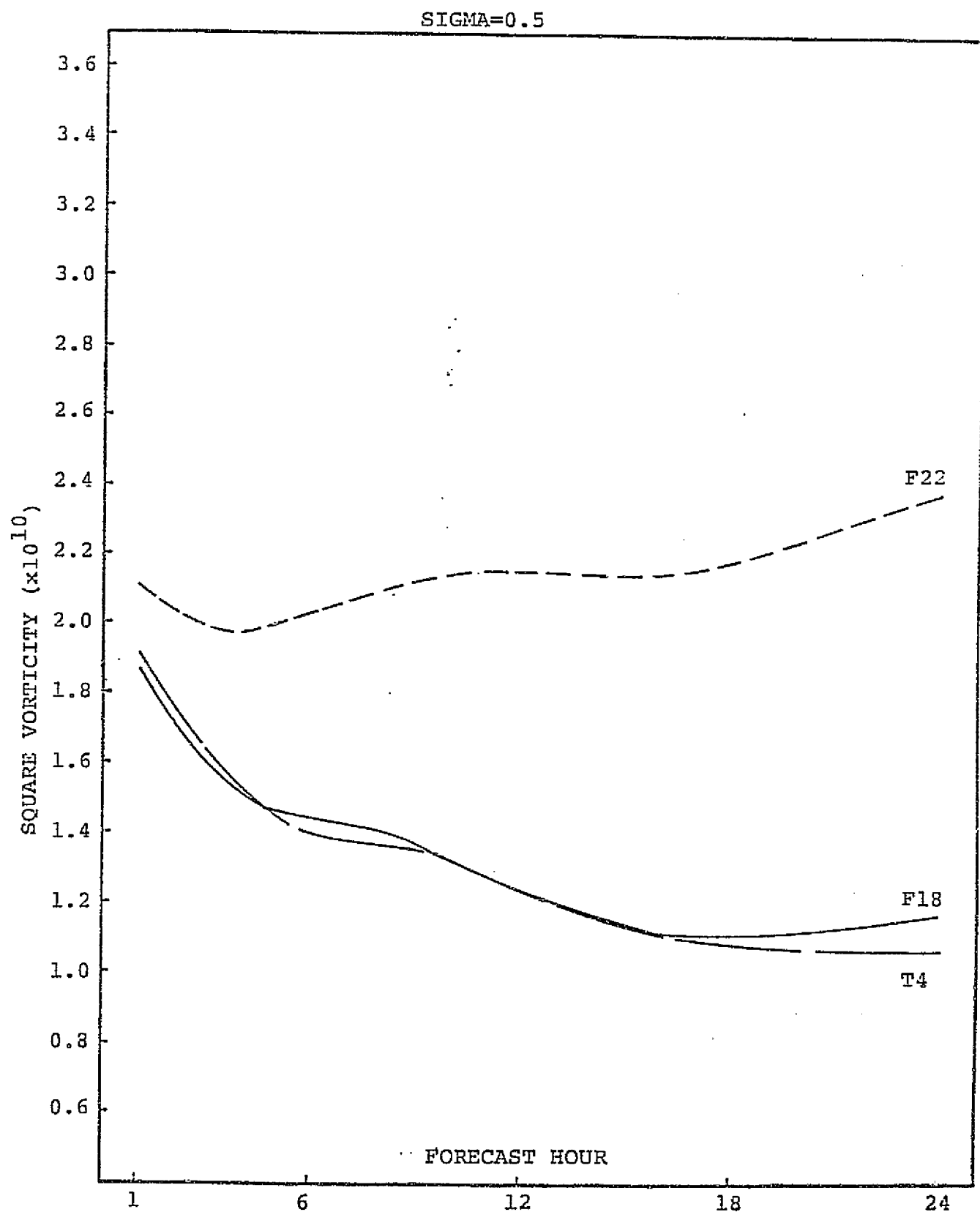


FIGURE VI-13: TIME VARIATION OF SQUARE VORTICITY FOR THREE MODEL VERSIONS AT SIGMA=0.5 LEVEL. SCENARIO A.

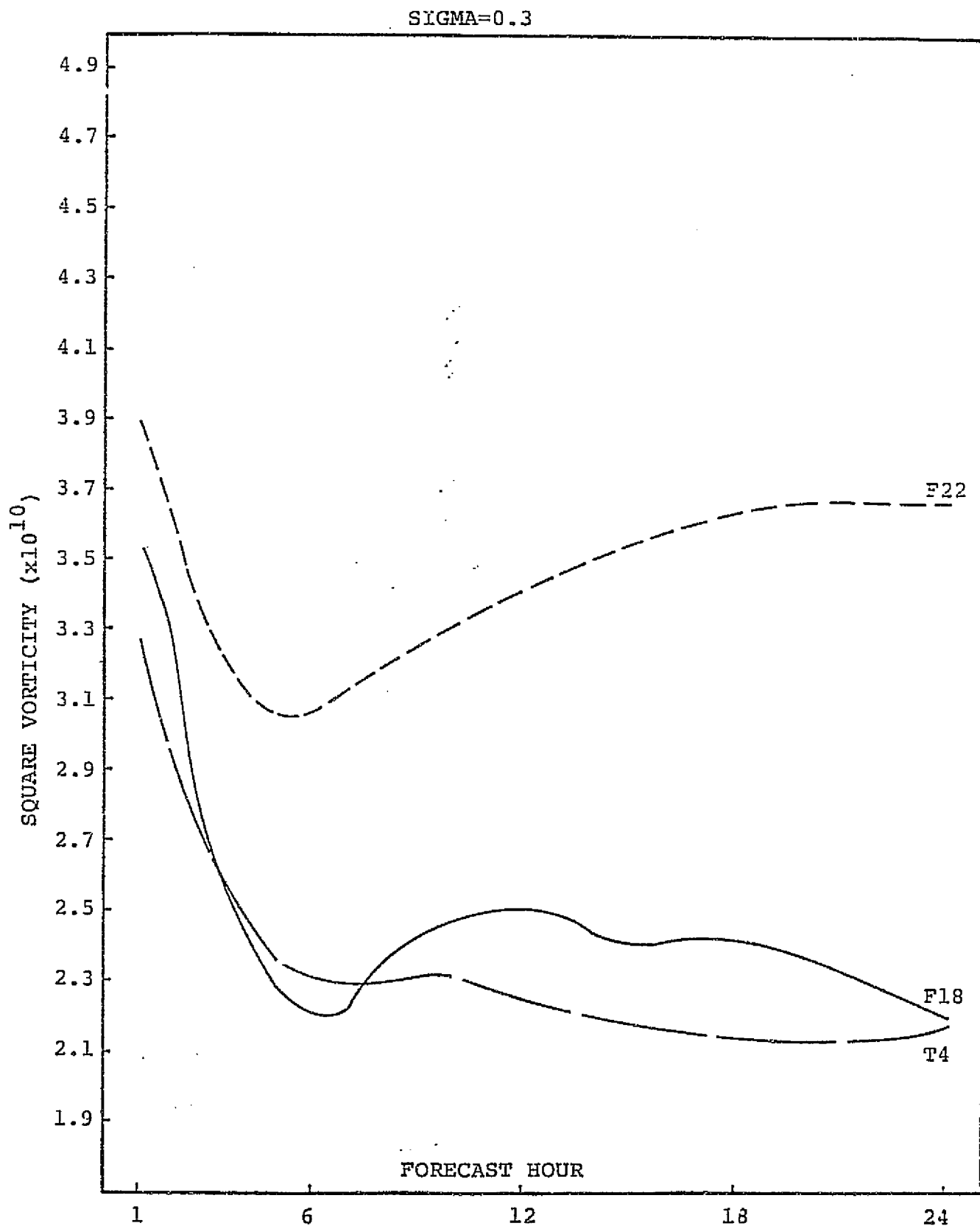


FIGURE VI-14: TIME VARIATION OF SQUARE VORTICITY FOR THREE MODEL VERSIONS AT SIGMA=0.3 LEVEL. SCENARIO A.

SIGMA=0.1

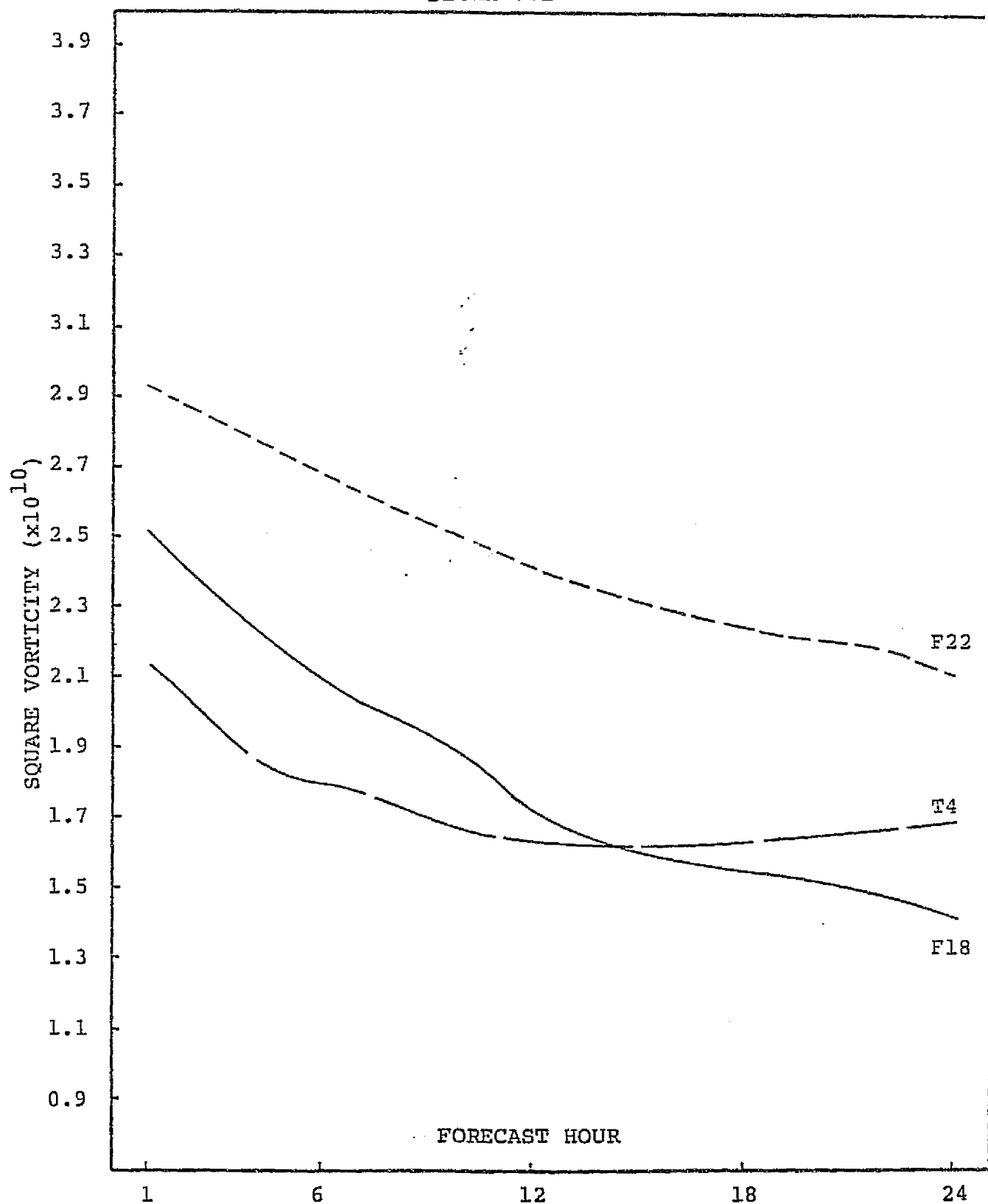


FIGURE VI-15: TIME VARIATION OF SQUARE VORTICITY FOR THREE MODEL VERSIONS AT SIGMA=0.1 LEVEL. SCENARIO A.

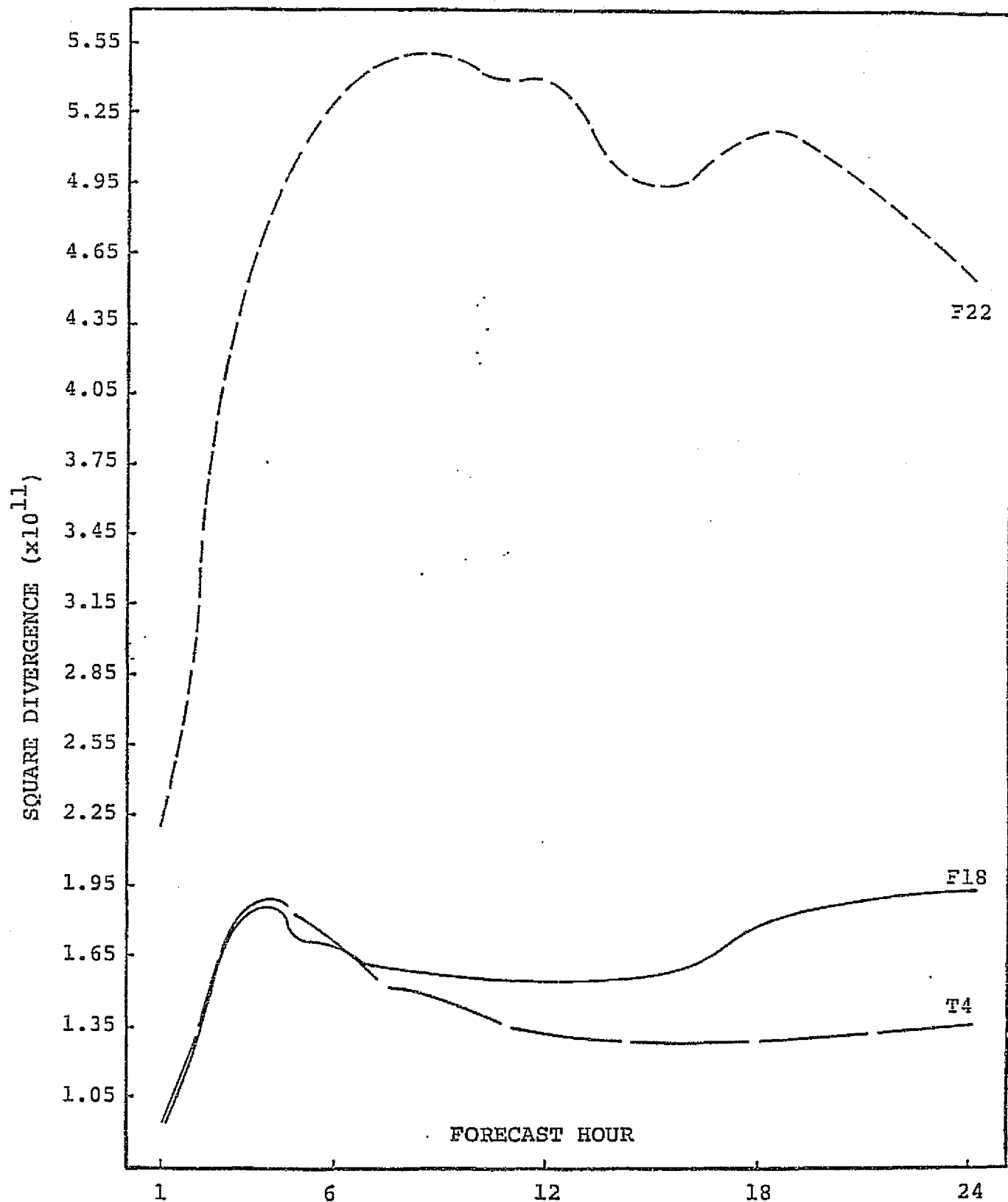


FIGURE VI-16: TIME VARIATION OF SQUARE DIVERGENCE FOR THREE MODEL VERSIONS AT SIGMA=0.9 LEVEL. SCENARIO A

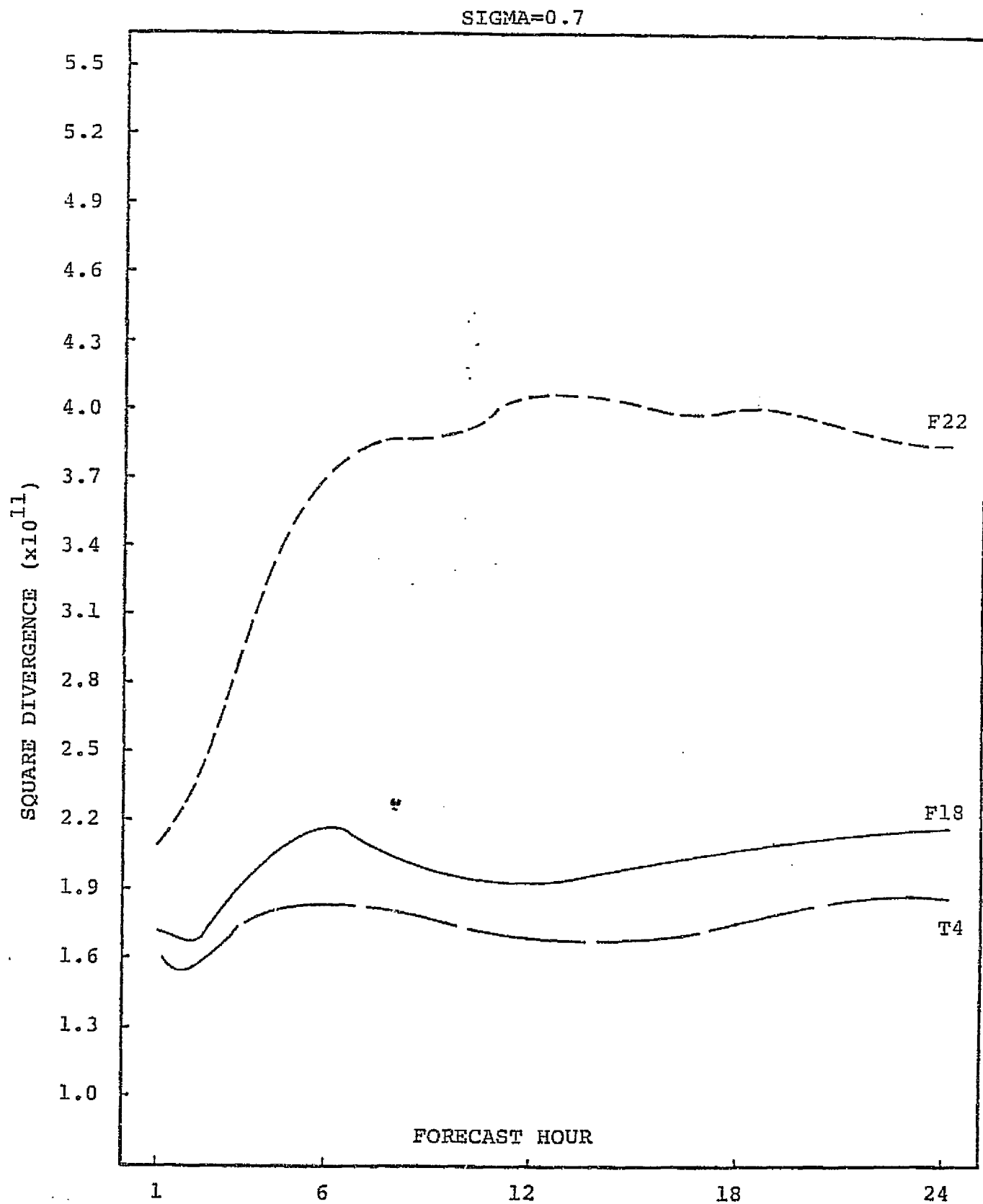


FIGURE VI-17: TIME VARIATION OF SQUARE DIVERGENCE FOR THREE MODEL VERSIONS AT SIGMA=0.7 LEVEL. SCENARIO A.

SIGMA=0.5

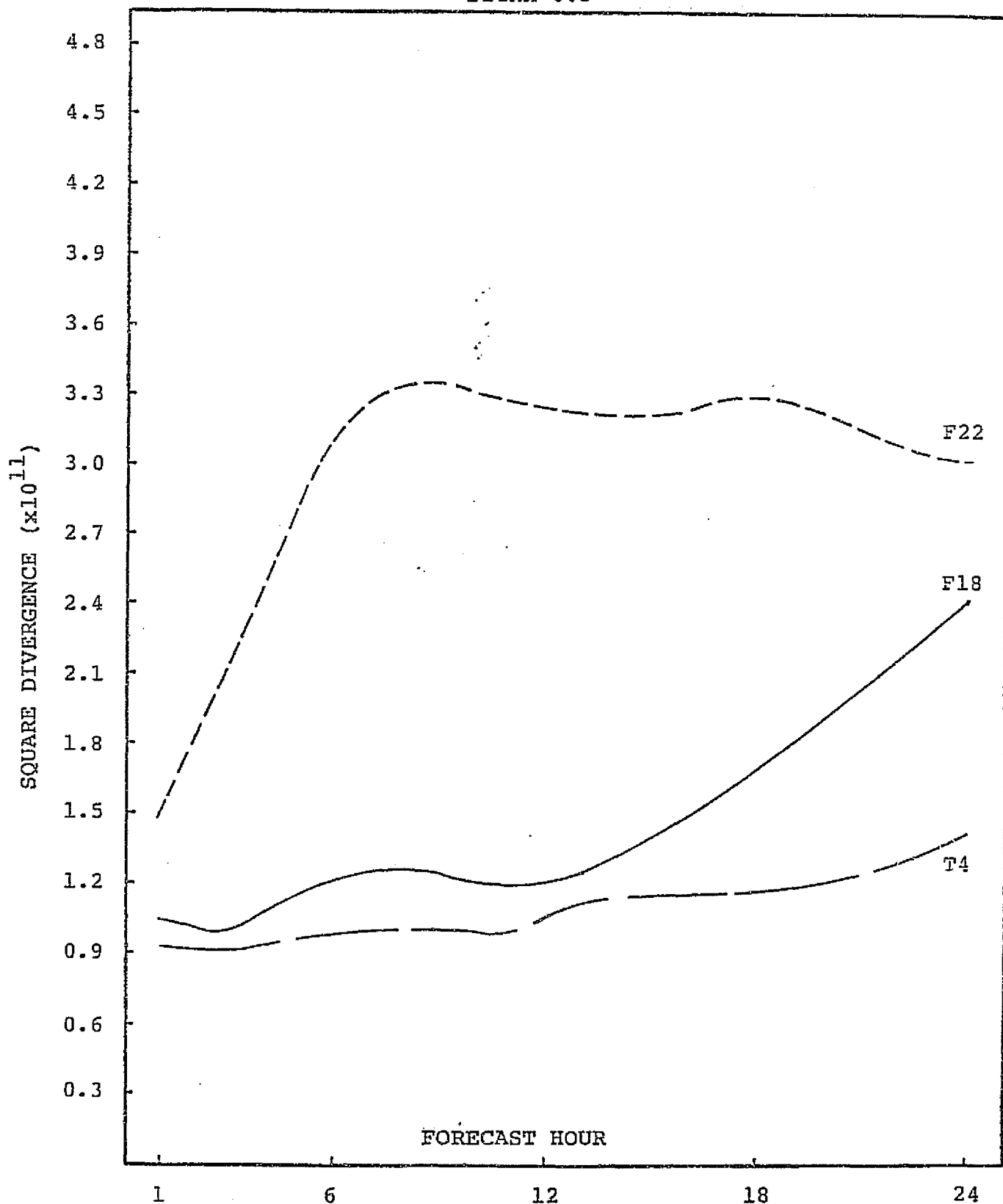


FIGURE VI-18: TIME VARIATION OF SQUARE DIVERGENCE FOR THREE MODEL VERSIONS AT SIGMA=0.5 LEVEL. SCENARIO A.

ORIGINAL PAGE IS
OF POOR QUALITY

SIGMA=0.3

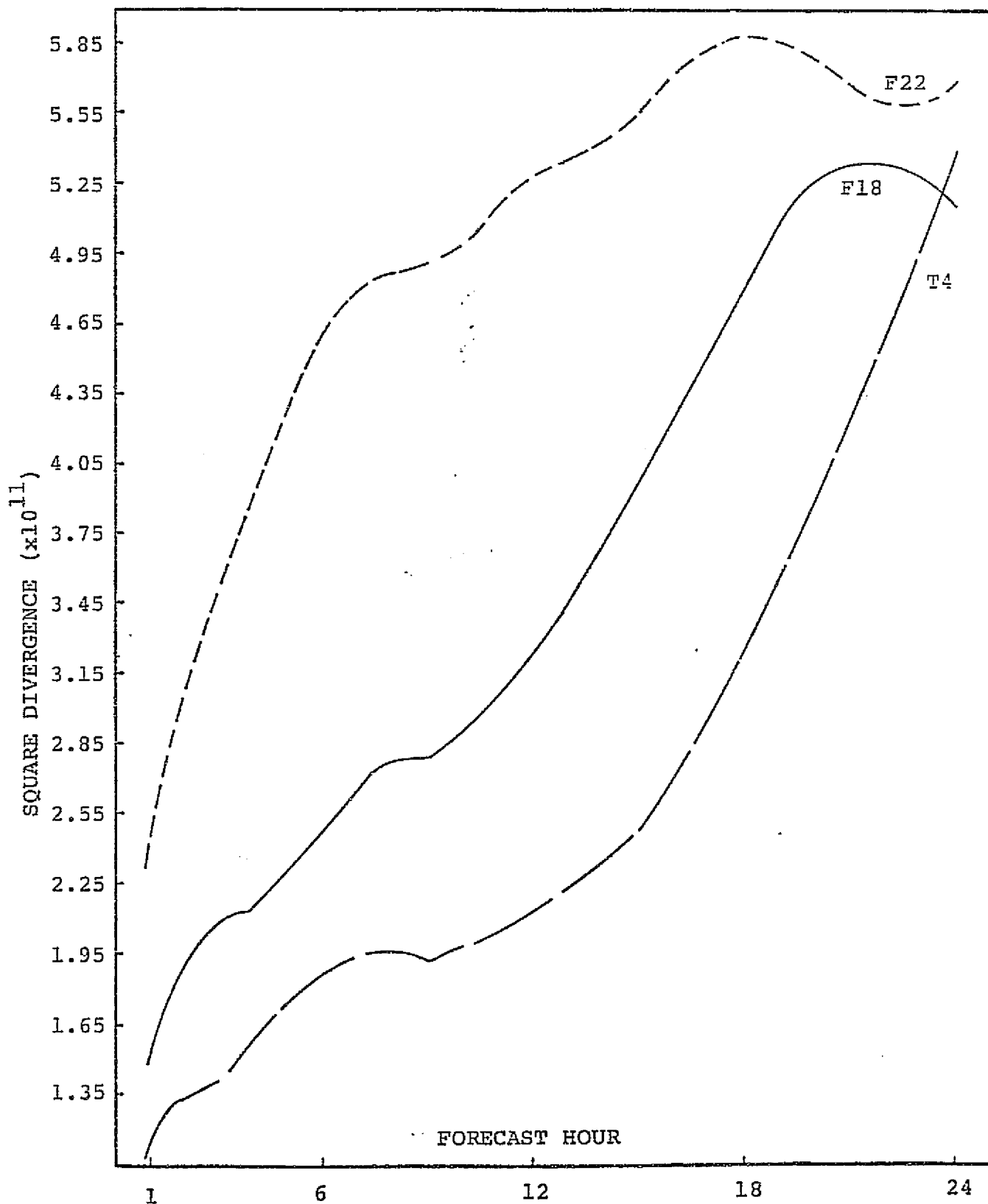


FIGURE VI-19: TIME VARIATION OF SQUARE DIVERGENCE FOR THREE MODEL VERSIONS AT SIGMA=0.3 LEVEL. SCENARIO A.

ORIGINAL PAGE IS
OF POOR QUALITY.

SIGMA=0.1

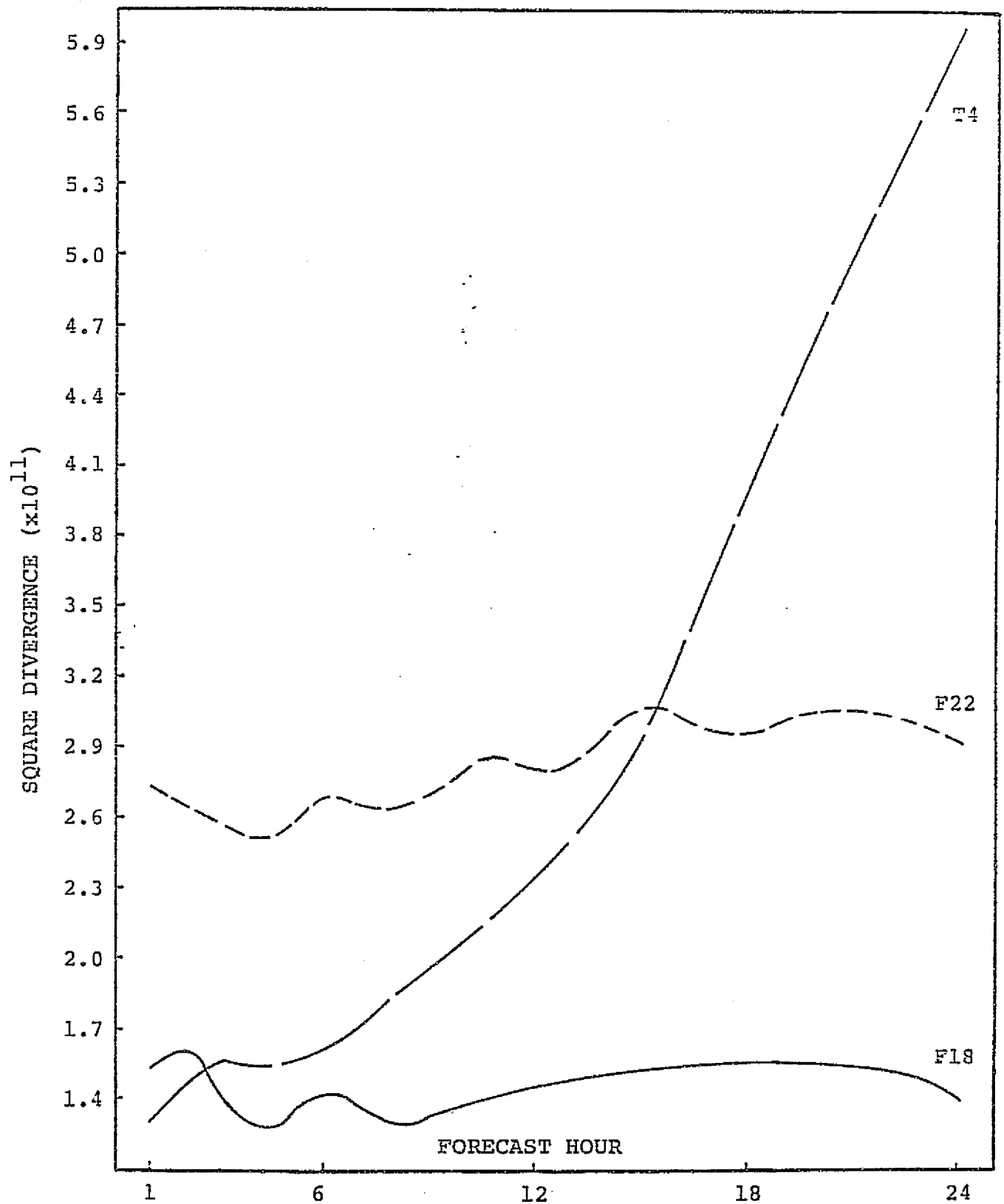


FIGURE VI-20: TIME VARIATION OF SQUARE DIVERGENCE FOR THREE MODEL VERSIONS AT SIGMA=0.1 LEVEL. SCENARIO A.

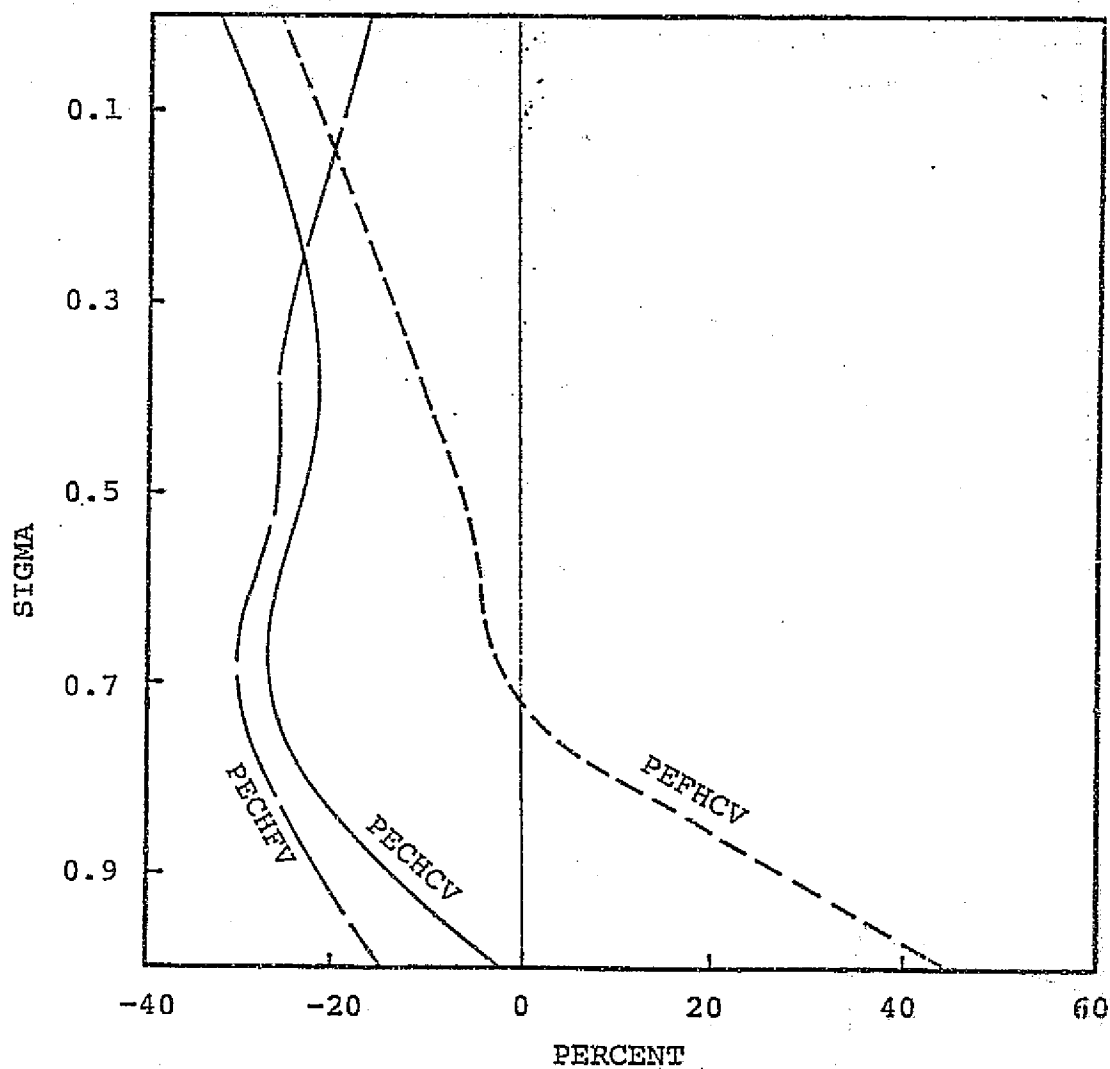


FIGURE VI-21: KINETIC ENERGY 24-HOUR FORECAST CHANGE (%), BY MODEL VERSION AND LEVEL. SCENARIO B.

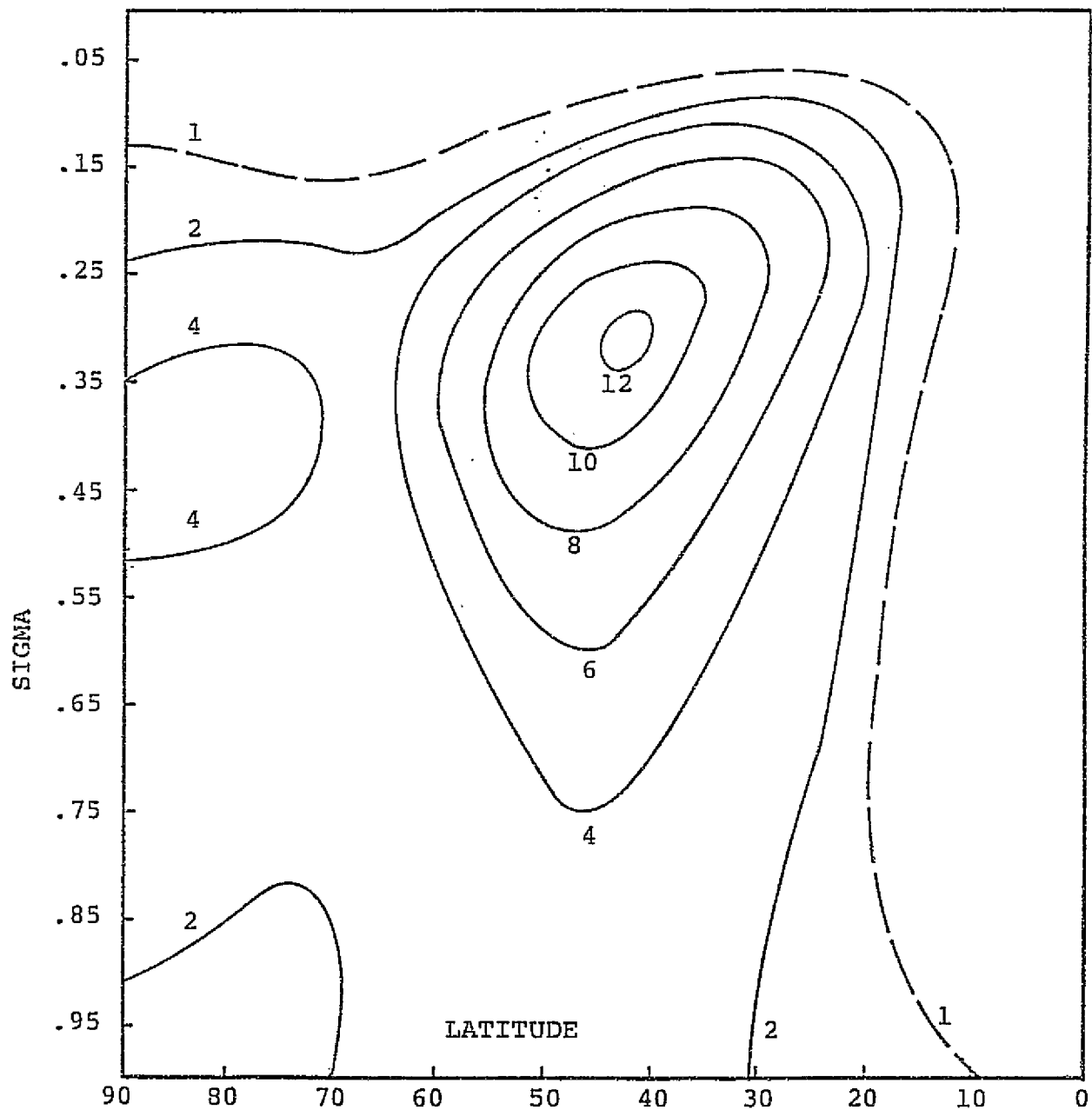


FIGURE VI-22: KINETIC ENERGY ($\times 10$) 24-HOUR FORECAST
CROSS-SECTION. RUN T5. MODEL PECHFV.
SCENARIO B.

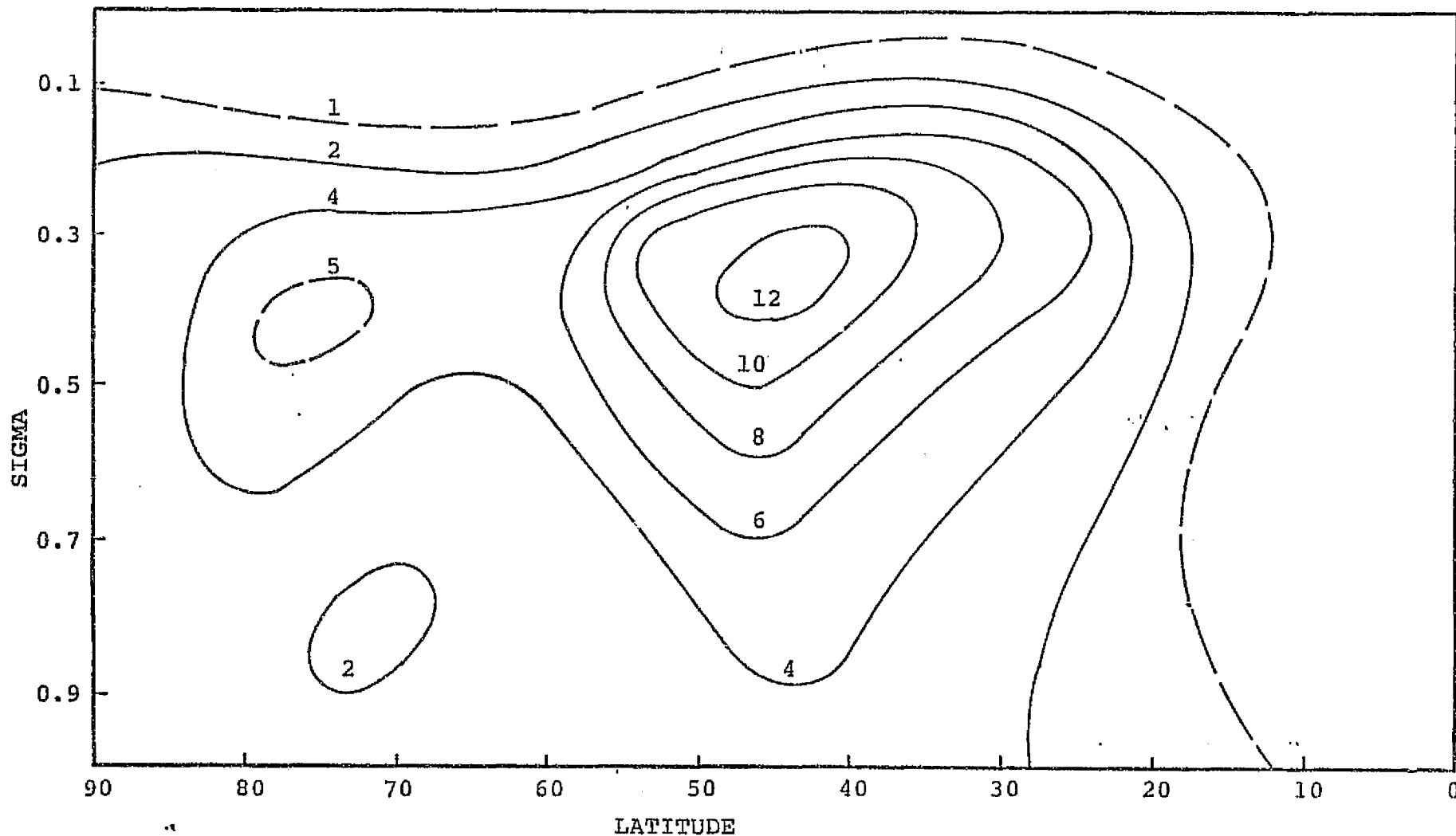


FIGURE VI-23: KINETIC ENERGY ($\times 10$) 24-HOUR FORECAST CROSS-SECTION.
 RUN F19. MODEL PECHCV. SCENARIO B.

ORIGINAL PAGE IS
 OF POOR QUALITY

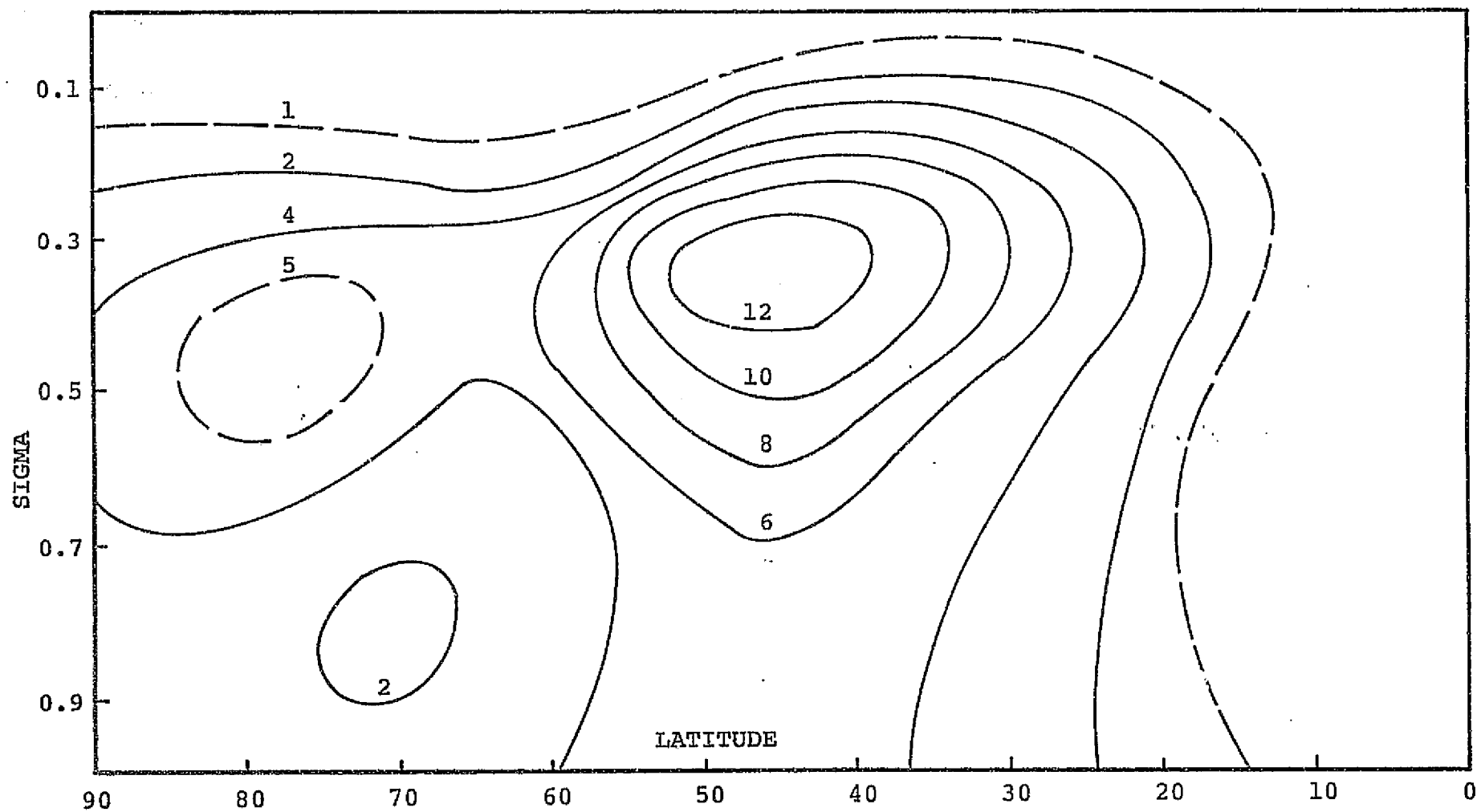


FIGURE VI-24: KINETIC ENERGY ($\times 10$) 24-HOUR FORECAST CROSS-SECTION.
RUN F24. MODEL PEFHCV. SCENARIO B.

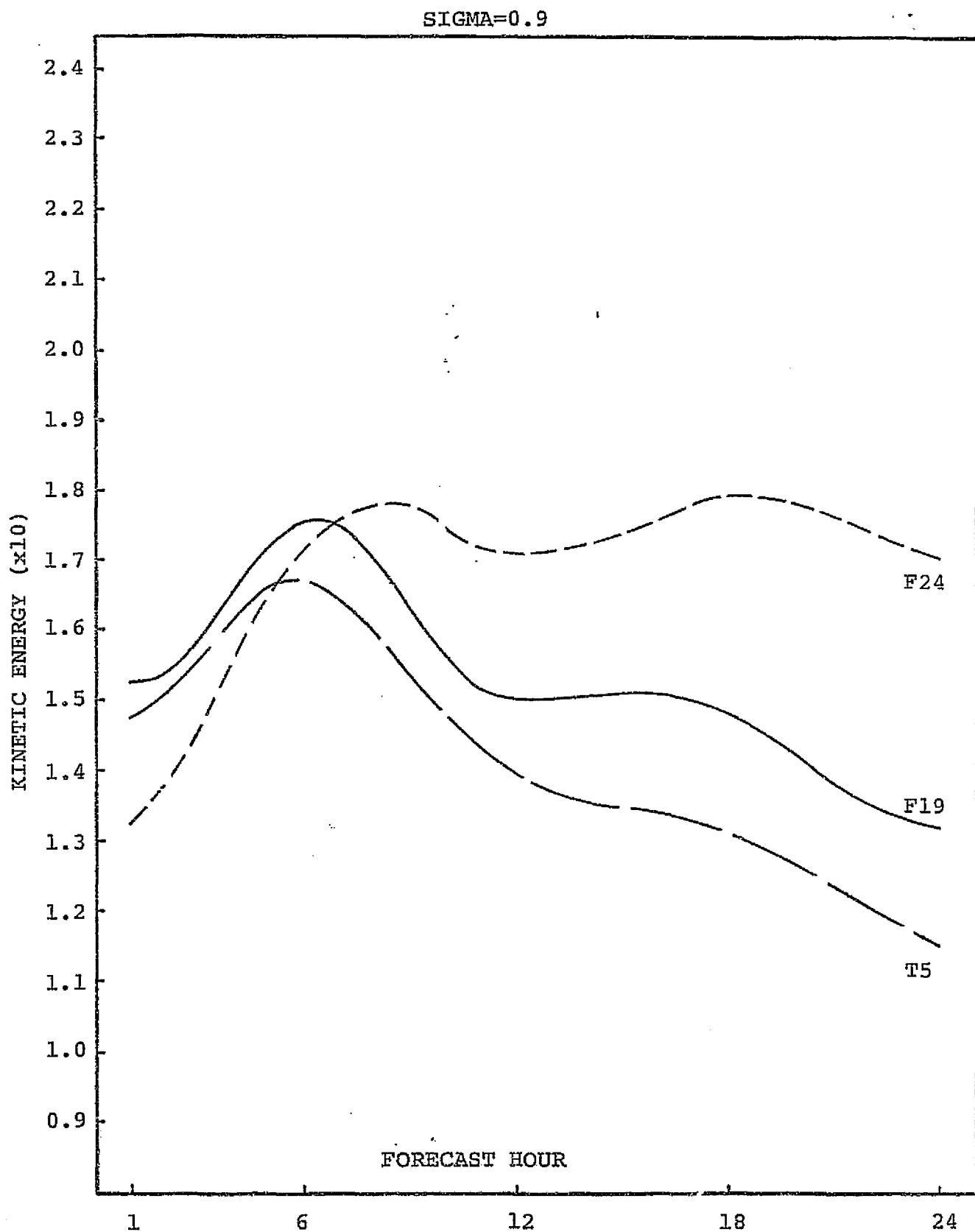


FIGURE VI-25: TIME VARIATION OF KINETIC ENERGY FOR THREE MODEL VERSIONS AT SIGMA=0.9 LEVEL. SCENARIO B.

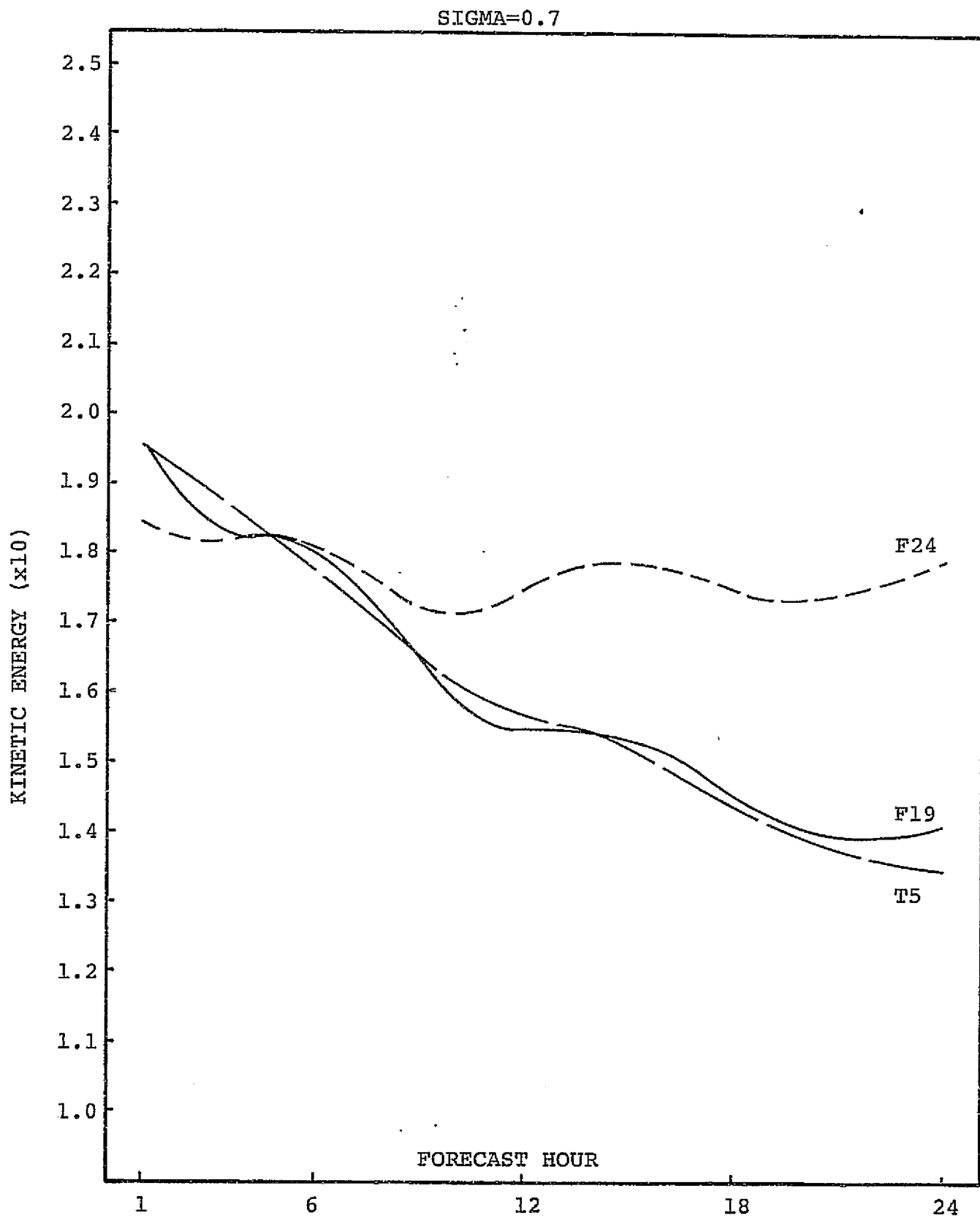


FIGURE VI-26: TIME VARIATION OF KINETIC ENERGY FOR THREE MODEL VERSIONS AT SIGMA=0.7 LEVEL. SCENARIO B.

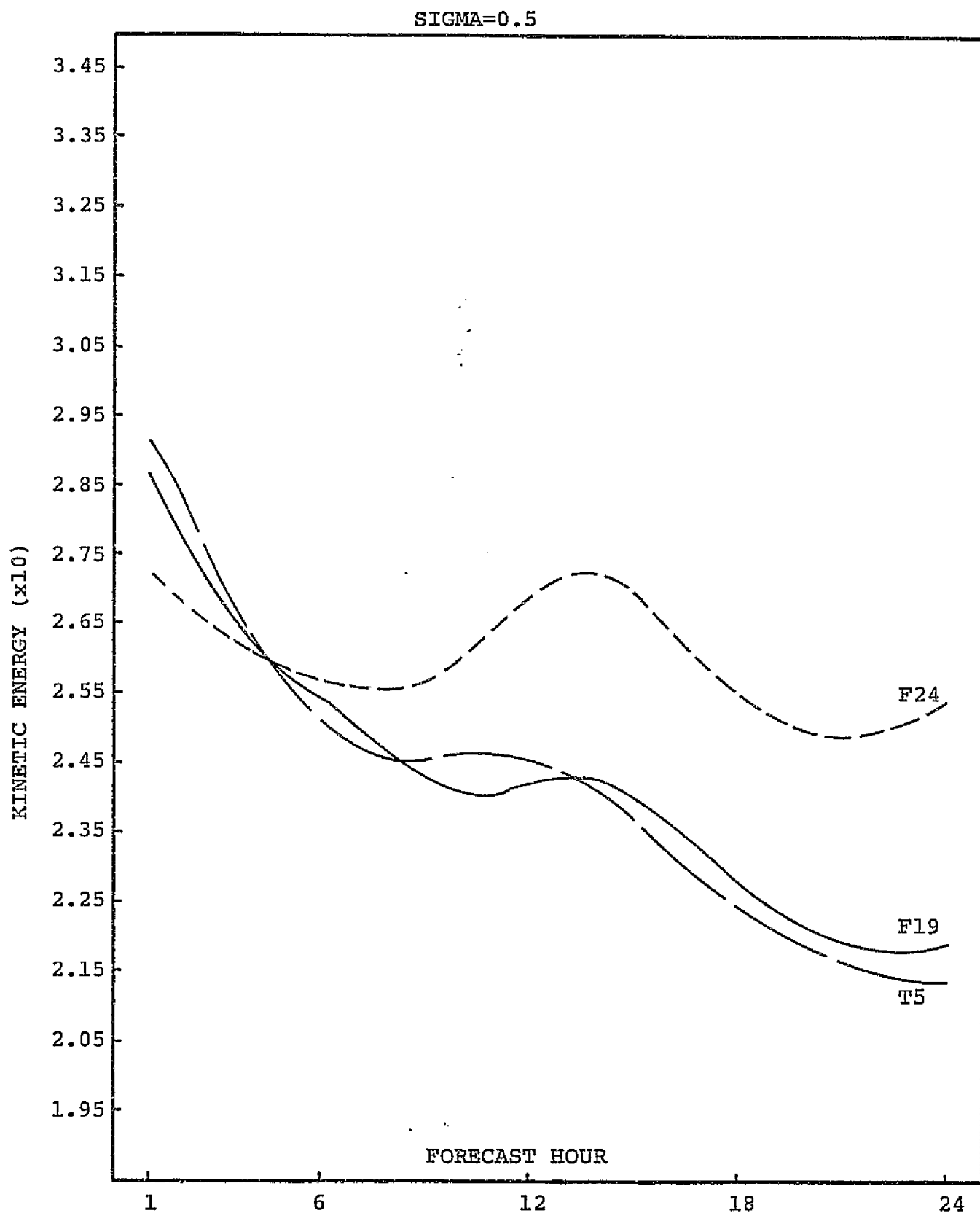


FIGURE VI-27: TIME VARIATION OF KINETIC ENERGY FOR THREE MODEL VERSIONS AT SIGMA=0.5 LEVEL. SCENARIO B.

SIGMA=0.3

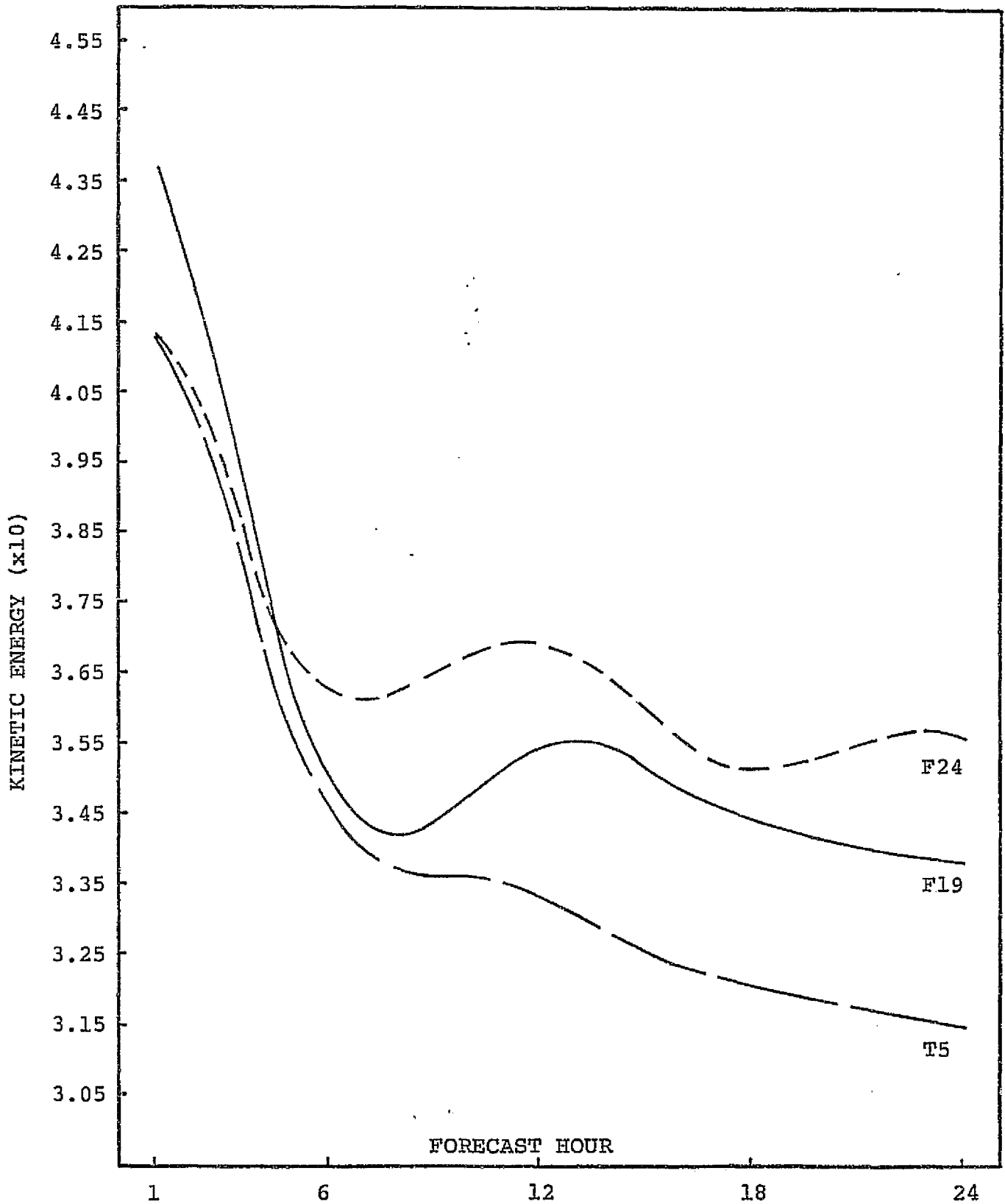


FIGURE VI-28: TIME VARIATION OF KINETIC ENERGY FOR THREE MODEL VERSIONS AT SIGMA=0.3 LEVEL. SCENARIO B.

SIGMA=0.1

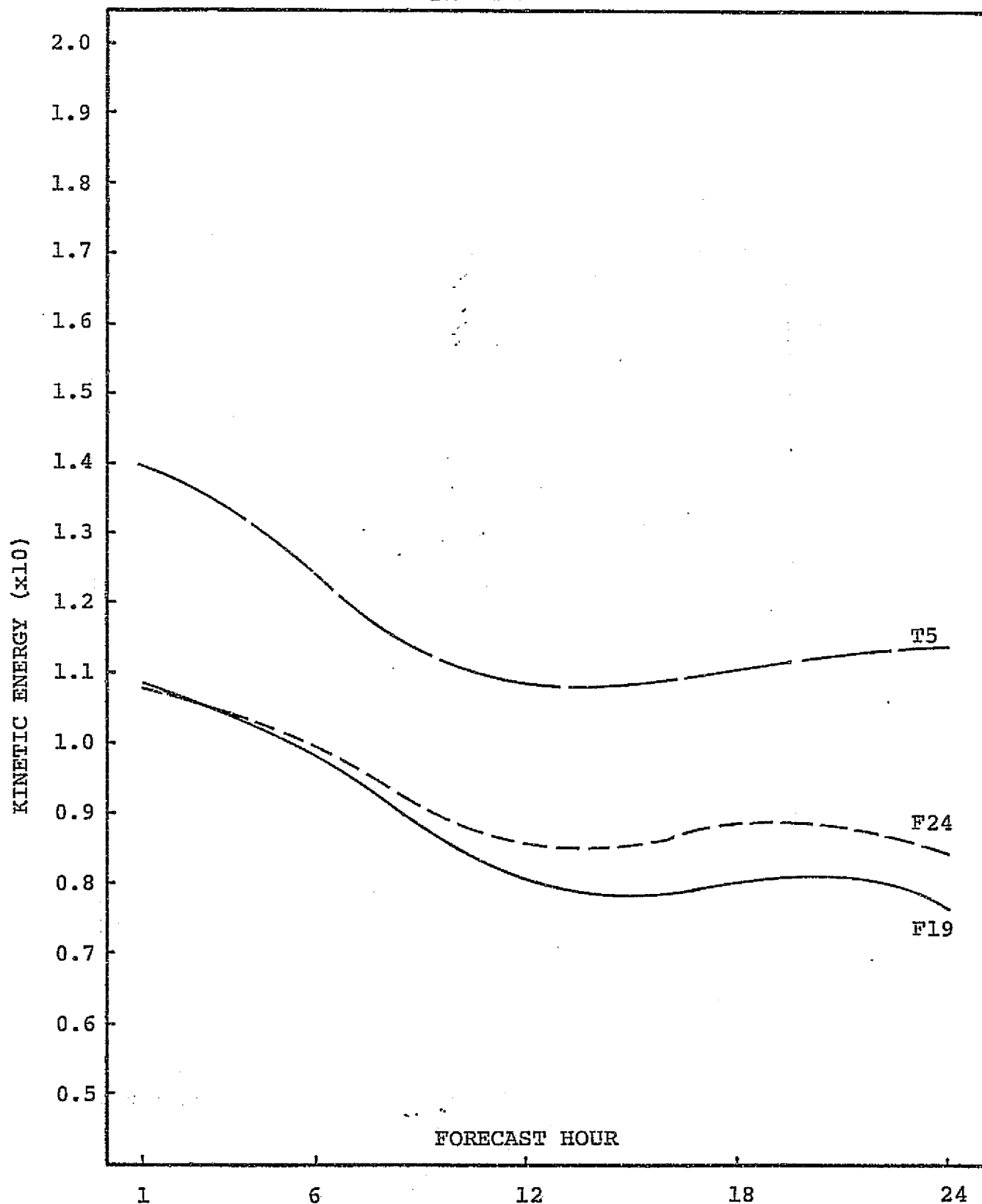


FIGURE VI-29: TIME VARIATION OF KINETIC ENERGY FOR THREE MODEL VERSIONS AT SIGMA=0.1 LEVEL. SCENARIO B.

ORIGINAL PAGE IS
OF POOR QUALITY

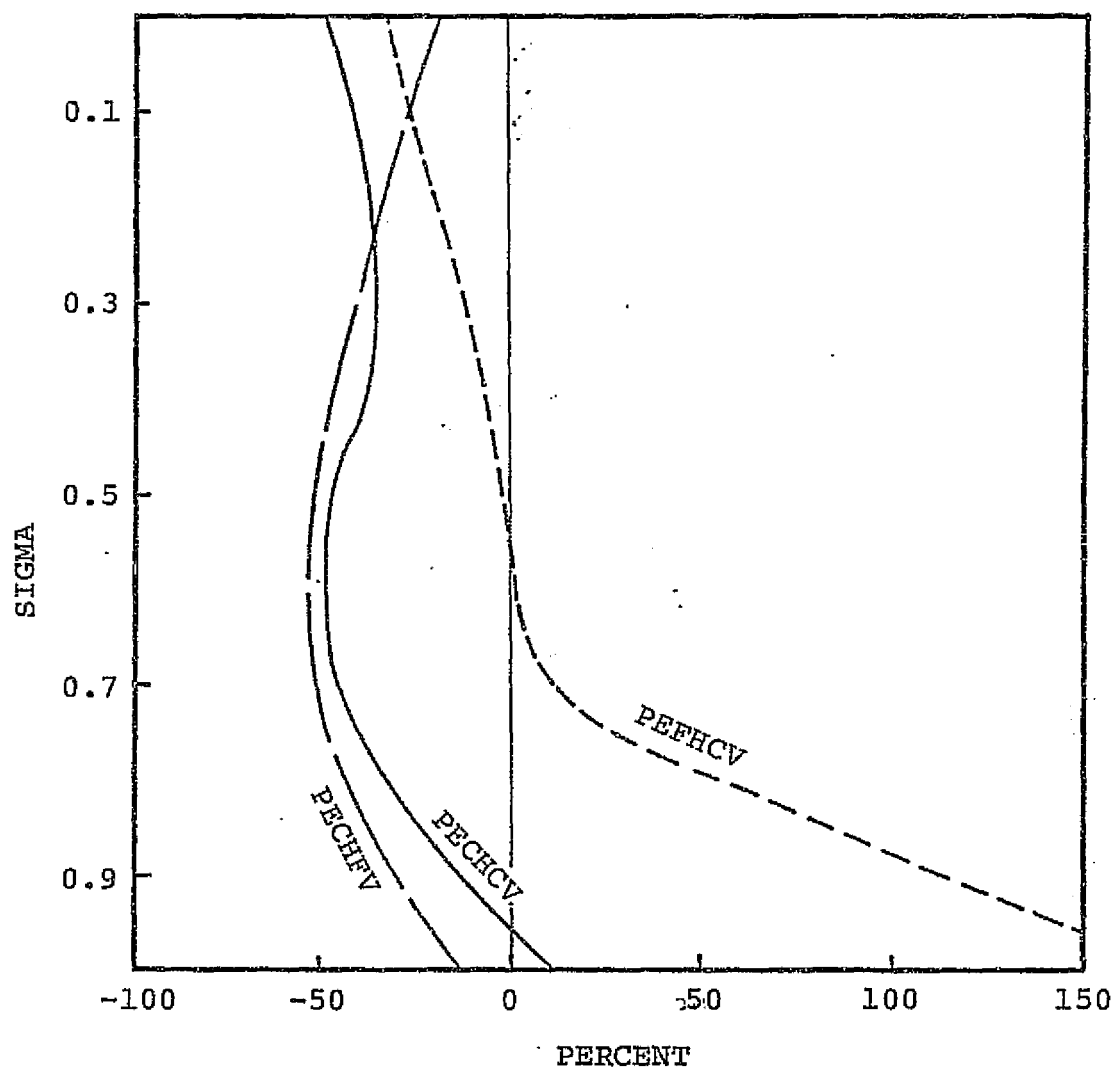


FIGURE VI-30: SQUARE VORTICITY 24-HOUR FORECAST CHANGE (%), BY MODEL VERSION AND LEVEL. SCENARIO B.

SIGMA=0.9

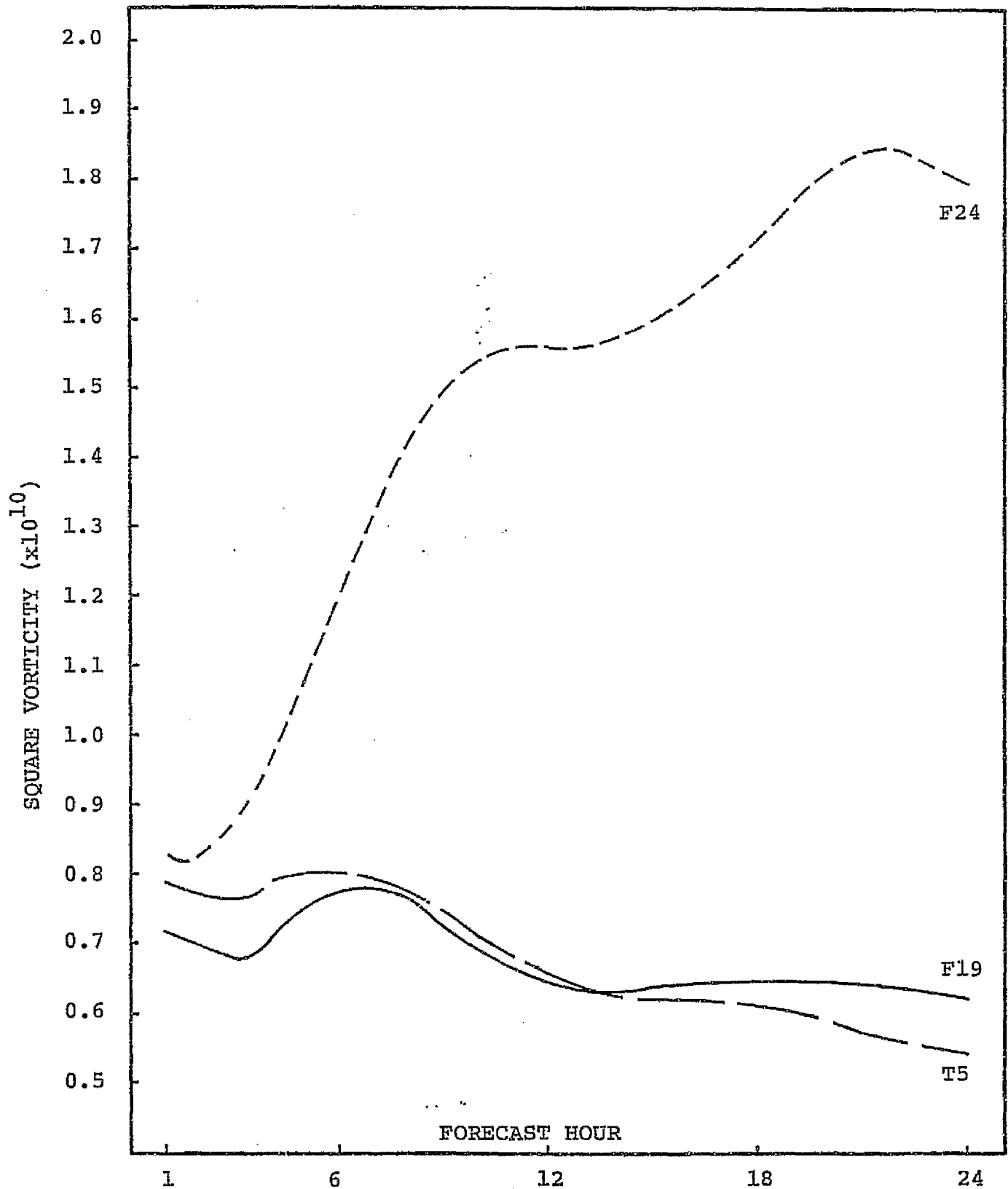


FIGURE VI-31: TIME VARIATION OF SQUARE VORTICITY FOR THREE MODEL VERSIONS AT SIGMA=0.9 LEVEL. SCENARIO B.

SIGMA=0.7

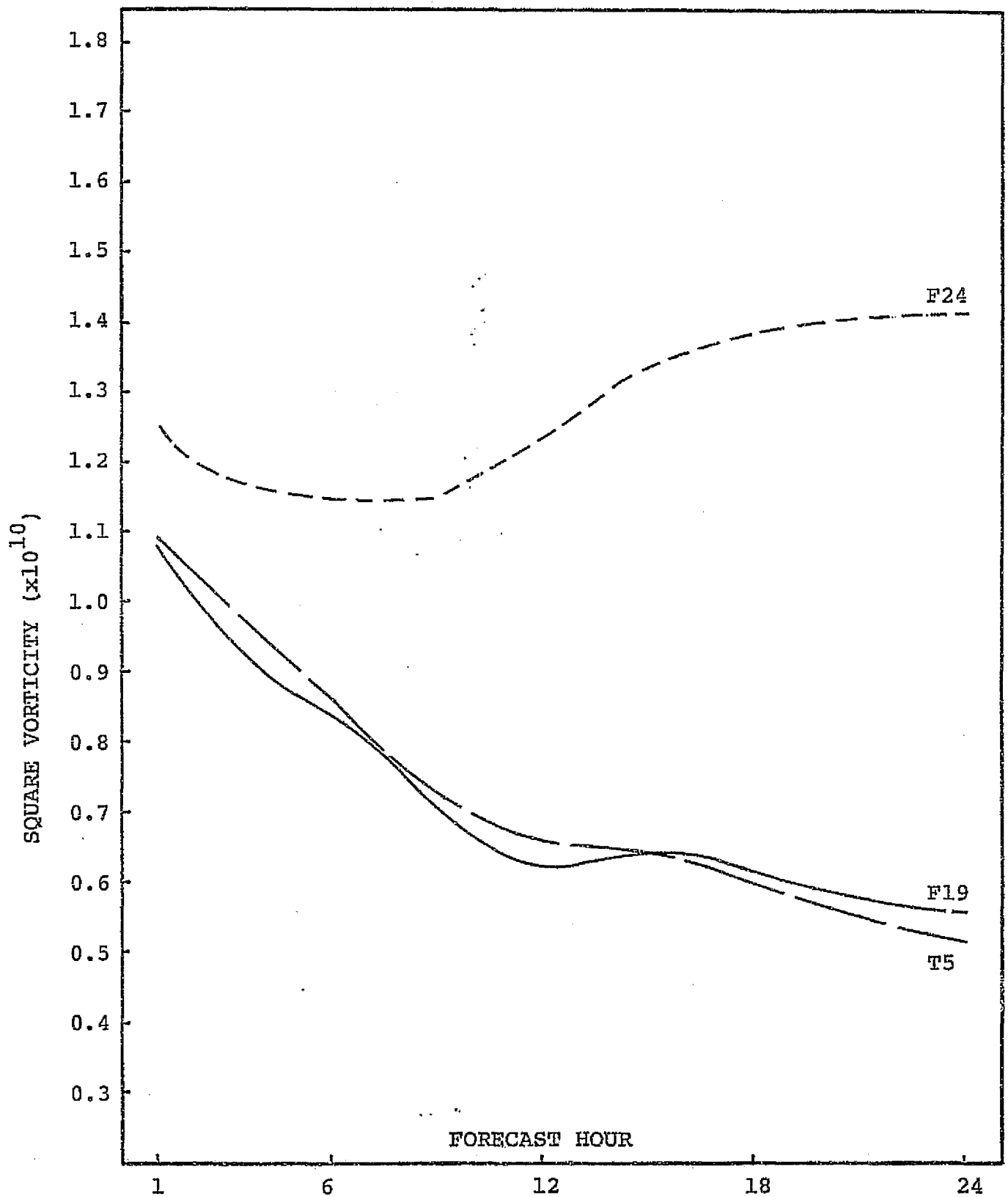


FIGURE VT-32: TIME VARIATION OF SQUARE VORTICITY FOR THREE MODEL VERSIONS AT SIGMA=0.7 LEVEL. SCENARIO B.

SIGMA=0.5

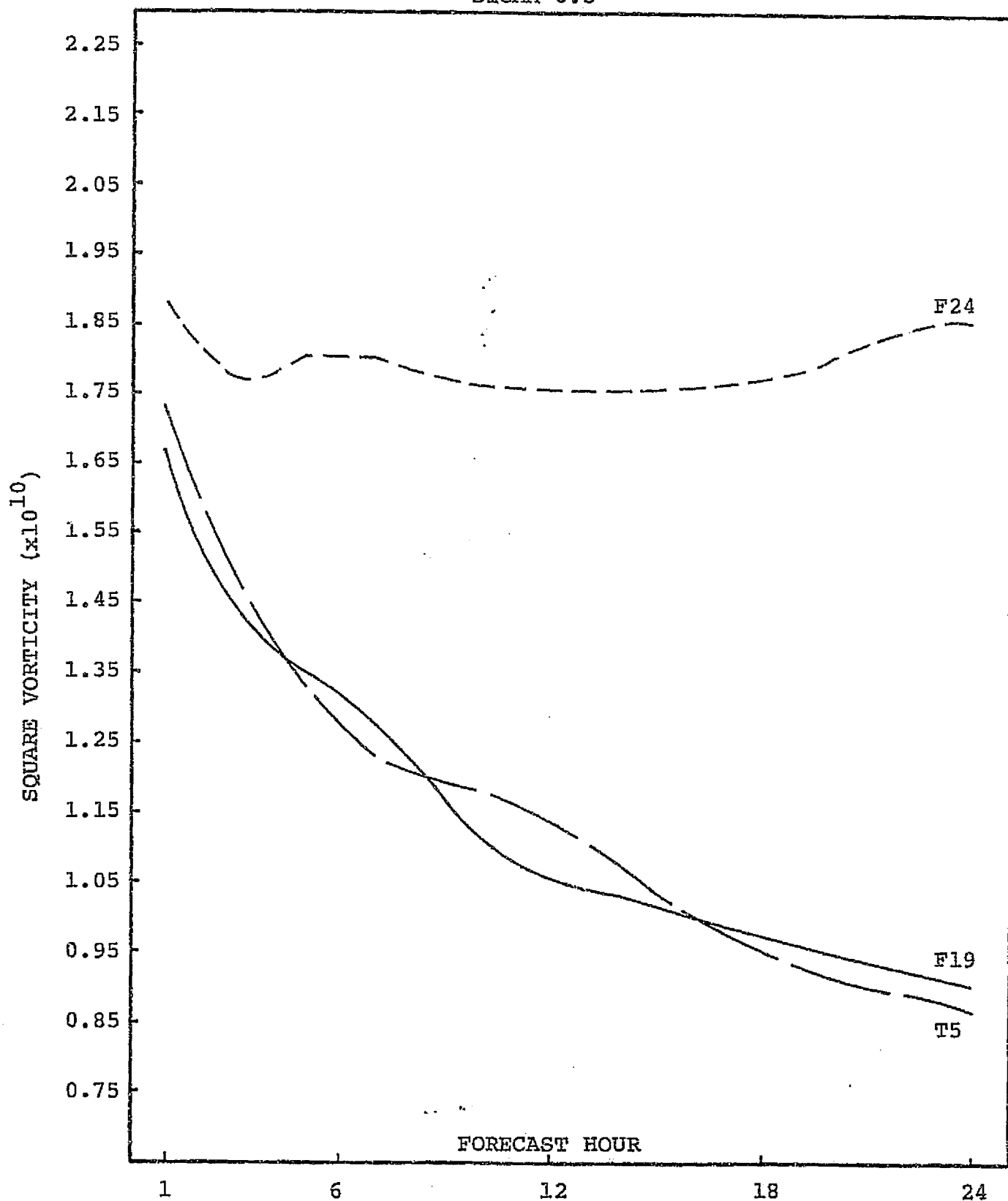


FIGURE VI-33: TIME VARIATION OF SQUARE VORTICITY FOR THREE MODEL VERSIONS AT SIGMA=0.5 LEVEL. SCENARIO B.

SIGMA=0.3

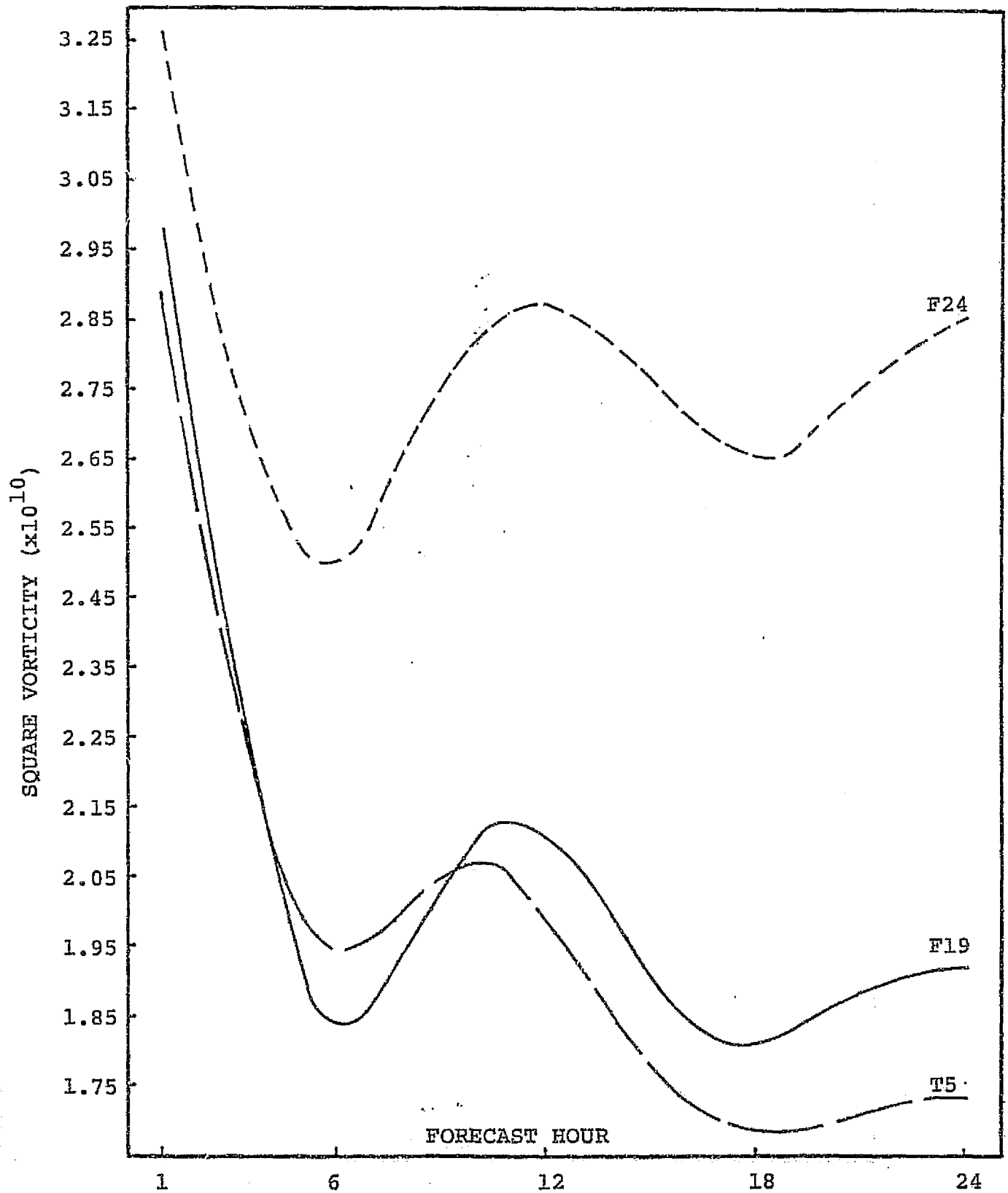


FIGURE VI-34: TIME VARIATION OF SQUARE VORTICITY FOR THREE MODEL VERSIONS AT SIGMA=0.3 LEVEL. SCENARIO B.

SIGMA=0.1

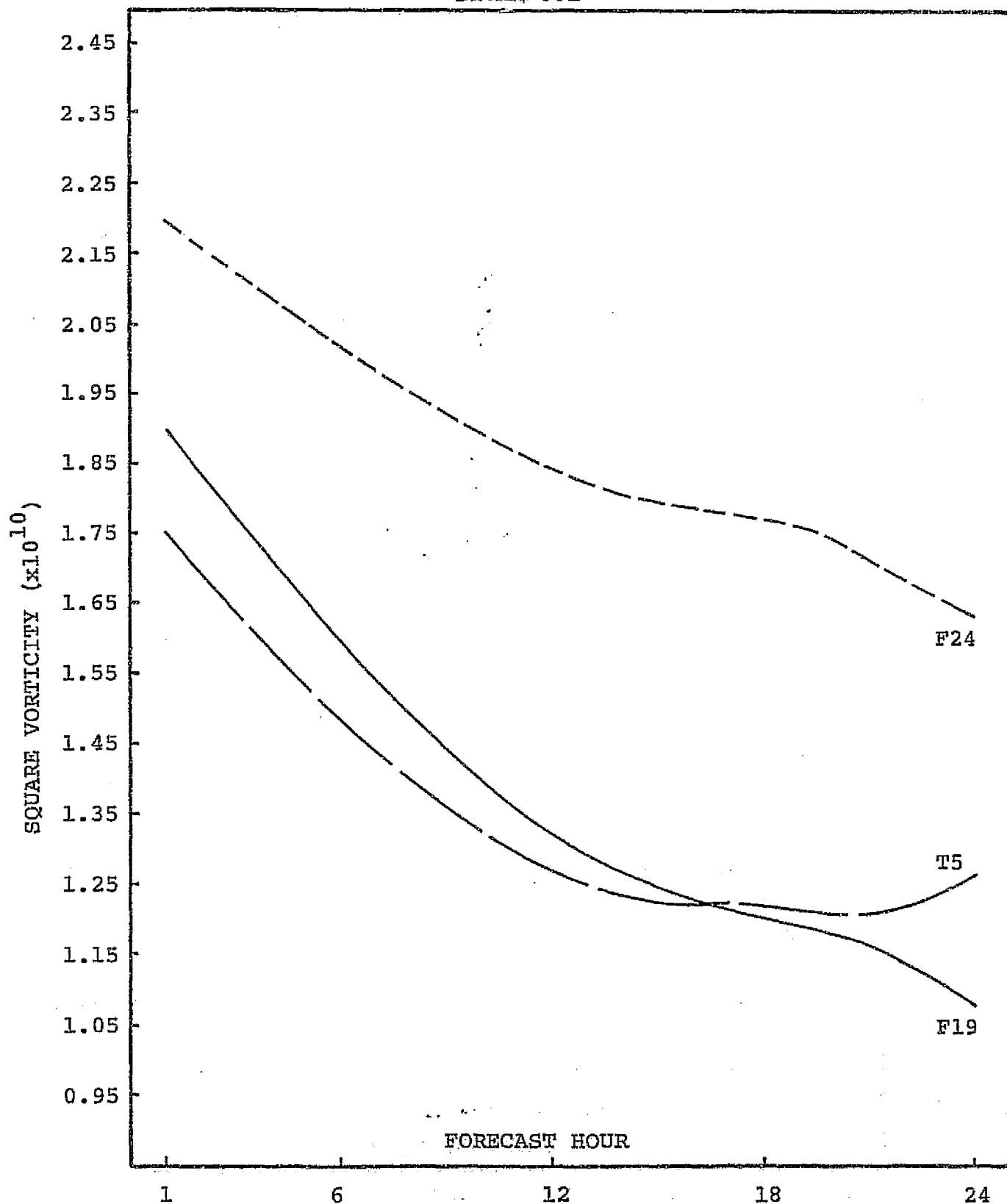


FIGURE VI-35: TIME VARIATION OF SQUARE VORTICITY FOR THREE MODEL VERSIONS AT SIGMA=0.1 LEVEL. SCENARIO B.

SIGMA=0.9

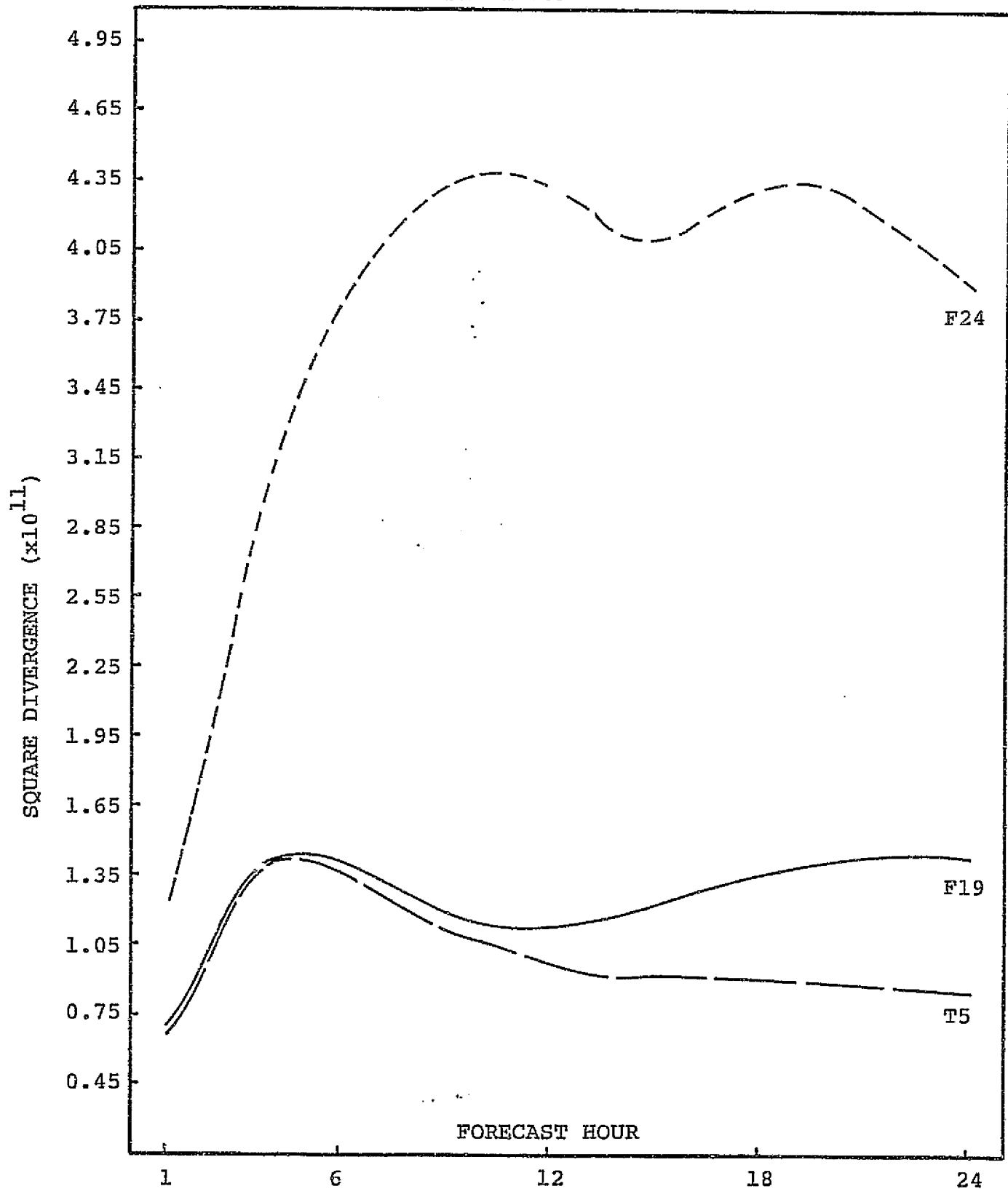


FIGURE VI-36: TIME VARIATION OF SQUARE DIVERGENCE FOR THREE MODEL VERSIONS AT SIGMA=0.9 LEVEL. SCENARIO B.

SIGMA=0.7

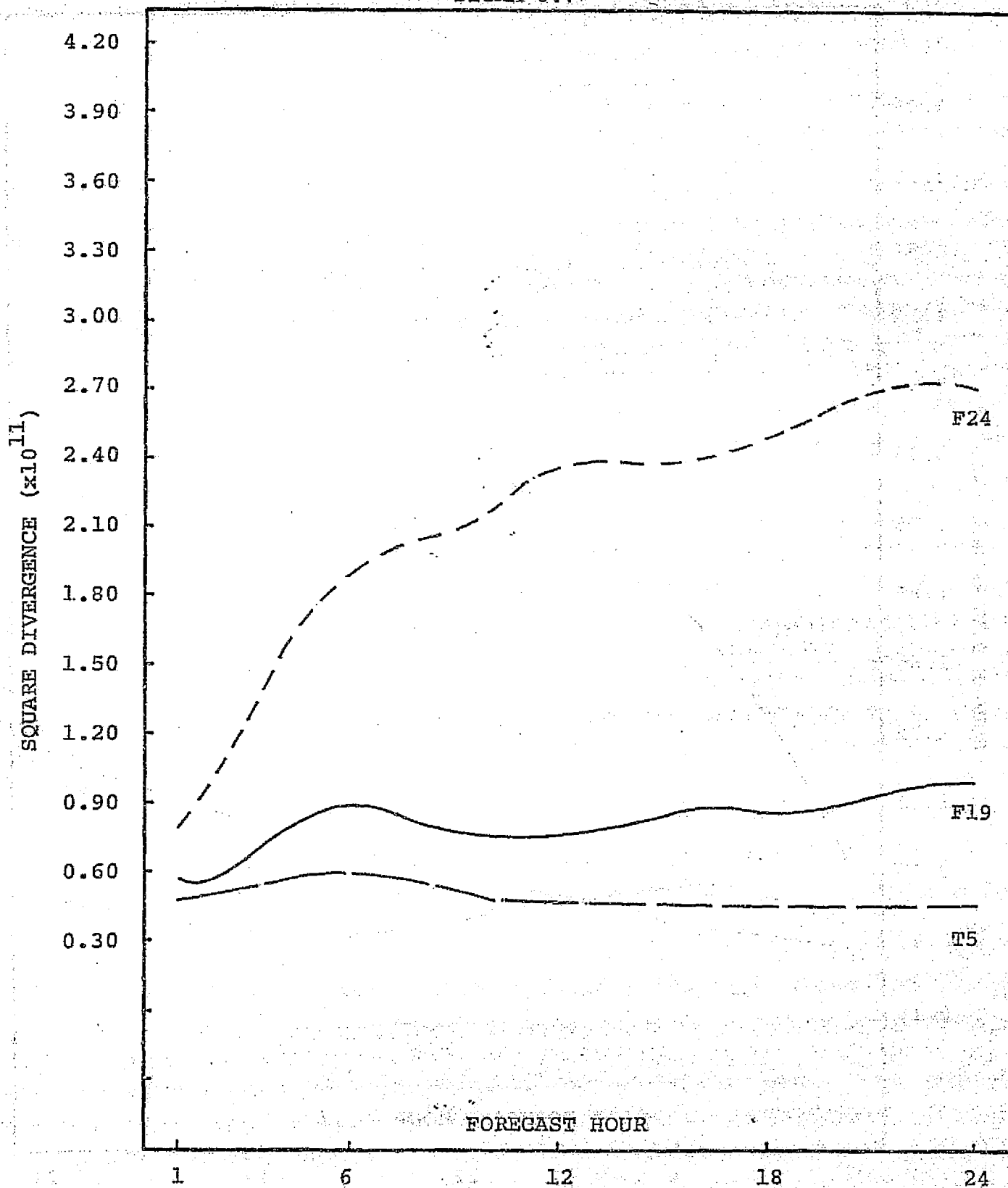


FIGURE VI-37: TIME VARIATION OF SQUARE DIVERGENCE FOR THREE MODEL VERSIONS AT SIGMA=0.7 LEVEL. SCENARIO B.

SIGMA=0.5

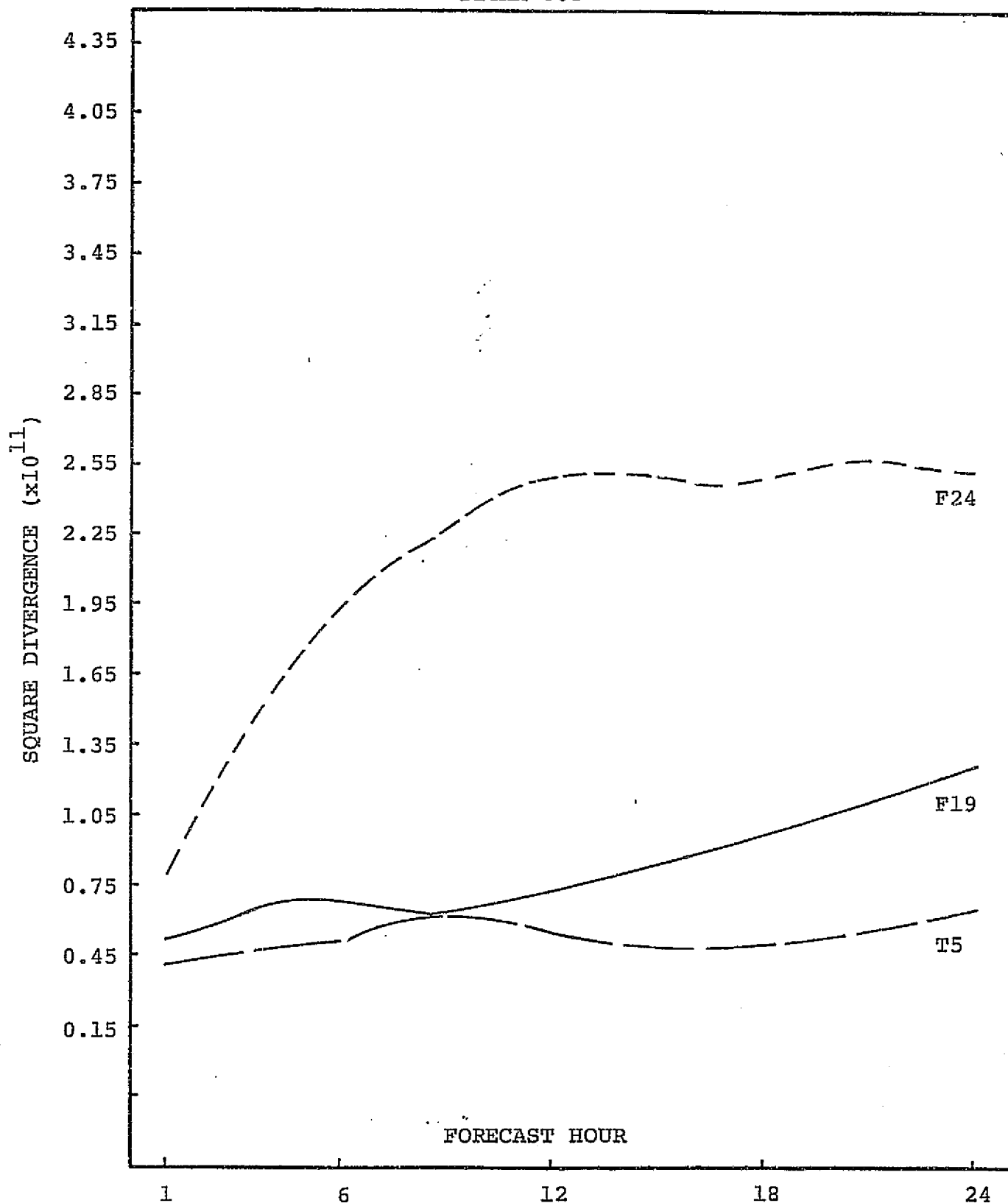


FIGURE VI-38: TIME VARIATION OF SQUARE DIVERGENCE FOR THREE MODEL VERSIONS AT SIGMA=0.5 LEVEL. SCENARIO B.

ORIGINAL PAGE IS
OF POOR QUALITY

SIGMA=0.3

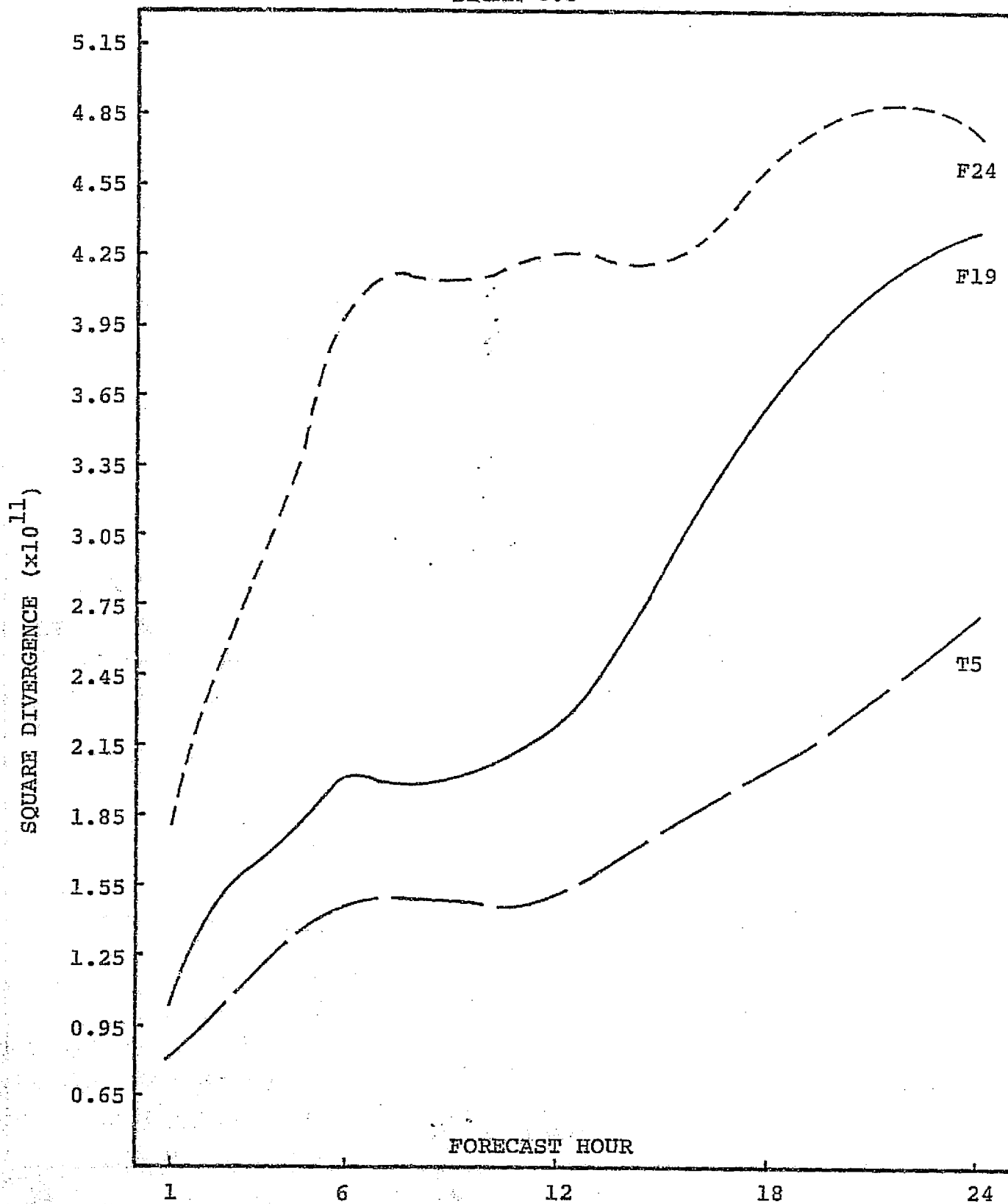


FIGURE VI-39: TIME VARIATION OF SQUARE DIVERGENCE FOR THREE MODEL VERSIONS AT SIGMA=0.3 LEVEL. SCENARIO B.

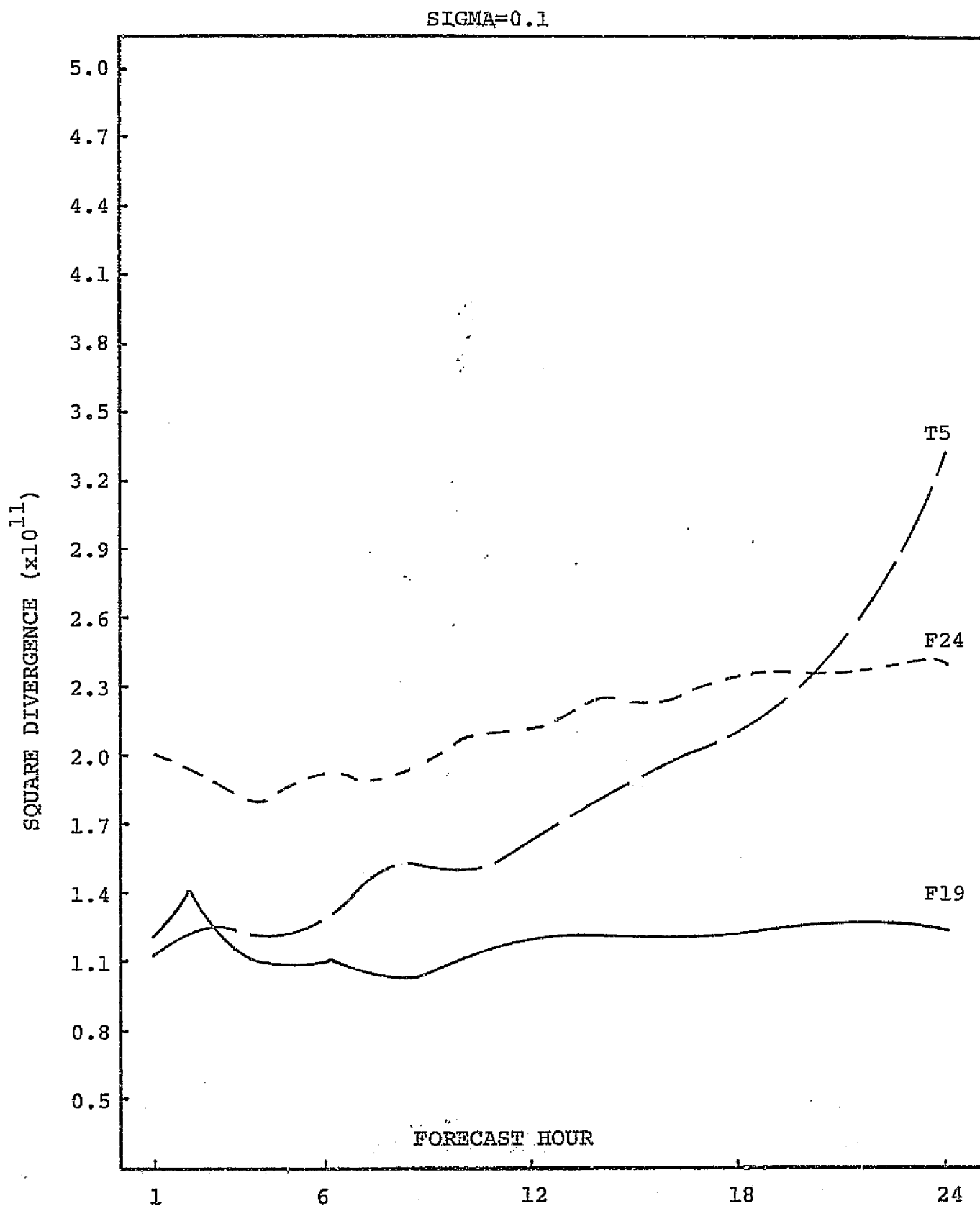


FIGURE VI-40: TIME VARIATION OF SQUARE DIVERGENCE FOR THREE MODEL VERSIONS AT SIGMA=0.1 LEVEL. SCENARIO B.

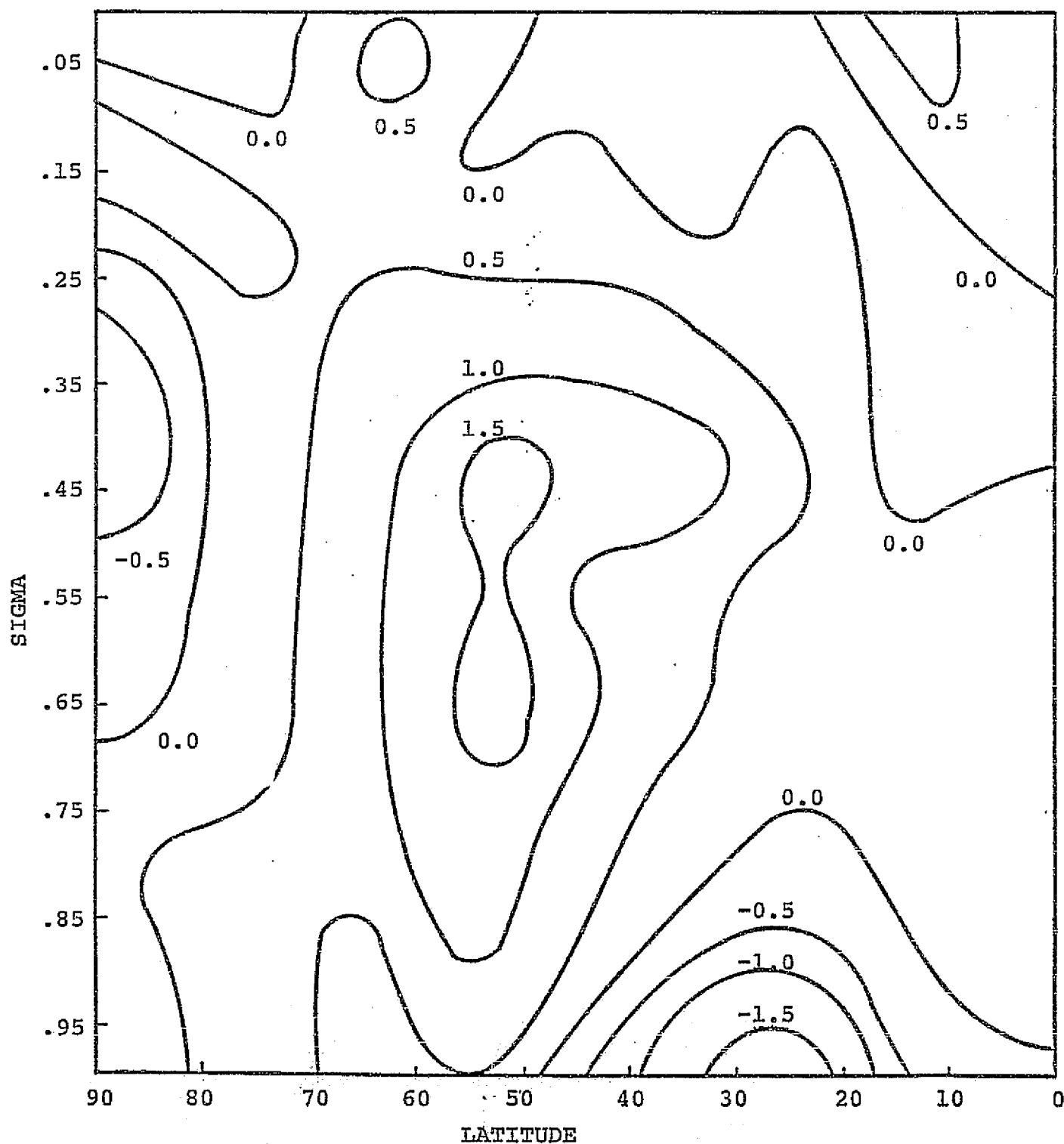


FIGURE VI-41: TEMPERATURE 24-HOUR FORECAST CHANGE ($^{\circ}\text{C}$),
BY LATITUDE AND LEVEL. RUN T4. MODEL
PECHFV. SCENARIO A.

ORIGINAL PAGE IS
OF POOR QUALITY

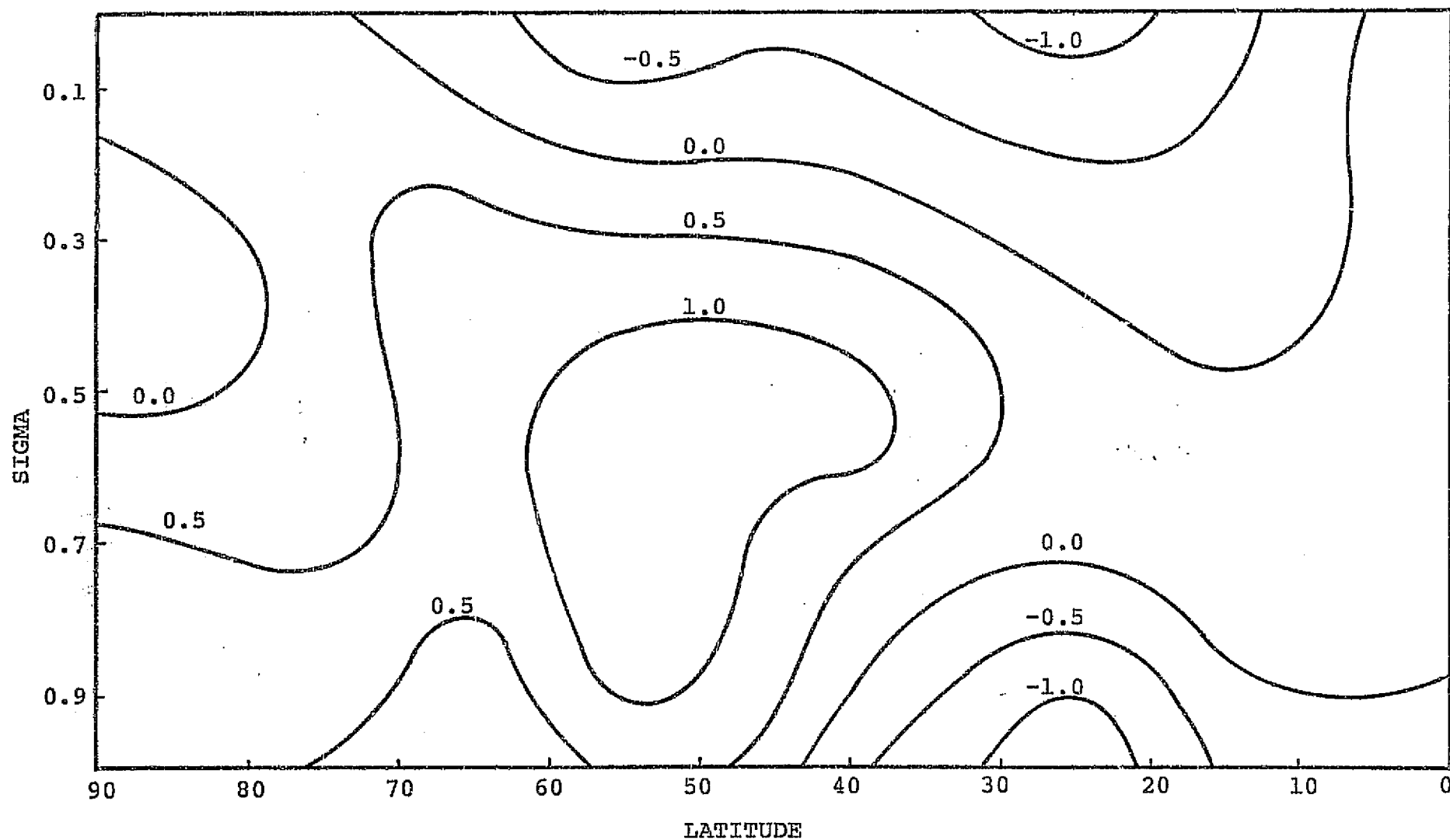


FIGURE VI-42: TEMPERATURE 24-HOUR FORECAST CHANGE ($^{\circ}\text{C}$), BY LATITUDE AND LEVEL. RUN F18. MODEL PECHCV. SCENARIO A.

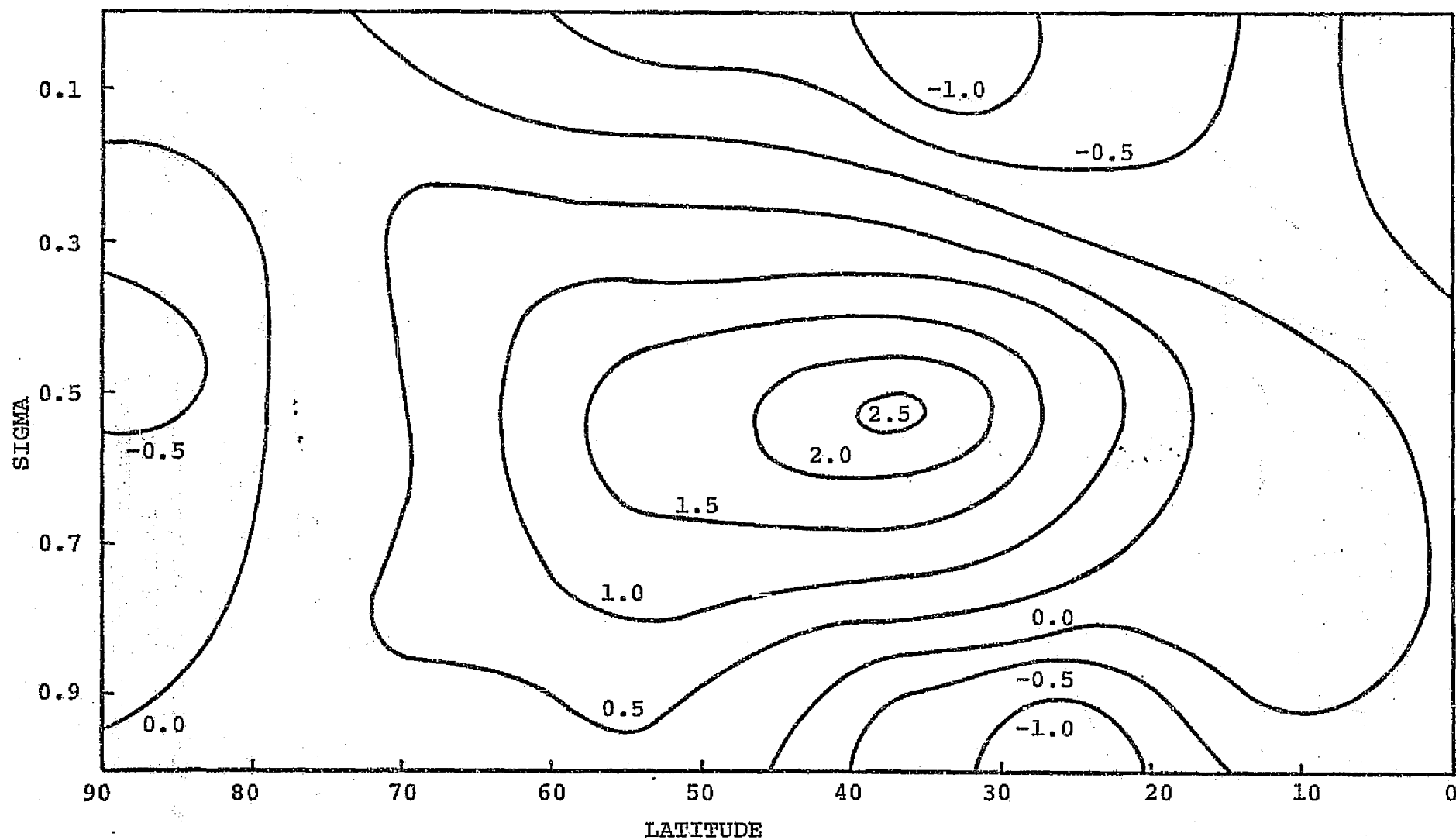


FIGURE VI-43: TEMPERATURE 24-HOUR FORECAST CHANGE ($^{\circ}\text{C}$), BY LATITUDE AND LEVEL. RUN F22. MODEL PEFHCV. SCENARIO A.

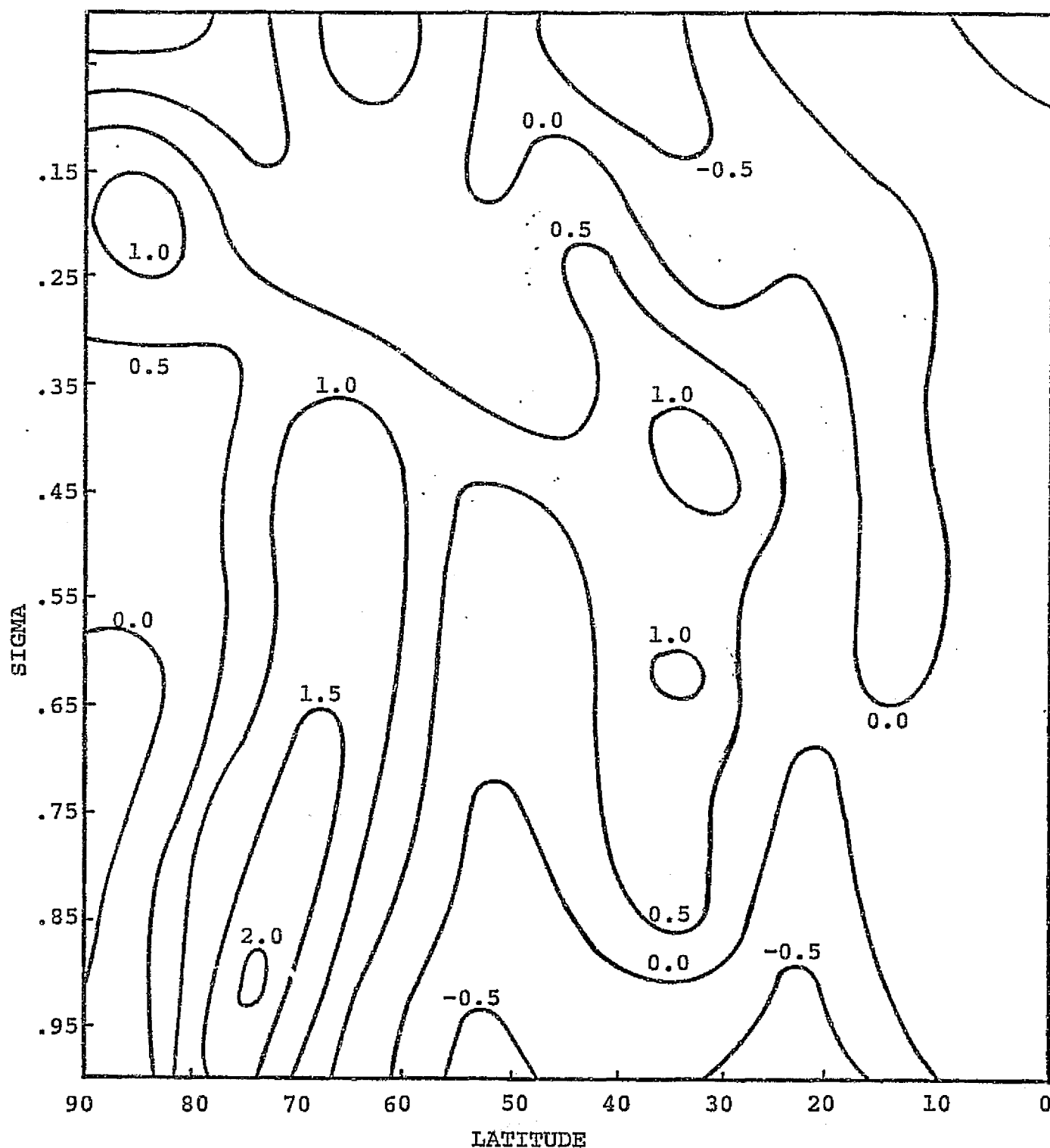


FIGURE VI-44: TEMPERATURE 24-HOUR FORECAST CHANGE ($^{\circ}\text{C}$),
BY LATITUDE AND LEVEL. RUN T5. MODEL
PECHFV. SCENARIO B.

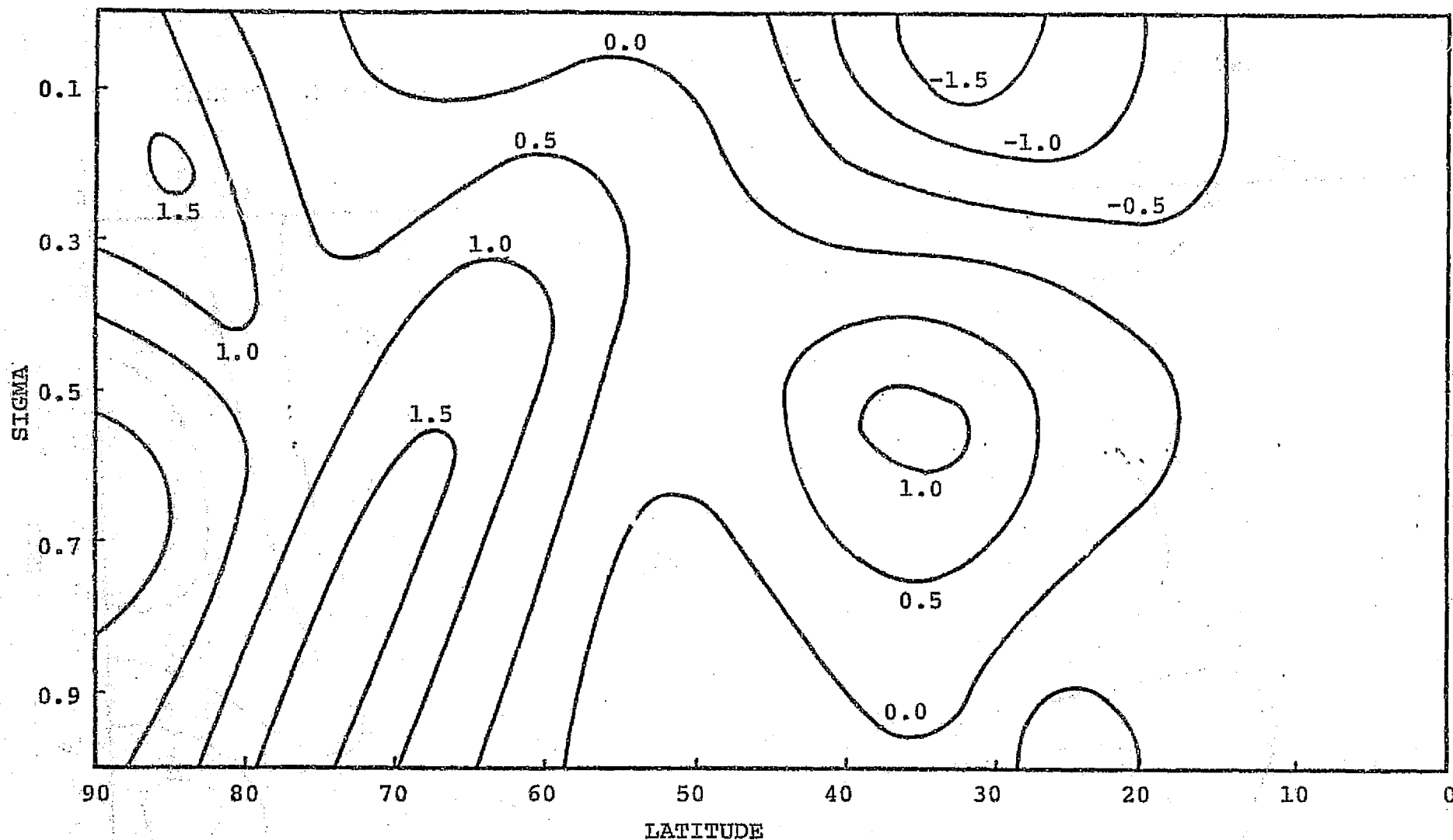


FIGURE VI-45: TEMPERATURE 24-HOUR FORECAST CHANGE ($^{\circ}\text{C}$), BY LATITUDE AND LEVEL. RUN F19. MODEL PECHCV. SCENARIO B.

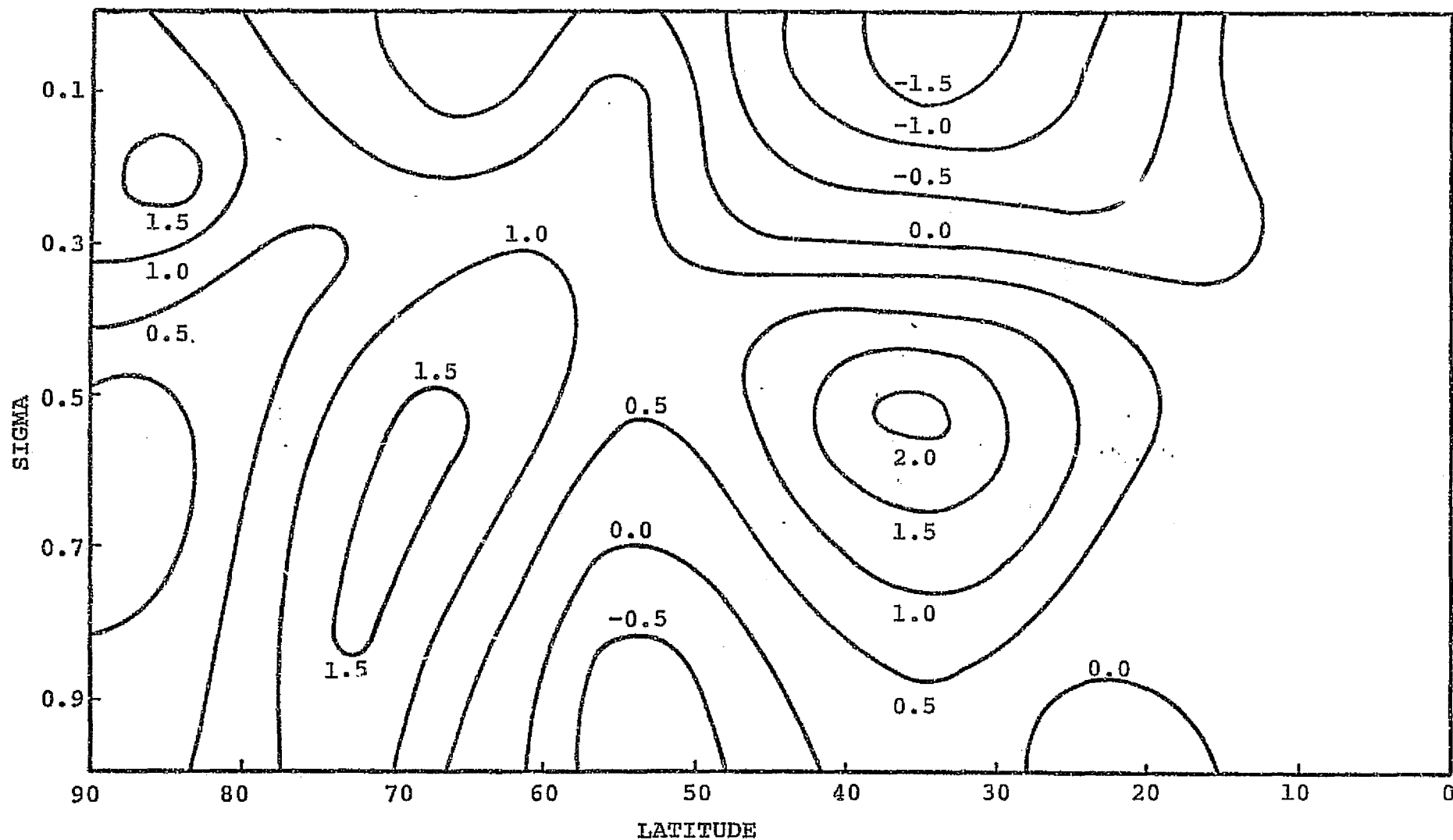


FIGURE VI-46: TEMPERATURE 24-HOUR FORECAST CHANGE ($^{\circ}\text{C}$), BY LATITUDE AND LEVEL. RUN F24. MODEL PEFHCV. SCENARIO B.

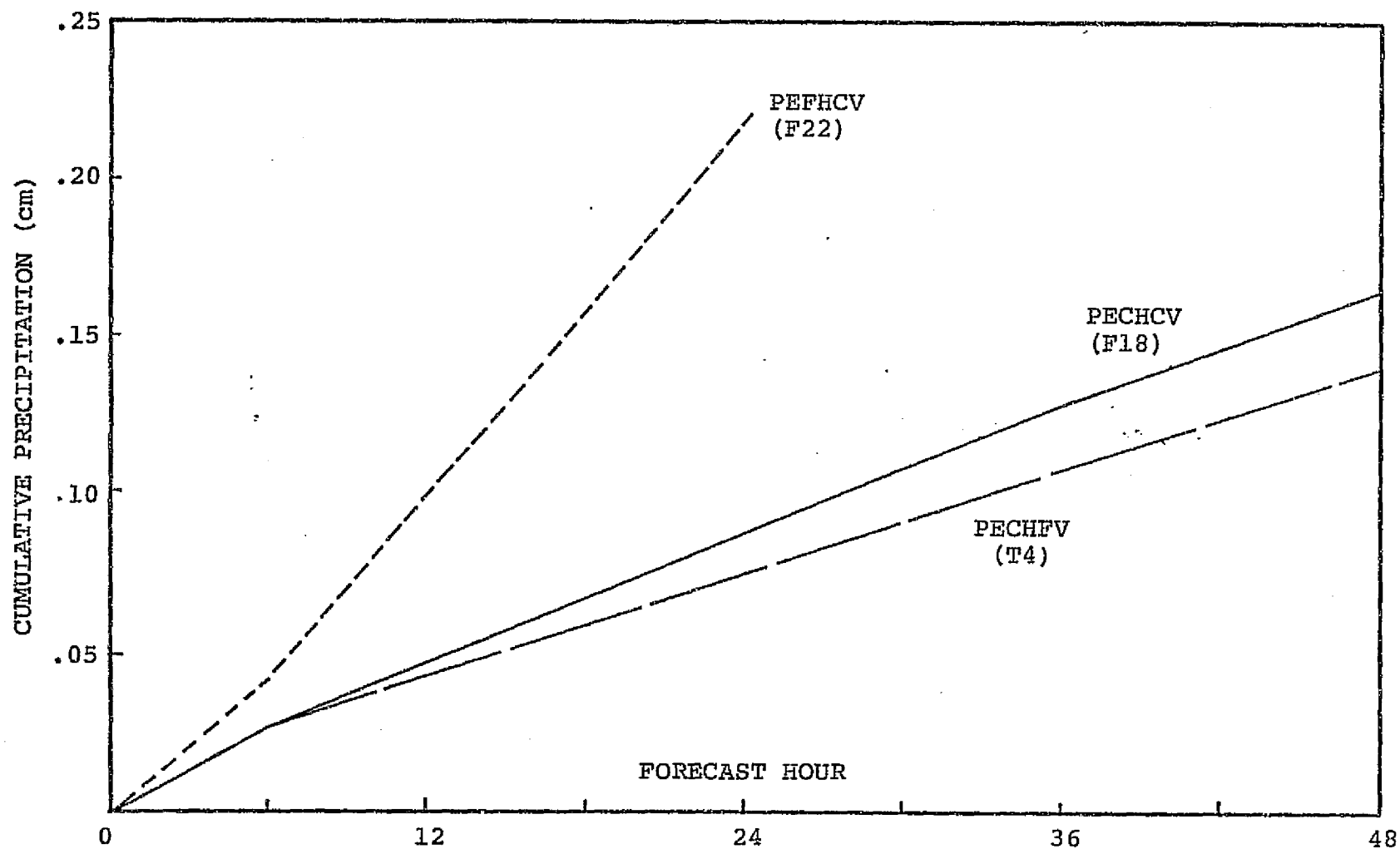


FIGURE VI-47: PRECIPITATION (PER GRID POINT) FOR THREE MODEL VERSIONS.
SCENARIO A.

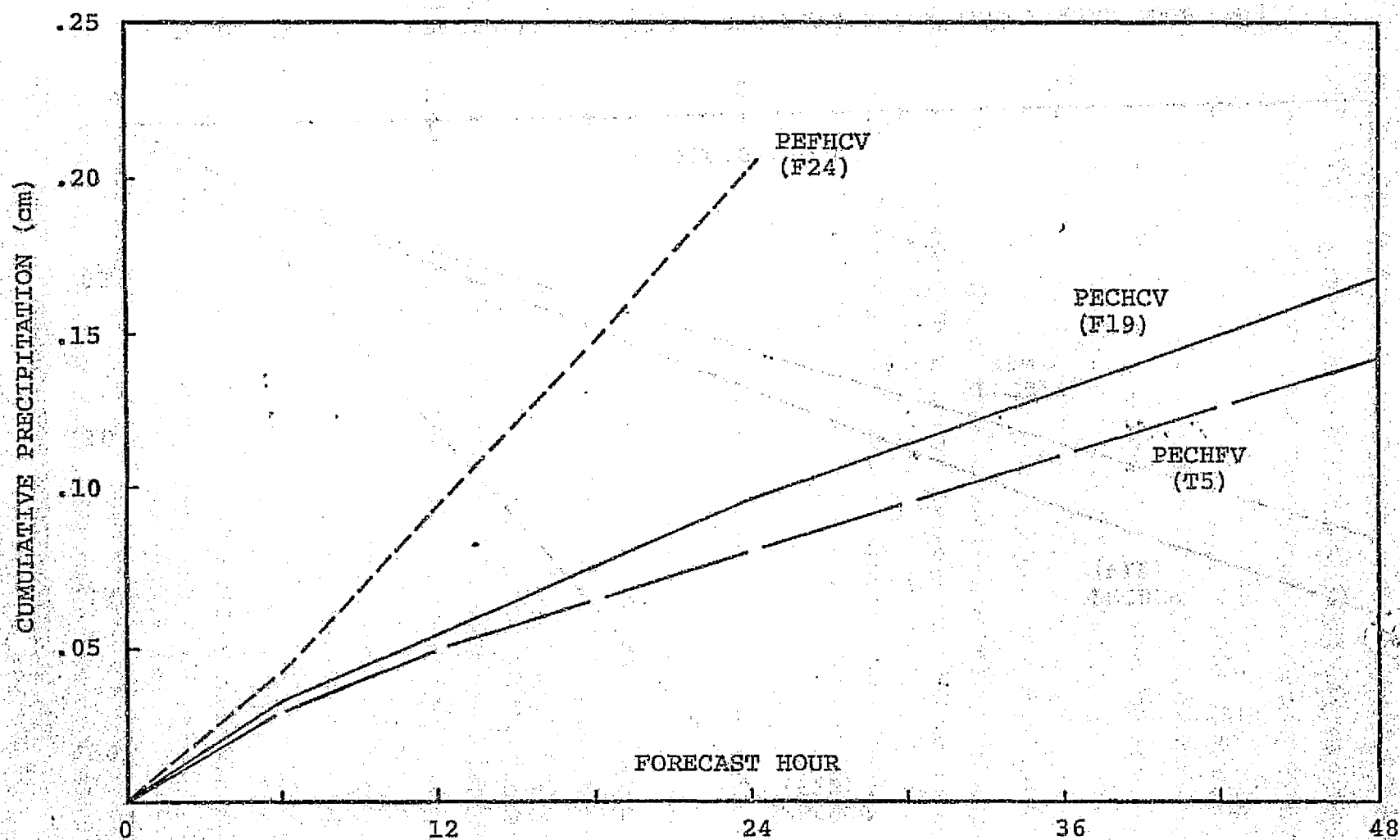


FIGURE VI-48: PRECIPITATION (PER GRID POINT) FOR THREE MODEL VERSIONS.
SCENARIO B.

VII. TABLES

TABLE VII-1: 24-HOUR FORECAST CENTRAL PRESSURES* (MBS) USING
THREE MODELS OF DIFFERING RESOLUTION.
SCENARIO A.

SCENARIO	RUN	LOW-PRESSURE CENTERS								AVERAGE ALGEBRAIC ERROR (MBS)
		CHINA	EAST OF KAMCHATKA	ALASKAN GULF	WEST ATLANTIC	MED	TEXAS - COLORADO	JAMES BAY	NOVAYA ZEMELA	
A	F22	975	1001	991	983	997	999	994	997	-0.8
	F18	986	1009	996	990	1001	1003	1002	1000	5.5
	T4	986	1009	996	990	1002	1004	1004	1000	6.0
STARTING ANALYSIS		1002	1003	1003	988	1004	1005	998	992	
VERIFICATION ANALYSIS		985	998	980	986	999	1003	1002	990	

* FROM 1200Z, 22 APRIL 1976

TABLE VII-2: 24-HOUR FORECAST CENTRAL PRESSURES* (MBS) USING
THREE MODELS OF DIFFERING RESOLUTION.
SCENARIO B.

SCENARIO	RUN	LOW-PRESSURE CENTERS						AVERAGE ALGEBRAIC ERROR (MBS)
		CHINA	EAST OF KAMCHATKA	ALASKAN GULF	MAINE	CENTRAL ATLANTIC	ICELAND- ENGLAND	
B	F24	975	992	1007	1002	1001	1000	-2.8
	F19	978	995	1008	1004	1005	1000	-0.7
	T5	978	996	1007	1006	1007	1000	0.0
STARTING ANALYSIS		988	988	1003	1001	1009	1004	
VERIFICATION ANALYSIS		988	992	1008	1004	1006	996	

* FROM 1200Z, 20 MAY 1976

TABLE VII-3: PERFORMANCE STATISTICS FOR FORECAST MODELS OF
DIFFERING RESOLUTION: 500 MB HEIGHTS (METERS).

			RMS DIFFERENCES					
SCENARIO	RUN	MODEL	24-HOUR			48-HOUR		
			ACTUAL CHANGE	FORECAST CHANGE	ERROR	ACTUAL CHANGE	FORECAST CHANGE	ERROR
A	F18	PECHCV		47.1	39.1		64.1	51.2
	T4	PECHFV	54.7	48.6	38.1	67.7	64.9	50.9
	F22	PEFHCV		53.7	36.3		-	-
B	F19	PECHCV		35.4	39.3		52.2	50.8
	T5	PECHFV	38.6	35.0	38.0	52.3	52.7	50.4
	F24	PEFHCV		36.5	38.2		-	-

TABLE VII-4: PERFORMANCE STATISTICS FOR FORECAST MODELS OF
DIFFERING RESOLUTION: SEA-LEVEL PRESSURE (MBS).

			RMS DIFFERENCES					
SCENARIO	RUN	MODEL	24-HOUR			48-HOUR		
			ACTUAL CHANGE	FORECAST CHANGE	ERROR	ACTUAL CHANGE	FORECAST CHANGE	ERROR
A	F18	PECHCV	4.81	4.19	3.54	6.01	5.74	4.16
	T4	PECHFV		4.21	3.47		5.81	4.15
	F22	PEFHCV		4.78	3.61		-	-
B	F19	PECHCV	3.34	3.14	3.55	4.35	4.27	3.83
	T5	PECHFV		2.99	3.34		4.18	3.70
	F24	PEFHCV		3.66	3.89		-	-

TABLE VII-5: KINETIC ENERGY 24-HOUR FORECAST CHANGES,
FOR MODELS OF VARYING RESOLUTION AND
TWO SCENARIOS (GIVEN IN PERCENT).

		SIGMA LEVEL				
SCENARIO	MODEL	0.9	0.7	0.5	0.3	0.1
A	PECHCV (F18)	-4.9	-13.1	-10.9	-19.5	-16.9
	PECHFV (T4)	-8.4	-12.5	-13.8	-18.4	-11.2
	PEFHCV (F22)	52.8	24.3	6.4	-9.8	-13.7
B	PECHCV (F19)	-13.7	-27.6	-23.7	-23.5	-29.4
	PECHFV (T5)	-22.3	-30.6	-26.8	-24.9	-19.3
	PEFHCV (F24)	27.8	-3.2	-6.6	-15.2	-22.2

TABLE VII-6: SQUARE VORTICITY 24-HOUR FORECAST CHANGES,
FOR MODELS OF VARYING RESOLUTION AND TWO
SCENARIOS (GIVEN IN PERCENT)

		SIGMA LEVEL				
SCENARIO	MODEL	0.9	0.7	0.5	0.3	0.1
A	PECHCV (F18)	-12.2	-43.2	-37.1	-37.4	-43.4
	PECHFV (T4)	-25.3	-44.2	-44.3	-33.5	-21.0
	PEFHCV (F22)	127.7	28.5	12.8	-5.9	-28.0
B	PECHCV (F19)	-13.9	-48.1	-46.1	-36.6	-43.1
	PECHFV (T5)	-31.6	-52.3	-50.3	-40.1	-28.0
	PEFHCV (F24)	115.7	12.8	-1.6	-13.9	-25.6

TABLE VII-7: THE EFFECT OF (FORECAST) MODEL
RESOLUTION ON PRECIPITATION.

AVERAGE PRECIPITATION PER GRID POINT*

SCENARIO		A			B		
MODEL		PECHCV	PECHFV	PEFHCV	PECHCV	PECHFV	PEFHCV
RUN IDENT		F18	T4	F22	F19	T5	F24
FORECAST HOUR	6	.028	.027	.042	.033	.030	.043
	12	.048	.044	.099	.057	.050	.096
	18	.068	.060	.159	.076	.066	.148
	24	.090	.077	.221	.098	.082	.205
	30	.109	.094	-	.116	.097	-
	36	.130	.112	-	.135	.114	-
	42	.147	.126	-	.151	.129	-
	48	.166	.142	-	.169	.144	-

* CUMULATIVE AMOUNTS, IN CENTIMETERS.

TABLE VII-8: STATISTICAL DIFFERENCES BETWEEN
187 x 187 AND 63 x 63 ANALYSES.

A. SEA-LEVEL PRESSURE (MBS)

SCENARIO	DIFFERENCE STATISTICS			
	RMS	MEAN	MAX	MIN
A ¹	0.35	-0.03	2.27	-3.59
B ²	0.37	-0.04	2.36	-3.15

B. 500 MB HEIGHT (METERS)

SCENARIO	DIFFERENCE STATISTICS			
	RMS	MEAN	MAX	MIN
A	7.46	-1.67	31.3	-45.3
B	9.03	-1.84	33.2	-98.8

1. A = 1200Z, 22 April 1976

2. B = 1200Z, 20 May 1976

TABLE VII-9: STATISTICAL DIFFERENCES BETWEEN
187 x 187 FORECAST AND 63 x 63
FORECAST. SCENARIO A.

A. SEA-LEVEL PRESSURE (MBS)

HOUR	DIFFERENCE STATISTICS			
	RMS	MEAN	MAX	MIN
24	2.01	-0.81	5.71	-16.5

B. 500 MB HEIGHT (METERS)

HOUR	DIFFERENCE STATISTICS			
	RMS	MEAN	MAX	MIN
24	14.1	0.20	89.3	-148.0

TABLE VII-10: STATISTICAL DIFFERENCES BETWEEN
187 x 187 FORECAST AND 63 x 63
FORECAST. SCENARIO B.

A. SEA-LEVEL PRESSURE (MBS)

HOUR	DIFFERENCE STATISTICS			
	RMS	MEAN	MAX	MIN
24	1.58	-0.68	4.50	-9.6

B. 500 MB HEIGHT (METERS)

HOUR	DIFFERENCE STATISTICS			
	RMS	MEAN	MAX	MIN
24	9.8	-0.44	61.0	-69.6

TABLE VII-11: ACTUAL CHANGES (FINAL MINUS
INITIAL ANALYSIS).
SCENARIO A.

A. SEA-LEVEL PRESSURE (MBS)

HOUR	DIFFERENCE STATISTICS			
	RMS	MEAN	MAX	MIN
24 ¹	4.81	0.13	21.0	-27.4
48 ²	6.01	-0.07	25.3	-34.6

B. 500 MB HEIGHT (METERS)

HOUR	DIFFERENCE STATISTICS			
	RMS	MEAN	MAX	MIN
24	54.7	3.1	242.0	-397.0
48	67.7	-2.59	359.0	-296.0

1. 4-23-76 MINUS 4-22-76
2. 4-24-76 MINUS 4-22-76

TABLE VII-12: MODEL STATISTICS. RUN F22. MODEL
PEFHCV. SCENARIO A. TEST SERIES
B ANALYSES.

A. SEA-LEVEL PRESSURE (MBS)

HOUR	TYPE	DIFFERENCE STATISTICS			
		RMS	MEAN	MAX	MIN
24	FORECAST CHANGE	4.78	0.06	16.9	-38.0
	ERROR	3.61	-0.42	20.4	-20.7
	ACTUAL CHANGE	4.81	0.13	21.0	-27.4

B. 500 MB HEIGHT (METERS)

HOUR	TYPE	DIFFERENCE STATISTICS			
		RMS	MEAN	MAX	MIN
24	FORECAST CHANGE	53.7	23.5	180.0	-424.0
	ERROR	36.3	6.5	207.0	-167.0
	ACTUAL CHANGE	54.7	3.1	242.0	-397.0

TABLE VII-13: MODEL STATISTICS. RUN F18. MODEL
PECHCV. SCENARIO A. TEST SERIES
B ANALYSES.

A. SEA-LEVEL PRESSURE (MBS)

HOUR	TYPE	DIFFERENCE STATISTICS			
		RMS	MEAN	MAX	MIN
24	FORECAST CHANGE ERROR	4.19	0.86	18.2	-24.8
		3.54	0.39	22.4	-13.8
48	FORECAST CHANGE	5.74	0.86	22.2	-37.2
	ERROR	4.16	0.58	19.6	-20.1
	ACTUAL CHANGE	6.01	-0.07	25.3	-34.6

B. 500 MB HEIGHT (METERS)

HOUR	TYPE	DIFFERENCE STATISTICS			
		RMS	MEAN	MAX	MIN
24	FORECAST CHANGE ERROR	47.1	23.3	173.0	-298.0
		39.1	6.3	241.0	-189.0
48	FORECAST CHANGE	64.1	24.9	278.0	-329.0
	ERROR	51.2	13.5	294.0	-194.0
	ACTUAL CHANGE	67.7	-2.59	359.0	-296.0

TABLE VII-14: MODEL STATISTICS. RUN T4. MODEL
PECFV. SCENARIO A. TEST SERIES
B ANALYSES.

A. SEA-LEVEL PRESSURE (MBS)

HOUR	TYPE	DIFFERENCE STATISTICS			
		RMS	MEAN	MAX	MIN
24	FORECAST CHANGE	4.21	1.06	18.1	-23.9
	ERROR	3.47	0.59	21.9	-12.9
48	FORECAST CHANGE	5.81	1.01	24.9	-38.1
	ERROR	4.15	0.73	18.4	-19.7
	ACTUAL CHANGE	6.01	-0.07	25.3	-34.6

B. 500 MB HEIGHT (METERS)

HOUR	TYPE	DIFFERENCE STATISTICS			
		RMS	MEAN	MAX	MIN
24	FORECAST CHANGE	48.6	23.9	176.0	-304.0
	ERROR	38.1	6.9	234.0	-175.0
48	FORECAST CHANGE	64.9	24.3	331.0	-330.0
	ERROR	50.9	13.0	294.0	-175.0
	ACTUAL CHANGE	67.7	-2.59	359.0	-296.0

TABLE VII-15: MODEL STATISTICS. RUN F20. MODEL
PECHCV. SCENARIO A. PRODUCTION
SERIES C ANALYSES.

A. SEA-LEVEL PRESSURE (MBS)

HOUR	TYPE	DIFFERENCE STATISTICS			
		RMS	MEAN	MAX	MIN
24	FORECAST CHANGE ERROR	4.01	-0.47	14.1	-27.2
		3.84	-0.94	22.5	-18.1
48	FORECAST CHANGE ERROR	5.63	-0.43	20.2	-31.6
		4.26	-0.71	20.2	-25.7
	ACTUAL CHANGE	6.01	-0.07	25.3	-34.6

B. 500 MB HEIGHT (METERS)

HOUR	TYPE	DIFFERENCE STATISTICS			
		RMS	MEAN	MAX	MIN
24	FORECAST CHANGE ERROR	40.5	-5.86	148.0	-316.0
		48.2	-22.8	255.0	-220.0
48	FORECAST CHANGE ERROR	60.4	-3.99	228.0	-314.0
		56.9	-15.3	310.0	-233.0
	ACTUAL CHANGE	67.7	-2.59	359.0	-296.0

TABLE VII-16: MODEL STATISTICS. RUN T6. MODEL
PECHFV. SCENARIO A. PRODUCTION
SERIES C ANALYSES.

A. SEA-LEVEL PRESSURE (MBS)

HOUR	TYPE	DIFFERENCE STATISTICS			
		RMS	MEAN	MAX	MIN
24	FORECAST CHANGE ERROR	3.94	-0.07	14.4	-23.6
		3.62	-0.54	21.8	-16.3
48	FORECAST CHANGE ERROR	5.62	-0.11	21.1	-32.3
		4.13	-.39	19.3	-19.8
	ACTUAL CHANGE	6.01	-0.07	25.3	-34.6

B. 500 MB HEIGHT (METERS)

HOUR	TYPE	DIFFERENCE STATISTICS			
		RMS	MEAN	MAX	MIN
24	FORECAST CHANGE ERROR	40.9	-4.61	150.0	-318.0
		46.7	-21.6	254.0	-214.0
48	FORECAST CHANGE ERROR	60.6	-4.01	291.0	-296.0
		56.6	-15.4	305.0	-234.0
	ACTUAL CHANGE	67.7	-2.59	359.0	-296.0

TABLE VII-17: ACTUAL CHANGES (FINAL MINUS
INITIAL ANALYSIS).
SCENARIO B.

A. SEA-LEVEL PRESSURE (MBS)

HOUR	DIFFERENCE STATISTICS			
	RMS	MEAN	MAX	MIN
24 ¹	3.24	-0.07	17.8	-17.9
48 ²	4.35	-0.18	26.0	-25.3

B. 500 MB HEIGHT (METERS)

HOUR	DIFFERENCE STATISTICS			
	RMS	MEAN	MAX	MIN
24	38.6	-1.50	201.0	-224.0
48	52.3	2.87	332.0	-338.0

1. 5-21-76 MINUS 5-20-76
2. 5-22-76 MINUS 5-20-76

TABLE VII-18: MODEL STATISTICS. RUN F24. MODEL
PEFHCV. SCENARIO B. PRODUCTION
SERIES C ANALYSES.

A. SEA-LEVEL PRESSURE (MBS)

HOUR	TYPE	DIFFERENCE STATISTICS			
		RMS	MEAN	MAX	MIN
24	FORECAST CHANGE	3.66	-0.86	15.2	-17.5
	ERROR	3.89	-1.06	19.6	-19.1
	ACTUAL CHANGE	3.34	-0.07	17.8	-17.9

B. 500 MB HEIGHT (METERS)

HOUR	TYPE	DIFFERENCE STATISTICS			
		RMS	MEAN	MAX	MIN
24	FORECAST CHANGE	36.5	-2.87	149.0	-273.0
	ERROR	38.2	-14.2	180.0	-143.0
	ACTUAL CHANGE	38.6	-1.50	201.0	-224.0

TABLE VII-19: MODEL STATISTICS. RUN F19. MODEL
PECHCV. SCENARIO B. PRODUCTION
SERIES C ANALYSES.

A. SEA-LEVEL PRESSURE (MBS)

HOUR	TYPE	DIFFERENCE STATISTICS			
		RMS	MEAN	MAX	MIN
24	FORECAST CHANGE ERROR	3.14	-0.18	13.7	-15.0
		3.55	-0.38	20.5	-14.4
48	FORECAST CHANGE ERROR	4.27	-0.14	23.1	-18.9
		3.83	-0.23	15.6	-14.6
	ACTUAL CHANGE	4.35	-0.18	26.0	-25.3

B. 500 MB HEIGHT (METERS)

HOUR	TYPE	DIFFERENCE STATISTICS			
		RMS	MEAN	MAX	MIN
24	FORECAST CHANGE ERROR	35.4	2.44	156.0	-216.0
		39.3	-13.8	183.0	-140.3
48	FORECAST CHANGE ERROR	52.2	-0.66	238.0	-194.0
		50.8	-16.4	256.0	-240.0
	ACTUAL CHANGE	52.3	2.87	332.0	-338.0

TABLE VII-20: MODEL STATISTICS. RUN T5. MODEL
PECHFV. SCENARIO B. PRODUCTION
SERIES C ANALYSES.

A. SEA-LEVEL PRESSURE (MBS)

HOUR	TYPE	DIFFERENCE STATISTICS			
		RMS	MEAN	MAX	MIN
24	FORECAST CHANGE ERROR	2.99	-0.04	13.7	-13.8
		3.24	-0.24	20.3	-14.6
48	FORECAST CHANGE ERROR	4.18	-0.10	24.0	-17.1
		3.70	-0.19	14.7	-14.4
	ACTUAL CHANGE	4.35	-0.18	26.0	-25.3

B. 500 MB HEIGHT (METERS)

HOUR	TYPE	DIFFERENCE STATISTICS			
		RMS	MEAN	MAX	MIN
24	FORECAST CHANGE ERROR	35.0	-3.56	146.0	-222.0
		38.0	-14.90	182.0	-138.0
48	FORECAST CHANGE ERROR	52.7	-3.19	248.0	-197.0
		50.4	-18.90	246.0	-246.0
	ACTUAL CHANGE	52.3	2.87	332.0	-338.0

TABLE VII-21: PECHV FORECAST MINUS PECHV
FORECAST. SCENARIO A. PRO-
DUCTION SERIES C ANALYSES.

A. SEA-LEVEL PRESSURE (MBS)

HOUR	DIFFERENCE STATISTICS			
	RMS	MEAN	MAX	MIN
24	0.96	0.40	5.15	-4.24
48	0.96	0.32	5.90	-4.54

B. 500 MB HEIGHT (METERS)

HOUR	DIFFERENCE STATISTICS			
	RMS	MEAN	MAX	MIN
24	8.34	1.25	38.4	-42.4
48	9.32	-0.02	67.0	-38.0

TABLE VII-22: PECHFV FORECAST MINUS PECHCV
FORECAST. SCENARIO A. TEST
SERIES B ANALYSES.

A. SEA-LEVEL PRESSURE (MBS)

HOUR	DIFFERENCE STATISTICS			
	RMS	MEAN	MAX	MIN
24	0.92	0.20	7.29	-3.77
48	1.02	0.15	9.35	-8.03

B. 500 MB HEIGHT (METERS)

HOUR	DIFFERENCE STATISTICS			
	RMS	MEAN	MAX	MIN
24	8.19	0.64	37.2	-38.5
48	9.79	-0.52	72.8	-54.8

TABLE VII-23: PECHFV FORECAST MINUS PECHCV
FORECAST. SCENARIO B. PRO-
DUCTION SERIES C ANALYSES.

A. SEA-LEVEL PRESSURE (MBS)

HOUR	DIFFERENCE STATISTICS			
	RMS	MEAN	MAX	MIN
24	0.76	0.14	4.88	-2.50
48	0.82	0.40	4.97	-4.21

B. 500 MB HEIGHT (METERS)

HOUR	DIFFERENCE STATISTICS			
	RMS	MEAN	MAX	MIN
24	7.27	-1.12	28.3	-23.4
48	8.66	-2.53	51.5	-42.2

VIII. CHARTS

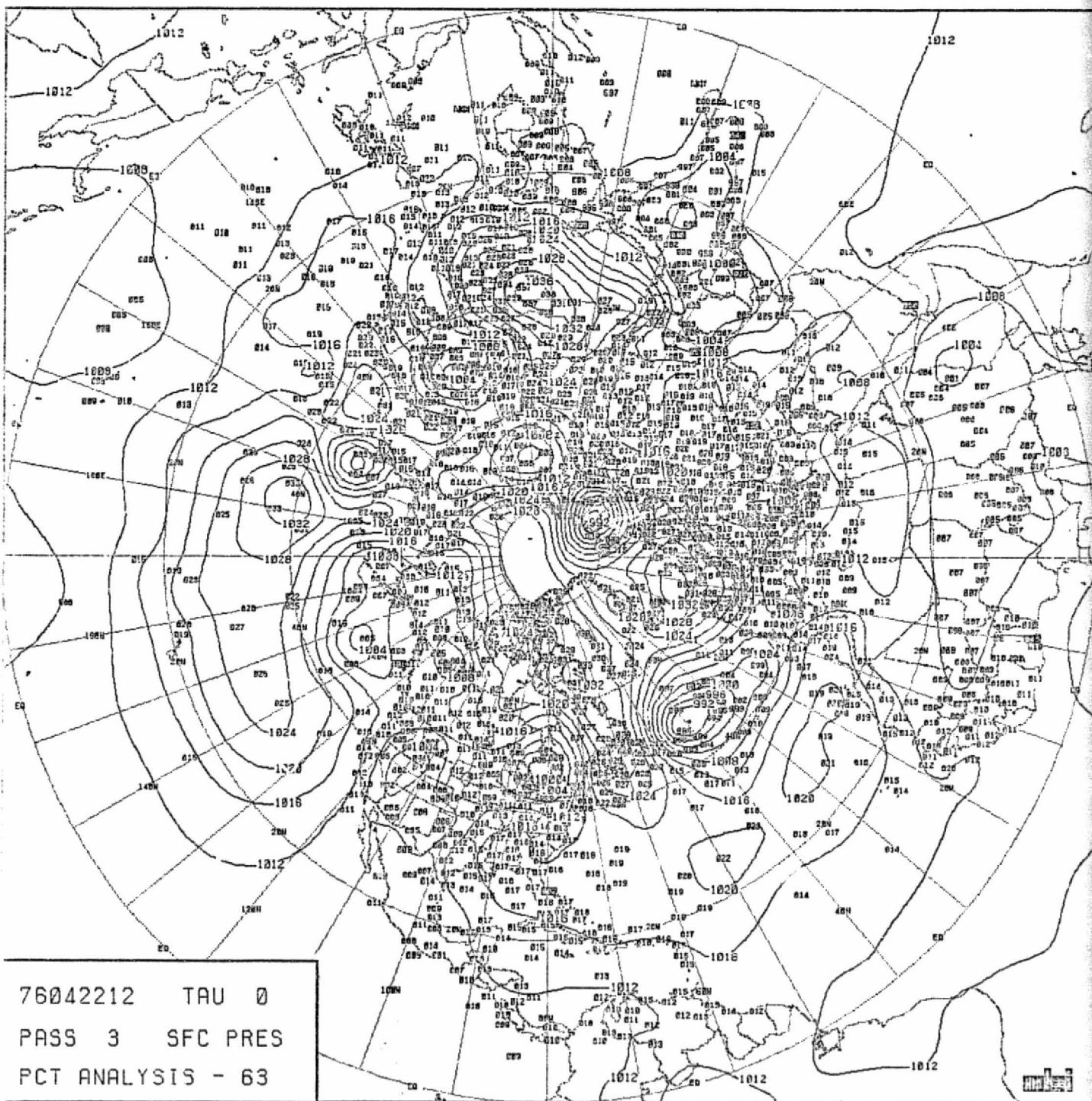


CHART VIII-1

SEA-LEVEL PRESSURE ANALYSIS, 63 x 63 GRID,
1200Z, 22 APRIL 1976

ORIGINAL PAGE IS
OF POOR QUALITY

ORIGINAL
OF POOR QUALITY

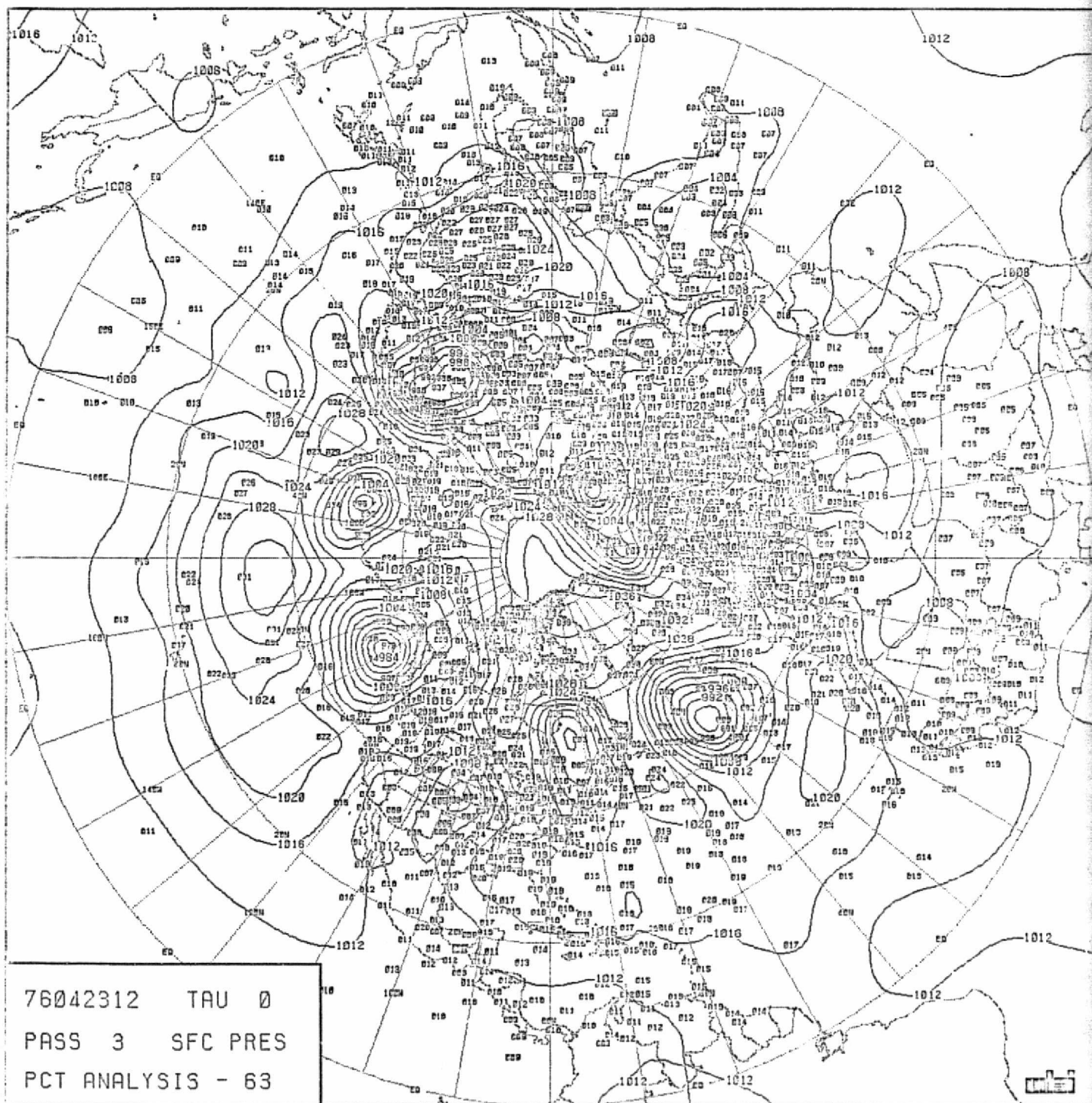
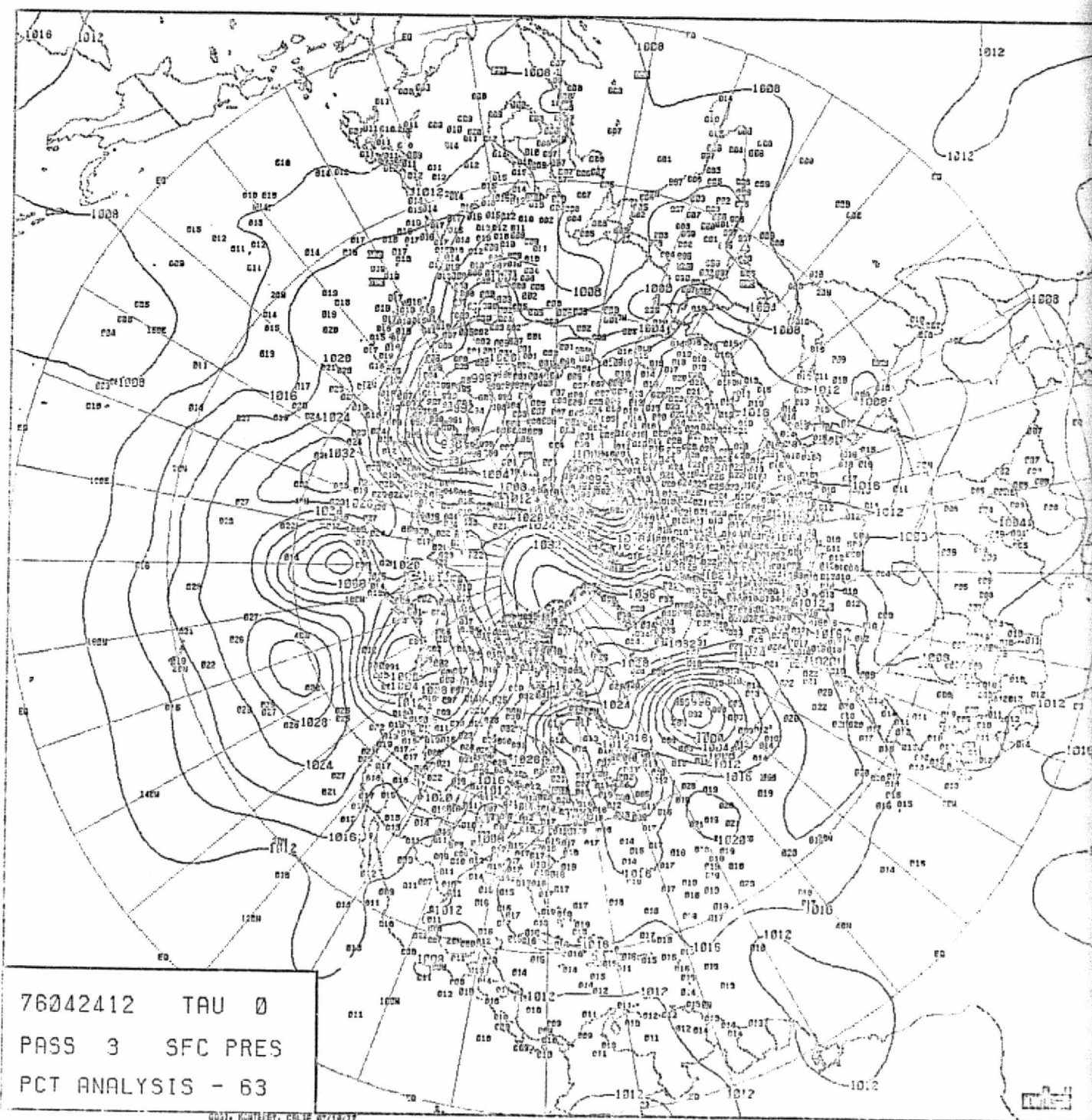


CHART VIII-2

SEA-LEVEL PRESSURE ANALYSIS, 63 x 63 GRID,
1200Z, 23 APRIL 1976.



ORIGINAL PAGE IS
DE POOR QUALITY

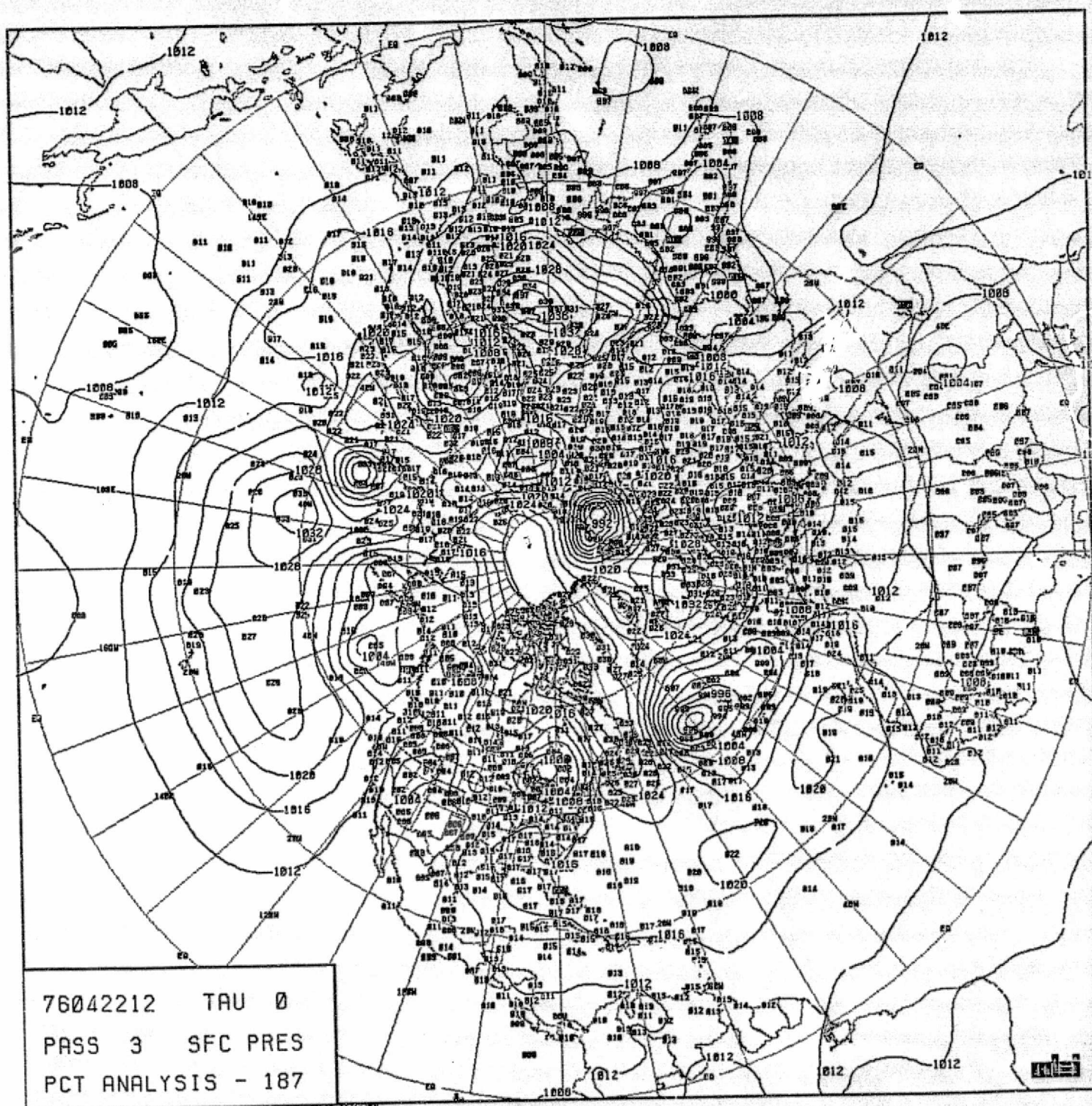


CHART VIII-4

SEA-LEVEL PRESSURE ANALYSIS, 187 x 187 GRID,
1200Z, 22 APRIL 1976.

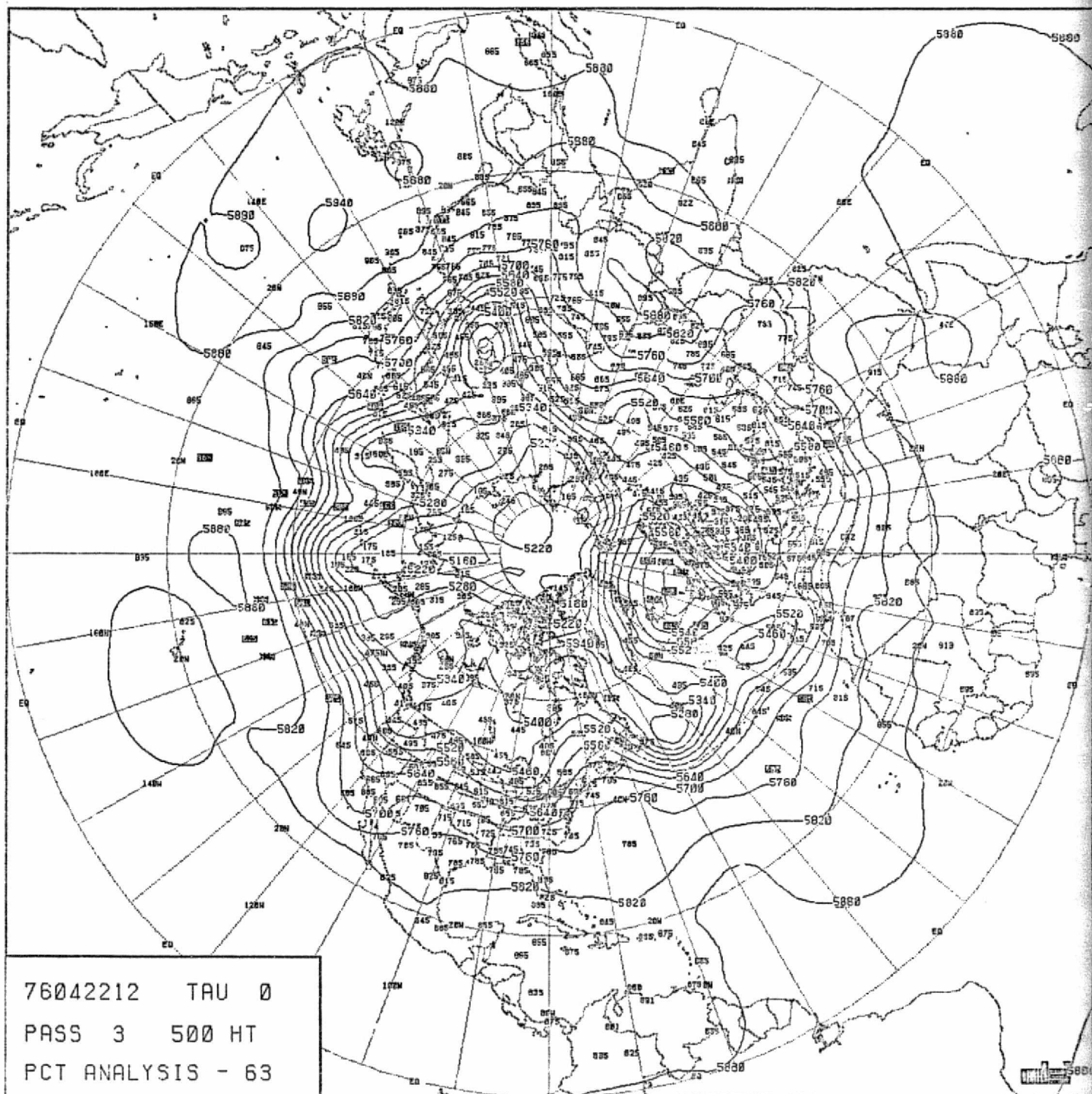
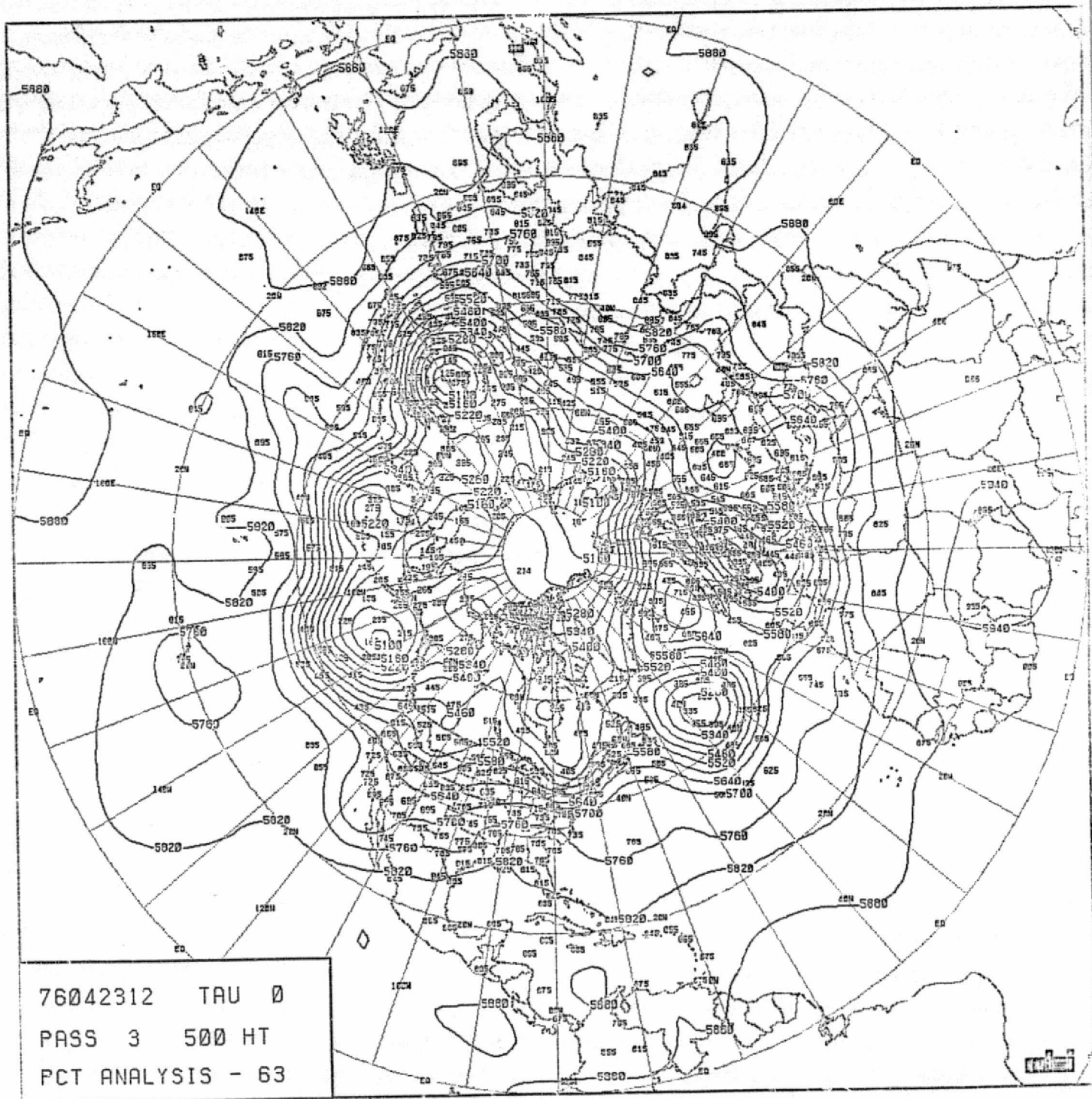


CHART VIII-5

500 MB HEIGHT ANALYSIS, 63 x 63 GRID, 1200Z,
22 APRIL 1976.

ORIGINAL PAGE 13
OF POOR QUALITY



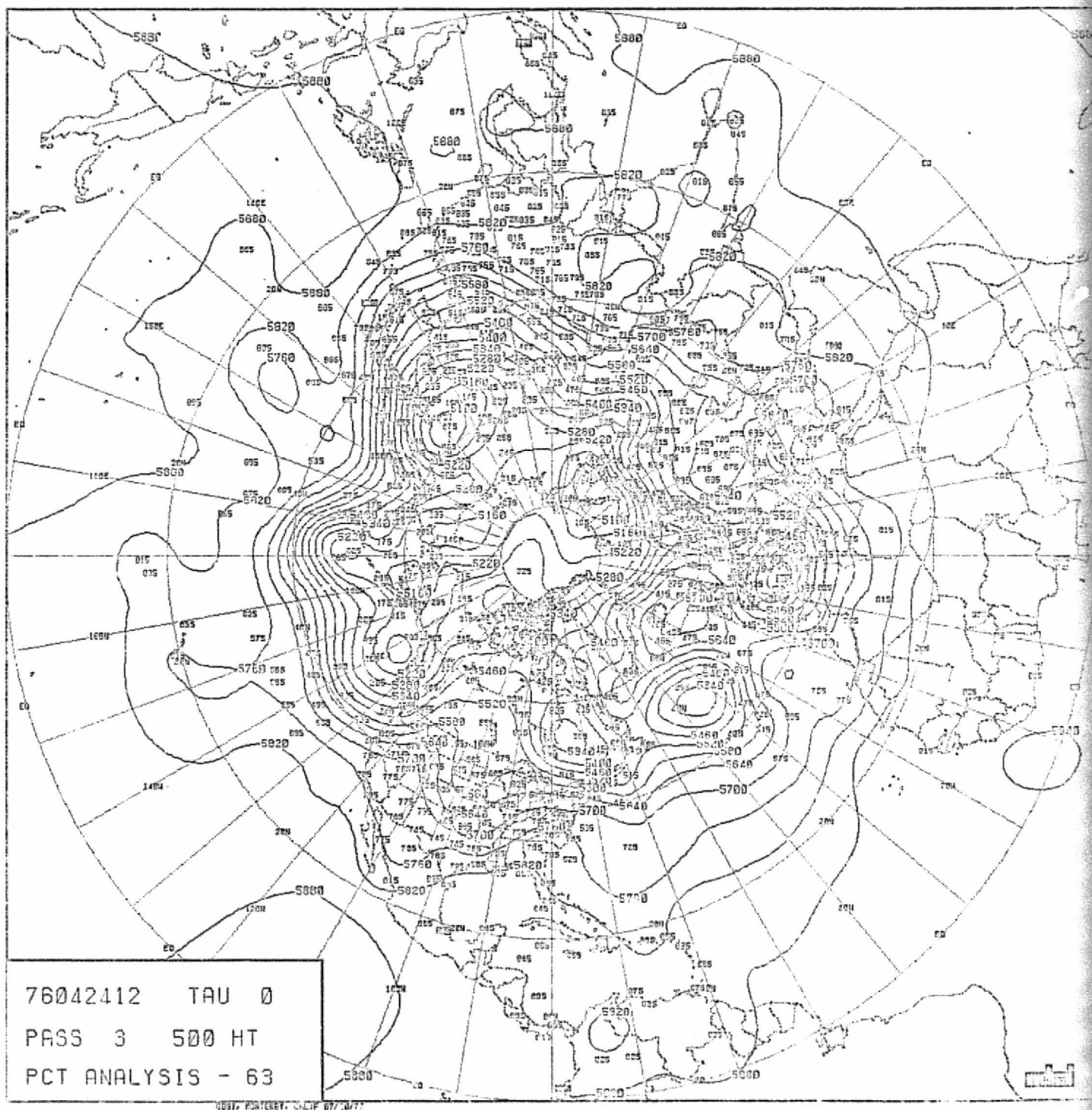
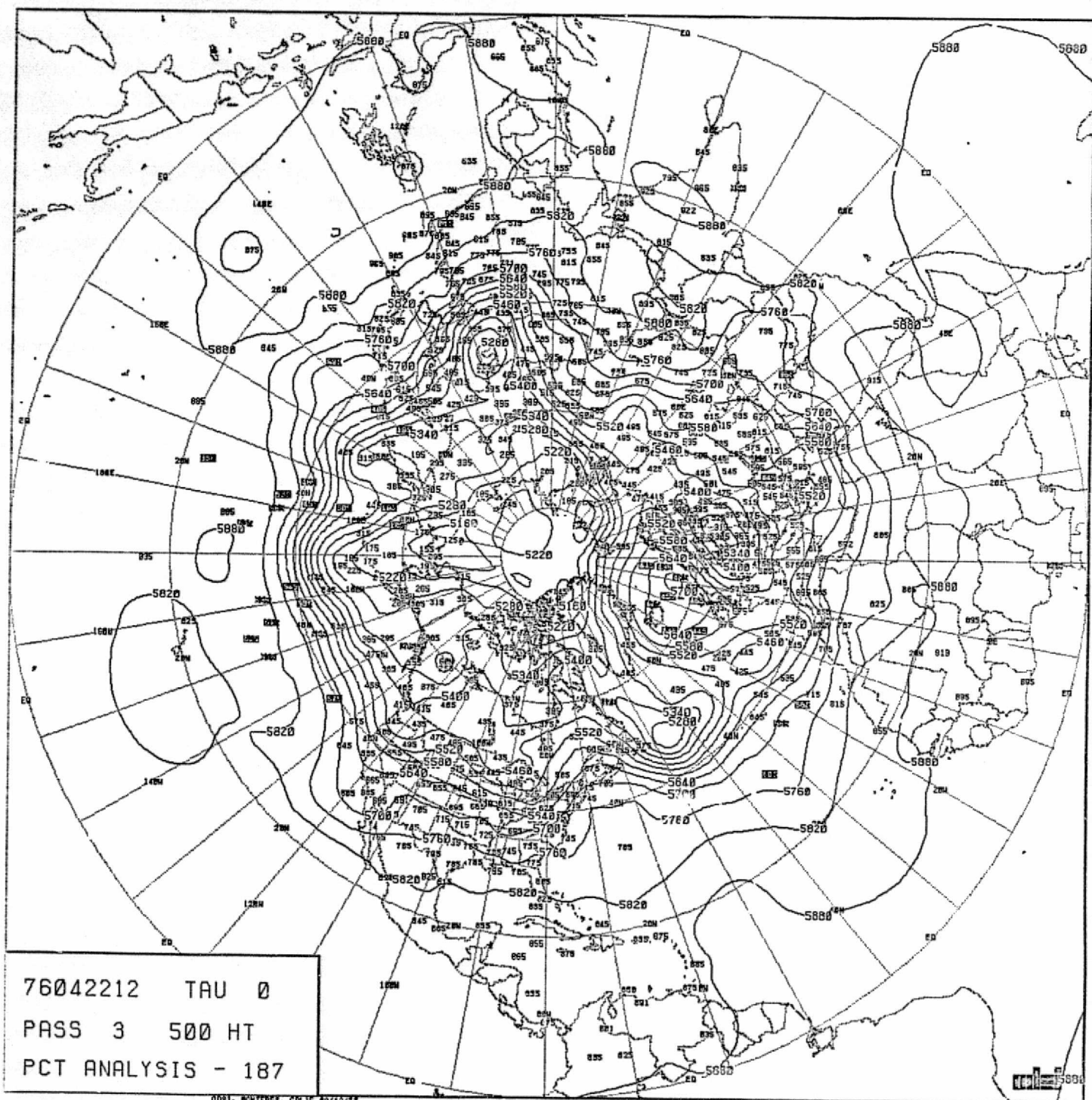


CHART VIII-7

500 MB HEIGHT ANALYSIS, 63 x 63 GRID, 1200Z,
24 APRIL 1976.

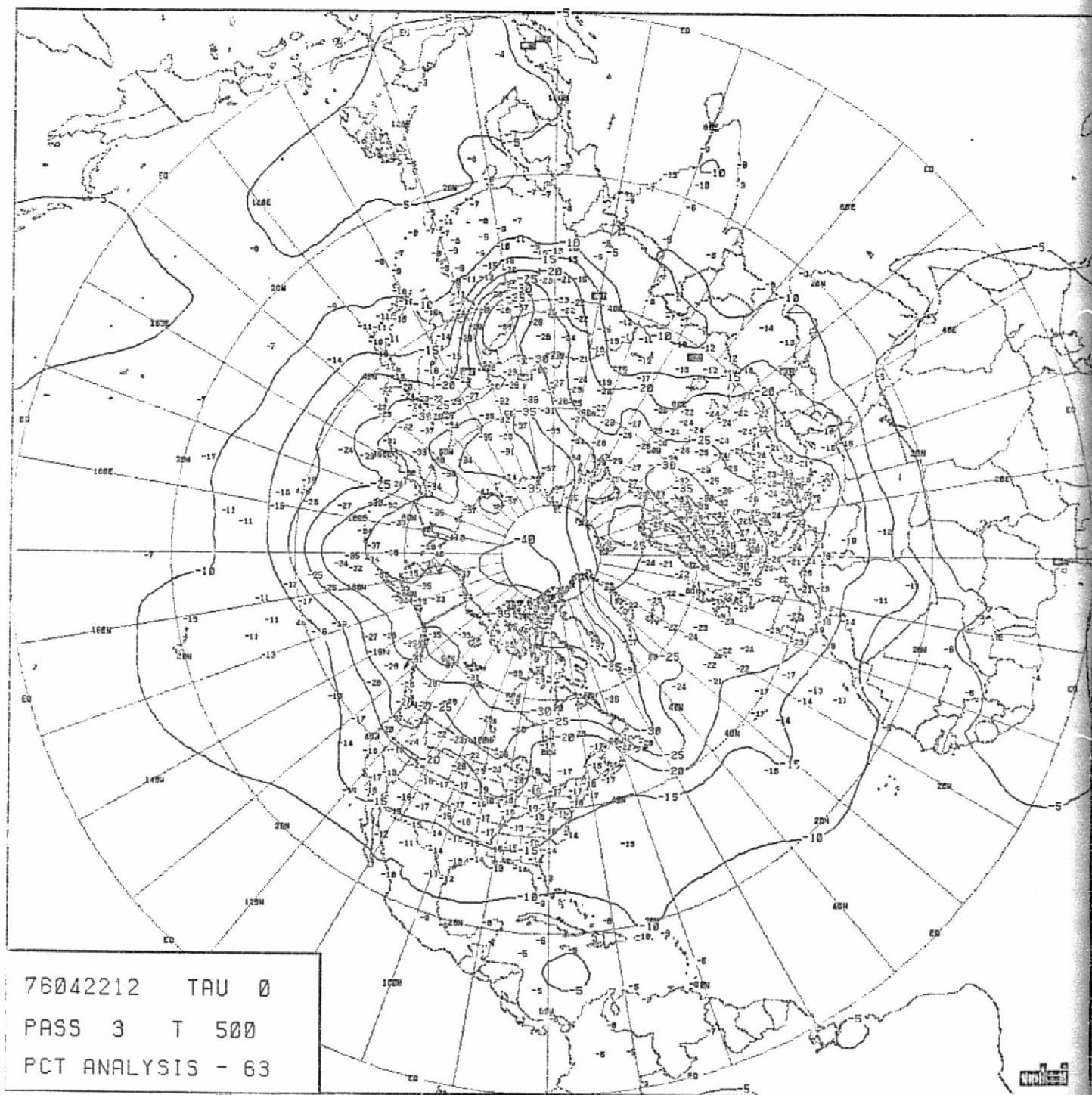


0031, MONTEREY, CALIF 00/12/77

CHART VIII-8

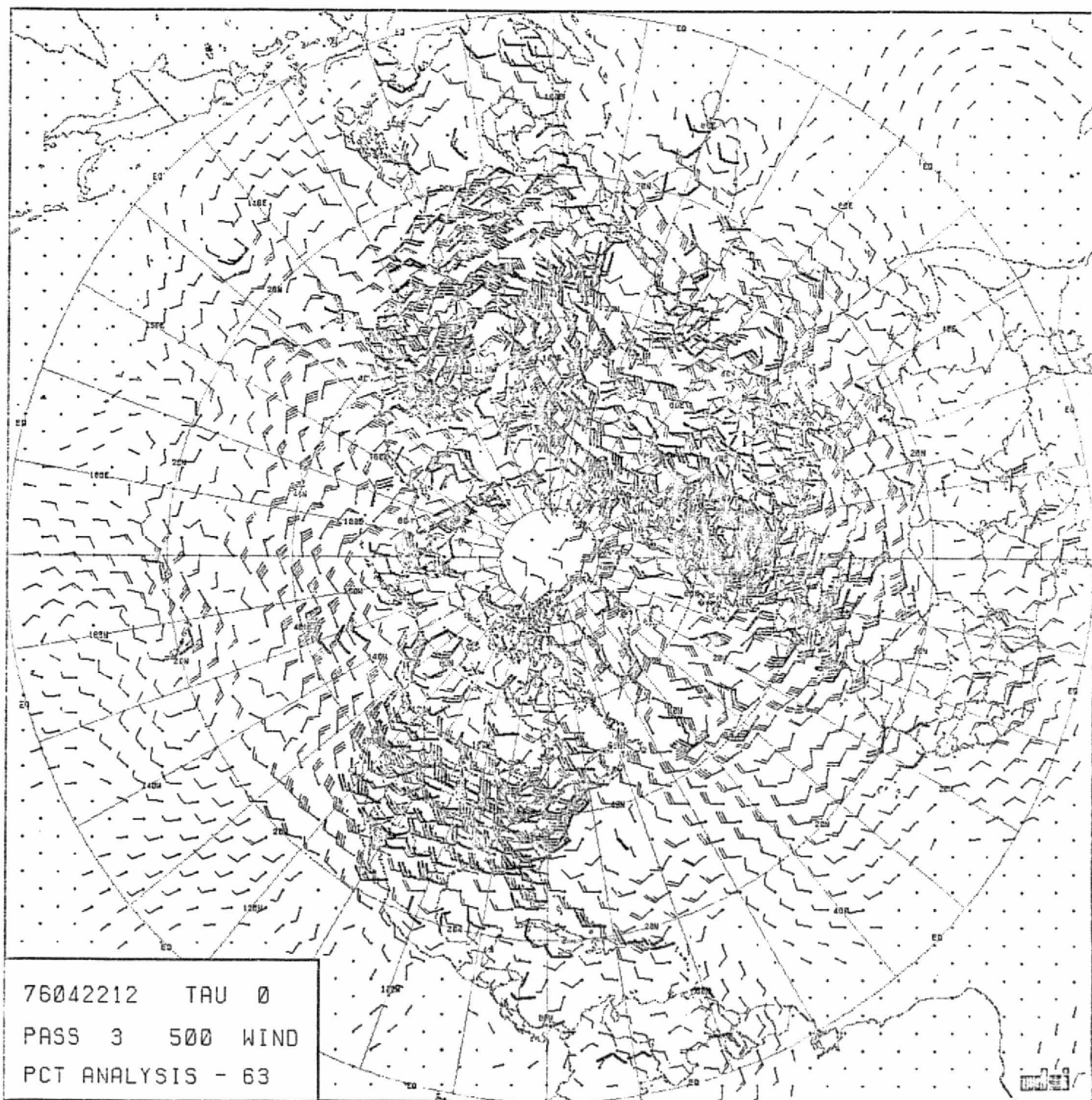
500 MB HEIGHT ANALYSIS, 187 x 187 GRID, 1200Z,
22 APRIL 1976.

ORIGINAL PAGE IS
OF POOR QUALITY



ORIGINAL PAGE IS
OF POOR QUALITY

53



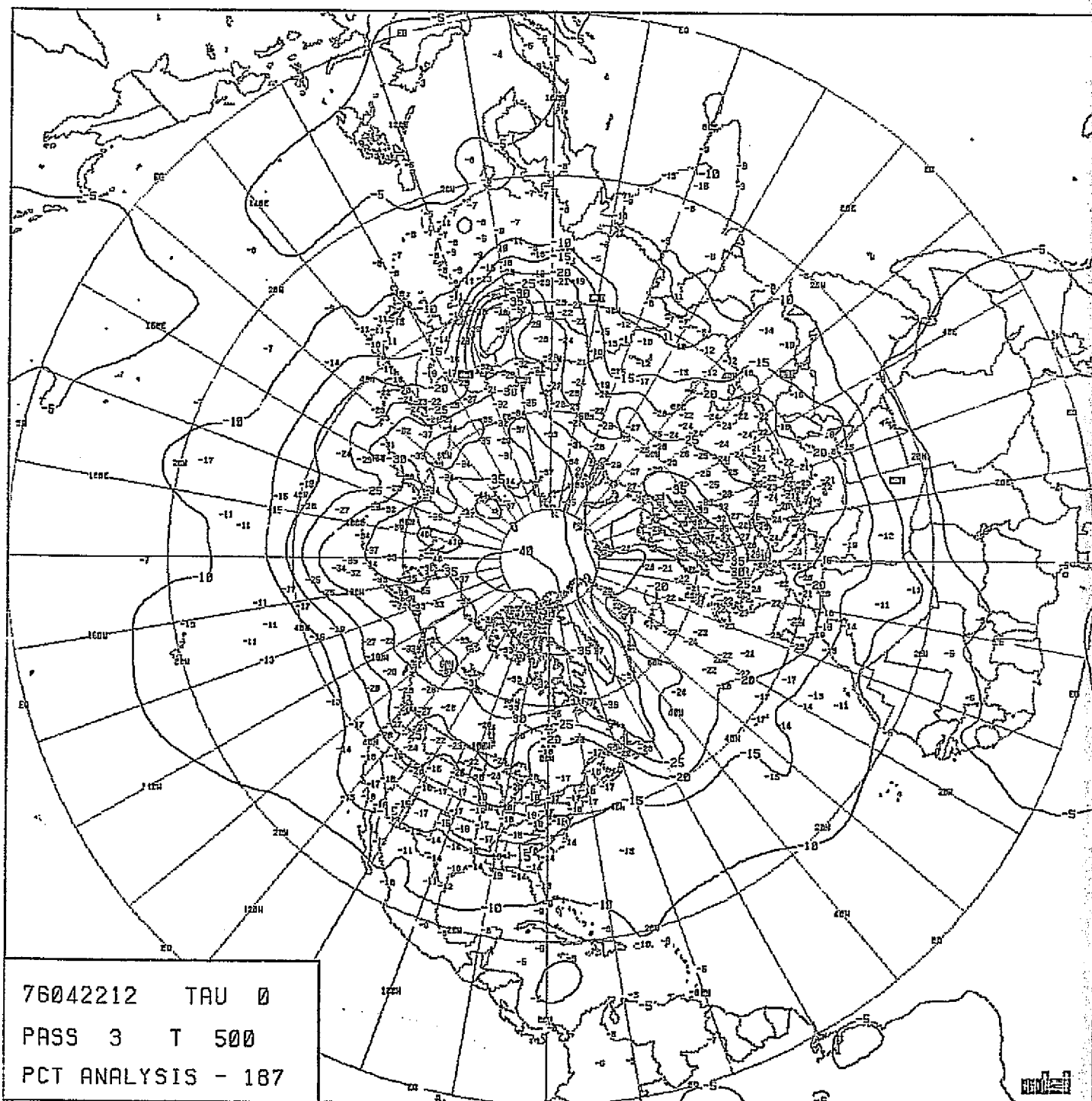
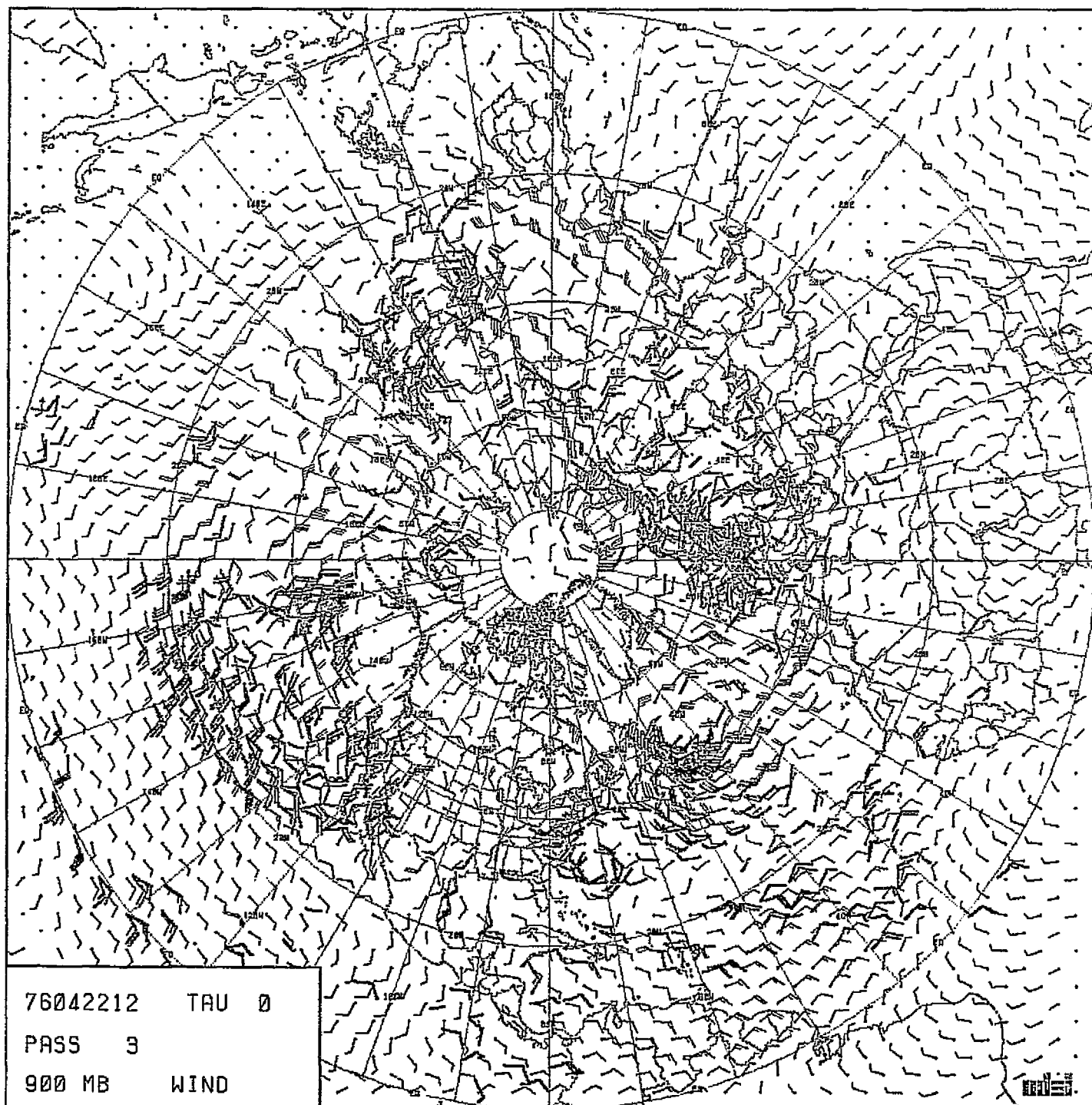


CHART VIII-11

500 MB TEMPERATURE ANALYSIS, 187 x 187 GRID,
1200Z, 22 APRIL 1976.

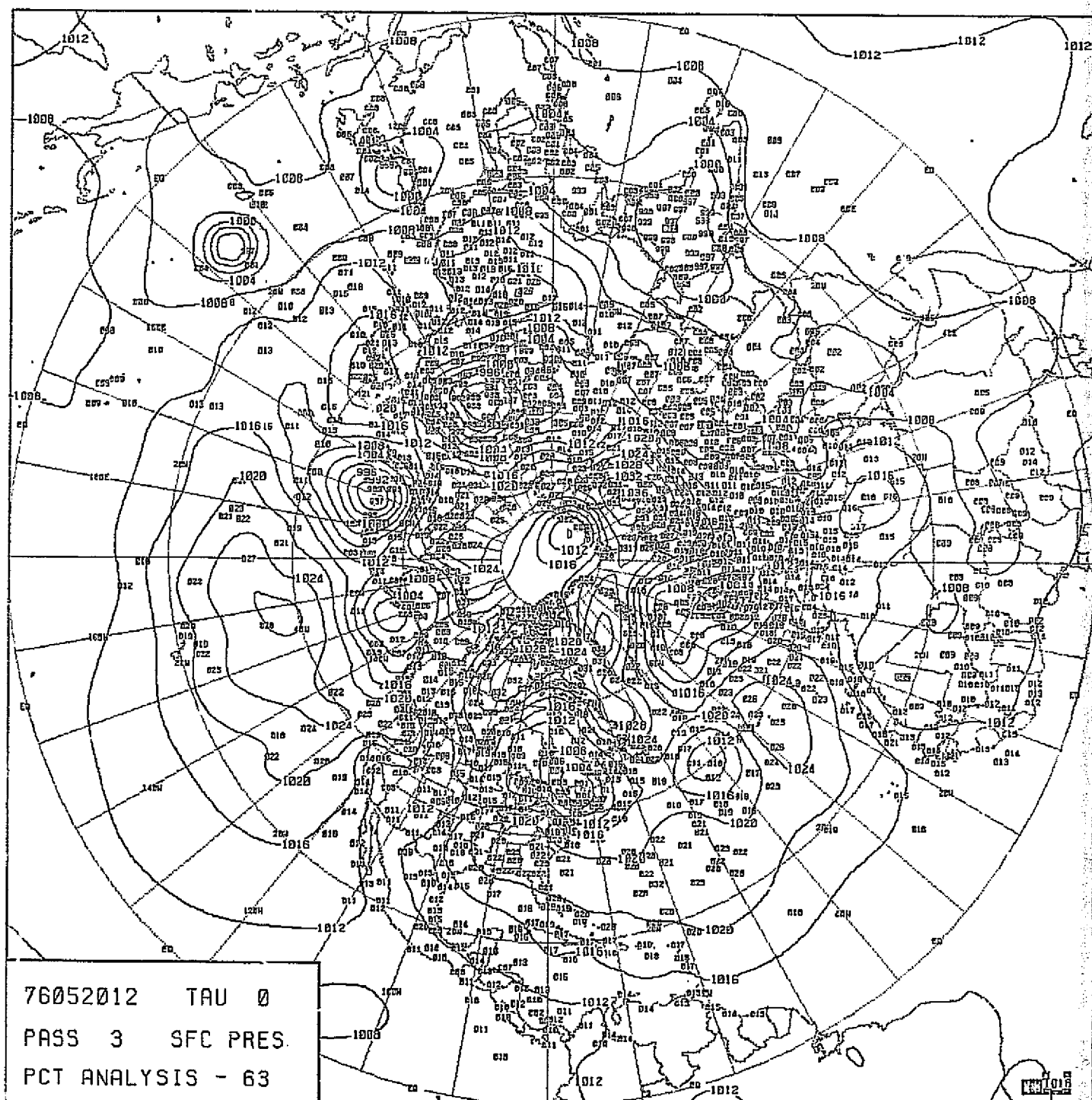
ORIGINAL PAGE IS
OF POOR QUALITY



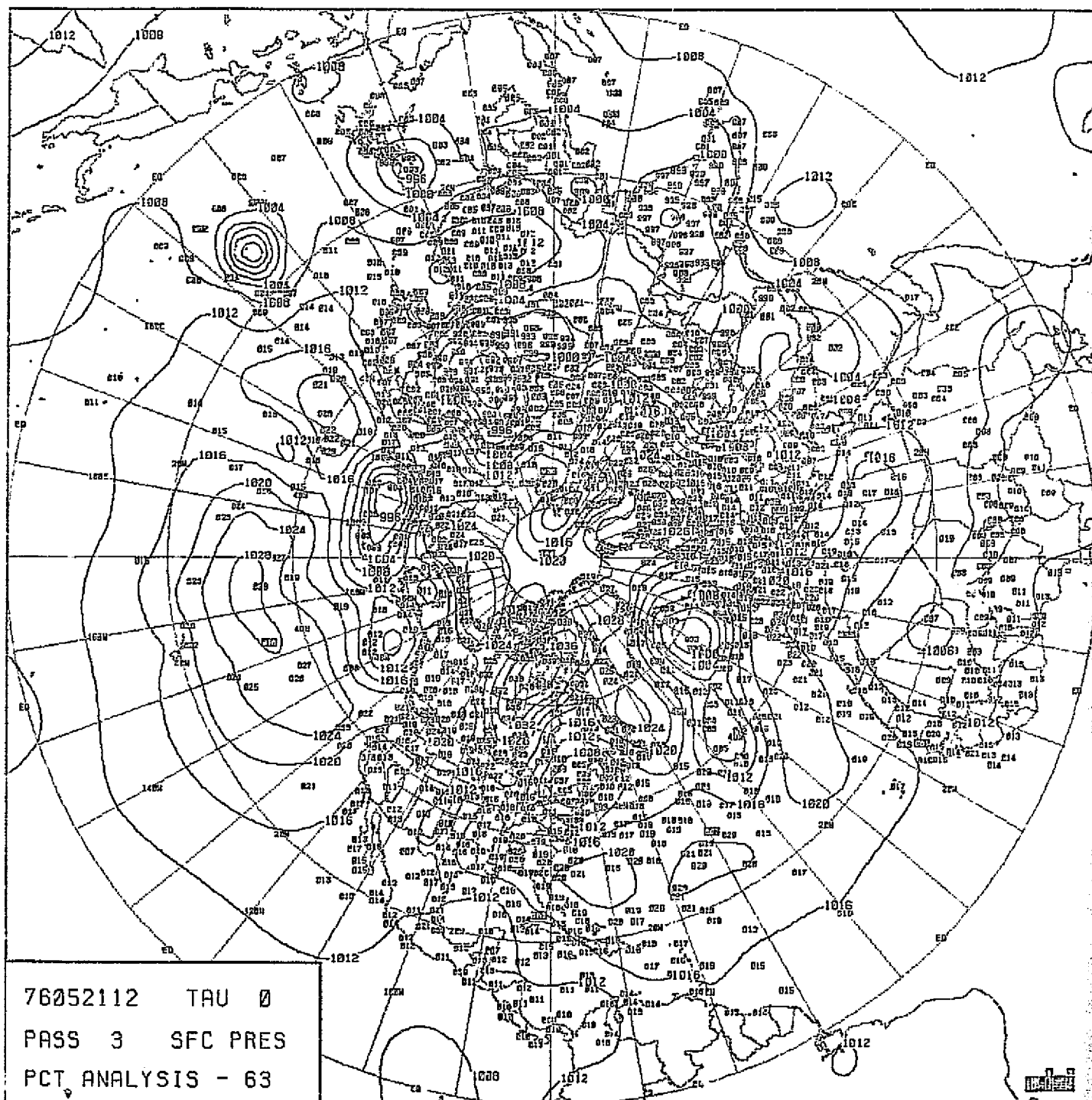
76042212 TAU 0
PASS 3
900 MB WIND

0001. MONTEREY, CALIF 11/11/76

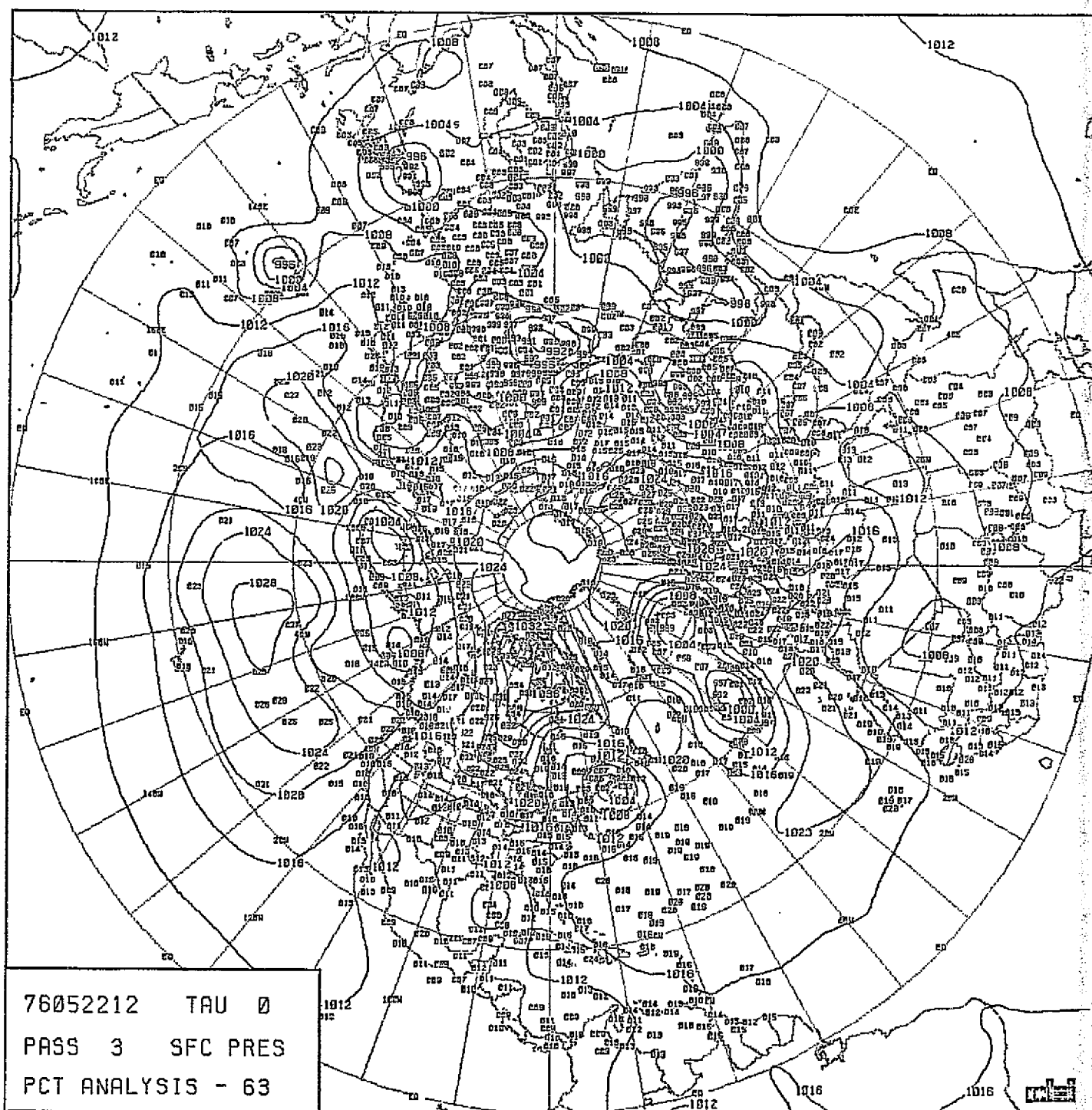
CHART VIII-12 : 900 MB WIND VECTOR ANALYSIS, 63 x 63 GRID,
1200Z, 22 APRIL 1976. WITH REPORTS.



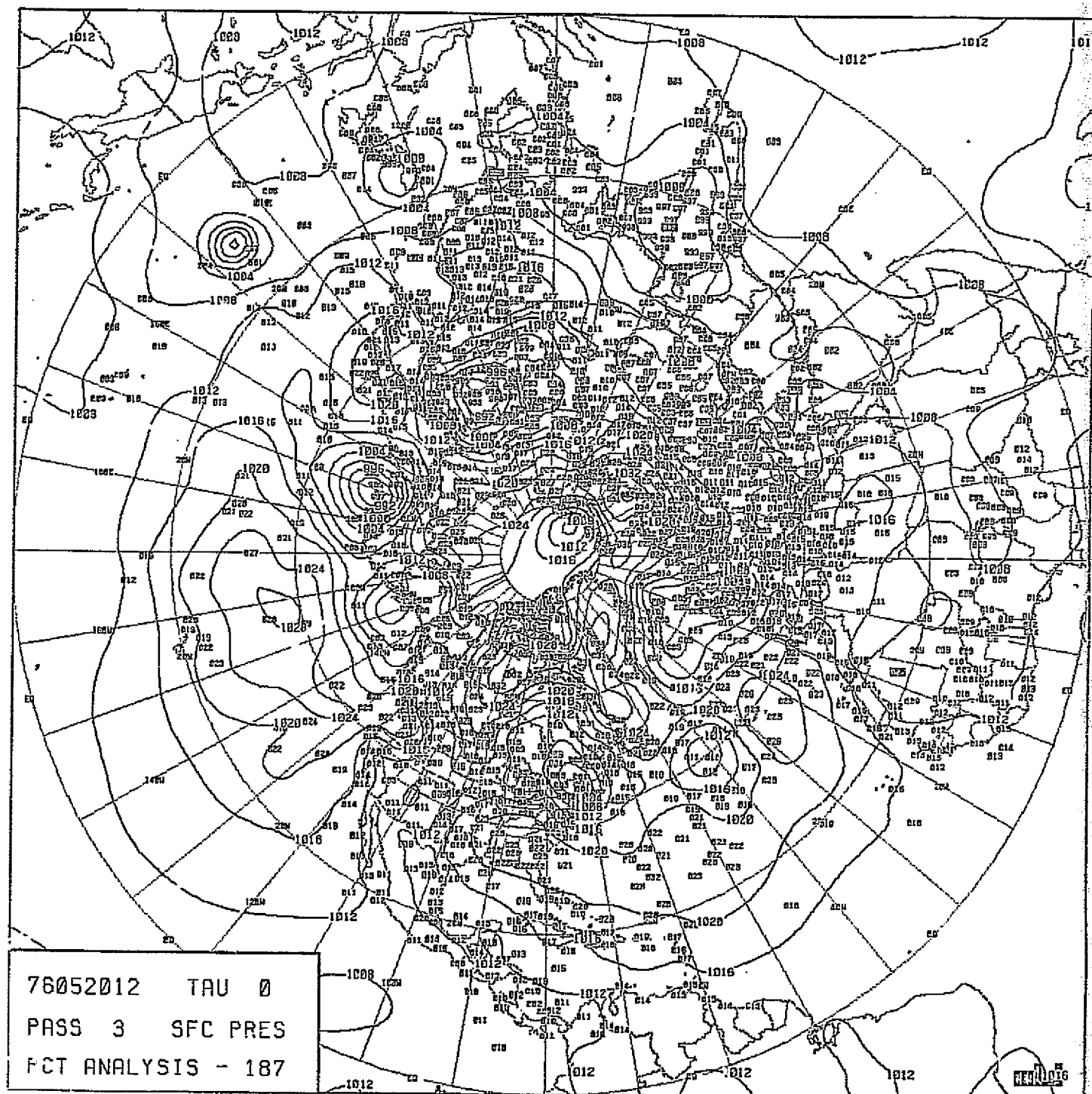
ORIGINAL PAGE IS
OF POOR QUALITY



ORIGINAL PAGE IS
OF POOR QUALITY



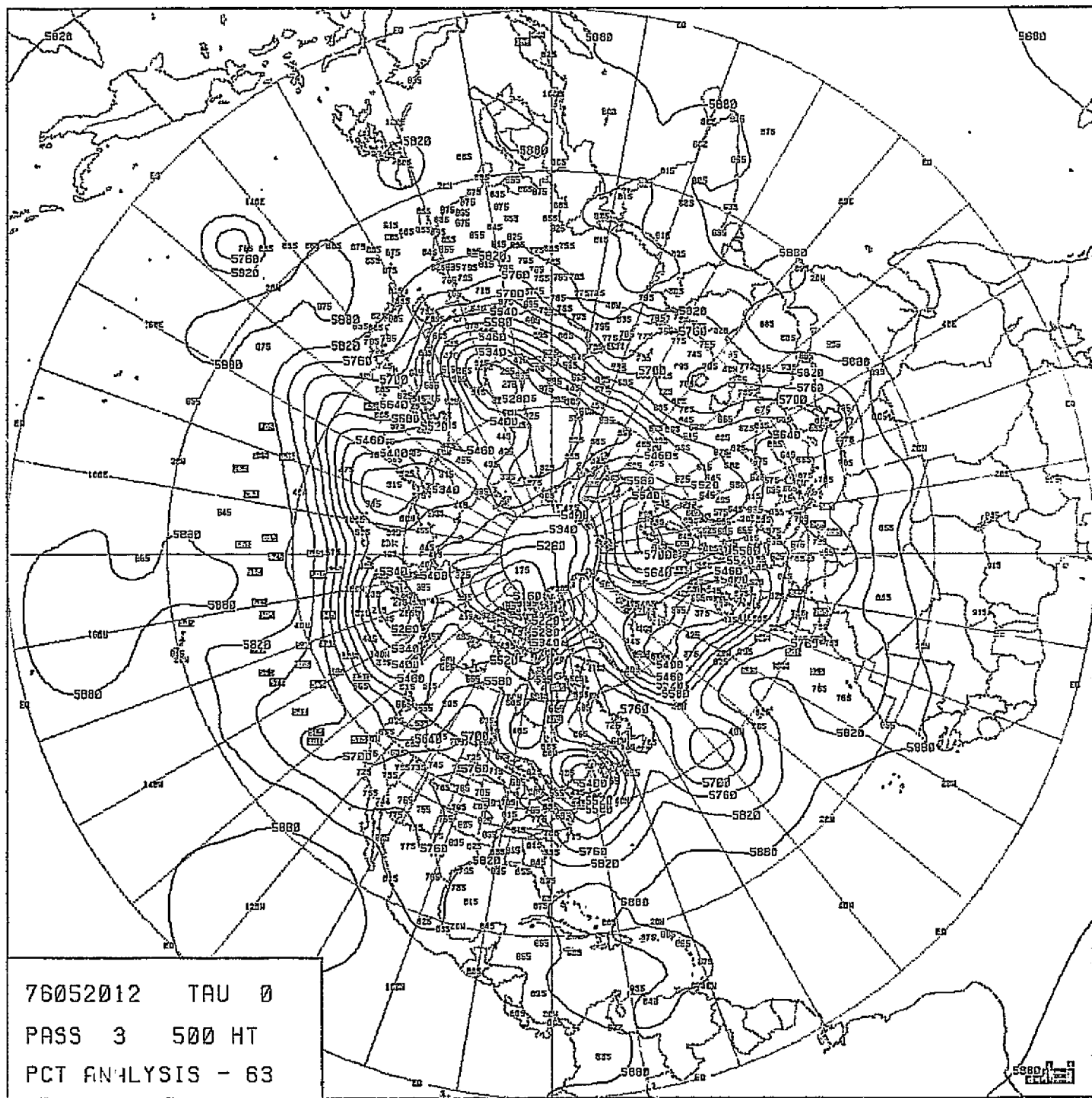
ORIGINAL PAGE IS
OF POOR QUALITY



CGO, ZAMREK, CHIF 68/13/77

CHART VIII-16

SEA-LEVEL PRESSURE ANALYSIS, 187 x 187 GRID,
1200Z, 20 MAY 1976.



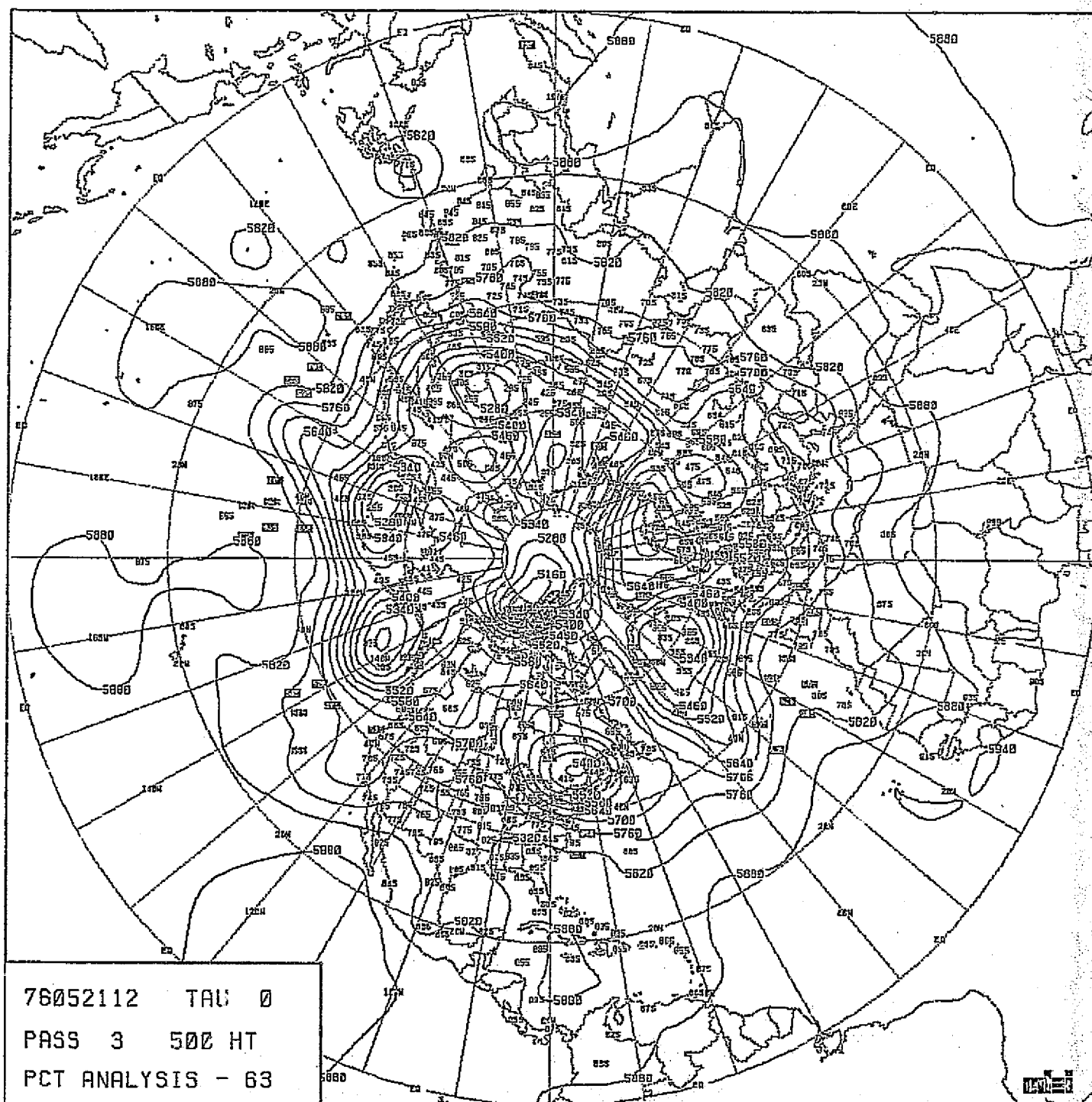


CHART VIII-18

500 MB HEIGHT ANALYSIS, 63 x 63 GRID, 1200Z,
21 MAY 1976.

ORIGINAL PAGE IS
OF POOR QUALITY

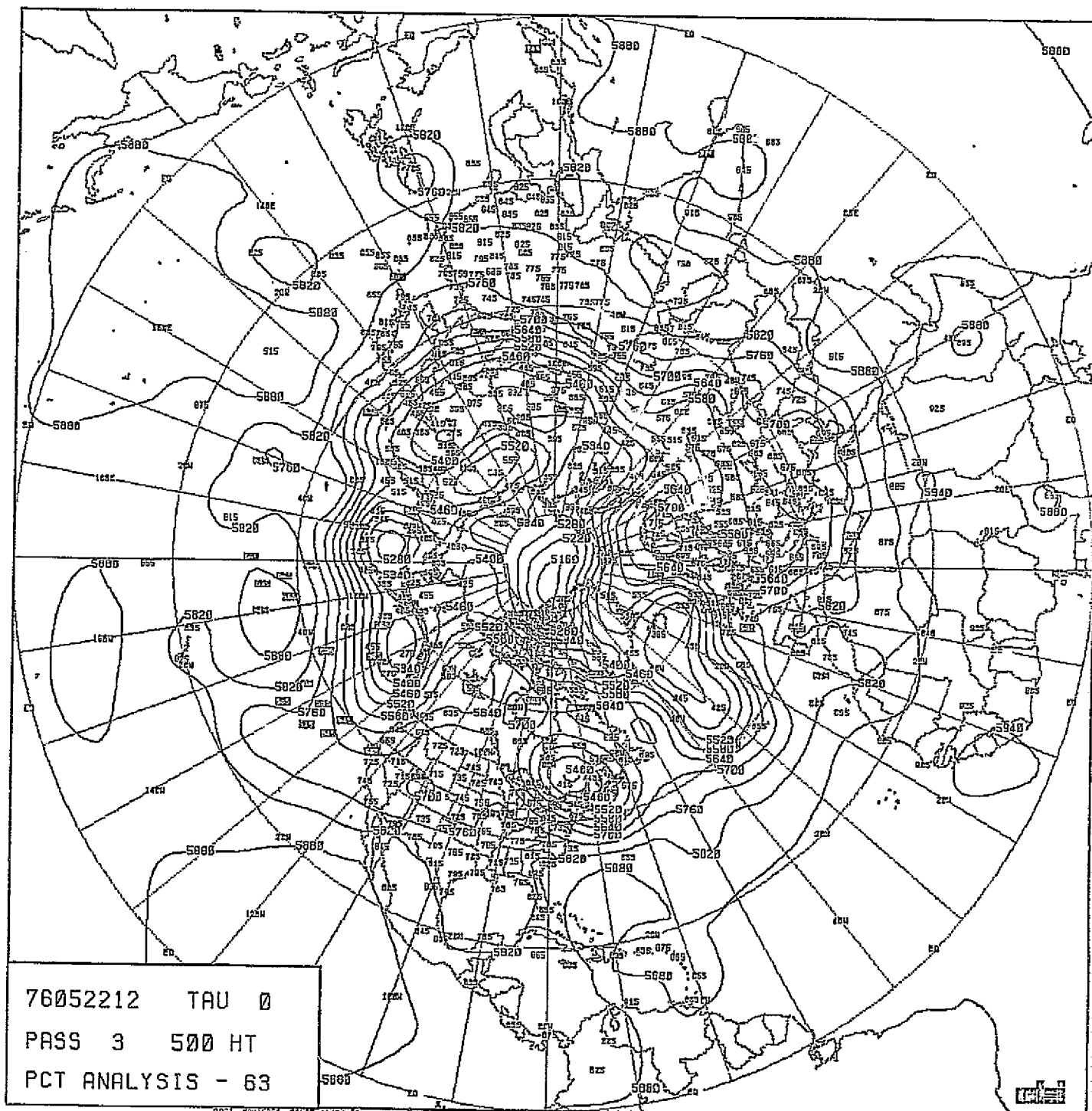


CHART VIII-19

500 MB HEIGHT ANALYSIS, 63 x 63 GRID, 1200Z,
22 MAY 1976.

ORIGINAL PAGE IS
POOR QUALITY

ORIGINAL PAGE IS
POOR QUALITY

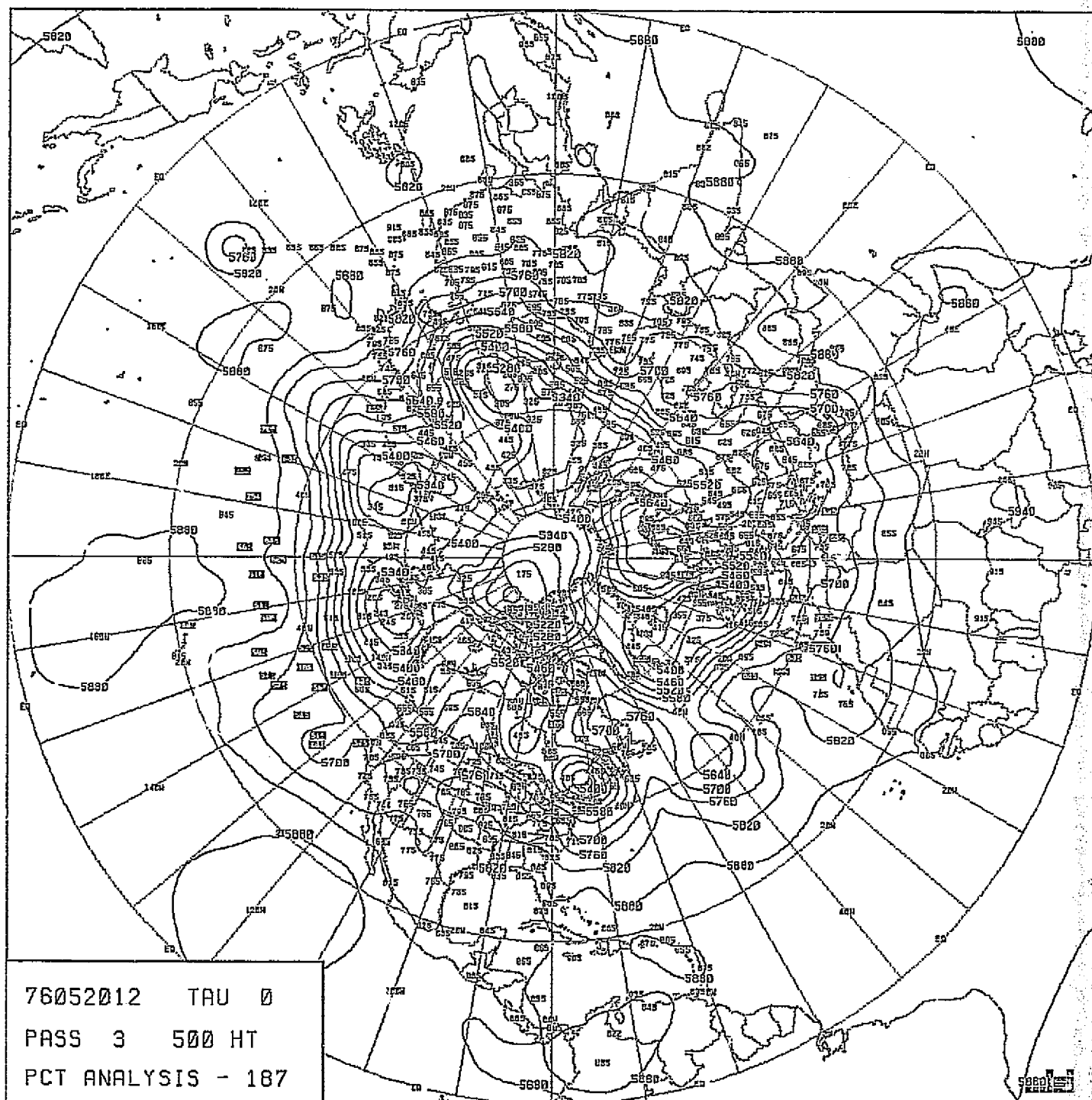
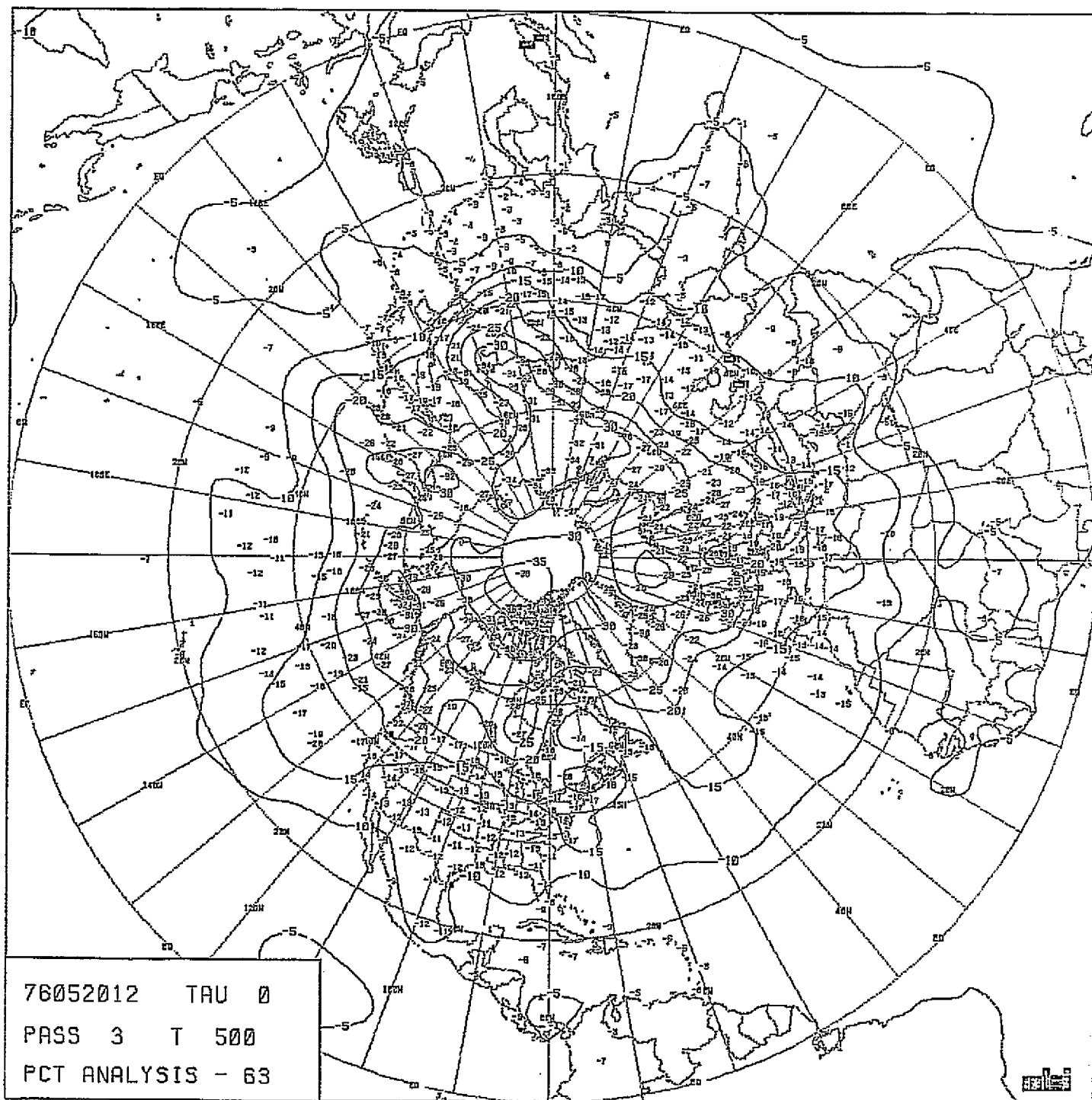


CHART VIII-20

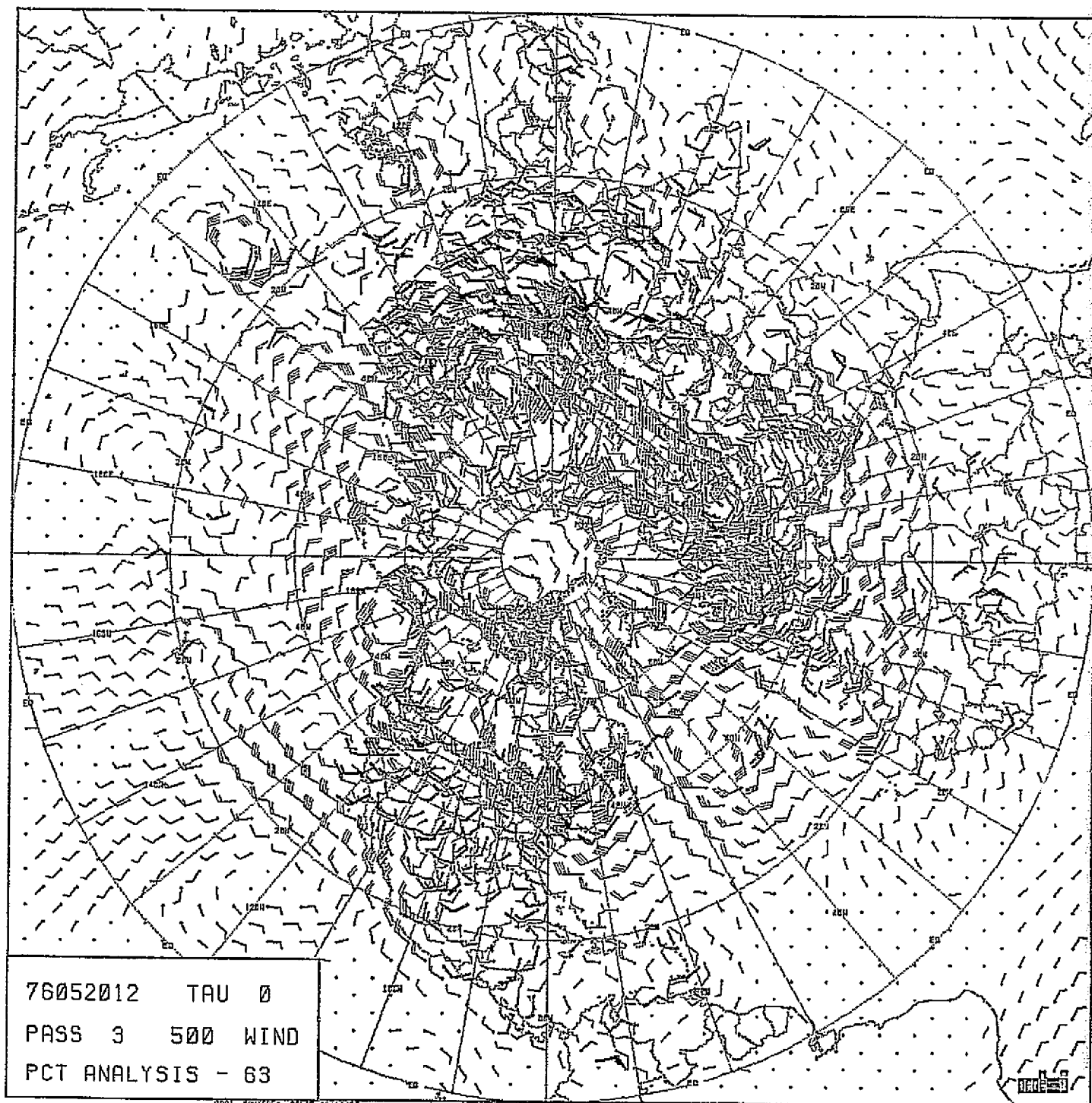
500 MB HEIGHT ANALYSIS, 187 x 187 GRID, 1200Z,
20 MAY 1976.



0031, 001000, 001000, 001000

CHART VIII-21

500 MB TEMPERATURE ANALYSIS, 63 x 63 GRID,
1200Z, 20 MAY 1976.



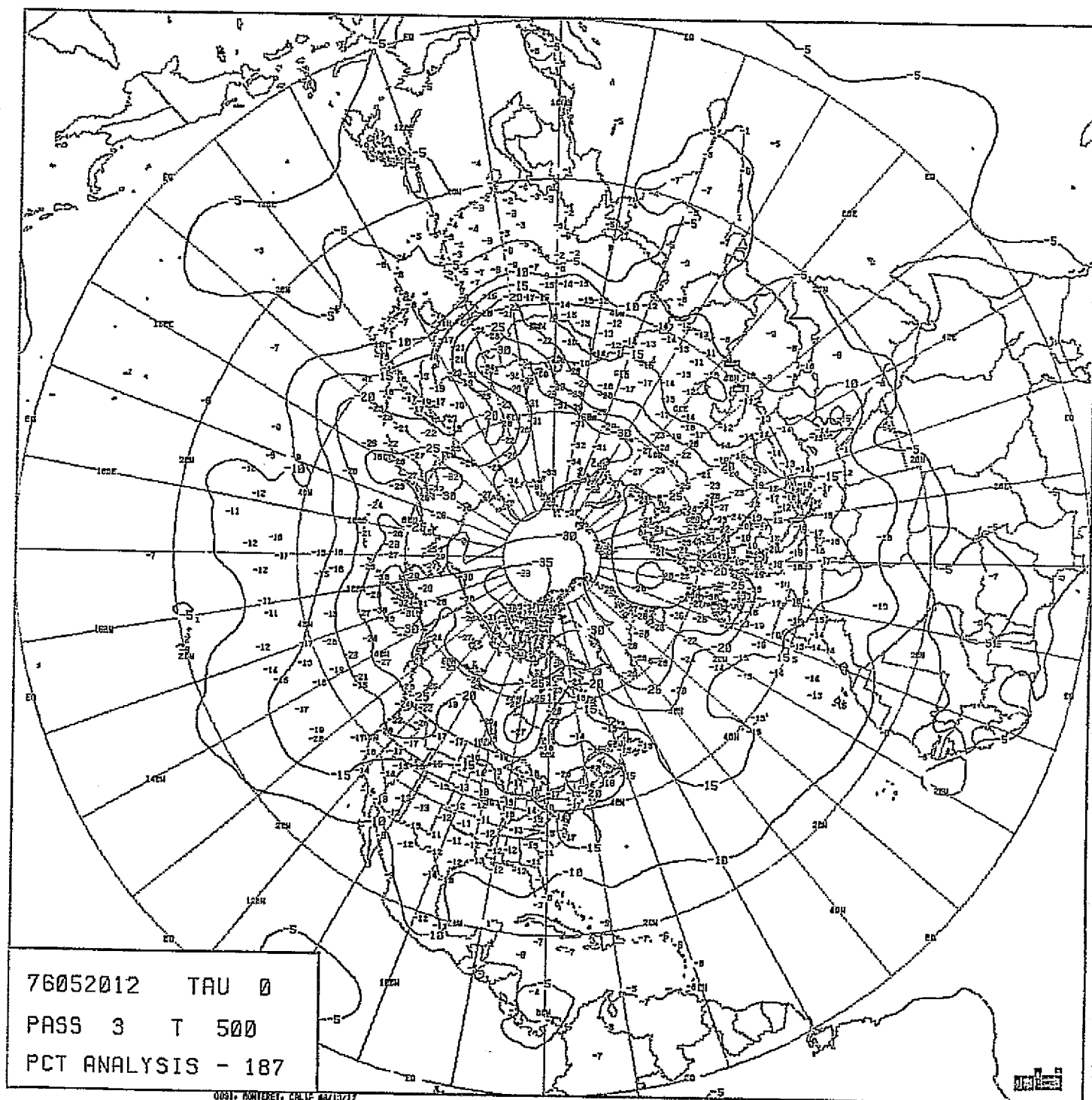
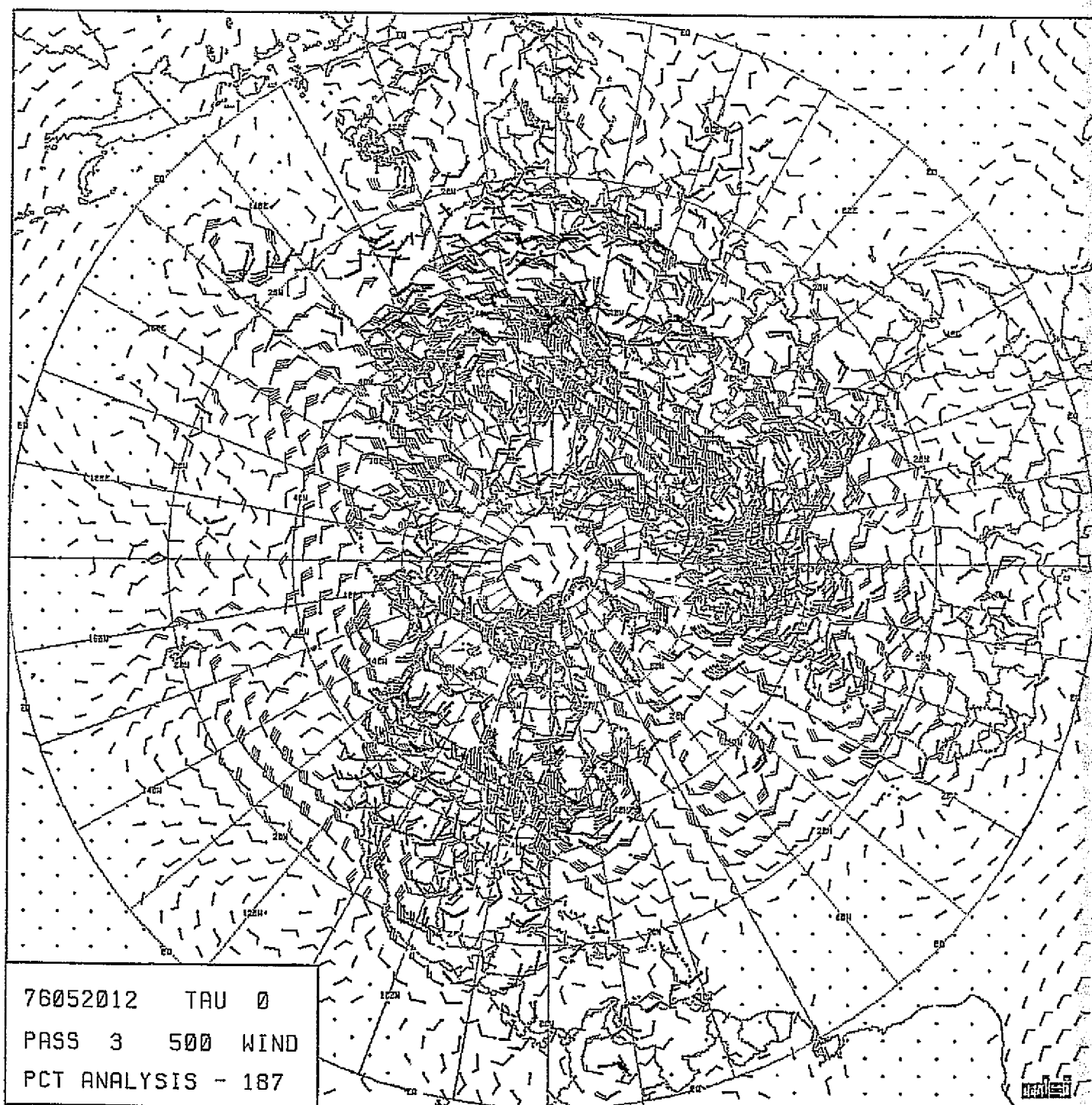


CHART VIII-23

500 MB TEMPERATURE ANALYSIS, 187 x 187 GRID,
1200Z, 20 MAY 1976.

**ORIGINAL PAGE IS
OF POOR QUALITY**



500 MB WIND VECTOR ANALYSIS, 187 x 187 GRID,
1200Z, 20 MAY 1976.

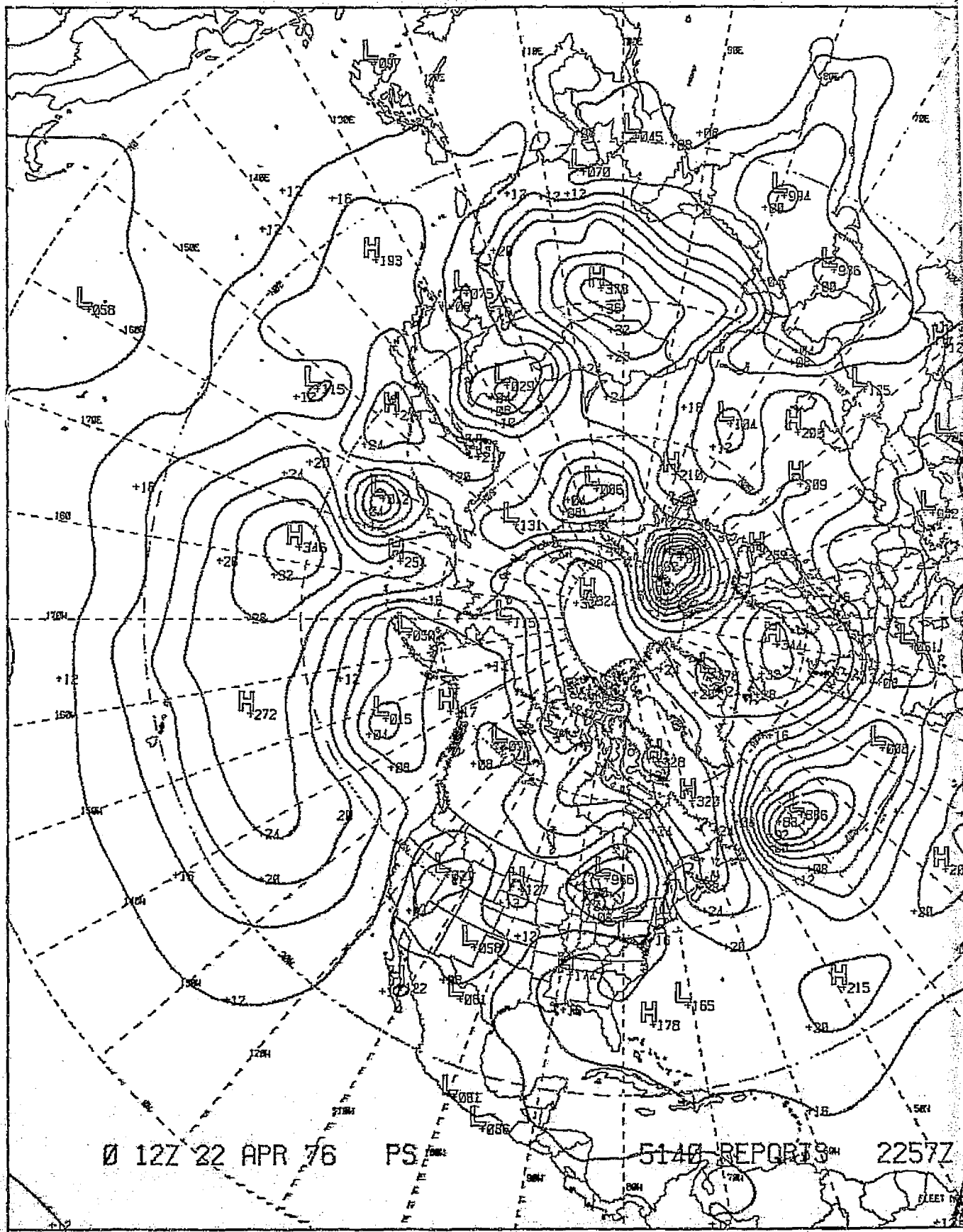


CHART VIII-25 : FNWC SEA-LEVEL PRESSURE ANALYSIS, 1200Z,
22 APRIL 1976.

ORIGINAL PAGE IS
OF POOR QUALITY

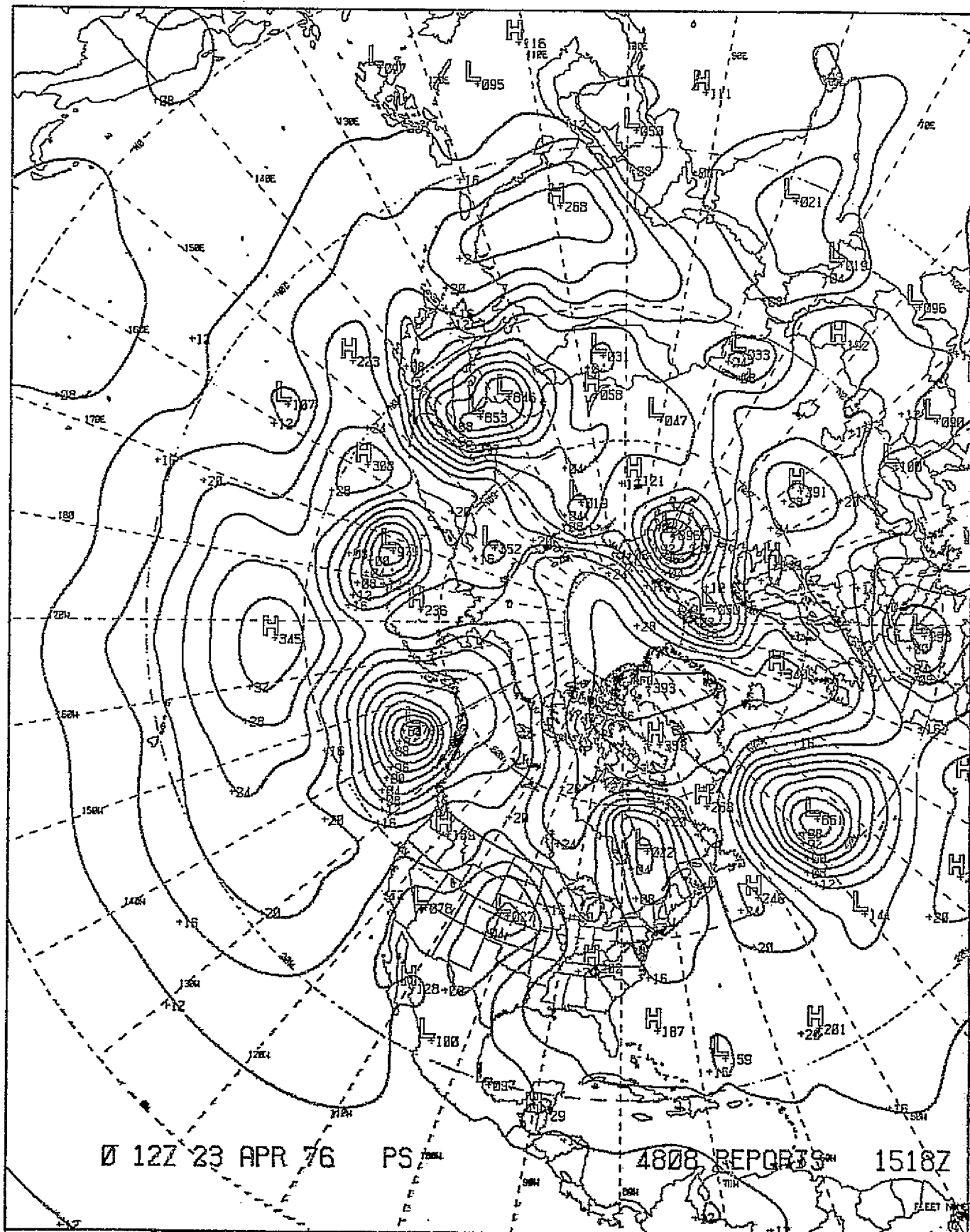
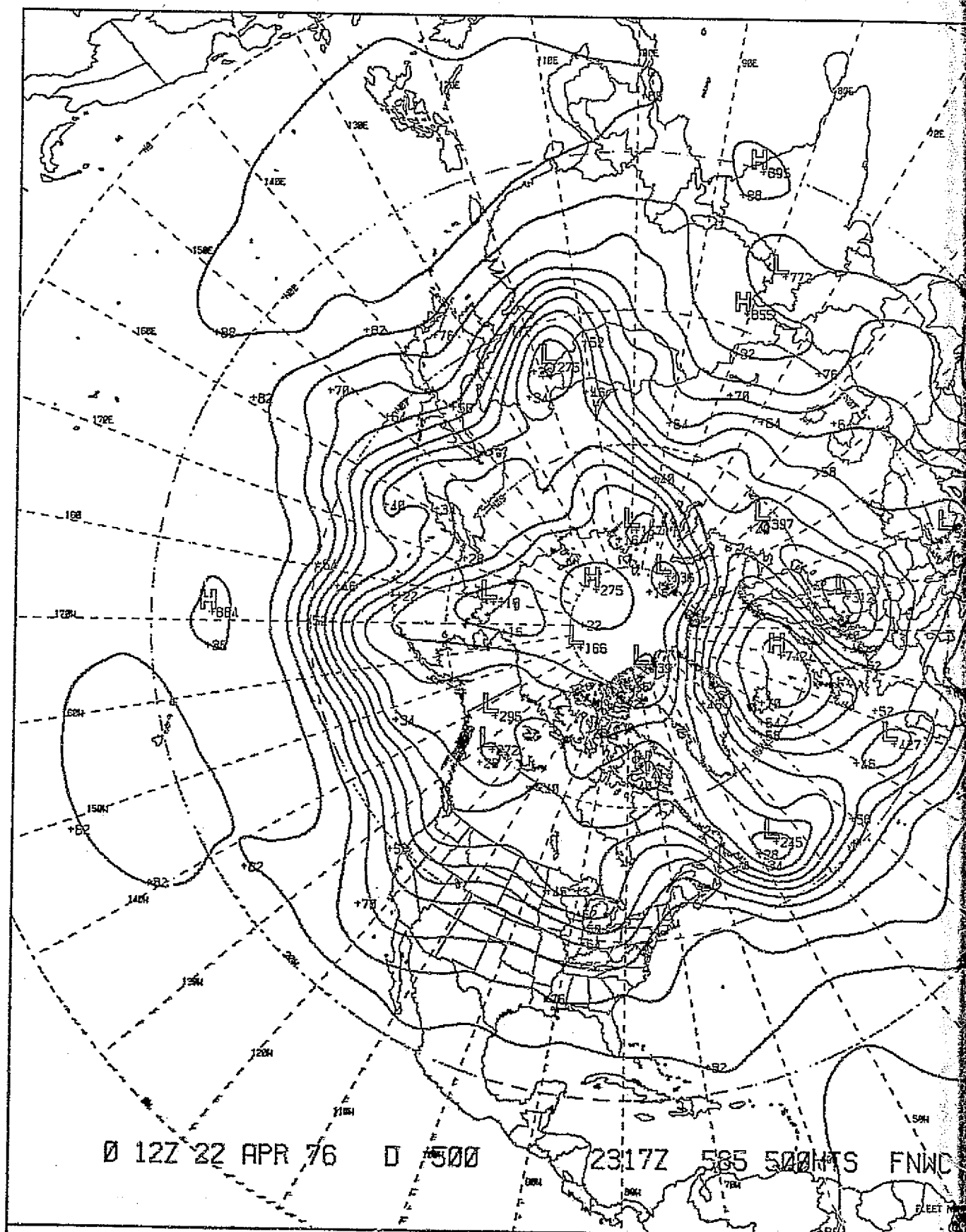


CHART VIII-26 : FNWC SEA-LEVEL PRESSURE ANALYSIS, 1200Z,
23 APRIL 1976.



0 12Z 22 APR 76

D 500

2317Z

585

500HRS

FNWC

CHART VIII-27 : FNWC 500 MB HEIGHT ANALYSIS, 1200Z,
22 APRIL 1976.

ORIGINAL PAGE IS
OF POOR QUALITY

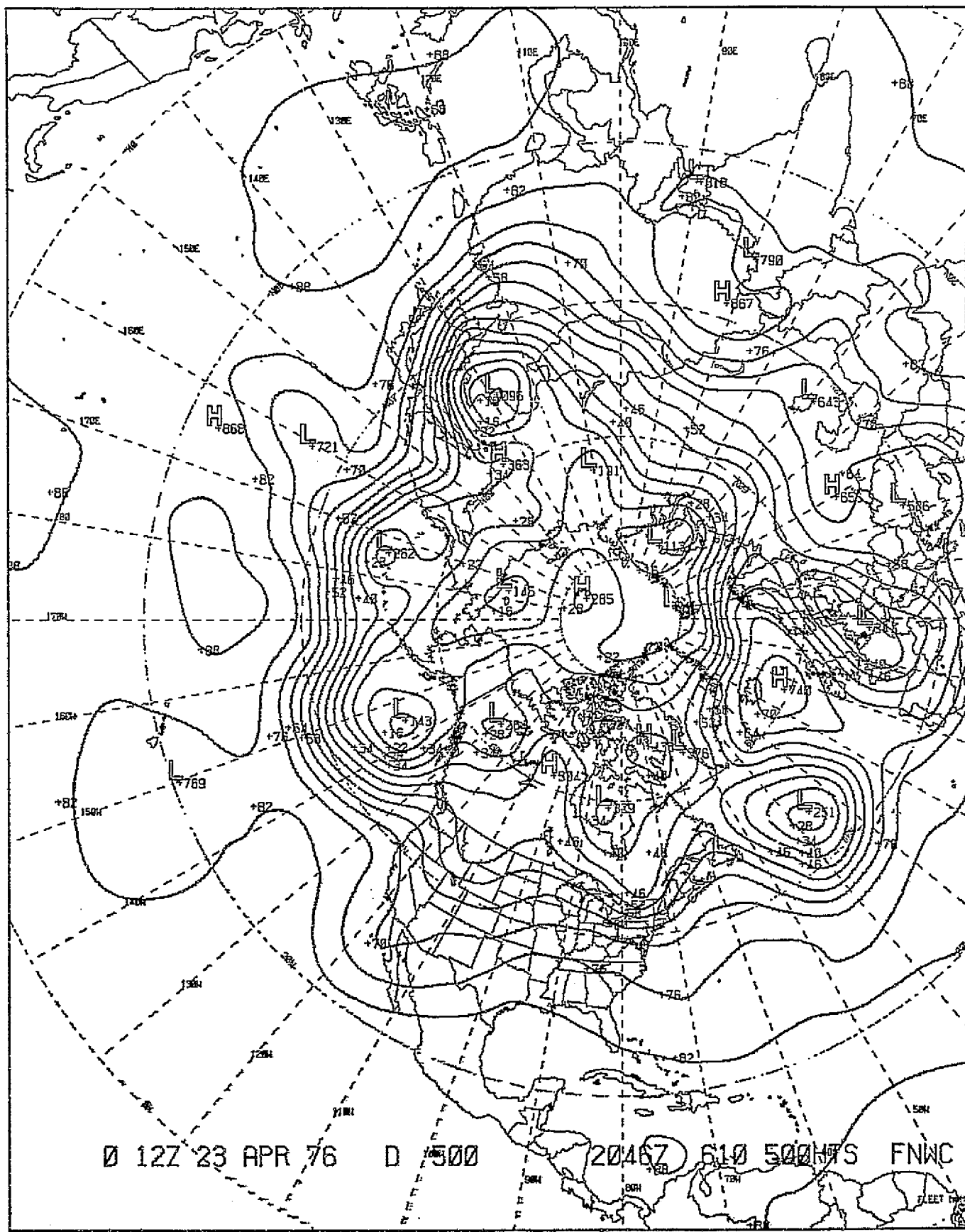


CHART VIII-28 : FNWC 500 MB HEIGHT ANALYSIS, 1200Z,
23 APRIL 1976.

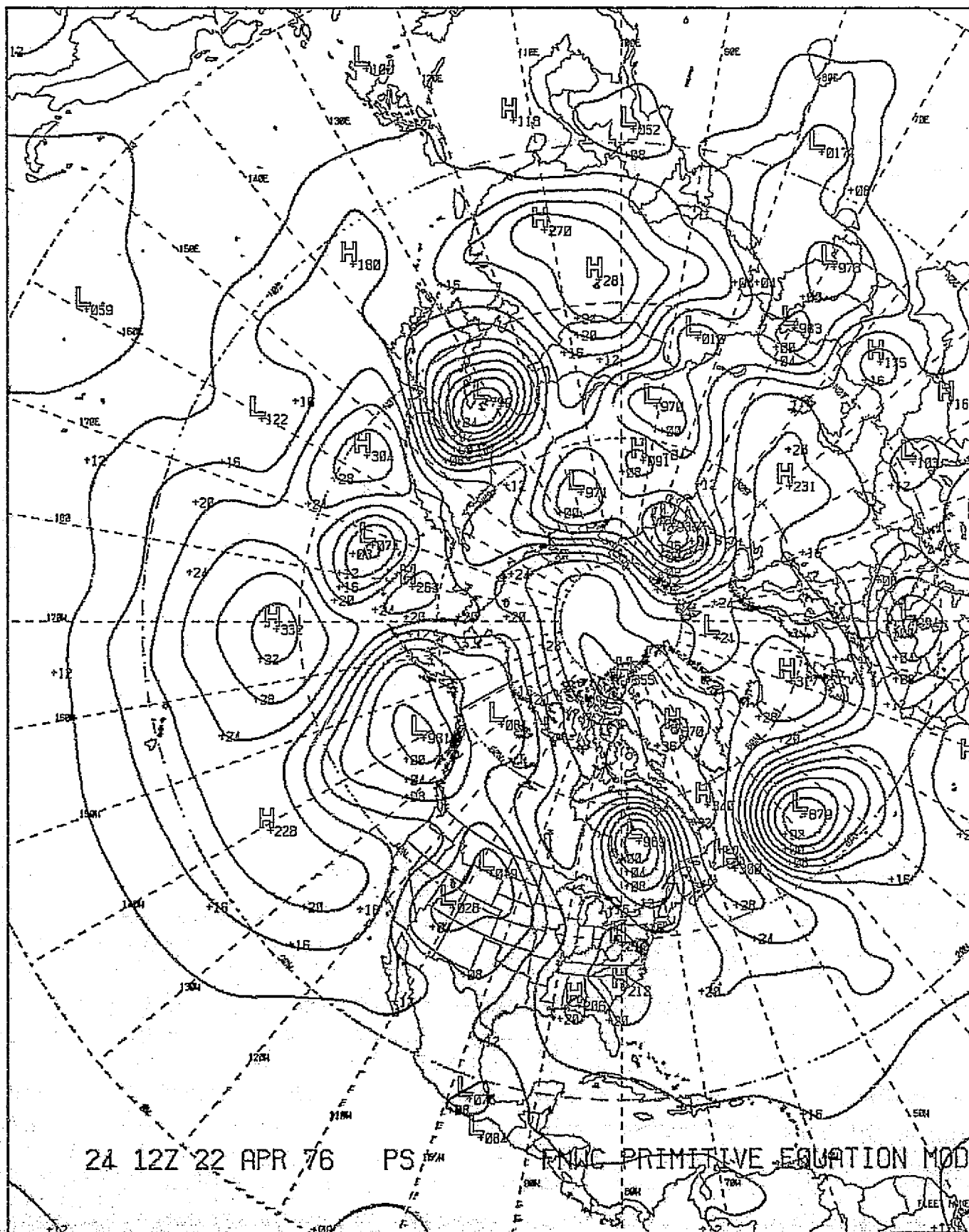


CHART VIII-29 : FNMC 24-HOUR SEA-LEVEL PRESSURE FORECAST
FROM 1200Z, 22 APRIL 1976.

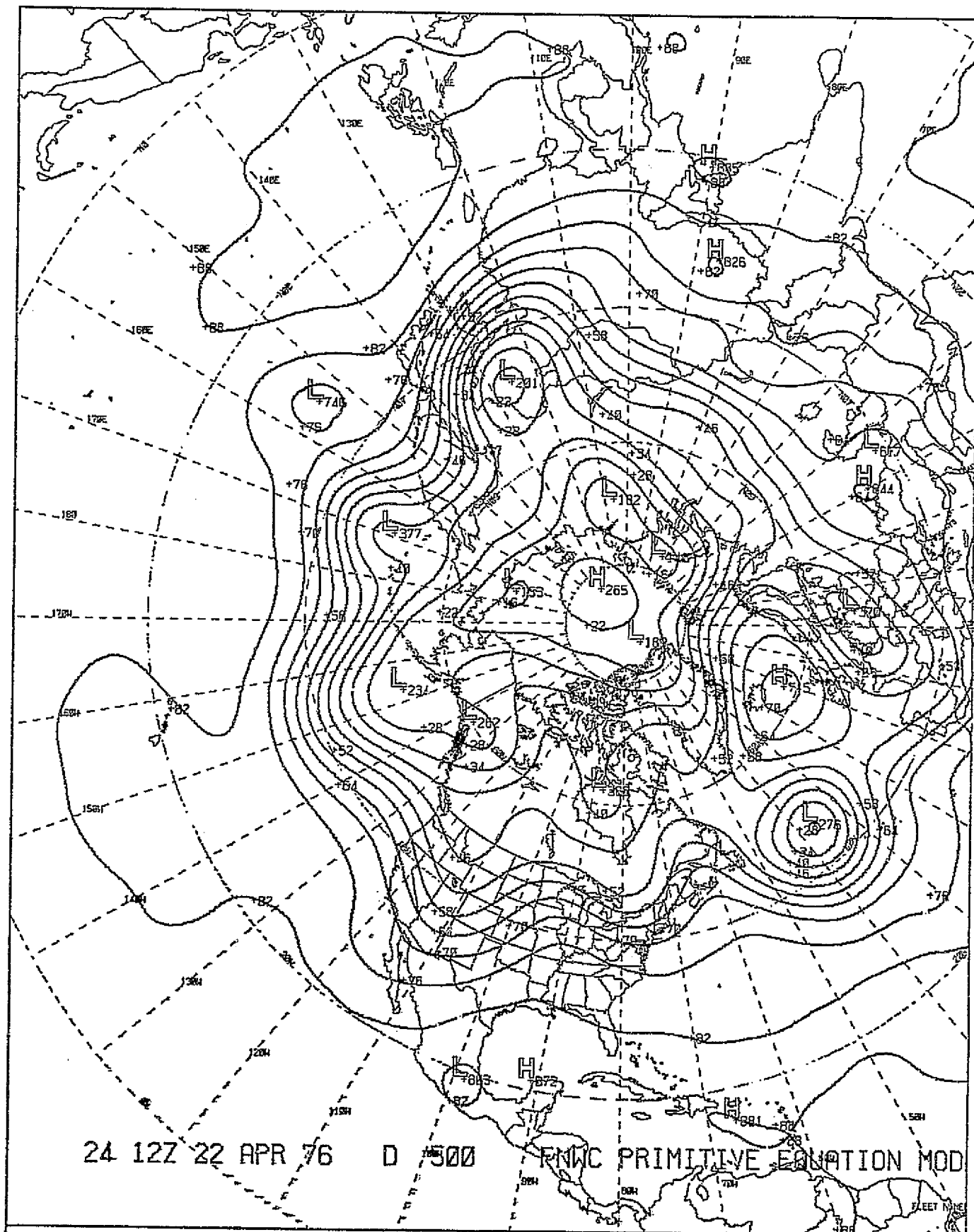


CHART VIII-30 : FNNC 24-HOUR 500 MB HEIGHT FORECAST FROM 1200Z, 22 APRIL 1976.

ORIGINAL PAGE IS
OF POOR QUALITY

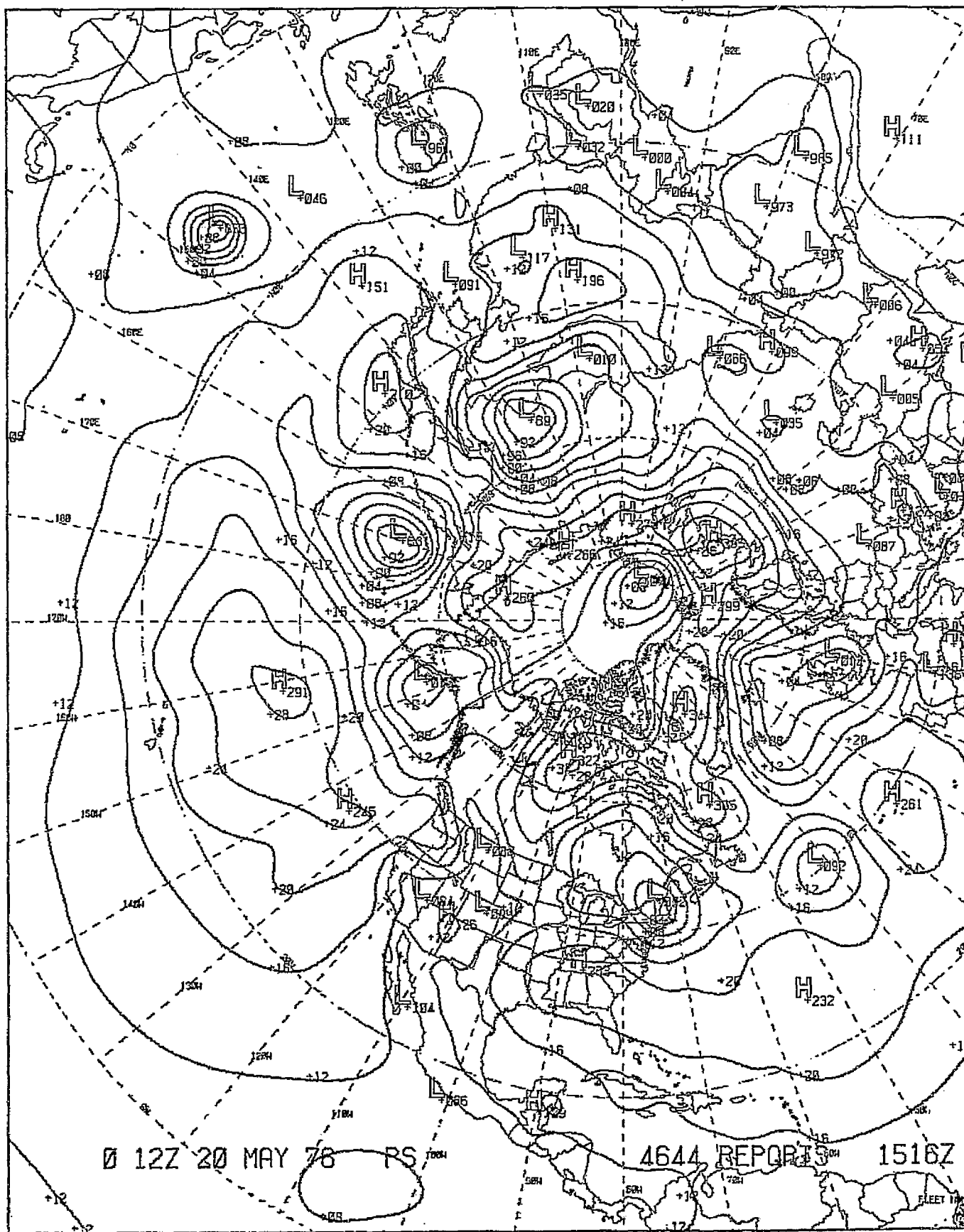


CHART VIII-31 : FNWC SEA-LEVEL PRESSURE ANALYSIS, 1200Z,
20 MAY 1976.

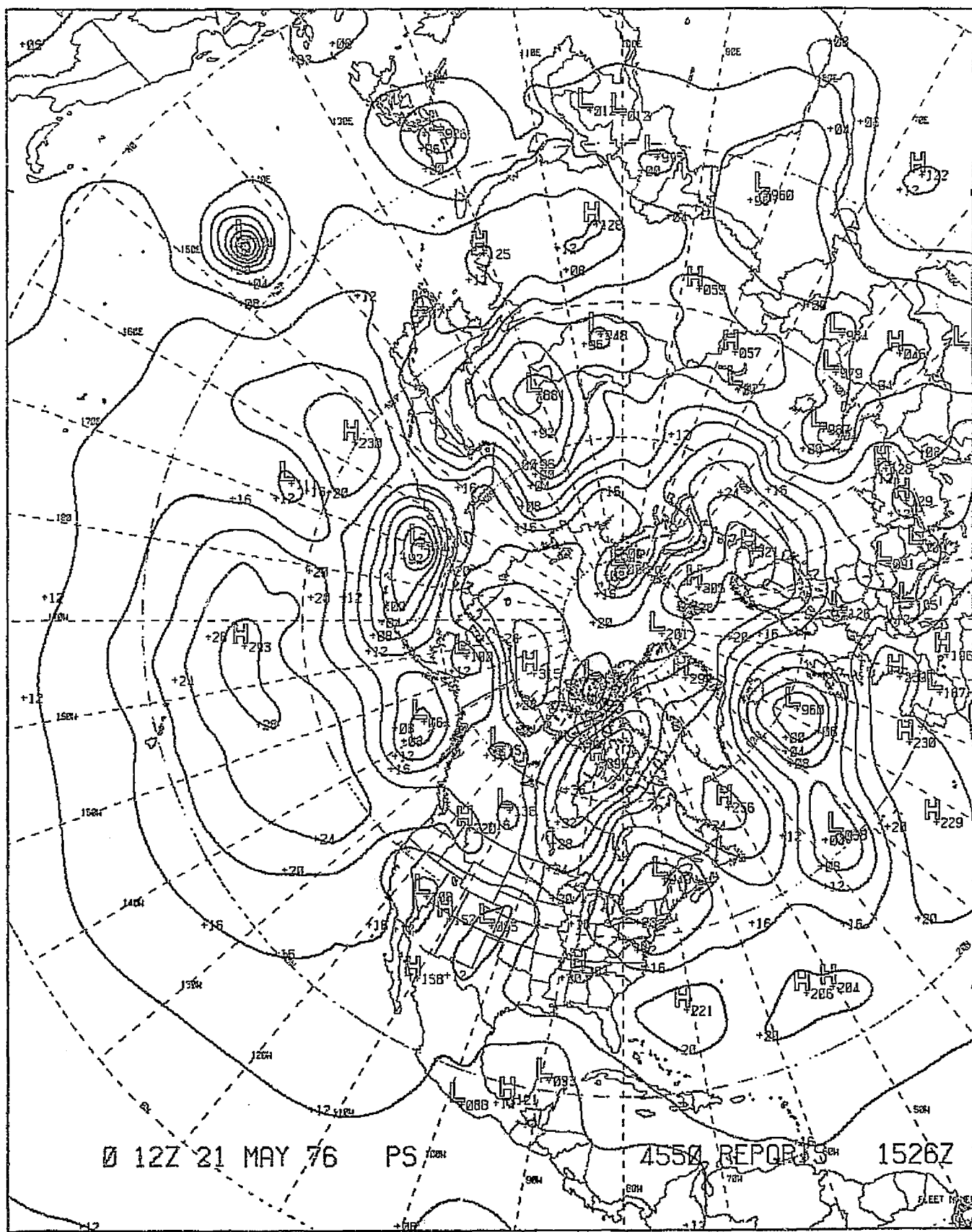


CHART VIII-32 : FNWC SEA-LEVEL PRESSURE ANALYSIS, 1200Z,
21 MAY 1976.

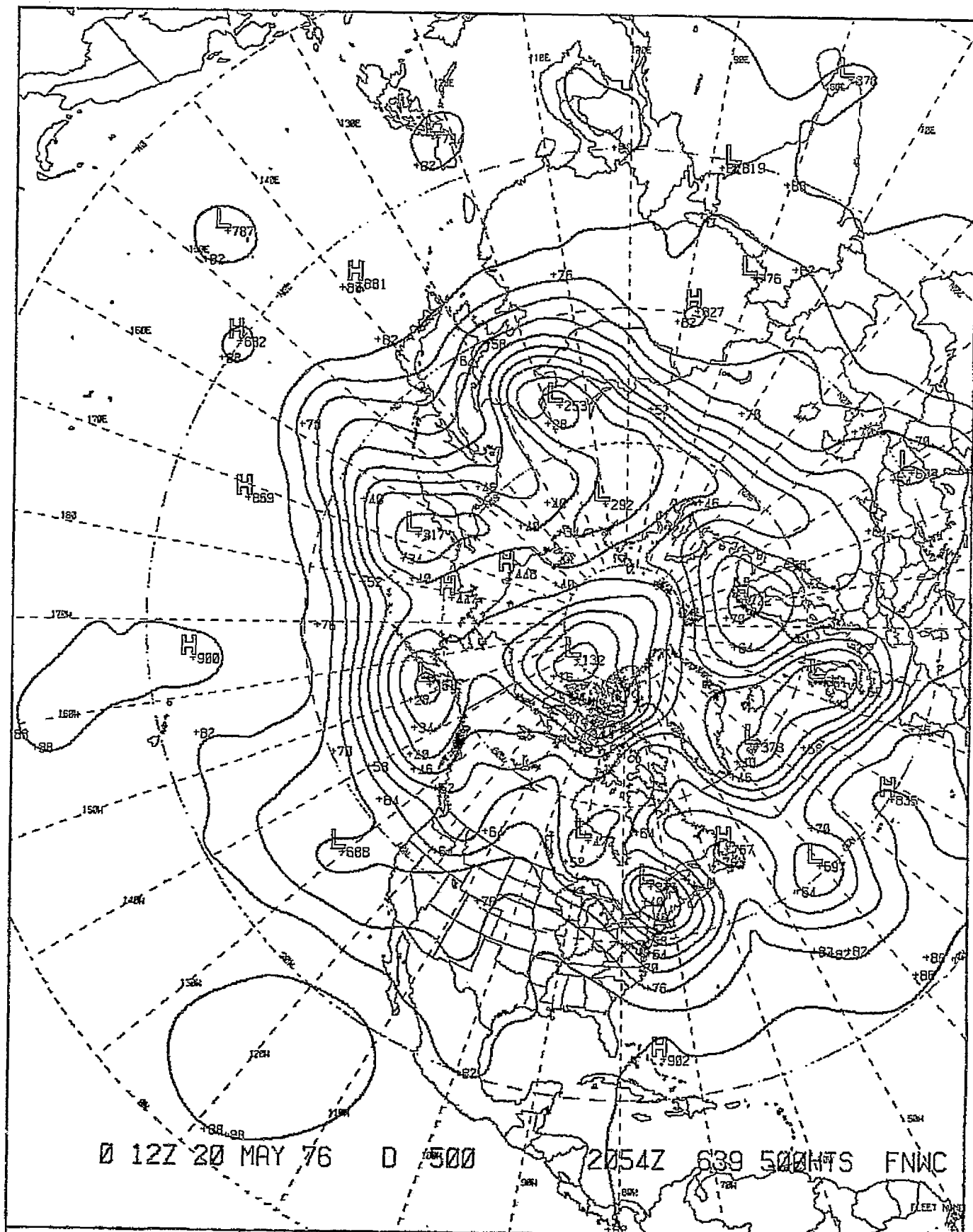
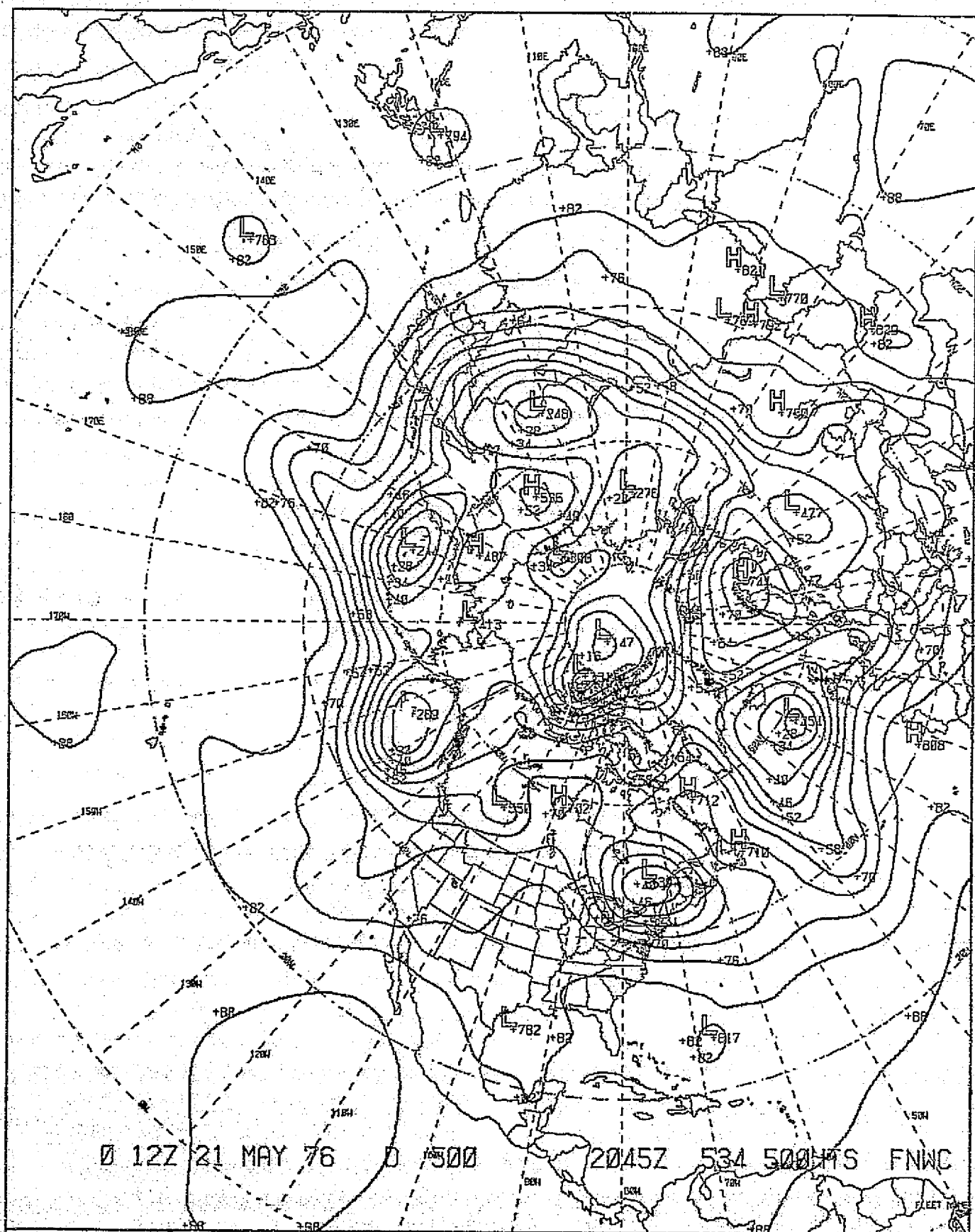


CHART VIII-33 : FNWC 500 MB HEIGHT ANALYSIS, 1200Z,
20 MAY 1976.

ORIGINAL PAGE IS
OF POOR QUALITY



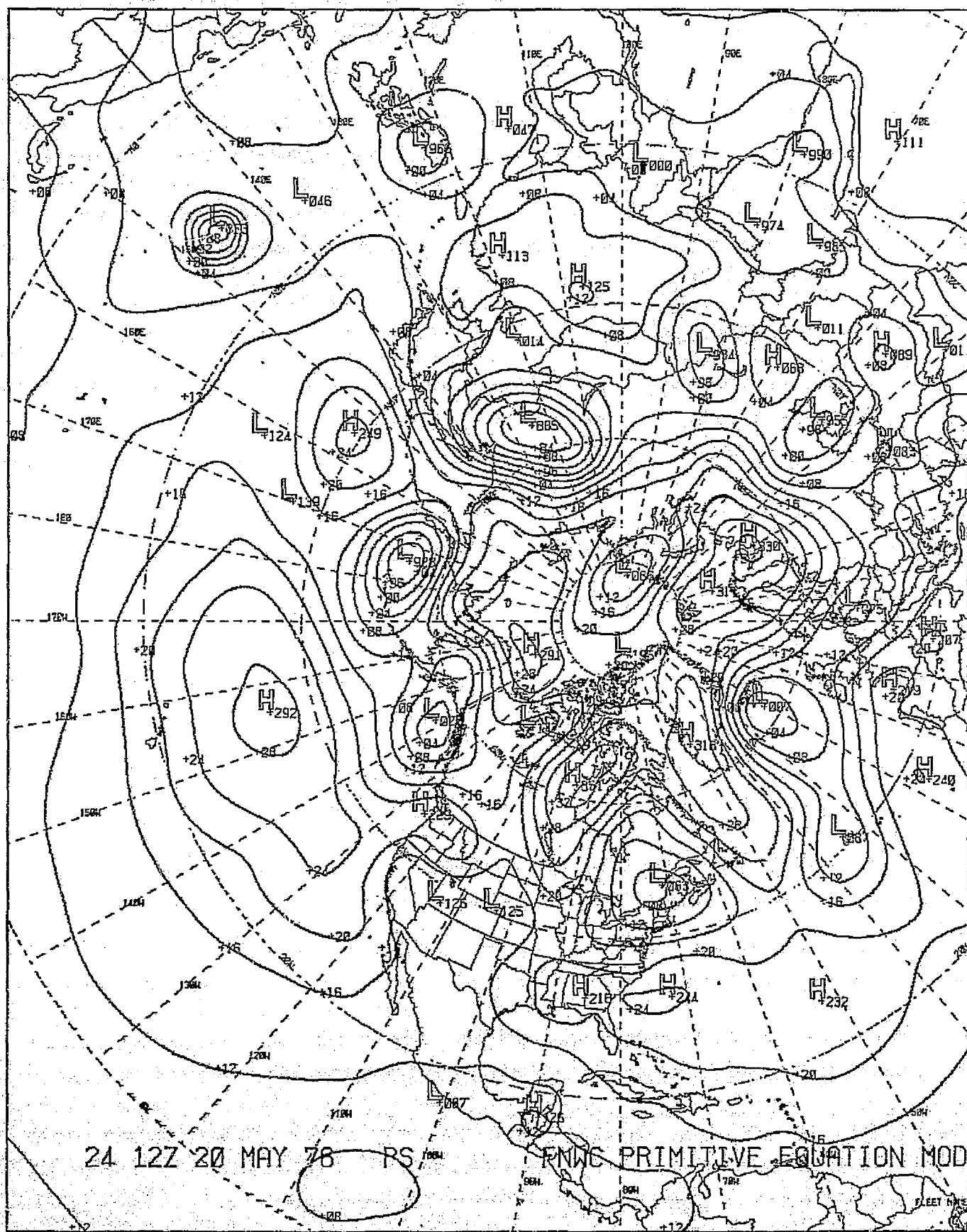


CHART VIII-35 : PNWC 24-HOUR SEA-LEVEL PRESSURE FORECAST
FROM 1200Z, 20 MAY 1976.

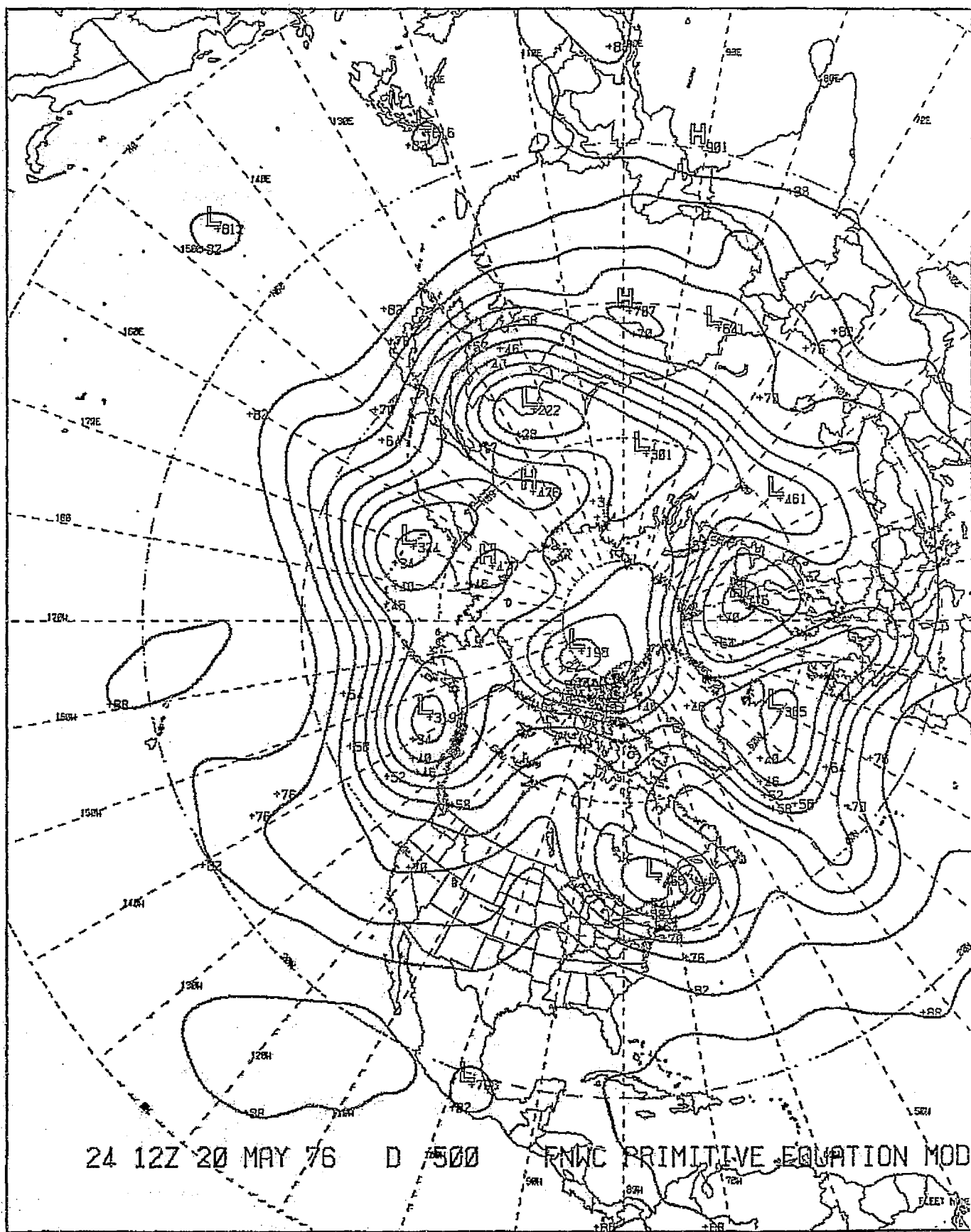


CHART VIII-36 : FNNC 24-HOUR 500 MB HEIGHT FORECAST FROM 1200Z, 20 MAY 1976.

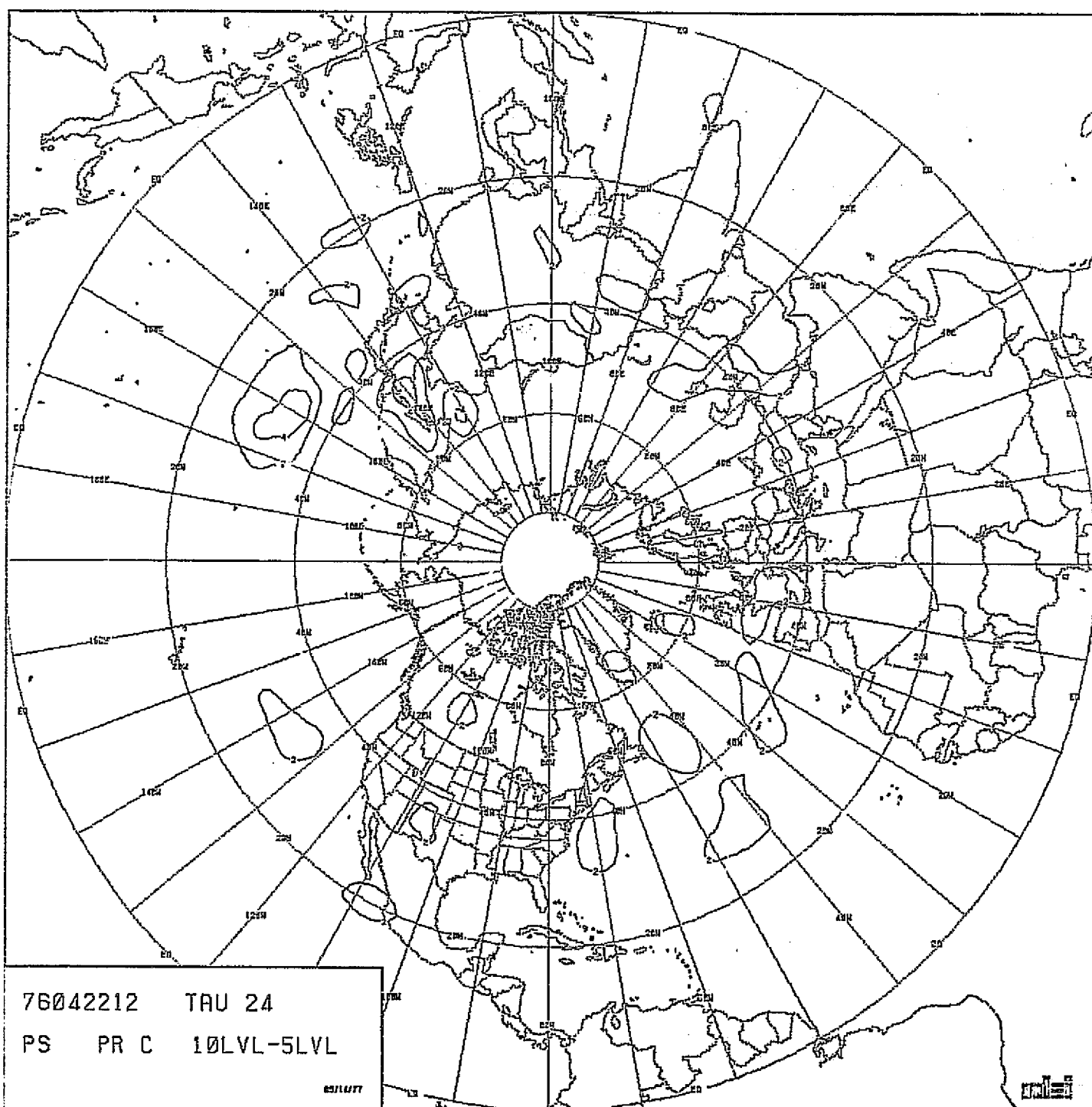


CHART VIII-37: DIFFERENCE BETWEEN TEN-LEVEL AND FIVE-LEVEL
24-HOUR SEA-LEVEL PRESSURE FORECASTS.
PRODUCTION SERIES C ANALYSES. SCENARIO A.

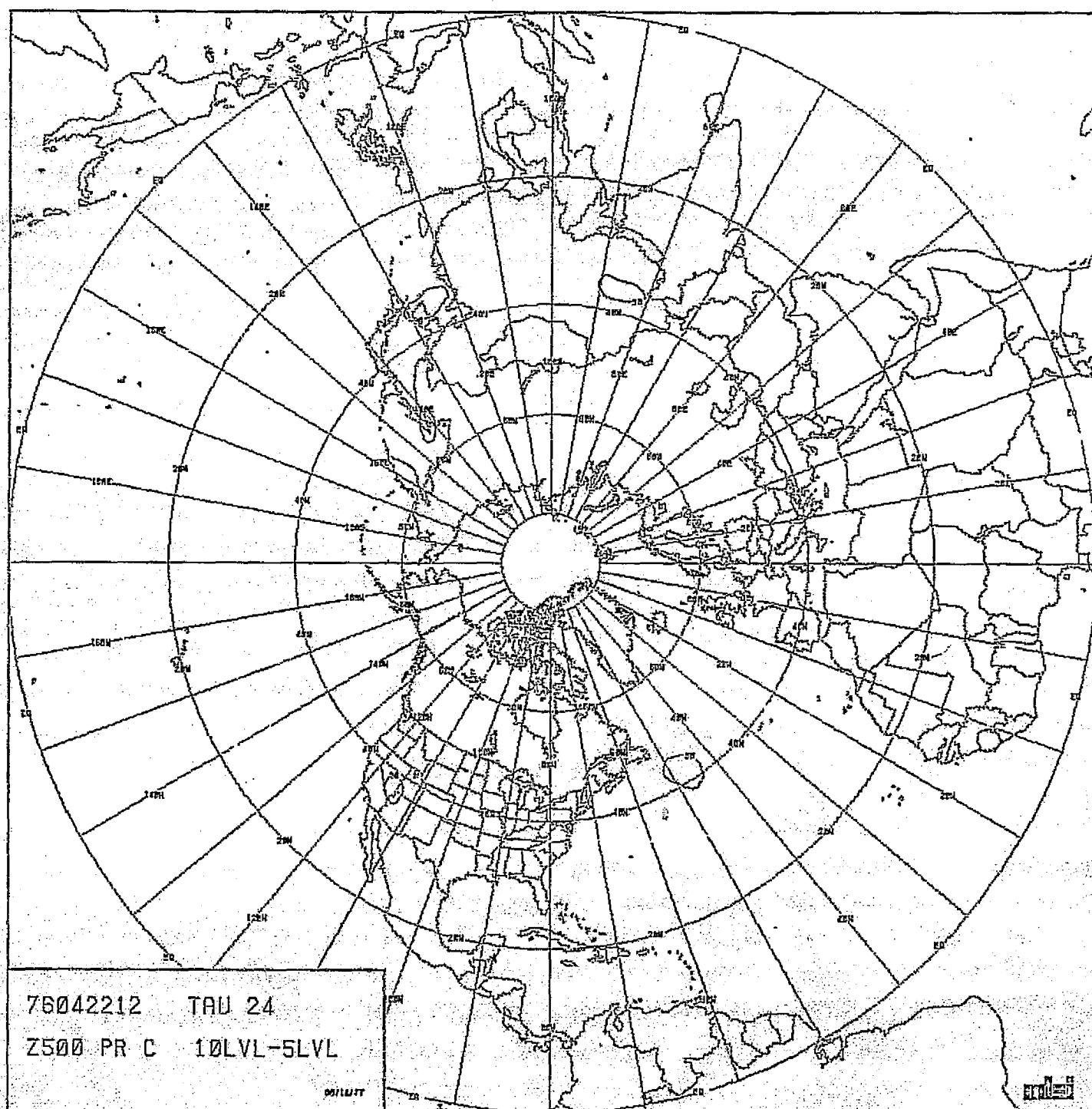


CHART VIII-38: DIFFERENCE BETWEEN TEN-LEVEL AND FIVE-LEVEL
24-HOUR 500 MB HEIGHT FORECASTS. PRODUCTION
SERIES C ANALYSES. SCENARIO A.

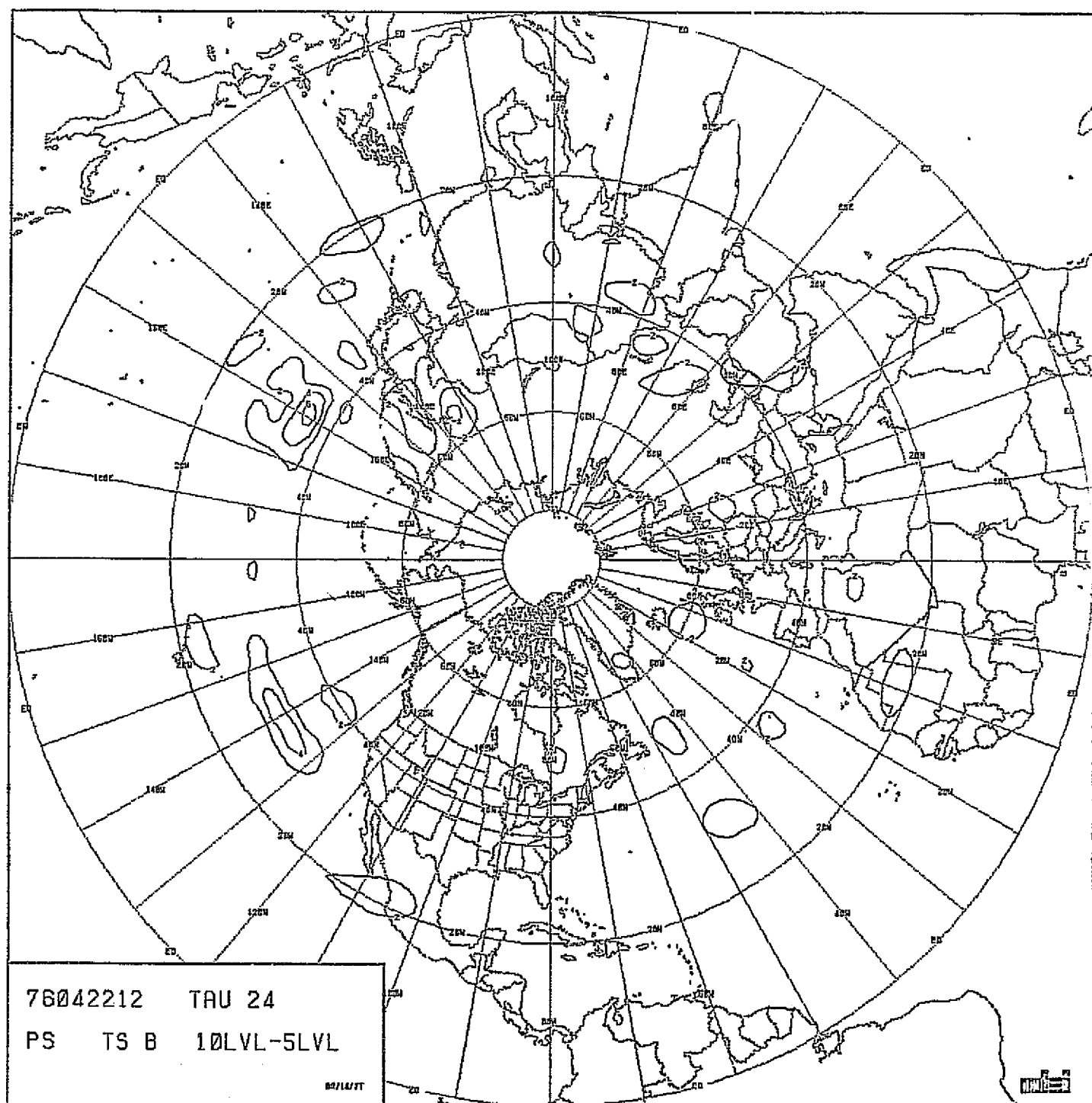


CHART VIII-39: DIFFERENCE BETWEEN TEN-LEVEL AND FIVE-LEVEL
24-HOUR SEA-LEVEL PRESSURE FORECASTS. TEST
SERIES B ANALYSES. SCENARIO A.

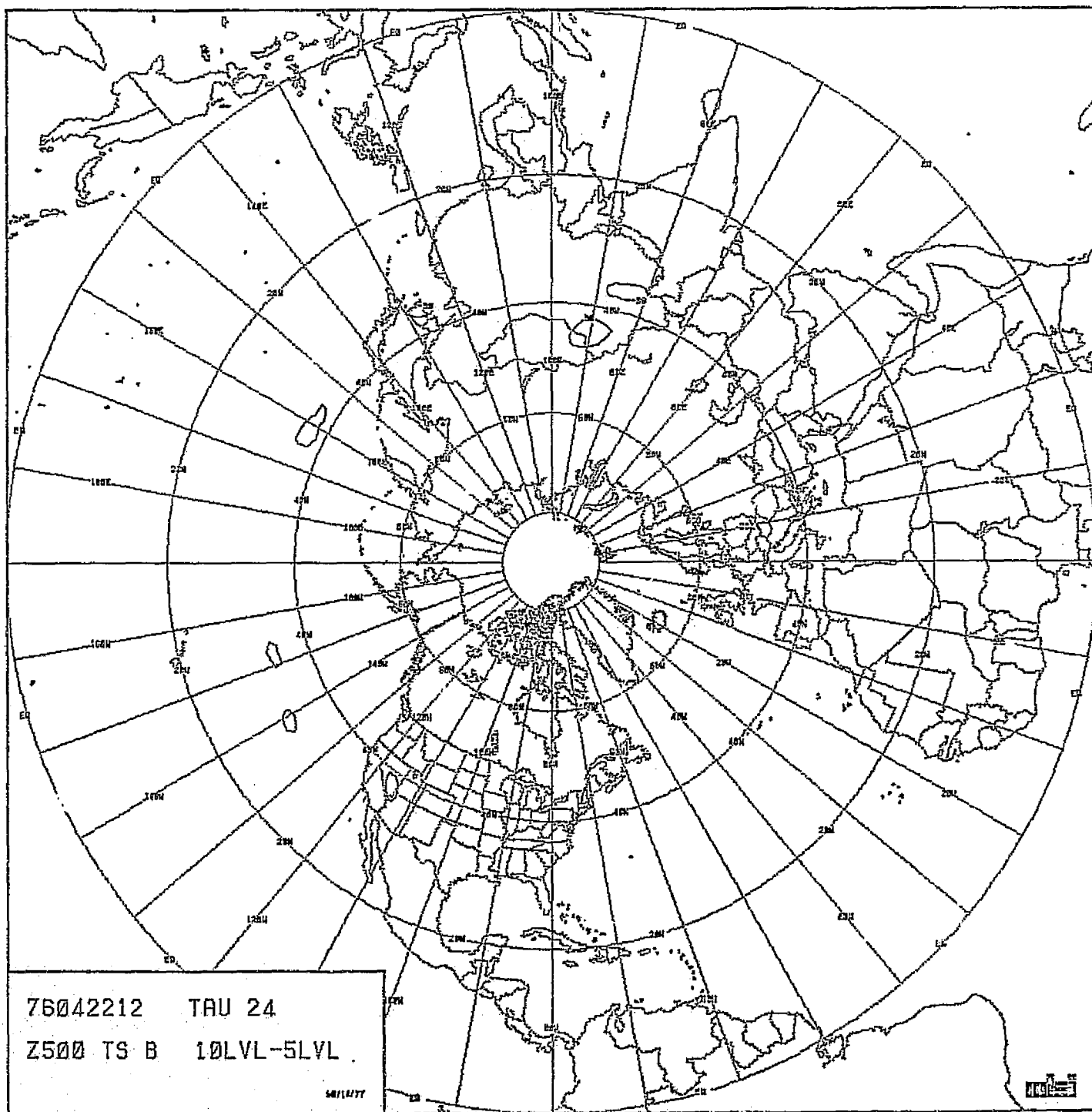
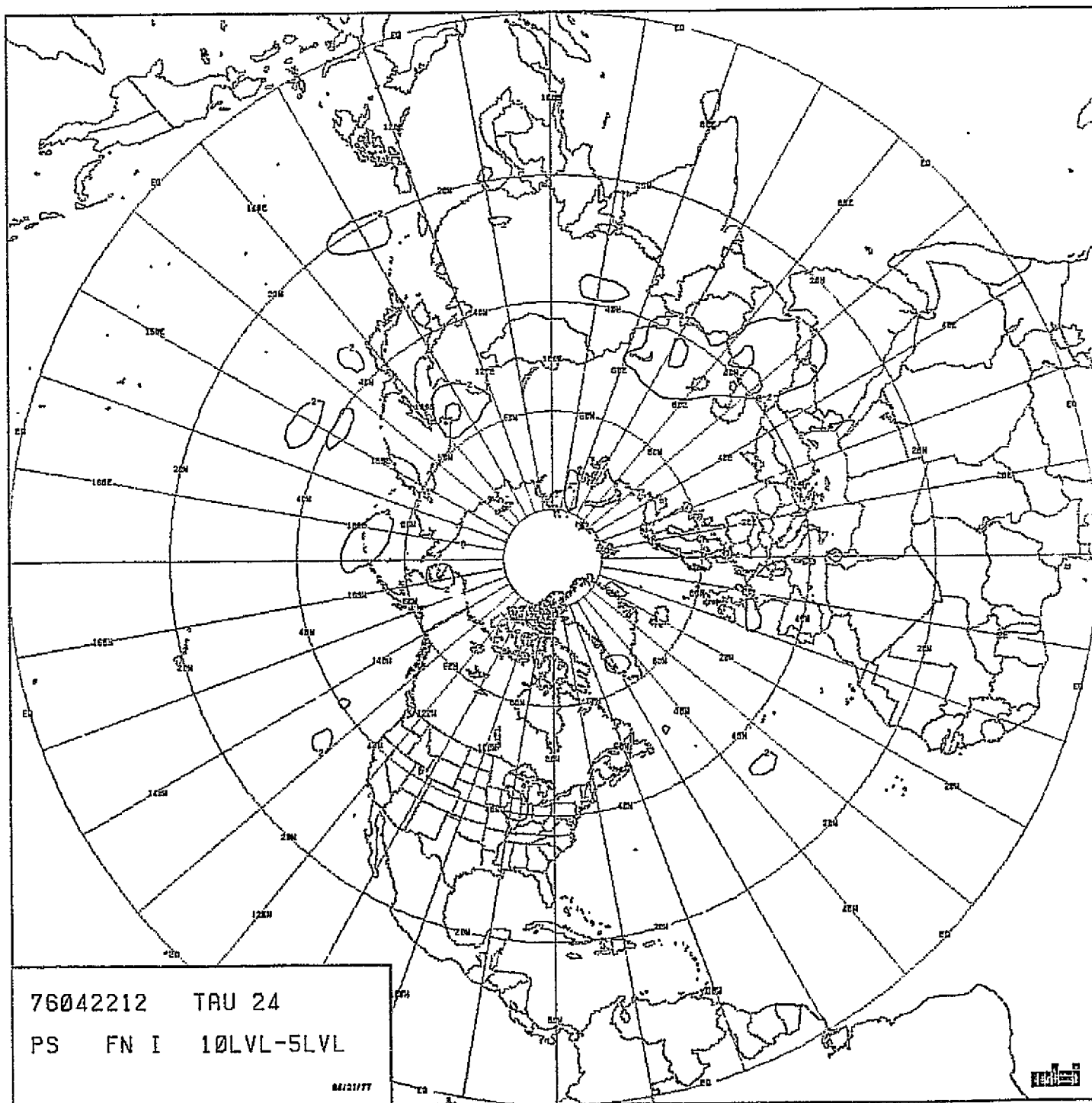


CHART VIII-40: DIFFERENCE BETWEEN TEN-LEVEL AND FIVE-LEVEL
24-HOUR 500 MB HEIGHT FORECASTS. TEST
SERIES B ANALYSES. SCENARIO A.



76042212 TAU 24
PS FN I 10LVL-5LVL

04121177

CHART VIII-41:

DIFFERENCE BETWEEN TEN-LEVEL AND FIVE-LEVEL
24-HOUR SEA-LEVEL PRESSURE FORECASTS. FMNC
GUESS-FIELD ANALYSES. SCENARIO A.

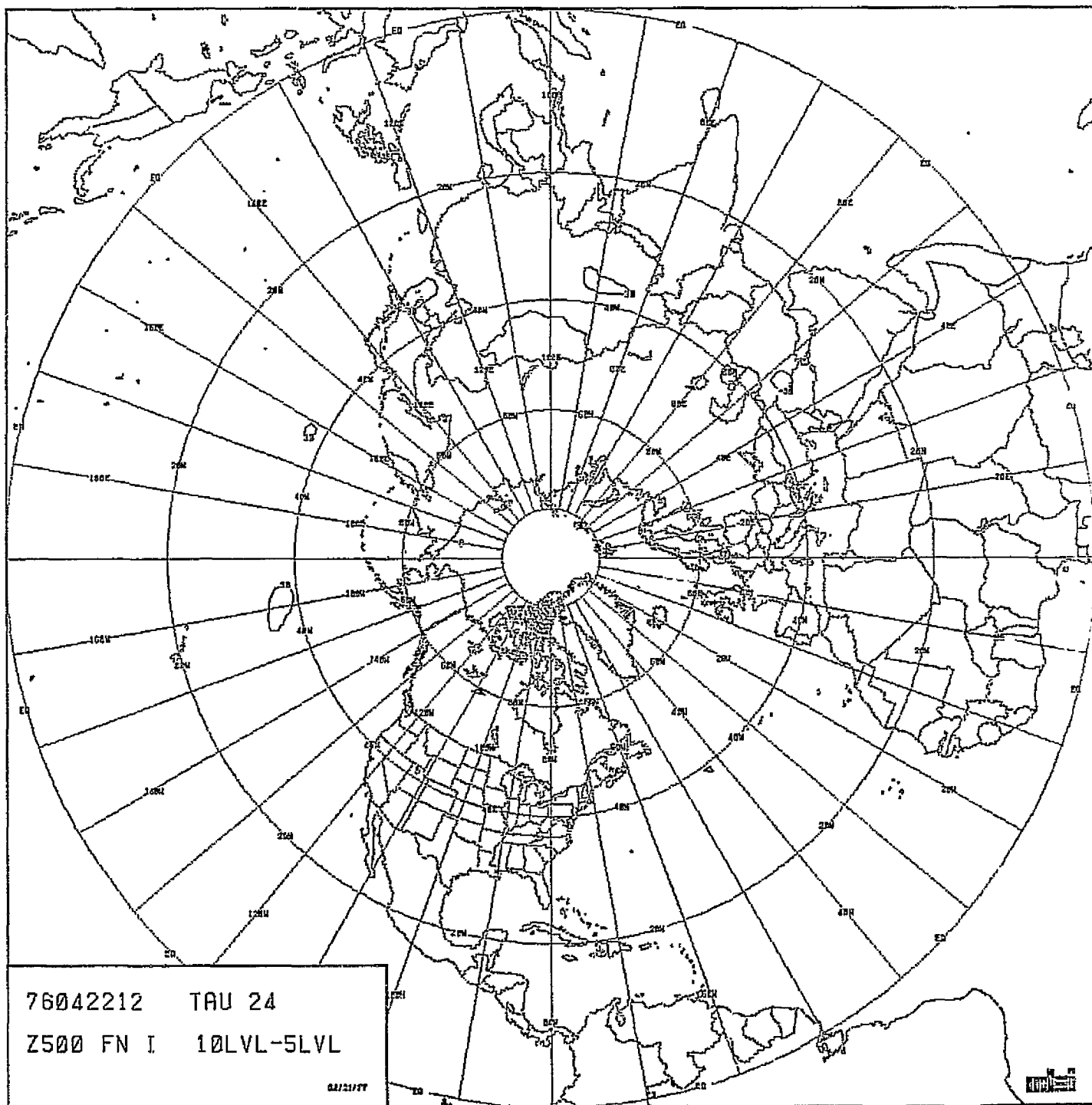
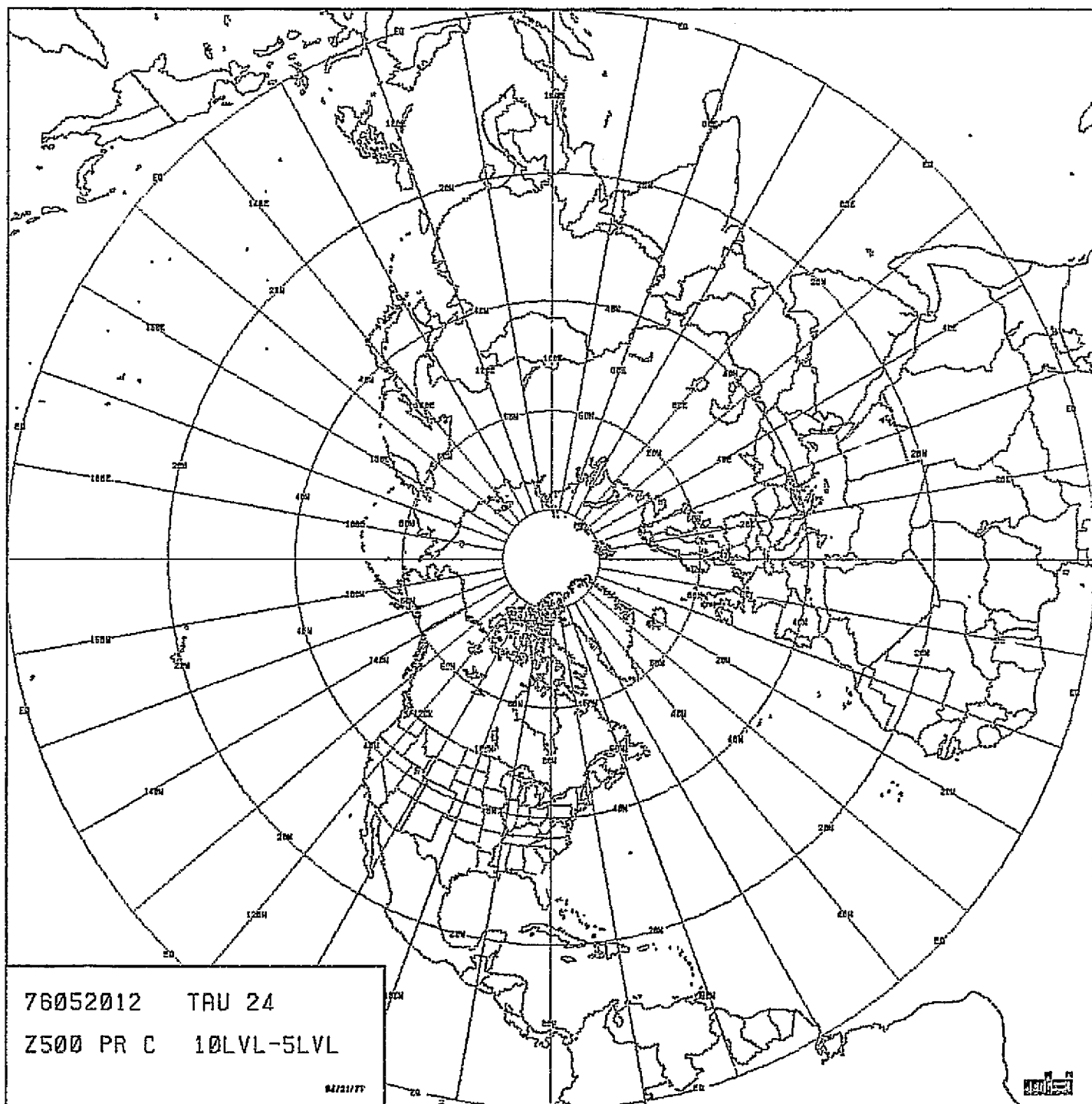


CHART VIII-42: DIFFERENCE BETWEEN TEN-LEVEL AND FIVE-LEVEL
24-HOUR 500 MB HEIGHT FORECASTS. FNWC
GUESS-FIELD ANALYSES. SCENARIO A.



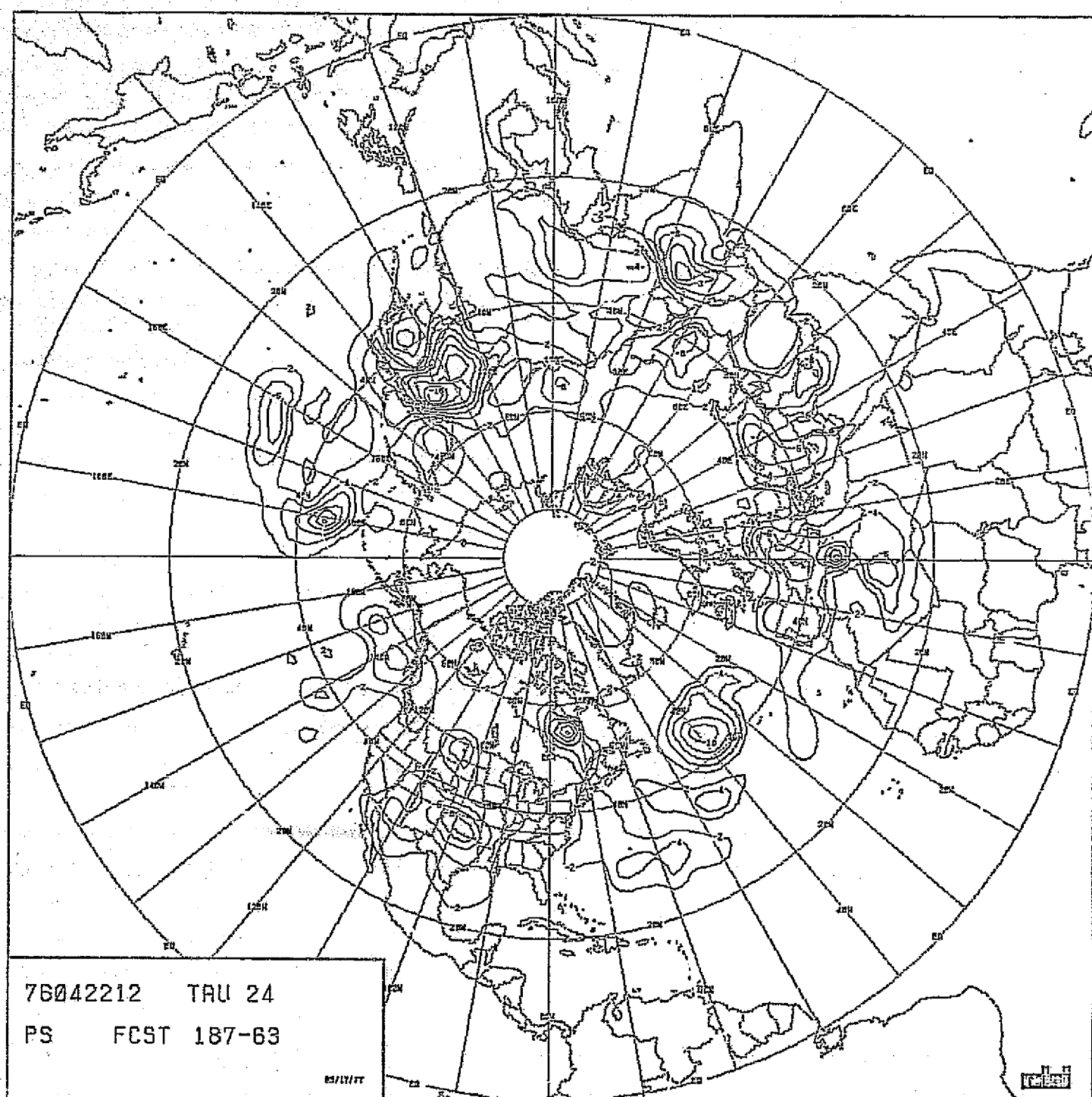


CHART VIII-45: DIFFERENCE BETWEEN 18" x 187 AND 63 x 63
FIVE-LAYER 24-HOUR FORECASTS. SEA-LEVEL
PRESSURE. SCENARIO A.

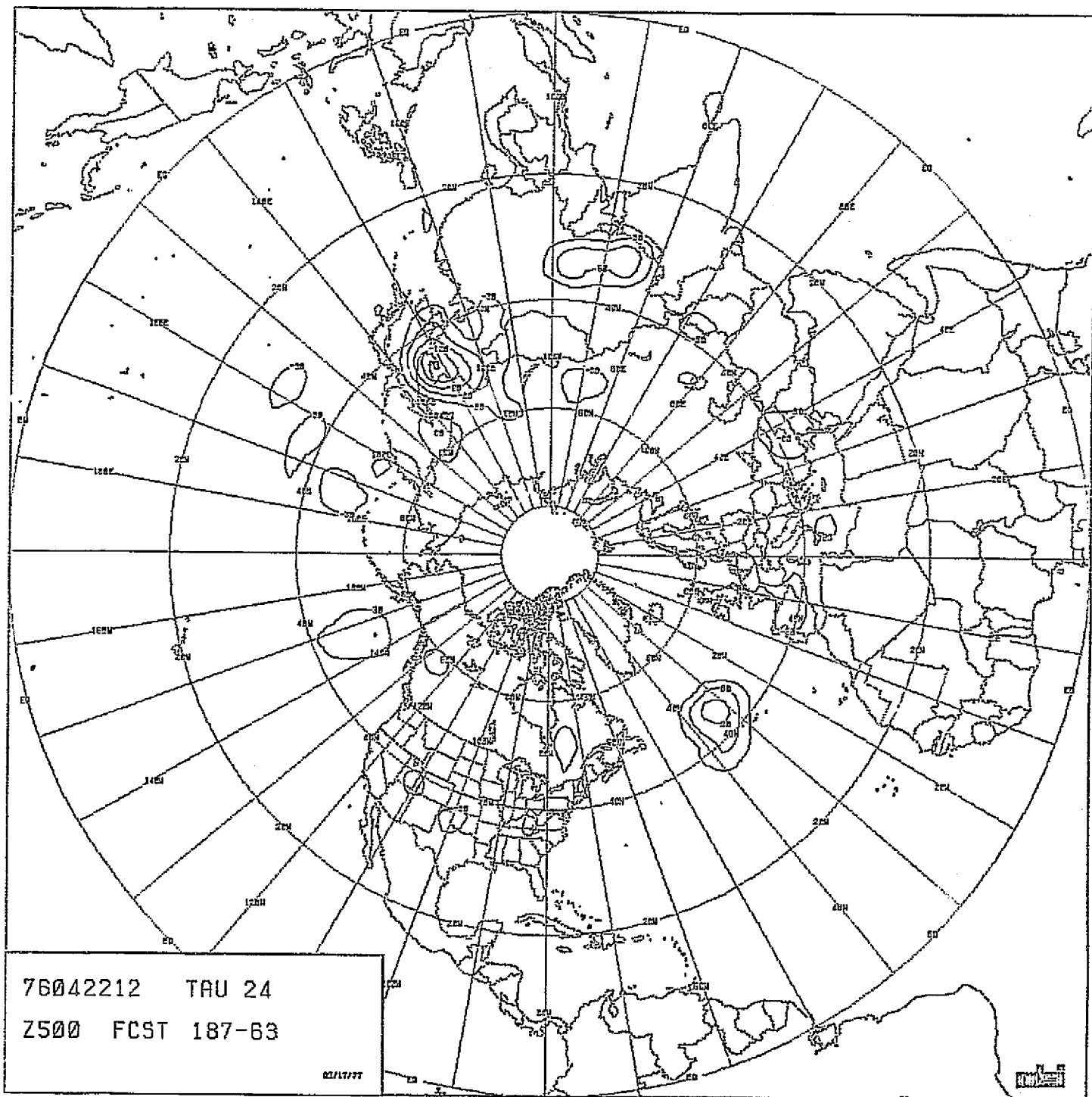


CHART VIII-46: DIFFERENCE BETWEEN 187 x 187 AND 63 x 63
FIVE-LAYER 24-HOUR FORECASTS. 500 MB HEIGHT.
SCENARIO A.

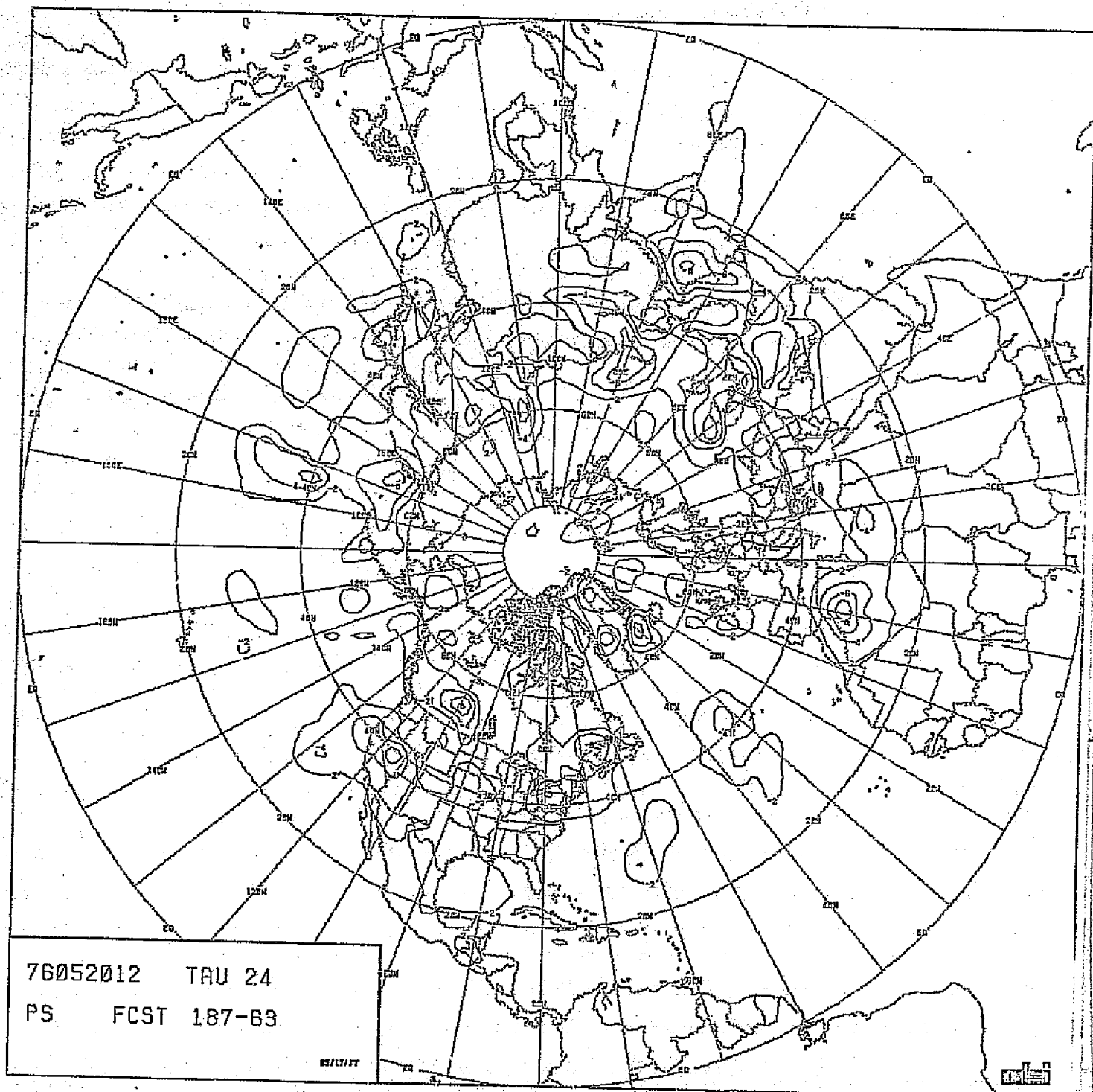


CHART VIII-47: DIFFERENCE BETWEEN 187 x 187 AND 63 x 63
FIVE-LAYER 24-HOUR FORECASTS. SEA-LEVEL
PRESSURE. SCENARIO B.

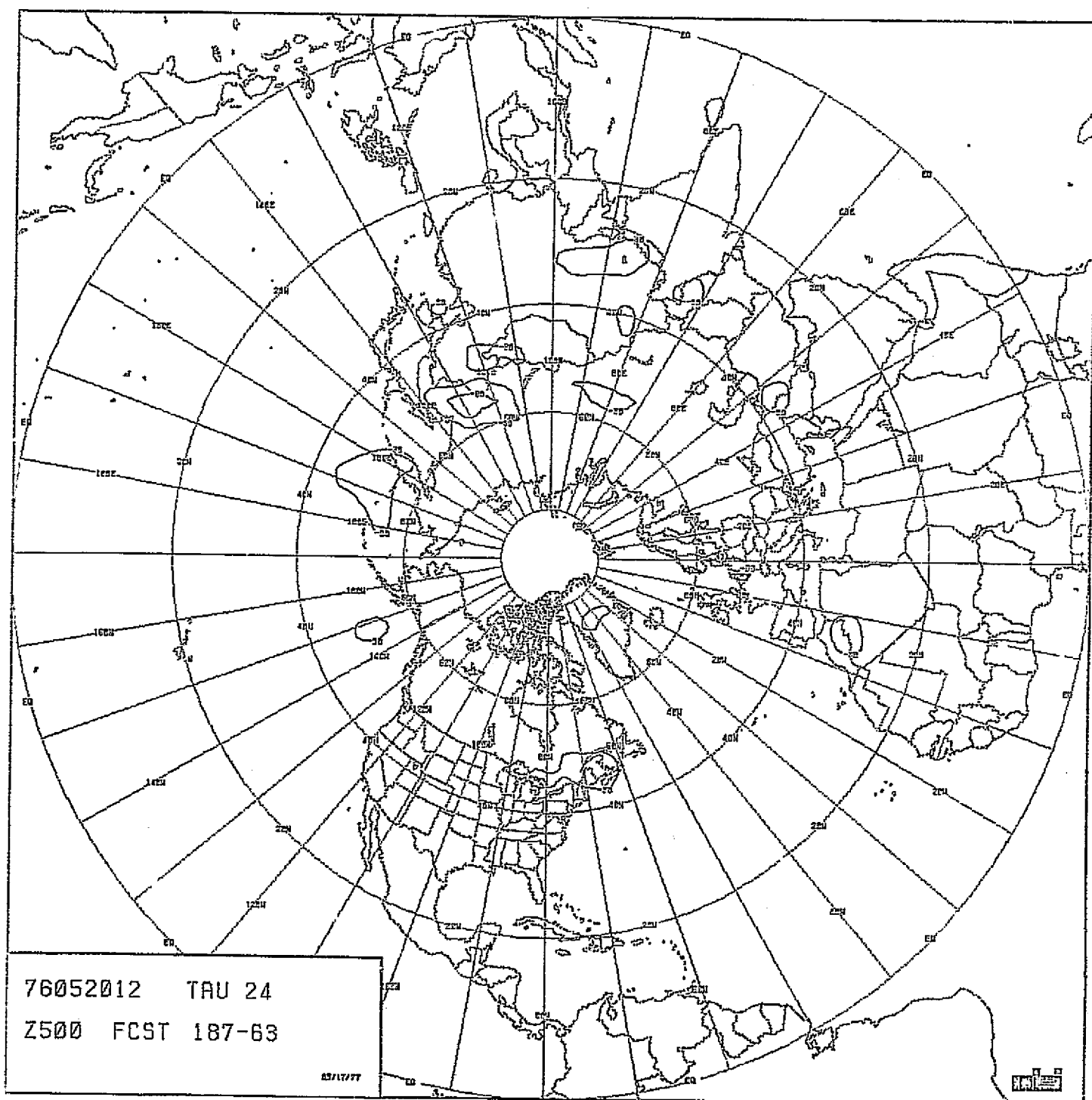
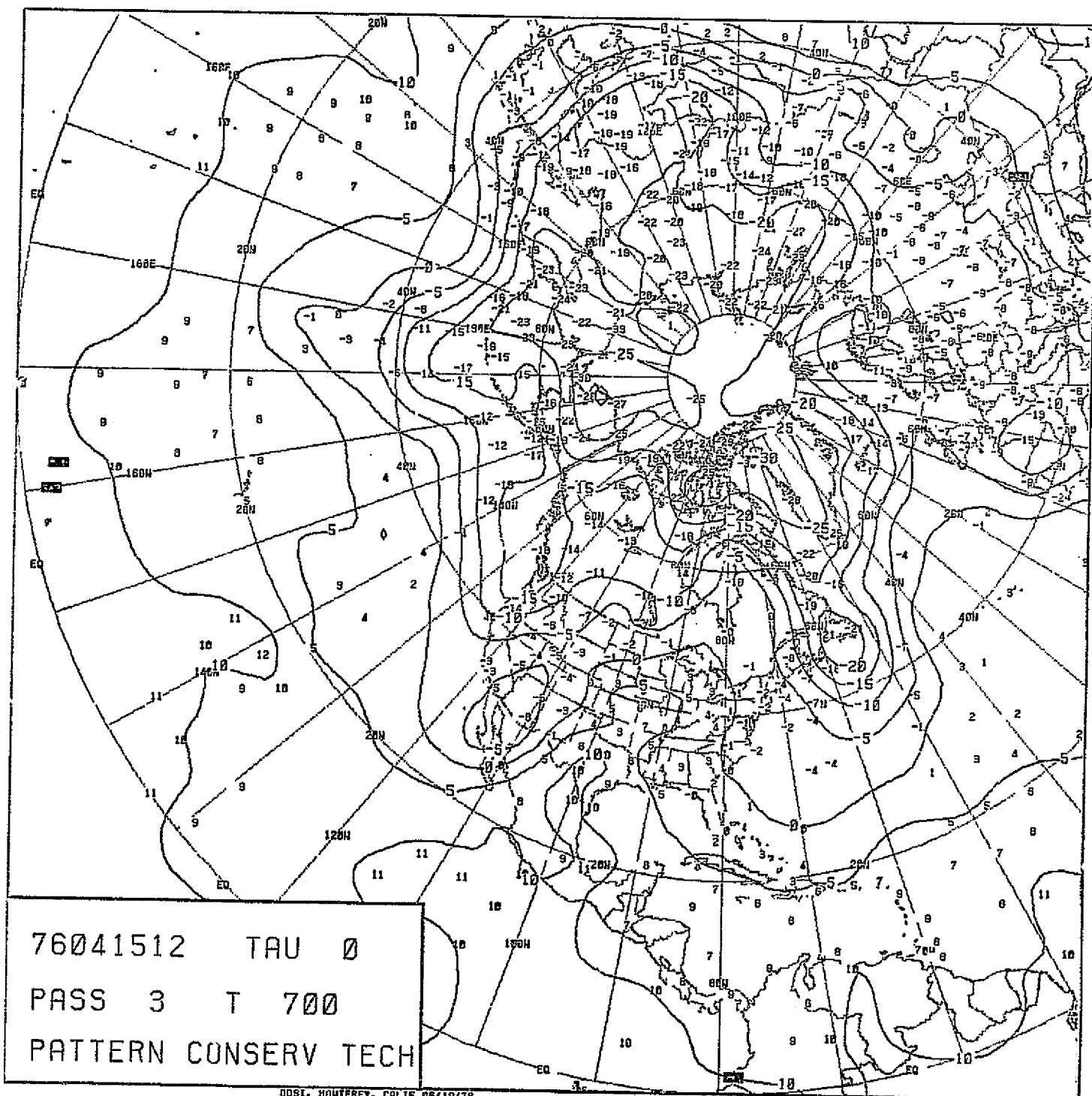


CHART VIII-48: DIFFERENCE BETWEEN 187 x 187 AND 63 x 63
FIVE-LAYER 24-HOUR FORECASTS. 500 MB HEIGHT.
SCENARIO B.

ORIGINAL PAGE IS
OF POOR QUALITY



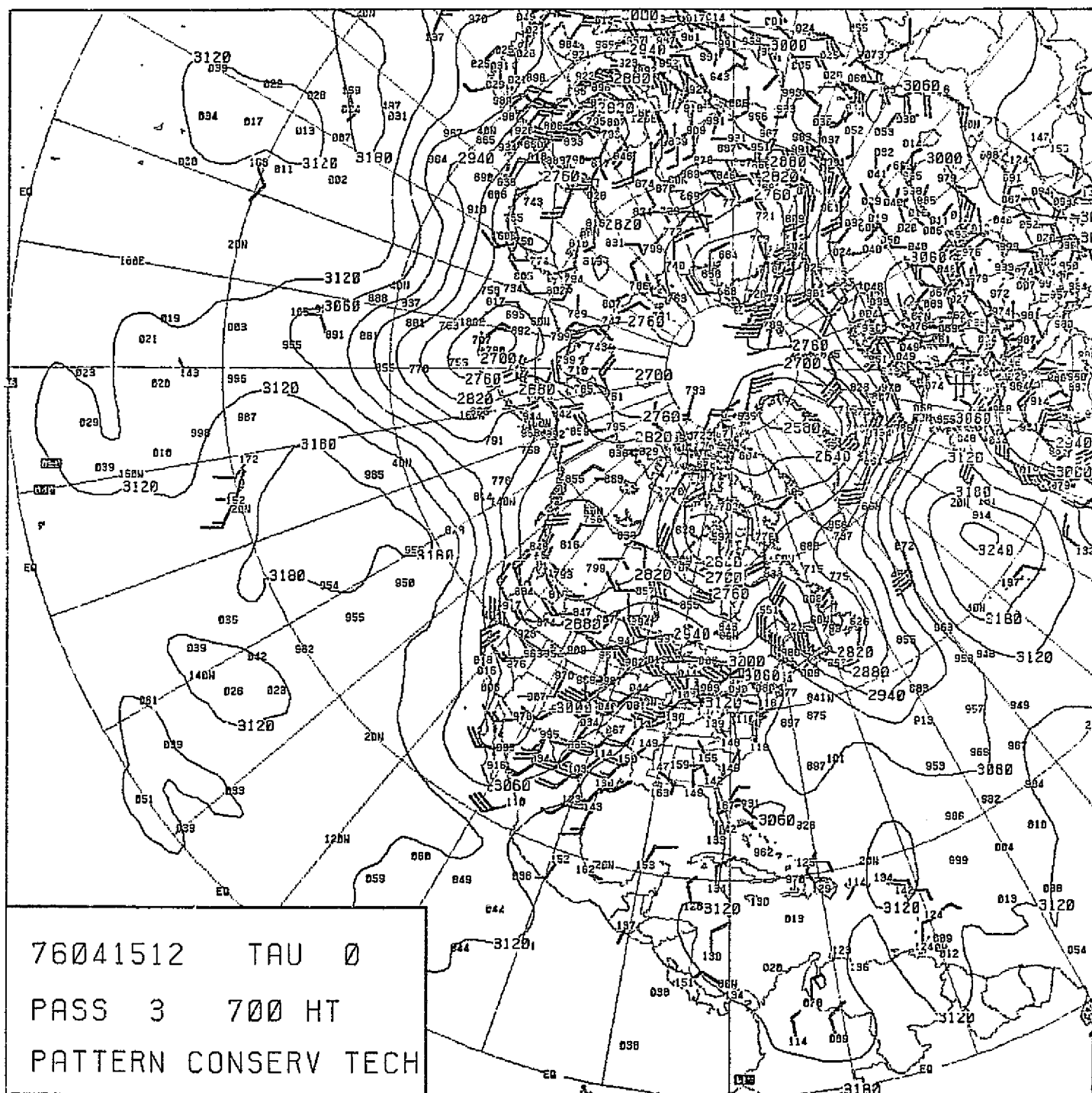
76041512 TAU 0
PASS 3 T 700
PATTERN CONSERV TECH

0051. MONTEREY, CALIF 08/19/76

CHART VIII-49

700 MB TEMPERATURE ANALYSIS FOR 1200Z,
15 APRIL 1976 (EARLY VERSION).

ORIGINAL PAGE IS
OF POOR QUALITY



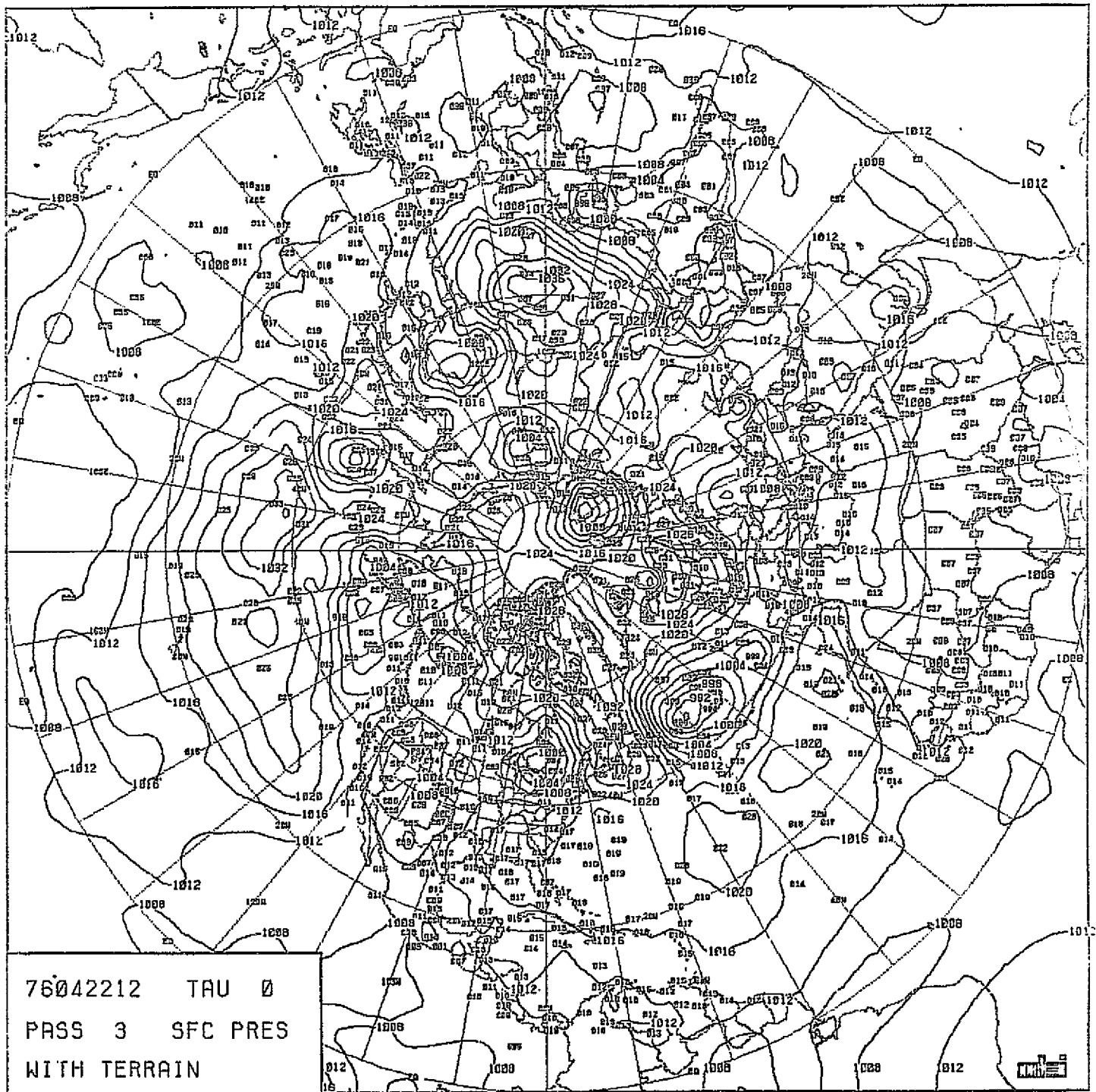
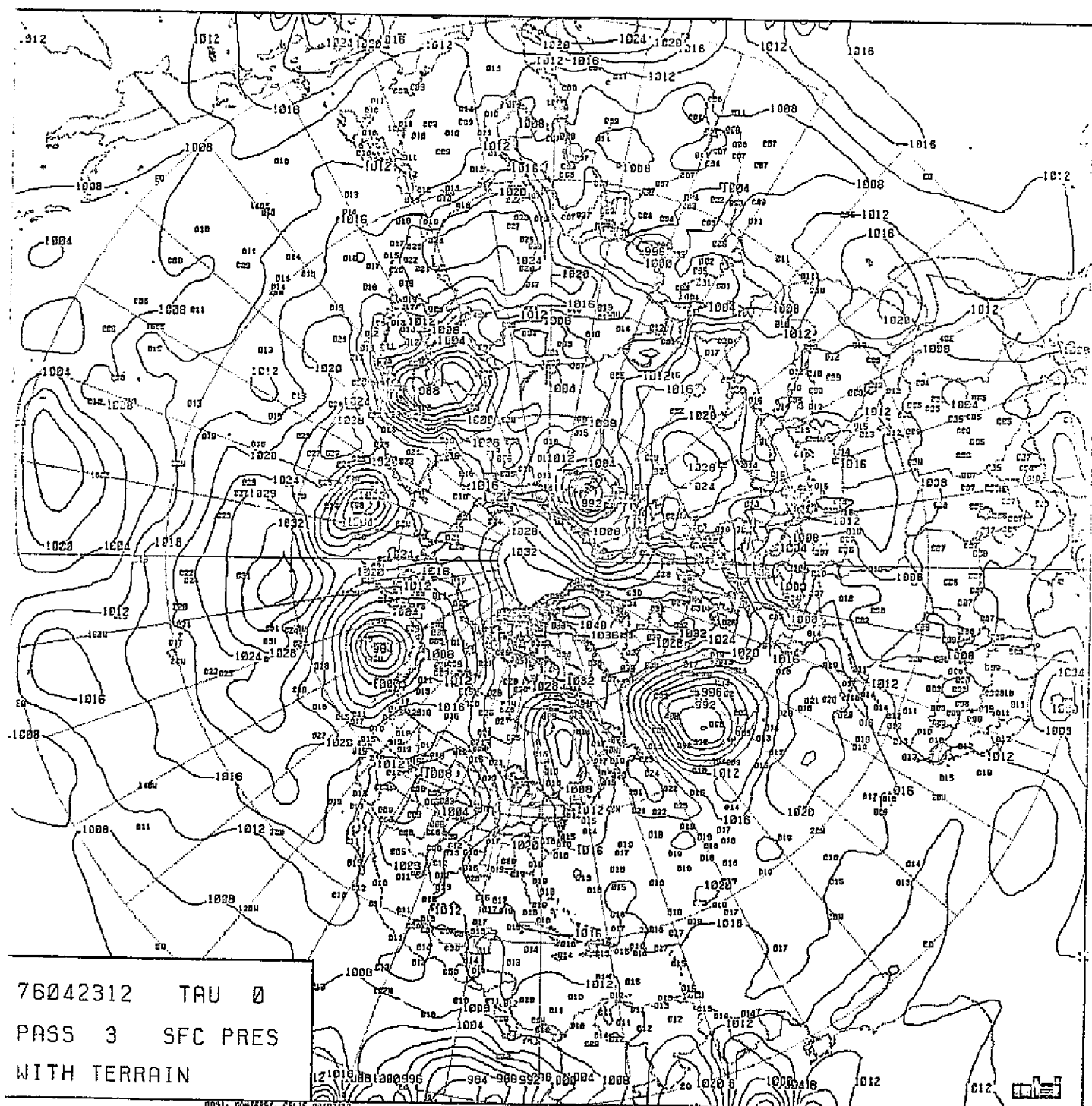
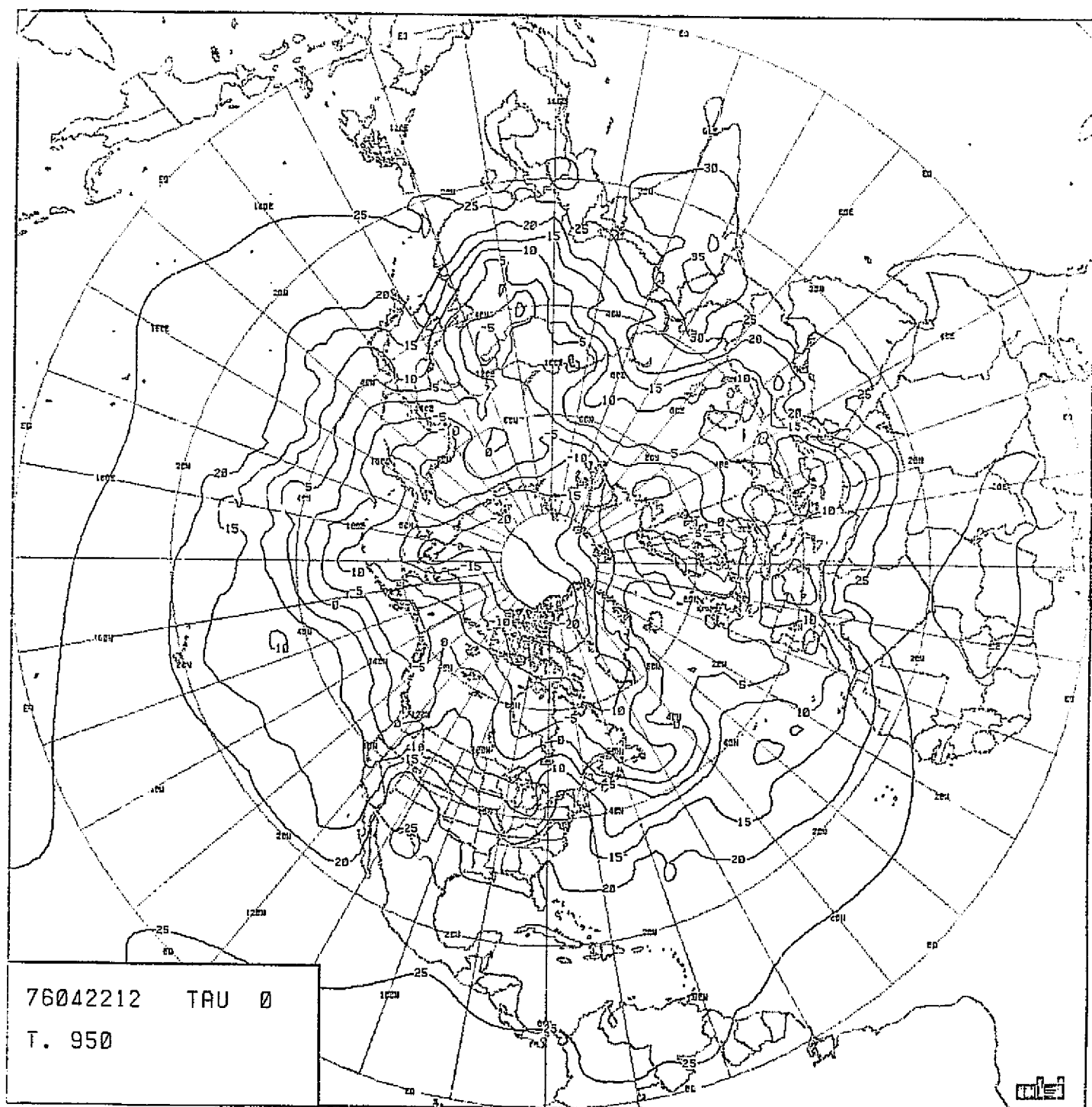


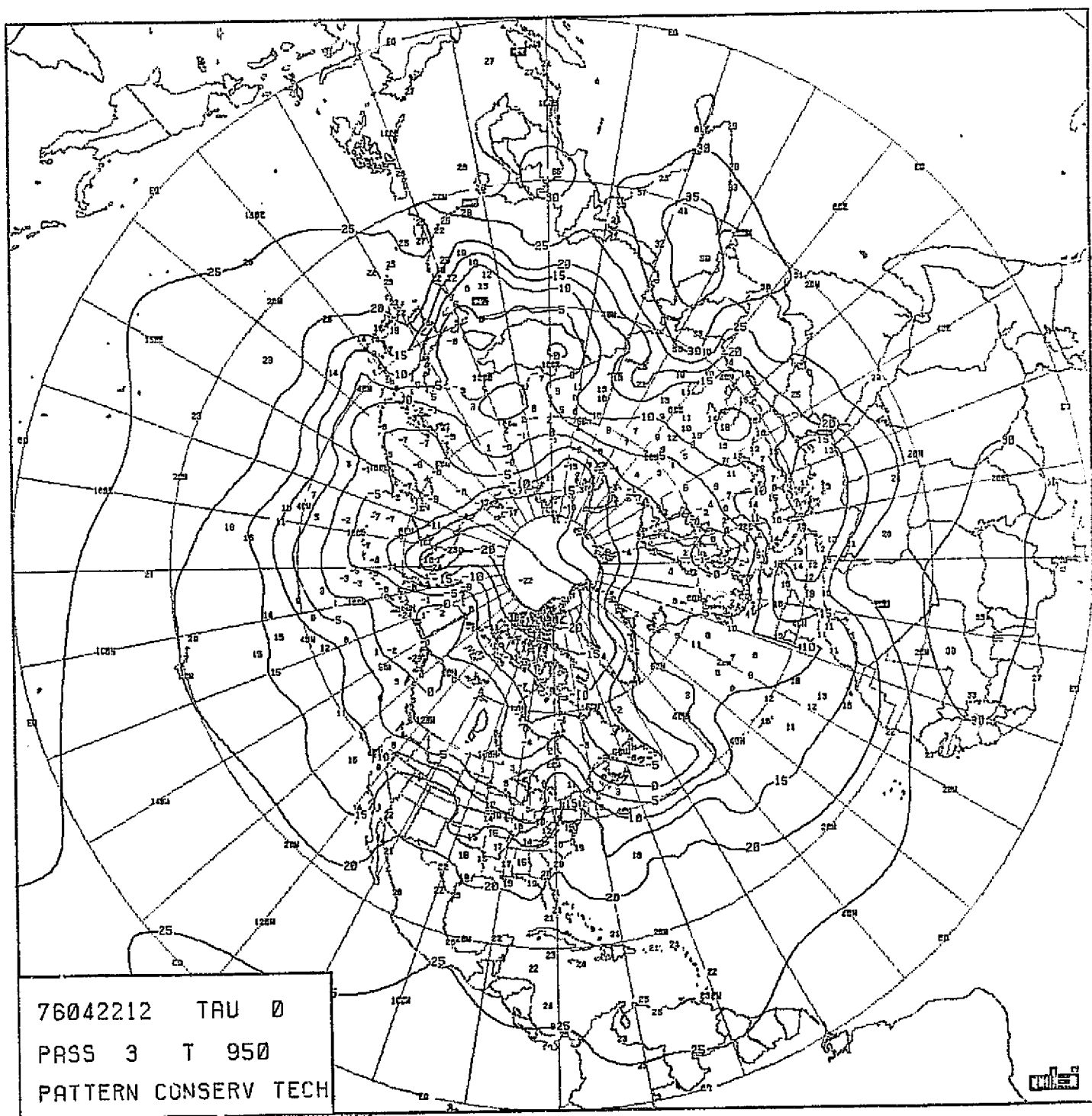
CHART VIII-51

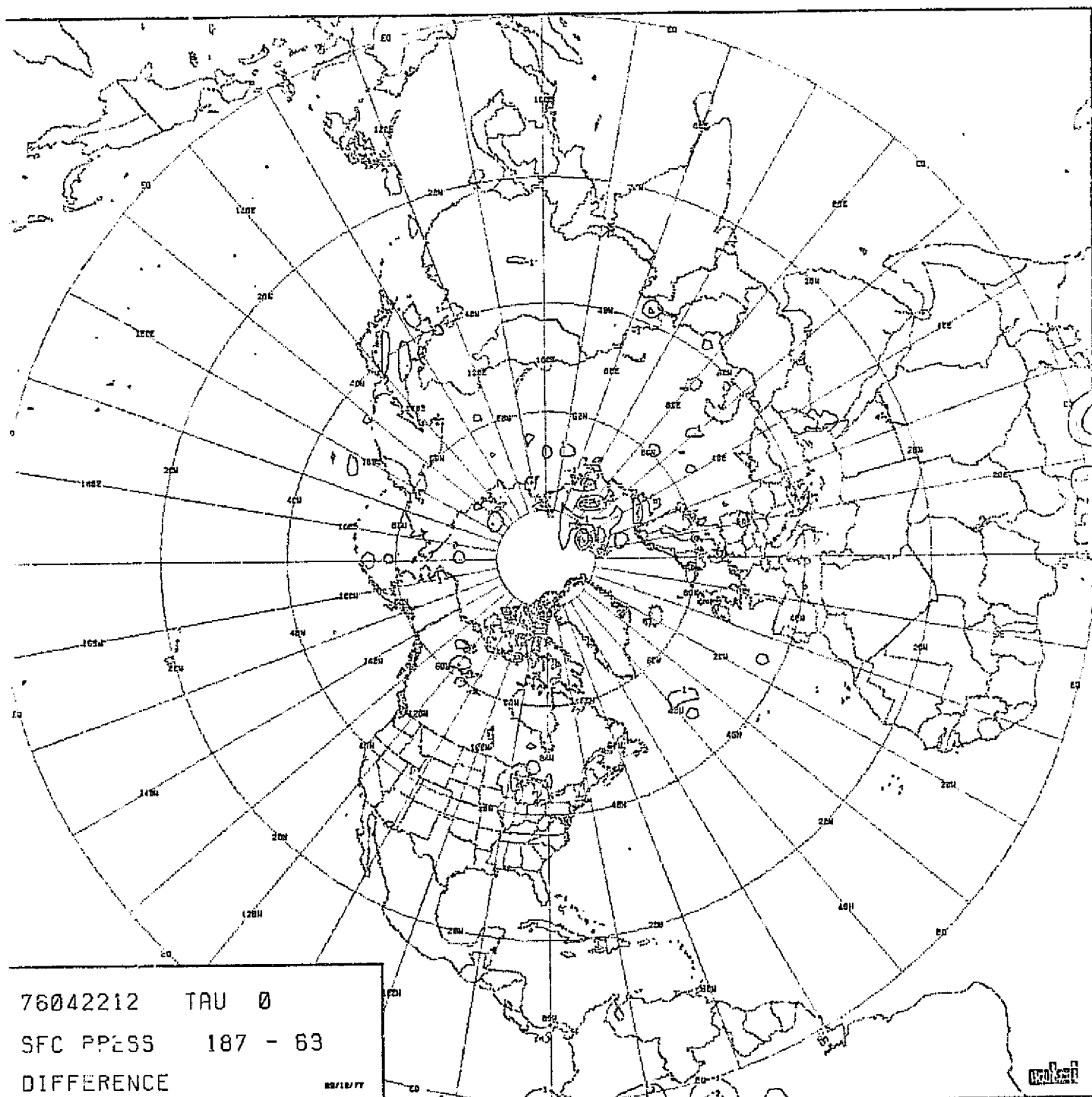
SEA-LEVEL PRESSURE ANALYSIS FOR 1200Z,
22 APRIL 1976 (EARLY VERSION).

ORIGINAL PAGE 2
OF FOUR QUALITY





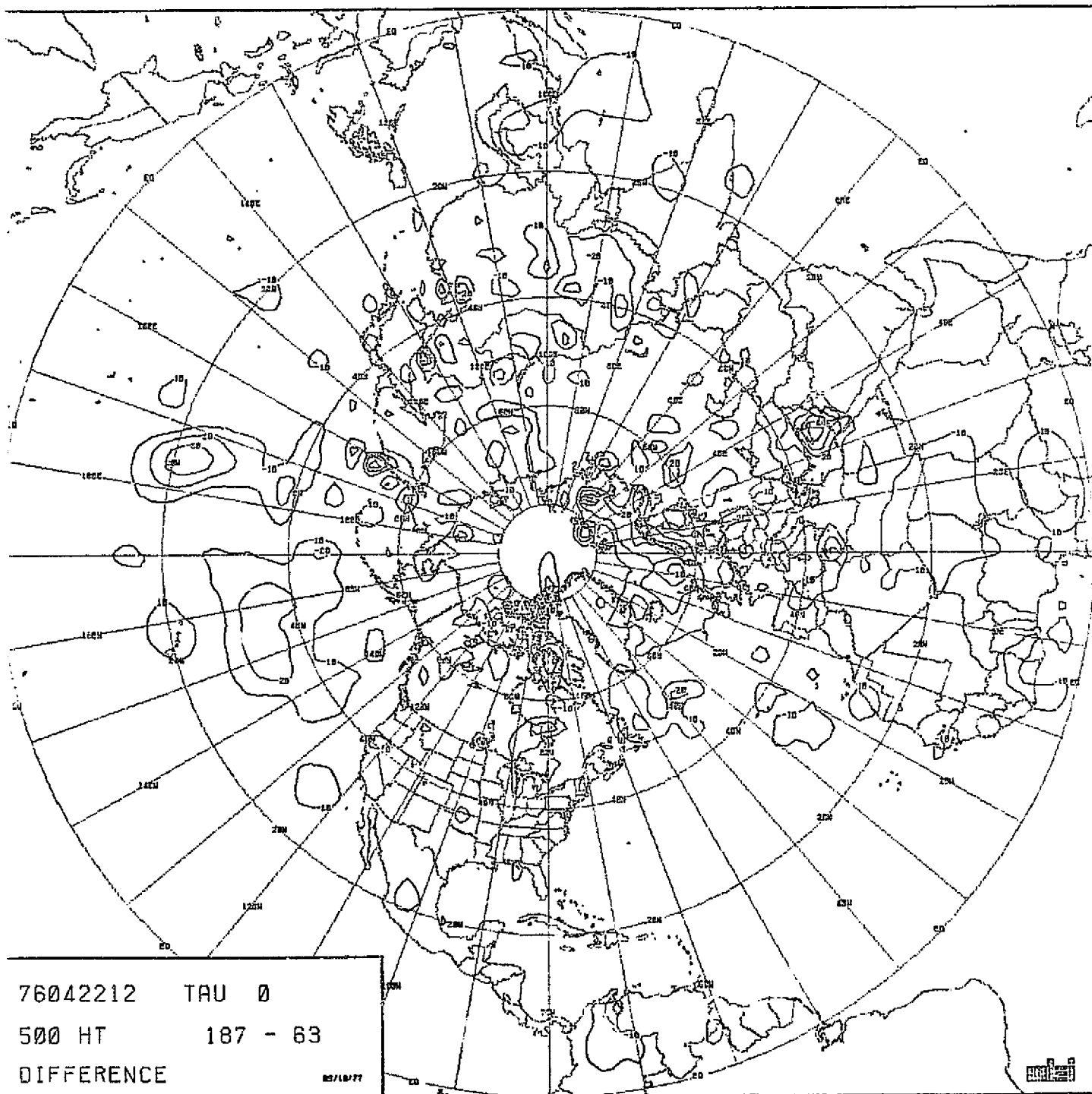




76042212 TAU 0
SFC PRESS 187 - 63
DIFFERENCE

CHART VIII-55

SEA-LEVEL PRESSURE ANALYSIS DIFFERENCE CHART:
187 x 187 GRID MINUS 63 x 63 GRID.
SCENARIO A.



76042212 TAU 0
500 HT 187 - 63
DIFFERENCE

05/10/77

CHART VIII-56

500 MB HEIGHT ANALYSIS DIFFERENCE CHART:
187 x 187 GRID MINUS 63 x 63 GRID.
SCENARIO A.

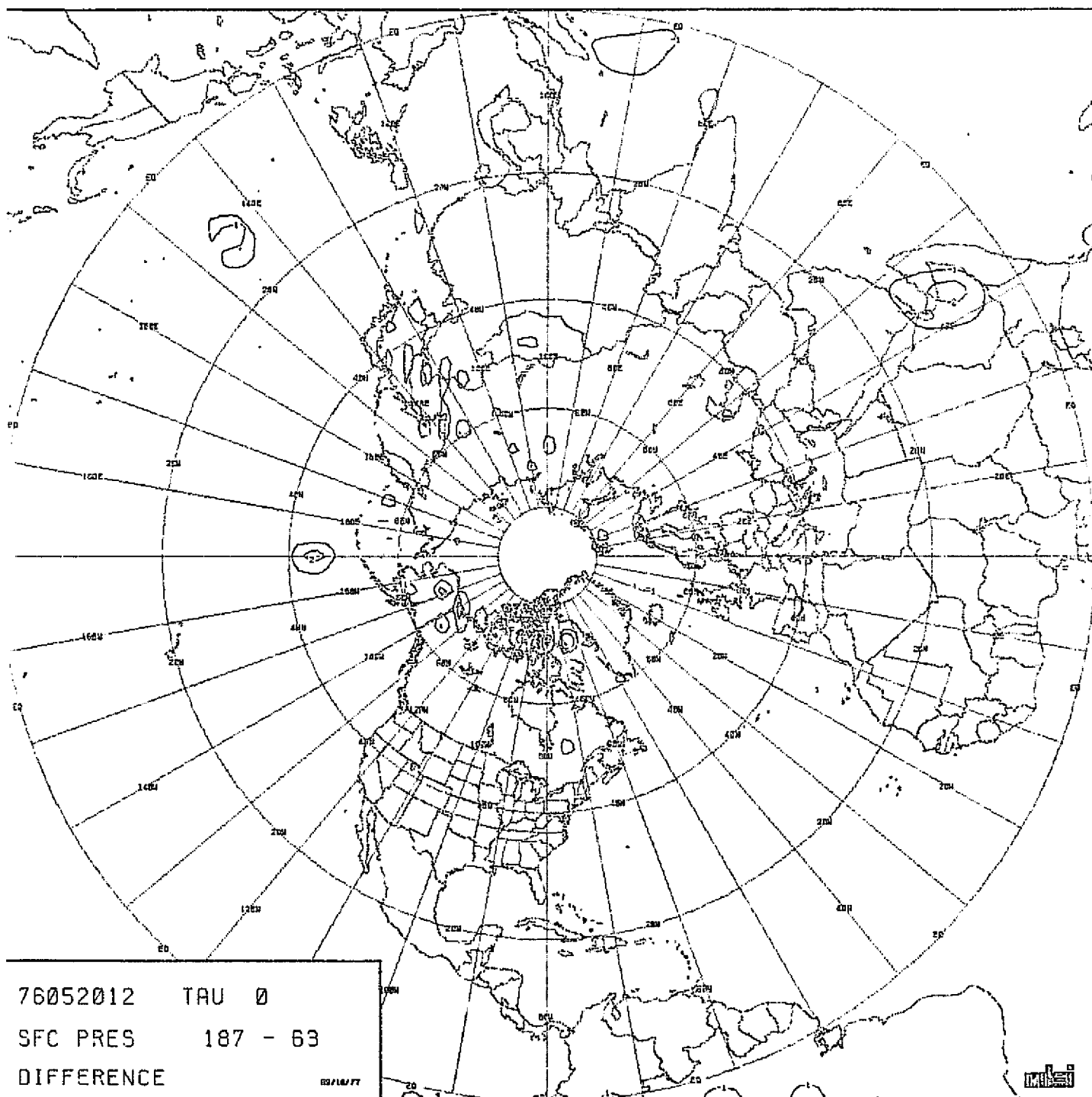


CHART VIII-57

SEA-LEVEL PRESSURE ANALYSIS DIFFERENCE CHART:
187 x 187 GRID MINUS 63 x 63 GRID.
SCENARIO B.

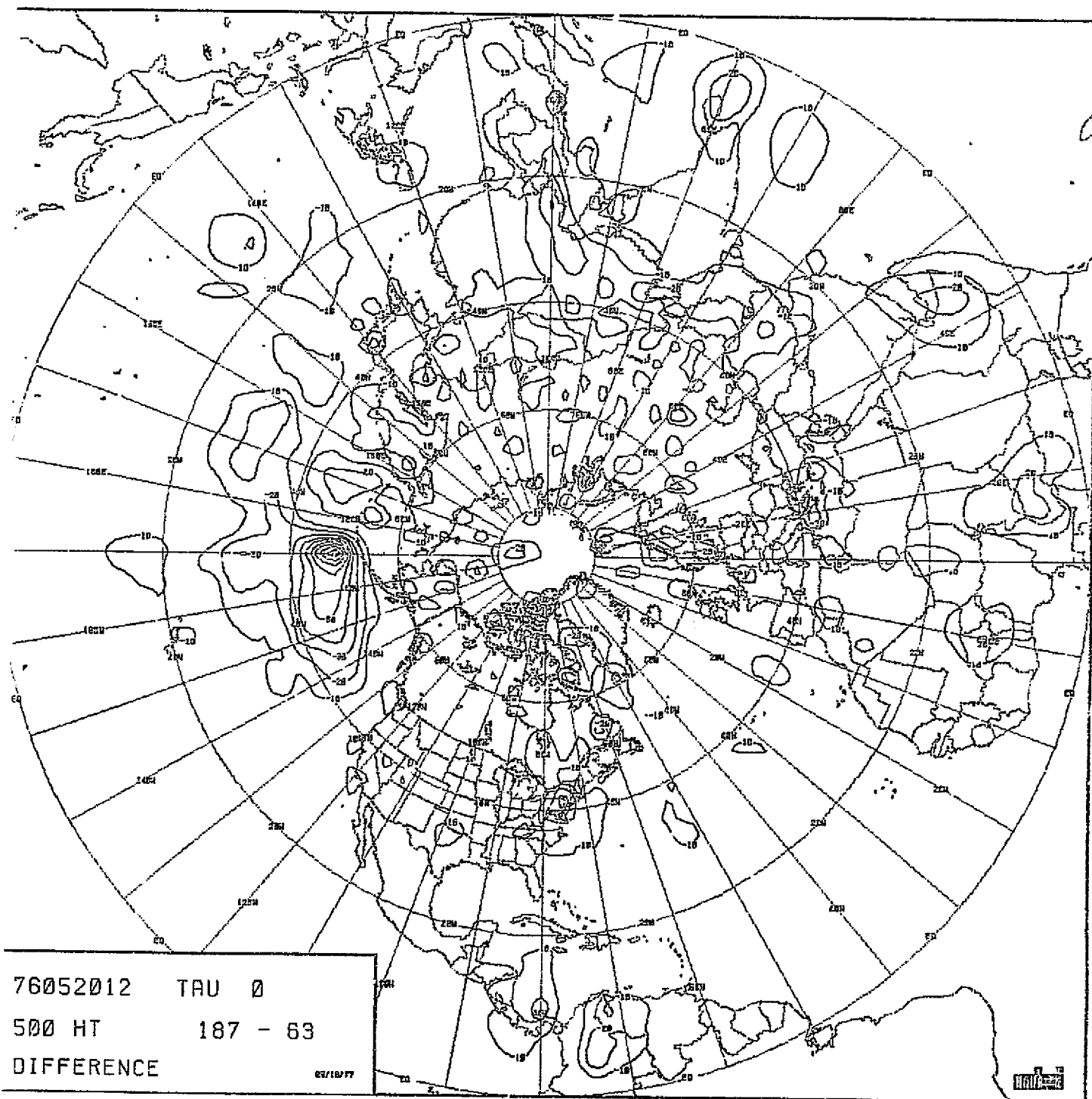
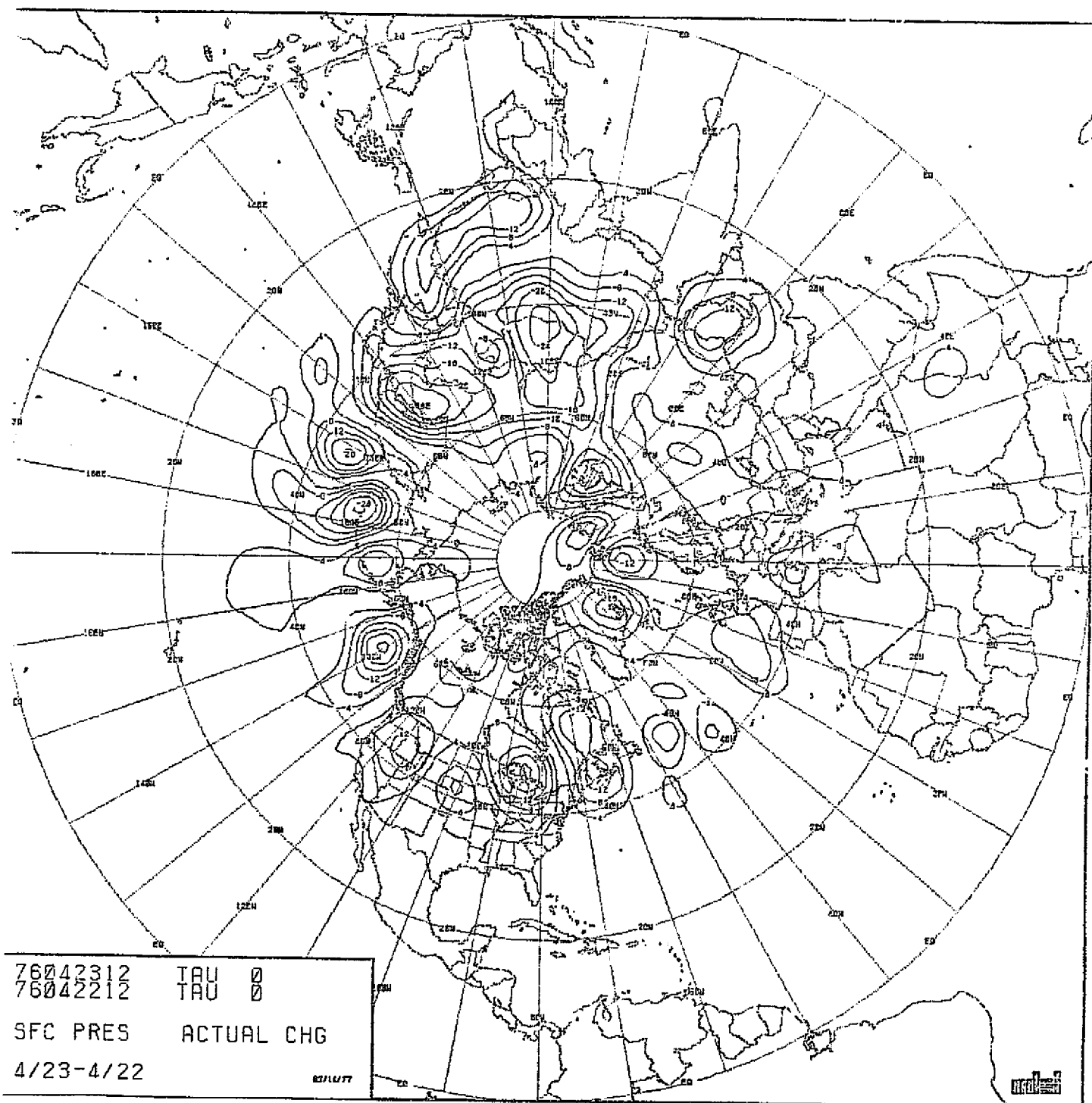


CHART VIII-58

500 MB HEIGHT ANALYSIS DIFFERENCE CHART:
187 x 187 GRID MINUS 63 x 63 GRID.
SCENARIO B.

ORIGINAL PAGE IS
OF POOR QUALITY



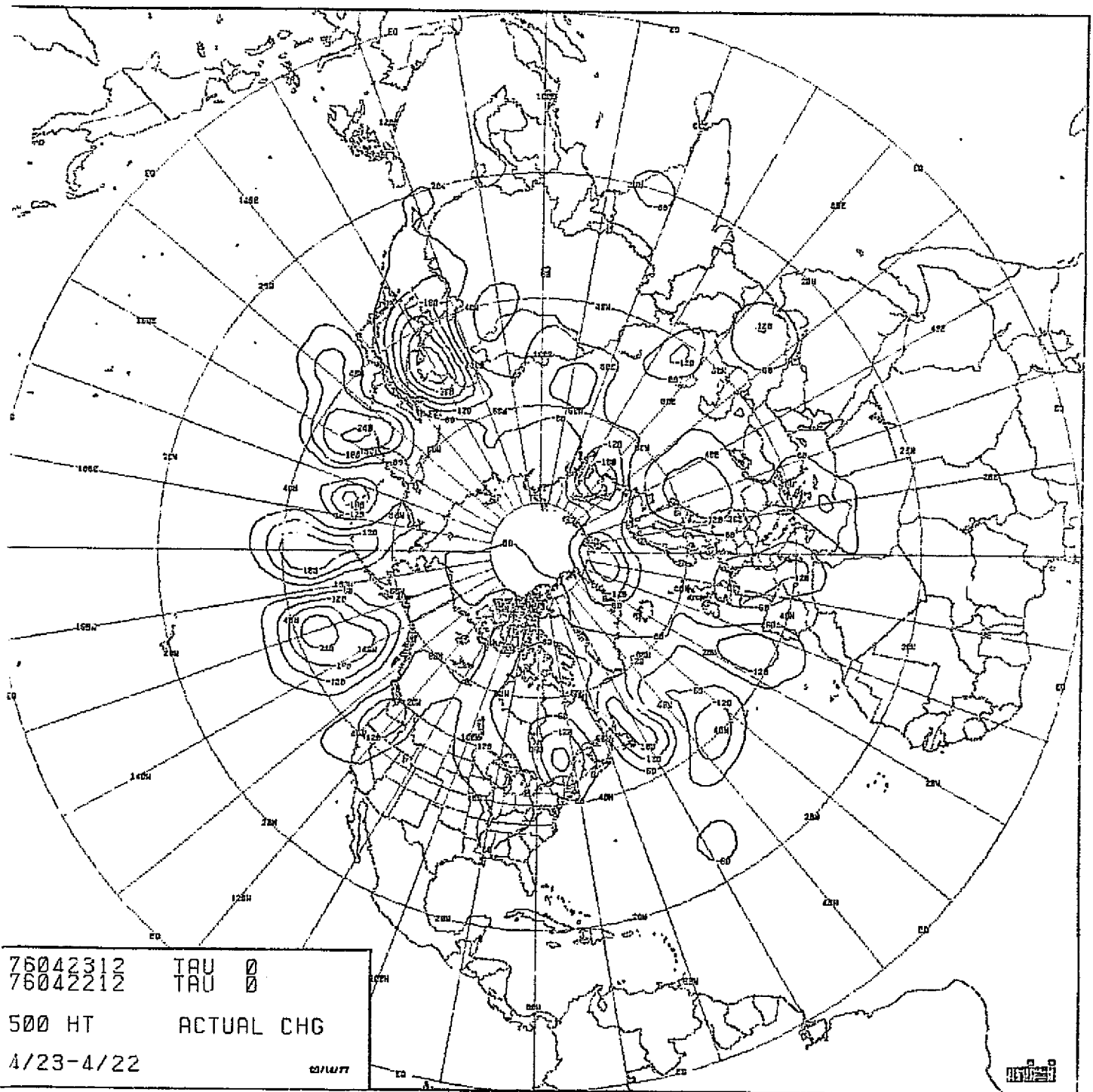


CHART VIII-60 500 MB HEIGHT ACTUAL CHANGES OVER 24 HOURS.
 SCENARIO A.

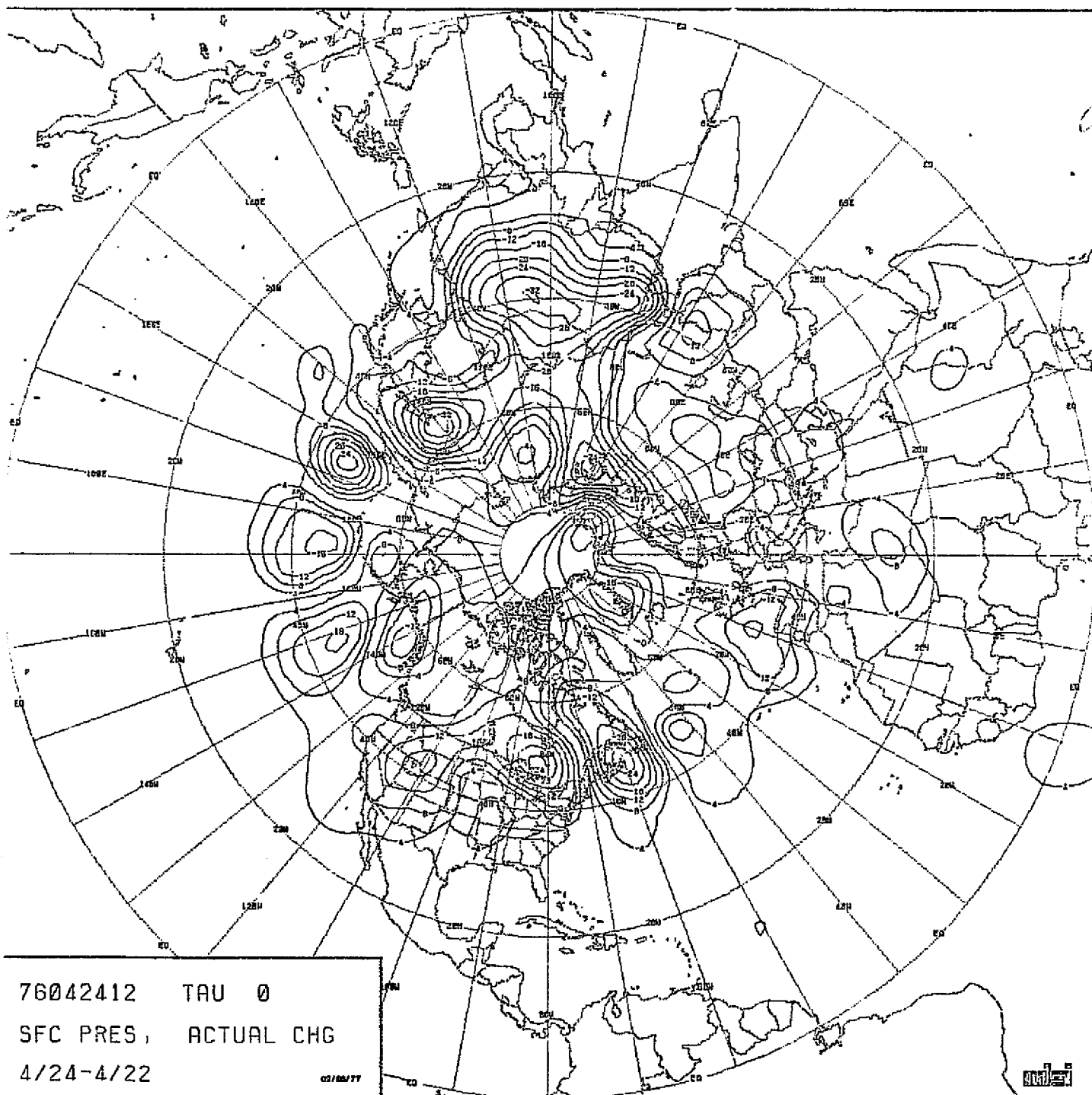


CHART VIII-61

SEA-LEVEL PRESSURE ACTUAL CHANGES OVER 48
HOURS. SCENARIO A.

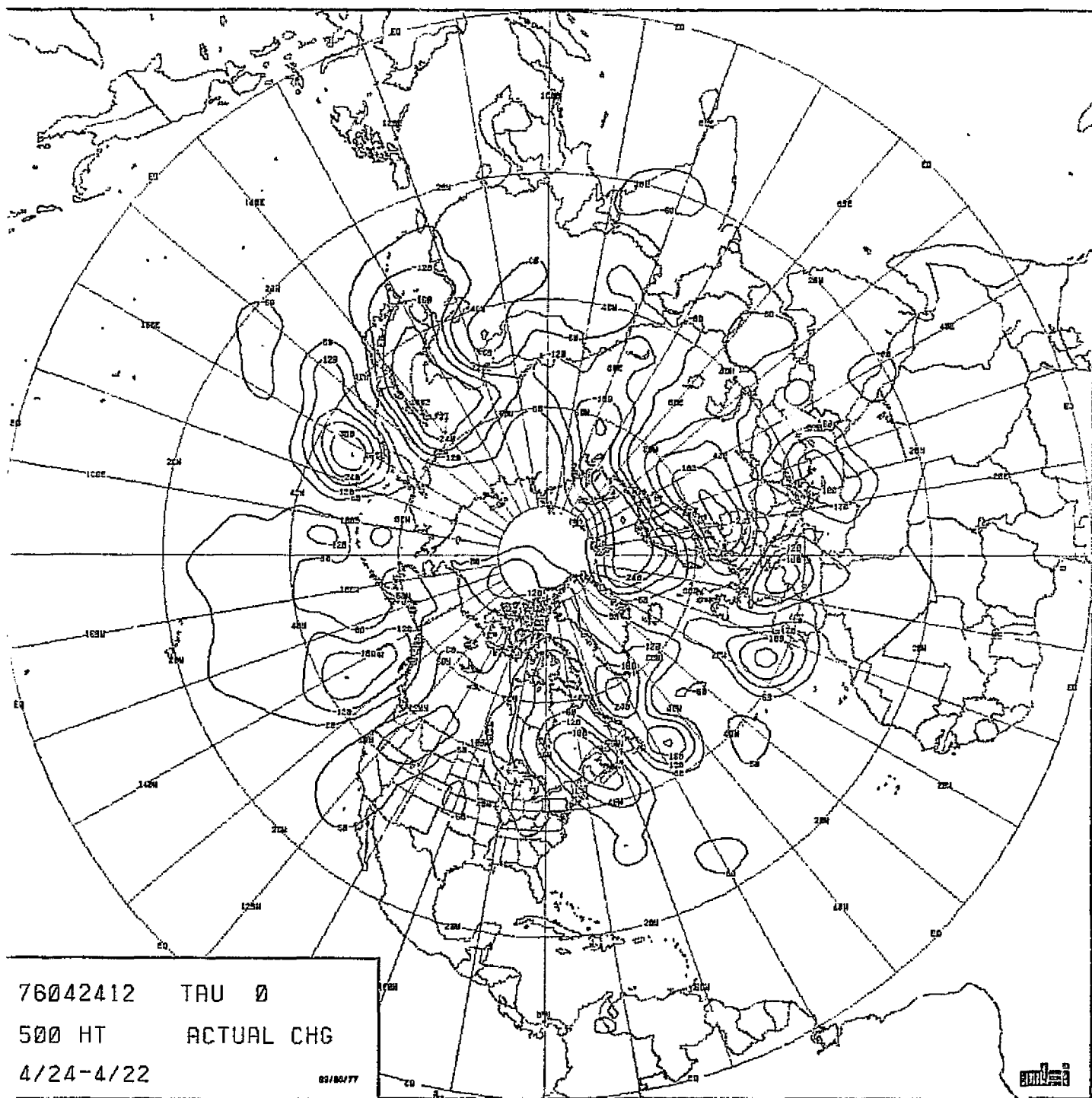


CHART VIII-62

500 MB HEIGHT ACTUAL CHANGES OVER 48 HOURS.
SCENARIO A.

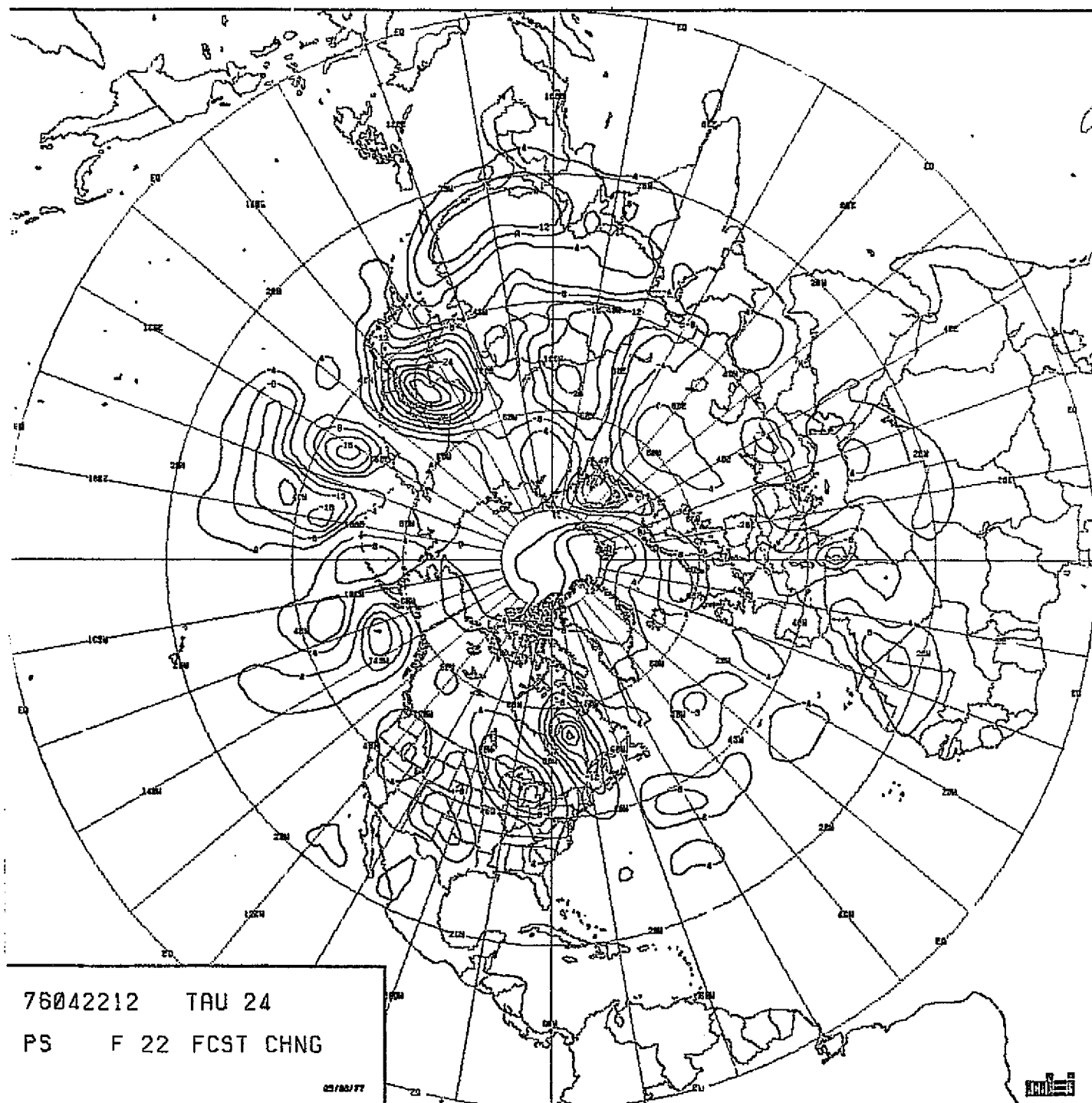
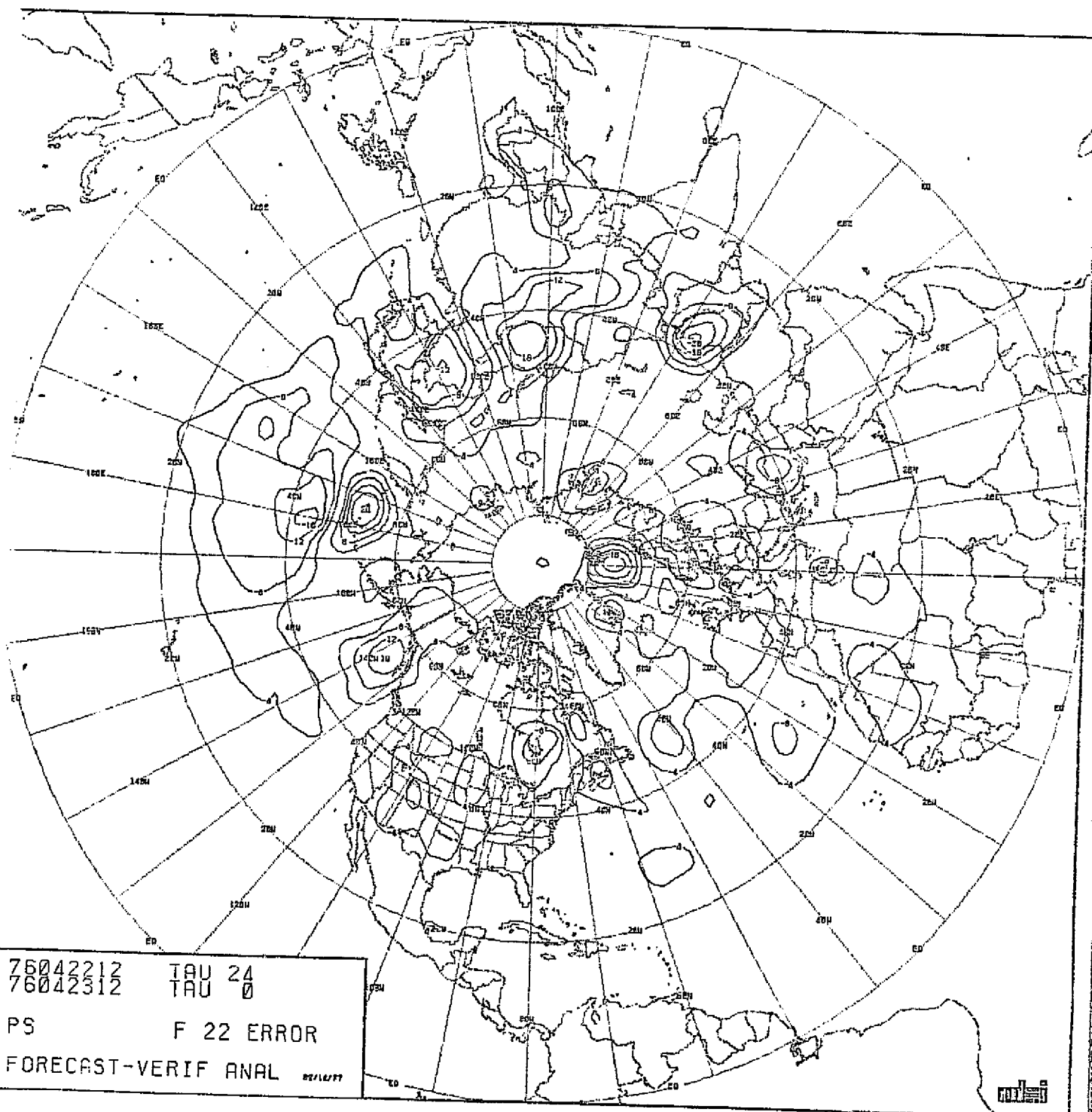
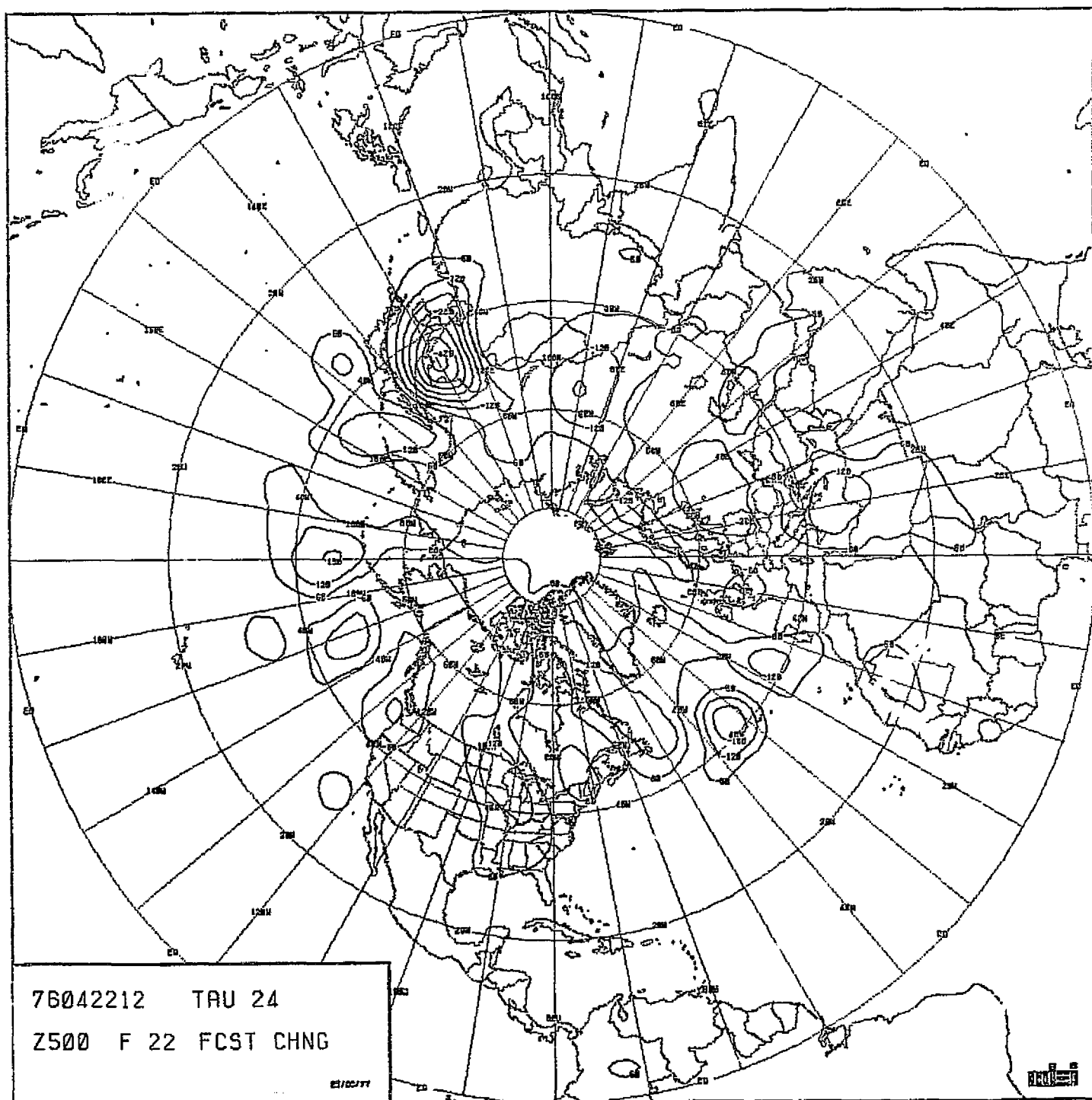
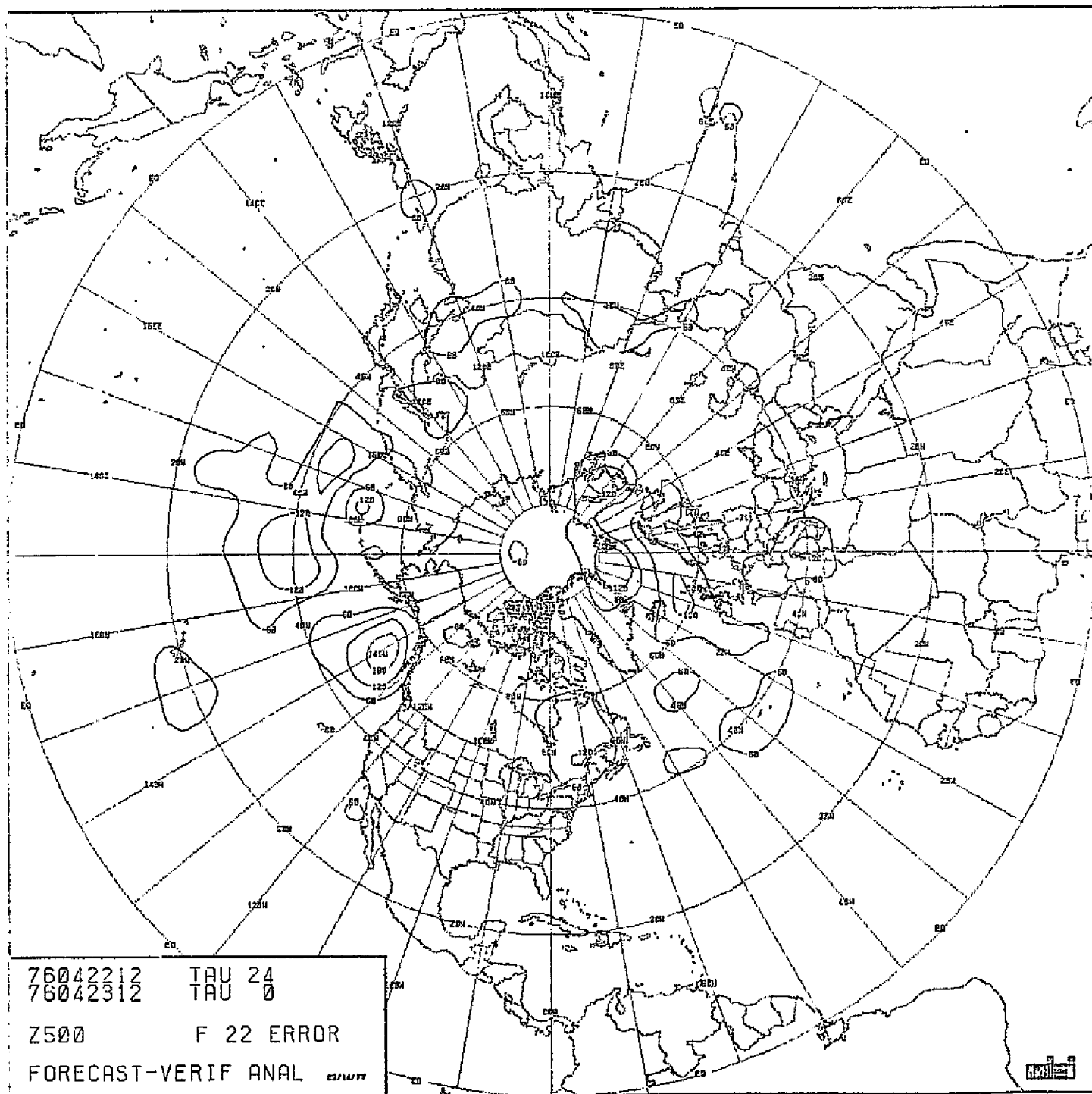


CHART VIII-63 : RUN F22. SCENARIO A. MODEL PEFHCV. 24-HOUR
FORECAST CHANGE IN SEA-LEVEL PRESSURE.







76042212 TAU 24
 76042312 TAU 0
 Z500 F 22 ERROR
 FORECAST-VERIF ANAL

CHART VIII-66

RUN F22. SCENARIO A. MODEL PEFHCY. 24-HOUR
 FORECAST ERROR IN 500 MB HEIGHT.

ORIGINAL PAGE IS
 OF POOR QUALITY

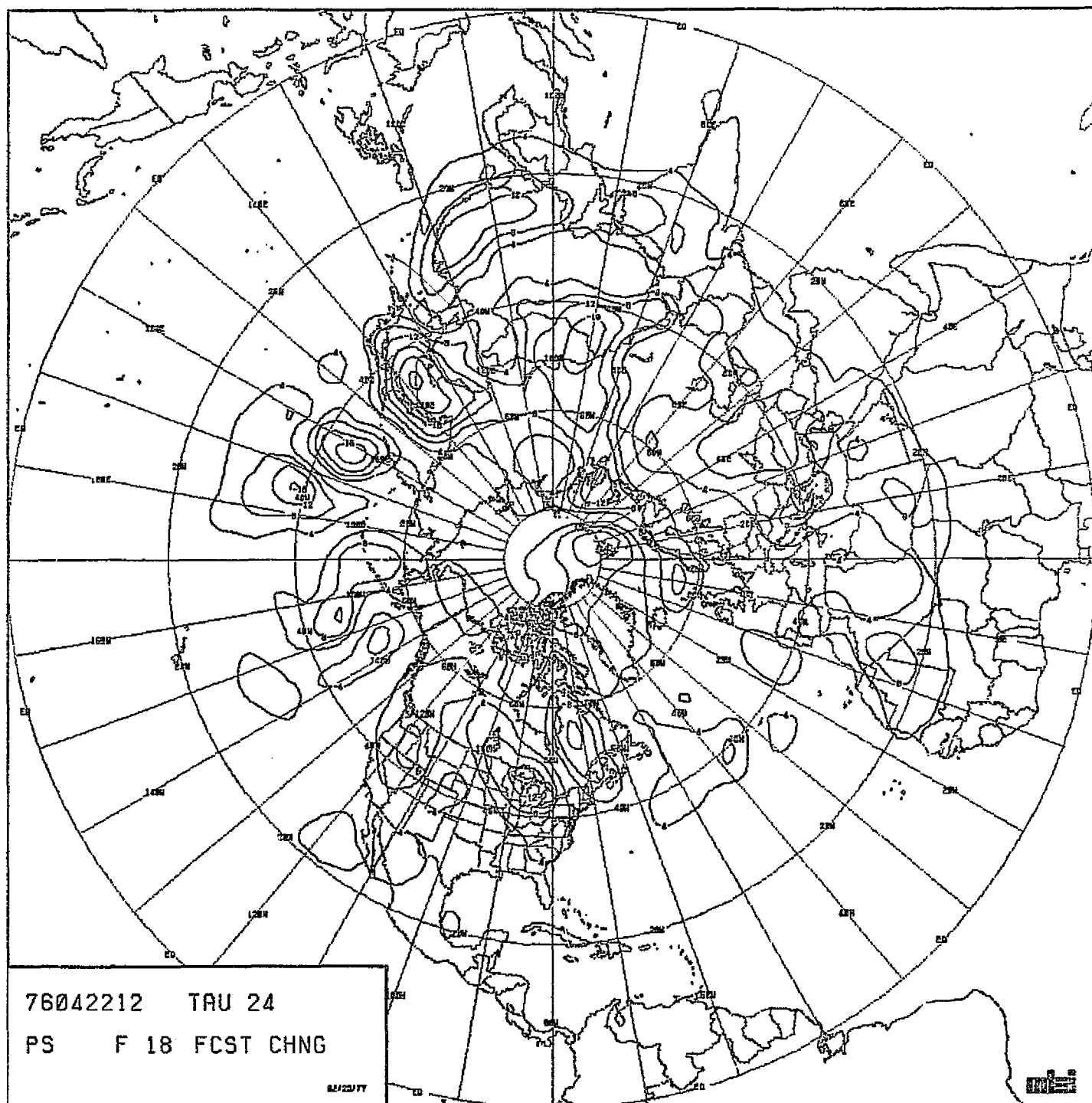
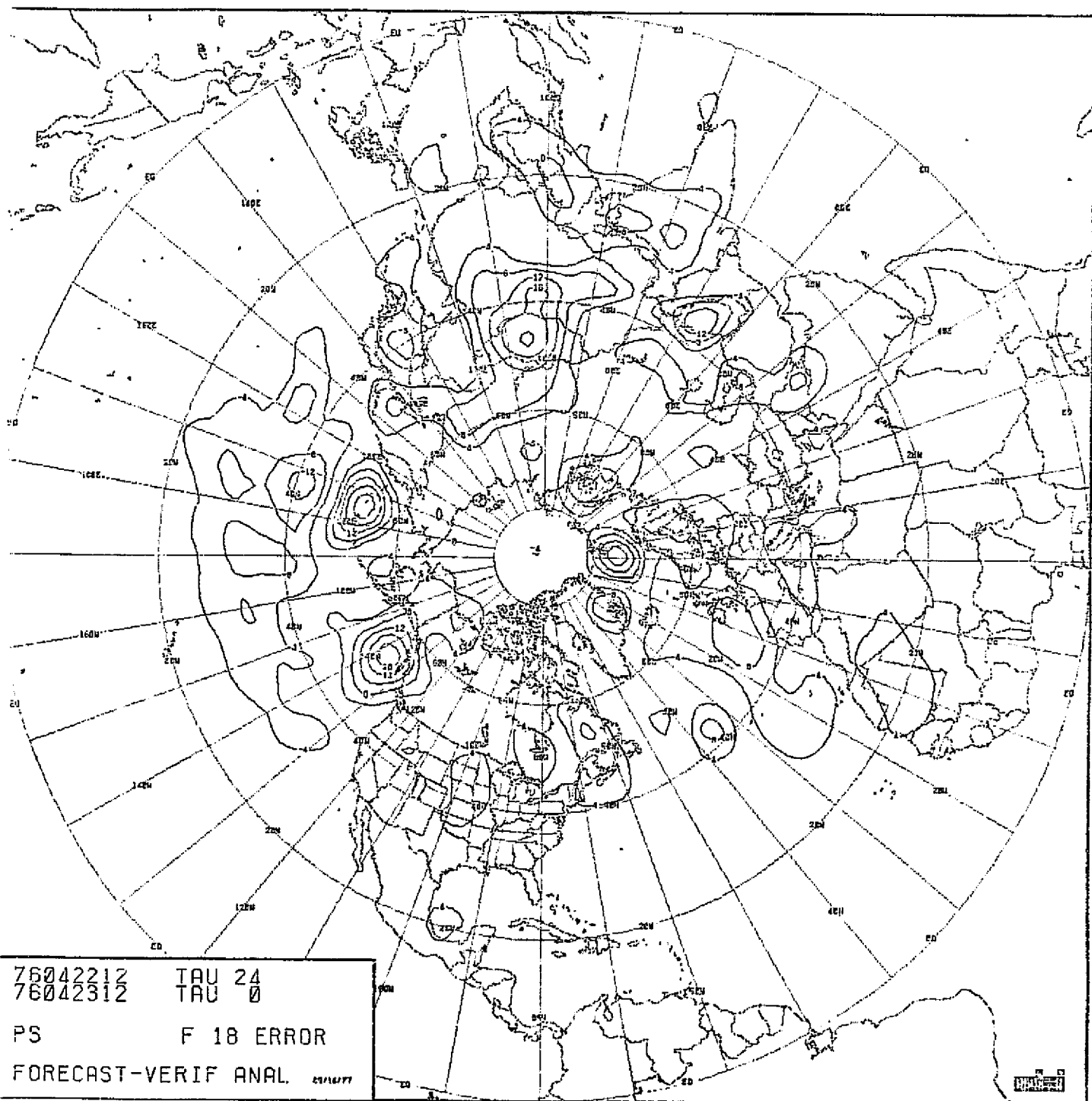


CHART VIII-67 : RUN F18. SCENARIO A. MODEL PECHCV. 24-HOUR
FORECAST CHANGE IN SEA-LEVEL PRESSURE.



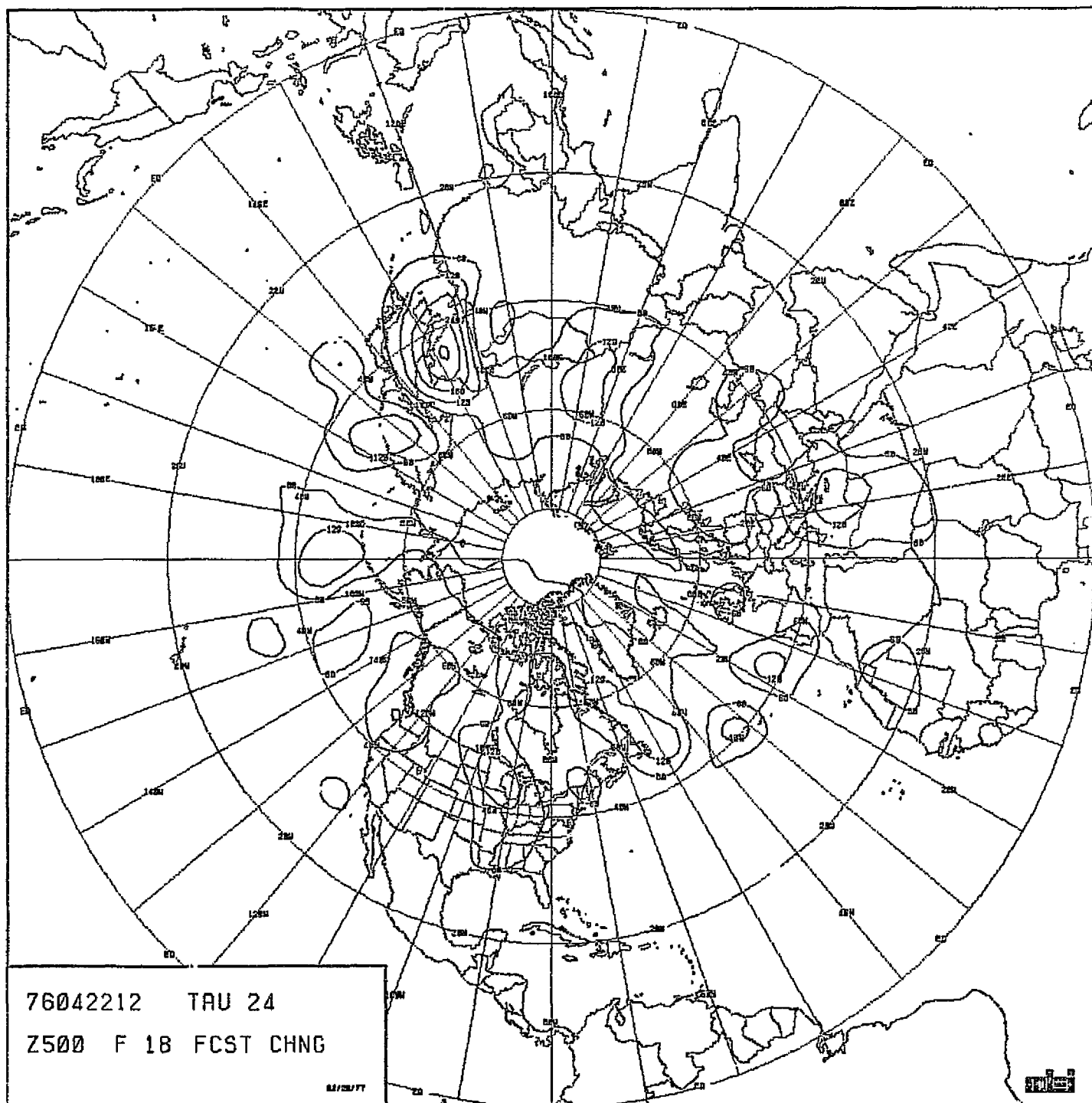


CHART VIII-69 : RUN F18. SCENARIO A. MODEL PECHCV. 24-HOUR
FORECAST CHANGE IN 500 MB HEIGHT.

ORIGINAL PAGE 10
OF POOR QUALITY

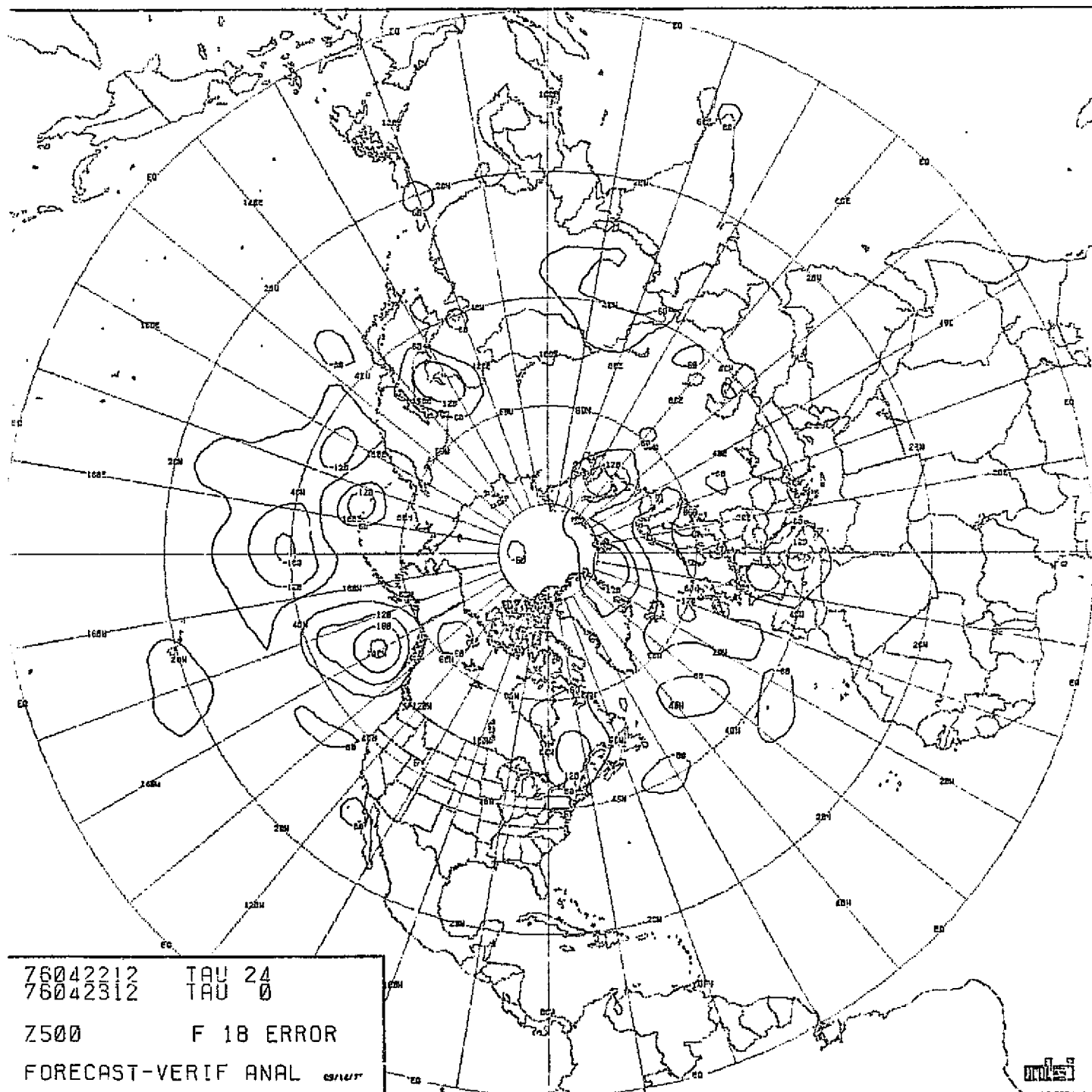


CHART VIII-70

RUN F18. SCENARIO A. MODEL PECHCV. 24-HOUR
FORECAST ERROR IN 500 MB HEIGHT.

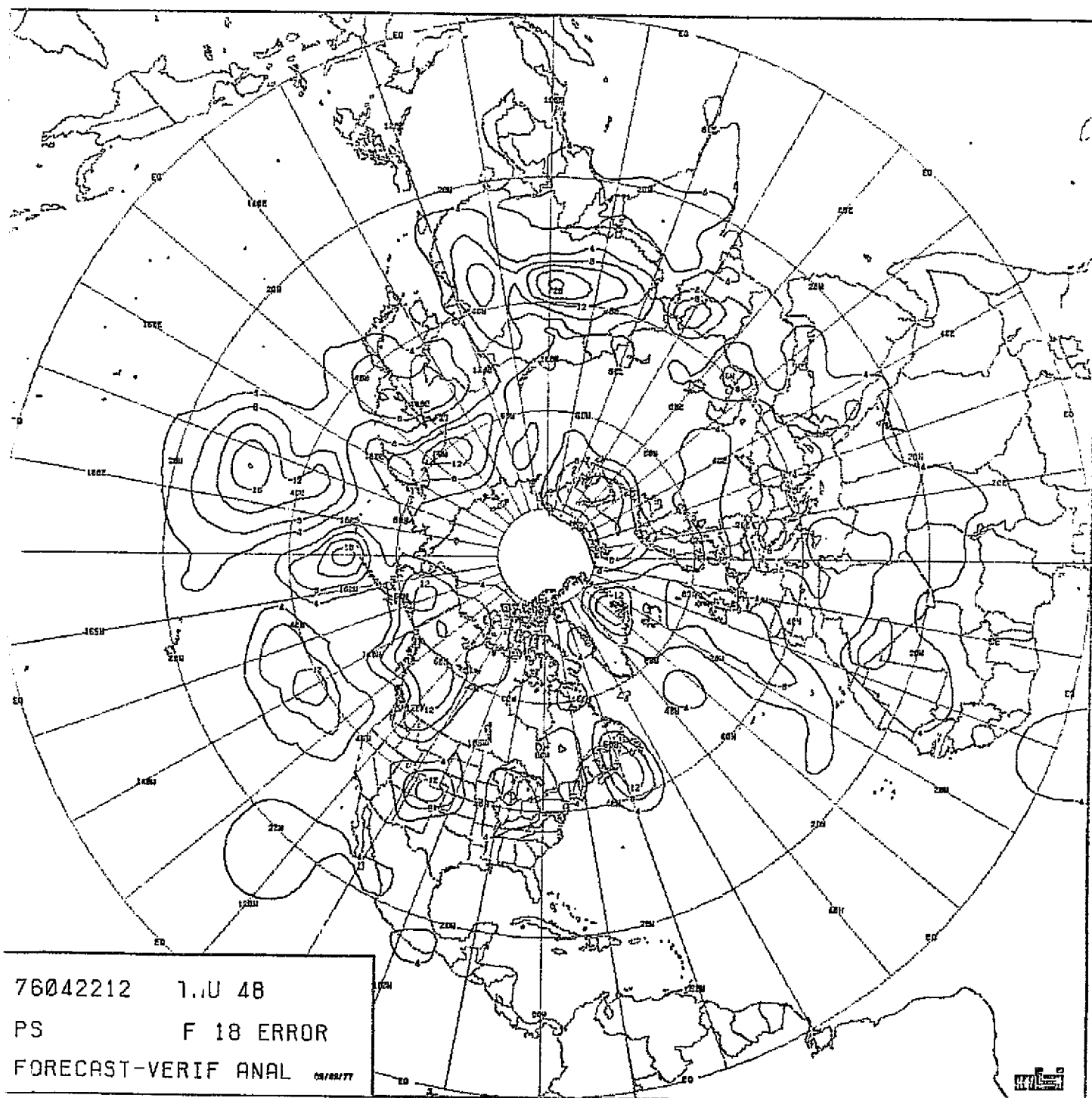


CHART VIII-72

RUN F18. SCENARIO A. MODEL PECHCV. 48-HOUR
FORECAST ERROR IN SEA-LEVEL PRESSURE.

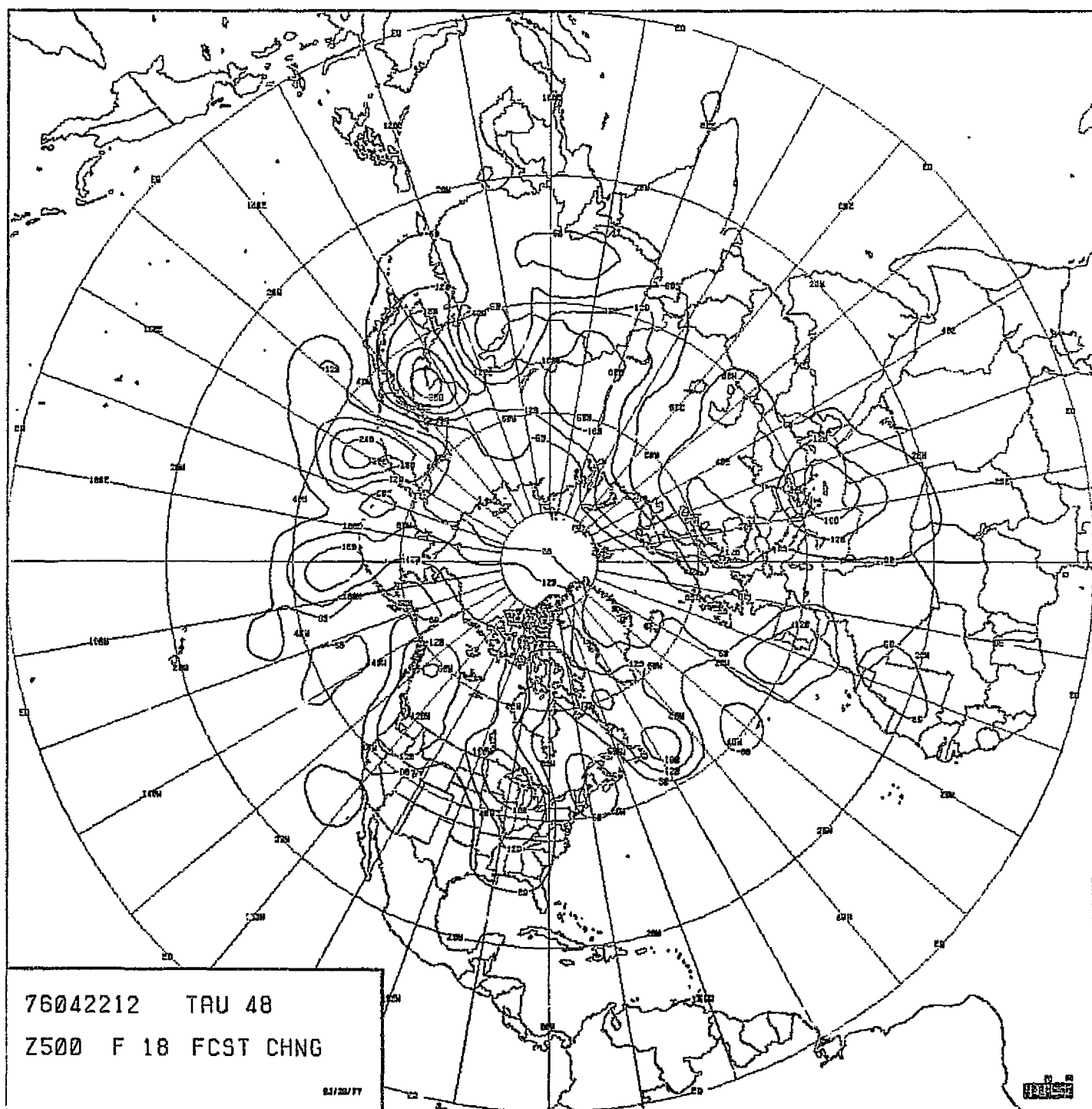
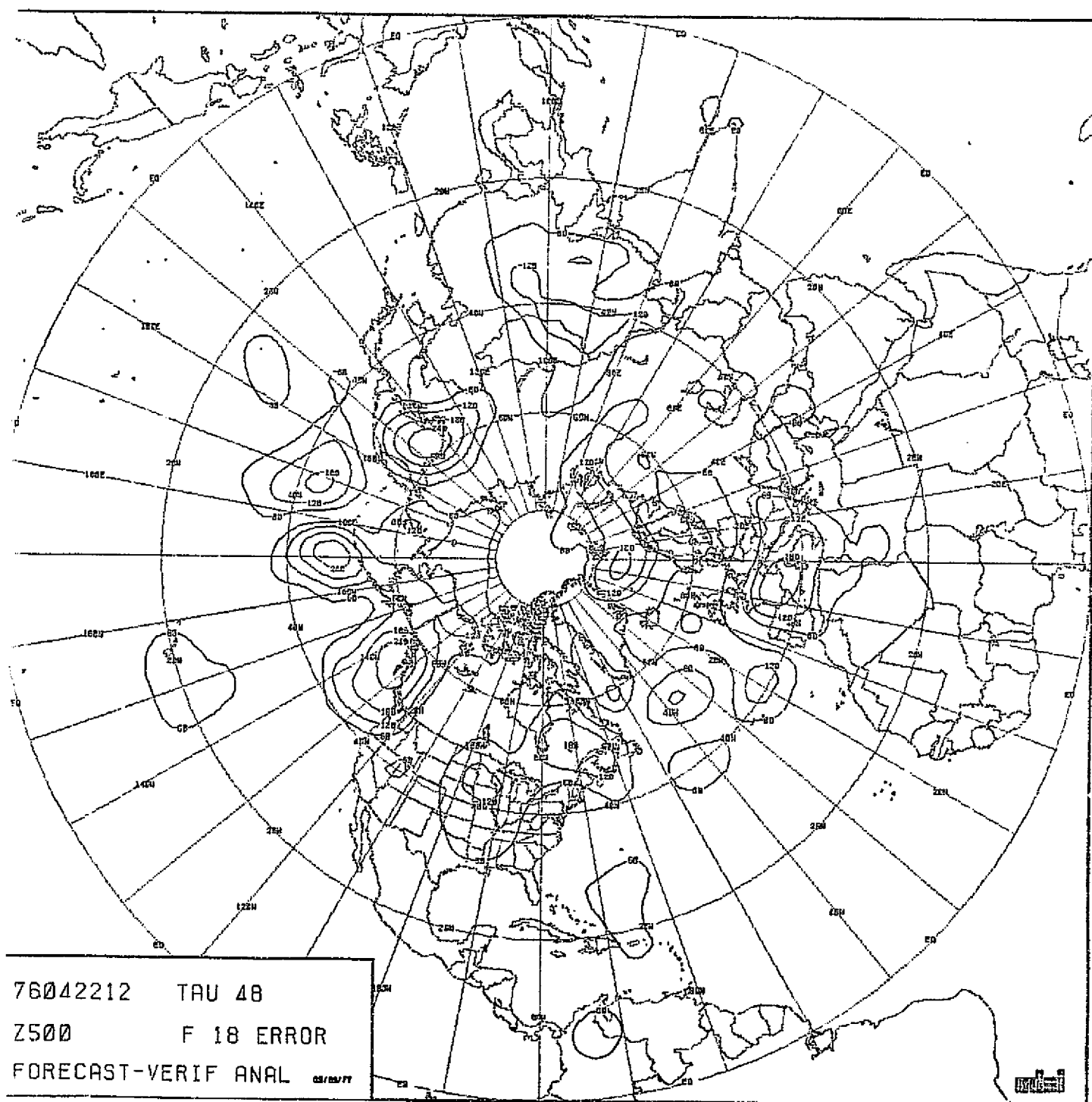


CHART VIII-73 : RUN F18. SCENARIO A. MODEL PECHCV. 48-HOUR
FORECAST CHANGE IN 500 MB HEIGHT.

ORIGINAL PAGE IS
OF POOR QUALITY



76042212 TAU 48
Z500 F 18 ERROR
FORECAST-VERIF ANAL

CHART VIII-74

RUN F18. SCENARIO A. MODEL PECHCV. 48-HOUR
FORECAST ERROR IN 500 MB HEIGHT.

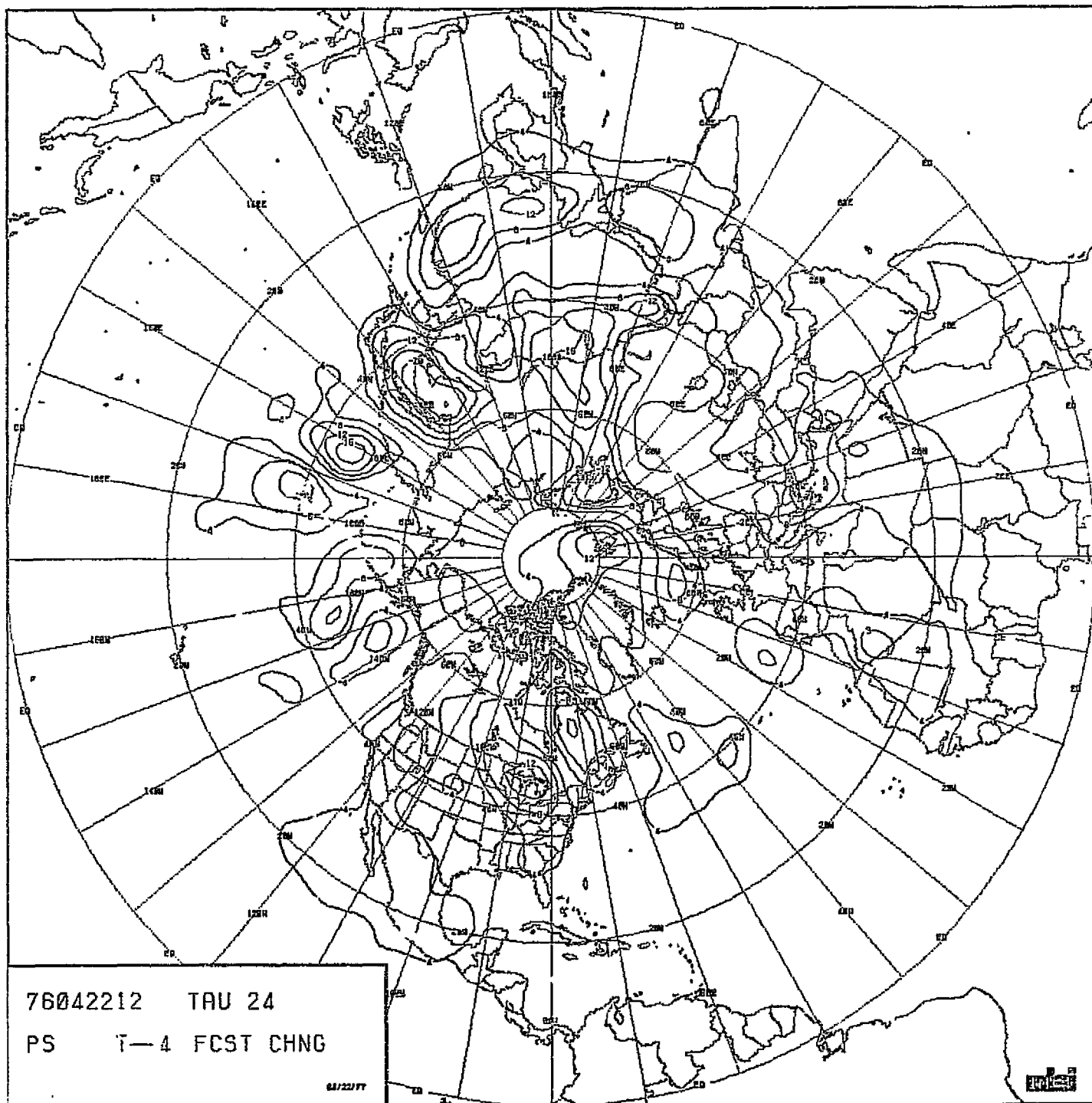


CHART VIII-75 : RUN T4. SCENARIO A. MODEL PECHFV. 24-HOUR
FORECAST CHANGE IN SEA-LEVEL PRESSURE.

ORIGINAL PAGE IS
OF POOR QUALITY

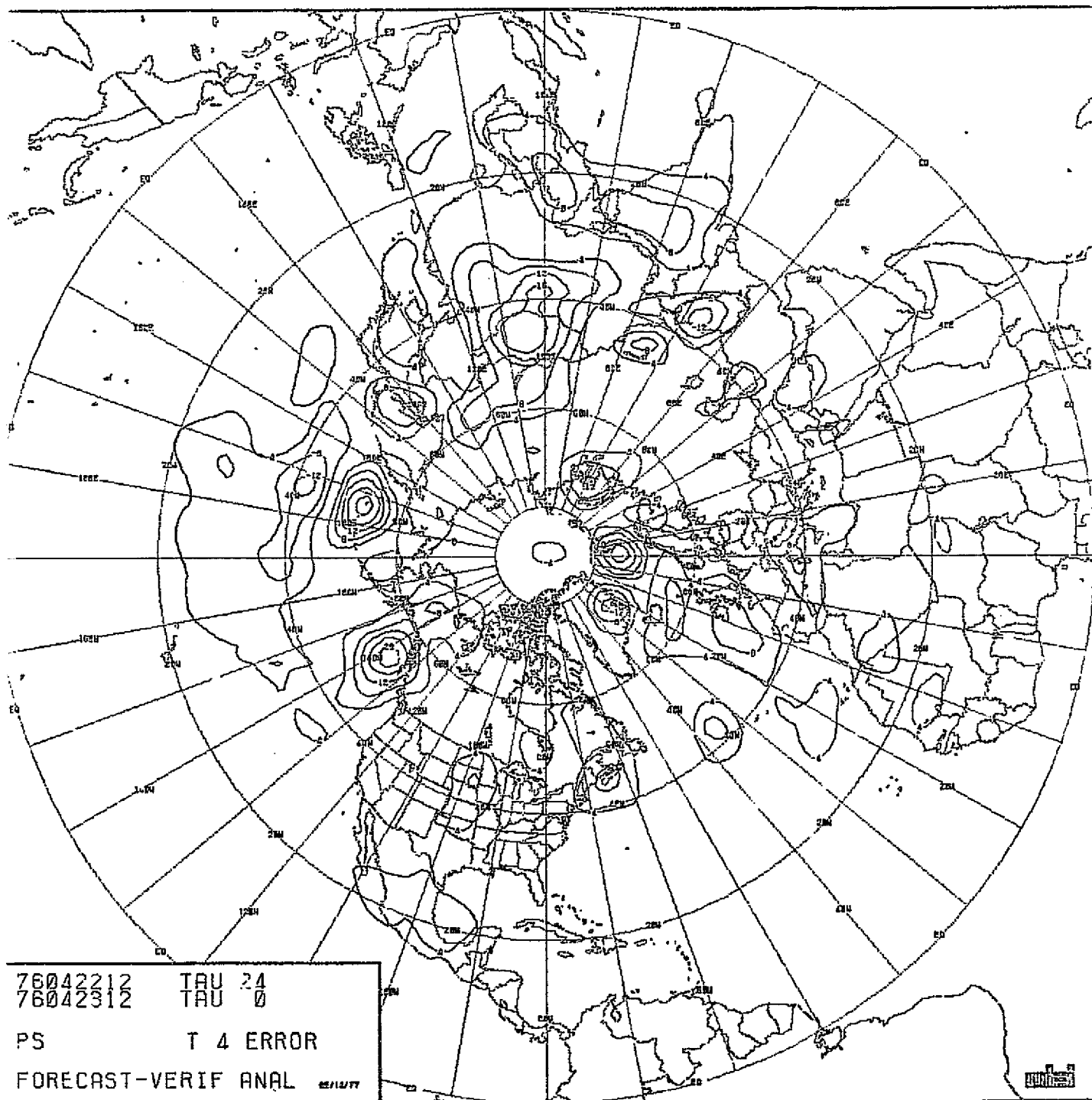


CHART VIII-76

RUN T4. SCENARIO A. MODEL PECHFV. 24-HOUR
FORECAST ERROR IN SEA-LEVEL PRESSURE.

PAGE 13
OF POOR QUALITY

ORIGINAL PAGE IS
OF POOR QUALITY

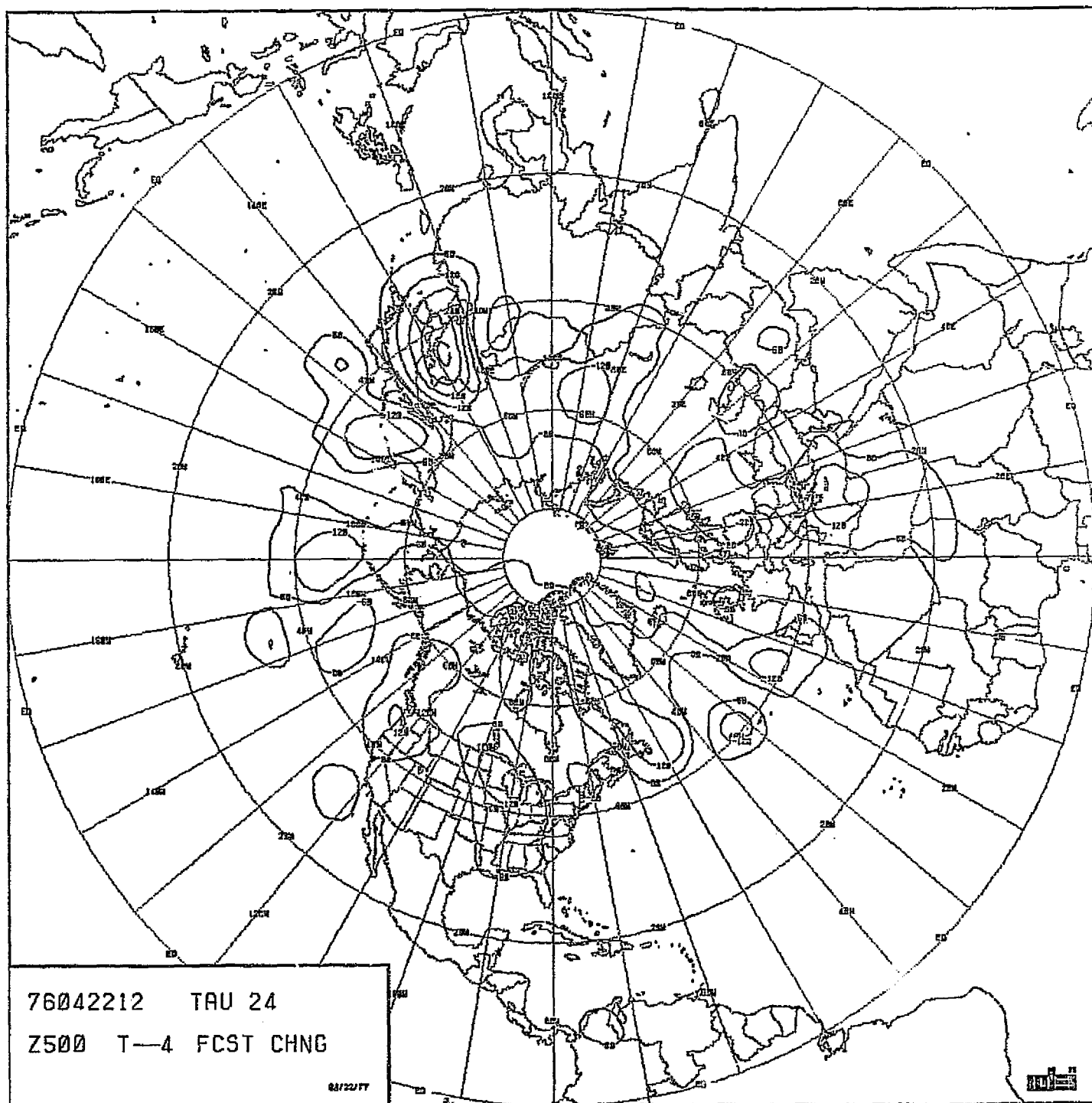


CHART VIII-77 : RUN T4. SCENARIO A. MODEL PECHEV. 24-HOUR
FORECAST CHANGE IN 500 MB HEIGHT.

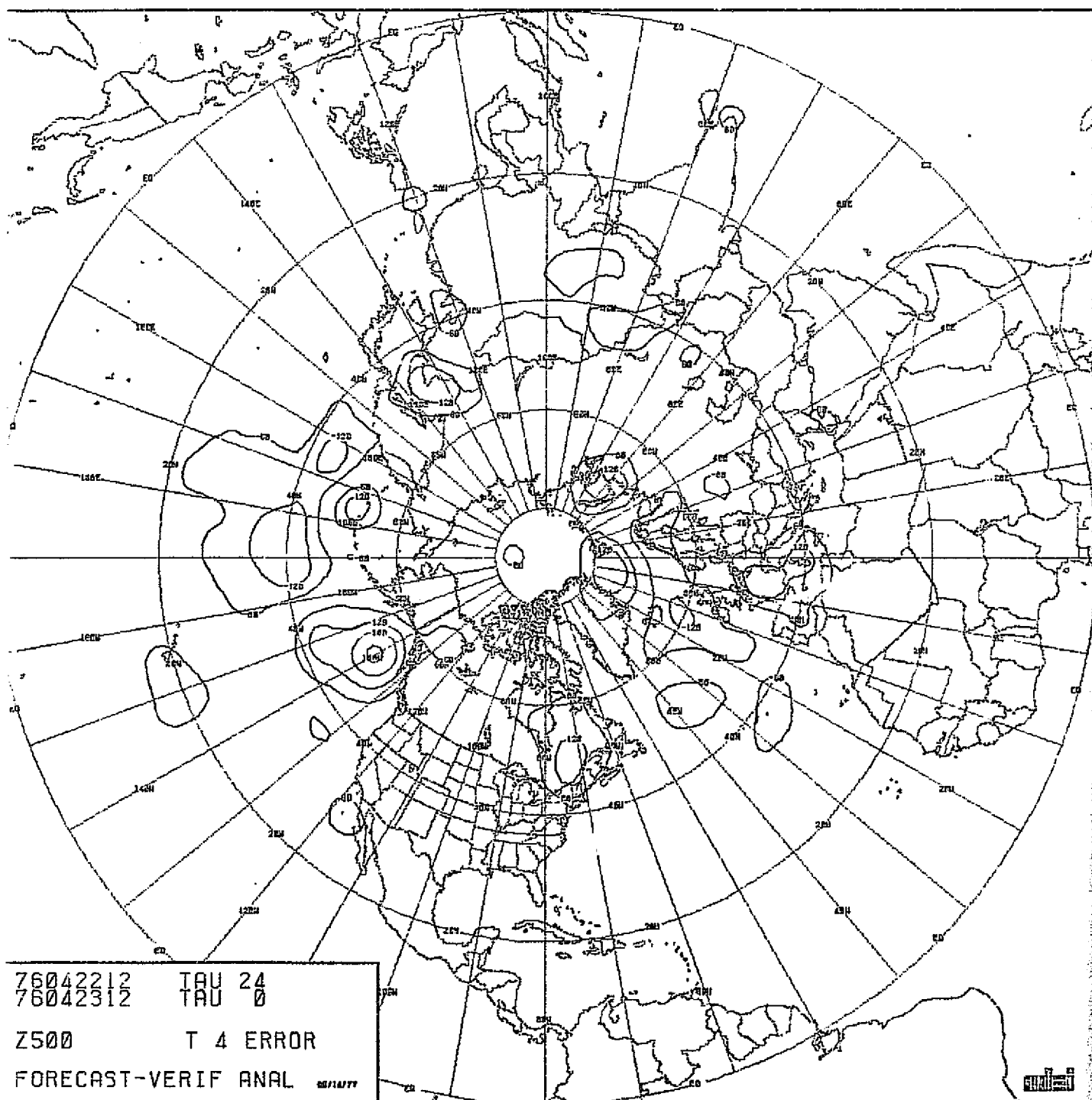


CHART VIII-78

RUN T4. SCENARIO A. MODEL PECHFV. 24-HOUR
FORECAST ERROR IN 500 MB HEIGHT.

ORIGINAL PAGE IS
OF POOR QUALITY

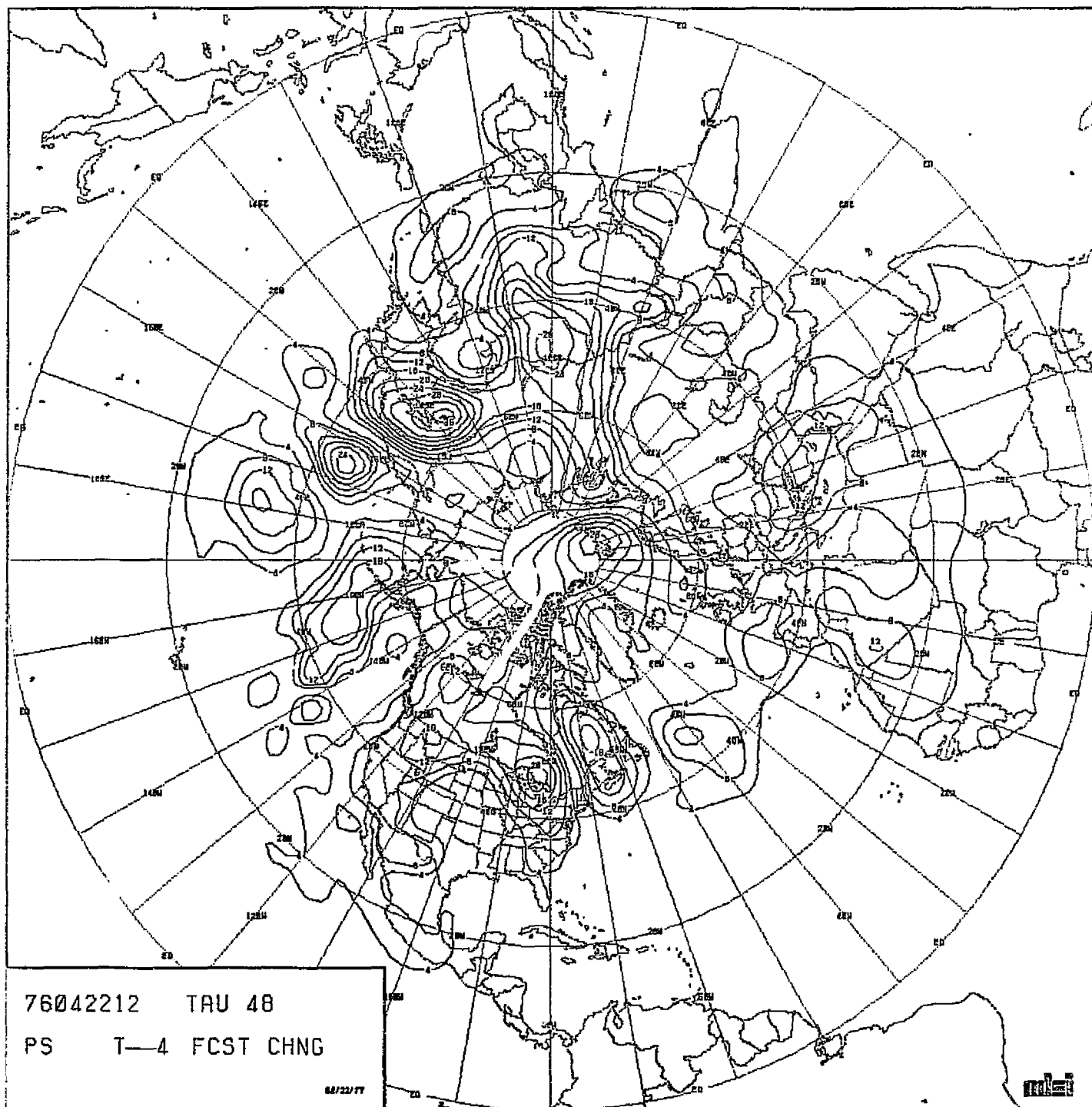


CHART VIII-79 : RUN T4. SCENARIO A. MODEL PECHFV. 48-HOUR
FORECAST CHANGE IN SEA-LEVEL PRESSURE.

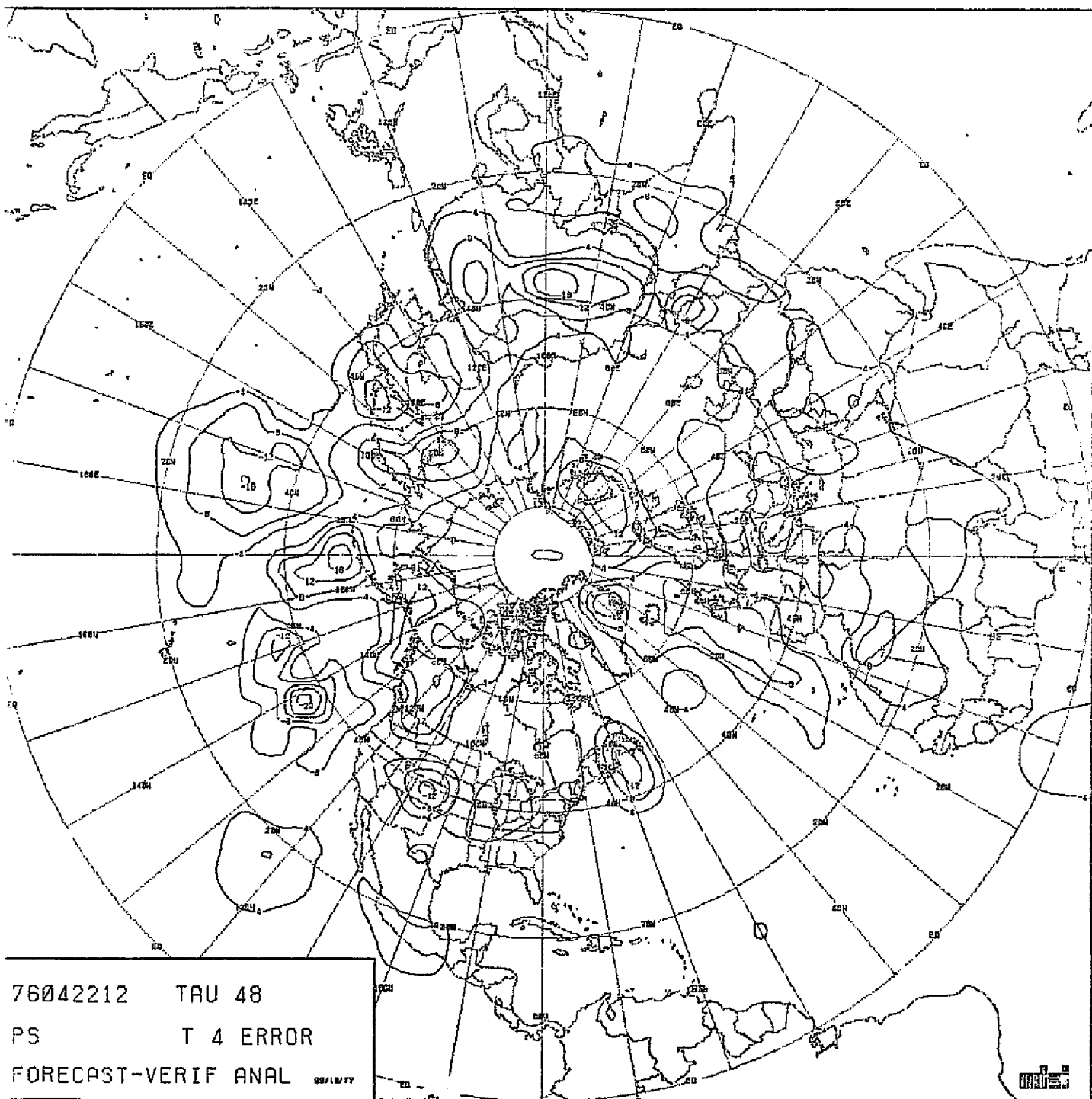


CHART VIII-80

RUN T4. SCENARIO A. MODEL PECHV. 48-HOUR
FORECAST ERROR IN SEA-LEVEL PRESSURE.

ORIGINAL PAGE IS
OF POOR QUALITY

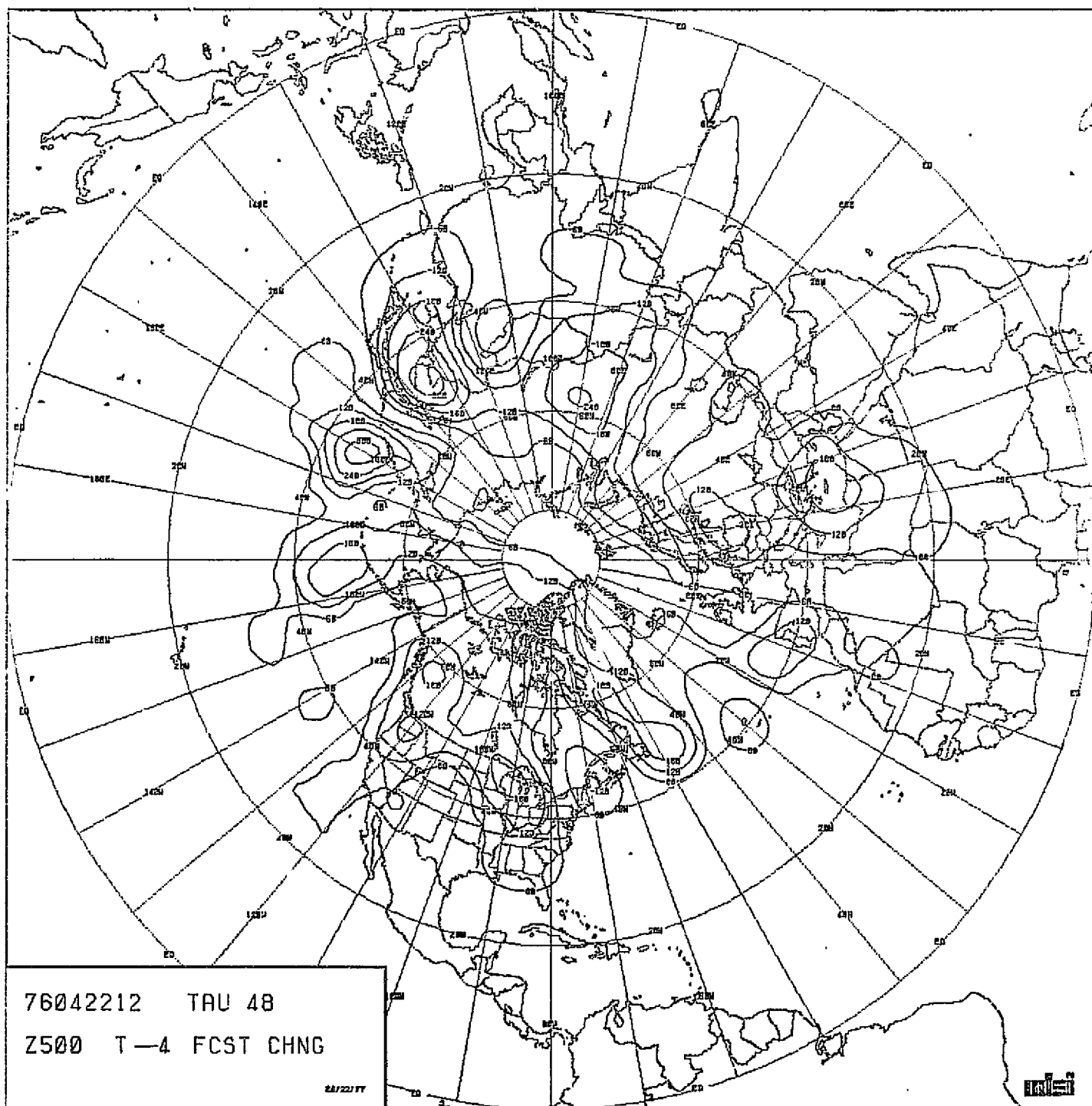


CHART VIII-81 : RUN T4. SCENARIO A. MODEL PECHFV. 48-HOUR
FORECAST CHANGE IN 500 MB HEIGHT.

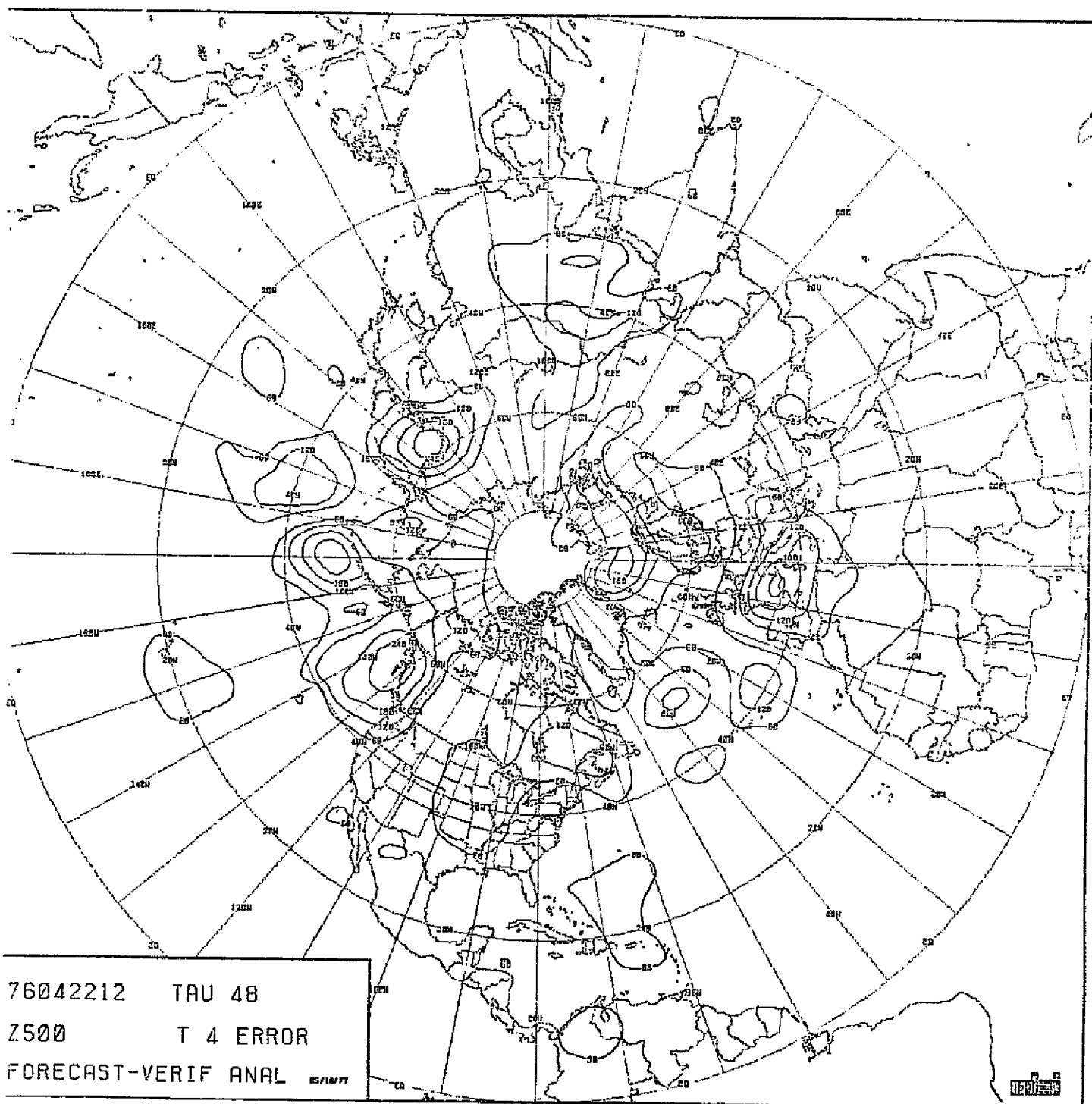


CHART VIII-82

RUN T4. SCENARIO A. MODEL PECHFV. 48-HOUR
FORECAST ERROR IN 500 MB HEIGHT.

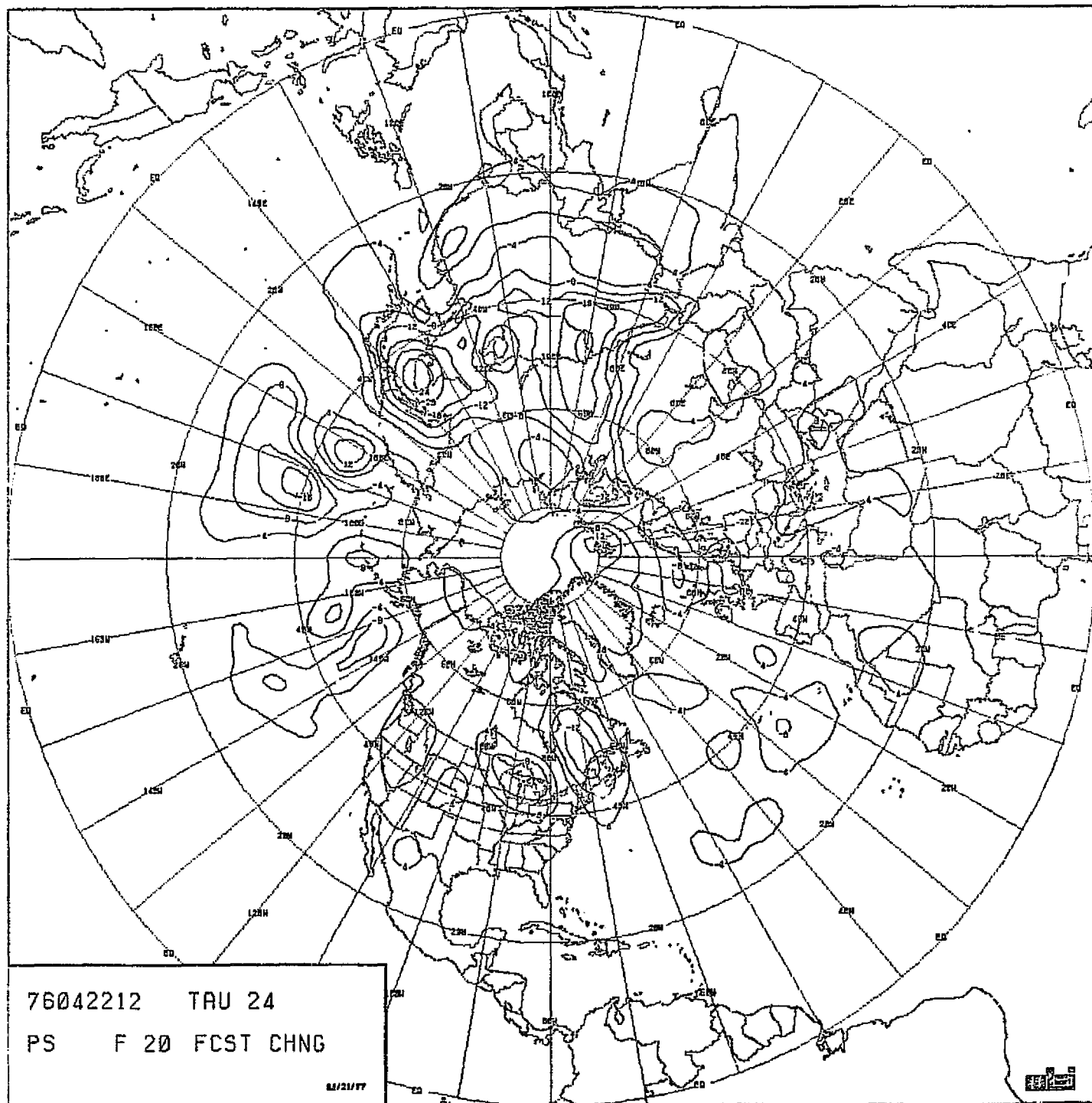


CHART VIII-83 : RUN F20. SCENARIO A. MODEL PECHCV. 24-HOUR
FORECAST CHANGE IN SEA-LEVEL PRESSURE.

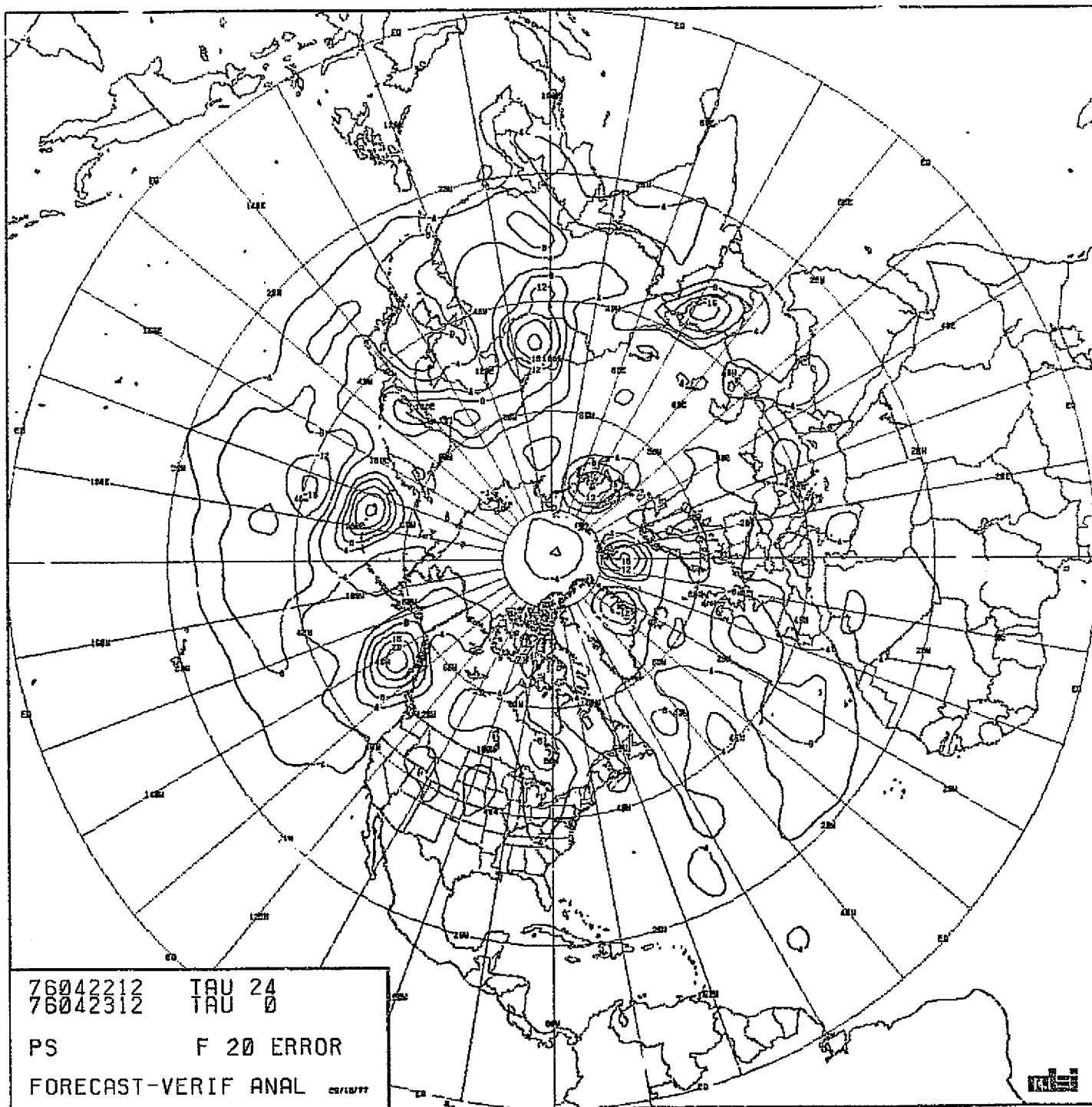


CHART VIII-84

RUN F20. SCENARIO A. MODEL PECHCV. 24-HOUR
 FORECAST ERROR IN SEA-LEVEL PRESSURE.

54

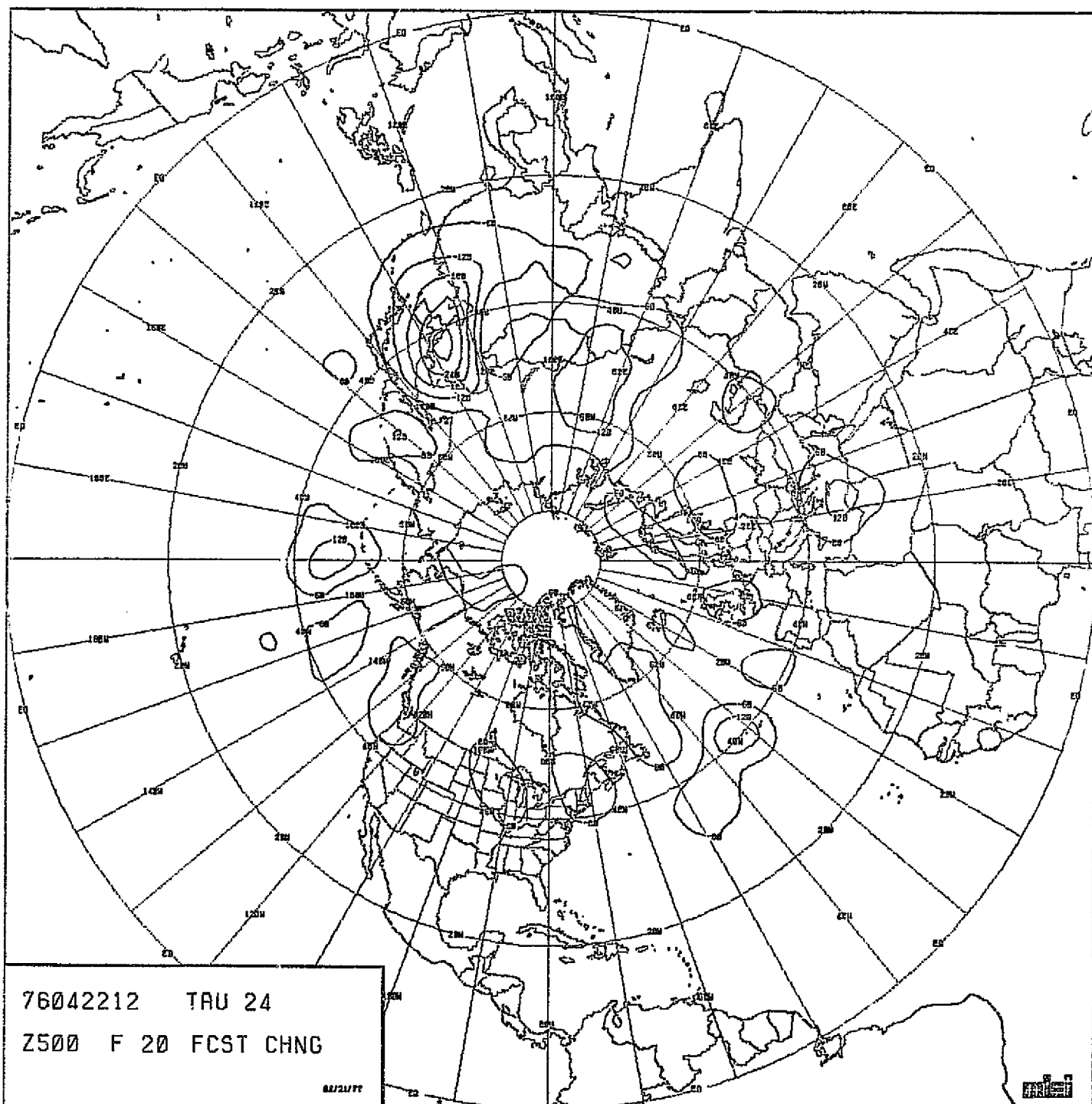


CHART VIII-85 : RUN F20. SCENARIO A. MODEL PECHCV. 24-HOUR
FORECAST CHANGE IN 500 MB HEIGHT.

ORIGINAL PAGE 48
OF POOR QUALITY

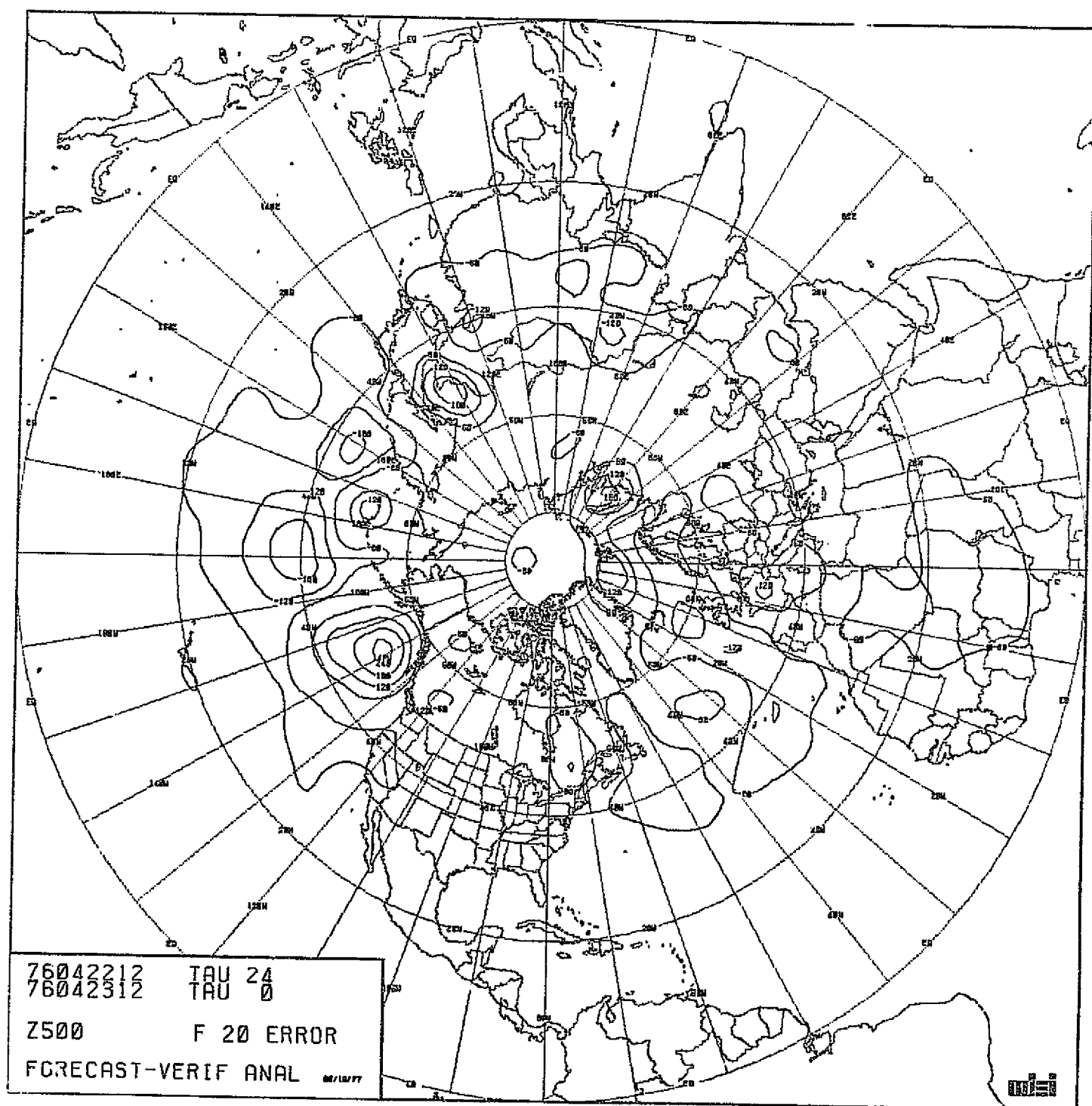


CHART VIII-86

RUN F20. SCENARIO A. MODEL PECHCV. 24-HOUR
 FORECAST ERROR IN 500 MB HEIGHT.

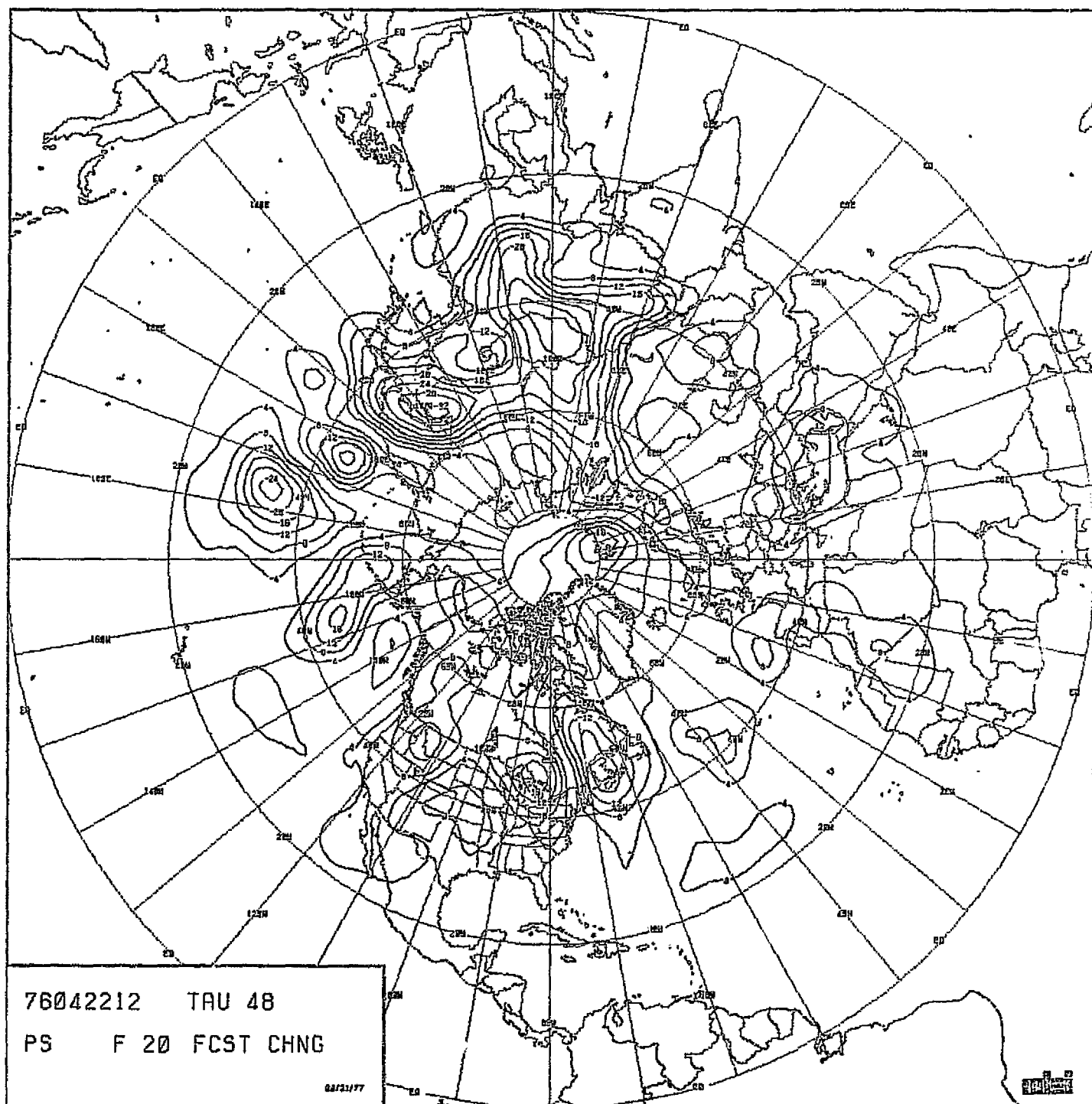


CHART VIII-87 : RUN F20. SCENARIO A. MODEL PECHCV. 48-HOUR
FORECAST CHANGE IN SEA-LEVEL PRESSURE.

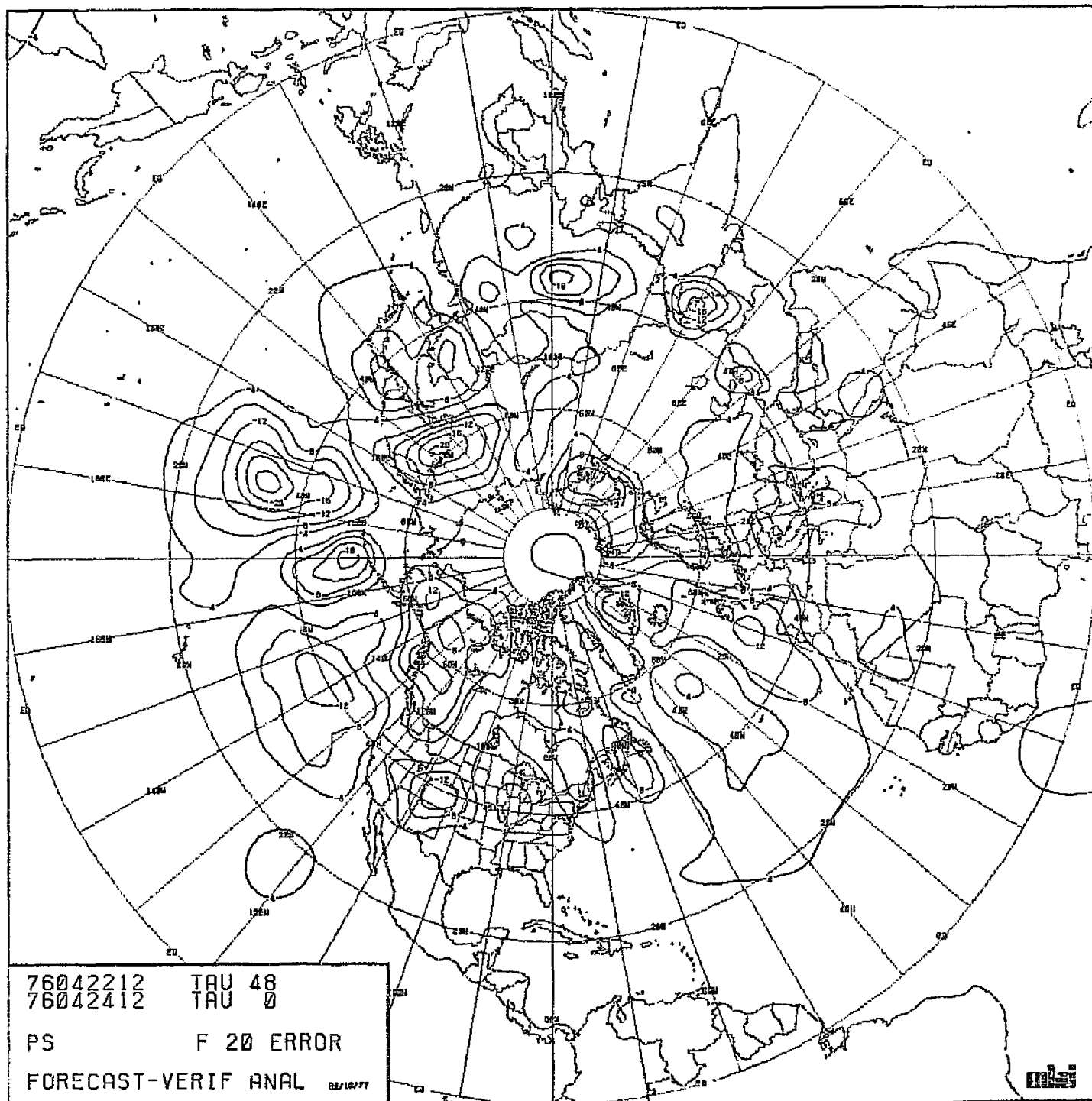


CHART VIII-88

RUN F20. SCENARIO A. MODEL PECHCV. 48-HOUR
 FORECAST ERROR IN SEA-LEVEL PRESSURE.

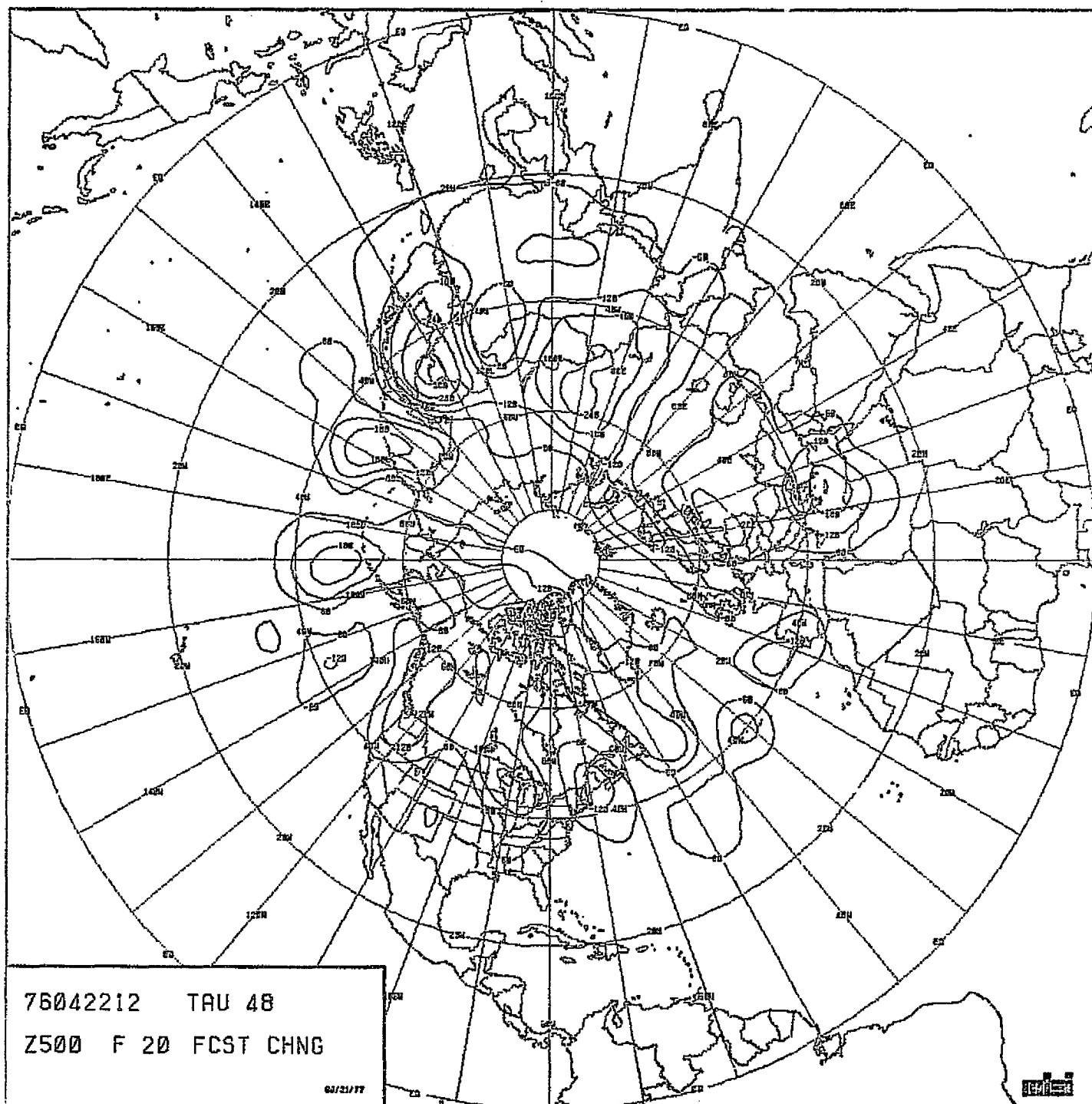


CHART VIII-89 : RUN F20. SCENARIO A. MODEL BECHCV. 48-HOUR
FORECAST CHANGE IN 500 MB HEIGHT.

ORIGINAL PAGE IS
OF POOR QUALITY

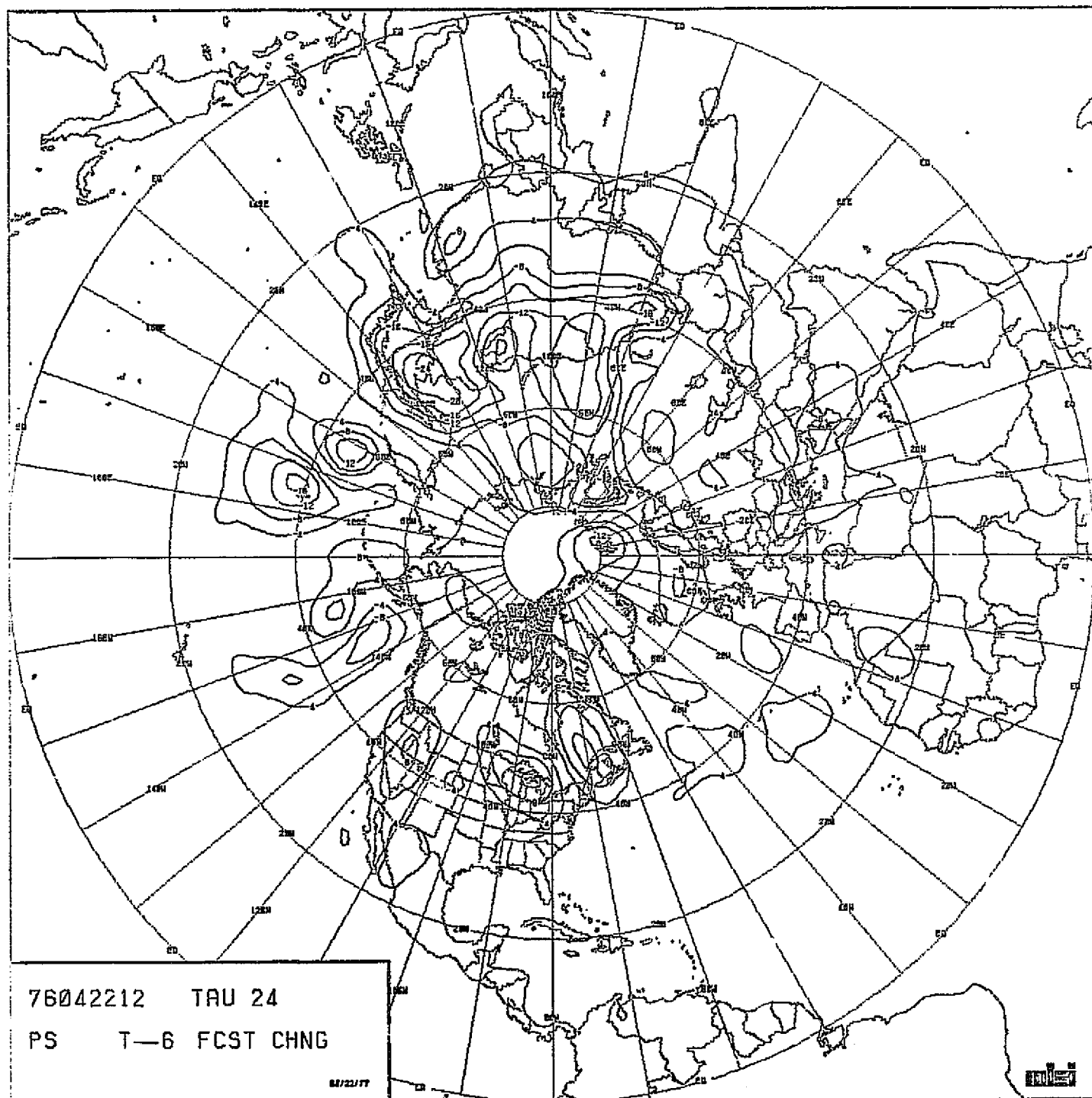


CHART VIII-91 : RUN T6. SCENARIO A. MODEL PECHV. 24-HOUR
FORECAST CHANGE IN SEA-LEVEL PRESSURE.

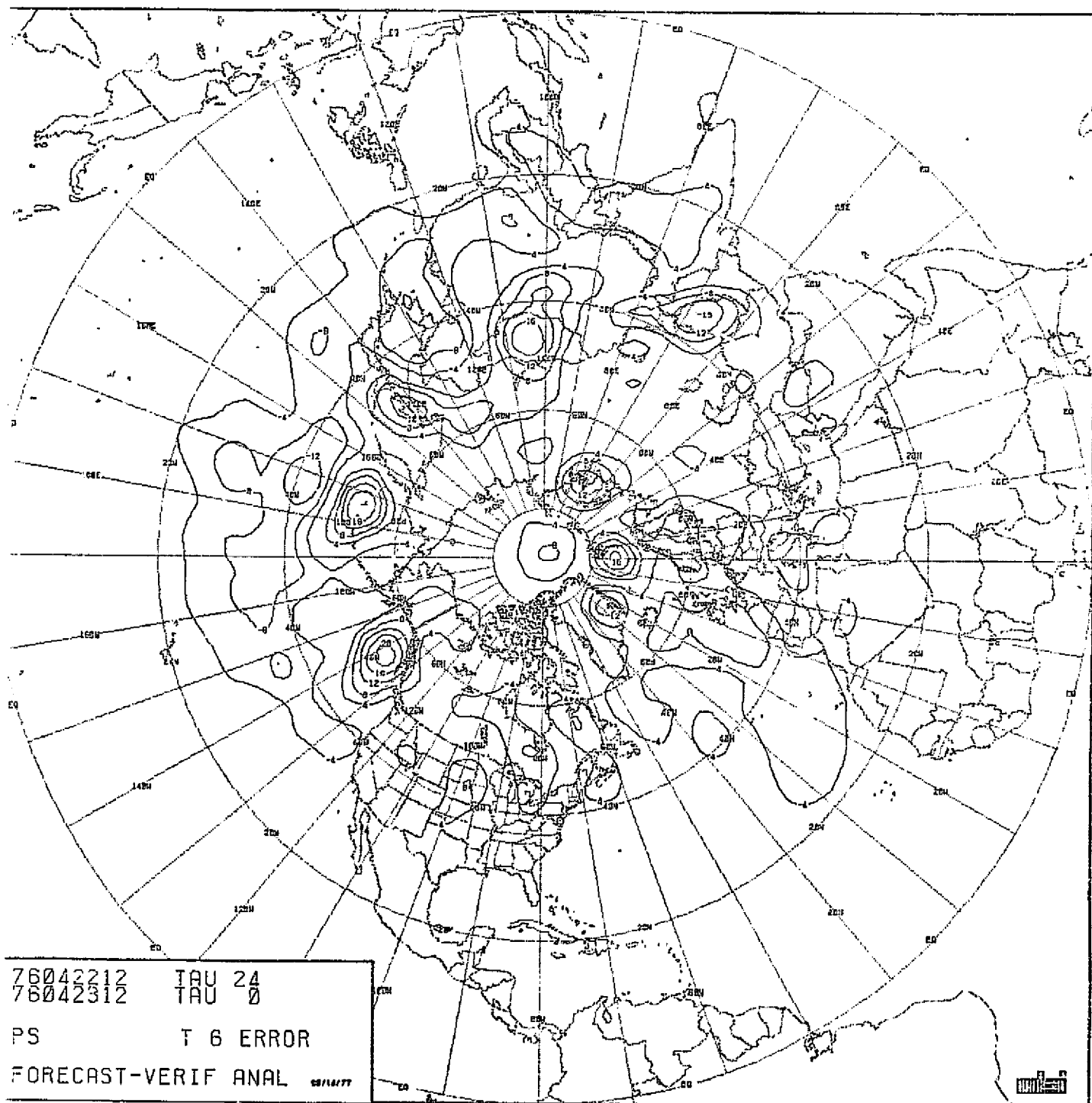


CHART VIII-92

RUN T6. SCENARIO A. MODEL PECHFV. 24-HOUR
FORECAST ERROR IN SEA-LEVEL PRESSURE.

**ORIGINAL PAGE IS
OF POOR QUALITY**

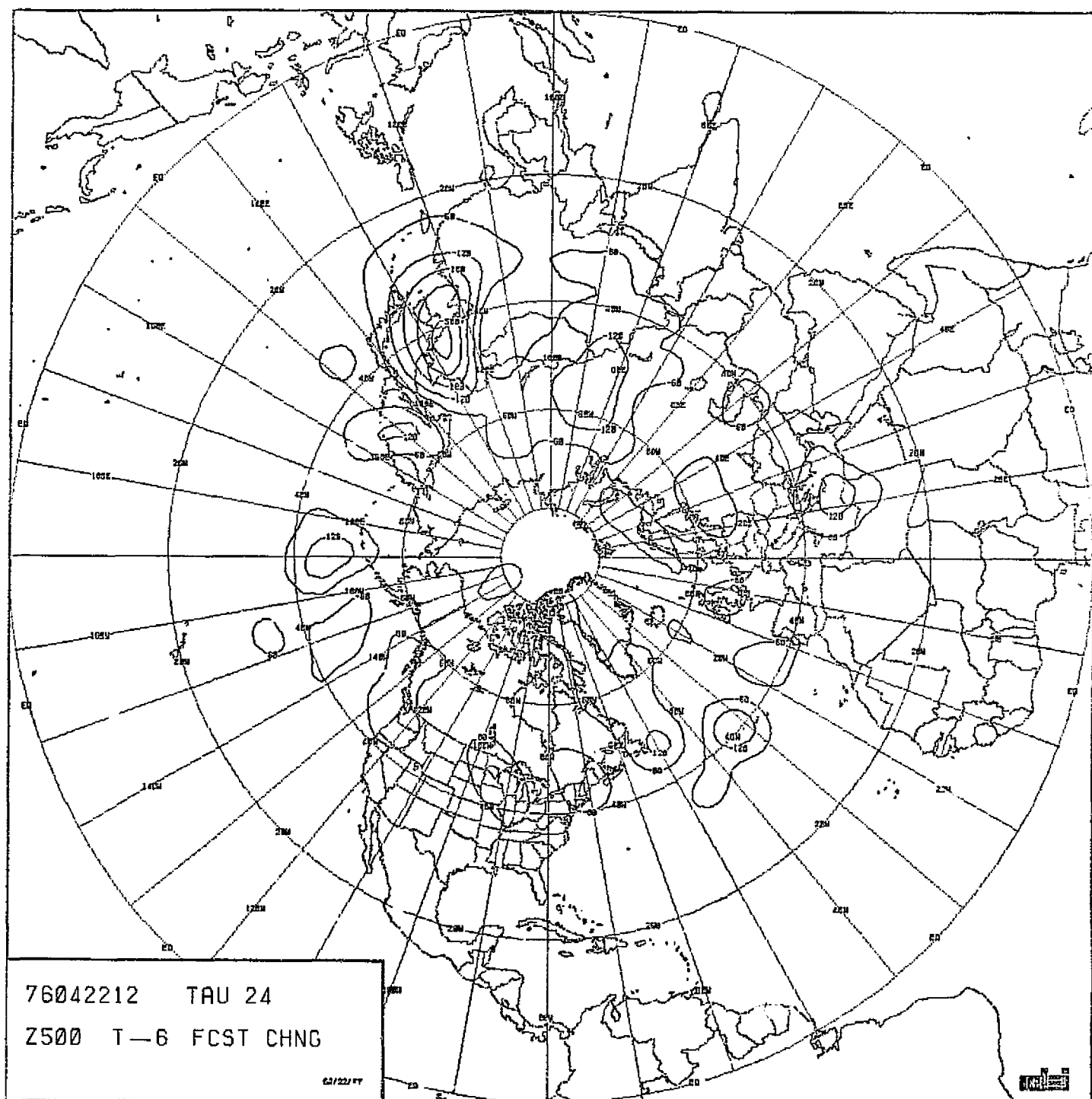


CHART VIII-93 : RUN T6. SCENARIO A. MODEL PECHFV. 24-HOUR
FORECAST CHANGE IN 500 MB HEIGHT.

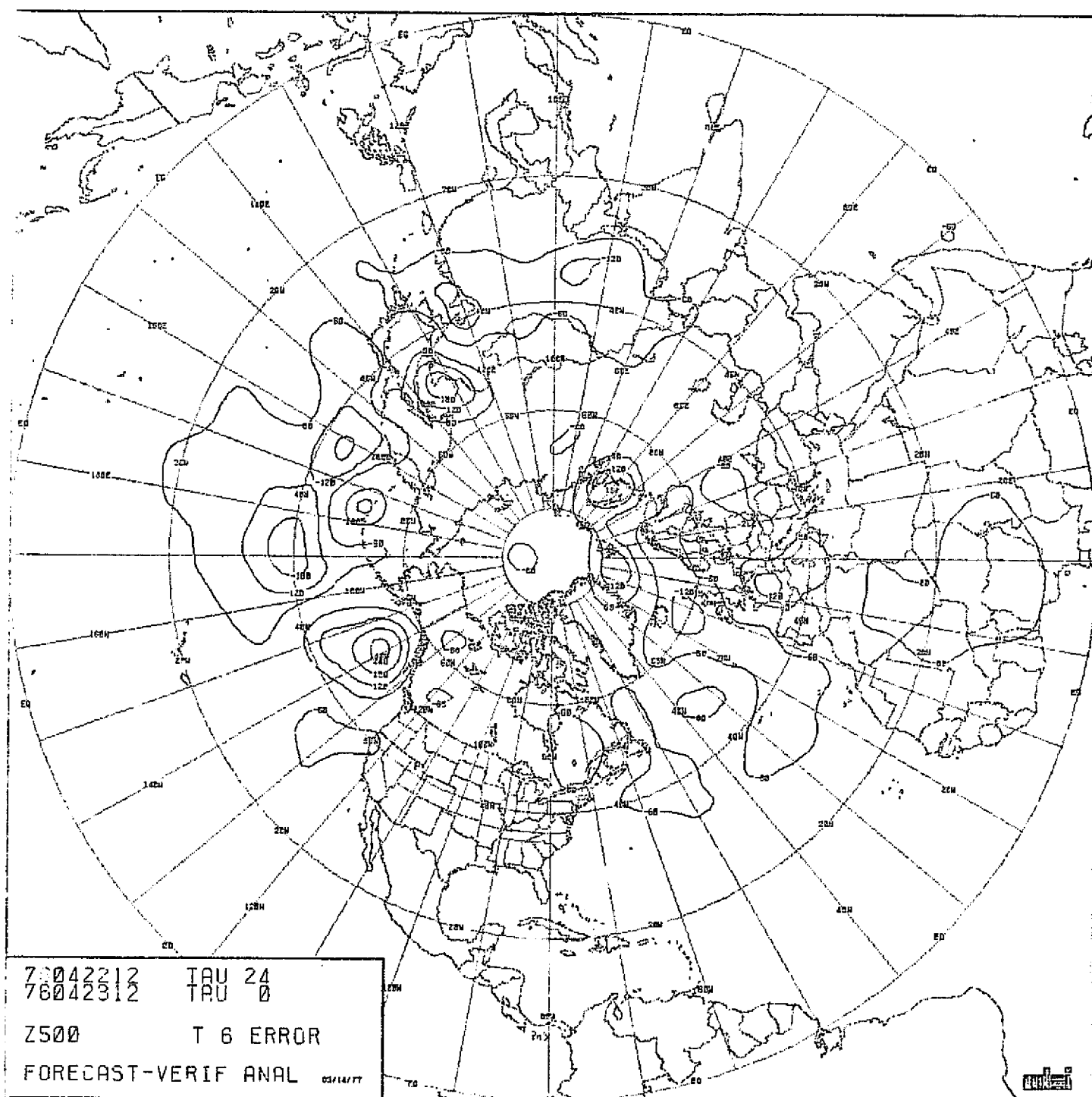


CHART VIII-94

RUN T6. SCENARIO A. MODEL PACHEV. 24-HOUR
FORECAST ERROR IN 500 MB HEIGHT.

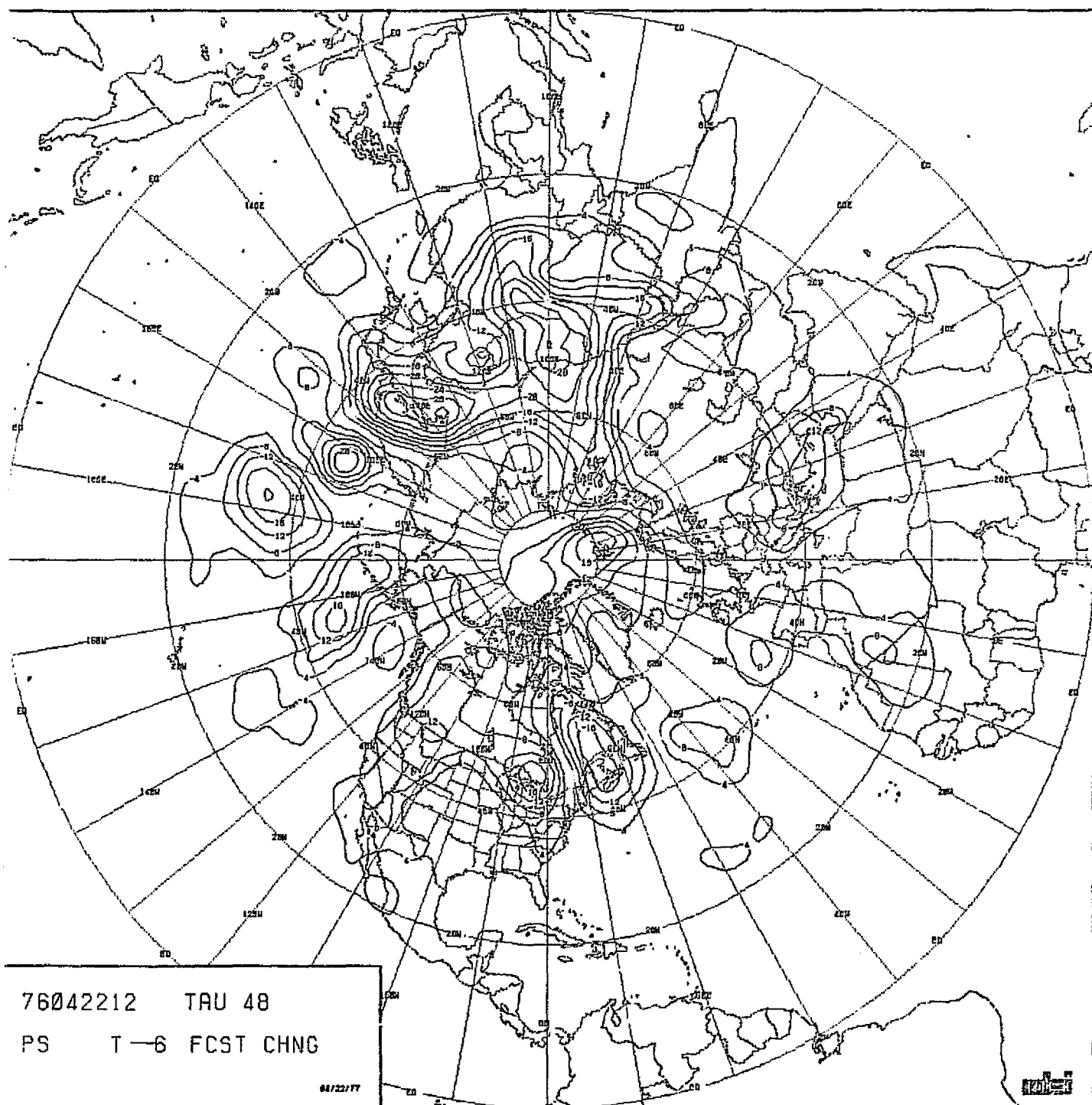
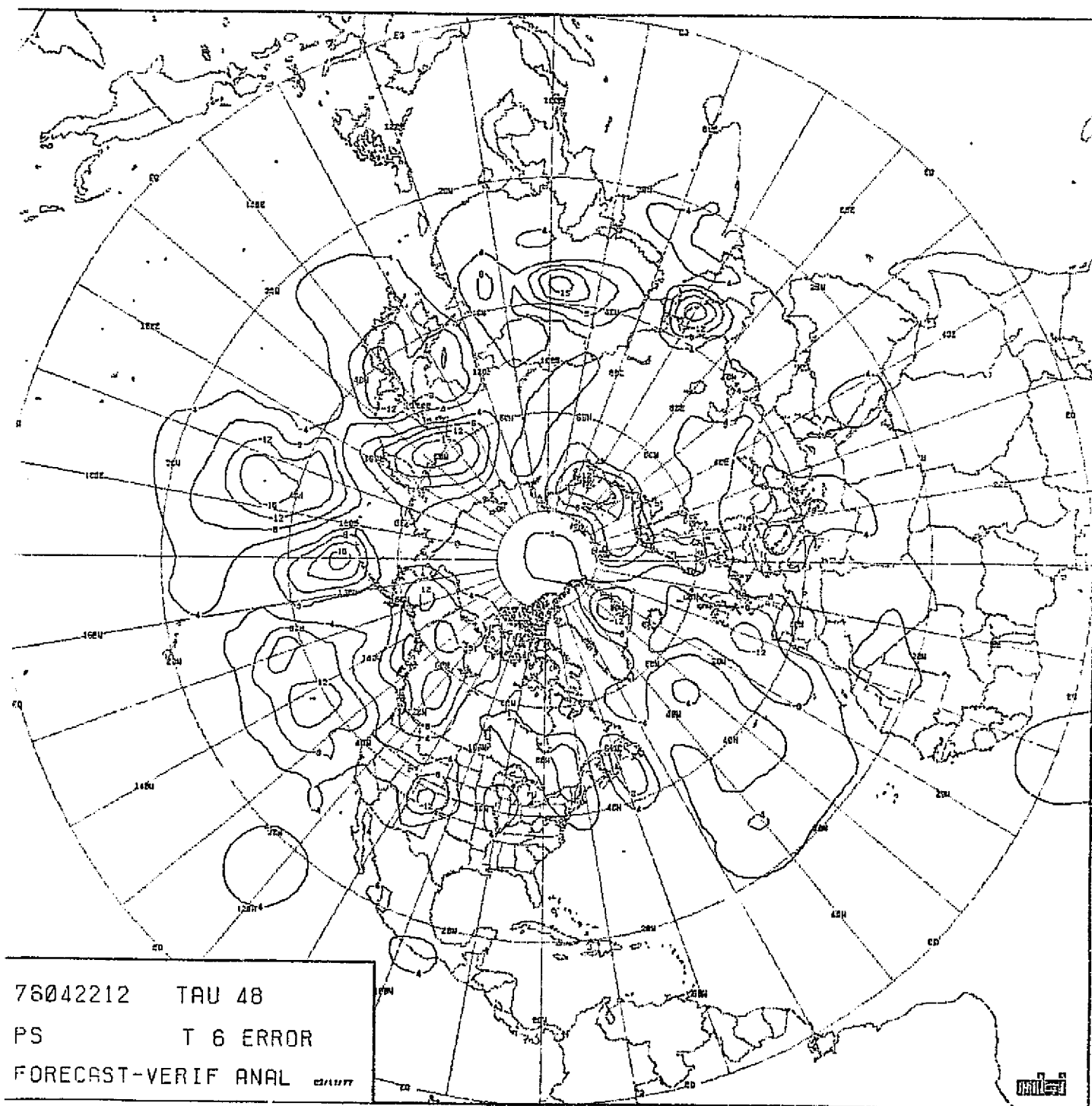


CHART VIII-95 : RUN T6. SCENARIO A. MODEL PECHFV. 48-HOUR
FORECAST CHANGE IN SEA-LEVEL PRESSURE.



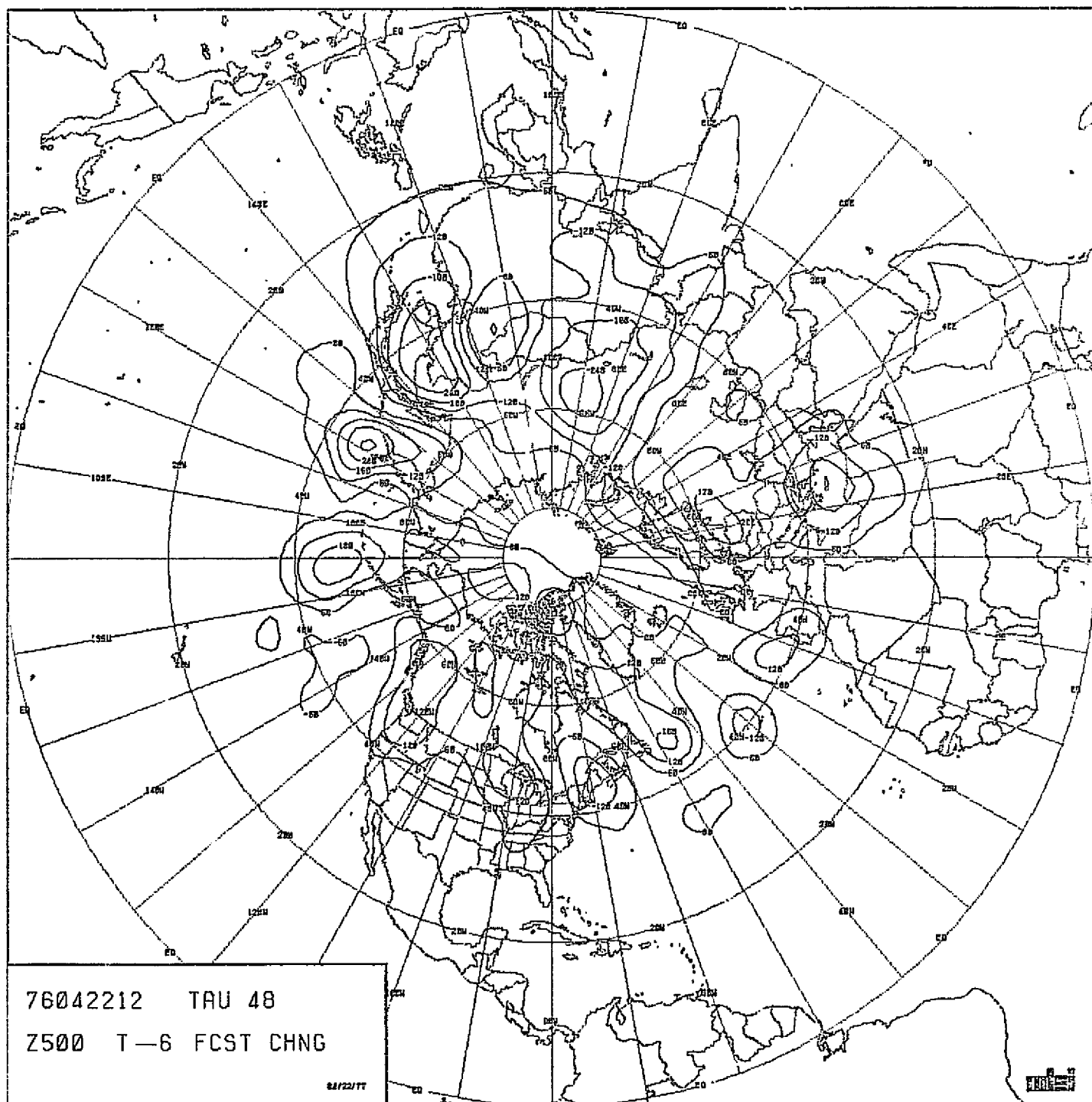


CHART VIII-97 : RUN T6. SCENARIO A. MODEL PECHFV. 48-HOUR
FORECAST CHANGE IN 500 MB HEIGHT.

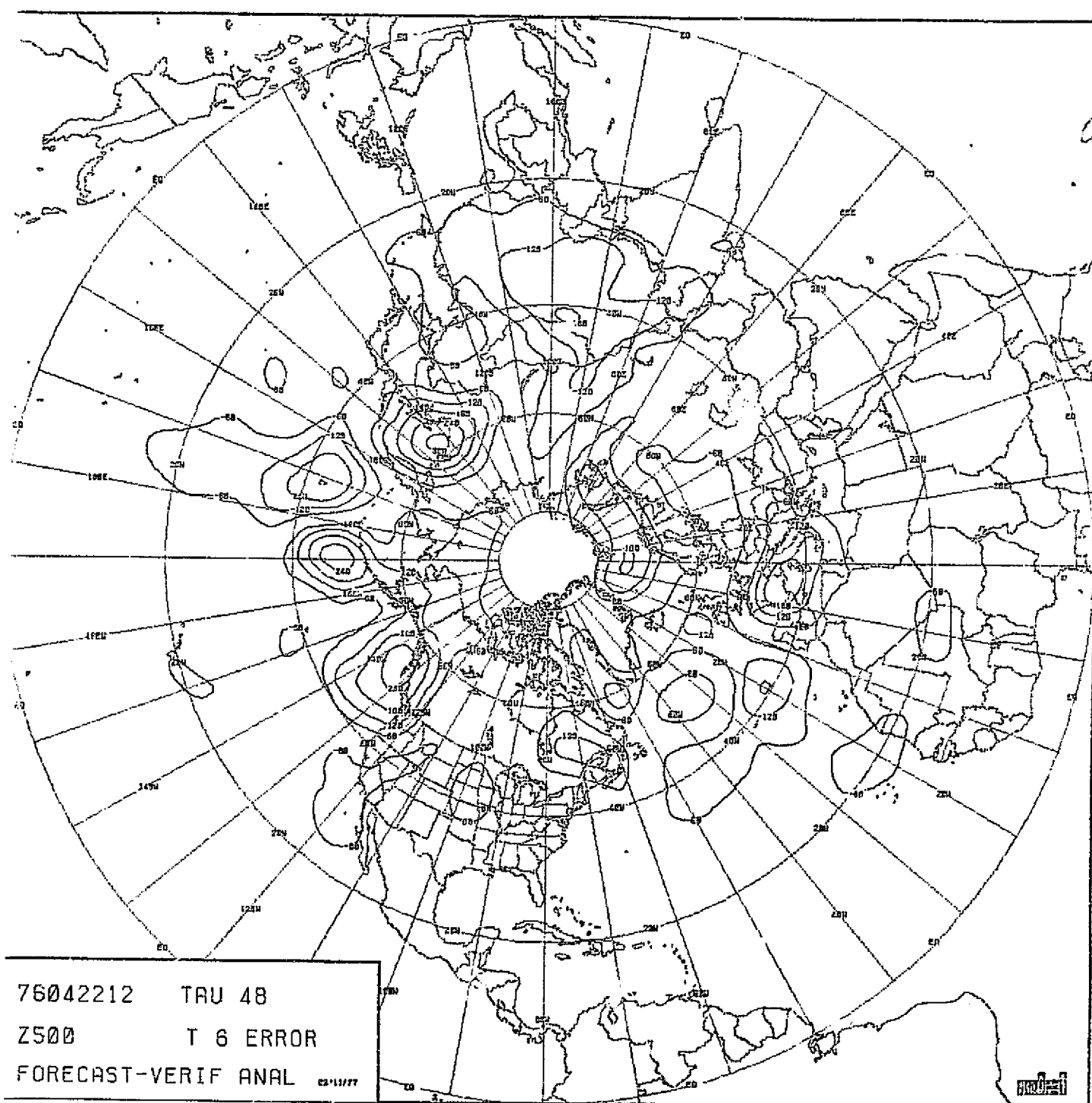


CHART VIII-98

RUN T6. SCENARIO A. MODEL PECHV. 48-HOUR
FORECAST ERROR IN 500 MB HEIGHT.

ORIGINAL PAGE IS
OF POOR QUALITY

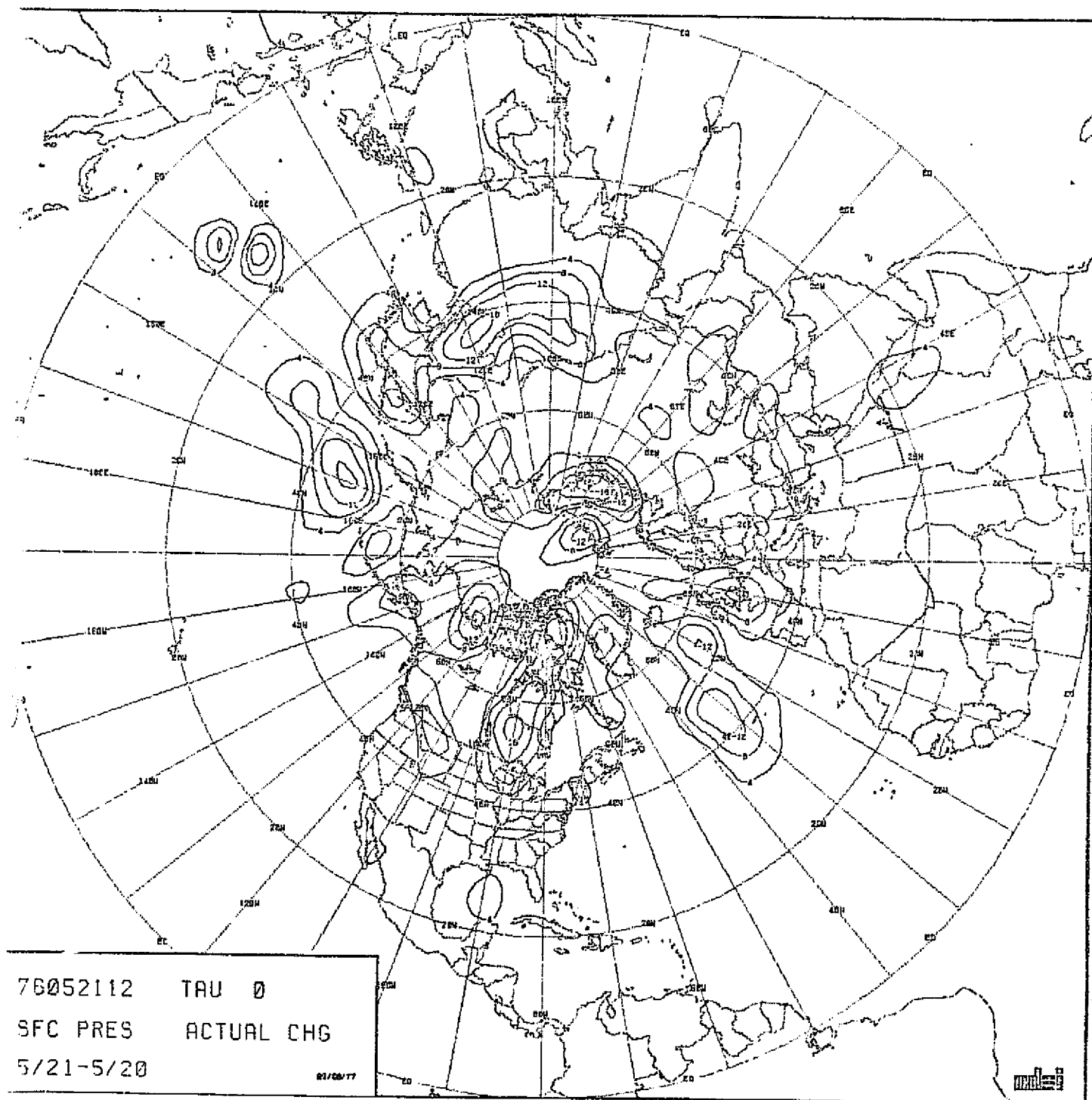


CHART VIII-99: SEA-LEVEL PRESSURE ACTUAL CHANGES OVER 24 HOURS. SCENARIO B.

ORIGINAL PAGE IS
OF POOR QUALITY

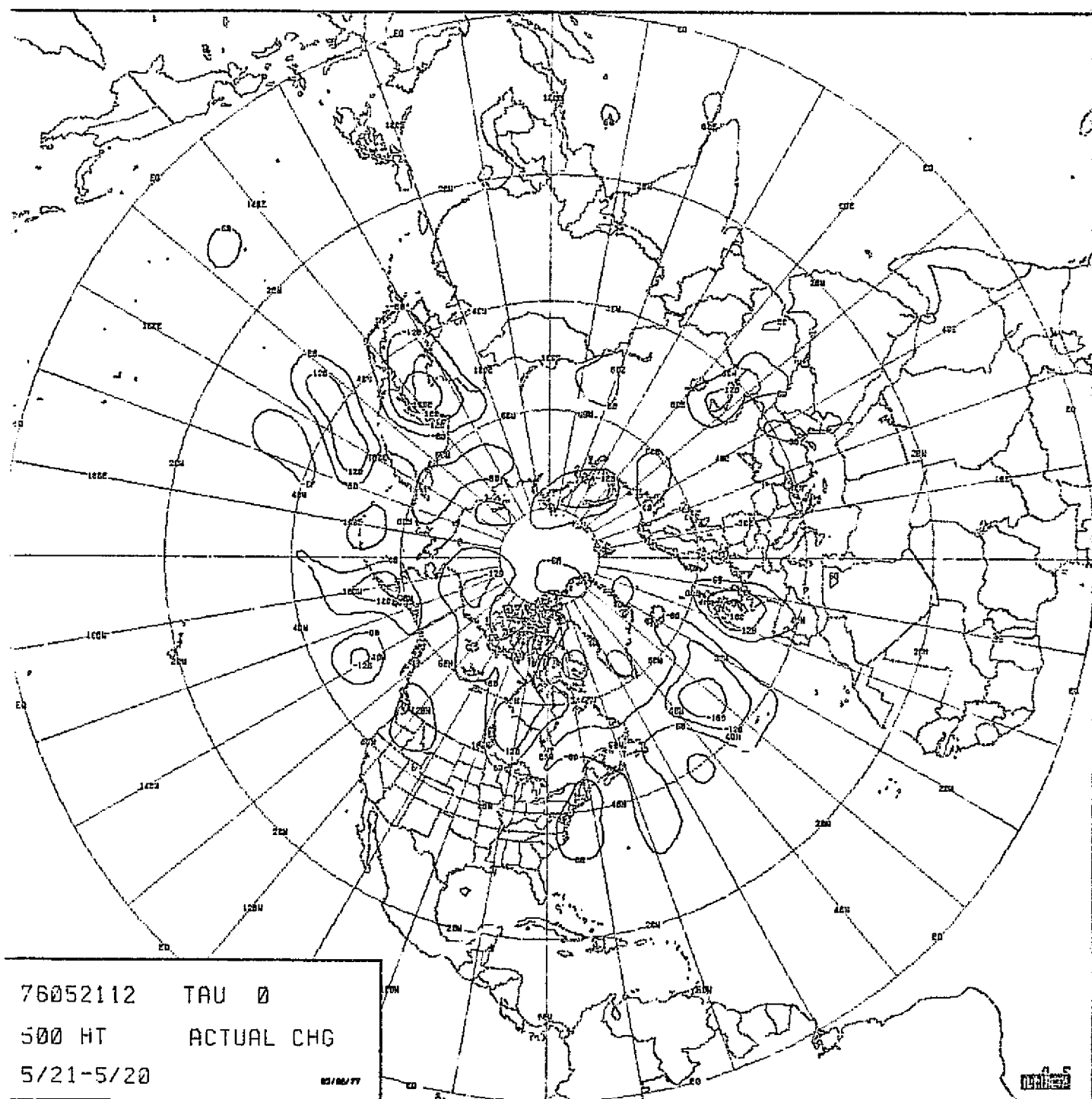


CHART VIII-100: 500 MB HEIGHT ACTUAL CHANGES OVER 24 HOURS.
SCENARIO B.

ORIGINAL PAGE IS
OF POOR QUALITY

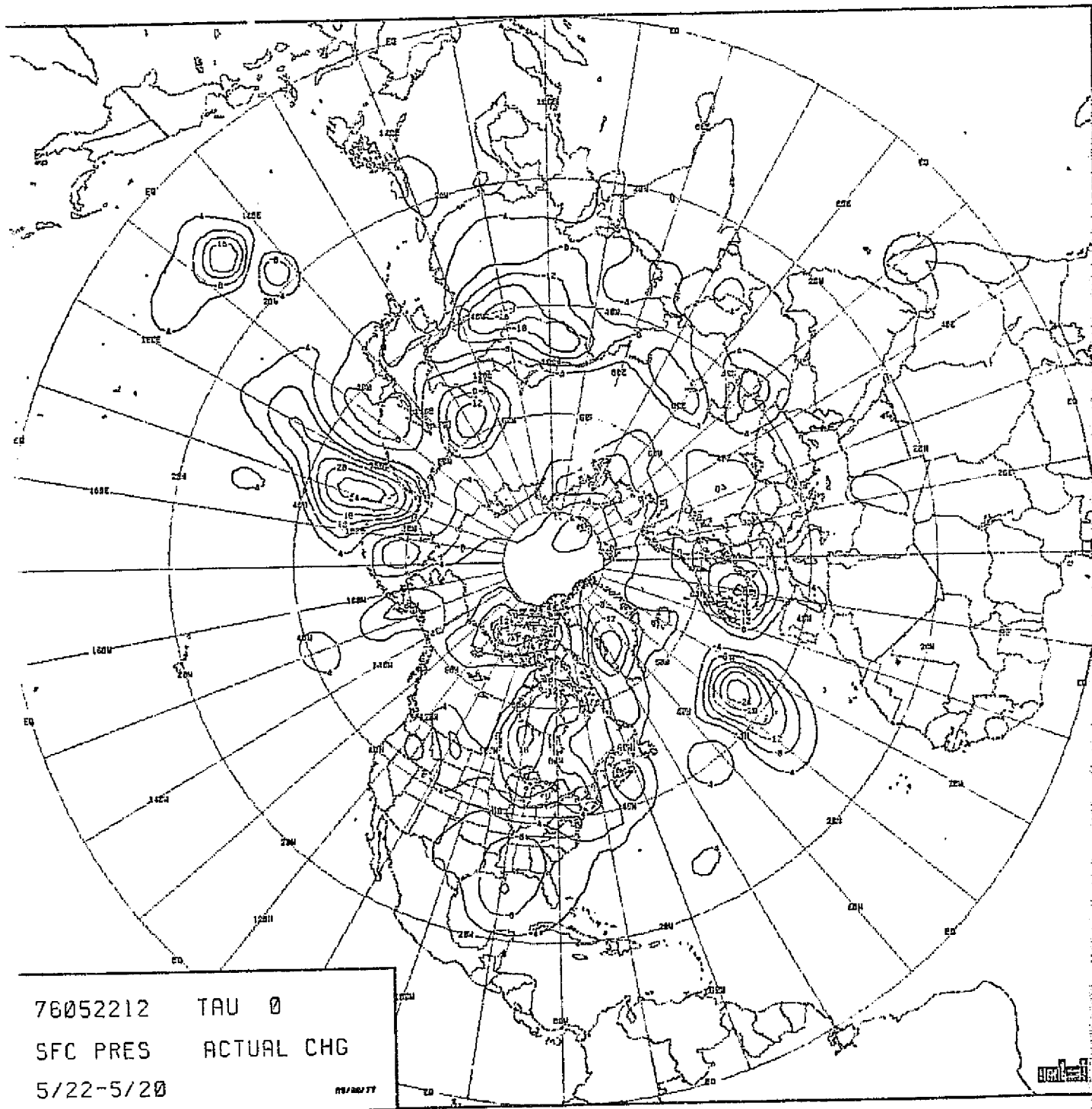


CHART VIII-101: SEA-LEVEL PRESSURE ACTUAL CHANGES OVER 48 HOURS. SCENARIO B.

ORIGINAL PAGE IS
OF POOR QUALITY

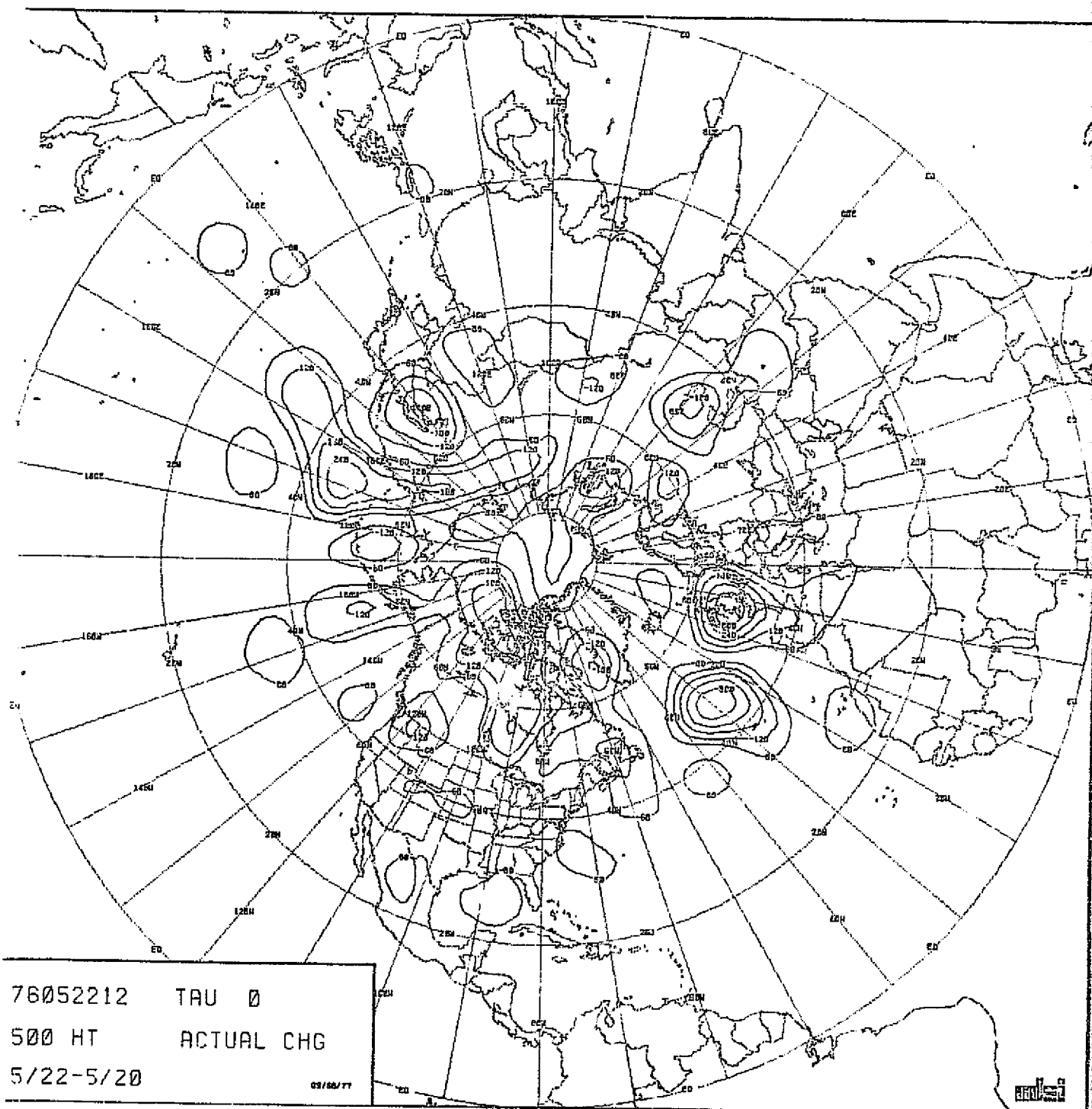


CHART VIII-102: 500 MB HEIGHT ACTUAL CHANGES OVER 48 HOURS.
SCENARIO B.

ORIGINAL PAGE IS
OF POOR QUALITY

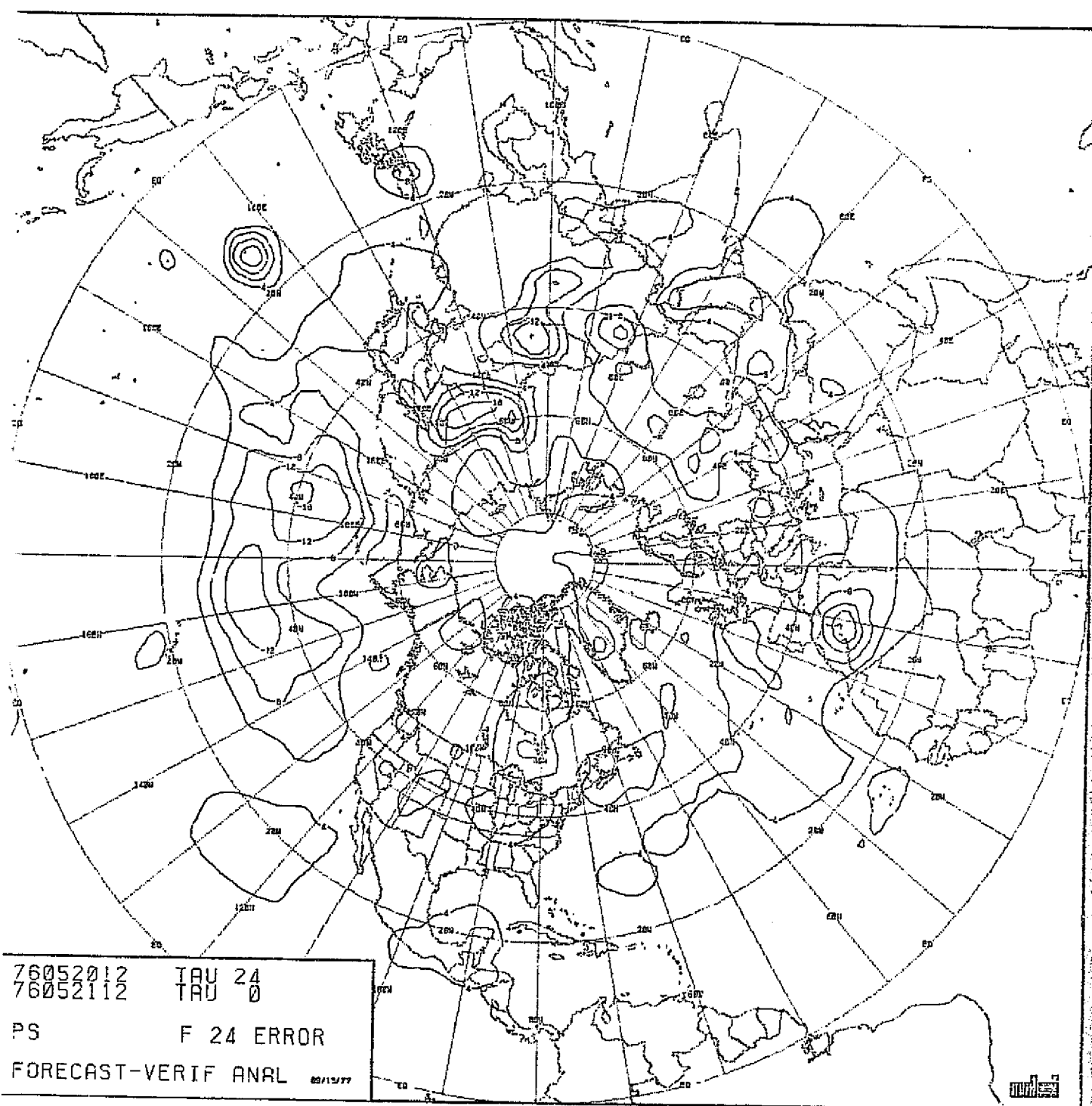


CHART VIII-104: RUN F24. SCENARIO B. MODEL PEFHCV. 24-HOUR
FORECAST ERROR IN SEA-LEVEL PRESSURE.

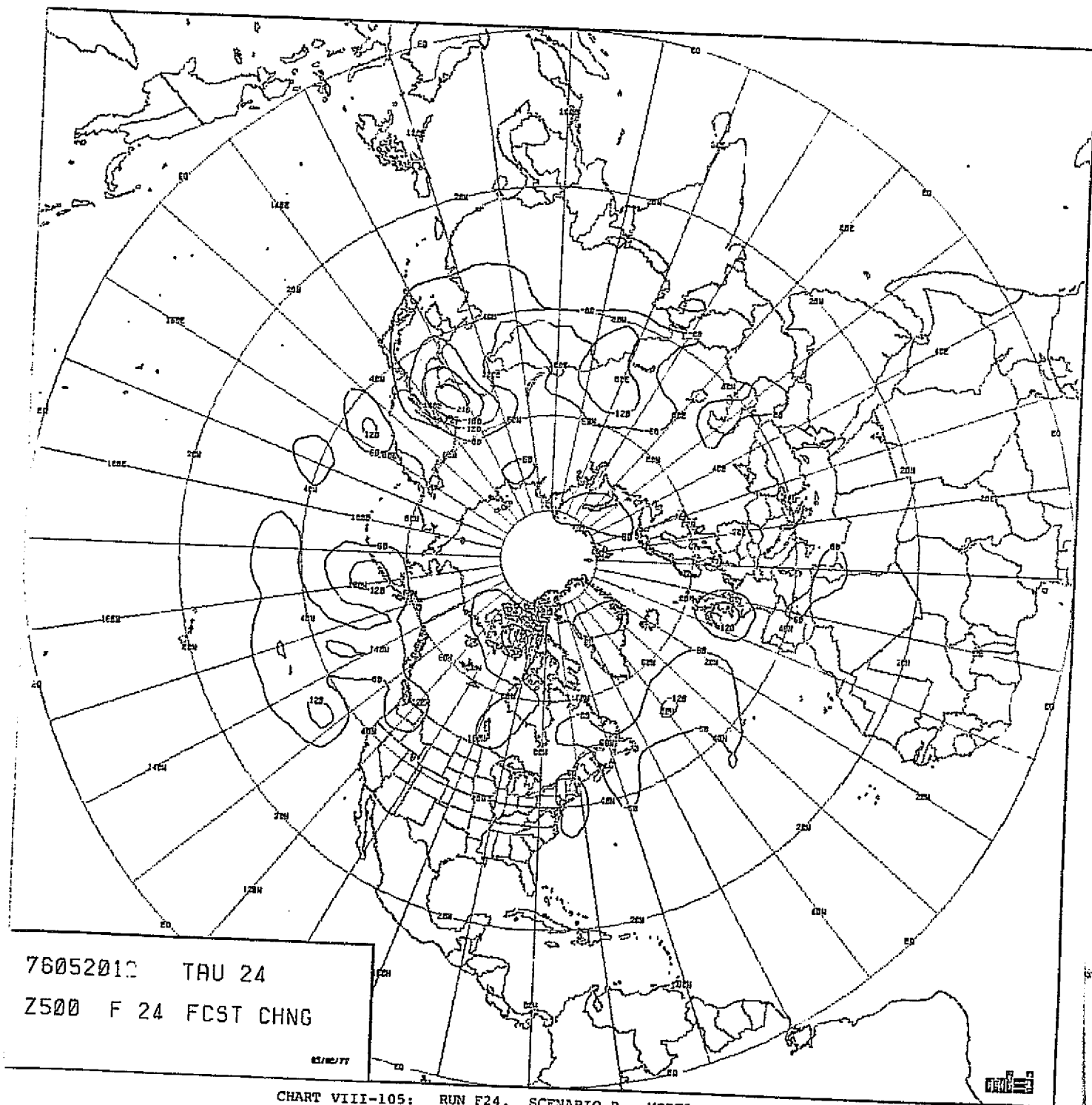


CHART VIII-105: RUN F24. SCENARIO B. MODEL PEFHCV. 24-HOUR
FORECAST CHANGE IN 500 MB HEIGHT.

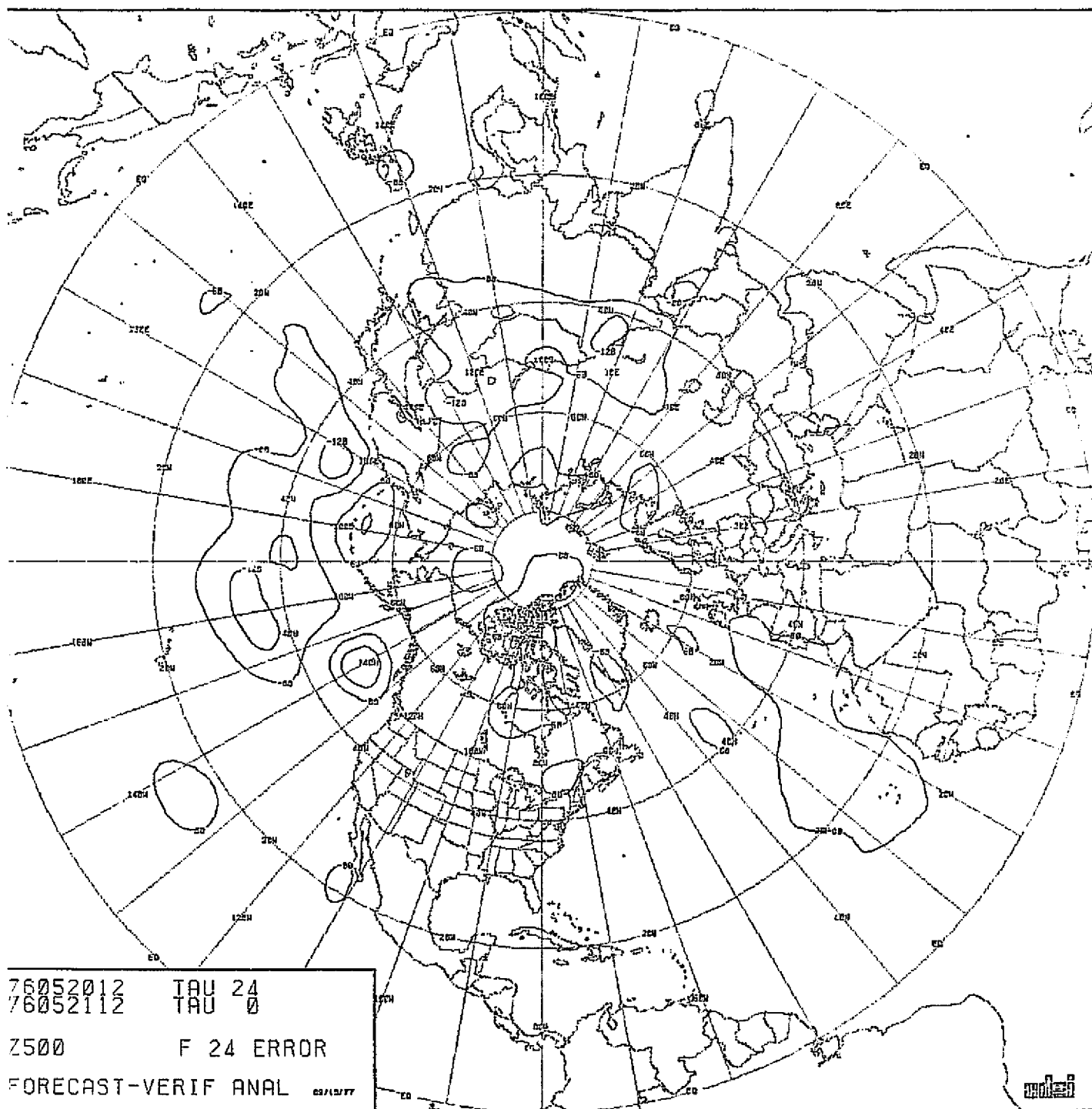


CHART VIII-106: RUN F24. SCENARIO B. MODEL PEFHCV. 24-HOUR
FORECAST ERROR IN 500 MB HEIGHT.

ORIGINAL PAGE IS
OF POOR QUALITY

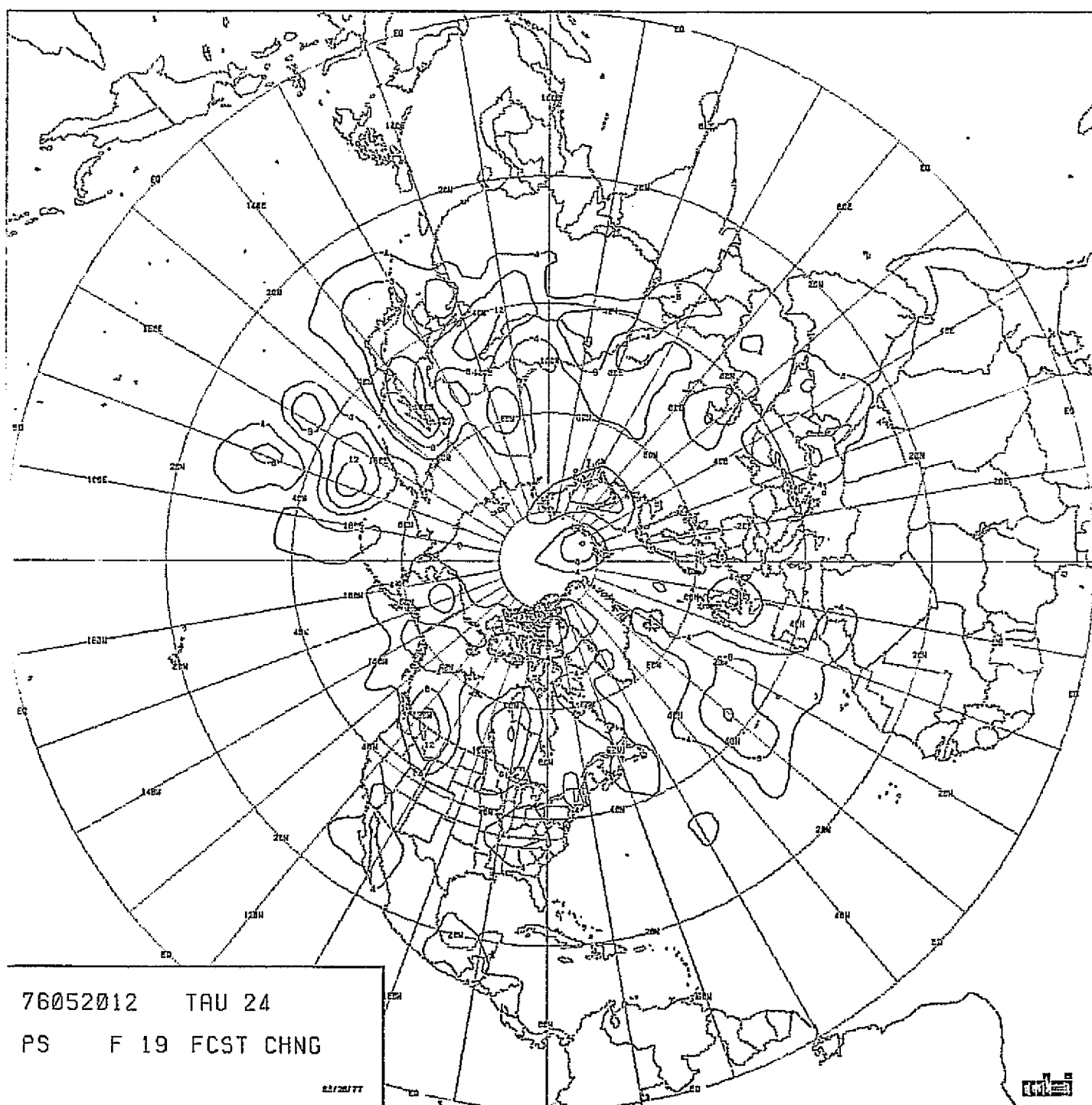


CHART VIII-107: RUN F19. SCENARIO B. MODEL PECHCV. 24-HOUR
FORECAST CHANGE IN SEA-LEVEL PRESSURE.

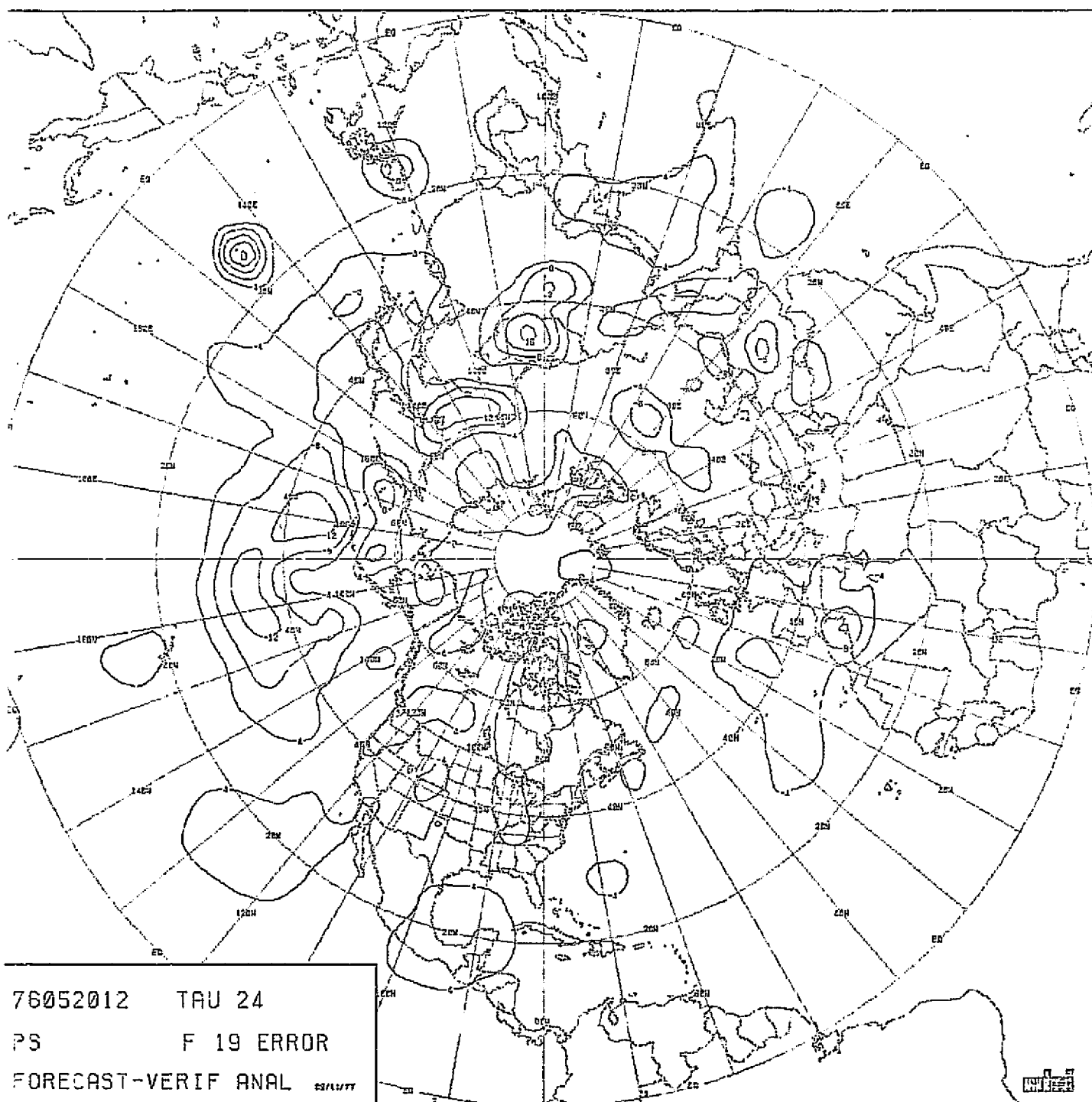


CHART VIII-108: RUN F19. SCENARIO B. MODEL PECHCV. 24-HOUR
FORECAST ERROR IN SEA-LEVEL PRESSURE.

ORIGINAL PAGE IS
OF POOR QUALITY

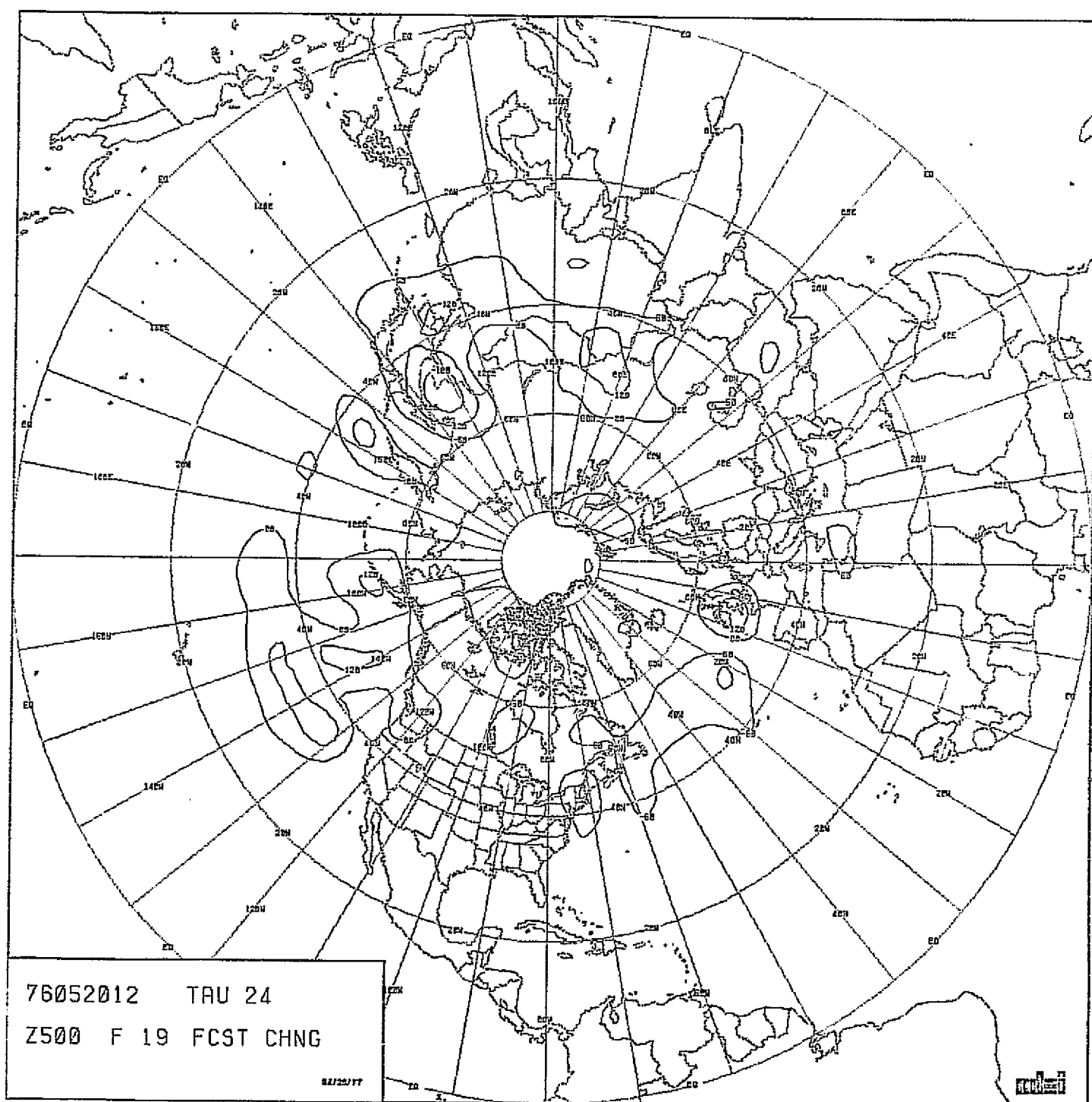


CHART VIII-109:: RUN F19. SCENARIO B. MODEL PECHCV. 24-HOUR
FORECAST CHANGE IN 500 MB HEIGHT.

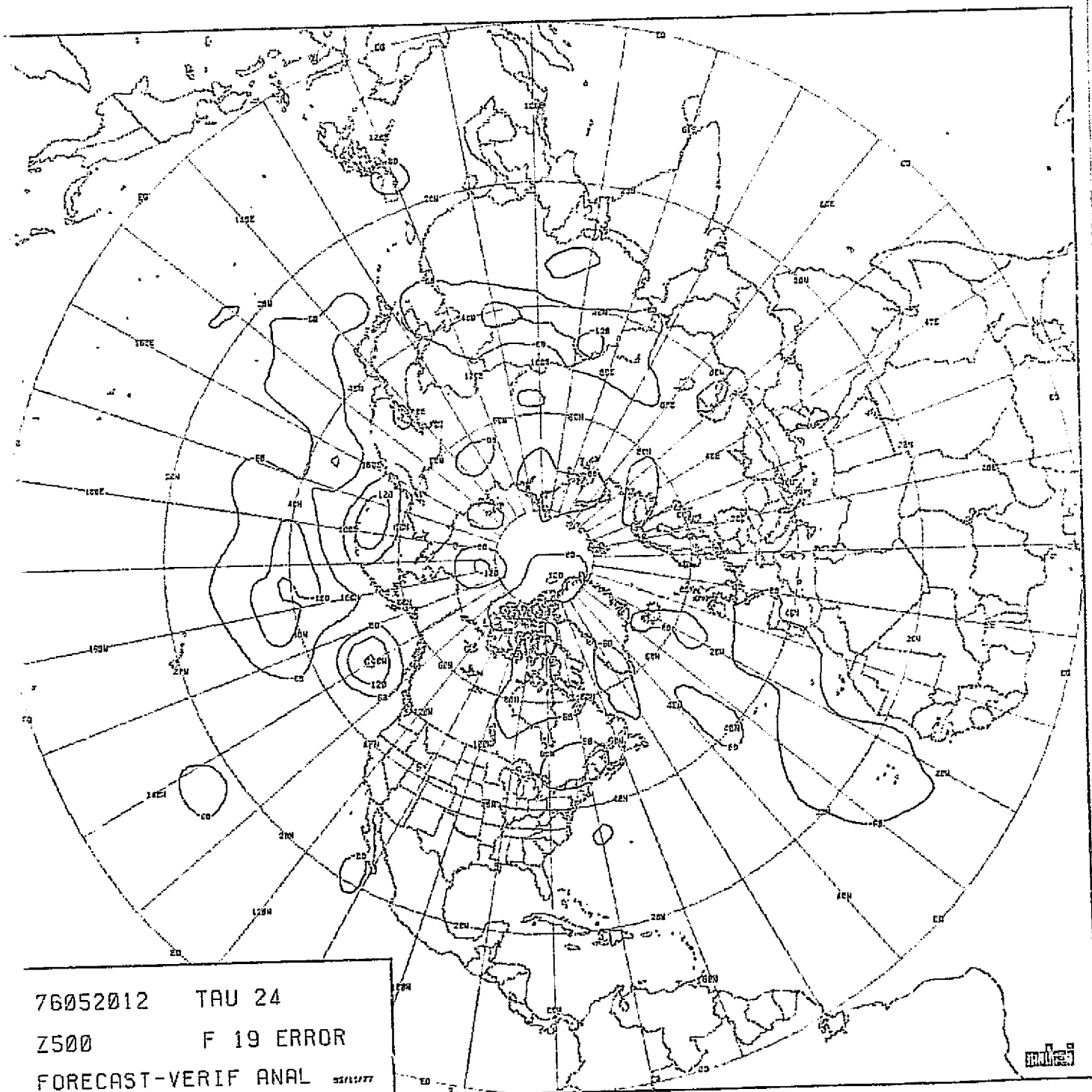


CHART VIII-110: RUN F19. SCENARIO B. MODEL PECHCV. 24-HOUR
FORECAST ERROR IN 500 MB HEIGHT.

ORIGINAL PAGE IS
OF POOR QUALITY

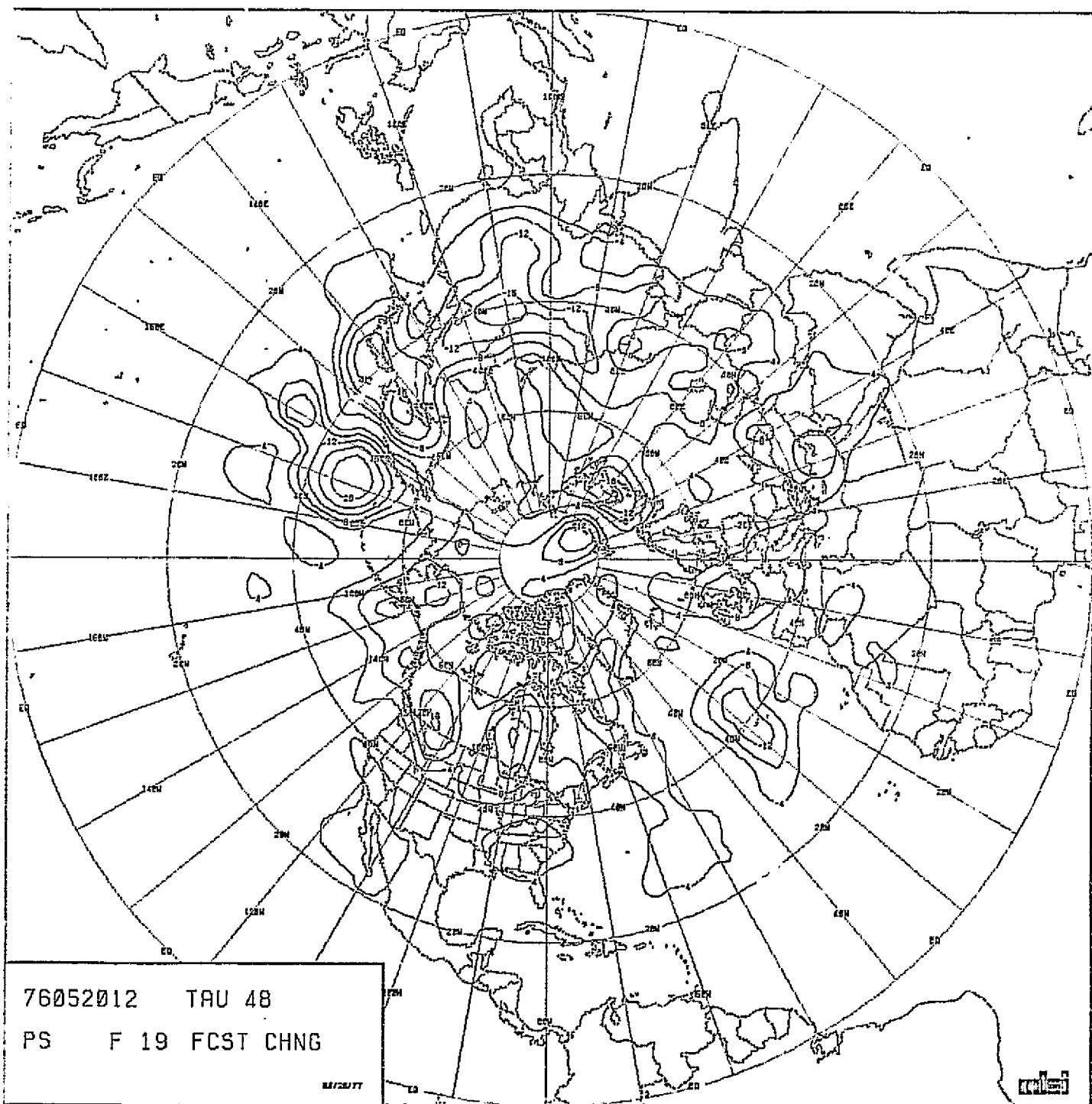


CHART VIII-111: RUN F19. SCENARIO B. MODEL PECHCV. 48-HOUR
FORECAST CHANGE IN SEA-LEVEL PRESSURE.

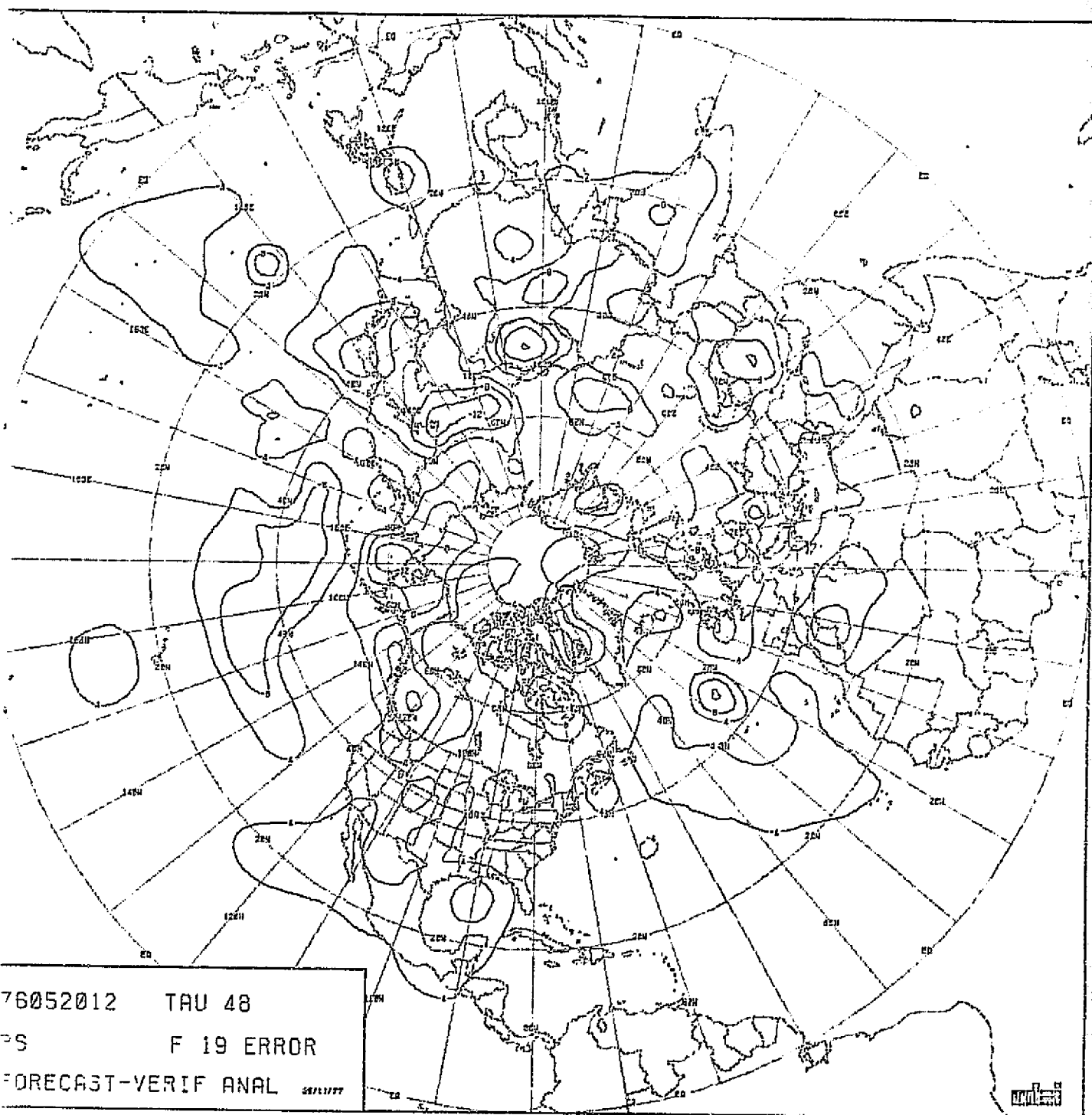


CHART VIII-112; RUN F19. SCENARIO B. MODEL PECHCV. 48-HOUR
FORECAST ERROR IN SEA-LEVEL PRESSURE.

ORIGINAL PAGE IS
OF POOR QUALITY

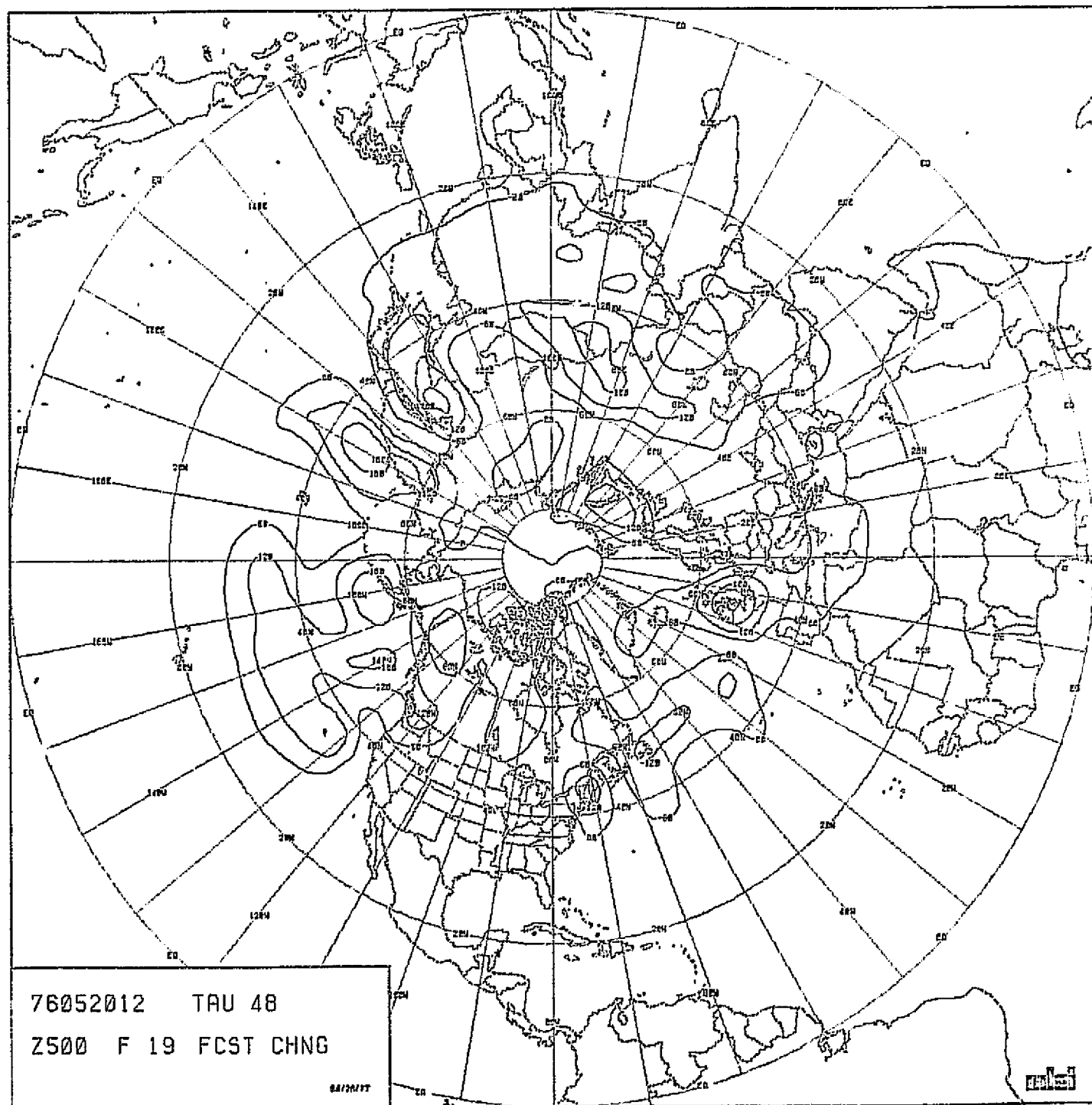


CHART VIII-113: RUN F19. SCENARIO B. MODEL PLSCHV. 48-HOUR
FORECAST CHANGE IN 500 MB HEIGHT.

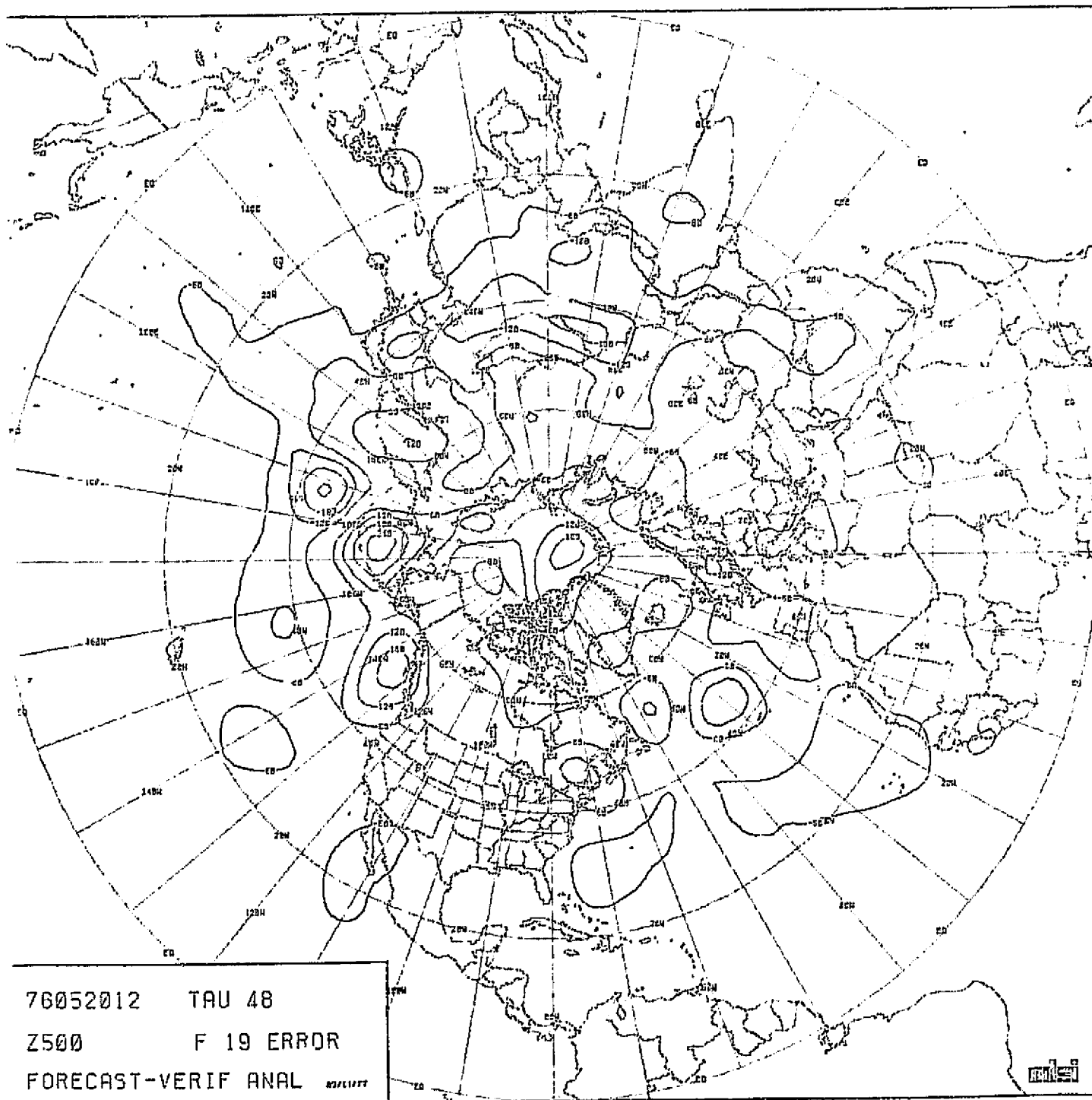


CHART VIII-114: RUN F19. SCENARIO B. MODEL PECHCV. 48-HOUR
FORECAST ERROR IN 500 MB HEIGHT.

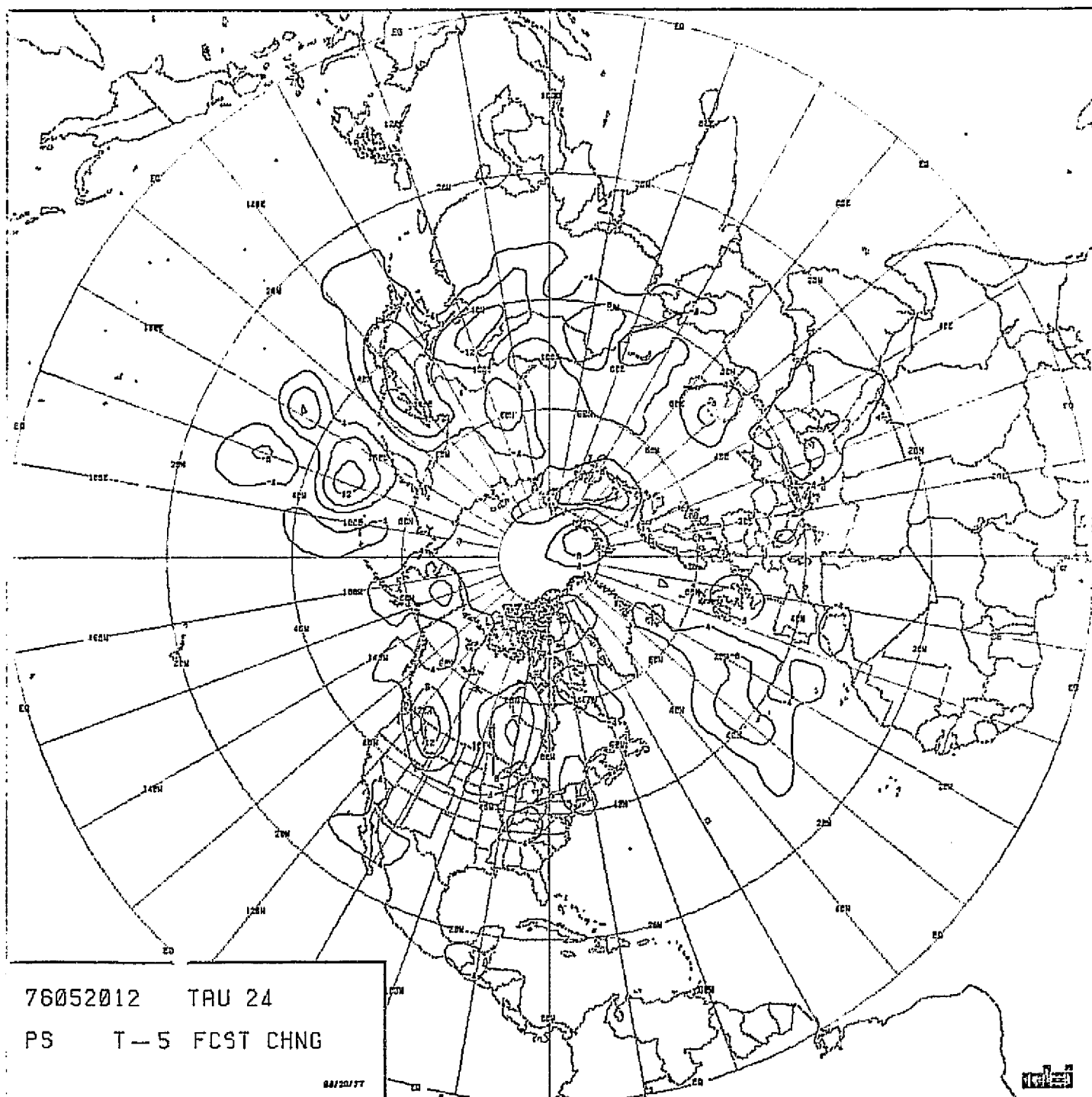


CHART VIII-115: RUN T5. SCENARIO 3. MODEL PECHFV. 24-HOUR
FORECAST CHANGE IN SEA-LEVEL PRESSURE.

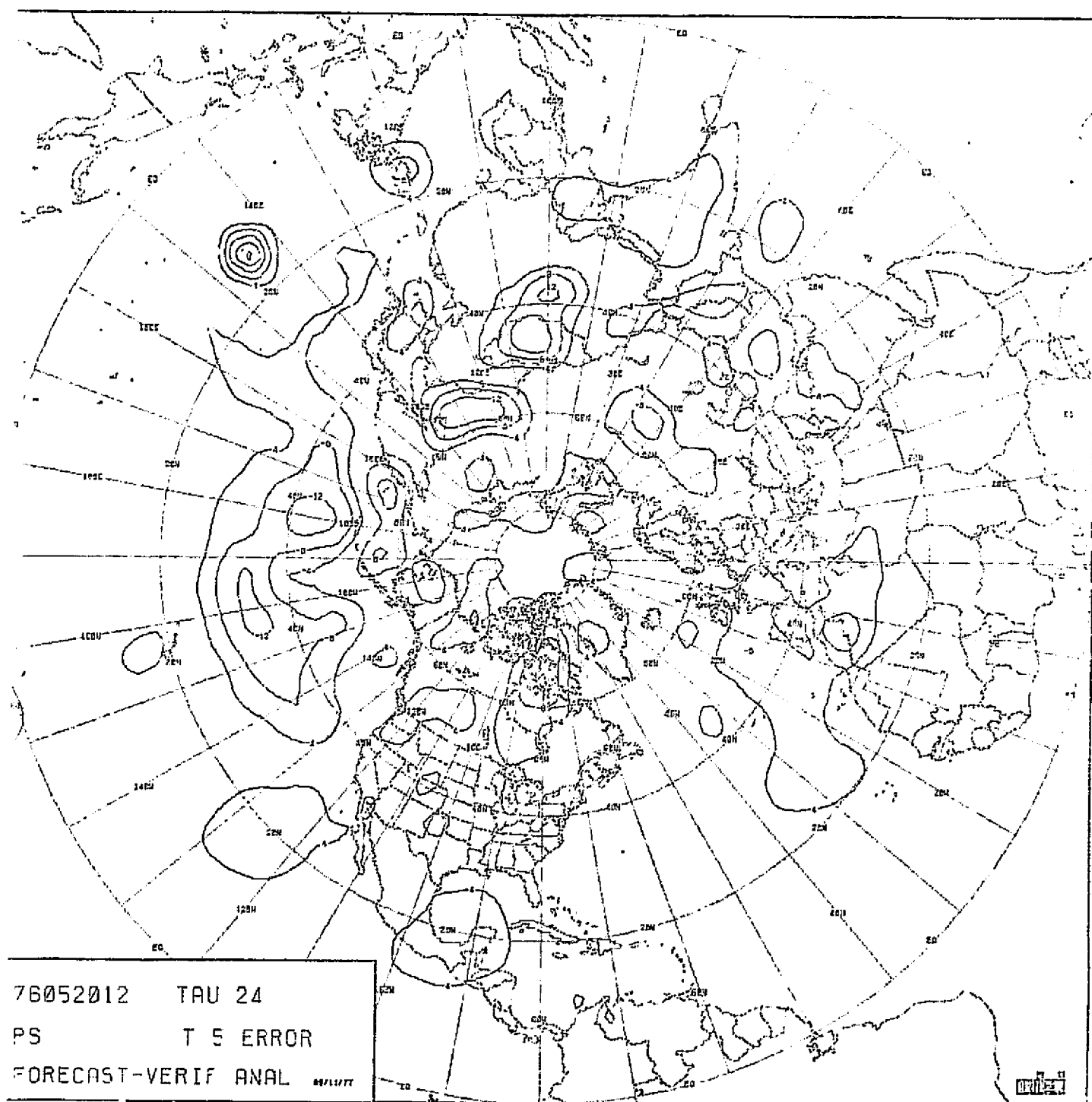


CHART VIII-116: RUN TS. SCENARIO B. MODEL PECHV. 24-HOUR
FORECAST ERROR IN SEA-LEVEL PRESSURE.

ORIGINAL PAGE IS
OF POOR QUALITY

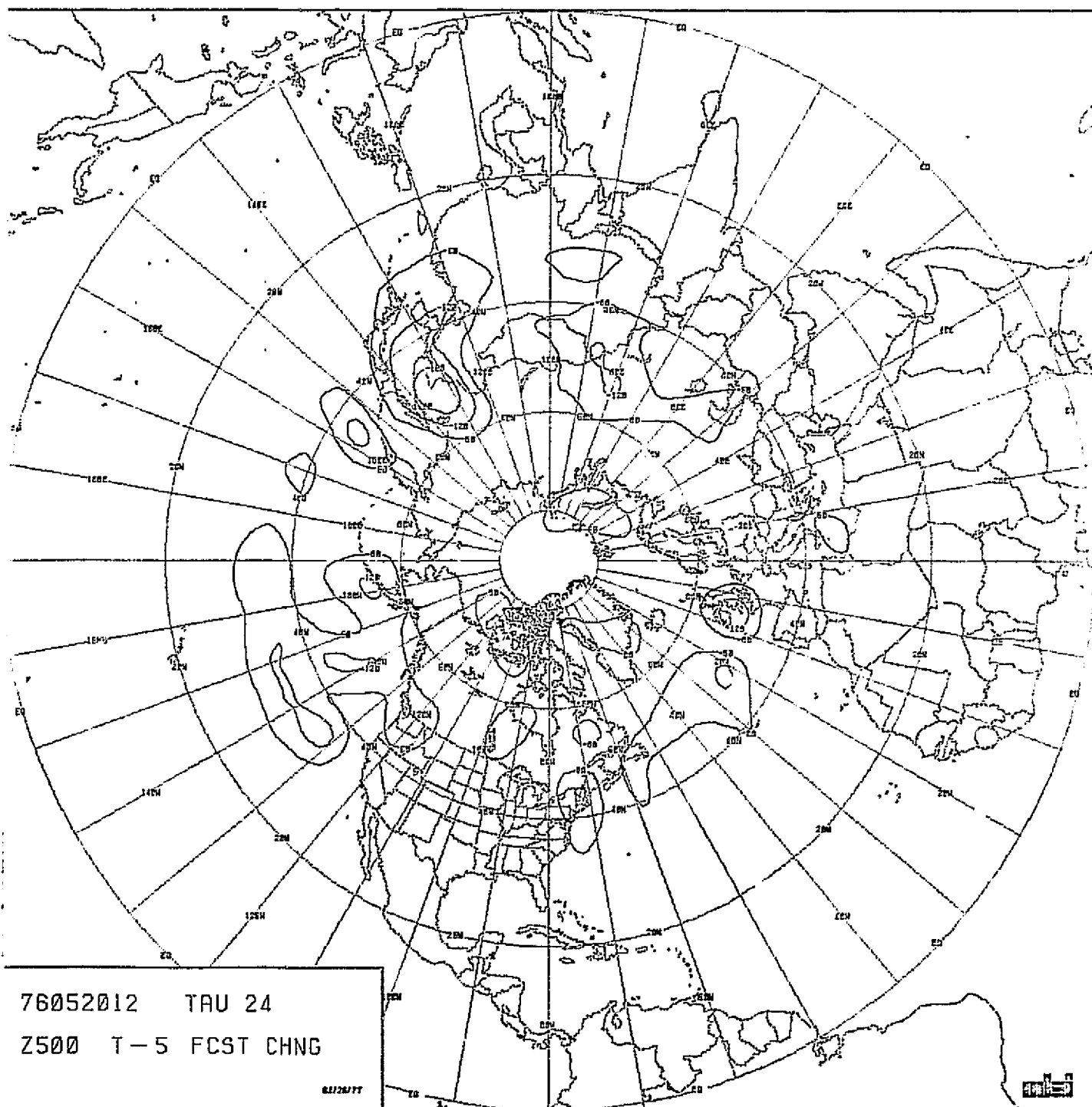


CHART VIII-117: RUN T5. SCENARIO B. MODEL PEFCHV. 24-HOUR
FORECAST CHANGE IN 500 MB HEIGHT.

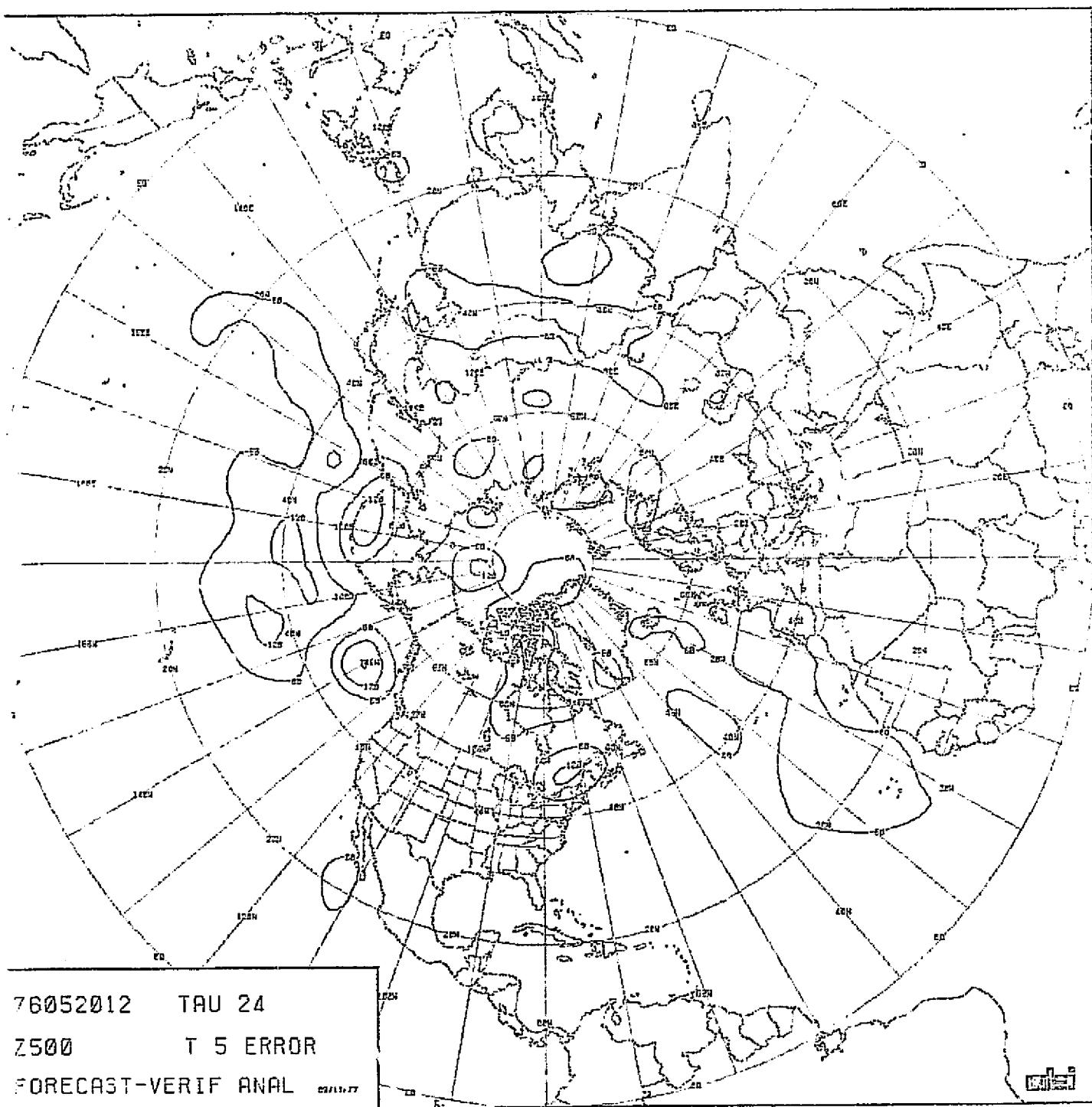


CHART VIII-118: RUN T5. SCENARIO B. MODEL PECHFV. 24-HOUR
FORECAST ERROR IN 500 MB HEIGHT.

ORIGINAL PAGE .
ON POOR QUALITY

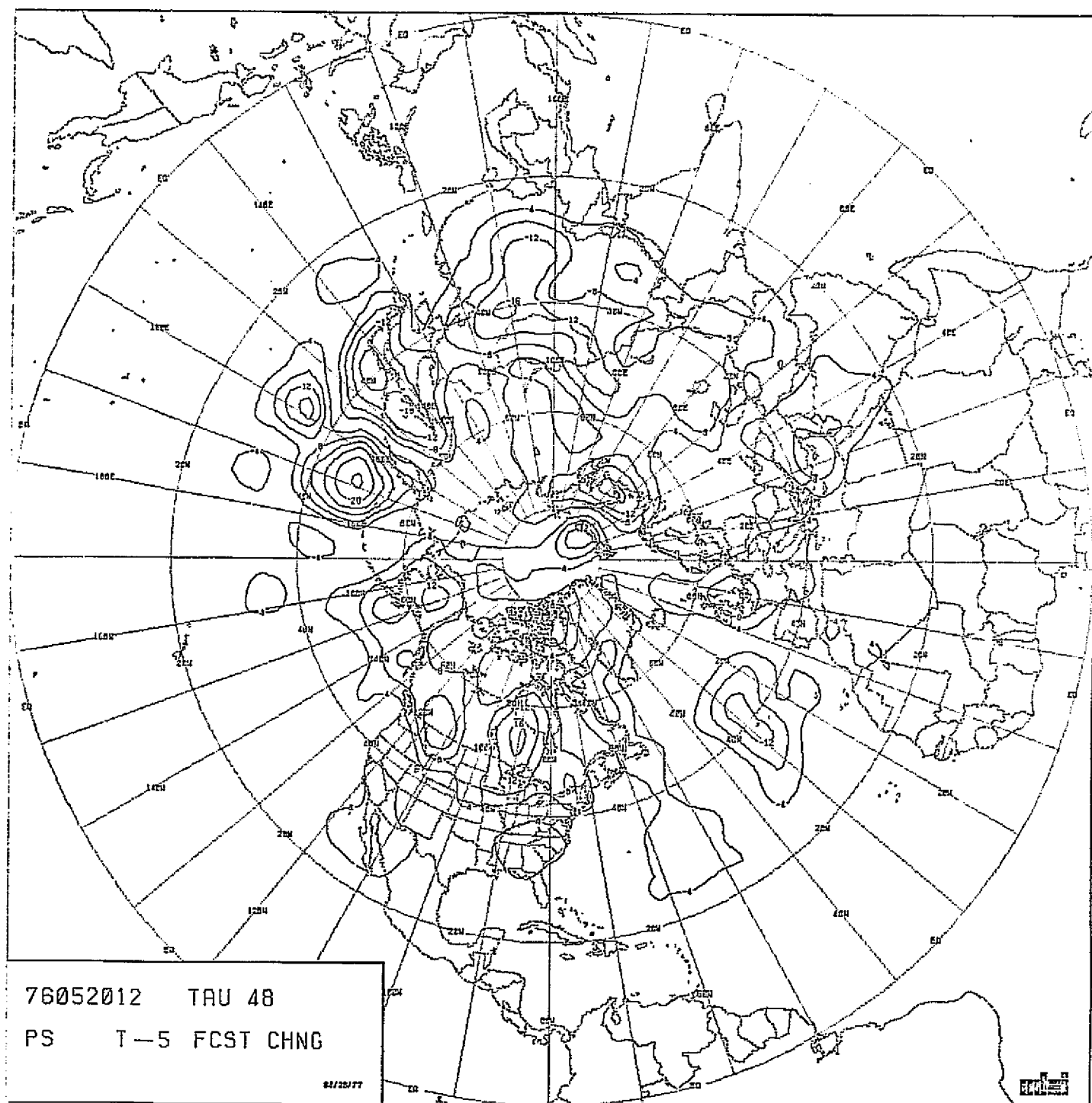


CHART VIII-119: RUN T5. SCENARIO B. MODEL PFCHEV. 48-HOUR
FORECAST CHANGE IN SEA-LEVEL PRESSURE.

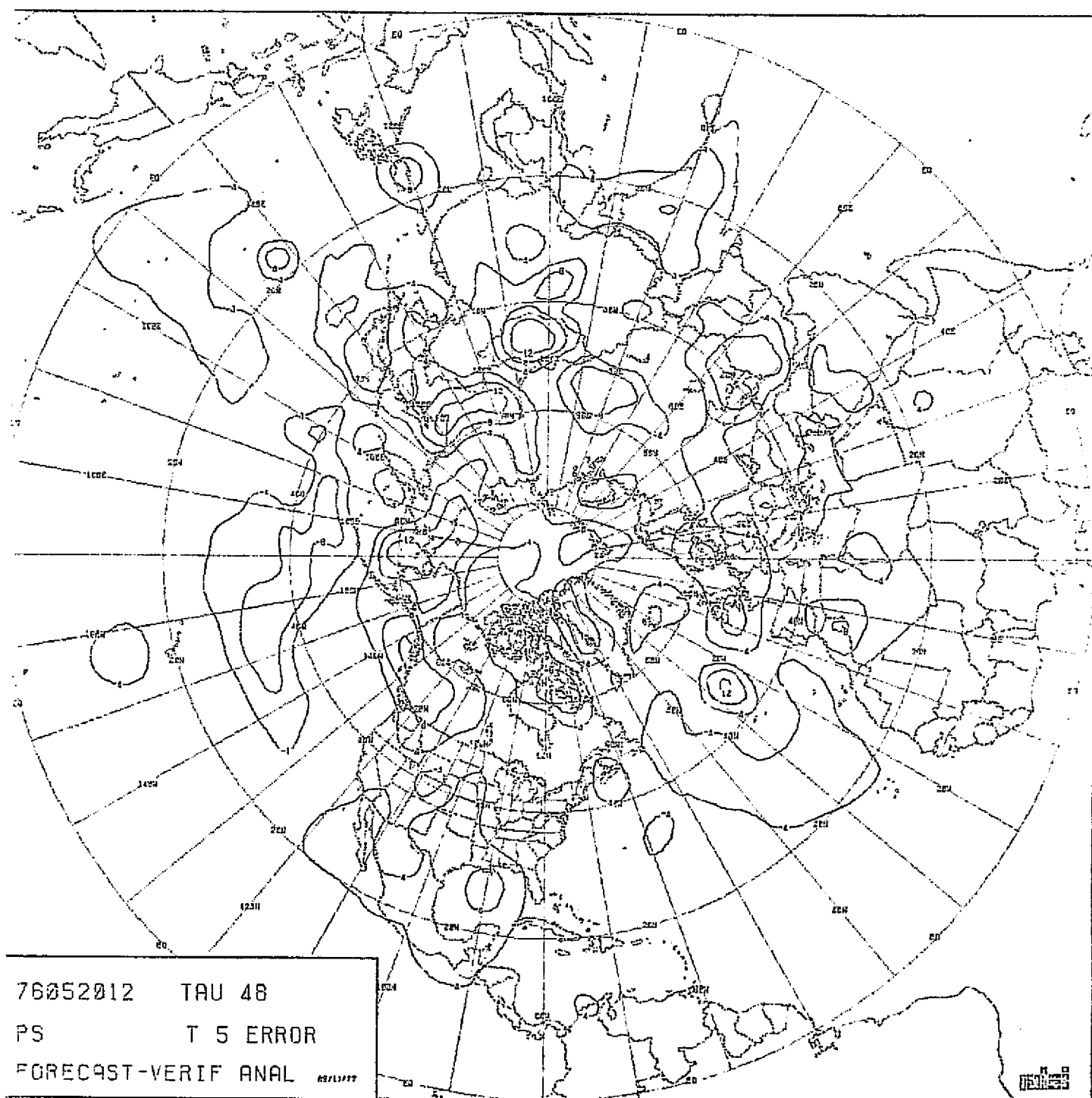


CHART VIII-120: RUN T5. SCENARIO B. MODEL PECHFV. 48-HOUR
FORECAST ERROR IN SEA-LEVEL PRESSURE.

ORIGINAL PAGE IS
OF POOR QUALITY

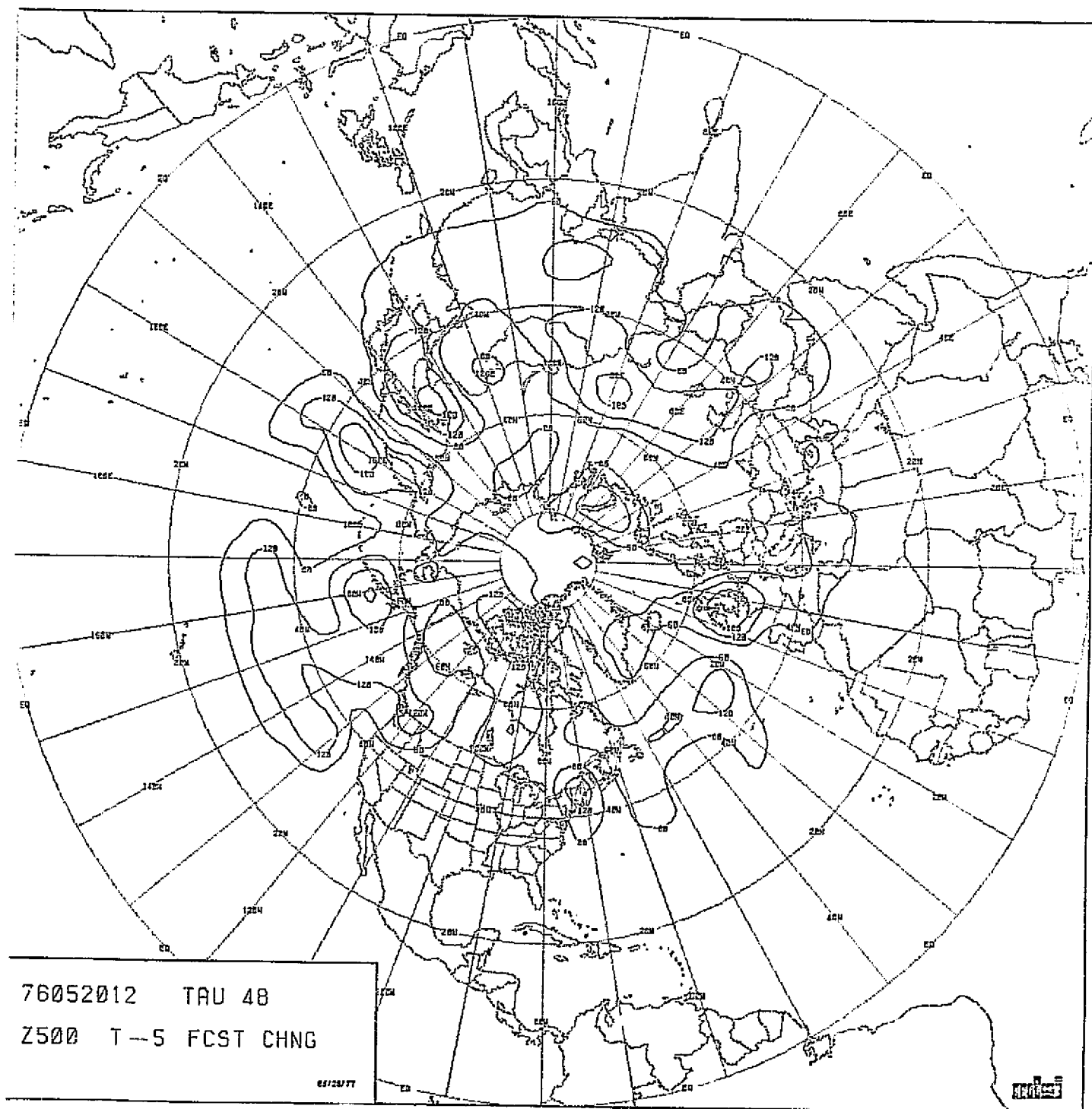


CHART VIII-121: RUN T5. SCENARIO B. MODEL PECHFY. 48-HOUR
FORECAST CHANGE IN 500 MB HEIGHT.

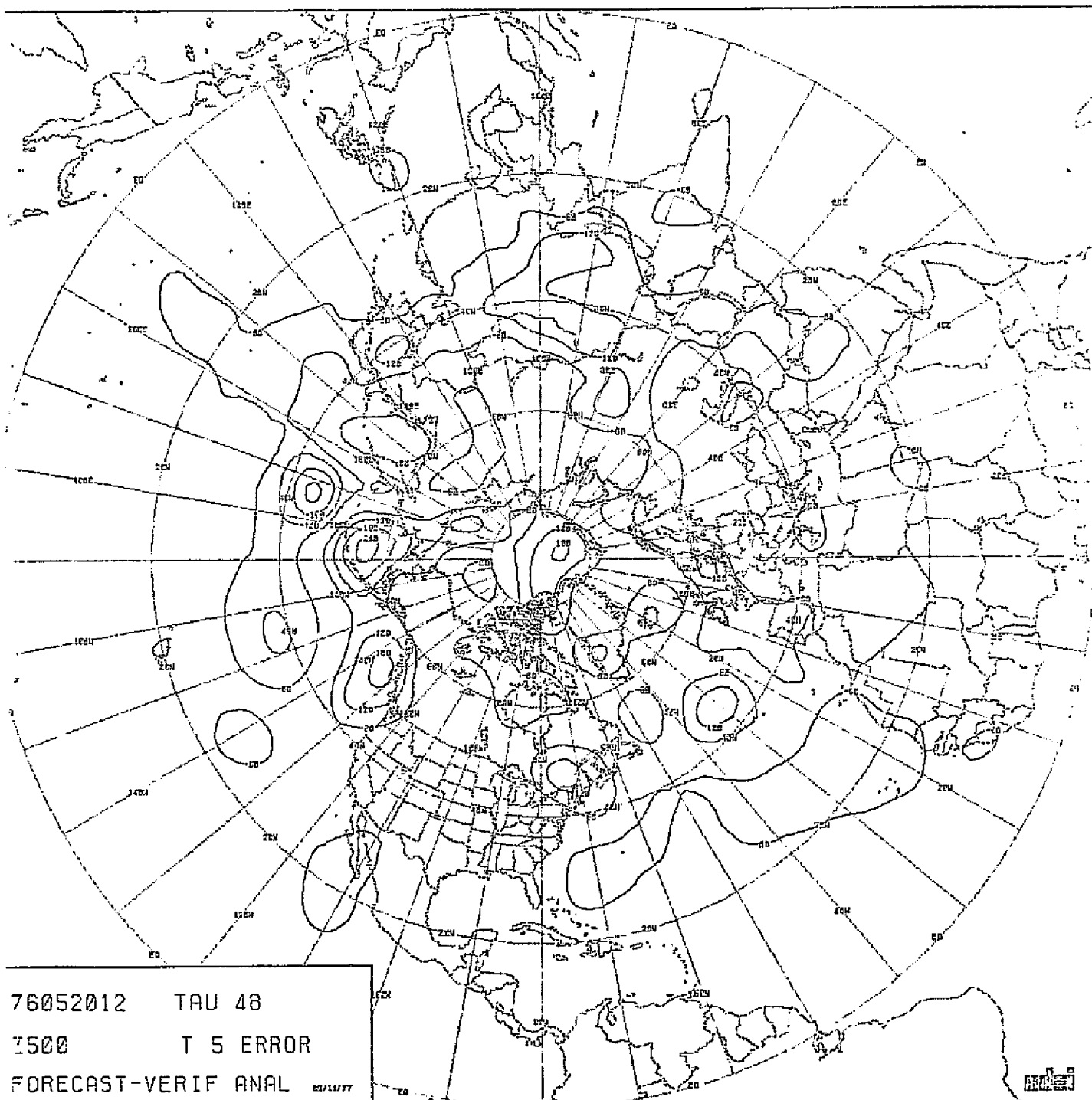


CHART VIII-122: RUN T5. SCENARIO B. MODEL PECHFV. 48-HOUR
FORECAST ERROR IN 500 MB HEIGHT.

ORIGINAL PAGE IS
OF POOR QUALITY

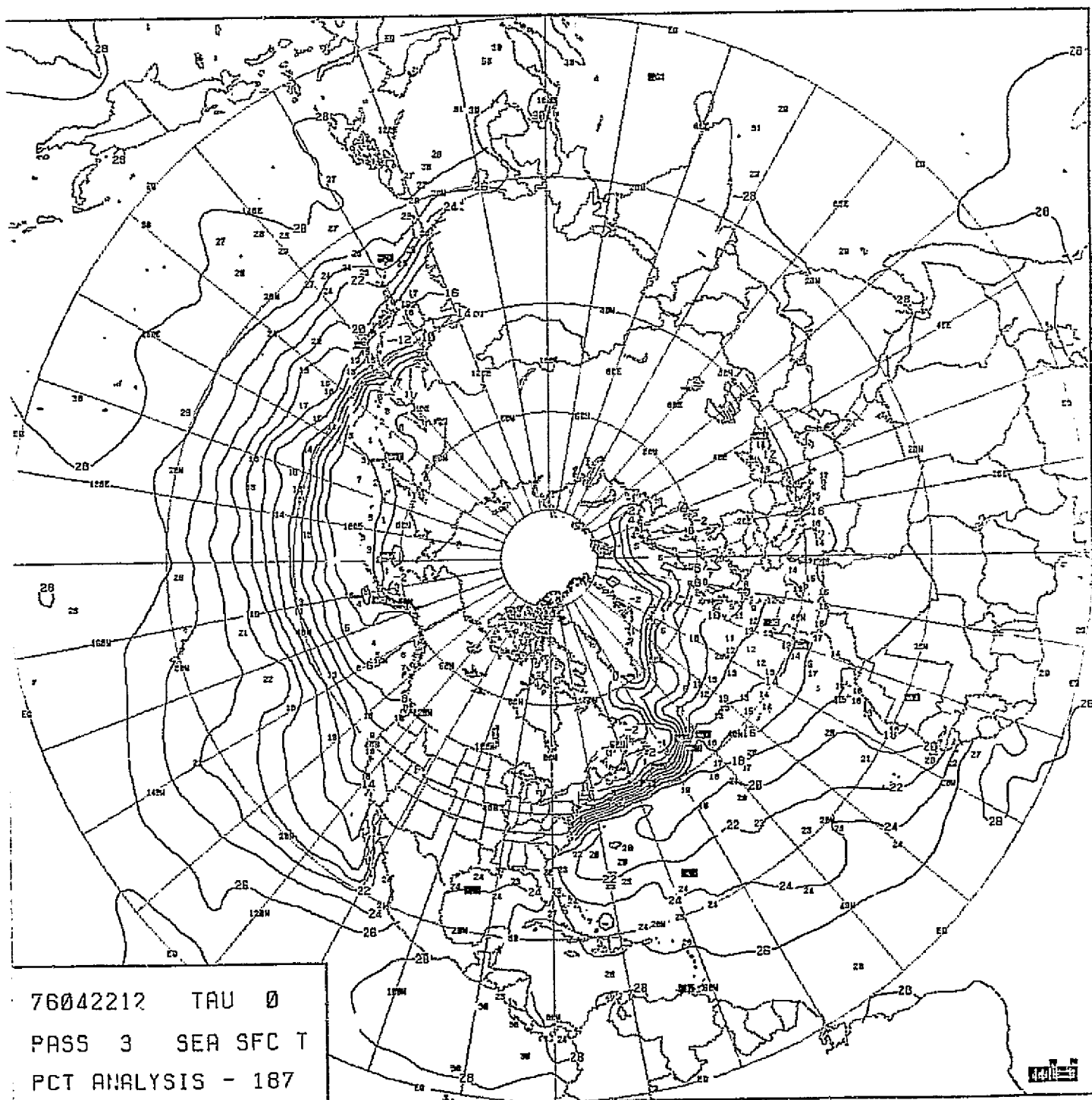
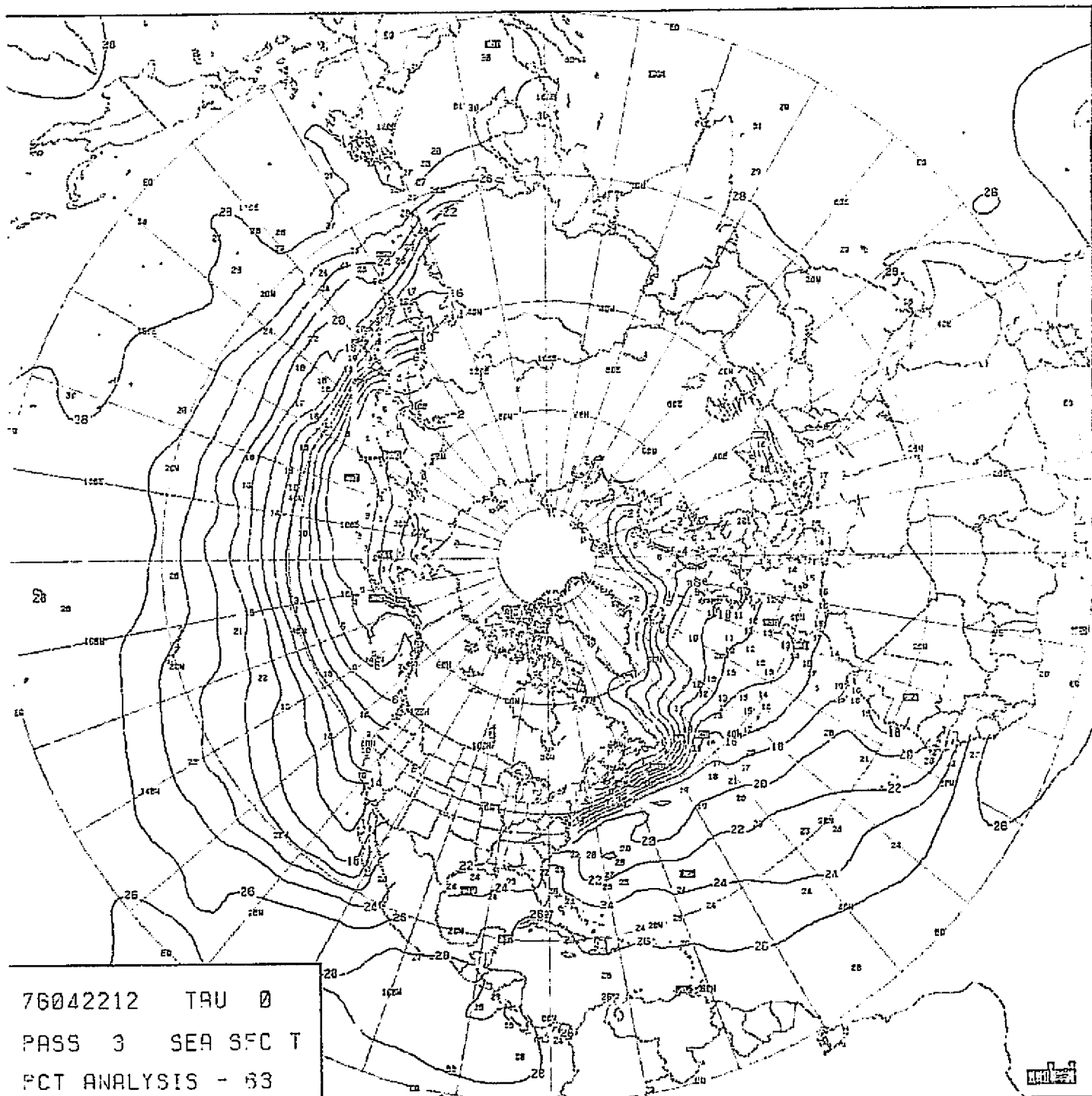
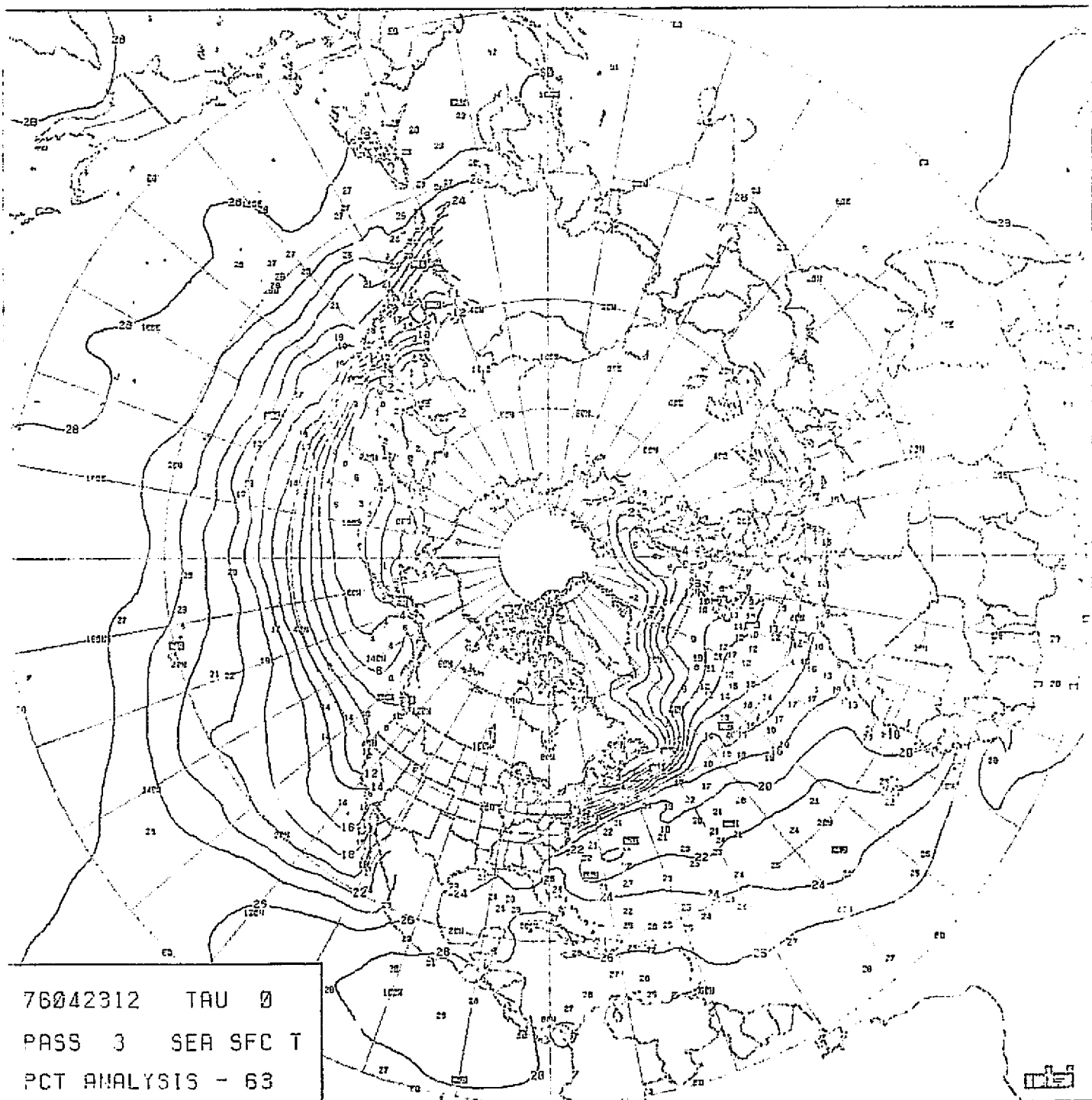


CHART VIII-123

SST ANALYSIS, 1200Z, 22 APRIL 1976,
187 x 187 GRID.



ORIGINAL PAGE
OF POOR QUALITY



0111. 00000000. 0000 000000

CHART VIII-125

SST ANALYSIS, 1200Z, 23 APRIL 1976,
63 x 63 GRID.

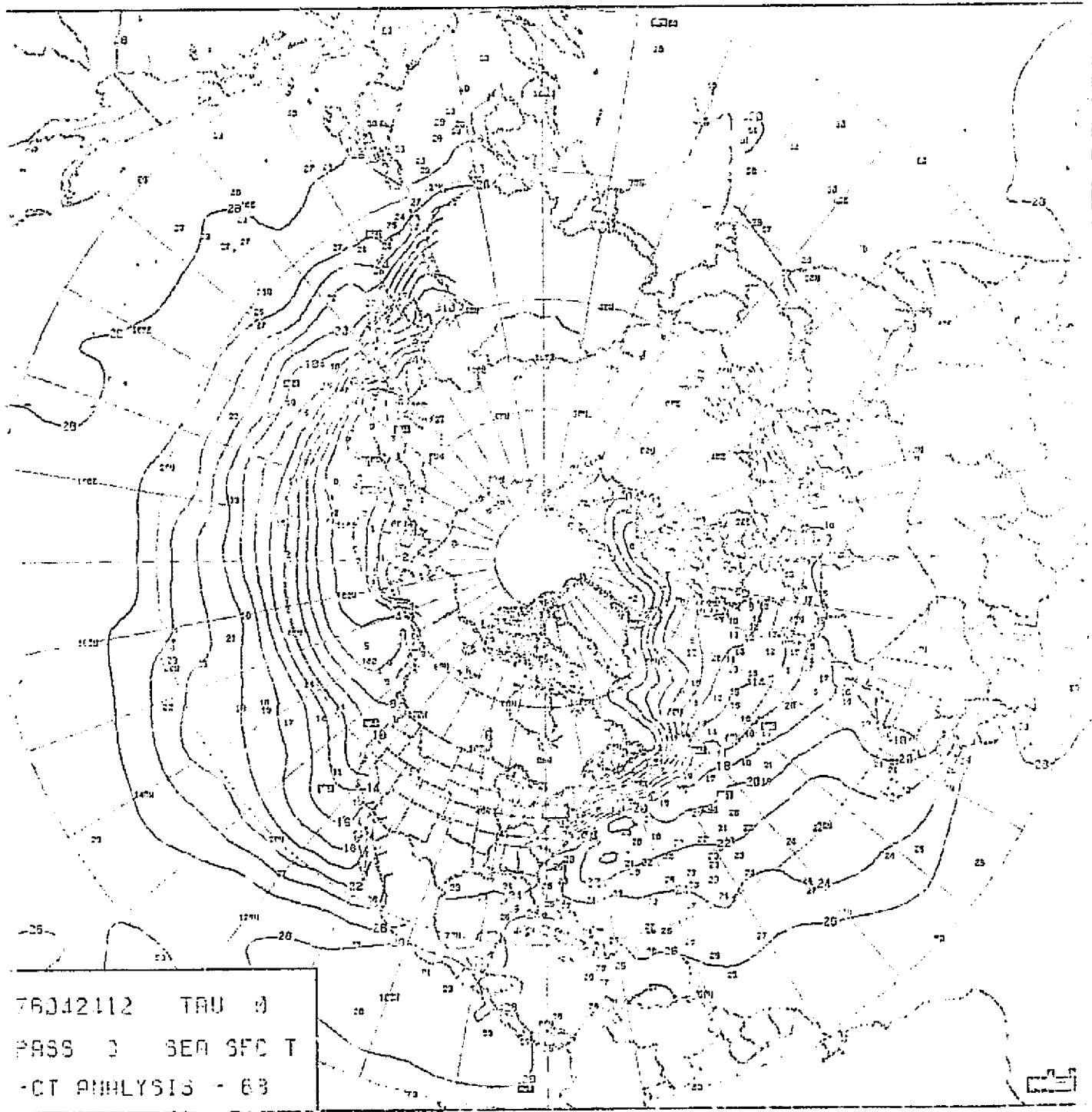
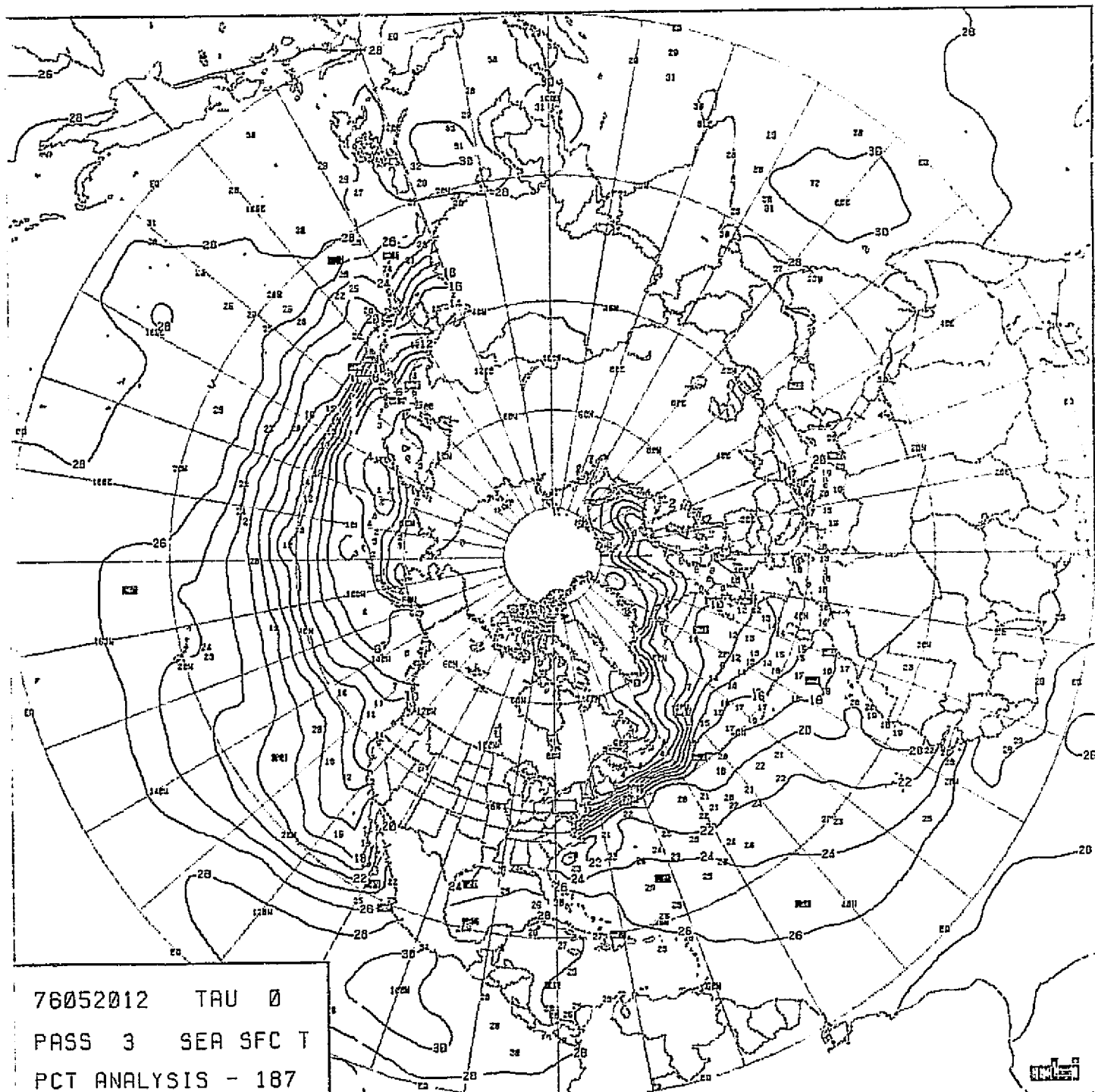


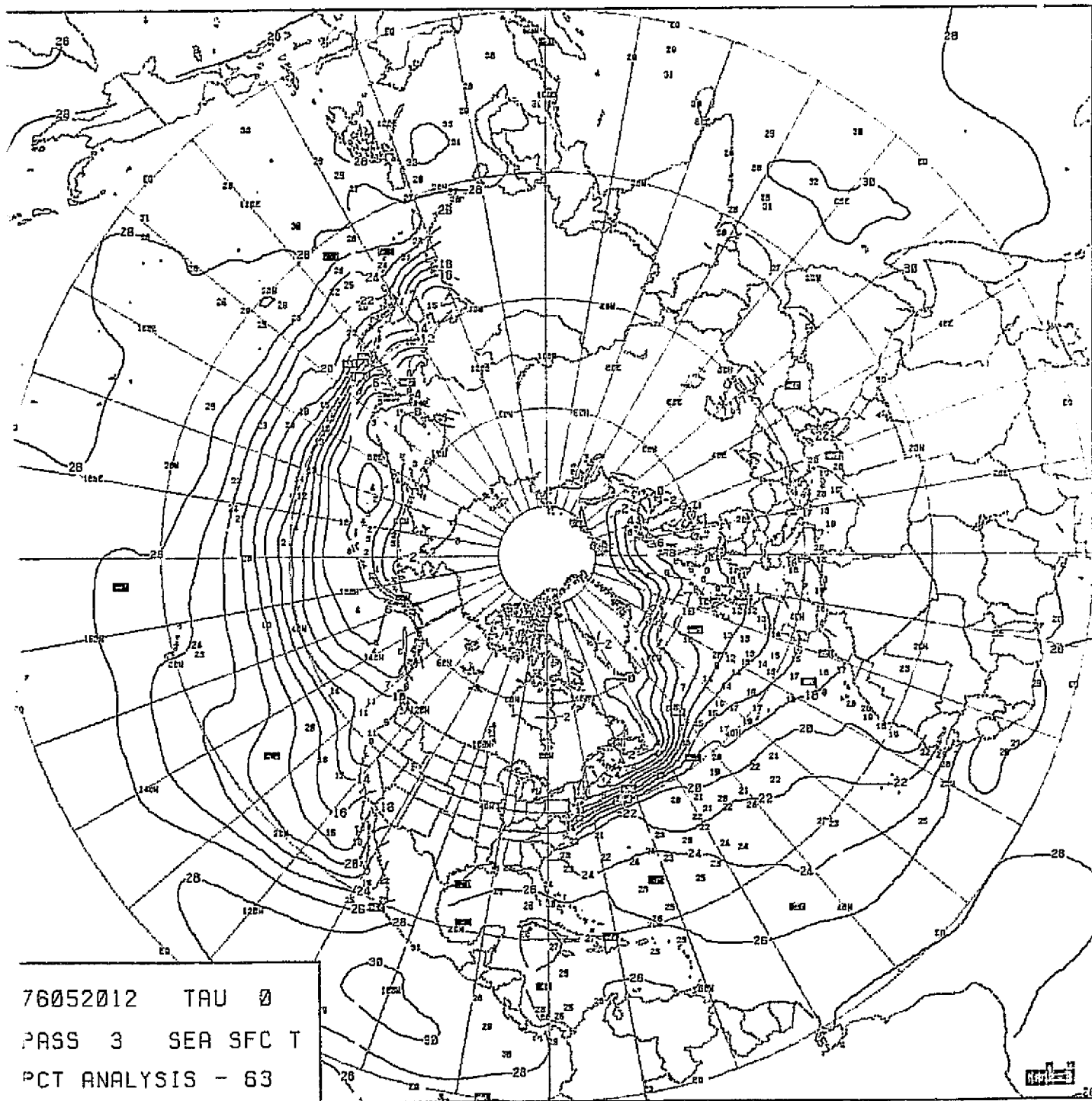
CHART VIII-126

SST ANALYSIS, 1200Z, 24 APRIL 1976,
63 x 63 GRID.

**ORIGINAL PAGE IS
OF POOR QUALITY**



ORIGINAL PAGE IS
OF POOR QUALITY



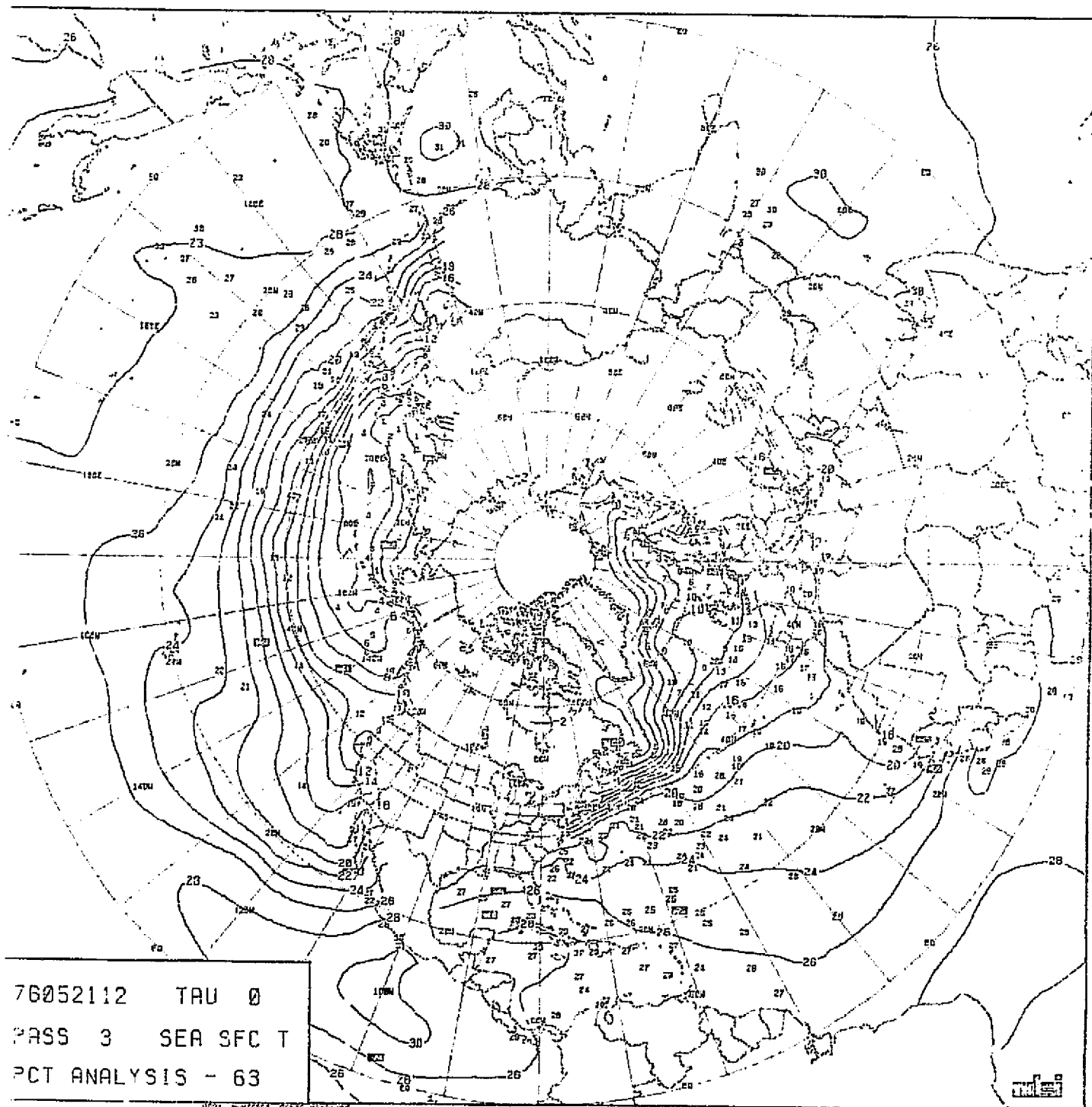


CHART VIII-129

SST ANALYSIS, 1200Z, 21 MAY 1976,
63 x 63 GRID.

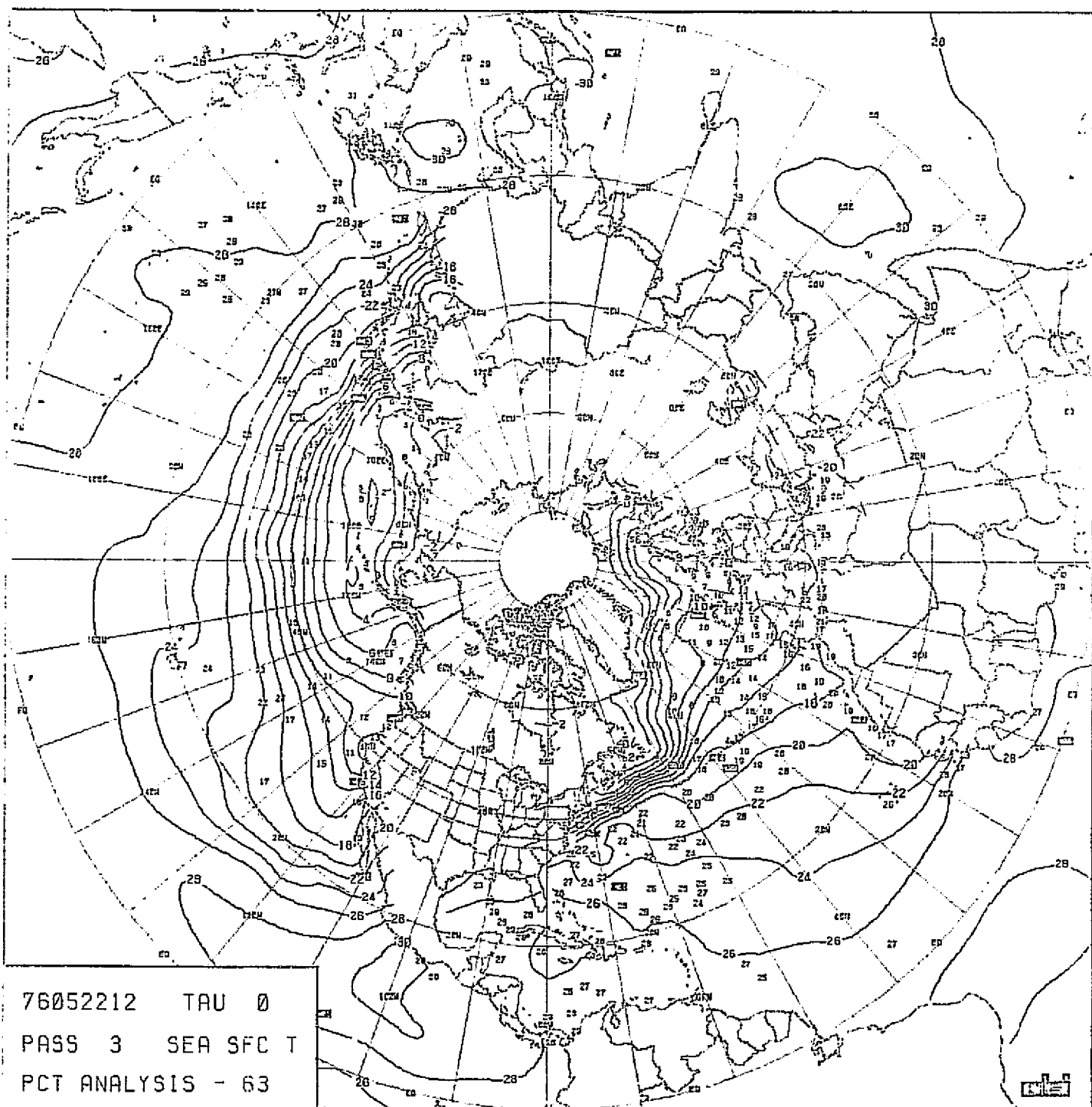
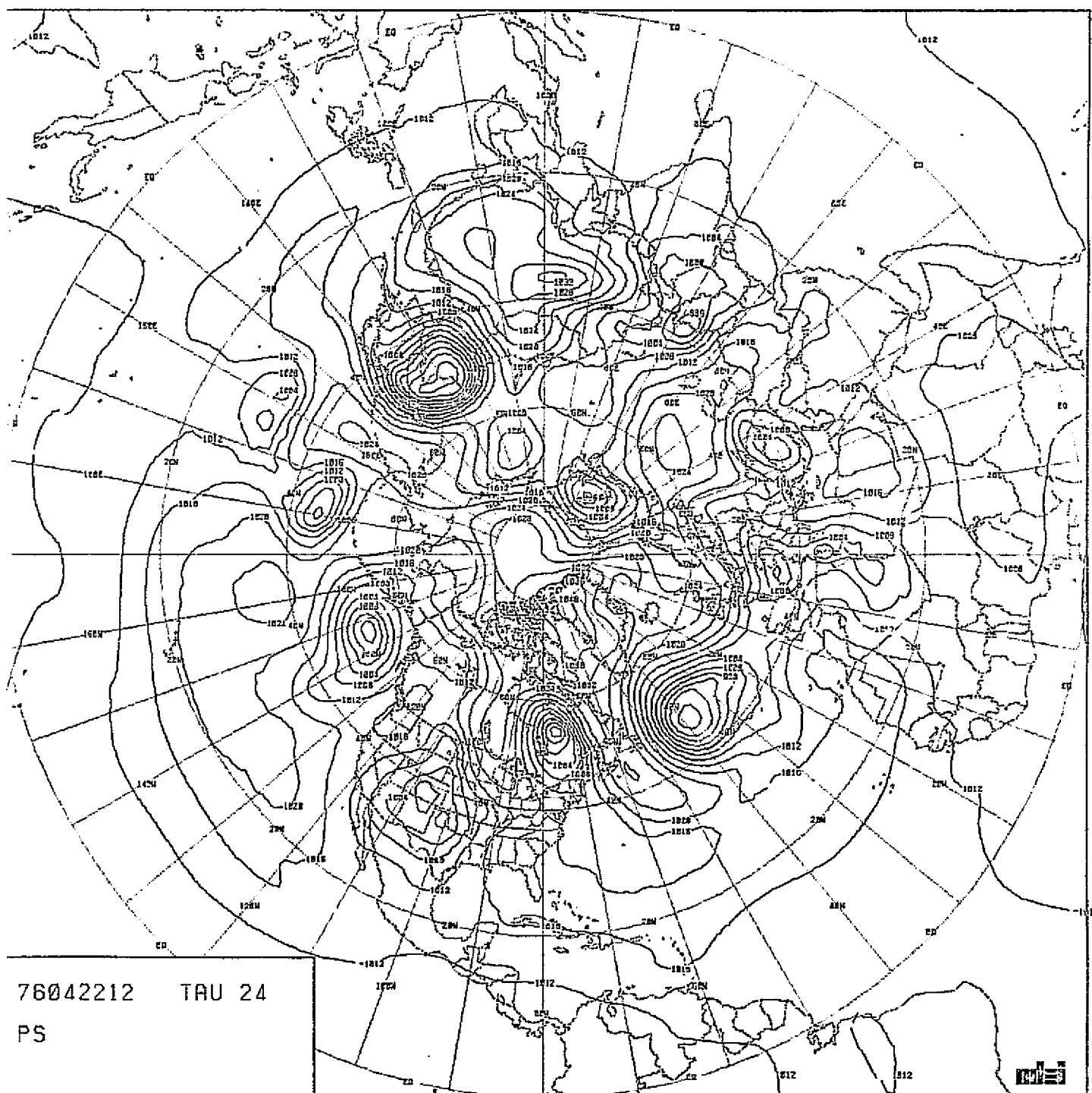


CHART VIII-130

CHART VIII-130

SST ANALYSIS, 1200Z, 22 MAY 1976,
63 x 63 GRID.

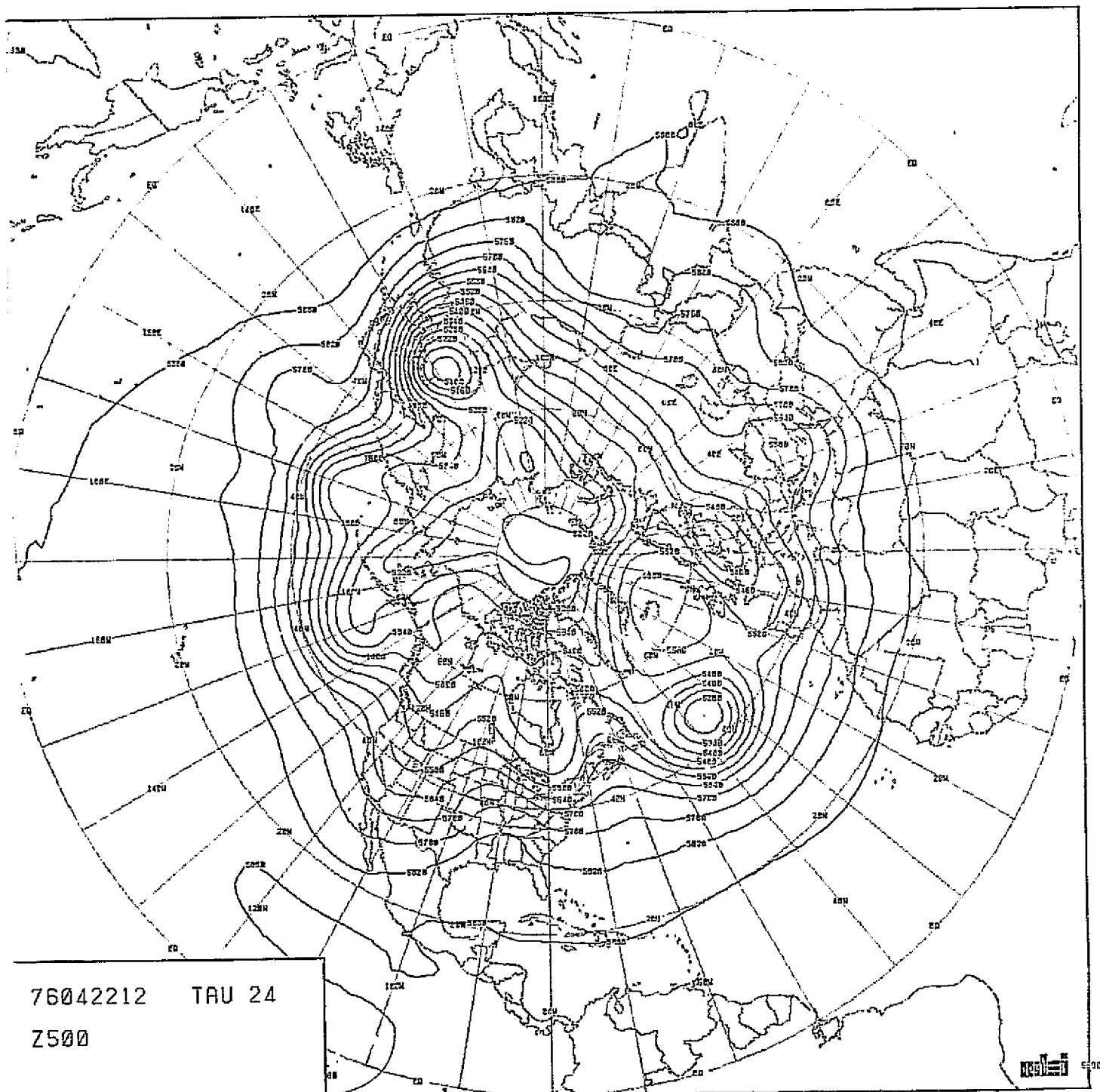
ORIGINAL PAGE IS
OF POOR QUALITY



GUSI. RANTREY. 7417 81/8177

CHART VIII-131 : SEA-LEVEL PRESSURE 24-HOUR FORECAST. RUN F22.
MODEL PEPHCY. SCENARIO A.

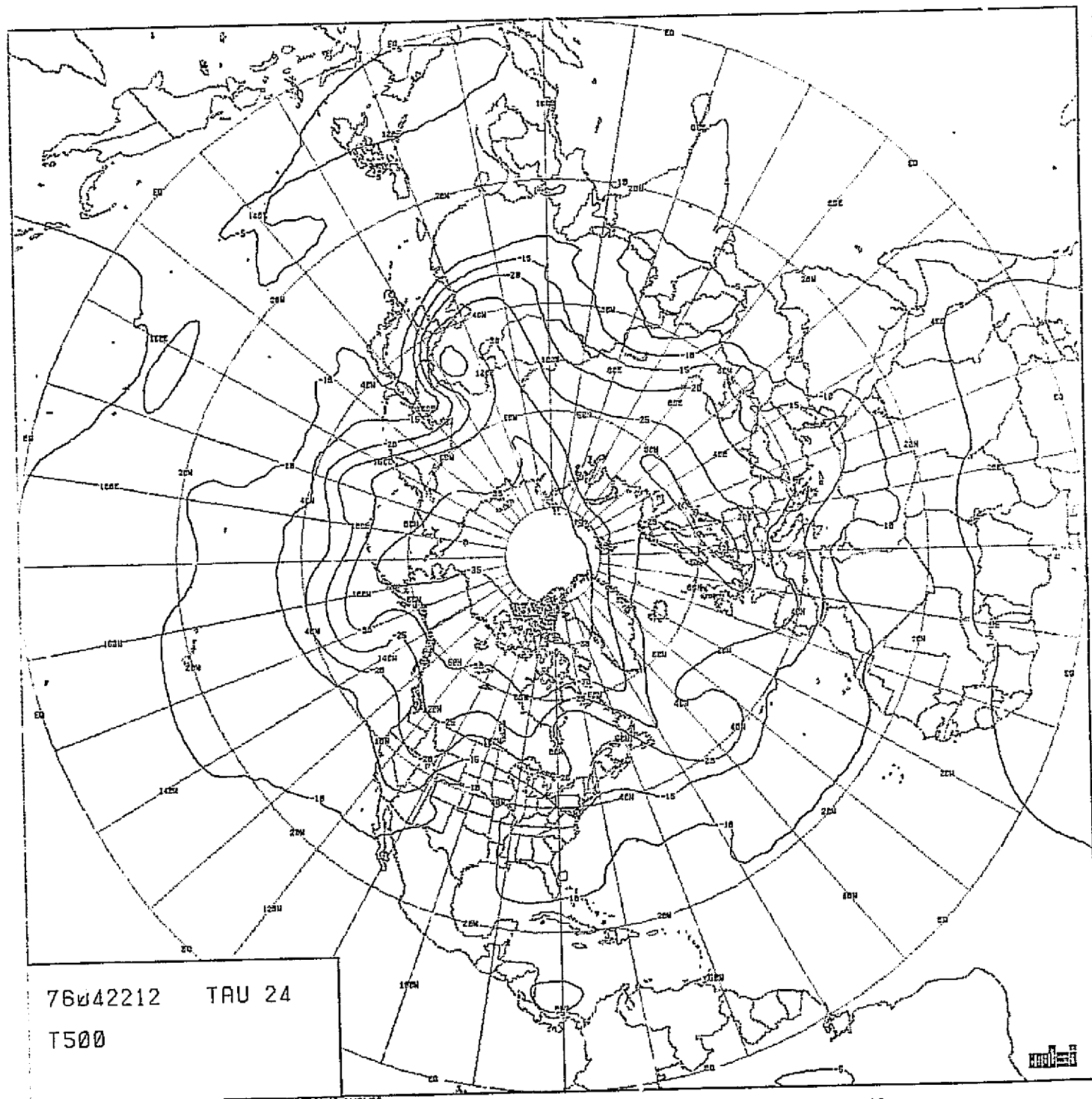
ORIGINAL PAGE IS
OF POOR QUALITY



76042212 TAU 24
Z500

CHART VIII-132 : 500 MB HEIGHT 24-HOUR FORECAST. RUN F22.
MODEL PEFHCV. SCENARIO A.

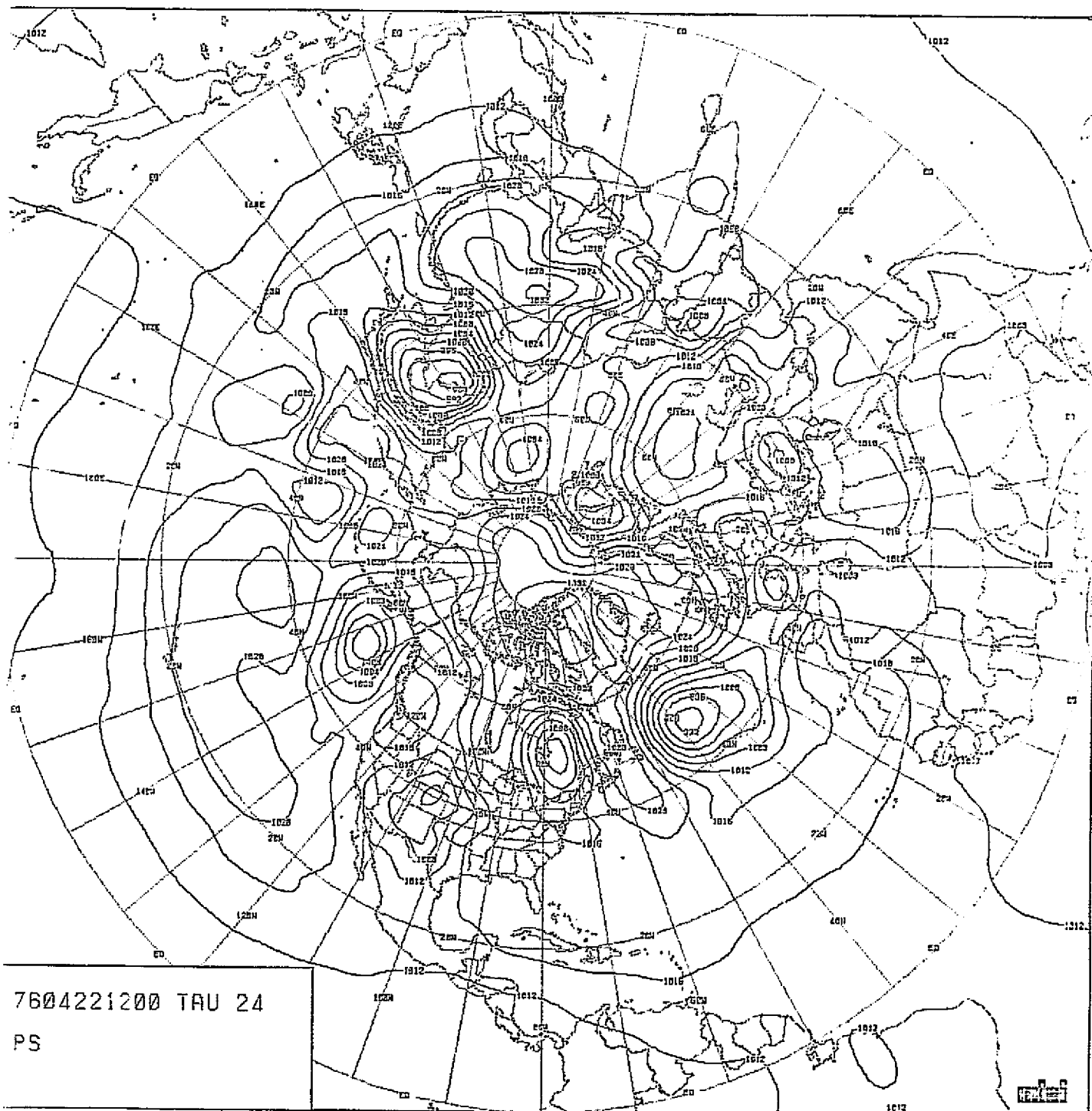
ORIGINAL PAGE IS
OF POOR QUALITY

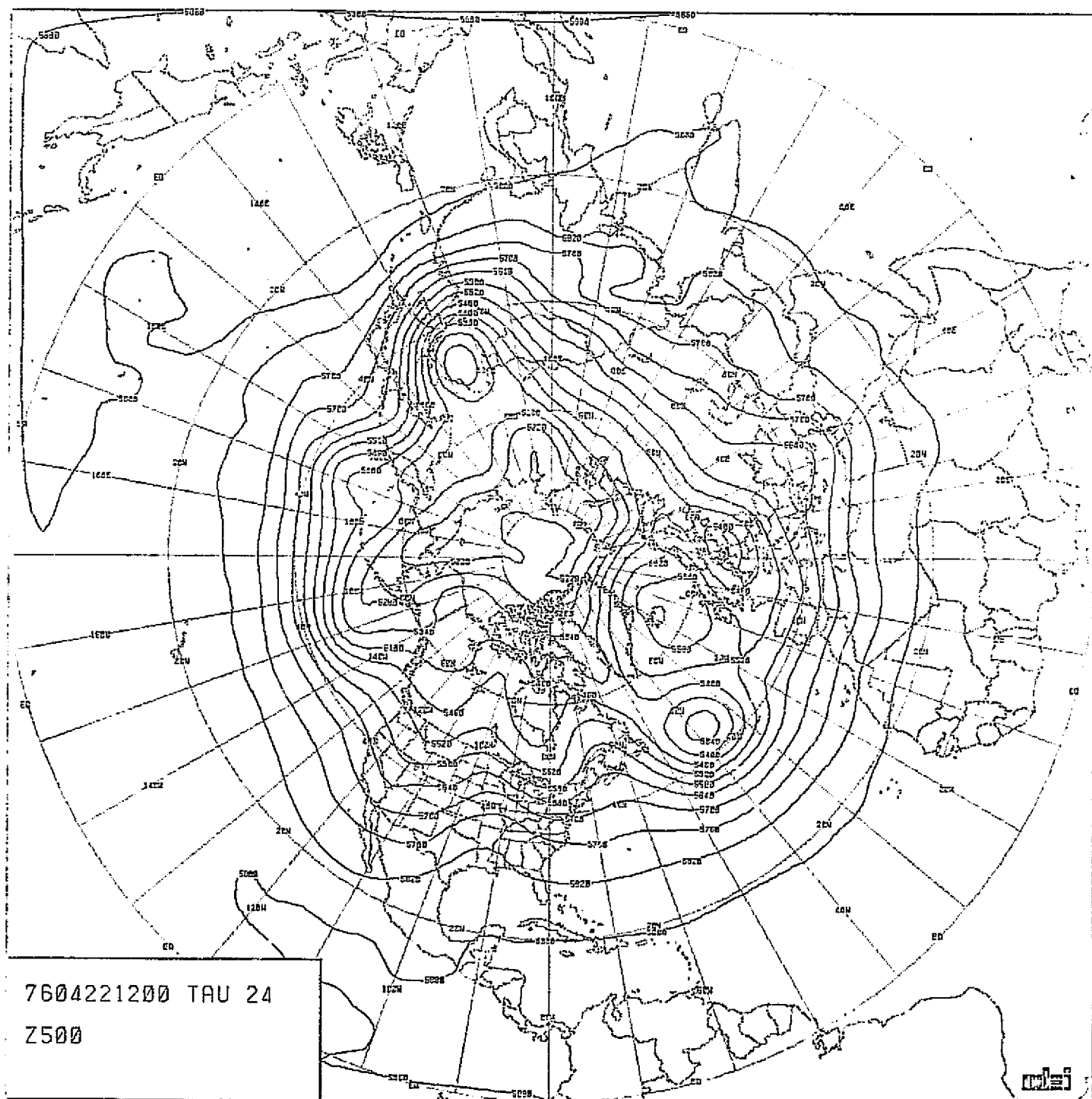


76042212 TAU 24
T500

CHART VIII-133 : 500 MB TEMPERATURE 24-HOUR FORECAST. RUN F22.
MODEL PEFHCV. SCENARIO A.

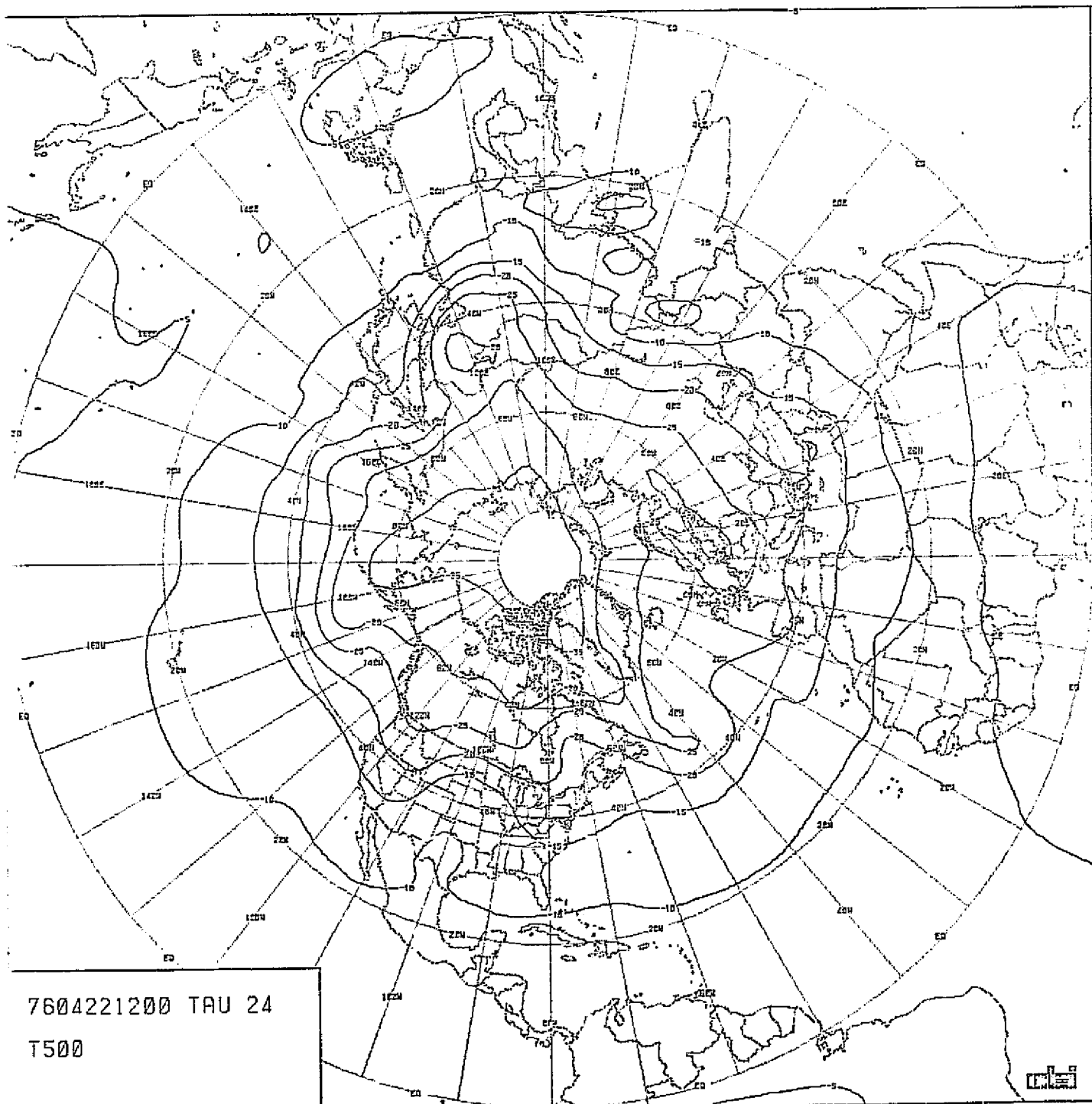
ORIGINAL PAGE IS
OF POOR QUALITY





7604221200 TAU 24
Z500

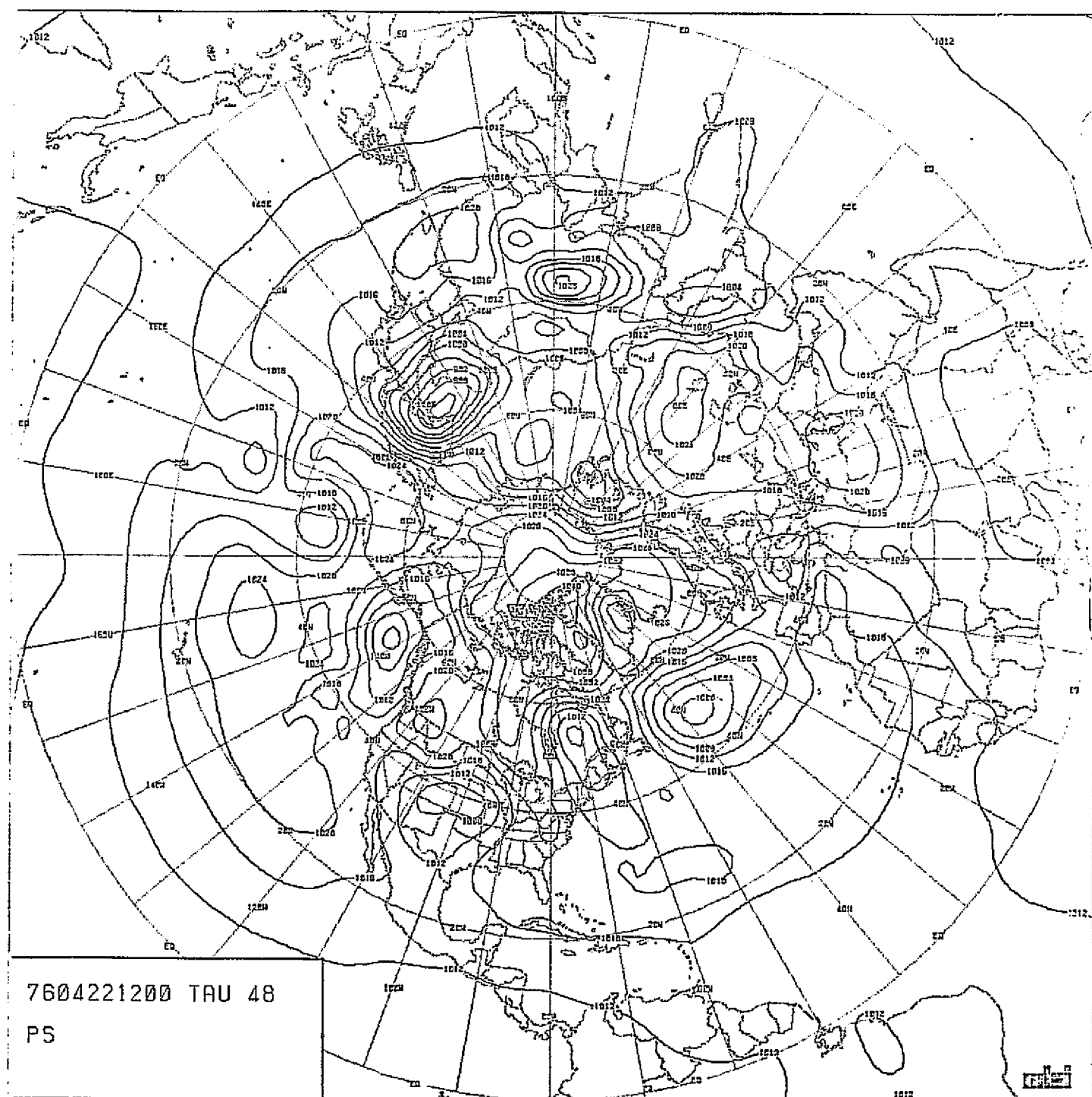
CHART VIII-135 : 500 MB HEIGHT 24-HOUR FORECAST. RUN F19.
MODEL PECHCV. SCENARIO A.



7604221200 TAU 24
T500

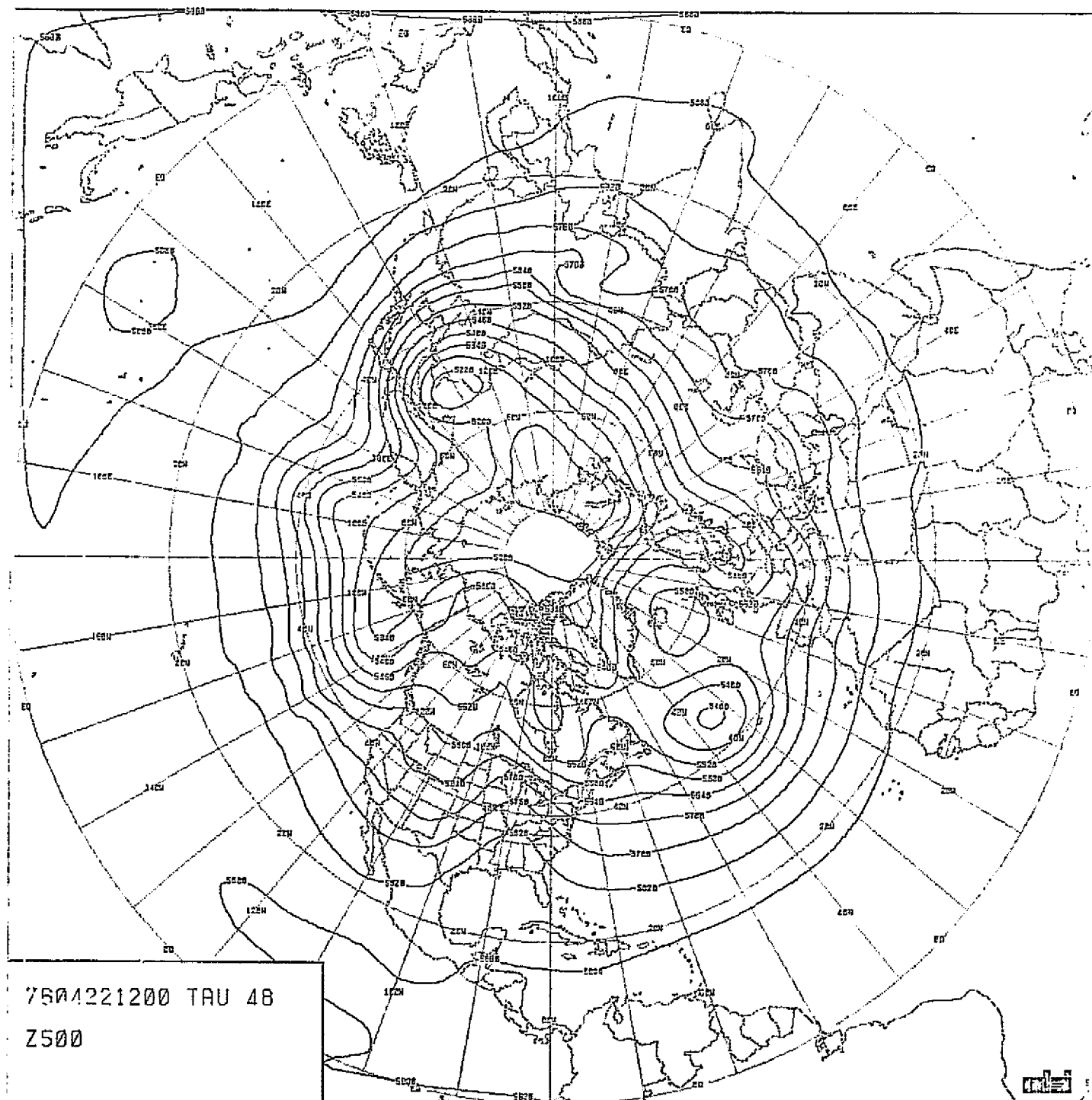
0001. CENTER, GULF 01/02/77

CHART VIII-136 : 500 MB TEMPERATURE 24-HOUR FORECAST. RUN F19.
MODEL PECHCV. SCENARIO A.



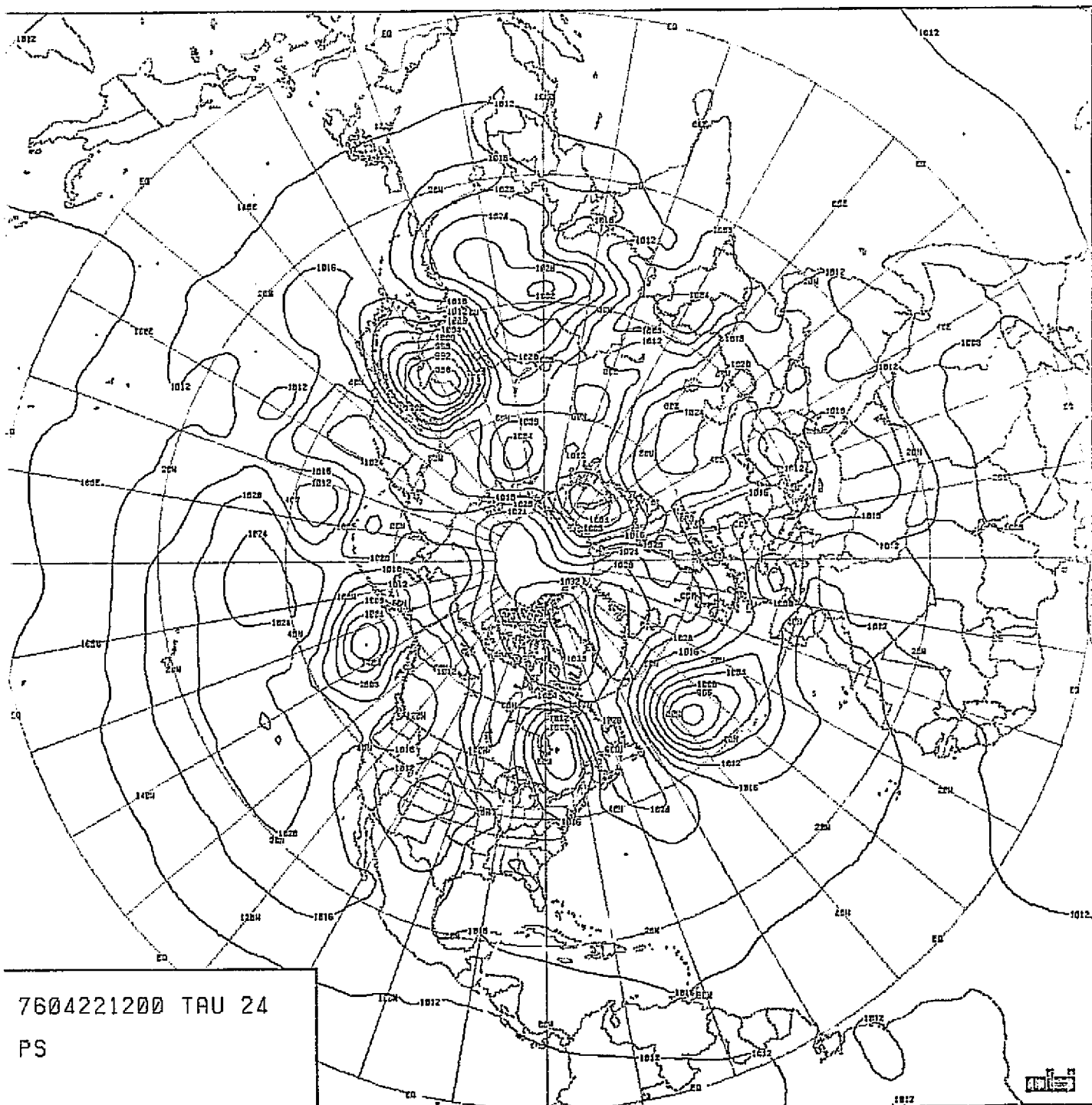
00311. R001087. CH. 04/02/77

CHART VIII-137 : SEA-LEVEL PRESSURE 48-HOUR FORECAST. RUN F13.
MODEL PECHCV. SCENARIO A.



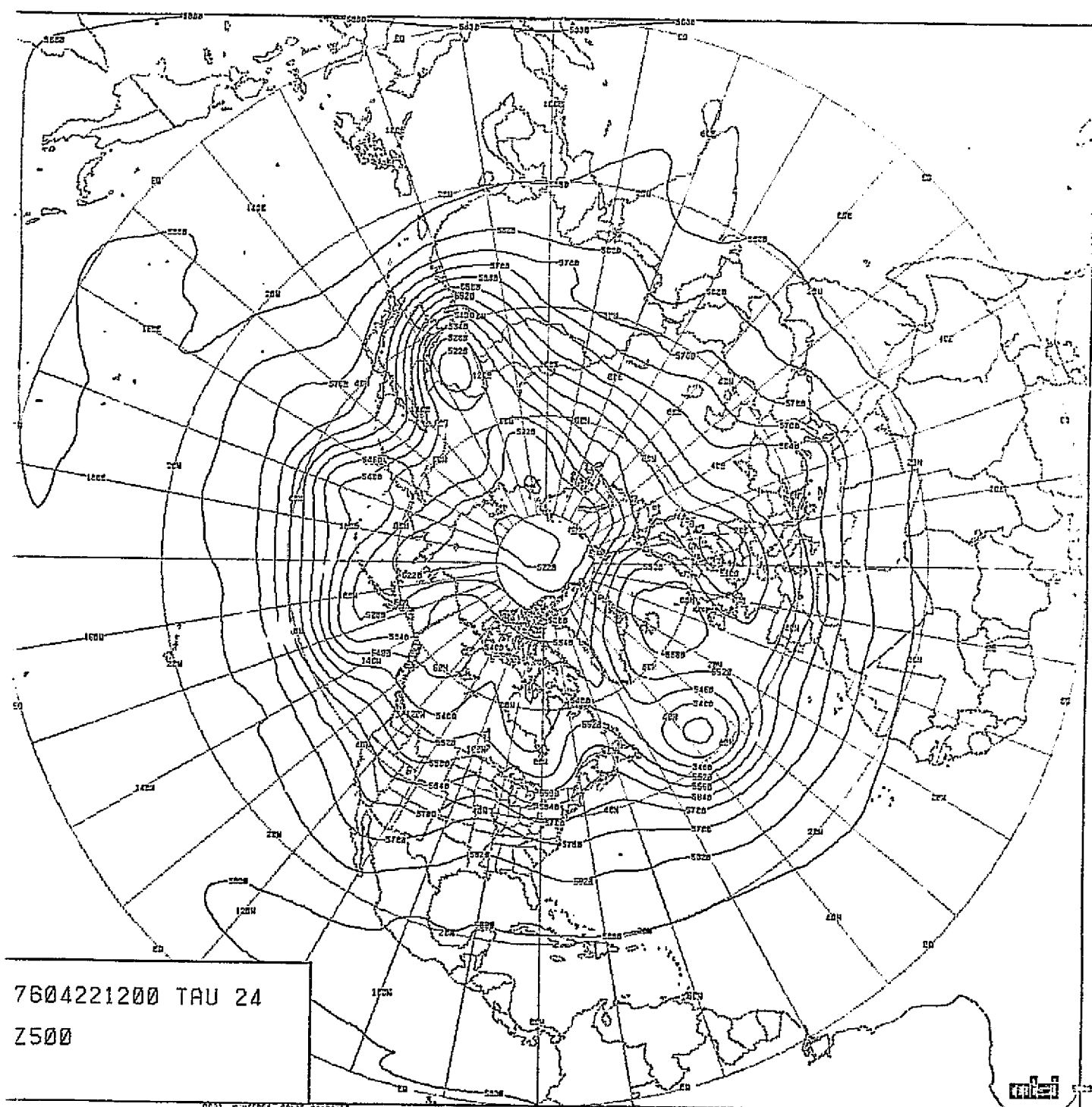
0031, PONTREY, CALIF 8/18/77

CHART VIII-138 : 500 MB HEIGHT 48-HOUR FORECAST. RUN F18.
MODEL PECHCV. SCENARIO A.



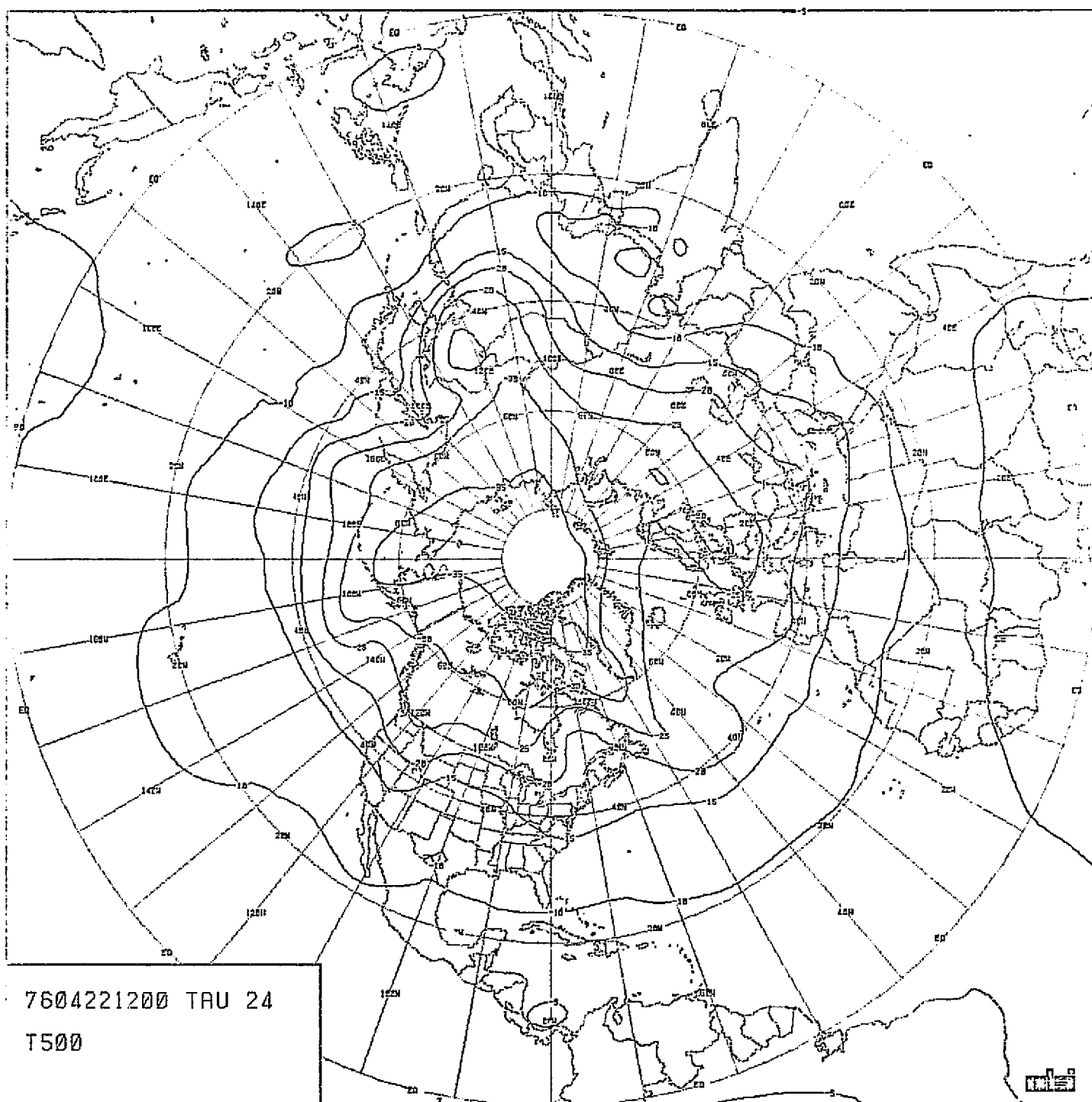
0031. FORTY-ONE. CHART VIII-140

CHART VIII-140 : SEA-LEVEL PRESSURE 24-HOUR FORECAST. RUN T4.
MODEL FICFV. SCENARIO A.



0031. 20011001. 0121P 0370717

CHART VIII-141 : 500 MB HEIGHT 24-HOUR FORECAST. RUN T4.
MODEL PECHFV. SCENARIO A.

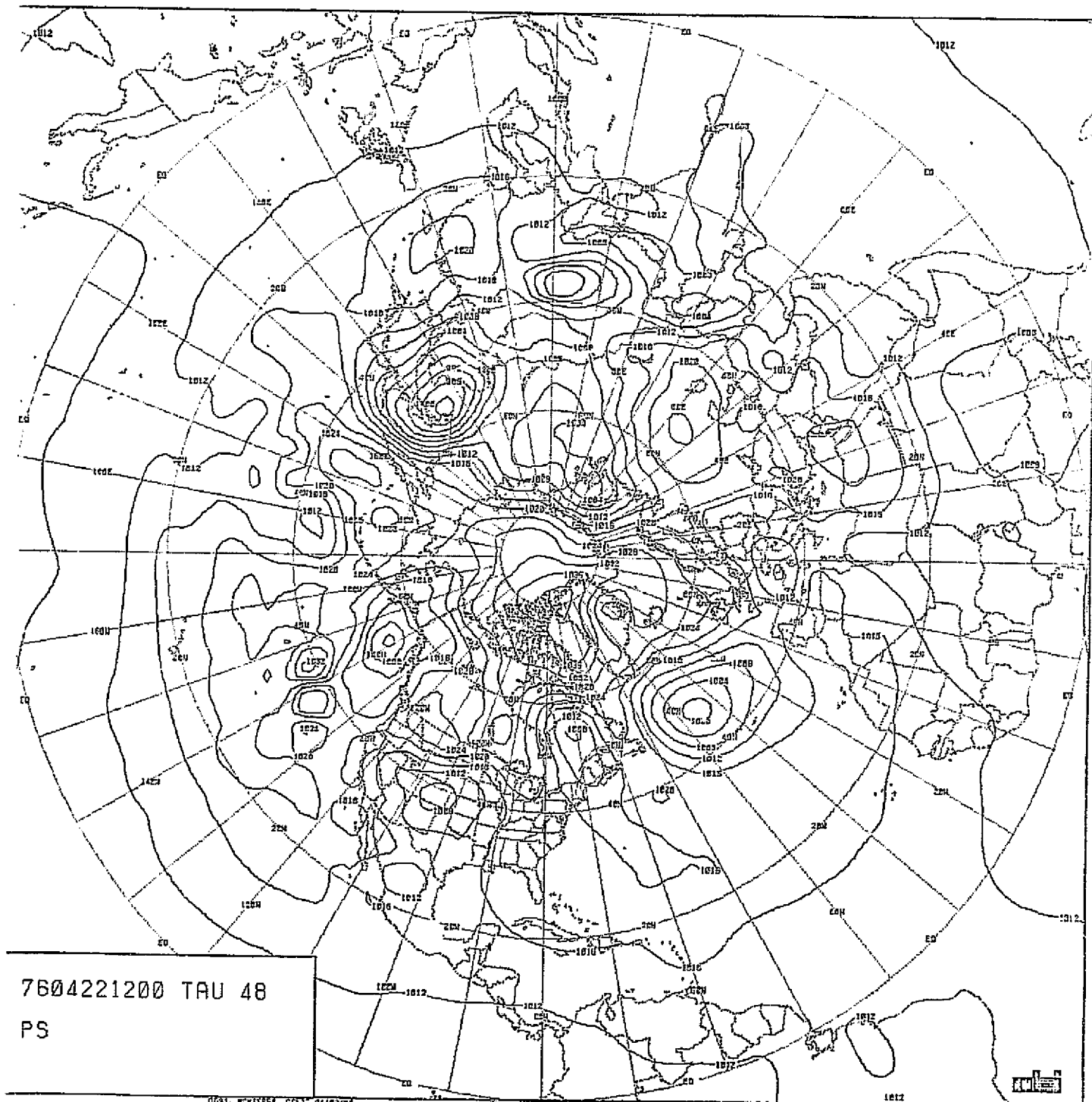


7604221200 TRU 24
T500

0001: FOM(ESF) CH(1P 01/02/77)

CHART VIII-142 : 500 MB TEMPERATURE 24-HOUR FORECAST. RUN T4.
MODEL PECHFV. SCENARIO A.

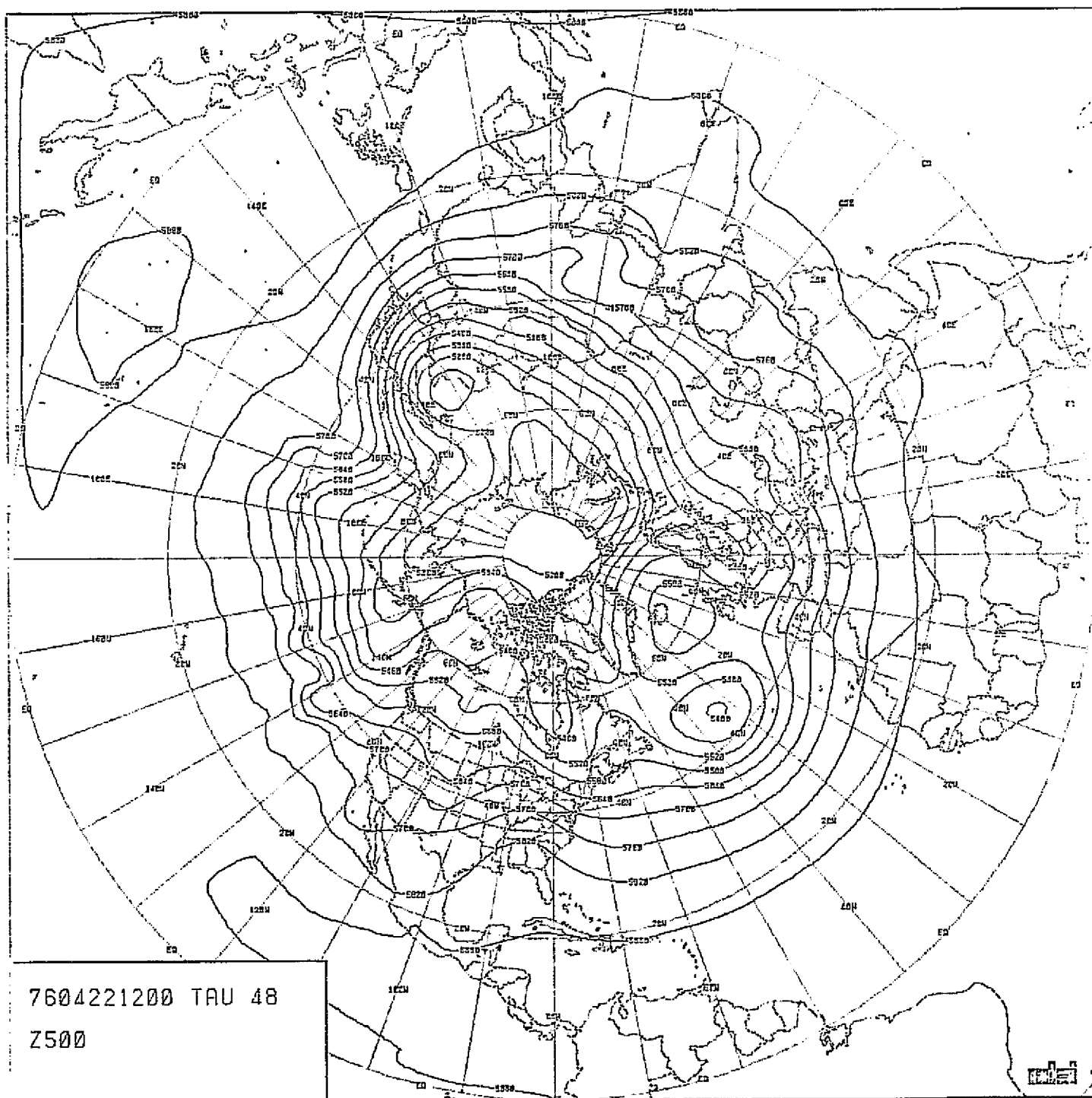
ORIGINAL PAGE IS
OF POOR QUALITY.



0031. NORTHERN. GRIFF 01/02/77

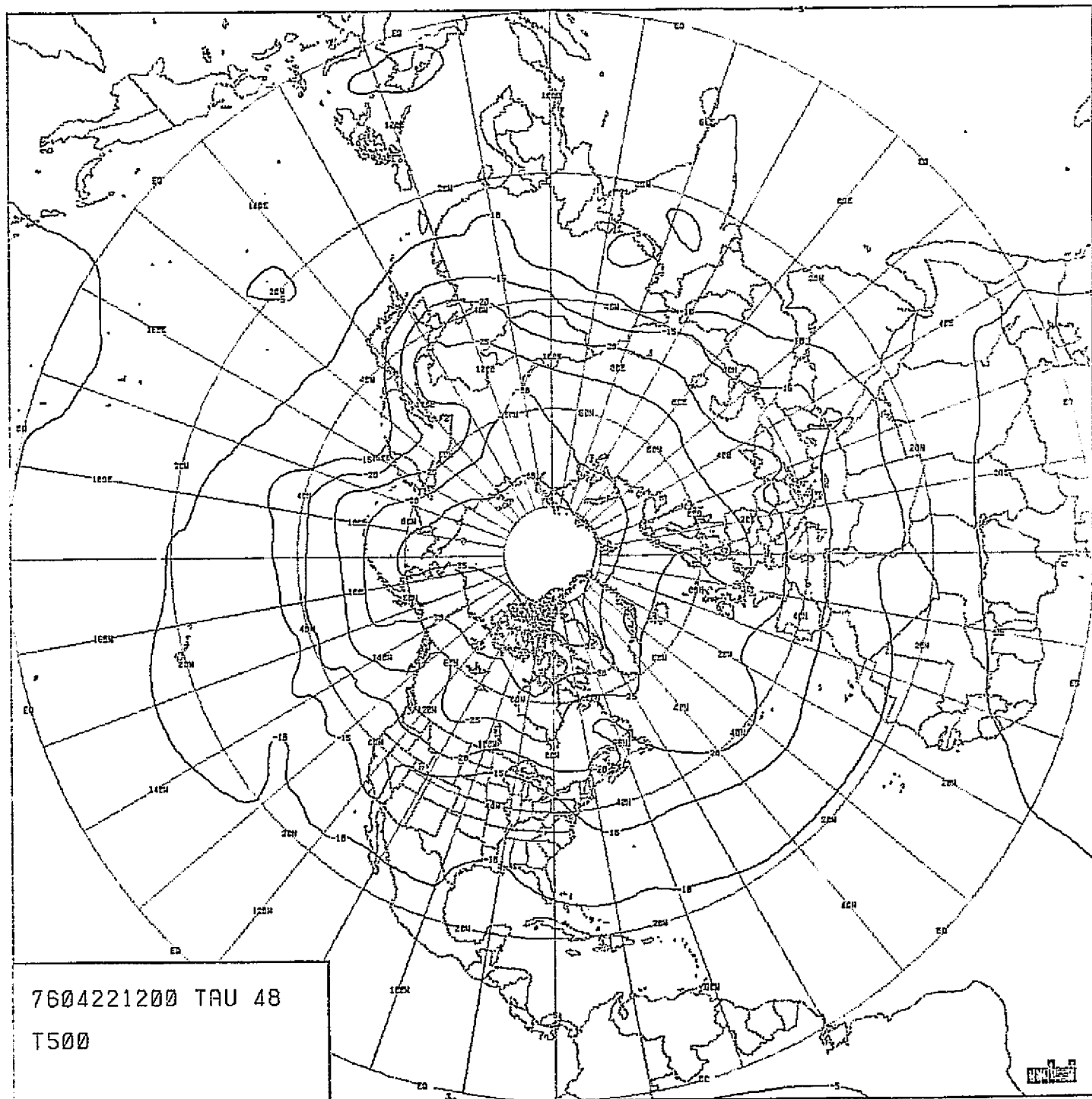
CHART VIII-143 : SEA-LEVEL PRESSURE 48-HOUR FORECAST. RUN T4.
MODEL PECHV. SCENARIO A.

ORIGINAL PAGE IS
OF POOR QUALITY



0051. 100122Z. CHATP 11/02/77

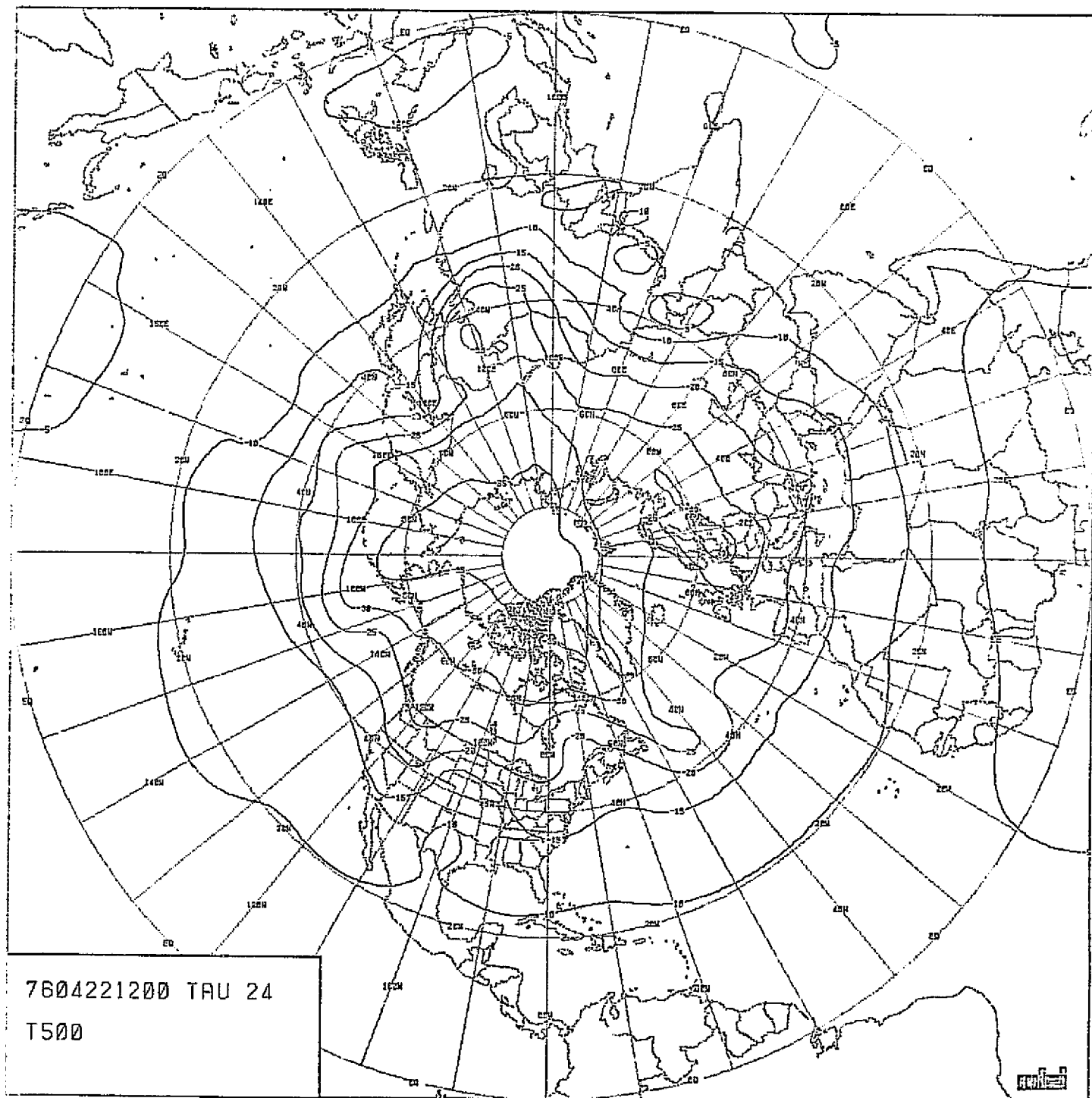
CHART VIII-144 : 500 MB HEIGHT 48-HOUR FORECAST. RUN T4.
MODEL PECHFV. SCENARIO A.



7604221200 TAU 48
T500

0001, 000000, 0001, 0001

CHART VIII-145 : 500 MB TEMPERATURE 48-HOUR FORECAST. RUN T4.
MODEL PECHFV. SCENARIO A.



0001, MONTESE, CHILP 01/01/77

CHART VIII-148 : 500 MB TEMPERATURE 24-HOUR FORECAST. RUN F20.
MODEL PECHCV. SCENARIO A.

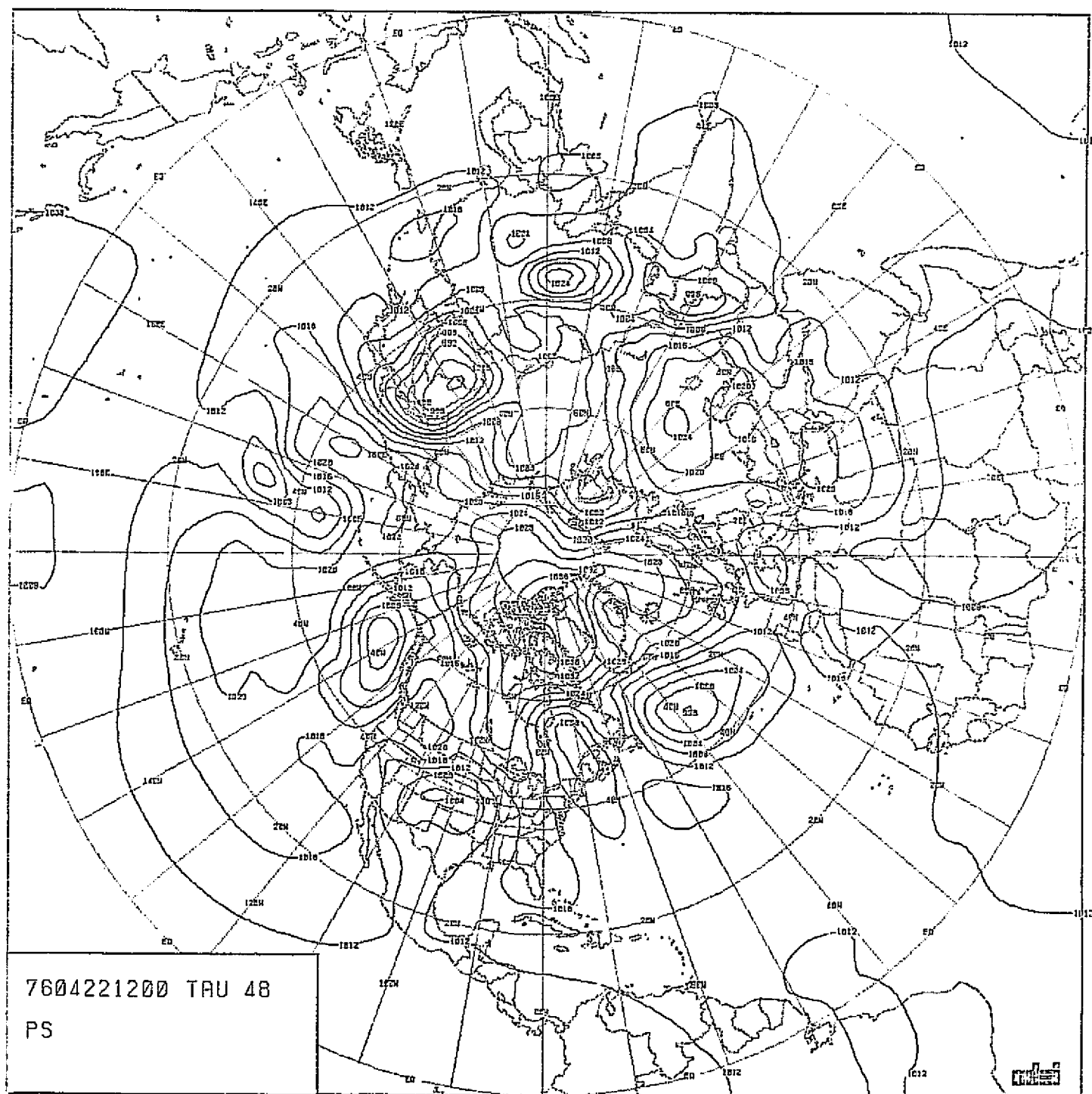
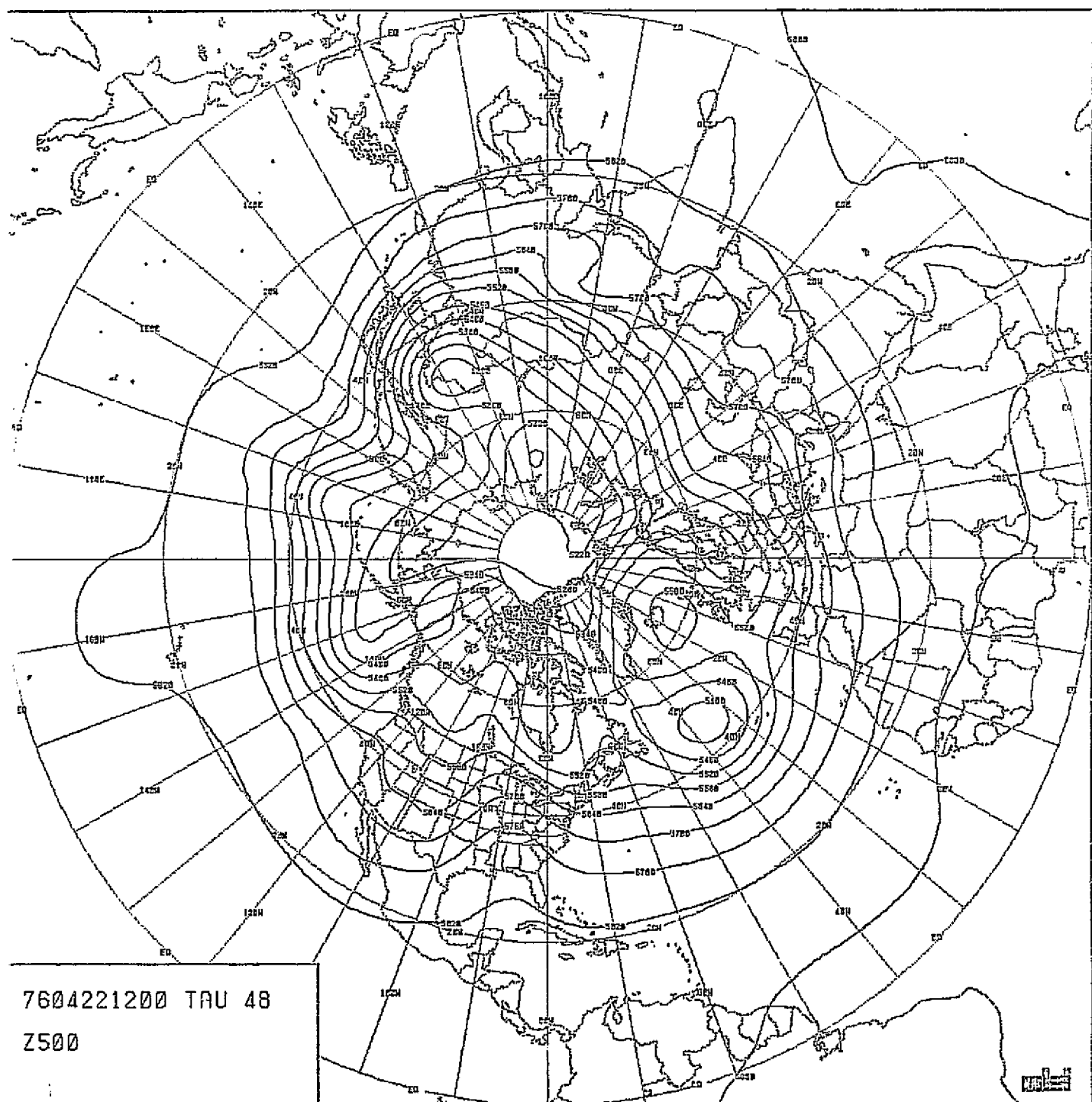


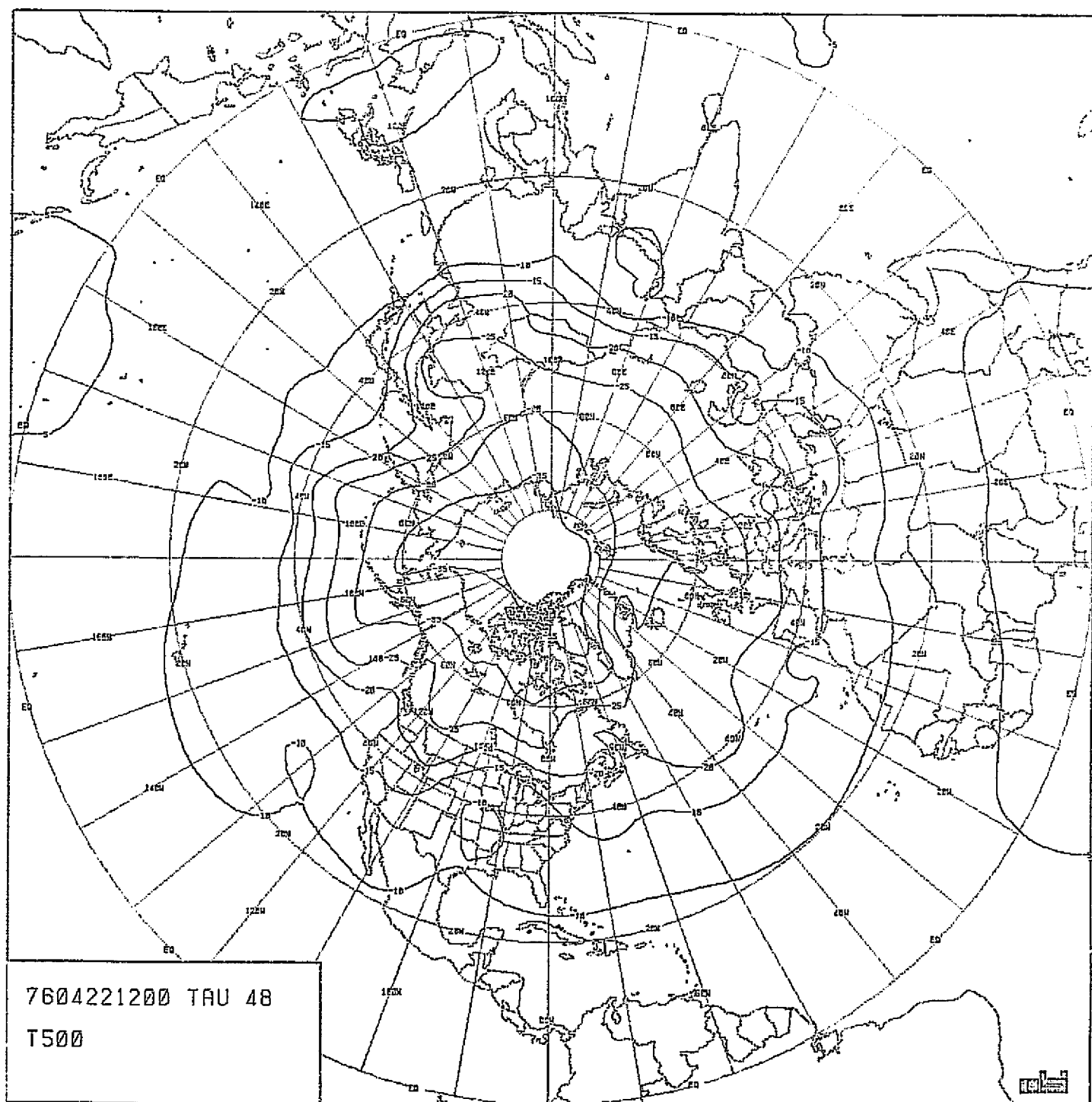
CHART VIII-149 : SEA-LEVEL PRESSURE 48-HOUR FORECAST. RUN F20.
MODEL PECHCV. SCENARIO A.

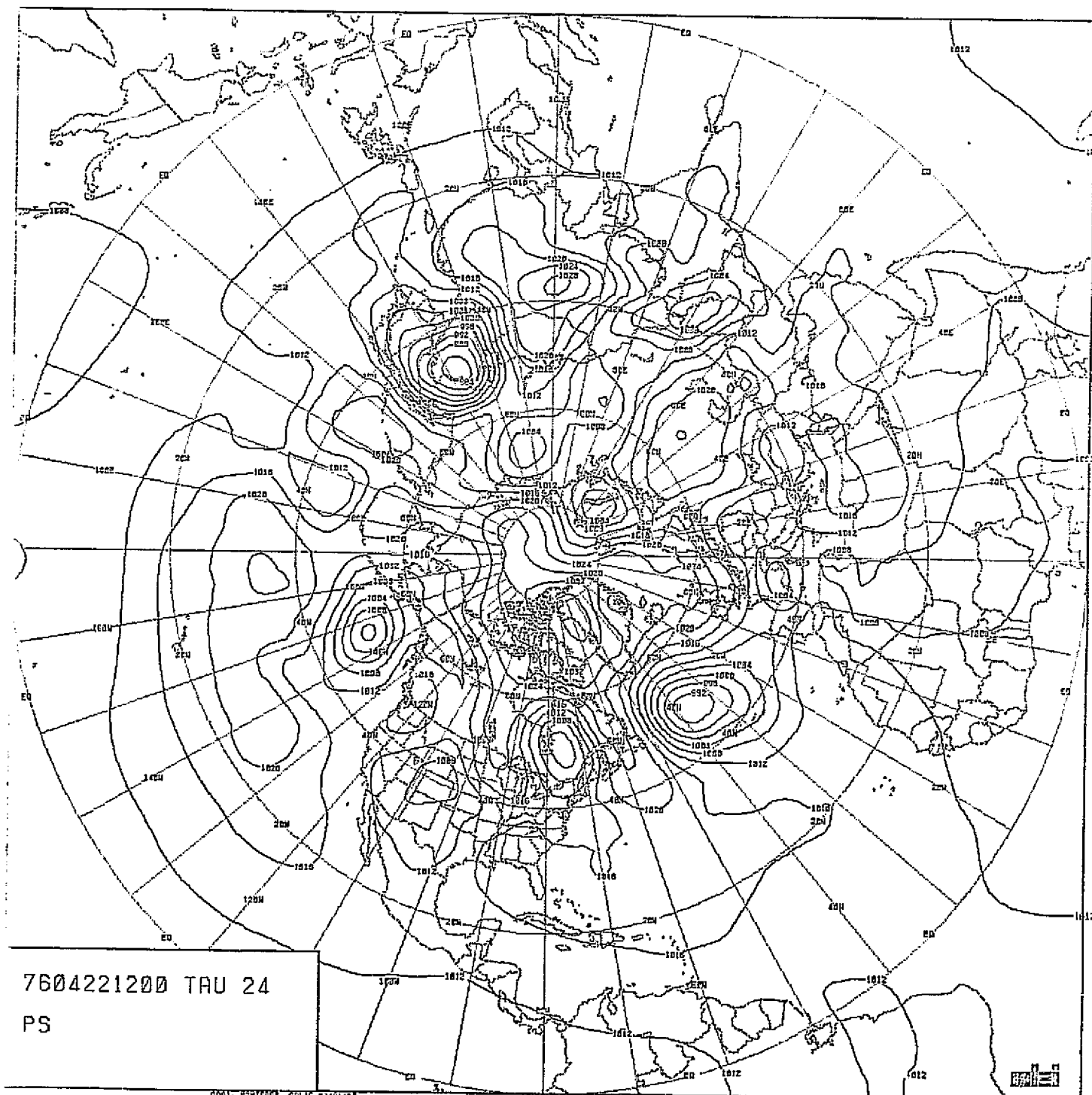
ORIGINAL PAGE IS
OF POOR QUALITY



0551, HORTERST, CRL16 C270177

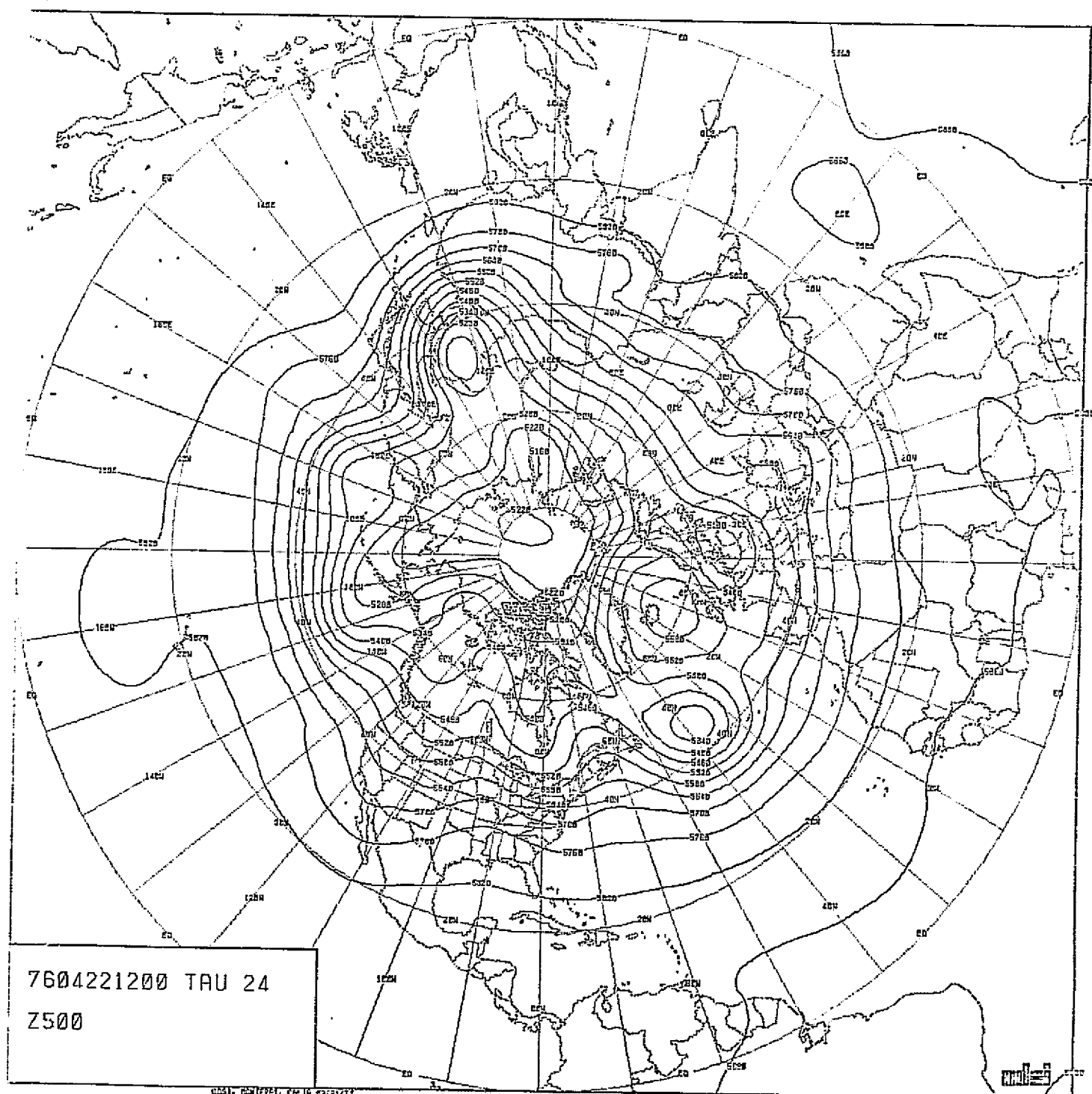
CHART VIII-150 : 500 MB HEIGHT 48-HOUR FORECAST. RUN F20.
MODEL PECHV. SCENARIO A.





0001. 05/01/77, CALIF 03/01/77

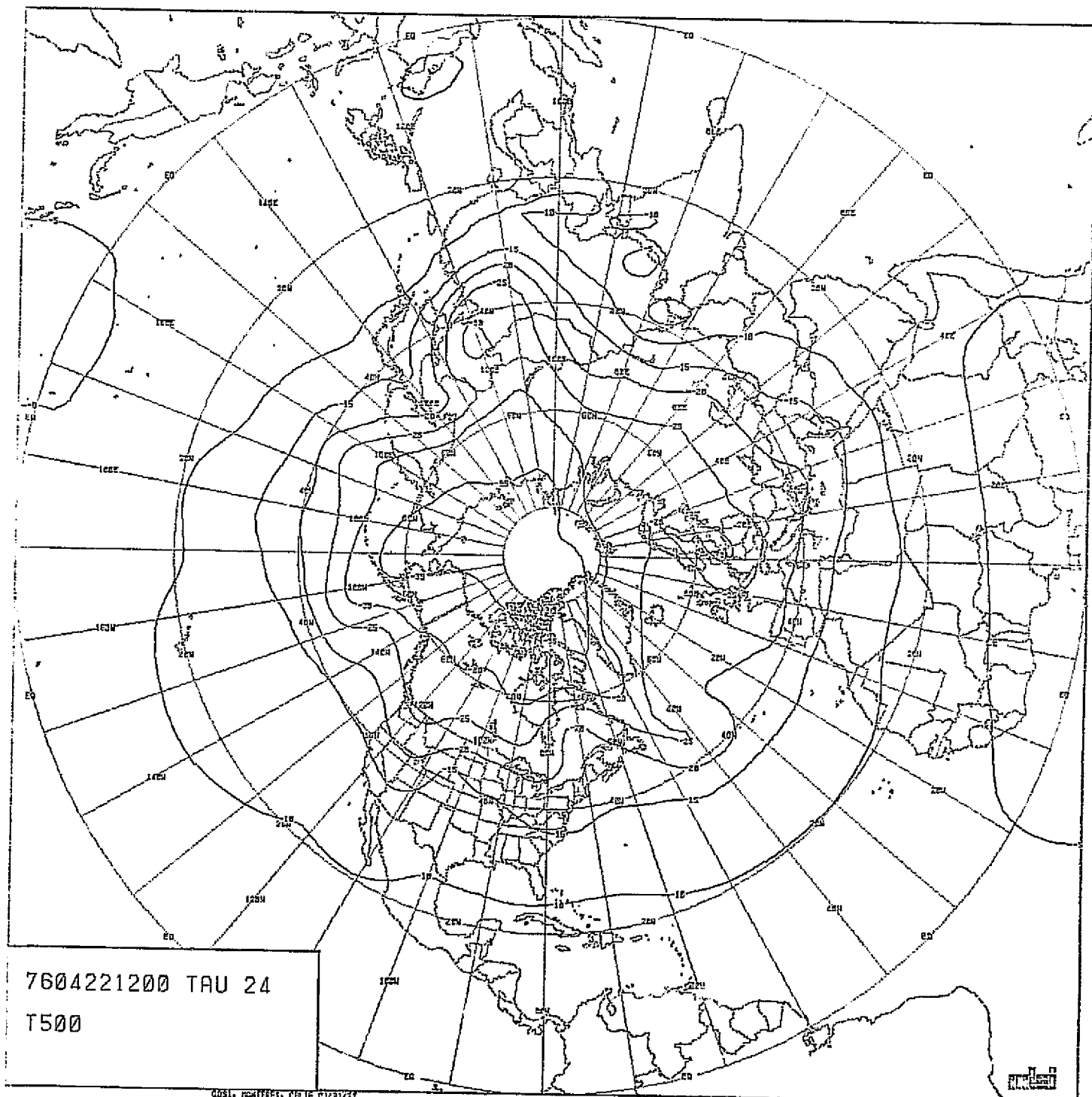
CHART VIII-152 : SEA-LEVEL PRESSURE 24-HOUR FORECAST. RUN T6.
MODFL PECHV. SCENARIO A.

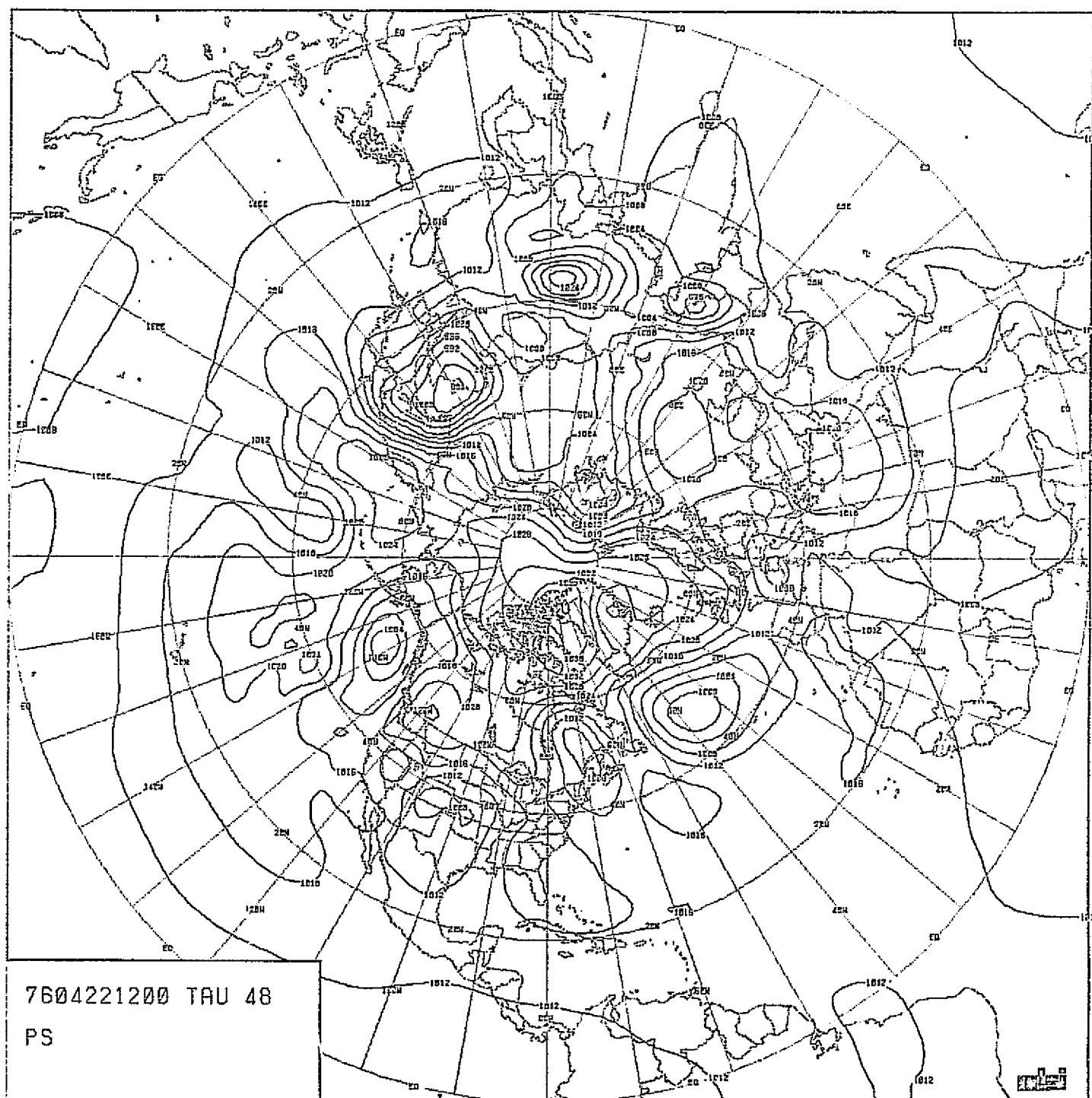


7604221200 TAU 24
Z500

CHART VIII-153 : 500 MB HEIGHT 24-HOUR FORECAST. RUN T6.
MODEL PECHFV. SCENARIO A.

ORIGINAL PAGE IS
OF POOR QUALITY





0001. 001555. 04.14 20/01/77

CHART VIII-155 : SEA-LEVEL PRESSURE 48-HOUR FORECAST. RUN T6.
MODEL PECHFV. SCENARIO A.

ORIGINAL PAGE IS
OF POOR QUALITY

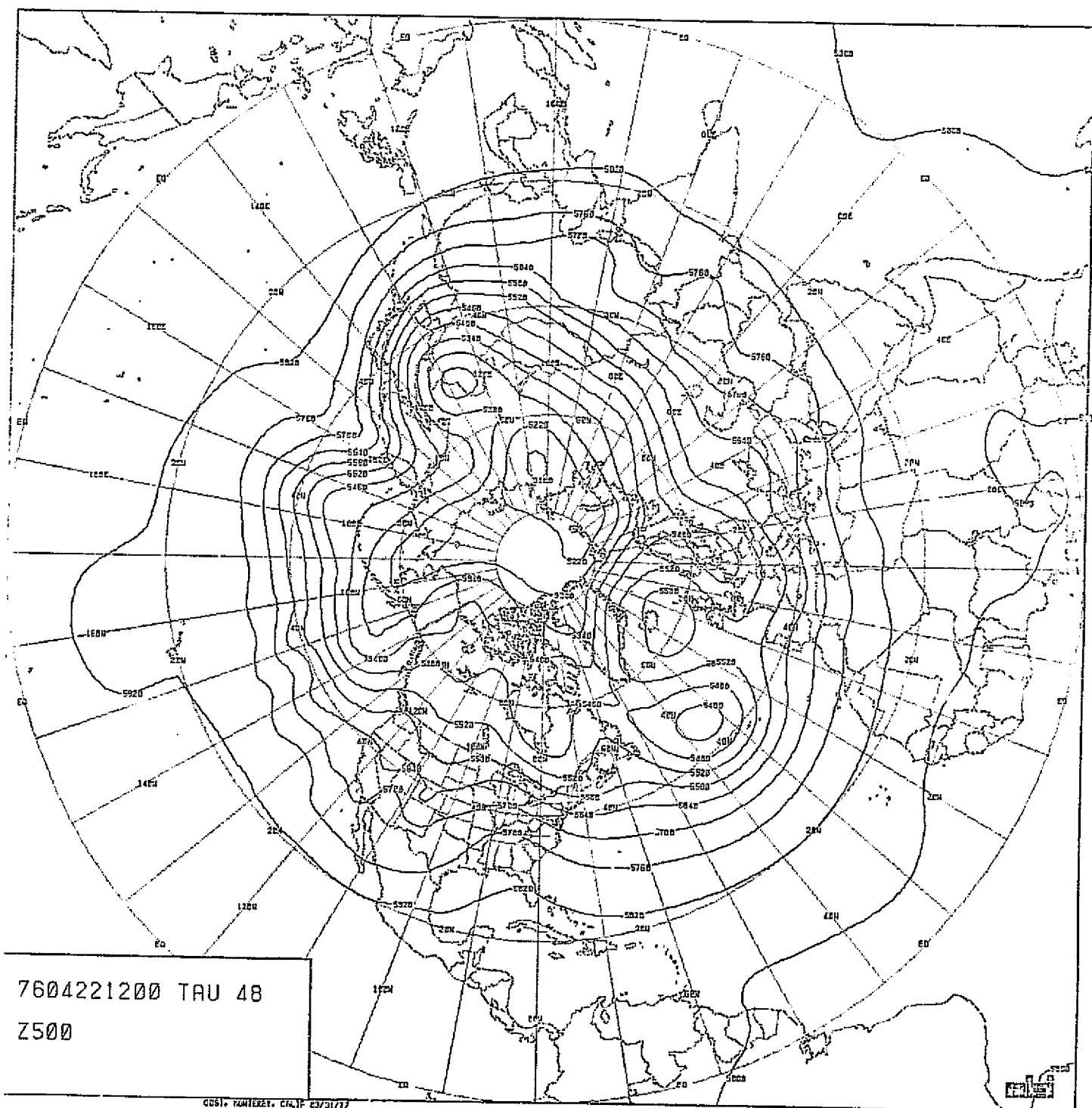
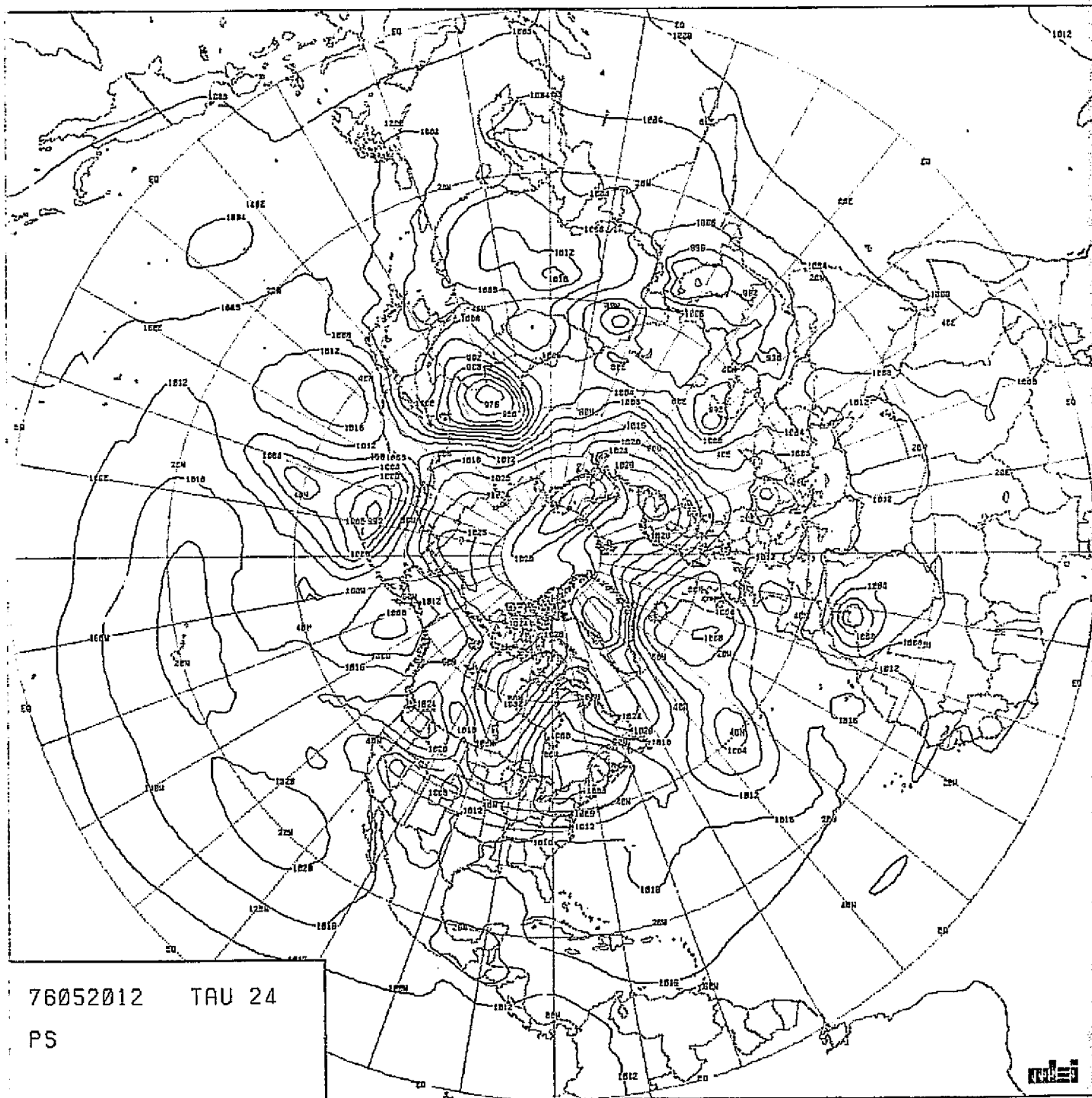


CHART VIII-156 : 500 MB HEIGHT 48-HOUR FORECAST. RUN T6.
MODEL PECHFV. SCENARIO A.

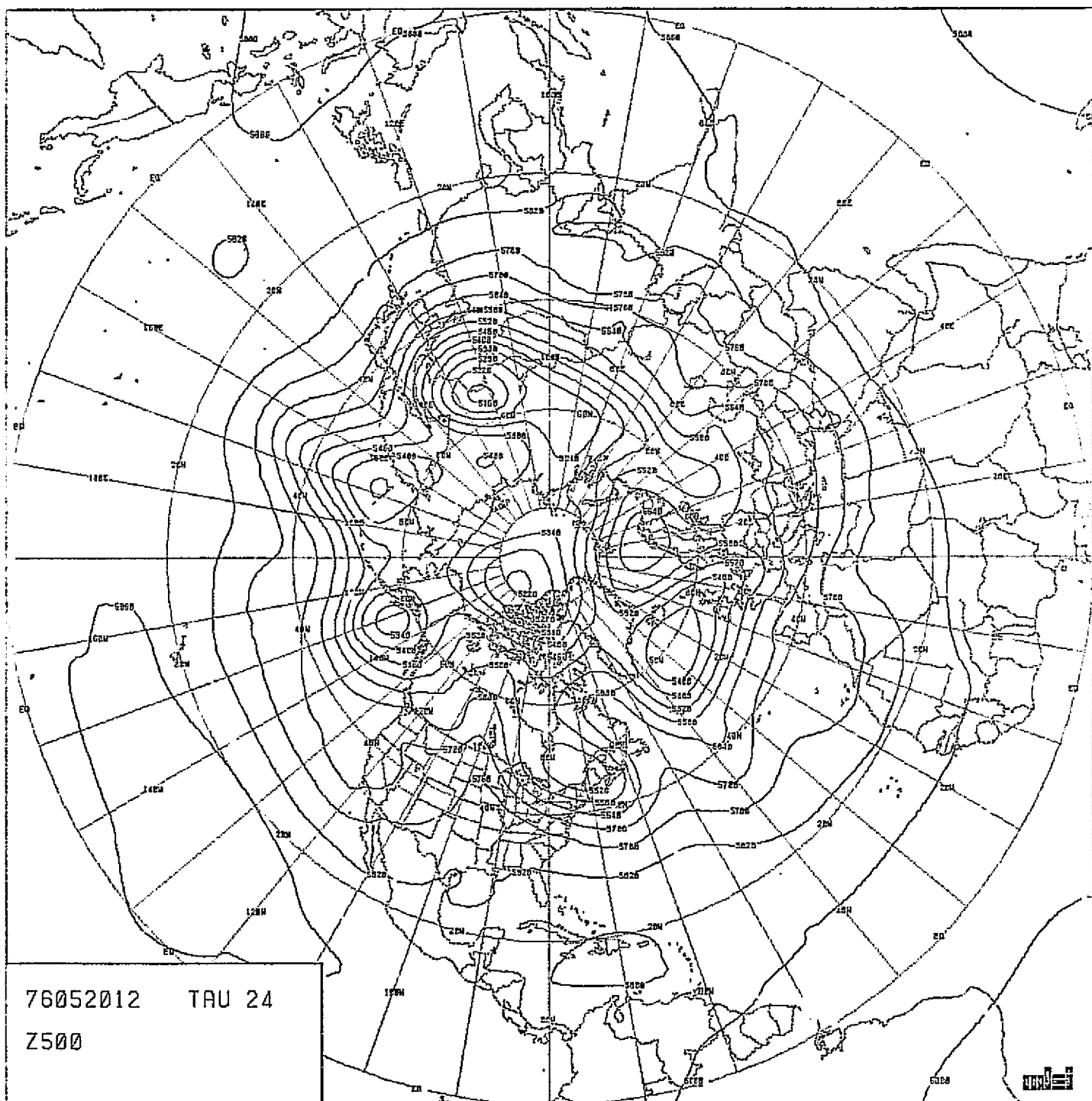


76052012 TAU 24
PS

0051, PANTREY, CALIF 02/14/77

CHART VIII-158: SEA-LEVEL PRESSURE 24-HOUR FORECAST. RUN F21.
MODEL PEFHCV. SCENARIO B.

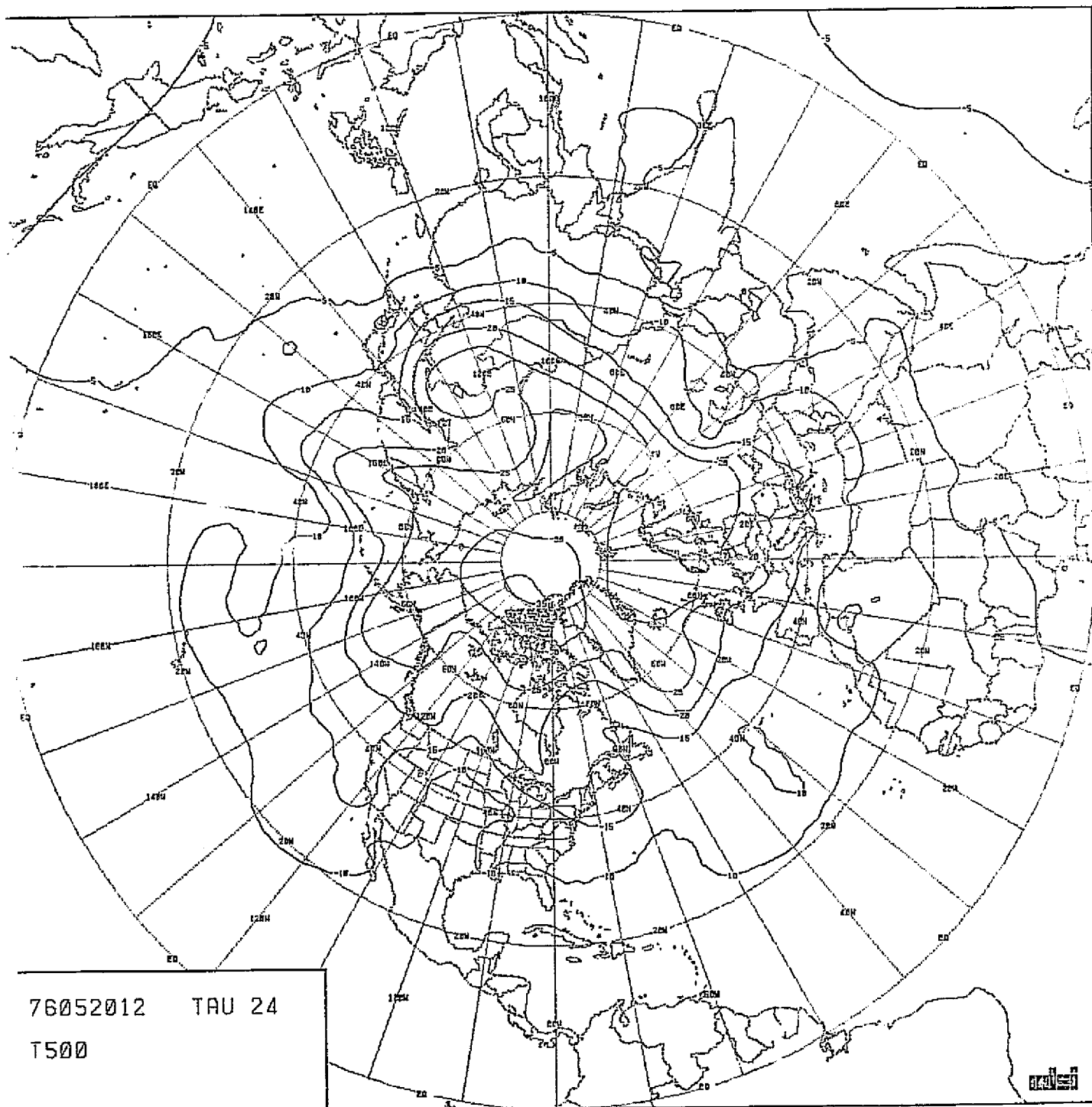
ORIGINAL PAGE IS
OF POOR QUALITY



0091, MONTEREY, CALIF 44/14/77

CHART VIII-159: 500 MB HEIGHT 24-HOUR FORECAST. RUN F24.
MODEL PEHFCV. SCENARIO B.

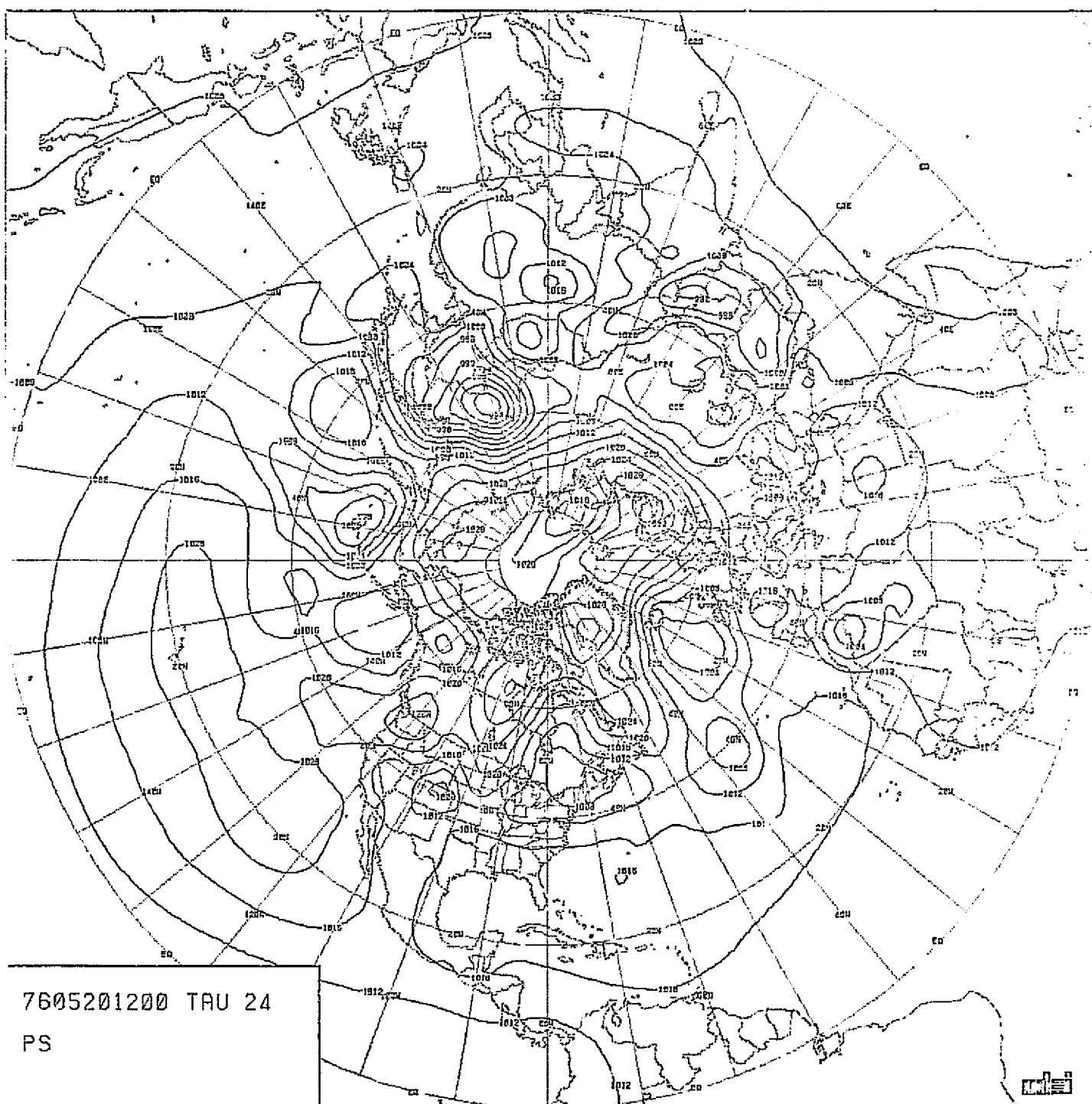
ORIGINAL PAGE IS
ON POOR QUALITY



76052012 TAU 24
T500

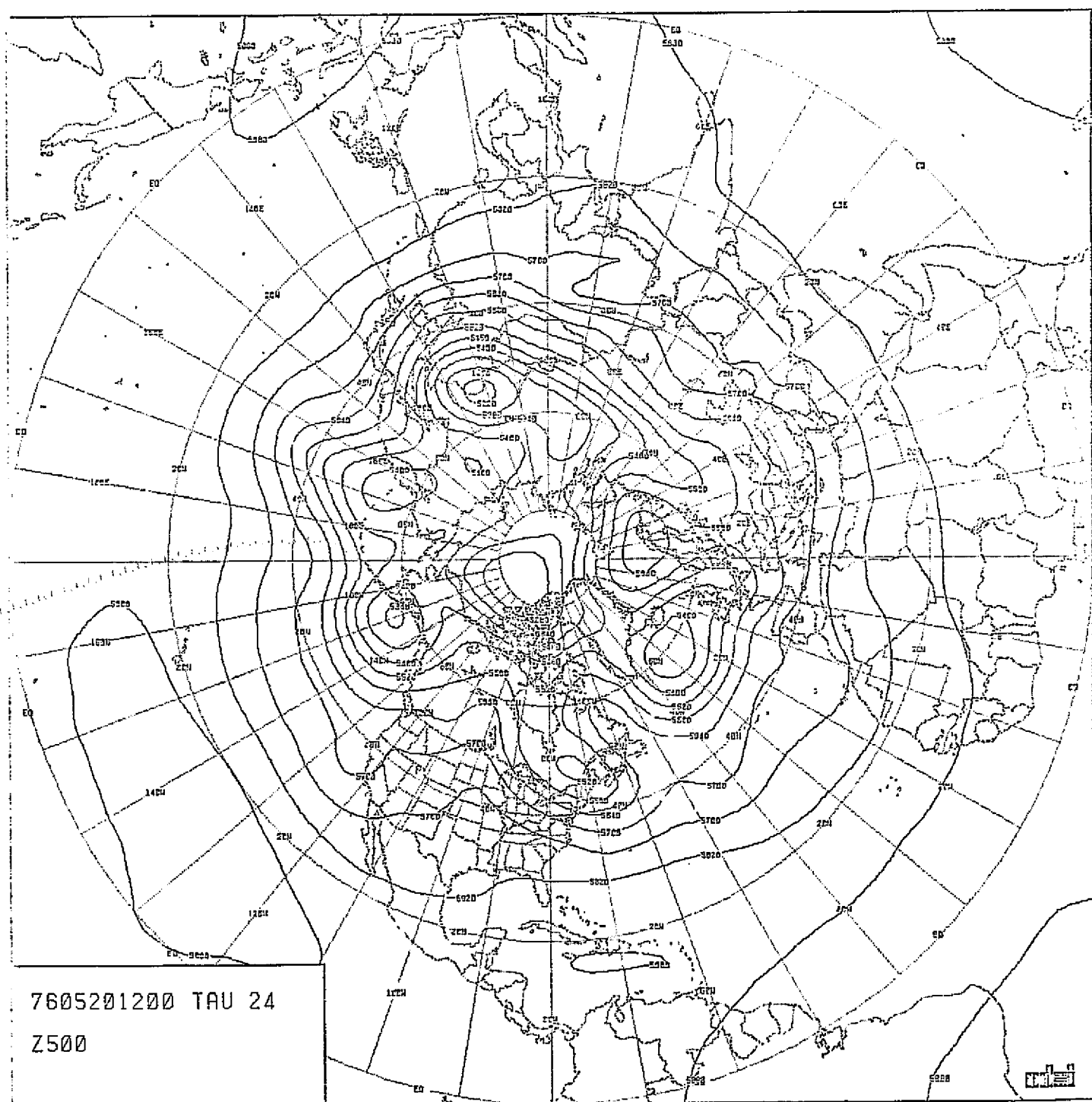
CHART VIII-160: 500 MB TEMPERATURE 24-HOUR FORECAST. RUN F24.
MODEL PEPHCV. SCENARIO B.

ORIGINAL PAGE IS
POOR QUALITY



0051, RUMBERY, CREF 01/02/77

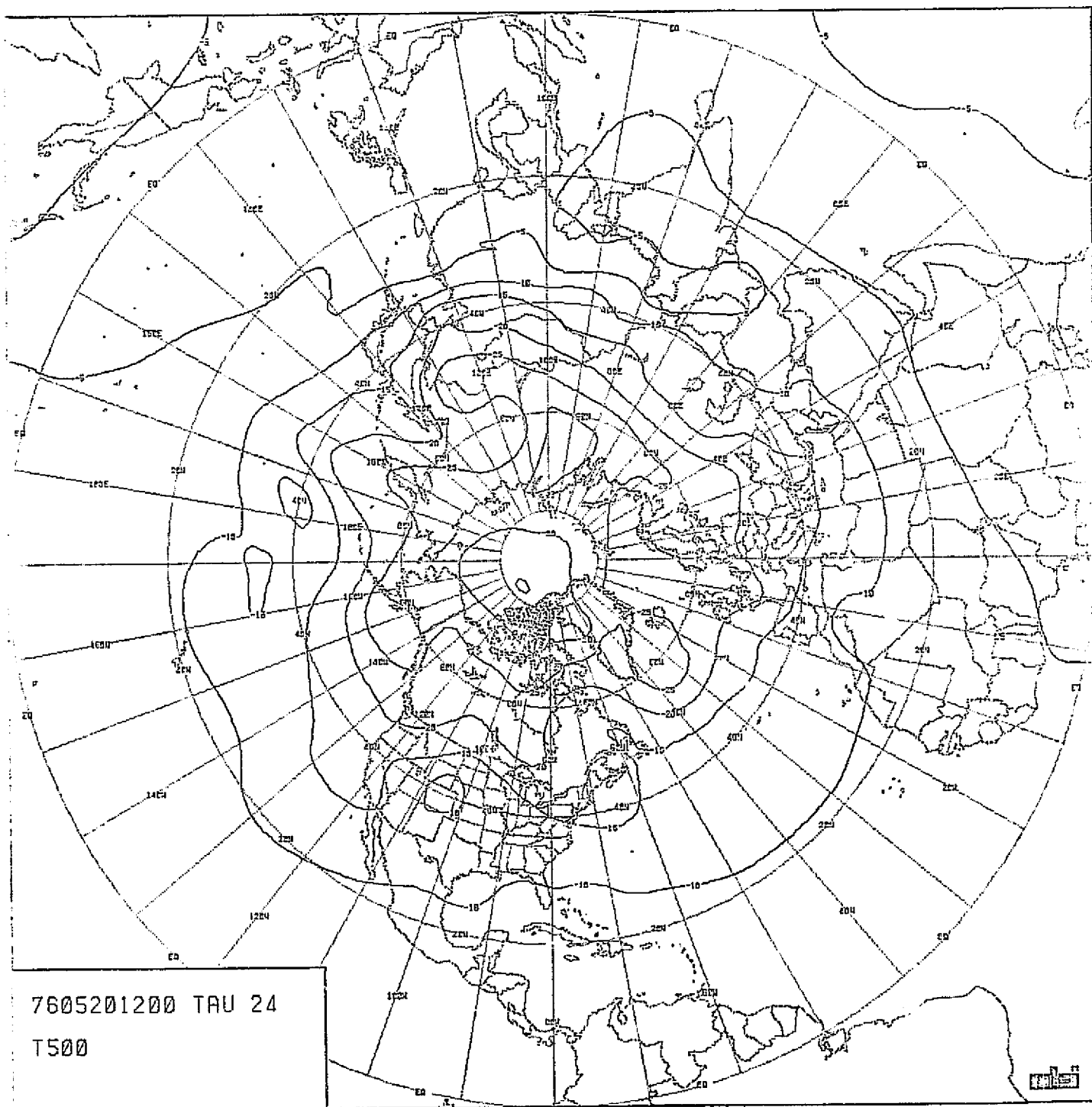
CHART VIII-161: SEA-LEVEL PRESSURE 24-HOUR FORECAST. RUN F19.
MODEL PECHCV. SCENARIO B.



0031. PIRETEST, CHIF 04/04/77

CHART VIII-162: 500 MB HEIGHT 24-HOUR FORECAST. RUN F19.
MODEL PECHCV. SCENARIO B.

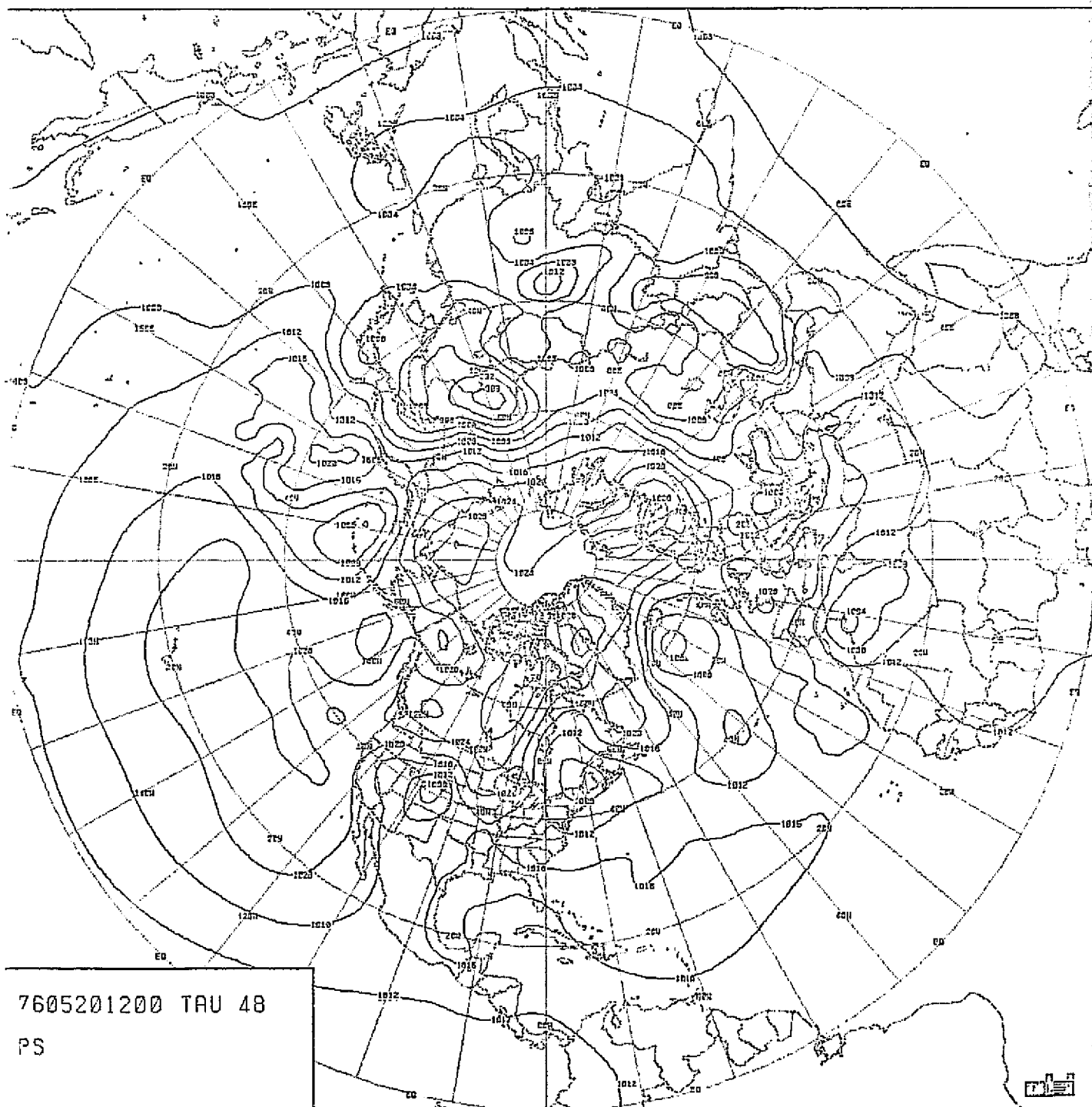
2
ORIGINAL PAGE
OF FOUR



7605201200 TAU 24
T500

CHART VIII-163: 500 MB TEMPERATURE 24-HOUR FORECAST. RUN F19.
MODEL PECHCV. SCENARIO B.

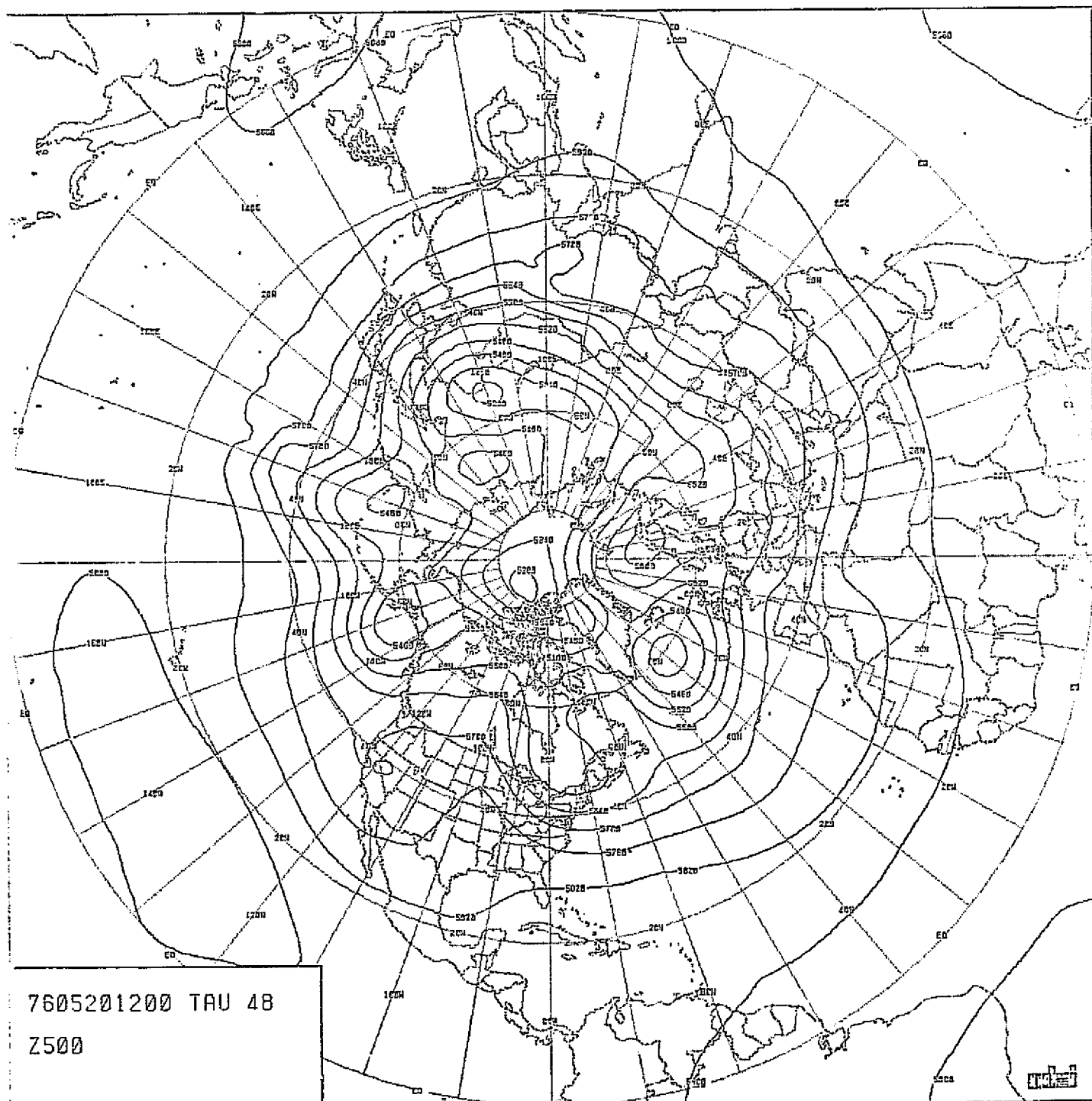
ORIGINAL PAGE 13
POOR QUALITY



0000, 0000000, CRIF 01/04/77

CHART VIII-164: SEA-LEVEL PRESSURE 48-HOUR FORECAST. RUN F19.
MODEL PECHCV. SCENARIO B.

ORIGINAL PAGE IS
OF POOR QUALITY

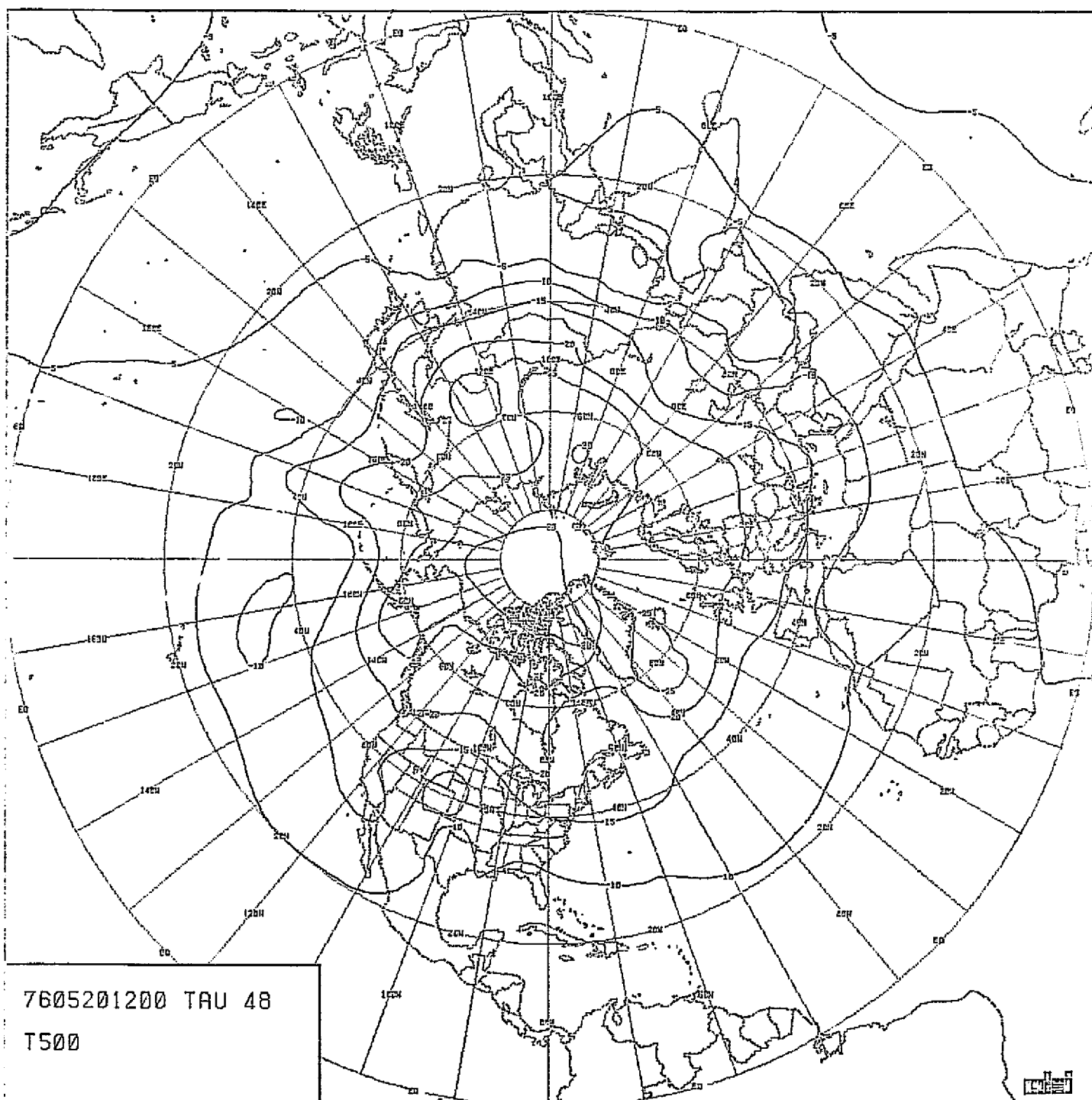


7605201200 TAU 48
Z500

0033, PORTCET, CRLIP 02/04/77

CHART VIII-165: 500-MB HEIGHT 48-HOUR FORECAST. RUN F19.
MODEL PECHCV. SCENARIO B.

ORIGINAL PAGE IS
OF POOR QUALITY



CDR: CENTER: CALIF 04/04/77

CHART VIII-166: 500 MB TEMPERATURE 48-HOUR FORECAST. RUN F19.
MODEL PECHCV. SCENARIO B.

ORIGINAL PAGE IS
OF POOR QUALITY

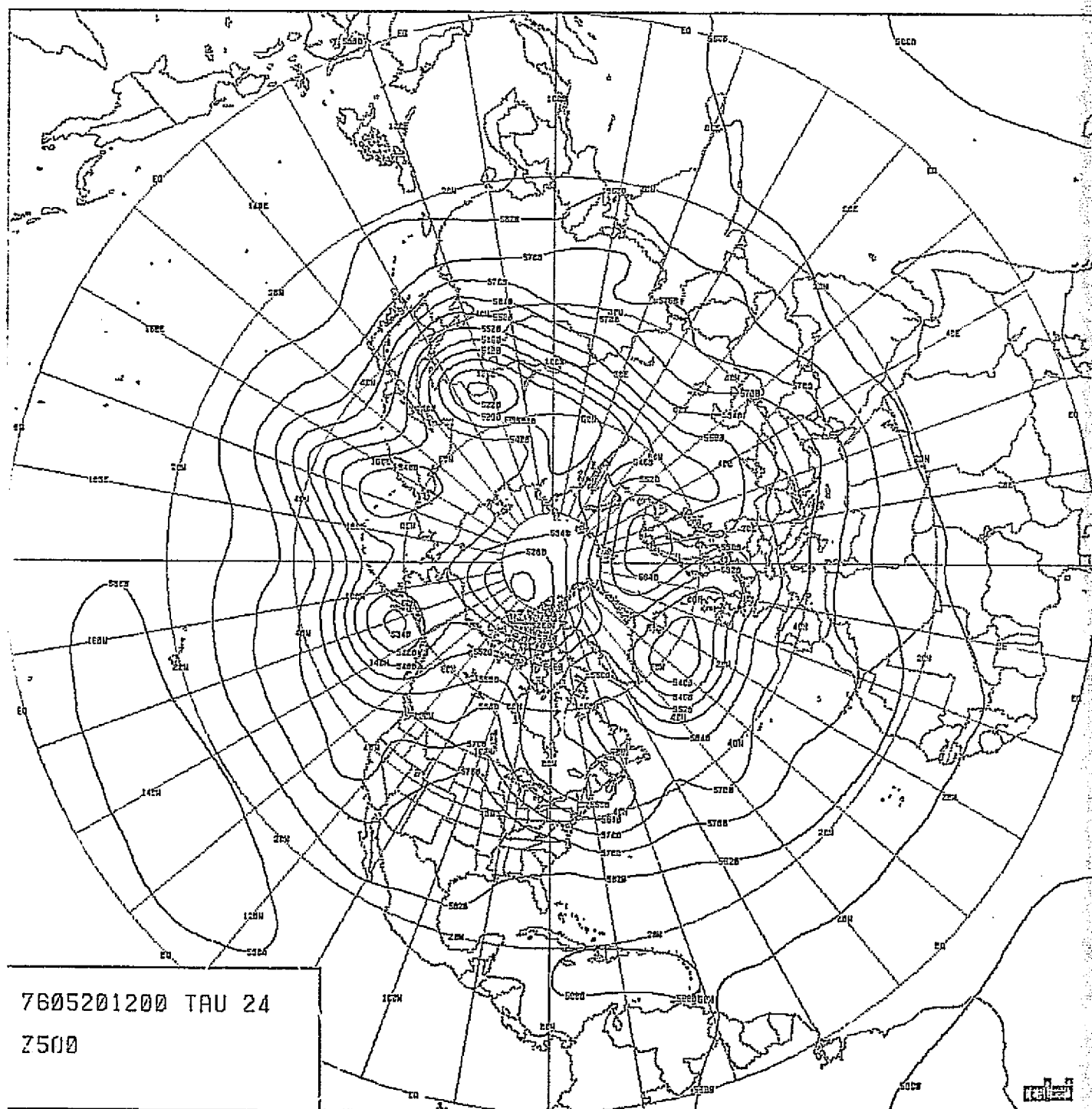
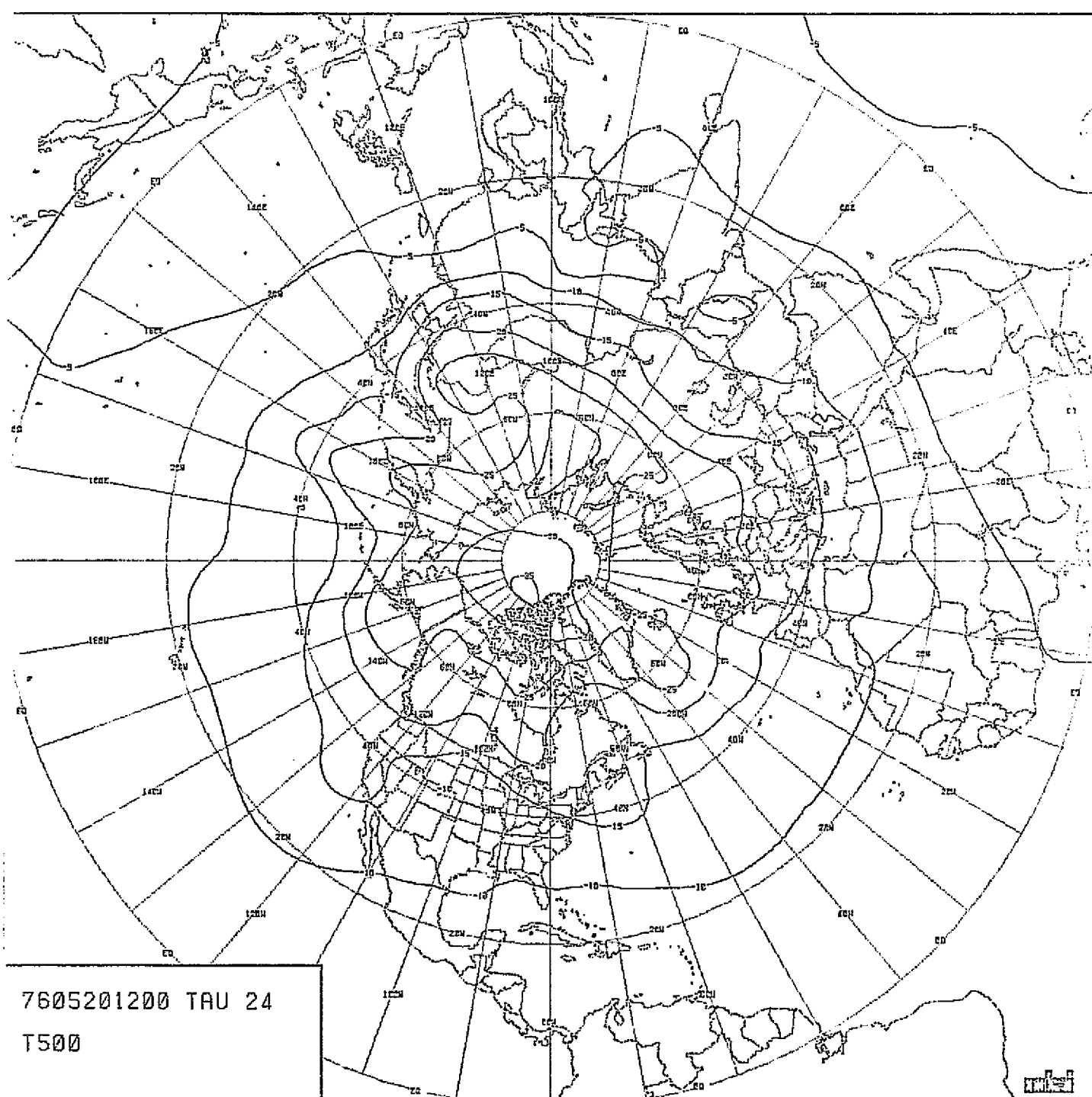


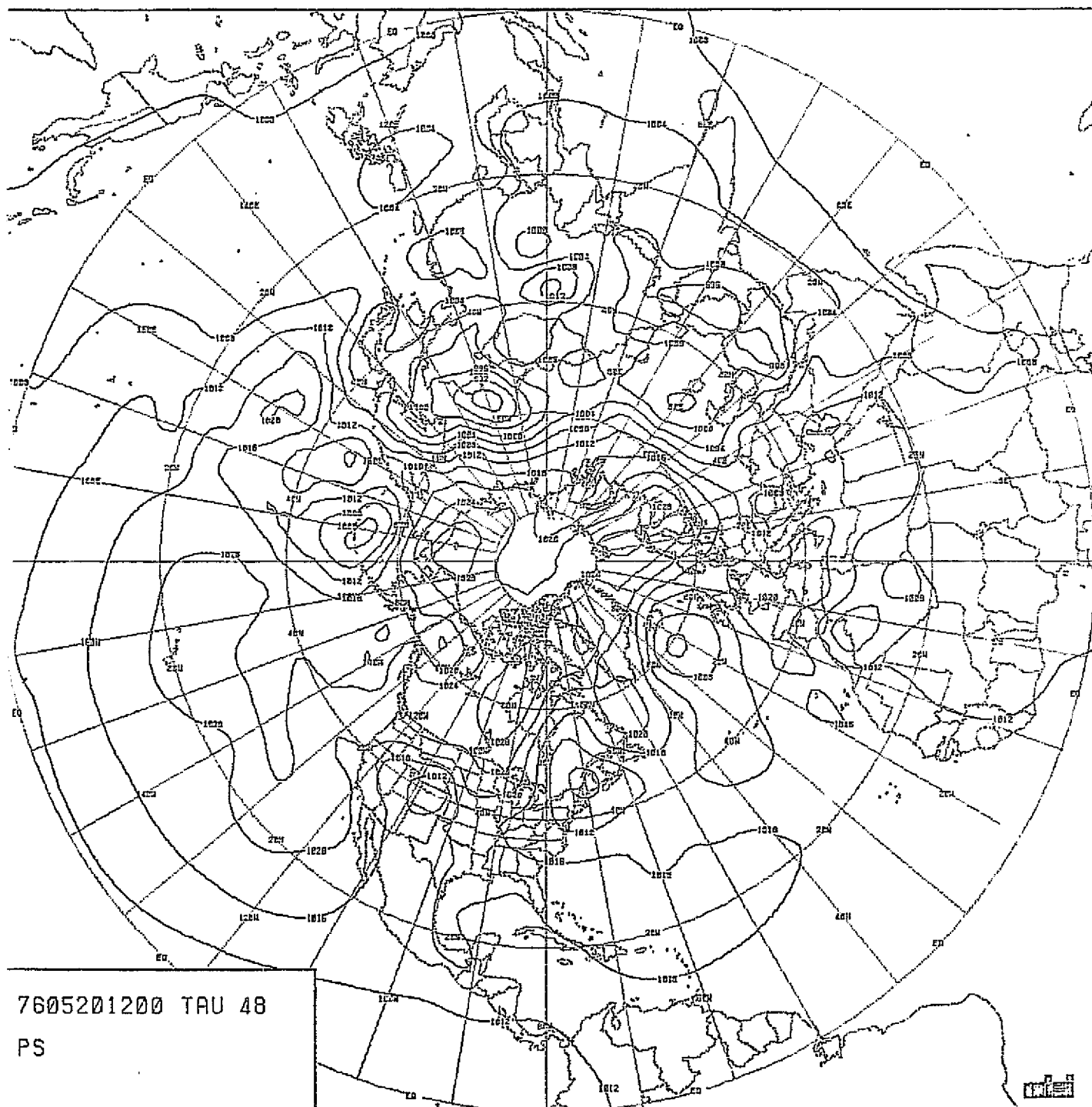
CHART VIII-168: 500 MB HEIGHT 24-HOUR FORECAST. RUN T5.
MODEL PECHPV. SCENARIO B.



7605201200 TAU 24
T500

0031, MONTESEY, CALIF 05/07/77

CHART VIII-169: 500 MB TEMPERATURE 24-HOUR FORECAST. RUN T5.
MODEL PECHFV. SCENARIO B.

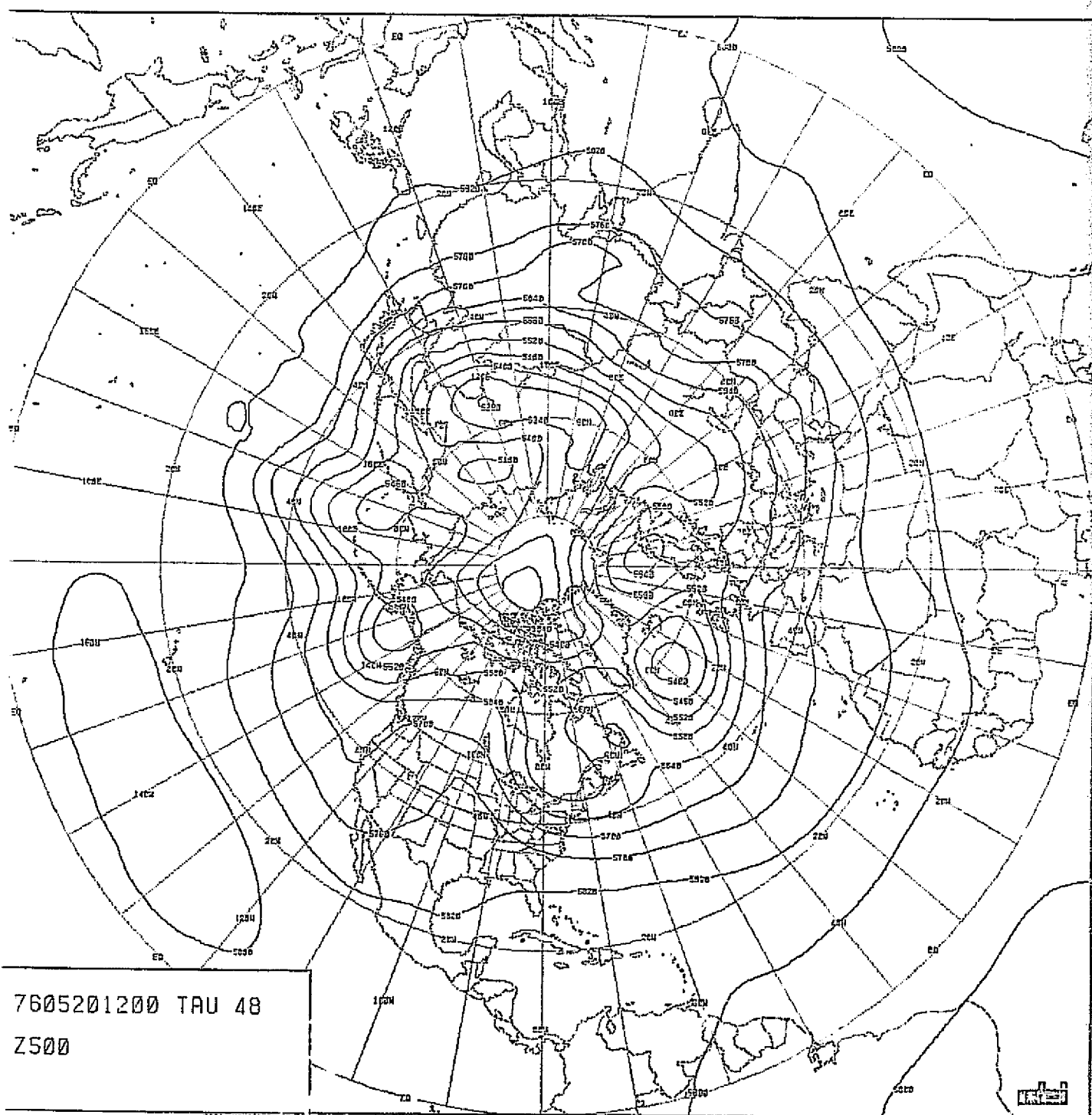


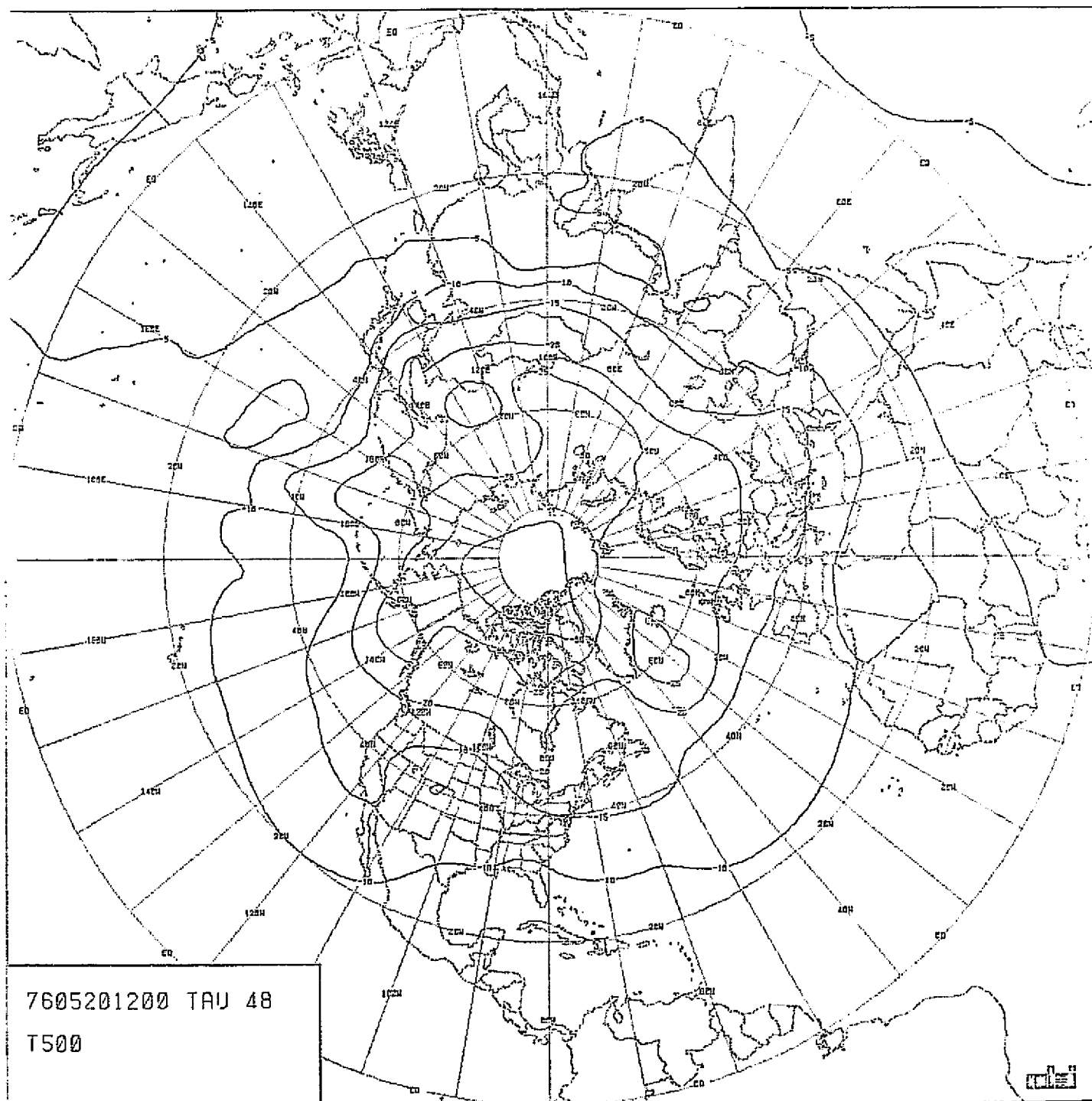
7605201200 TAU 48

PS

0091, RANTERT, CALIF 04/01/77

CHART VIII-170: SEA-LEVEL PRESSURE 48-HOUR FORECAST. RUN T5.
MODEL PECHFV. SCENARIO B.





7605201200 TRJ 48
T500

CSST, MONTREAL, CRTC 66/11/17

CHART VIII-172: 500 MB TEMPERATURE 48-HOUR FORECAST. RUN T5.
MODEL PECHFV. SCENARIO B.

ORIGINAL T
OF POOR QUALITY